

Brookhaven National Laboratory

Brookhaven Science Associates

Upton, New York 11973

Muon g-2 Note No. 446

Title: Multiparameter ω_a Analysis of the g-2 Data from 2001

Author: M. Deile

Affiliation: Yale University

Date: March 4, 2004

Multiparameter ω_a Analysis of the g-2 Data from 2001

M. Deile
Yale University

March 5, 2004

Version 1.1

Abstract

The present report describes an ω_a analysis for the g-2 data of the run period in the year 2001. The muon spin precession frequency ω_a was determined by fitting a multiparameter function to the combined electron time spectrum from all 23 usable calorimeters in the g-2 ring.

Two fit functions were applied to the data and compared. The first of them neglects the modulations of g-2 asymmetry and phase by coherent betatron oscillations, whereas the second – the so-called full physics function – implements these effects.

In this document the fit results for R are given with our own secret offset. To convert these numbers into the ones with the official offset, you need to subtract 17.91 ppm. [Addition after opening the box: To obtain the result without any offset, subtract 10.11 ppm from the numbers with our private offset.]

The smallest total uncertainty was obtained with the full physics function. With the official offset the result of this analysis is

$$R = (108.31 \pm 0.71 \pm 0.19) \text{ ppm.}$$

Without offset it is

$$R = (116.11 \pm 0.71 \pm 0.19) \text{ ppm.}$$

Contents

1	Data Production	4
2	Run Selection and Division into Subsets	4
3	Fill Selection	4
3.1	Quadrupole Cuts	4
3.2	T0 Cuts	7
3.3	Laser Cut	7
4	Construction of the Electron Decay Time Spectra	8
4.1	Energy calibration	8
4.2	T0 subtraction	8
4.3	Binning and Randomisation	8
4.4	Pileup Subtraction	8
4.5	Energy Scale Correction	12
4.6	Electrons after Pileup Subtraction	12
5	Fit of the Time Spectra	13
5.1	Fourier Spectra after 5-Parameter Fits	13
5.2	Fit Function	15
5.2.1	Overview	15
5.2.2	Free and Fixed Fit Parameters	17
5.2.3	The CBO Envelope	18
5.2.4	Implementation of the Muon Loss Function	18
5.3	Fit Procedure	20
5.4	Fit Results	24
5.4.1	Fits without Asymmetry/Phase Modulation (1999 Style)	24
5.4.2	Fits with Asymmetry Modulation but without Phase Modulation	33
5.4.3	Fits with Asymmetry and Phase Modulation	41
5.4.4	Energy-Binned Fits with the Full Physics Function	51
5.4.5	Comparison of Fit Results with Different Functions	58
6	Systematic Errors at 31.8 μs Fit Start Time	60
6.1	Time-Varying CBO Frequency	60
6.2	Main (Acceptance) CBO	64
6.3	Acceptance Double CBO	66
6.4	Asymmetry and Phase CBO – Half-Ring Effect	68
6.4.1	1999-Style Function	68
6.4.2	Full Physics Function	70
6.5	Residual Pileup	72
6.5.1	Residual Pileup Fraction from Early and Late Energy Spectra	72
6.5.2	Influence of Residual Pileup on R	74
6.5.3	Shift in R due to the Pileup Phase (Underwater Effect)	75
6.5.4	Unseen Pileup	75
6.6	Gain Changes and Residual Slow Effects	77
6.6.1	Gain Correction with Upper Energy Cut	77
6.6.2	Artificial Enhancement of Gain Variations	80
6.6.3	Effects of an R.S.E. Term	86
6.7	Investigation of the Asymmetry Instability by Energy-Binned Fits	89

6.8	Muon losses	96
6.9	Binning Effects	97
6.10	Randomisation	98
7	Summary	101
7.1	Systematic Error Table	101
7.2	Combined Result from the two Run Sets	102
7.2.1	Averaging Central Values and Systematic Errors with Statistical Weights	102
7.2.2	Optimal Weighting including Correlations of Systematic Errors . . .	102
7.2.3	Purely Statistical Weights but Error Analysis with Correlations . . .	103
7.2.4	Preferred Result	104
A	Fit Results for the 1999-Style Function	106
A.1	Start Time Scans for the Sum of Detectors	106
A.2	Start Time Scans for the Two Half Rings	110
A.3	Individual Detector Fits Starting at $31.8 \mu\text{s}$	114
B	Fit Results for the Physics Function without Phase Modulation	118
B.1	Start Time Scans for the Sum of Detectors	118
B.2	Start Time Scans for the Two Half Rings	122
B.3	Individual Detector Fits Starting at $31.8 \mu\text{s}$	126
C	Fit Results for the Full Physics Function	130
C.1	Start Time Scans for the Sum of Detectors	130
C.2	Start Time Scans for the Two Half Rings	134
C.3	Individual Detector Fits Starting at $31.8 \mu\text{s}$	138
D	Results from the Energy-Binned Fits with the Full Physics Function	142
E	Results from the Gain Study	145
E.1	Average Energy / Gain Sensitivity Factors	145
E.2	Gain versus Time	147

1 Data Production

This analysis is based on the g2off data production [2].

2 Run Selection and Division into Subsets

The run selection by C. Polly and X. Huang [3] with field input from E. Sichtermann – with some further modifications by E. Sichtermann and myself – was used. Runs with low kicker amplitude ($< 97\%$) were discarded while runs with a scraping amplitude of 4 kV instead of 7 kV were kept. Both scraping times used ($7\mu\text{s}$ and $15\mu\text{s}$) were kept.

The data set was divided in two parts reflecting the two quadrupole voltages 21.7 kV and 25.3 kV which result in very distinct coherent betatron oscillation frequencies (418.4 kHz and 490.3 kHz respectively). The run periods constituting the two data sub-sets are defined in Table 1.

Subset	Runs	V_{Quad} [kV]	Comments
A	9423 - 9754	21.7	B_r changed
B	9755 - 9989	25.3	
A	9990 - 10272	21.7	
B	10273 - 10710	25.3	
A	10711 - 10780	21.7	
A	10788 - 10963	21.7	
B	10964 - 11019	25.3	
A	11026 - 11356	21.7	
B	11357 - 11384	25.3	
0	all runs	–	

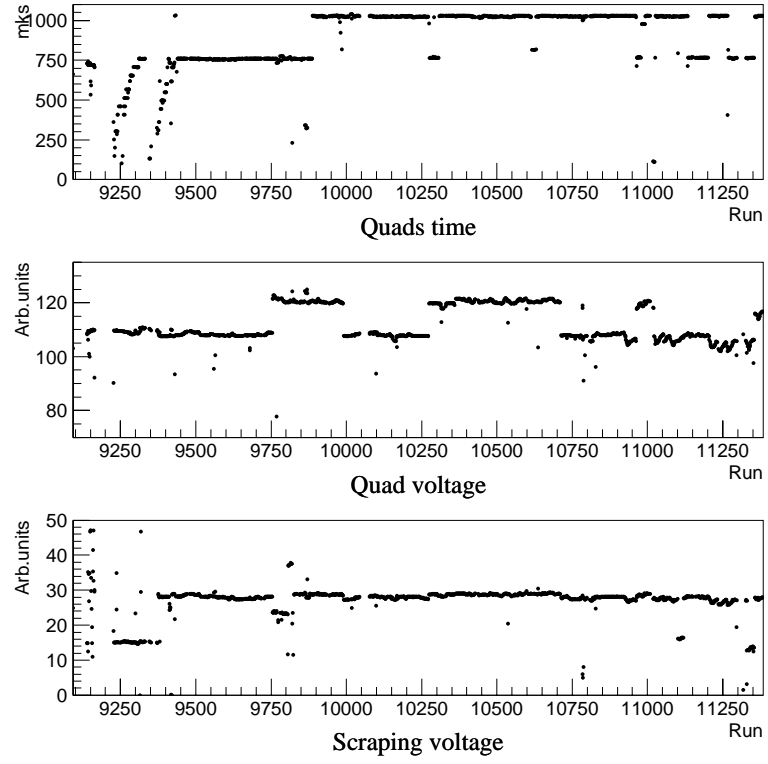
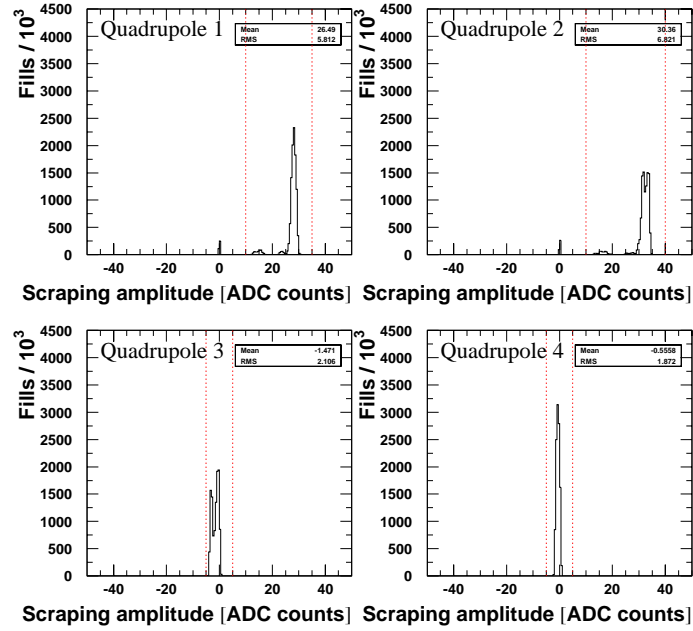
Table 1: *Run periods and the reasons for their distinction.*

3 Fill Selection

3.1 Quadrupole Cuts

A fill passes the quadrupole selection if the following criteria are met:

- The quadrupoles are on for at least $600\mu\text{s}$ after injection. The distribution of quadrupole switch-off times is shown in Figure 1.
- The scraping amplitudes (second minus first quadrupole voltage reading) must be within the limits shown in Figure 2.
- The second and third quadrupole reading must be equal within the limits shown in Figure 3. This requirement discards fills with quadrupole sparks.
- The individual quadrupole readings must lie within $5 \times \text{RMS}$ of their distributions.

Figure 1: *CBO parameters versus run.*Figure 2: *Distribution of the scraping amplitudes in the four quadrupoles. The dotted lines represent the cuts applied.*

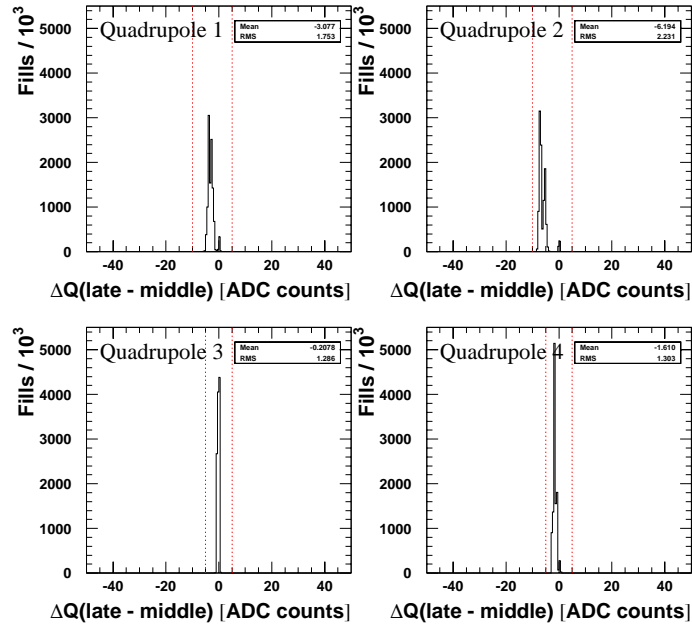


Figure 3: *Distribution of the difference between the third and the second voltage measurement in the four quadrupoles. The dotted lines represent the cuts applied.*

3.2 T0 Cuts

T0 cuts were derived from the distributions of T0 pulse amplitudes and mean times. Outlier fills are discarded.

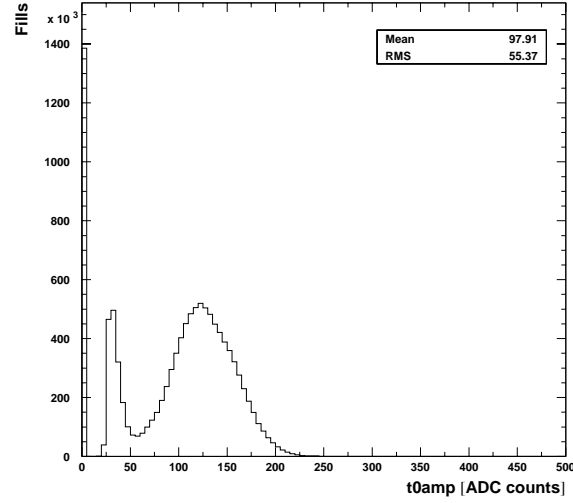


Figure 4: *Distribution of the T0 pulse amplitude. Each entry corresponds to one fill.*

- The pulse amplitude is required to be greater than 10 (see Figure 4).
- The pulse mean time must lie between 59000 ns and 59500 ns (Figure 5). This cut is not very tight and mainly designed for discarding fills without T0 pulse (`t0mean` = 0).

3.3 Laser Cut

Fills with laser pulses in the analysed time window ($20\ \mu\text{s}$ to $600\ \mu\text{s}$) were discarded.

4 Construction of the Electron Decay Time Spectra

4.1 Energy calibration

Energy-spectrum end-points (corresponding to 3.2 GeV) were determined for each run by straight-line fits to the trailing parts of the energy spectra later than $200\ \mu\text{s}$. The raw run-by-run end-points were then plotted as a function of the run number and fitted to straight lines in run intervals.

4.2 T0 subtraction

To obtain the electron pulse times with respect to the T0 pulse, the mean time of the T0 pulse (ntuple variable **t0mean**) was subtracted from the raw pulse times.

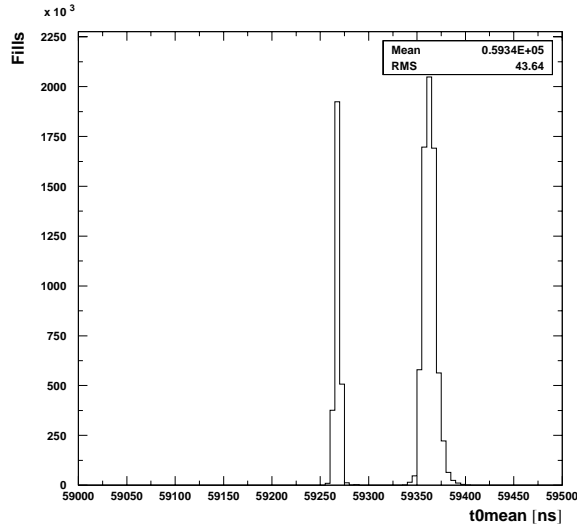


Figure 5: *Distributions of the mean time of the T0 pulse. Each entry corresponds to one fill. There are two peaks because after run 10827 the G10 kicker timing changed.*

4.3 Binning and Randomisation

For each detector and each run a time spectrum was created. The bin width of the time spectra was $149.2\ \text{ns}$, i.e. the fast rotation period determined by A. Lam with a Fourier analysis [4]. Before filling the individual electron times into their histograms, they were randomised by adding a fill-specific random number taken from a flat distribution in the range $[-\frac{149.2\ \text{ns}}{2}, +\frac{149.2\ \text{ns}}{2}]$. This was done to remove the fast rotation structure from the data.

4.4 Pileup Subtraction

Pileup was subtracted with the “Mediterranean Method” [5]. The lower energy cut was 1.8 GeV.

The time window where shadow pulses (“S2”) for the construction of the artificial pileup were looked for, had its centre 13 ns after the trigger pulse (“S1”). The window width was twice the g2off pulse fitter dead-time. This dead-time is detector-specific and depends on the energy E_{S2} of the shadow pulse. It is typically about 2.9 ns. The detector

and energy dependence of the dead-time (Figure 6) was provided by Vanya [6] who had obtained them from a simulation.

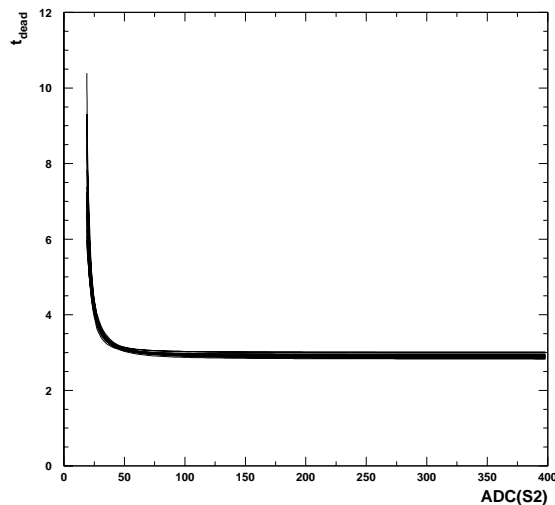


Figure 6: *Dead-time of the pulse finding algorithm as a function of the pulse height of S2 in terms of ADC counts. The conversion from ADC to energy is detector dependent (Section 4.1). Typically $ADC = 60$ corresponds to 1 GeV . The curves for all detectors are superimposed.*

Also, the energy E_D of a constructed double pulse was calculated from the energies E_{S1} and E_{S2} of the two individual overlapping pulses, using Vanya’s simulation results:

$$E_D = f_L(E_{S1}, E_{S2}) \cdot (E_{S1} + E_{S2}) \quad , \quad (1)$$

where the function $f_L(E_{S1}, E_{S2})$ replaces the constant “Logashenko coefficient” of 0.96 which had been used in the past. This function is shown in Figures 7 and 8.

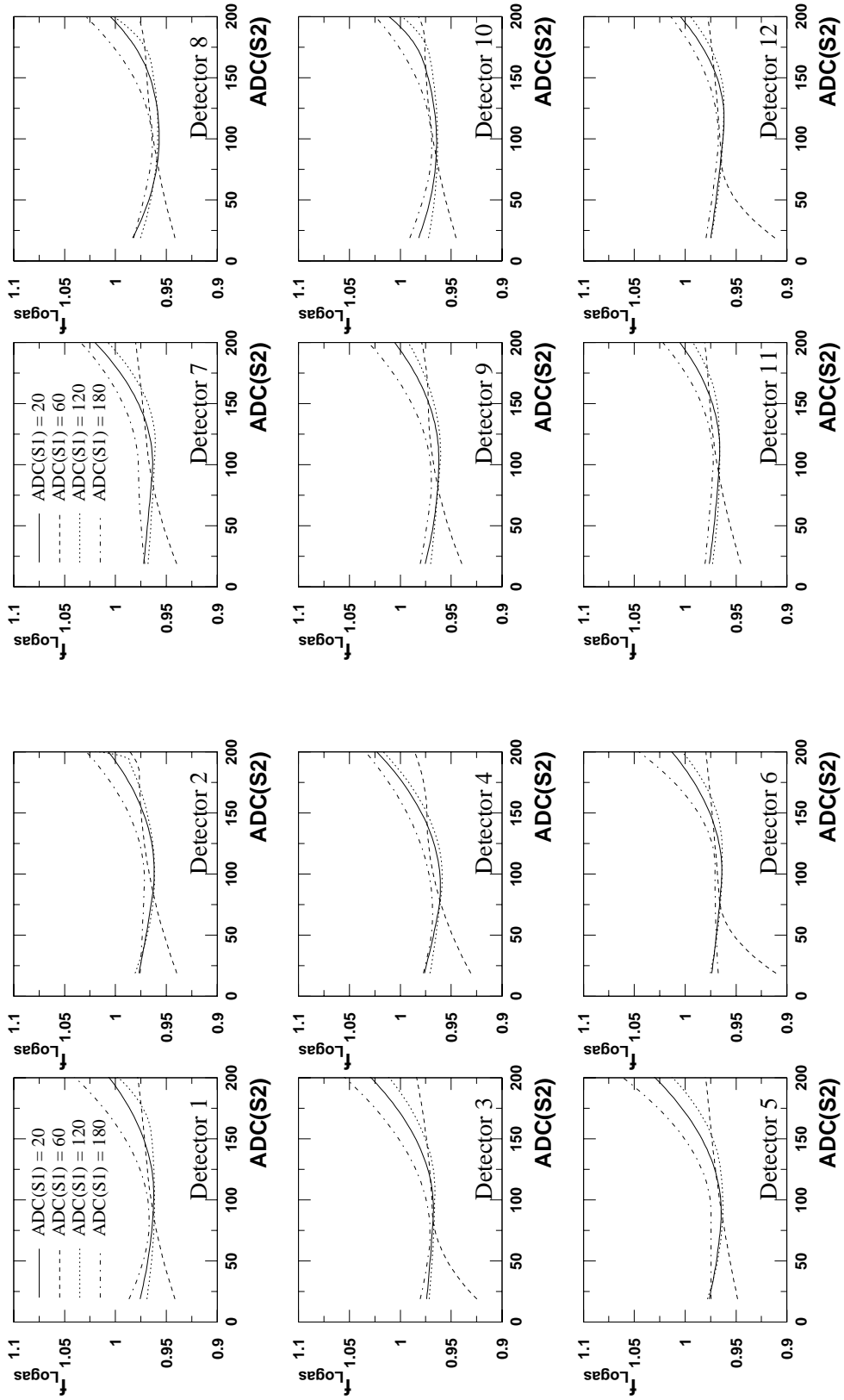


Figure 7: *Logashenko function for detectors 1 to 12. Typically $\text{ADC} = 60$ corresponds to 1 GeV .*

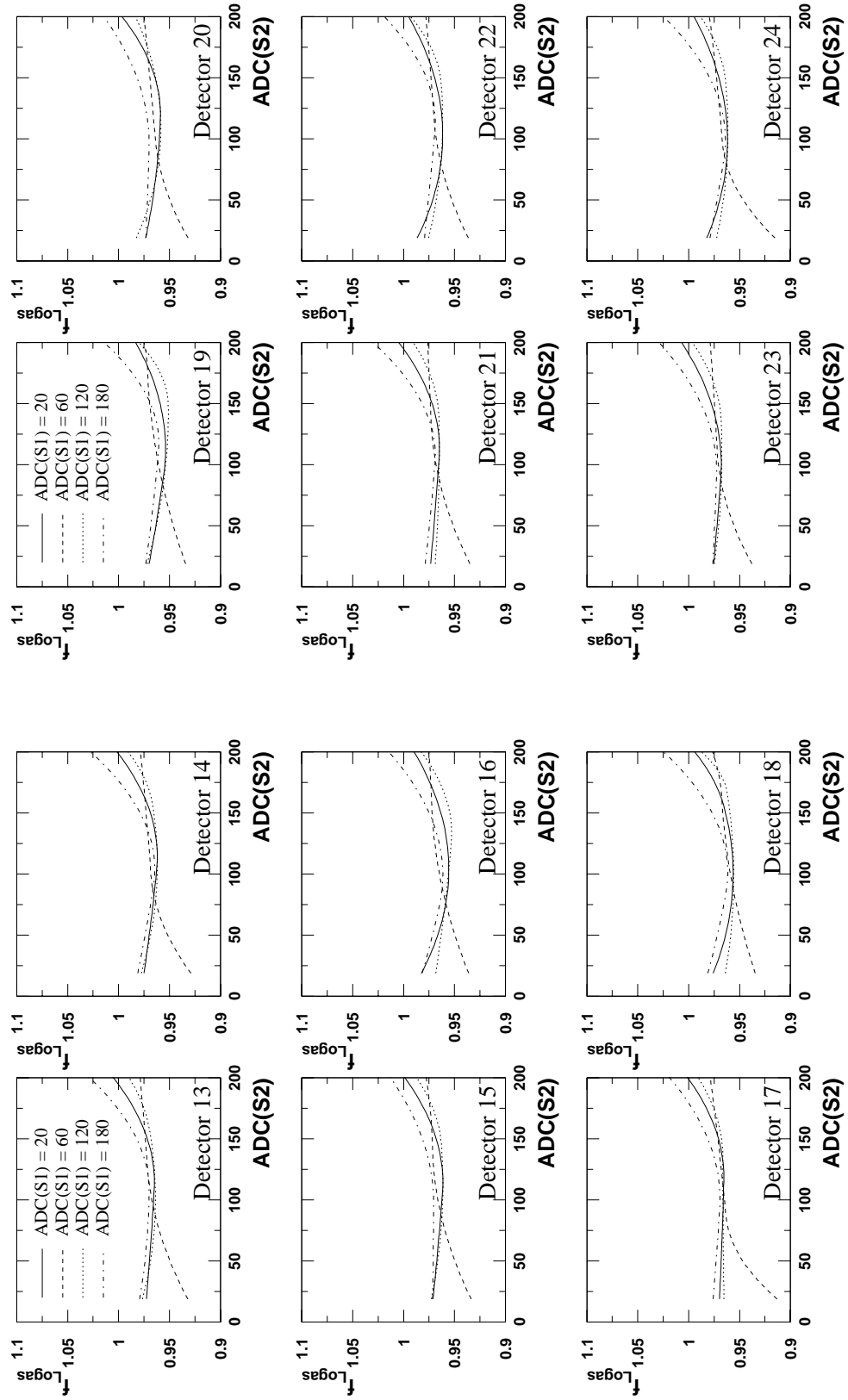


Figure 8: *Logashenko function for detectors 13 to 24. Typically $\text{ADC} = 60$ corresponds to 1 GeV .*

4.5 Energy Scale Correction

Gain variations were corrected for by using the time evolution of the average energy between 1.8 GeV and 3.4 GeV. Method and impact on the fit results are explained in Section 6.6.

4.6 Electrons after Pileup Subtraction

The final number of analysable electrons per detector between $31.8 \mu\text{s}$ and $600 \mu\text{s}$ after all cuts and pileup subtraction is given in Table 2.

Detector	Set A	Set B	Sum
1	104 598 794	70 865 274	
2	103 722 204	70 326 373	
3	103 772 927	70 143 333	
4	104 718 612	70 870 106	
5	101 670 393	68 768 646	
6	92 808 150	62 612 199	
7	89 486 798	60 444 400	
8	84 002 245	56 946 686	
9	90 529 440	61 384 216	
10	94 882 887	64 436 026	
11	101 510 607	68 760 995	
12	93 472 178	63 470 416	
13	103 069 423	69 830 759	
14	96 542 080	65 562 645	
15	103 111 415	70 100 276	
16	90 659 893	61 548 018	
17	98 442 277	66 990 281	
18	95 187 966	65 085 152	
19	101 657 780	69 125 511	
20	(60 966 748)	(40 588 896)	
21	102 012 193	68 873 798	
22	94 927 638	64 246 414	
23	94 084 851	63 798 012	
24	93 891 155	63 771 855	
0	2 238 761 906	1 517 961 391	3 756 723 297

Table 2: *Number of electrons between $31.8 \mu\text{s}$ and $600 \mu\text{s}$ after all cuts and pileup subtraction.*

5 Fit of the Time Spectra

5.1 Fourier Spectra after 5-Parameter Fits

Figures 9 and 10 show the Fourier spectra of residuals after fits to the 5-parameter function

$$\dot{N}(t) = \frac{N_0}{\tau} e^{-t/\tau} [1 + A \cos(\omega_a t + \phi_a)] \quad (2)$$

with a start time of 31.8 μs .

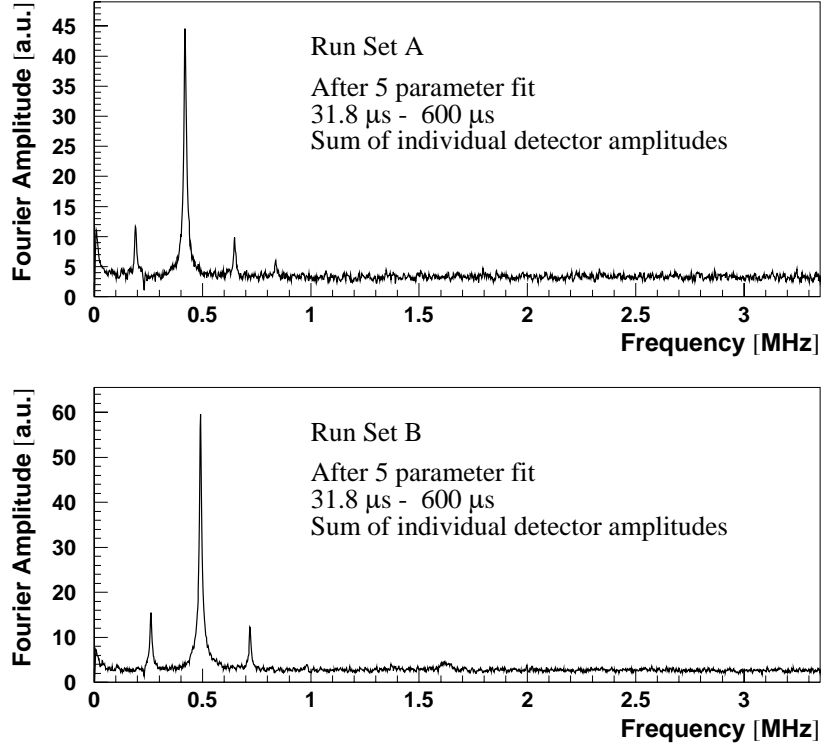


Figure 9: All detectors were fitted separately to a 5-parameter function in the fit interval 31.8 μs - 600 μs . The residuals after the fit were Fourier-analysed; then the Fourier amplitudes were added.

This study tells us which perturbation effects need to be accounted for by the fit function. In the first figure, the individual detector residuals were Fourier-analysed and then their Fourier amplitudes added; in the second figure, the residuals from the fit to the sum of detectors were Fourier-analysed.

All spectra shown are dominated by the CBO peak and its satellites from beating with ω_a . Furthermore, there is a peak at zero frequency which is mainly caused by muon losses but also by residual slow effects from gain variations and unsubtracted pileup.

The double CBO is significant for Set A, mainly in the sum of individual Fourier amplitudes. In the spectrum from the fit to the sum of detector it is less pronounced because of cancellation around the ring, but it is still visible. Therefore the DCBO was included in the fit function. In the sum of individual Fourier amplitudes a small peak for the vertical waist (VW) is visible in Set A (around 1.63 MHz). In Set B the VW peak

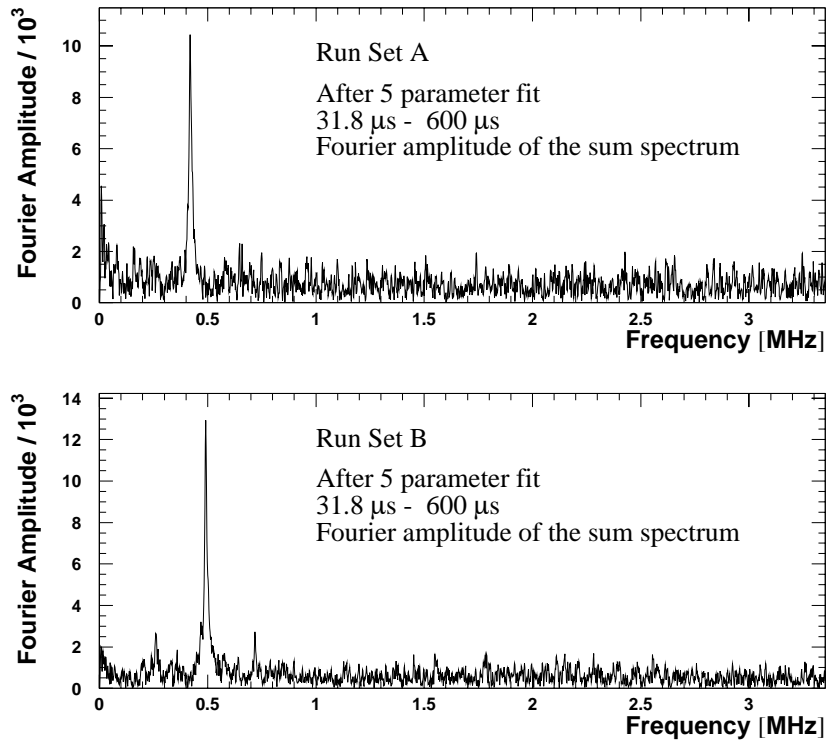


Figure 10: *The sum of detectors was fitted to a 5-parameter function in the fit interval 31.8 μ s - 600 μ s. The residuals after the fit were Fourier-analysed.*

would be expected around 2.0 MHz but is not observed. The vertical oscillations (VO, expected around 2.3 MHz in Set A and around 2.5 MHz in Set B) are invisible. Both VW and VO were neglected in the fits.

5.2 Fit Function

5.2.1 Overview

The analysis is based on the following function. Some of its features were only switched on for certain studies.

$$\dot{N}(t) = \frac{N_0}{\tau} A_N(t) \cdot e^{-t/\tau} \cdot [1 + A \cdot A_R(t) \cdot \cos(\omega_a t + \phi_a \cdot A_J(t))] \cdot V(t) \cdot g_{\text{slow}}(t) \quad (3)$$

with

$$\omega_a = 2\pi \cdot 0.2291 \text{ MHz} \cdot [1 - (R - \Delta R) \cdot 10^{-6}] \quad (4)$$

where R is the actual fit parameter and ΔR a secret offset.

This function accounts for horizontal (radial) CBO oscillations modulating the acceptance $A_N(t)$, the asymmetry A and the g-2 phase ϕ_a . There are contributions from oscillations of the beam centre and from width variations. The latter are not harmonic oscillations with the CBO frequency f_{CBO} but also contain components with the frequency $2f_{\text{CBO}}$. However, this double CBO decays with about half the CBO life time (i.e. roughly $50 \mu\text{s}$) and plays a role only at early times. The following functional forms were used for the CBO terms:

- Acceptance modulation by CBO:

$$A_N(t) = 1 + A_{\text{CBO}} \cdot g_{\text{CBO}}(t) \cdot \cos(\phi_{\text{CBO}}(t)) + A_{\text{DCBO}} \cdot g_{\text{CBO}}^2(t) \cdot \cos(\phi_{\text{DCBO}}(t)) \quad (5)$$

The oscillation is described by the terms $\phi_{\text{CBO}}(t)$ (single CBO frequency) and $\phi_{\text{DCBO}}(t)$ (double CBO frequency) which will be further specified below. The time envelope $g_{\text{CBO}}(t)$ was determined as described in Section 5.2.3, and found to be exponential in good approximation. For the double CBO envelope the square of $g_{\text{CBO}}(t)$ was used, i.e. an exponential with half the CBO life time.

- Asymmetry modulation by CBO (“Rob effect”):

$$A_R(t) = 1 + A_R \cdot g_{\text{CBO}}(t) \cdot \cos(\phi_R(t)) \quad (6)$$

For a single detector, this effect is roughly five times smaller than the acceptance CBO. The same exponential time envelope $g_{\text{CBO}}(t)$ was used as for the acceptance CBO. In principle, there is also a double CBO component like for the acceptance CBO. However, it is very small and can be neglected.

- Phase modulation by CBO (“Jim effect”):

$$A_J(t) = 1 + A_J \cdot g_{\text{CBO}}(t) \cdot \cos(\phi_J(t)) \quad (7)$$

Again, the same exponential envelope $g_{\text{CBO}}(t)$ was used.

Vertical waist and vertical oscillation are small, short-lived effects and only observable at very early times. The dominant acceptance part is given by

$$V(t) = 1 + A_{\text{VW}} \cdot e^{-t^2/2\tau_{\text{VW}}^2} \cdot \cos(\phi_{\text{VW}}(t)) + A_{\text{VO}} \cdot e^{-t^2/2\tau_{\text{VO}}^2} \cdot \cos(\phi_{\text{VO}}(t)) \quad (8)$$

if the time envelopes are approximated by gaussians. This expression was only implemented for systematic studies whereas for the regular fitting function, $V(t)$ was set to 0.

The quadrupole voltage V_Q and thus the field index n were not constant during the fill:

- After the end of scraping, V_Q and n increase with a RC saturation time constant τ_{rise} of about $5\ \mu\text{s}$:

$$n(t) = n_{\text{sat}} \left[1 - A_{\text{rise}} e^{-(t-t_{\text{scrap}})/\tau_{\text{rise}}} \right] \quad (9)$$

In 2000, the parameter values were $A_{\text{rise}} = 0.13$, $\tau_{\text{rise}} = 4.3\ \mu\text{s}$ and $t_{\text{scrap}} = 15\ \mu\text{s}$ [1]. Since τ_{rise} is determined by hardware, it is the same in 2001. A_{rise} depends slightly on the quadrupole-plate voltages during and after scraping, but the order of magnitude is the same in 2000 and 2001. The scraping time however was only $t_{\text{scrap}} = 7\ \mu\text{s}$ in 2001. Therefore, the end-of-scraping effect on f_{CBO} which had already been negligible in 2000 after about $30\ \mu\text{s}$, was even smaller in 2001 and hence not included in the fitting function.

- After $50\ \mu\text{s}$ the quadrupole plates discharge with a time constant of the order 200 ms:

$$n(t) = n(50\ \mu\text{s}) e^{-(t-50\ \mu\text{s})/\tau_{\text{droop}}} \quad (10)$$

In 2000, χ^2 minimisation gave an empirical optimum of τ_{droop} at 140 ms. It was used for the 2001 analysis as well since it depends only on the quadrupole circuitry. This parameter is always fixed in the final fits. A systematic error will be assigned.

The time dependence of n translates into a time dependence of the frequencies

$$f_{\text{CBO}}(t) \approx (1 - \sqrt{1 - n(t)}) f_{\text{cyc}} \quad (11)$$

$$f_{\text{VO}}(t) \approx \sqrt{n(t)} f_{\text{cyc}} \quad (12)$$

$$f_{\text{VW}}(t) \approx (1 - 2\sqrt{n(t)}) f_{\text{cyc}} \quad (13)$$

(for a rigorous treatment see [8]). Therefore the arguments $\phi_{\text{CBO}}(t)$, $\phi_{\text{DCBO}}(t)$, $\phi_{\text{VO}}(t)$ and $\phi_{\text{VW}}(t)$ of the horizontal and vertical oscillation cosines are not simply $\omega_{\text{CBO}}t + \phi_{\text{CBO}}(0)$ etc., but have to be obtained from time integration of the respective frequencies, e.g.

$$\phi_{\text{CBO}}(t) = \int_{50\ \mu\text{s}}^t dt' 2\pi f_{\text{CBO}}(t') + \phi_{\text{CBO}}(50\ \mu\text{s}) \quad (14)$$

As fit parameters the frequencies and phases at the reference time $50\ \mu\text{s}$ are chosen. Acceptance, asymmetry and phase modulation share the same CBO frequency parameter. By definition, the double CBO frequency was implemented as $2 f_{\text{CBO}}$ and is not an additional free parameter.

The electron time spectrum is further modulated by slow effects $g_{\text{slow}}(t)$ which are dominated by muon losses and residual detector gain variations and pileup. These effects correlate strongly with each other and are difficult to separate. Their individual functional forms are not very well known. In the final fitting function we implement only the muon loss function $g_{\text{loss}}(t)$ derived from FSD triple coincidence measurements [9]. This function is known to about 10 %. The details of the implementation of $g_{\text{loss}}(t)$ are explained in Section 5.2.4. To avoid phase pulling in R entirely, an empirical correction term would have to be included:

$$g_{\text{slow}}(t) = (1 + g_{\text{loss}}(t) - A_{\text{rse}} \cdot e^{-t/\tau_{\text{rse}}}) \quad (15)$$

The correction term accounts for lacking knowledge about $g_{\text{loss}}(t)$, for imperfections in the gain correction and pileup subtraction. Therefore it is called “residual slow effects” (“r.s.e.”; if this concept is unclear to you see Figure 16 in [1] for a comprehensive explanation). In the final fits no such term is used, but it was included for studies.

5.2.2 Free and Fixed Fit Parameters

- N_0 : always free.
- τ : always free.
- A : always free.
- R : always free.
- ϕ_a : always free.
- $f_{\text{CBO}}(50\mu\text{s})$: always free.
- A_{CBO} : always free.
- $\phi_{\text{CBO}}(50\mu\text{s})$: always free.
- A_{DCBO} : free for start times up to $80\mu\text{s}$, then fixed.
- $\phi_{\text{DCBO}}(50\mu\text{s})$: free for start times up to $80\mu\text{s}$, then fixed.
- A_{R} : fixed to 0 in the 1999-style function, otherwise free.
- $\phi_{\text{R}}(50\mu\text{s})$: fixed to 0 in the 1999-style function, otherwise free.
- A_{J} : free in the “full physics function”, otherwise fixed to 0.
- $\phi_{\text{J}}(50\mu\text{s})$: free in the “full physics function”, otherwise fixed to 0.
- A_{VO} : free for systematic studies; otherwise fixed to 0.
- $f_{\text{VO}}(50\mu\text{s})$: only used for systematic studies; fixed; determined from a Fourier spectrum.
- τ_{VO} : only used for systematic studies; fixed; determined by manual χ^2 minimisation at early times.
- $\phi_{\text{VO}}(50\mu\text{s})$: only used for systematic studies where it is free; otherwise fixed to 0.
- A_{VW} : free for systematic studies; otherwise fixed to 0.
- $f_{\text{VW}}(50\mu\text{s})$: only used for systematic studies; fixed; determined from a Fourier spectrum.
- τ_{VW} : only used for systematic studies; fixed; determined by manual χ^2 minimisation at early times.
- $\phi_{\text{VW}}(50\mu\text{s})$: only used for systematic studies where it is free; otherwise fixed to 0.
- $\tau_{\text{droop}} = 140\text{ ms}$: always fixed.
- A_{loss} : free at the earliest start time for the sum of all detectors, otherwise fixed to that result.
- A_{rse} : free in special studies, otherwise fixed to 0.
- τ_{rse} : free in special studies, otherwise irrelevant.

There are 12 free parameters if the “1999-style function” is used; the “physics function without phase modulation” has 14 free parameters, and the “full physics function” including the phase modulation has 16 free parameters. In studies at very early start times the inclusion of the vertical oscillation and waist increases the number of parameters to 20.

5.2.3 The CBO Envelope

The CBO envelope was determined as described in the 2000 analysis report [1] (Section 5.1.3). The results for the two data sets are shown in Figure 11 together with exponential fits.

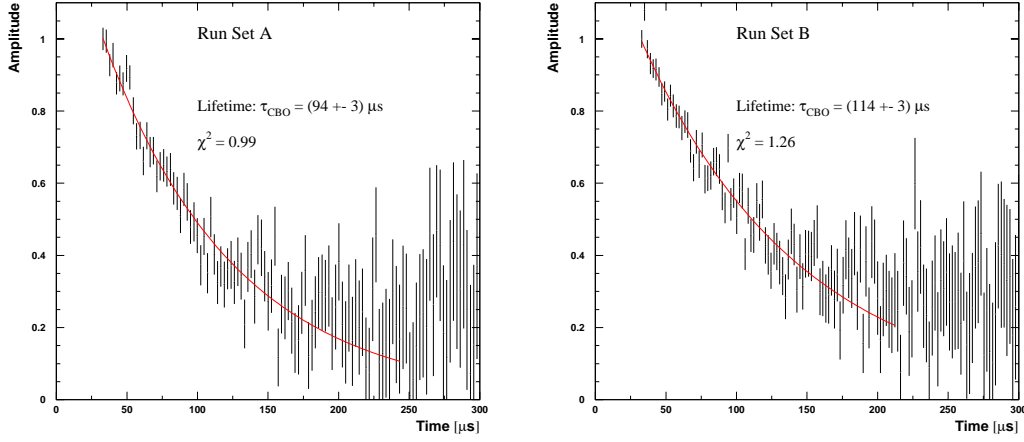


Figure 11: *CBO envelopes for the two run sets, normalised to the value at 31.8 μs. The lines superimposed represent exponential fits.*

Unlike in 2000, the CBO envelopes are sufficiently well parametrised by exponentials, and we do not need empirical envelopes.

5.2.4 Implementation of the Muon Loss Function

Following a suggestion by Chris, the implementation of the muon loss function was slightly changed w.r.t. 2000.

Neglecting the muon spin precession, the time spectrum of the detected electrons $\dot{N}_\mu(t)$ is given by the differential equation

$$\dot{N}_\mu(t) = -\varepsilon_d \lambda_\mu N(t) \quad (16)$$

where $\lambda = 1/\tau$, $N(t)$ is the total number of muons in the ring at the time t , and ε_d is an efficiency and acceptance factor for the electron detection. The muon losses $L(t)$ measured via FSD triple coincidences [9, 10] obey the equation

$$L(t) = -\varepsilon_l \dot{N}_l(t) \quad (17)$$

where ε_l an efficiency and acceptance factor for the detection of muons. The number of muons in the ring follows from combining (16) and (17):

$$\dot{N}(t) = -\lambda_\mu N(t) + \dot{N}_l(t) = -\lambda_\mu N(t) - \frac{1}{\varepsilon_l} L(t) \quad (18)$$

The solution is

$$N(t) = N_0 e^{-\lambda_\mu t} \left(1 - \frac{1}{\varepsilon_l} \int_0^t L(t') e^{\lambda_\mu t'} dt' \right) \quad (19)$$

Hence, the detected electron spectrum is

$$\dot{N}_\mu(t) = -\varepsilon_d \lambda_\mu N_0 e^{-\lambda_\mu t} \left(1 - \frac{1}{\varepsilon_l} \int_0^t L(t') e^{\lambda_\mu t'} dt' \right) \quad (20)$$

With a different choice of constants, this equation can be rewritten as

$$\dot{N}_\mu(t) = \tilde{N}_{\mu,0} \lambda_\mu e^{-\lambda_\mu t} \left(1 - A_l \frac{\int_{t_0}^t L(t') e^{\lambda_\mu t'} dt'}{\int_{t_0}^{t_{max}} L(t') e^{\lambda_\mu t'} dt'} \right) \quad (21)$$

where t_0 is an arbitrary reference time which for this analysis was chosen to be $30 \mu\text{s}$. After the cut-off time $t_{max} = 325 \mu\text{s}$ the measured losses $L(t)$ are taken to be zero because anti-proton losses start to dominate.

In (21) we identify

$$g_{\text{loss}}(t) = \left(1 - A_l \frac{\int_{t_0}^t L(t') e^{\lambda_\mu t'} dt'}{\int_{t_0}^{t_{max}} L(t') e^{\lambda_\mu t'} dt'} \right) \quad (22)$$

5.3 Fit Procedure

The fitting technique was the same as for the 2000 data set [1]. However, due to earlier gate-on times, the fits are also started earlier:

The latest detectors to be gated on were 4 and 5. They are available after about $30 \mu\text{s}$. The closest (g-2) zero-crossing is at $31.8 \mu\text{s}$ which was chosen as the start time for individual detector fits, and as the earliest point of start-time scans for fits to the sum of all detector spectra (excluding detector 20). In these scans, the start times were varied in 150 ns steps before $45 \mu\text{s}$ to look for phase pulling. After $45 \mu\text{s}$ the step size was $5 \mu\text{s}$.

Like in the previous analysis, the fit stop time was $600 \mu\text{s}$ or the time when the number of entries per bin went below 42, whichever was earlier. The latter criterion ensures gaussian statistics in each time bin. However, thanks to the big statistics of the data set, this cut was never active.

Again, the error on the N_i entries of a time bin i was corrected for correlations from our pileup subtraction method:

$$\sigma_i = \sqrt{N_i \cdot (1 + \gamma \cdot X \cdot e^{-\frac{t-34.1 \mu\text{s}}{\tau}})} \quad (23)$$

in the first call to the fitting routine (NAGLIB e04ycf). In later iterations, N_i was replaced by the function value from the previous fit. The values of the parameters γ and X are given in Tables 3 and 4.

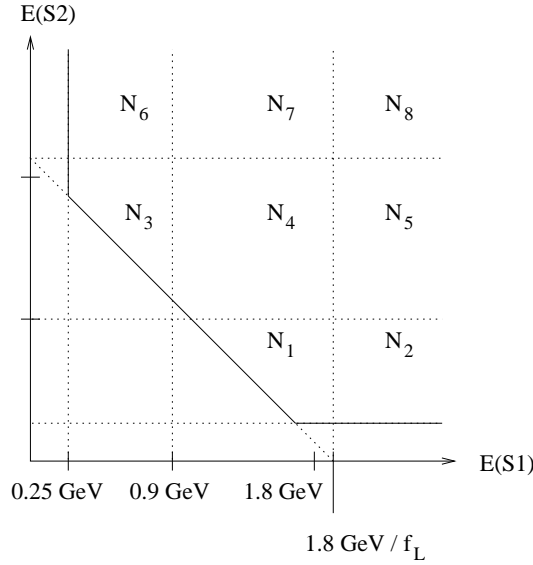


Figure 12: *Illustration of the construction of pileup pulses from single pulses with energies $E(S1)$ and $E(S2)$. For all points above the diagonal line the energy of the constructed double pulse is greater than 1.8 GeV .*

Detector	Set A	Set B
1	1.11	1.10
2	1.12	1.11
3	1.14	1.12
4	1.14	1.13
5	1.13	1.13
6	1.16	1.15
7	1.20	1.20
8	1.22	1.21
9	1.18	1.17
10	1.14	1.13
11	1.13	1.13
12	1.16	1.15
13	1.12	1.12
14	1.14	1.14
15	1.11	1.11
16	1.16	1.16
17	1.13	1.12
18	1.13	1.14
19	1.10	1.10
(20)	(1.31)	(1.32)
21	1.13	1.13
22	1.16	1.16
23	1.15	1.15
24	1.15	1.15
0	1.14	1.14

Table 3: Values of $\gamma \equiv \frac{6N_1+2N_4+2N_8}{2(N_1+N_2)+N_4+N_5+N_7+N_8}$ for all detectors and the two data subsets. Detector 0 stands for the sum of all detectors. For the notation used in the definition of gamma and its derivation see [7] and Figure 12.

Detector	Set A	Set B
1	0.0055	0.0060
2	0.0059	0.0063
3	0.0061	0.0065
4	0.0060	0.0065
5	0.0060	0.0064
6	0.0063	0.0068
7	0.0072	0.0077
8	0.0089	0.0097
9	0.0072	0.0078
10	0.0059	0.0064
11	0.0060	0.0065
12	0.0066	0.0072
13	0.0059	0.0064
14	0.0065	0.0071
15	0.0053	0.0057
16	0.0069	0.0075
17	0.0058	0.0062
18	0.0070	0.0075
19	0.0061	0.0066
(20)	(0.0087)	(0.0094)
21	0.0061	0.0065
22	0.0064	0.0070
23	0.0061	0.0065
24	0.0065	0.0070
0	0.0063	0.0068

Table 4: Values of $X = \frac{\text{doubles at } 34.1 \mu\text{s}}{\text{singles at } 34.1 \mu\text{s}}$ for all detectors and run subsets. Single pulses $N - D + S1 + S2$ and double pulses D are counted over one g -2 period centred at $34.1 \mu\text{s}$. See also Figure 13.

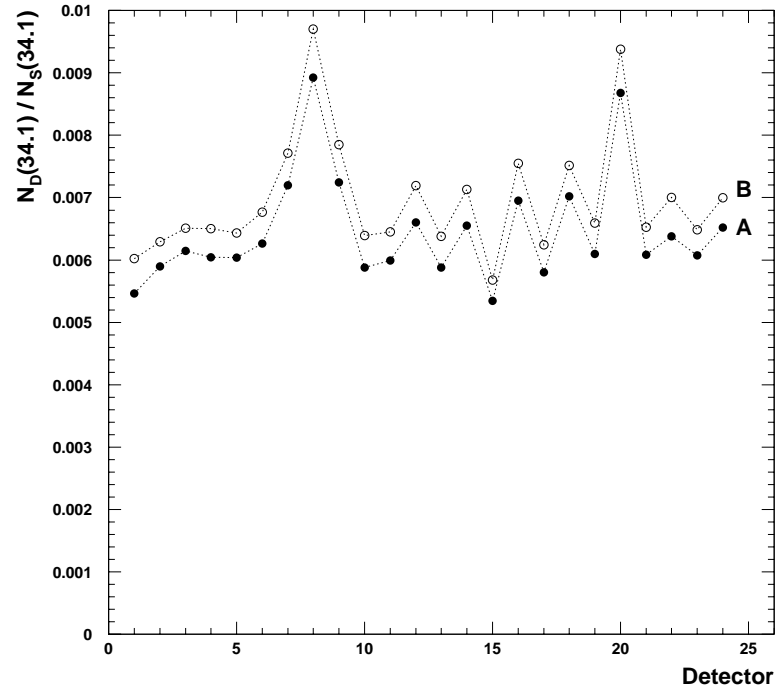


Figure 13: Values of $X = \frac{\text{doubles at } 34.1 \mu\text{s}}{\text{singles at } 34.1 \mu\text{s}}$ as in Table 4. The energy spectra of the kicker detectors 7, 8, 9 have a different shape which impacts the pileup fraction.

5.4 Fit Results

All results in this section are based on a single random seed. More seeds will only be used for a systematic study (Section 6.10).

5.4.1 Fits without Asymmetry/Phase Modulation (1999 Style)

We define the “1999-style function” as Function (3) with the following parameters fixed:

- No asymmetry modulation by CBO: $A_{\text{Rob}} = \phi_{\text{Rob}} = 0$.
- No phase modulation by CBO: $A_{\text{Jim}} = \phi_{\text{Jim}} = 0$.

Thus, the remaining function is

$$\dot{N}(t) = \frac{N_0}{\tau} e^{-t/\tau} [1 + A_{\text{CBO}} \cdot g_{\text{CBO}}(t) \cdot \cos(\phi_{\text{CBO}}(t)) + A_{\text{DCBO}} \cdot g_{\text{CBO}}^2(t) \cdot \cos(\phi_{\text{DCBO}}(t))] \cdot [1 + A \cdot \cos(\omega_a t + \phi_a)] \cdot g_{\text{slow}}(t) \quad (24)$$

The individual terms are explained in Section 5.2.1. For the fits discussed here, $g_{\text{slow}}(t)$ only incorporates the muon losses, no rse term.

Set A	N_0	A	τ	ϕ_a	R	f_{CBO}	τ_{CBO}	A_{CBO}	ϕ_{CBO}	A_{DCBO}	ϕ_{DCBO}	A_{loss}
N_0	1.000	-0.040	0.816	-0.001	-0.001	0.018	-0.021	0.029	-0.026	-0.009	0.019	0.982
A	-0.040	1.000	-0.025	-0.009	-0.005	0.009	0.006	-0.008	-0.012	-0.002	0.003	-0.037
τ	0.816	-0.025	1.000	-0.001	-0.001	0.011	-0.013	0.018	-0.016	-0.006	0.012	0.873
ϕ_a	-0.001	-0.009	-0.001	1.000	0.833	0.014	-0.029	0.040	-0.021	0.001	0.011	-0.002
R	-0.001	-0.005	-0.001	0.833	1.000	0.010	-0.021	0.029	-0.015	0.001	0.008	-0.001
f_{CBO}	0.018	0.009	0.011	0.014	0.010	1.000	-0.004	0.007	-0.321	-0.011	0.016	0.016
τ_{CBO}	-0.021	0.006	-0.013	-0.029	-0.021	-0.004	1.000	-0.902	0.003	-0.462	0.017	-0.019
A_{CBO}	0.029	-0.008	0.018	0.040	0.029	0.007	-0.902	1.000	-0.006	0.416	-0.023	0.027
ϕ_{CBO}	-0.026	-0.012	-0.016	-0.021	-0.015	-0.321	0.003	-0.006	1.000	0.014	-0.016	-0.024
A_{DCBO}	-0.009	-0.002	-0.006	0.001	0.001	-0.011	-0.462	0.416	0.014	1.000	-0.015	-0.008
ϕ_{DCBO}	0.019	0.003	0.012	0.011	0.008	0.016	0.017	-0.023	-0.016	-0.015	1.000	0.017
A_{loss}	0.982	-0.037	0.873	-0.002	-0.001	0.016	-0.019	0.027	-0.024	-0.008	0.017	1.000

Set B	N_0	A	τ	ϕ_a	R	f_{CBO}	τ_{CBO}	A_{CBO}	ϕ_{CBO}	A_{DCBO}	ϕ_{DCBO}	A_{loss}
N_0	1.000	-0.036	0.820	-0.002	-0.001	0.025	-0.004	0.005	-0.033	0.006	0.014	0.982
A	-0.036	1.000	-0.022	-0.009	-0.005	0.001	0.007	-0.010	-0.002	0.004	0.004	-0.033
τ	0.820	-0.022	1.000	-0.002	-0.001	0.015	-0.002	0.003	-0.020	0.002	0.009	0.877
ϕ_a	-0.002	-0.009	-0.002	1.000	0.833	0.023	-0.008	0.011	-0.030	0.003	0.012	-0.002
R	-0.001	-0.005	-0.001	0.833	1.000	0.016	-0.006	0.008	-0.022	0.002	0.009	-0.001
f_{CBO}	0.025	0.001	0.015	0.023	0.016	1.000	0.003	-0.005	-0.422	-0.003	0.005	0.023
τ_{CBO}	-0.004	0.007	-0.002	-0.008	-0.006	0.003	1.000	-0.887	-0.006	-0.027	0.016	-0.003
A_{CBO}	0.005	-0.010	0.003	0.011	0.008	-0.005	-0.887	1.000	0.009	0.022	-0.022	0.004
ϕ_{CBO}	-0.033	-0.002	-0.020	-0.030	-0.022	-0.422	-0.006	0.009	1.000	0.003	-0.010	-0.030
A_{DCBO}	0.006	0.004	0.002	0.003	0.002	-0.003	-0.027	0.022	0.003	1.000	0.001	0.005
ϕ_{DCBO}	0.014	0.004	0.009	0.012	0.009	0.005	0.016	-0.022	-0.010	0.001	1.000	0.013
A_{loss}	0.982	-0.033	0.877	-0.002	-0.001	0.023	-0.003	0.004	-0.030	0.005	0.013	1.000

Table 5: Correlation matrix $\frac{\text{cov}(p_i, p_j)}{\sigma_i \sigma_j}$ from fits to the sum of detectors starting at $31.8 \mu\text{s}$; 1999-style function.

With the 1999-style function the fit results for R decouple well from the other fit parameters, as the correlation matrices in Table 5 demonstrate. We shall see that this makes the results relatively insensitive to gain variations and other effects influencing the asymmetry. The disadvantage of this function is that by neglecting the CBO modulations

of $g-2$ asymmetry and phase it does not fully describe the physics. The missing effects need to be addressed in systematic error studies.

Fits to the Sum of Detectors

Start time scans for R is shown in Figure 14 for the two data sets. Figure 15 shows zooms for start times up to $45 \mu\text{s}$ with a step of 150 ns . For both run sets there is phase pulling with the $g-2$ frequency and an amplitude of about 0.3 ppm which suggests that the muon-loss function alone is not quite adequate to describe the slow varying term $g_{\text{slow}}(t)$. In Section 6.6.3 the resulting systematic error and the effects of including an r.s.e. term will be discussed.

The weighted average of the R values for the two subsets is shown in Figure 16 and Table 6. Figure 17 shows start-time scans for the asymmetry A . Like in 2000, A droops below the allowed 1σ error band, suggesting imperfections in pileup subtraction and/or gain correction.

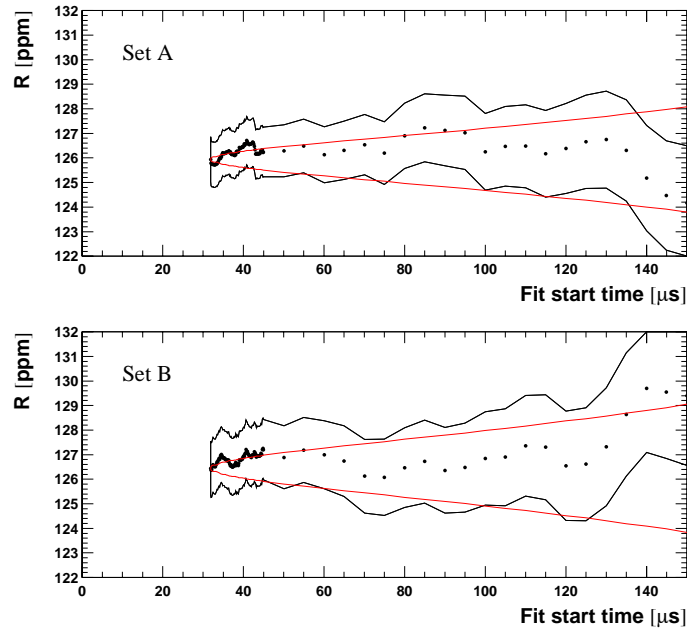
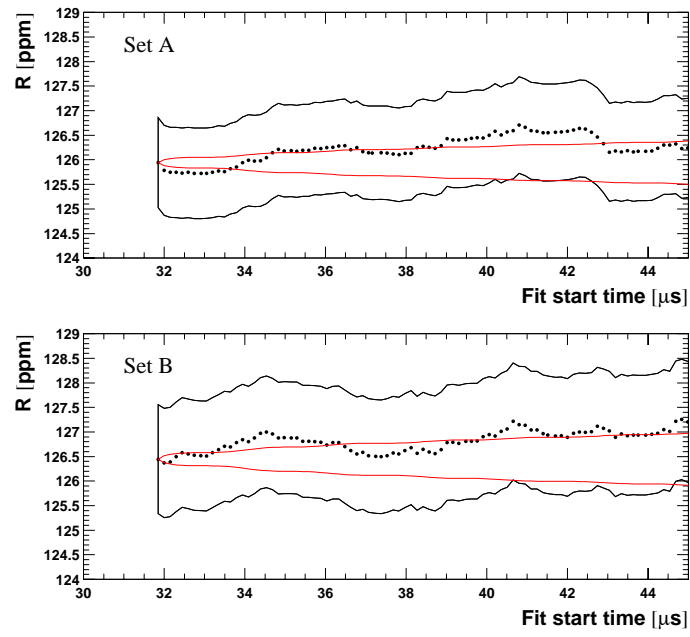
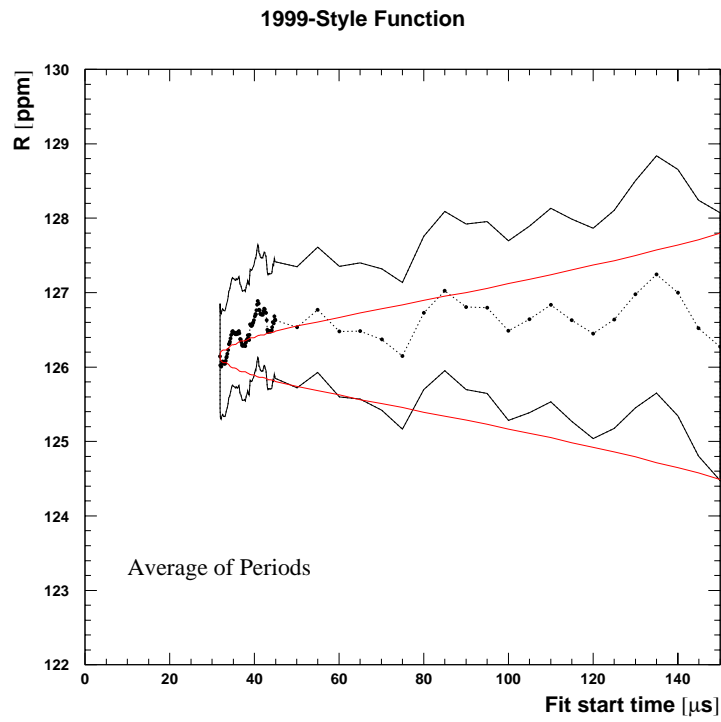
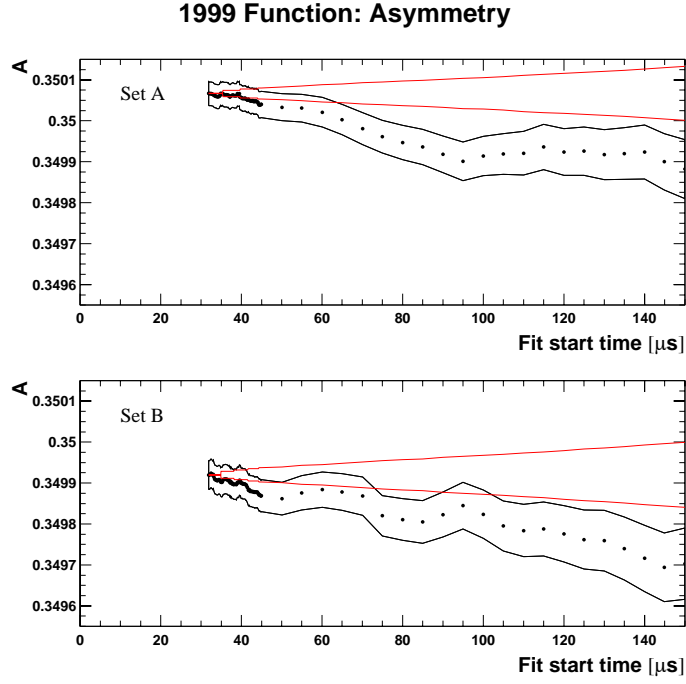


Figure 14: *Start time scans for the sum of all detector spectra of all runs fitted with the 1999-style function.*

Figure 15: *Early-time zoom of Figure 14.*Figure 16: R averaged over the two run sets.

Figure 17: *Start-time scans for A, sum of all detector spectra.*

Period	Sum of all detectors	First half	Second half	Average of the halves
A	125.9420 ± 0.9138	125.5806 ± 1.2748	126.3616 ± 1.3079	125.9611 ± 0.9129
B	126.4448 ± 1.1098	128.0083 ± 1.5491	124.8792 ± 1.5874	126.4820 ± 1.1087
avr.	126.1452 ± 0.7054	126.5608 ± 0.9843	125.7622 ± 1.0094	126.1716 ± 0.7047
A - B	0.5028 ± 1.4376	2.4277 ± 2.0062	1.4824 ± 2.0568	0.5209 ± 1.4362

Table 6: *Fit results for R in ppm in the two run periods with a start time of $31.8 \mu s$. The fits were done with the 1999-style function.*

The omission of the asymmetry and phase modulation manifests itself in the halfring effect on both R and A , see Figures 18 and 19.

Start time scans for all other parameters and for the different run periods are shown in Appendix A.1. Appendix A.2 shows the same for the first and second half of the ring.

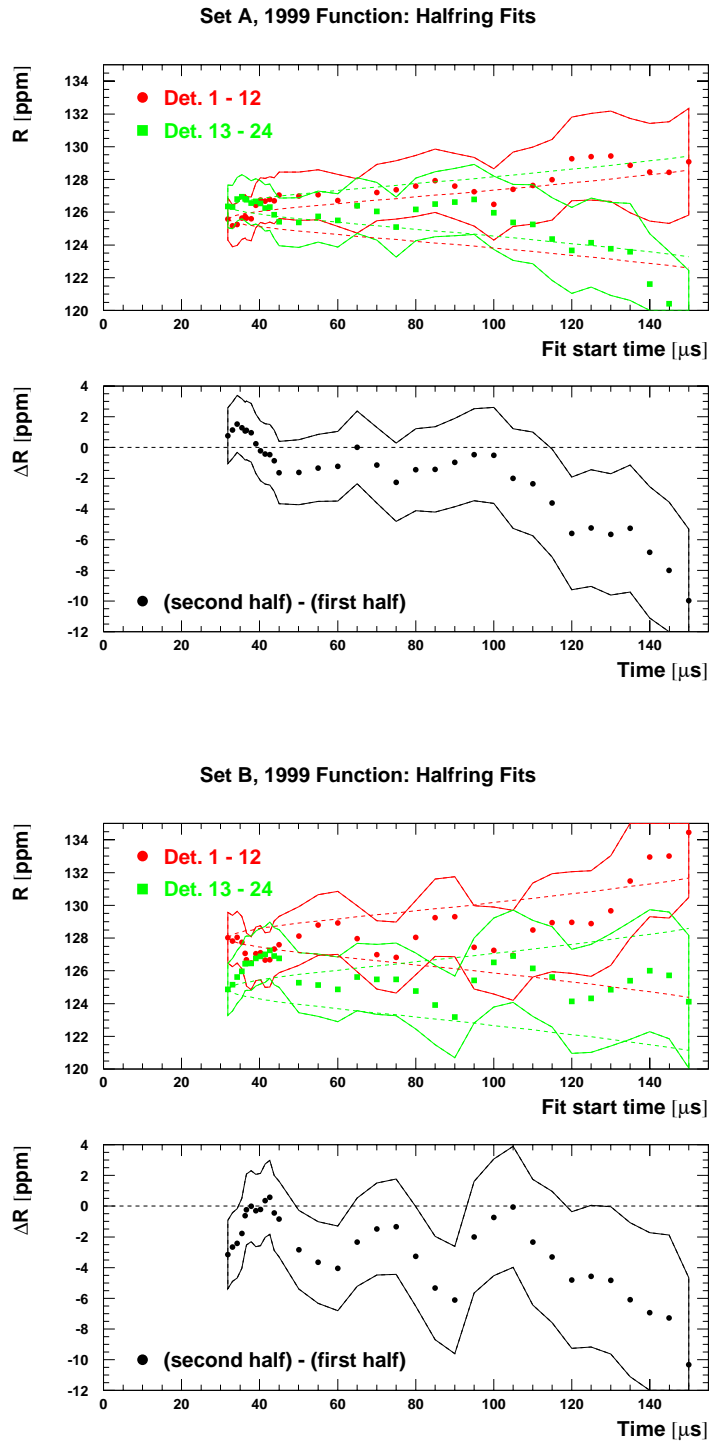
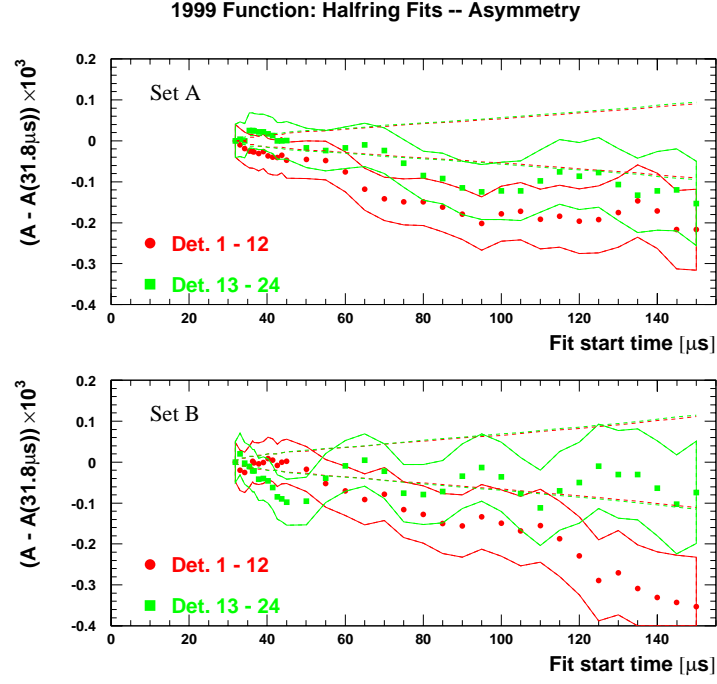


Figure 18: *Fit results for R in the two halves of the ring.*

Figure 19: *Fit results for A in the two halves of the ring.*

The CBO parameters are listed in Table 7.

Period	$A_{\text{CBO}} \times 10^3$	ϕ_{CBO}	f_{CBO} [kHz]	τ_{CBO} [μs]
A	1.32 ± 0.15	-0.29 ± 0.05	418.46 ± 0.27	98.28 ± 16.17
B	1.91 ± 0.13	2.41 ± 0.04	490.48 ± 0.15	146.17 ± 20.23

Table 7: *CBO parameters from fits to the sum of all detectors with a start time of $31.8 \mu\text{s}$. The fits were done with the 1999-style function.*

Fits to the Individual Detectors

The fit results for individual detectors at a start time of $31.8 \mu\text{s}$ are shown in the figures of Appendix A.3. A bigger version of R versus detector is displayed in Figure 20.

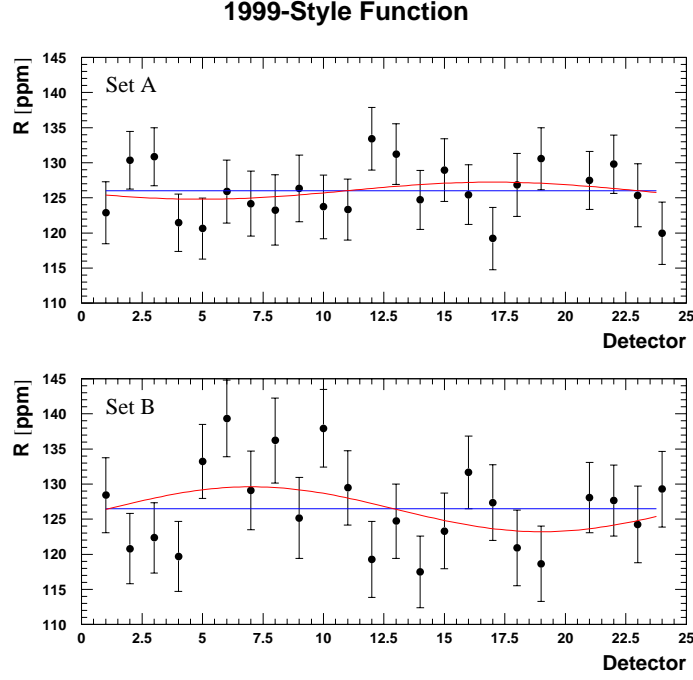


Figure 20: R versus detector with the 1999-style function.

As a consequence of omitting the asymmetry and phase modulation in the fit function, R versus detector may not be constant but follow a sine wave

$$R(d) = R_0 + A_{Rc} \cos(2\pi \frac{d}{24}) + A_{Rs} \sin(2\pi \frac{d}{24}). \quad (25)$$

We find an average amplitude of (0.76 ± 1.00) ppm. The centroid value R_0 of this wave differs by (0.01 ± 0.02) ppm from the weighted average $\langle R \rangle$ (see Table 10).

Set	$\langle R \rangle$	χ^2/dof (fit to a constant)
A	125.9958 ± 0.9133	17.95 / 22
B	126.4789 ± 1.1091	28.77 / 22
avr.	126.1910 ± 0.7050	

Table 8: Average R from the individual detector fits, for the different run periods with a start time of $31.8 \mu\text{s}$. Detector 20 was excluded. The fits were done with the 1999-style function.

Set	R_0	A_{Rc}	A_{Rs}	$\sqrt{A_{Rc}^2 + A_{Rs}^2}$	χ^2/dof
A	126.0255 ± 0.9139	-0.3203 ± 1.2736	-1.1763 ± 1.3175	1.2191 ± 1.3145	17.05 / 20
B	126.4110 ± 1.1097	-0.8365 ± 1.5476	3.0848 ± 1.5990	3.1962 ± 1.5955	24.88 / 20
avr.	126.1813 ± 0.7055	-0.5287 ± 0.9834	0.5468 ± 1.0168	0.7606 ± 1.0008	

Table 9: R versus detector was fitted with Function (25). The table gives the fit parameters for the two run sets with a start time of $31.8 \mu\text{s}$. Detector 20 was excluded. The underlying individual detector fits were done with the 1999-style function.

Set	$\langle R \rangle - R_0$
A	-0.0297 ± 0.0331
B	0.0679 ± 0.0365
avr.	0.0143 ± 0.0245

Table 10: Difference between fitting R versus detector to a constant and to a wave (Tables 8 and 9).

Table 11 lists the CBO amplitude averaged over all detectors for the two run sets.

As an additional detector consistency check, the CBO vectors ($A_{\text{CBO}}, \phi_{\text{CBO}}$) are added coherently (“vector sum” in Table 11) and compared with the result for the sum. This vector sum follows from the addition of the time spectra whose relevant part can be written as

$$N_0 A_{\text{CBO, sum}} \cos(\omega_{\text{CBO}} t + \phi_{\text{CBO, sum}}) = \sum_{d=1}^{24} N_d A_{\text{CBO}, d} \cos(\omega_{\text{CBO}} t + \phi_{\text{CBO}, d}) \quad (26)$$

In complex notation the amplitude $A_{\text{CBO, sum}}$ and phase $\phi_{\text{CBO, sum}}$ of the sum are given by

$$N_0 A_{\text{CBO, sum}} (\cos \phi_{\text{CBO, sum}} + i \sin \phi_{\text{CBO, sum}}) = \sum_{d=1}^{24} N_d A_{\text{CBO}, d} (\cos \phi_{\text{CBO}, d} + i \sin \phi_{\text{CBO}, d}) \quad (27)$$

These vector sums are in rather good agreement with the results from the fits to the sum of detectors given in Table 7.

Set	$\langle A_{\text{CBO}} \rangle \times 10^3$	vector sum over all detectors	
		$A_{\text{CBO}} \times 10^3$	ϕ_{CBO}
A	6.41 ± 0.17	1.37 ± 0.15	-0.30 ± 0.09
B	10.31 ± 0.16	2.08 ± 0.13	2.27 ± 0.06

Table 11: First column: CBO parameters from fits to the individual detectors, averaged over all detectors. Second and third columns: vector sum of the CBO parameters over all detectors. Amplitude and phase of the vector sum should be consistent with the corresponding parameters obtained from the summed spectra (cf. Table 7).

Comparison between Fits to the Sum and the Average of Individual Fits

The R -value from a fit to the sum of detector spectra should agree with the average $\langle R \rangle$ over the results from individual detector fits. Discrepancies between R_{sum} and the sine wave centroid R_0 are less surprising because the 1999-style function does not include any information about the presence of this sine wave.

Set	$ \langle R \rangle - R_{\text{sum}} $	$ R_0 - R_{\text{sum}} $
A	0.0538 ± 0.0302	0.0835 ± 0.0135
B	0.0341 ± 0.0394	0.0338 ± 0.0149

Table 12: *Difference between R from fits to the sum of all detector spectra and the averages $\langle R \rangle$ or R_0 from fits to individual detector spectra. The 1999 function was used.*

5.4.2 Fits with Asymmetry Modulation but without Phase Modulation

This section describes fits using Function (3) including the asymmetry modulation term (6), but not the phase modulation term (7) (we fix the parameters $A_{\text{Jim}} = \phi_{\text{Jim}} = 0$). This function is only used for a study of fit results. No systematic errors will be determined for it, and it will not be considered for the final result.

A look at the correlation matrices (Table 13) reveals that – unlike in 2000 – the inclusion of the asymmetry modulation into the fit does not lead to additional correlations: neither A nor R correlates strongly with A_{Rob} or ϕ_{Rob} . The reason for the weak correlations is the larger difference $\frac{1}{2}\omega_{\text{CBO}} - \omega_a$ as compared to the 2000 data. R decouples well from all parameters except ϕ .

Fits to the Sum of Detectors

Start time scans for R are shown in Figure 21 for the two data sets. Figure 22 shows a zoom for start times up to $45 \mu\text{s}$ with a step of 150 ns .

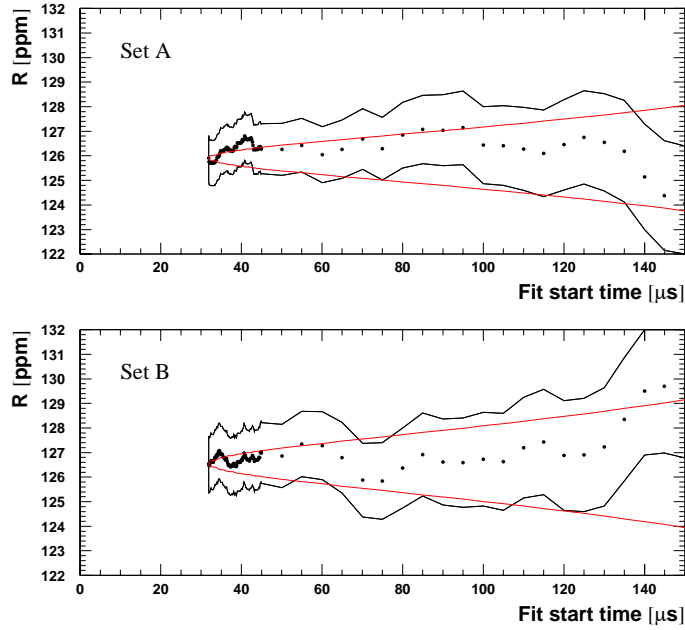


Figure 21: *Start-time scan for the sum of all detector spectra of all runs fitted with the physics function without phase modulation.*

The weighted average of the fit results for R from the two run sets is shown in Figure 23 and Table 14. Figure 24 shows start-time scans for A .

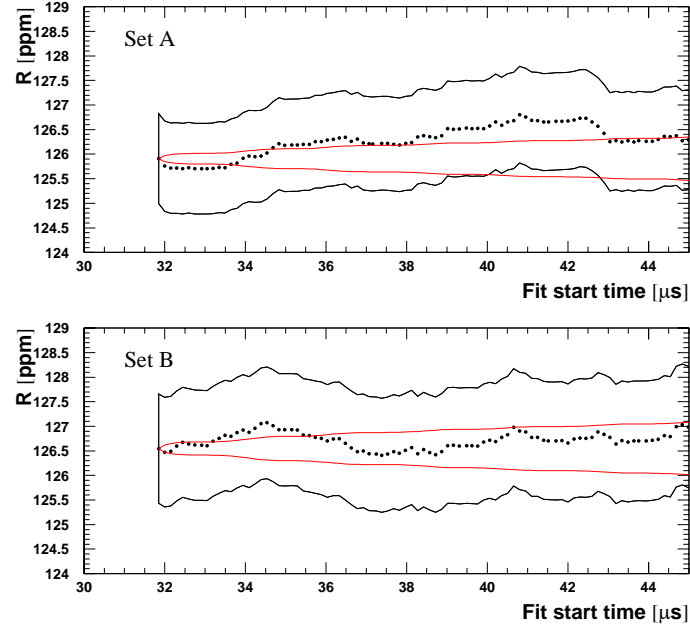
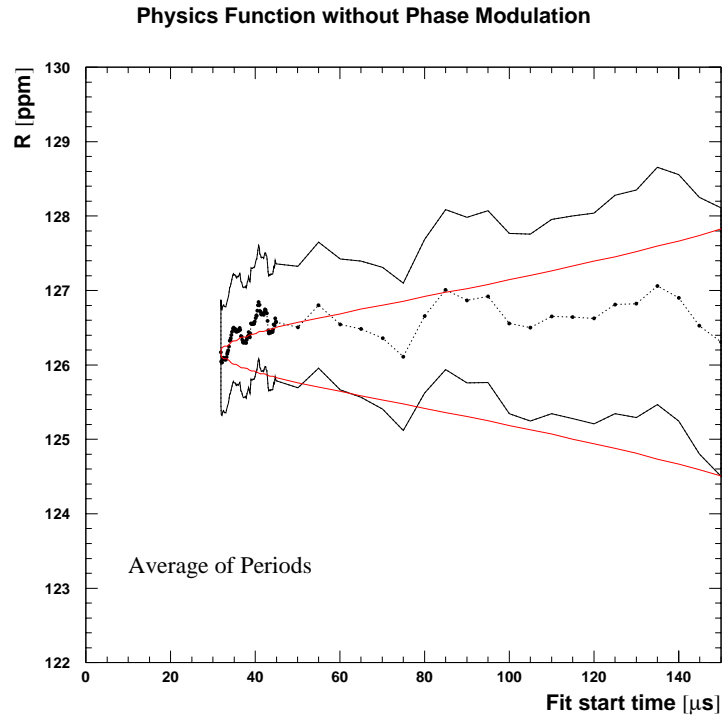
Inclusion of the asymmetry modulation into the fit function almost eliminates the halfring effect, see Figures 25 and 26.

Start time scans for the other parameters and for the different run periods are shown in Appendix B.1. Appendix B.2 shows them for the first and second half of the ring.

Set A	N_0	A	τ	ϕ_a	R	f_{CBO}	τ_{CBO}	A_{CBO}	ϕ_{CBO}	A_{Rob}	ϕ_{Rob}	A_{DCBO}	ϕ_{DCBO}	A_{loss}
N_0	1.000	-0.040	0.816	-0.005	-0.003	0.015	-0.022	0.031	-0.024	-0.021	0.028	-0.008	0.019	0.982
A	-0.040	1.000	-0.025	-0.009	-0.005	0.006	0.011	-0.014	-0.011	0.066	0.037	-0.005	0.003	-0.037
τ	0.816	-0.025	1.000	-0.004	-0.003	0.009	-0.014	0.019	-0.015	-0.013	0.018	-0.005	0.012	0.873
ϕ_a	-0.005	-0.009	-0.004	1.000	0.834	0.019	-0.024	0.035	-0.025	0.053	-0.082	-0.002	0.009	-0.005
R	-0.003	-0.005	-0.003	0.834	1.000	0.014	-0.017	0.025	-0.018	0.039	-0.058	-0.001	0.007	-0.003
f_{CBO}	0.015	0.006	0.009	0.019	0.014	1.000	-0.004	0.008	-0.320	0.002	0.132	-0.134	0.003	-0.020
τ_{CBO}	-0.022	0.011	-0.014	-0.024	-0.017	-0.004	1.000	-0.903	0.003	0.132	0.005	-0.049	-0.011	-0.021
A_{CBO}	0.031	-0.014	0.019	0.035	0.025	0.008	-0.903	1.000	-0.006	-0.134	-0.007	0.419	-0.015	0.028
ϕ_{CBO}	-0.024	-0.011	-0.015	-0.025	-0.018	-0.320	0.003	-0.006	1.000	-0.003	0.046	0.015	-0.016	-0.022
A_{Rob}	-0.021	0.066	-0.013	0.053	0.039	0.002	0.132	-0.134	-0.003	1.000	-0.006	-0.073	-0.003	-0.020
ϕ_{Rob}	0.028	0.037	0.018	-0.082	-0.058	-0.049	0.005	-0.007	0.046	-0.006	1.000	0.005	0.019	0.026
A_{DCBO}	-0.008	-0.005	-0.005	-0.002	-0.001	-0.011	-0.465	0.419	0.015	-0.073	0.005	1.000	-0.015	-0.007
ϕ_{DCBO}	0.019	0.003	0.012	0.009	0.007	0.016	0.017	-0.022	-0.016	-0.003	0.019	-0.015	1.000	0.018
A_{loss}	0.982	-0.037	0.873	-0.005	-0.003	0.014	-0.021	0.028	-0.022	-0.020	0.026	-0.007	0.018	1.000

Set B	N_0	A	τ	ϕ_a	R	f_{CBO}	τ_{CBO}	A_{CBO}	ϕ_{CBO}	A_{Rob}	ϕ_{Rob}	A_{DCBO}	ϕ_{DCBO}	A_{loss}
N_0	1.000	-0.036	0.820	0.001	0.000	0.026	-0.005	0.006	-0.033	0.010	-0.018	0.007	0.014	0.982
A	-0.036	1.000	-0.022	-0.009	-0.005	0.006	0.012	-0.013	-0.006	-0.066	-0.027	0.004	0.003	-0.033
τ	0.820	-0.022	1.000	-0.000	-0.000	0.016	-0.003	0.004	-0.020	0.006	-0.011	0.003	0.008	0.877
ϕ_a	0.001	-0.009	-0.000	1.000	0.834	0.029	-0.016	0.019	-0.033	0.046	-0.090	0.005	0.011	0.000
R	0.000	-0.005	-0.000	0.834	1.000	0.021	-0.011	0.014	-0.024	0.035	-0.064	0.004	0.008	0.000
f_{CBO}	0.026	0.006	0.016	0.029	0.021	1.000	0.003	-0.004	-0.426	-0.026	-0.052	-0.002	0.005	0.024
τ_{CBO}	-0.005	0.012	-0.003	-0.016	-0.011	0.003	1.000	-0.885	-0.008	-0.177	0.028	-0.027	0.014	-0.005
A_{CBO}	0.006	-0.013	0.004	0.019	0.014	-0.004	-0.885	1.000	0.010	0.155	-0.037	0.021	-0.021	0.006
ϕ_{CBO}	-0.033	-0.006	-0.020	-0.033	-0.024	-0.426	-0.008	0.010	1.000	0.035	0.030	0.002	-0.009	-0.030
A_{Rob}	0.010	-0.066	0.006	0.046	0.035	-0.026	-0.177	0.155	0.035	1.000	-0.005	0.010	0.007	0.009
ϕ_{Rob}	-0.018	-0.027	-0.011	-0.090	-0.064	-0.052	0.028	-0.037	0.030	-0.005	1.000	-0.006	0.003	-0.017
A_{DCBO}	0.007	0.004	0.003	0.005	0.004	-0.002	-0.027	0.021	0.002	0.010	-0.006	1.000	0.001	0.006
ϕ_{DCBO}	0.014	0.003	0.008	0.011	0.008	0.005	0.014	-0.021	-0.009	0.007	0.003	0.001	1.000	0.012
A_{loss}	0.982	-0.033	0.877	0.000	0.000	0.024	-0.005	0.006	-0.030	0.009	-0.017	0.006	0.012	1.000

Table 13: Correlation matrix $\frac{\text{cov}(\mathbf{p}_i, \mathbf{p}_j)}{\sigma_i \sigma_j}$ from a fit to the sum of detectors starting at 31.8 μs ; physics function without phase modulation.

Figure 22: *Early-time zoom of Figure 21.*Figure 23: *R averaged over the run sets.*

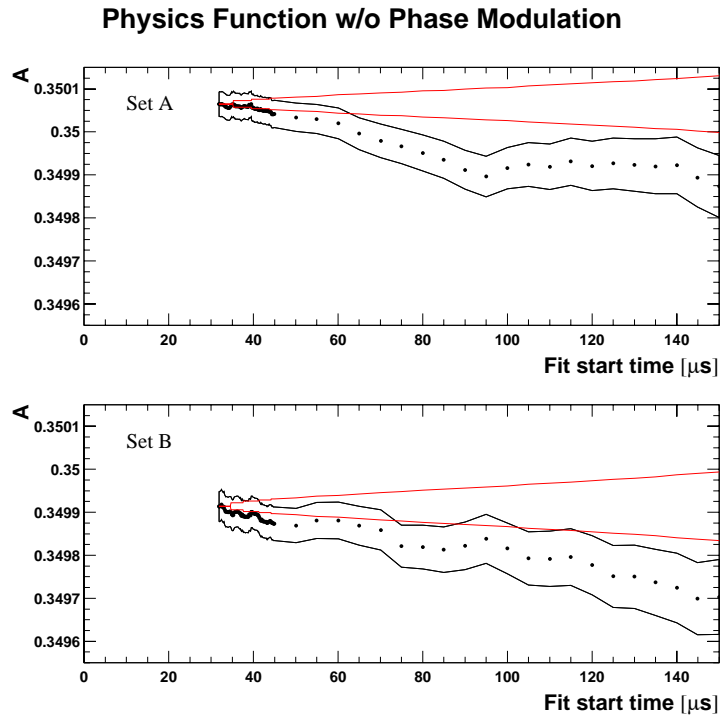


Figure 24: *Start-time scans for A, sum of all detector spectra.*

Set A, Physics Function w/o Phase Mod.: Halfring Fits

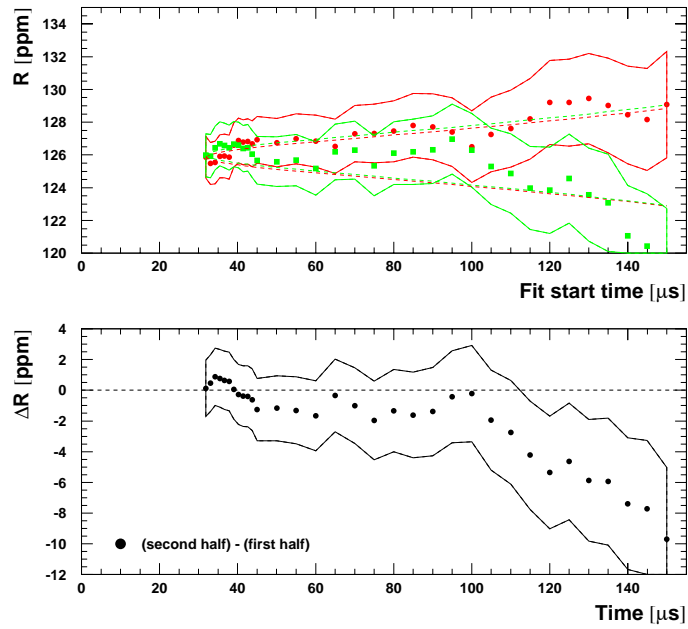


Figure 25: *Fit results for R in the two halves of the ring for Set A.*

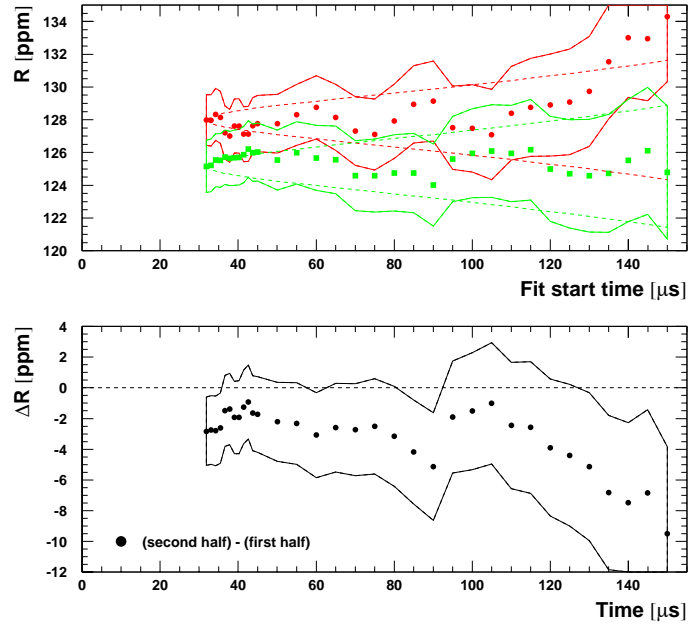
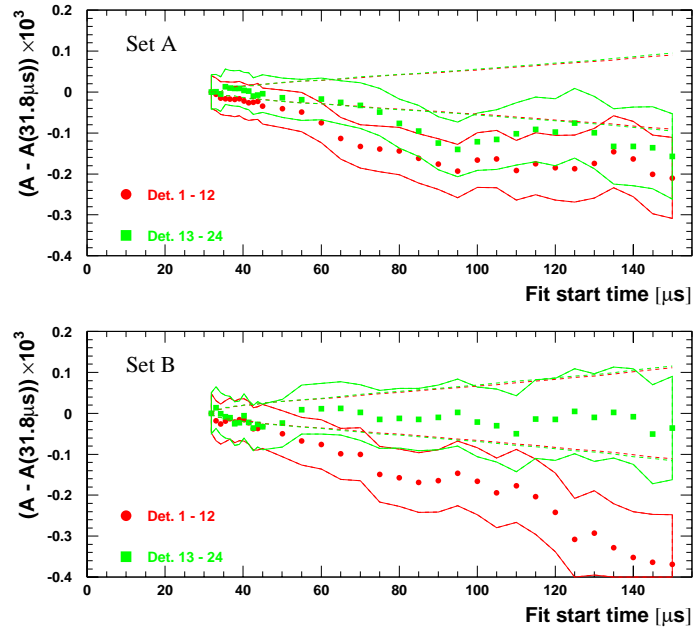
Set B, Physics Function w/o Phase Mod.: Halfring FitsFigure 26: *Fit results for R in the two halves of the ring for Set B.***Physics Function w/o Phase Mod.: Halfring Fits**Figure 27: *Fit results for A in the two halves of the ring.*

Table 14 (last line) shows that the results from the two independent run sets are consistent within about 1σ .

Period	Sum of all detectors	First half	Second half	Average of the halves
A	125.9080 ± 0.9161	125.8438 ± 1.2785	126.0064 ± 1.3112	125.9231 ± 0.9154
B	126.5474 ± 1.1128	127.9847 ± 1.5528	125.1480 ± 1.5936	126.6031 ± 1.1121
avr.	126.1663 ± 0.7073	126.7088 ± 0.9870	125.6599 ± 1.0125	126.1977 ± 0.7068
A - B	0.6394 ± 1.4414	2.1409 ± 2.0114	0.8584 ± 2.0637	0.6800 ± 1.4404

Table 14: *Fit results for R in the individual run periods with a start time of $31.8\mu\text{s}$. The physics function without phase modulation was used.*

The CBO parameters are shown in Table 15.

Period	$A_{\text{CBO}} \times 10^3$	ϕ_{CBO}	$A_{\text{Rob}} \times 10^3$	ϕ_{Rob}	f_{CBO}	τ_{CBO}
A	1.33 ± 0.15	-0.29 ± 0.05	0.23 ± 0.25	2.91 ± 1.07	418.48 ± 0.27	97.41 ± 15.97
B	1.89 ± 0.13	2.41 ± 0.04	0.69 ± 0.24	0.81 ± 0.35	490.45 ± 0.15	149.53 ± 20.87

Table 15: *CBO parameters from fits to the sum of all detectors.*

Fits to the Individual Detectors

The fit results for individual detectors at a start time of $31.8\mu\text{s}$ are shown in the figures of Appendix B.3. A bigger version of R versus detector is displayed in Figure 28.

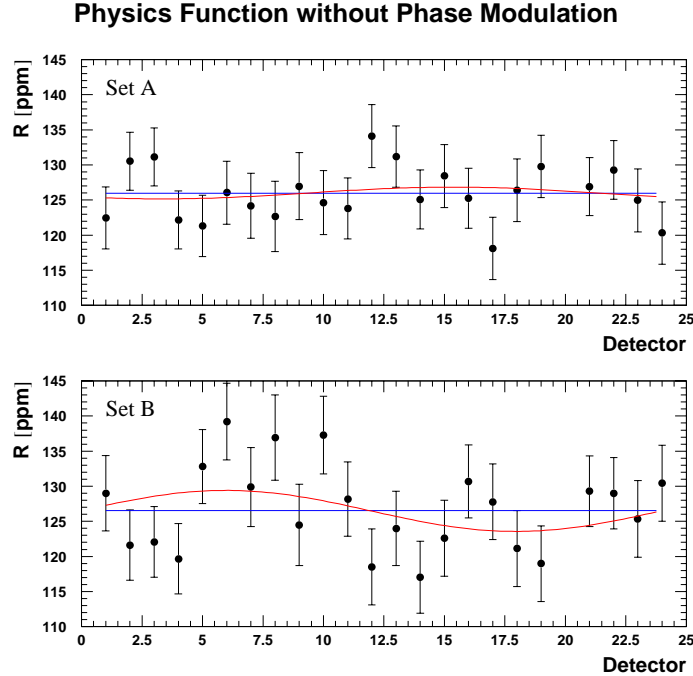


Figure 28: *R versus detector with the physics function without phase modulation.*

R versus detector can be fitted either to a constant or to a sine wave. In both cases satisfactory χ^2 are achieved. The wave amplitude is slightly smaller than for the 1999-style

function. In Set A it decreased from (1.2 ± 1.3) ppm to (0.8 ± 1.2) ppm, in Set B from (3.2 ± 1.6) ppm to (2.9 ± 1.6) ppm. The remaining effect of almost 2σ in Set B is not really a wave but rather a constant statistical shift between detectors 1-12 and 13-24, as can be seen by the rather flat difference in Figure 26.

Period	$\langle R \rangle$	χ^2/ndof (fit to a constant)
A	125.9847 ± 0.9158	17.72 / 22
B	126.5537 ± 1.1127	29.05 / 22
avr.	126.2145 ± 0.7071	

Table 16: Average R from the individual detector fits, for the different run periods with a start time of $31.8\mu\text{s}$. Detector 20 was excluded. The physics function without g -2 phase modulation was used.

Period	R_0	A_{Rc}	A_{Rs}	$\sqrt{A_{Rc}^2 + A_{Rs}^2}$	χ^2/ndof
A	126.0031 ± 0.9164	-0.5328 ± 1.2770	-0.6455 ± 1.3212	0.8370 ± 1.3035	17.28 / 20
B	126.4857 ± 1.1134	0.0304 ± 1.5528	2.9219 ± 1.6046	2.9221 ± 1.6046	25.71 / 20
avr.	126.1980 ± 0.7076	-0.3056 ± 0.9863	0.7959 ± 1.0200	0.8526 ± 1.0157	

Table 17: R versus detector fitted with a sine + cosine function like in Table 9, but for ω_a fits including the asymmetry CBO modulation. The start time was $31.8\mu\text{s}$. As always, detector 20 was excluded.

Period	$\langle R \rangle - R_0$
A	-0.0184 ± 0.0332
B	0.0680 ± 0.0395

Table 18: Difference between fitting R versus detector to a constant and to a wave (Tables 16 and 17).

In Table 19 we give the average CBO amplitudes and the CBO vector sums like in Table 11, except that the weights N_d in Eq. (27) are replaced by $N_d A_d \cos \phi_{a,d}$.

Period	$\langle A_{\text{CBO}} \rangle \times 10^3$	$\langle A_{\text{Rob}} \rangle \times 10^3$
A	6.31 ± 0.17	2.84 ± 0.28
B	10.24 ± 0.16	4.08 ± 0.28

Period	vector sum over all detectors			
	$A_{\text{CBO}} \times 10^3$	ϕ_{CBO}	$A_{\text{Rob}} \times 10^3$	ϕ_{Rob}
A	1.35 ± 0.15	5.98 ± 0.09	0.20 ± 0.29	2.27 ± 1.43
B	2.09 ± 0.13	2.28 ± 0.06	0.84 ± 0.28	0.90 ± 0.34

Table 19: Upper table: CBO parameters from fits to the individual detectors, averaged over all detectors. Lower Table: coherent sum of the CBO parameters over all detectors. The results should be consistent with the fit parameters obtained from the summed spectra (cf. Table 15).

We want to point out the following observations:

- Inclusion of the asymmetry modulation into the fit has very little influence on $\langle A_{\text{CBO}} \rangle$: For Set A we find $(6.31 \pm 0.17) \times 10^{-3}$ instead of $(6.41 \pm 0.17) \times 10^{-3}$ (Table 11); for Set B we find $(10.24 \pm 0.16) \times 10^{-3}$ instead of $(10.31 \pm 0.16) \times 10^{-3}$.
- The same holds for the vector sum of $(A_{\text{CBO}}, \phi_{\text{CBO}})$.
- The agreement between the vector sum $(A_{\text{CBO}}, \phi_{\text{CBO}})$ and the parameter values obtained by fitting the sum of detector spectra is good (compare with Table 15).
- The same is true for $(A_{\text{Rob}}, \phi_{\text{Rob}})$.

Comparison between Fits to the Sum and the Average of Individual Fits

Period	$ \langle R \rangle - R_{\text{sum}} $	$ R_0 - R_{\text{sum}} $
A	0.0767 ± 0.0234	0.0951 ± 0.0234
B	0.0063 ± 0.0149	-0.0617 ± 0.0365

Table 20: *Difference between R from fits to the sum of all detector spectra and the averages $\langle R \rangle$ and R_0 from fits to individual detector spectra.*

5.4.3 Fits with Asymmetry and Phase Modulation

In this section we fit for all three CBO effects: acceptance, asymmetry and phase modulation.

The correlation matrices (Tables 21 and 22) confirm what we have already seen after including the asymmetry modulation into the fit: neither A nor R correlates strongly with A_{Jim} or ϕ_{Jim} .

Fits to the Sum of Detectors

Start time scans for R are shown in Figure 29 for the two data subsets. Figure 30 shows a zoom for start times up to $45 \mu\text{s}$ with a step of 150 ns .

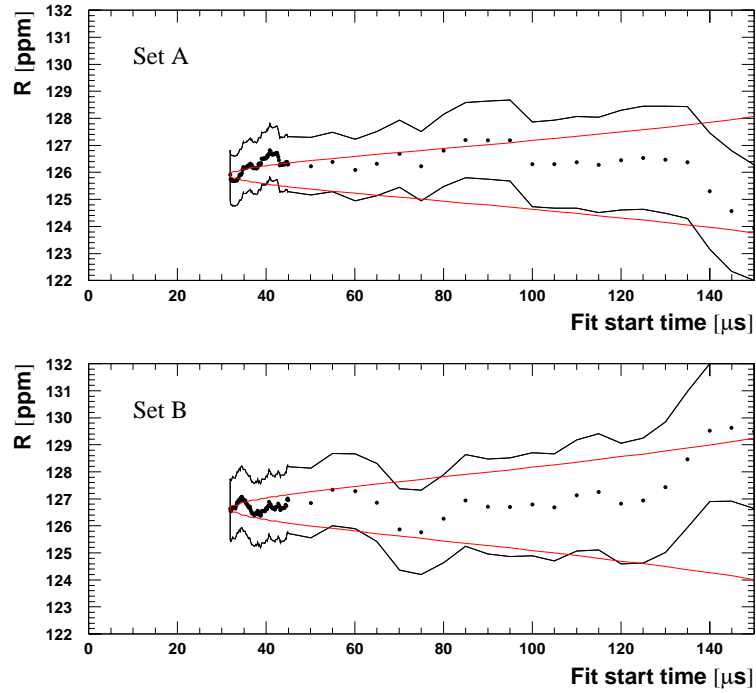


Figure 29: *Start time scans for the sum of all detector spectra fitted with the physics function including phase modulation by CBO.*

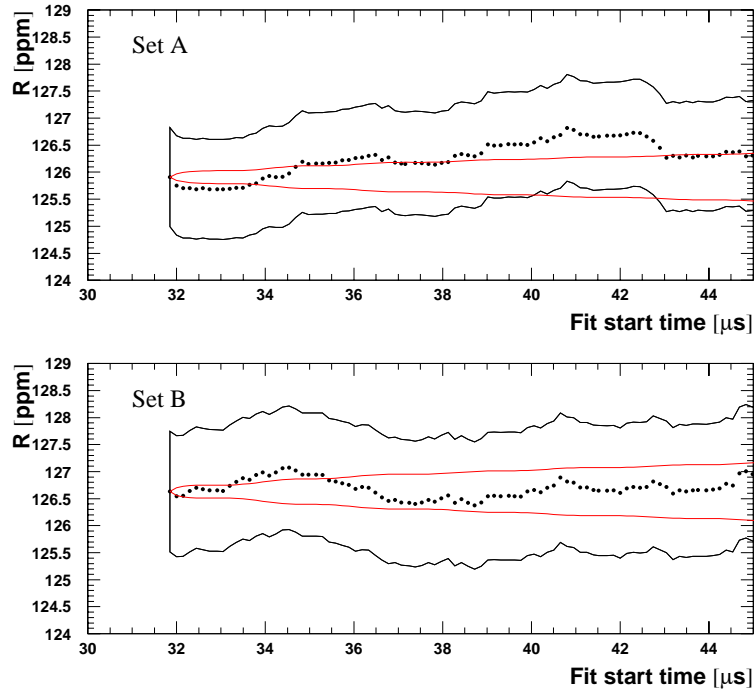
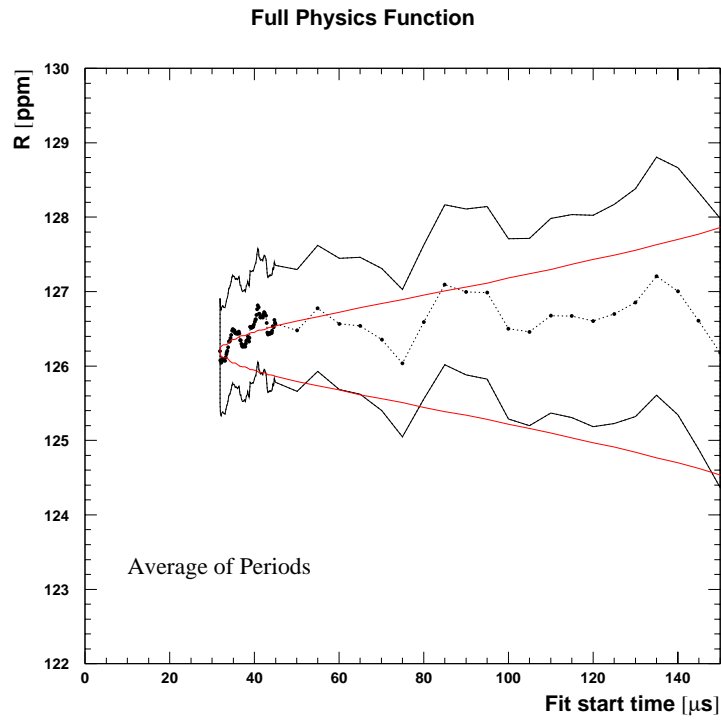
The weighted average of the fit results for R from the two run sets is shown in Figure 31 and Table 23 for R . Scans of the fit stop-time are shown in Figure 32.

Set A	N_0	A	τ	ϕ_a	R	f_{CBO}	τ_{CBO}	A_{CBO}	ϕ_{CBO}	A_{Rob}	ϕ_{Rob}	A_{Jim}	ϕ_{Jim}	A_{DCBO}	ϕ_{DCBO}	A_{loss}
N_0	1.000	-0.040	0.816	-0.010	-0.007	0.017	-0.022	0.030	-0.025	-0.023	0.028	-0.013	-0.071	-0.009	0.018	0.982
A	-0.040	1.000	-0.025	-0.008	-0.004	0.006	0.011	-0.014	-0.010	0.066	0.038	-0.068	0.016	-0.003	0.001	
τ	0.816	-0.025	1.000	-0.007	-0.005	0.010	-0.013	0.018	-0.015	-0.014	0.018	-0.010	-0.044	-0.006	0.011	
ϕ_a	-0.010	-0.008	-0.007	1.000	0.834	0.018	-0.025	0.035	-0.024	-0.017	-0.014	0.004	0.068	-0.000	0.010	
R	-0.007	-0.004	-0.005	0.834	1.000	0.013	-0.018	0.026	-0.017	0.040	-0.058	0.002	0.050	-0.012	0.016	
f_{CBO}	0.017	0.006	0.010	0.018	0.013	1.000	-0.004	0.007	-0.319	0.002	-0.049	-0.002	-0.016	-0.012	0.016	
τ_{CBO}	-0.022	0.011	-0.013	-0.025	-0.018	-0.004	1.000	-0.903	0.003	0.132	0.005	0.016	-0.007	-0.466	0.017	
A_{CBO}	0.030	-0.014	0.018	0.035	0.026	0.007	-0.903	1.000	-0.006	-0.134	-0.007	-0.010	0.008	0.420	-0.022	
ϕ_{CBO}	-0.025	-0.010	-0.015	-0.024	-0.017	-0.319	0.003	-0.006	1.000	-0.003	0.046	-0.001	0.014	0.015	0.015	
A_{Rob}	-0.023	0.066	-0.014	0.054	0.040	0.002	0.132	-0.134	-0.003	1.000	-0.006	0.009	0.023	-0.073	-0.002	
ϕ_{Rob}	0.028	0.038	0.018	-0.082	-0.058	-0.049	0.005	-0.007	0.046	-0.006	1.000	-0.007	0.005	0.005	0.019	
A_{Jim}	-0.013	-0.068	-0.010	0.004	0.002	-0.002	0.016	-0.010	-0.001	0.009	-0.007	1.000	-0.015	-0.034	0.029	
ϕ_{Jim}	-0.071	0.016	-0.044	0.068	0.050	-0.016	-0.007	0.008	0.014	0.023	0.005	-0.015	1.000	0.024	0.015	
A_{DCBO}	-0.009	-0.003	-0.006	-0.000	-0.000	-0.012	-0.466	0.420	0.015	-0.073	0.005	-0.034	1.000	1.000	-0.016	
ϕ_{DCBO}	0.018	0.001	0.011	0.010	0.007	0.016	0.017	-0.022	-0.016	-0.002	0.019	0.029	0.015	-0.016	1.000	
A_{loss}	0.982	-0.037	0.873	-0.009	-0.007	0.015	-0.020	0.028	-0.023	-0.021	0.026	-0.013	-0.065	-0.008	0.016	

Table 21: Correlation matrix $\frac{\text{cov}(\text{B}, \text{P})}{\sigma_i \sigma_j}$ from a fit to the sum of detector spectra of Set A starting at 31.8 μs .

Set B	N_0	A	τ	ϕ_a	R	f_{CBO}	τ_{CBO}	A_{CBO}	ϕ_{CBO}	A_{Rob}	ϕ_{Rob}	A_{Jim}	ϕ_{Jim}	A_{DCBO}	ϕ_{DCBO}	A_{loss}
N_0	1.000	-0.036	0.820	0.006	0.004	0.028	-0.006	0.007	-0.034	0.010	-0.019	0.024	-0.039	-0.005	0.014	0.982
A	-0.036	1.000	-0.022	-0.010	-0.006	0.009	0.014	-0.016	-0.007	-0.067	-0.027	-0.063	-0.035	-0.004	0.006	-0.033
τ	0.820	-0.022	1.000	0.003	0.002	0.017	-0.003	0.004	-0.021	0.006	-0.012	0.015	-0.023	-0.002	0.009	0.877
ϕ_a	0.006	-0.010	0.003	1.000	0.835	0.034	-0.019	0.021	-0.035	0.046	-0.091	0.066	-0.096	-0.002	0.012	0.005
R	0.004	-0.006	0.002	0.835	1.000	0.024	-0.014	0.015	-0.025	0.035	-0.065	0.050	-0.068	-0.001	0.009	0.004
f_{CBO}	0.028	0.009	0.017	0.034	0.024	1.000	0.003	-0.004	-0.424	-0.027	-0.053	-0.003	-0.033	0.004	0.006	0.026
τ_{CBO}	-0.006	0.014	-0.003	-0.019	-0.014	0.003	1.000	-0.885	-0.008	-0.177	0.028	-0.092	-0.005	0.026	0.016	-0.005
A_{CBO}	0.007	-0.016	0.004	0.021	0.015	-0.004	-0.885	1.000	0.010	0.156	-0.038	0.081	0.007	-0.021	-0.023	0.006
ϕ_{CBO}	-0.034	-0.007	-0.021	-0.035	-0.025	-0.424	-0.008	0.010	1.000	0.035	0.030	0.005	0.021	-0.003	-0.010	-0.031
A_{Rob}	0.010	-0.067	0.006	0.046	0.035	-0.027	-0.177	0.156	0.035	1.000	-0.006	0.022	0.012	-0.009	0.007	0.009
ϕ_{Rob}	-0.019	-0.027	-0.012	-0.091	-0.065	-0.053	0.028	-0.038	0.030	-0.006	1.000	-0.019	0.011	0.006	0.002	-0.018
A_{Jim}	0.024	-0.063	0.015	0.066	0.050	-0.003	-0.092	0.081	0.005	0.022	-0.019	1.000	0.000	0.006	-0.024	0.022
ϕ_{Jim}	-0.039	-0.035	-0.023	-0.096	-0.068	-0.033	-0.005	0.007	0.021	0.012	0.011	0.000	1.000	-0.011	-0.015	-0.035
A_{DCBO}	-0.005	-0.004	-0.002	-0.002	-0.001	0.004	0.026	-0.021	-0.003	-0.009	0.006	0.006	-0.011	1.000	-0.001	-0.004
ϕ_{DCBO}	0.014	0.006	0.009	0.012	0.009	0.006	0.016	-0.023	-0.010	0.007	0.002	-0.024	-0.015	-0.001	1.000	0.013
A_{loss}	0.982	-0.033	0.877	0.005	0.004	0.026	-0.005	0.006	-0.031	0.009	-0.018	0.022	-0.035	-0.004	0.013	1.000

Table 22: Correlation matrix $\frac{\text{cov}(\text{p}_i, \text{p}_j)}{\sigma_i \sigma_j}$ from a fit to the sum of detector spectra of Set B starting at $31.8 \mu\text{s}$.

Figure 30: *Early-time zoom of Figure 29.*Figure 31: R averaged over the two run sets.

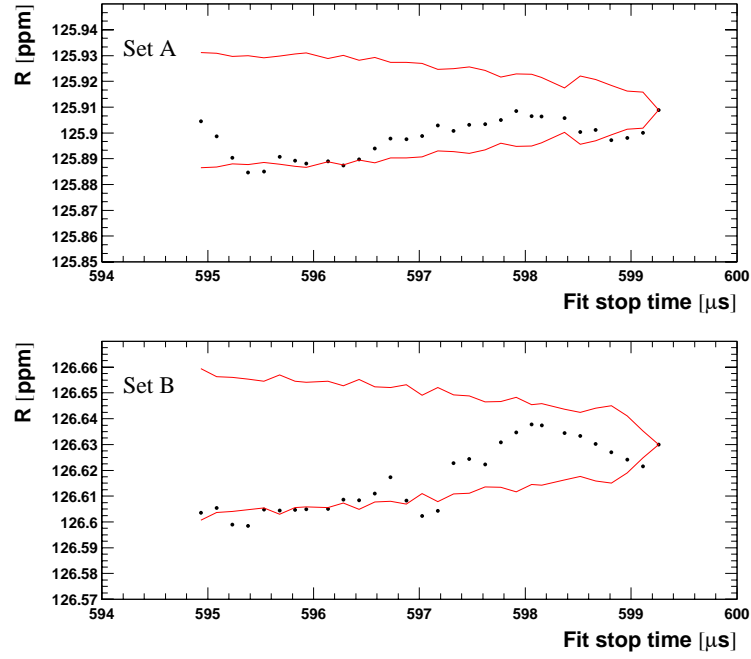
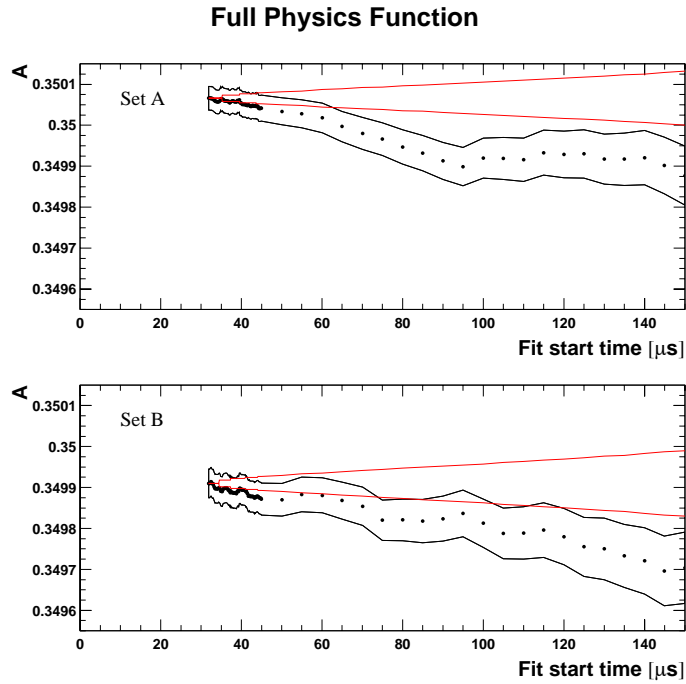
Figure 32: *Fit stop-time scans for R .*

Figure 33 shows start-time scans for A . Unlike in 2000, the start-time stability of A does not improve when amplitude and phase modulation are switched on. This reflects the absence of strong correlations between A and A_{Rob} , A_{Jim} . The reason of the asymmetry sag may be a combination of imperfections in pileup subtraction and energy-scale correction.

Figure 33: *Start-time scans for A , sum of all detector spectra.*

The halfring effect that had already been reduced by inclusion of the asymmetry modulation is mostly eliminated when also the phase modulation is fitted for, see Figures 34 and 35 for R and Figures 36 for A .

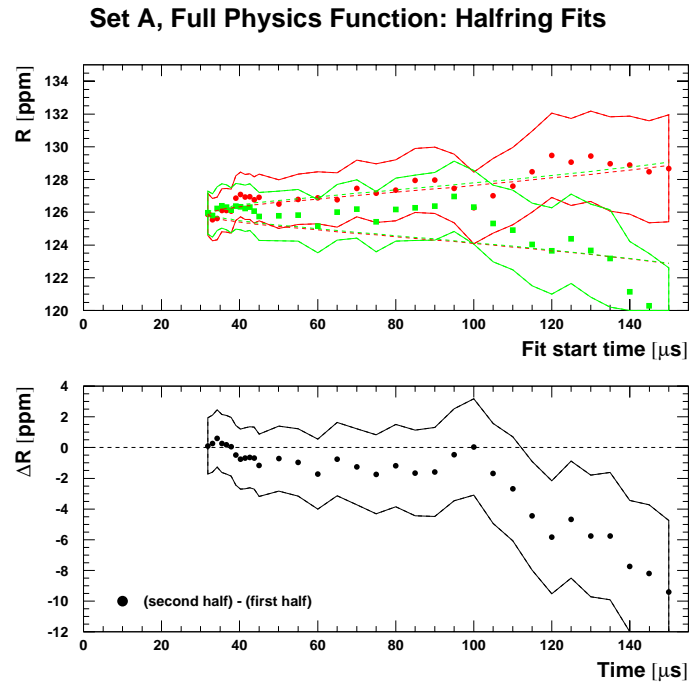


Figure 34: *Fit results for R in the two halves of the ring for Set A.*

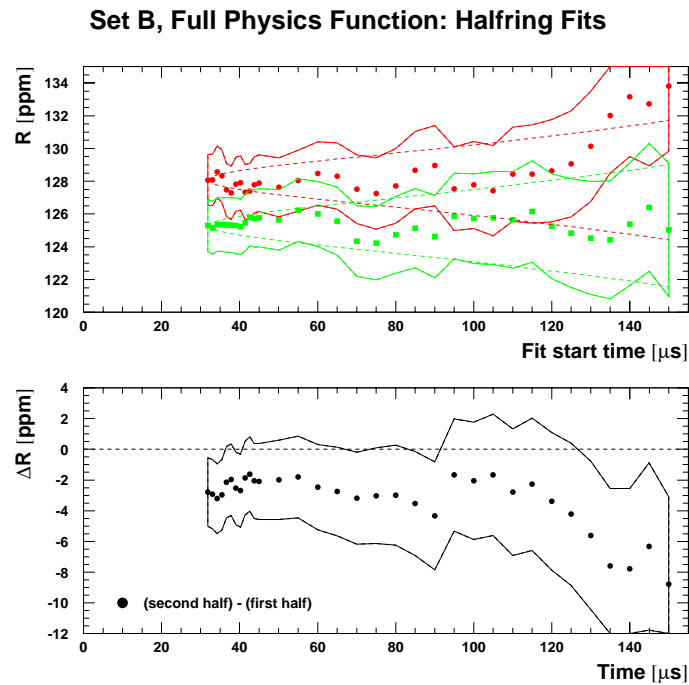


Figure 35: *Fit results for R in the two halves of the ring for Set B.*

Period	Sum of all detectors	First half	Second half	Average of the halves
A	125.9085 ± 0.9172	125.8337 ± 1.2802	126.0115 ± 1.3131	125.9203 ± 0.9166
B	126.6301 ± 1.1169	128.0963 ± 1.5583	125.2315 ± 1.6010	126.7026 ± 1.1167
A _{vr.}	126.1991 ± 0.7088	126.7454 ± 0.9892	125.6978 ± 1.0153	126.2352 ± 0.7085
A - B	0.7216 ± 1.4452	2.2626 ± 2.0167	0.7800 ± 2.0706	0.7823 ± 1.4447

Table 23: R for the sum of all detectors and for the two half rings. The fits were done with the full physics function. The start time was $31.8 \mu\text{s}$.

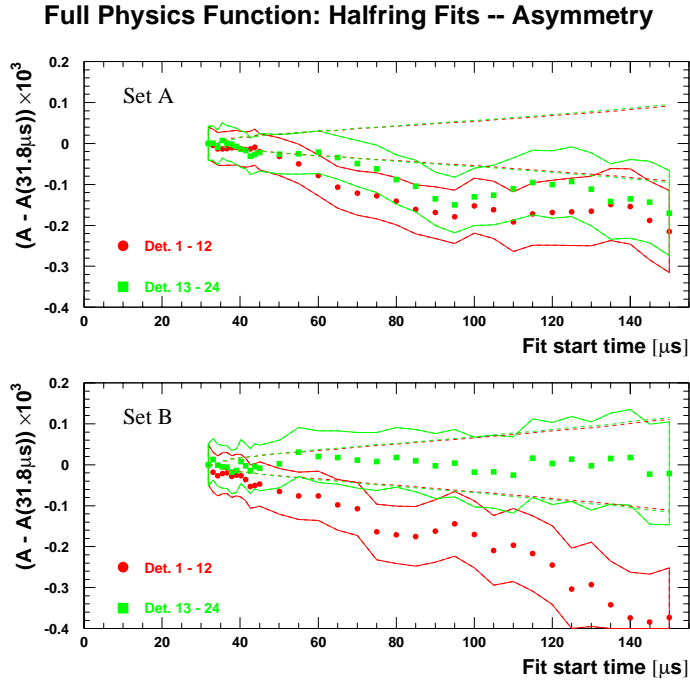


Figure 36: Fit results for A in the two halves of the ring.

Start time scans for the other parameters and for the different run periods are shown in Appendix C.1. Appendix C.2 shows them for the first and second half of the ring.

Period	$A_{\text{CBO}} \times 10^3$	ϕ_{CBO}	$A_{\text{Rob}} \times 10^3$	ϕ_{Rob}	$A_{\text{Jim}} \times 10^3$	ϕ_{Jim}
A	1.33 ± 0.15	-0.29 ± 0.05	0.23 ± 0.25	2.91 ± 1.07	0.02 ± 0.09	0.65 ± 5.03
B	1.89 ± 0.13	2.42 ± 0.04	0.69 ± 0.24	0.81 ± 0.35	0.13 ± 0.08	2.27 ± 0.66
Period	$f_{\text{CBO}} [\text{kHz}]$		$\tau_{\text{CBO}} [\mu\text{s}]$			
A	418.48 ± 0.27		97.09 ± 15.90			
B	490.44 ± 0.15		148.29 ± 20.58			

Table 24: CBO parameters from fits to the sum of all detectors.

Fits to the Individual Detectors

The fit results for individual detectors at a start time of $49.2\,\mu\text{s}$ are shown in the figures of Appendix C.3. A bigger version of R versus detector is displayed in Figure 37.

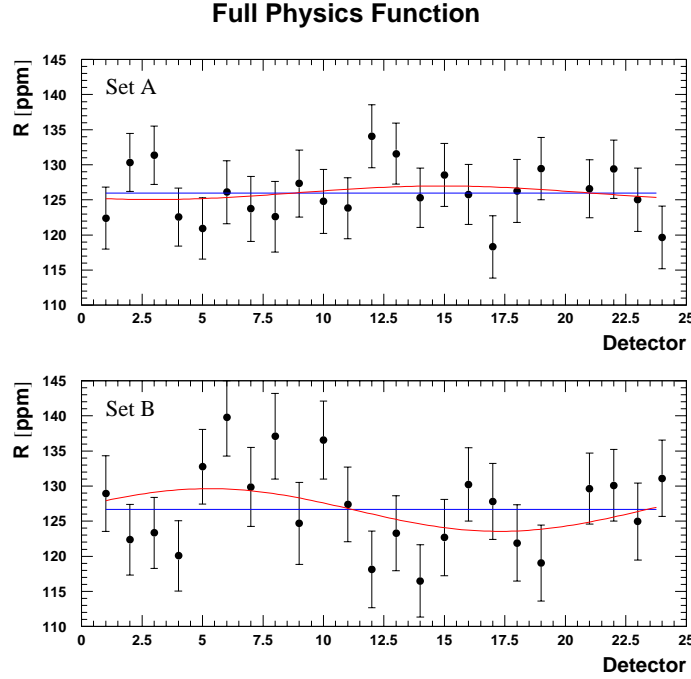


Figure 37: R versus detector with the full physics function.

With the full physics function, R versus detector is very similar to its behaviour for the physics function without phase modulation because the latter is a very small effect. The wave amplitude (Table 26) is reduced from (1.2 ± 1.3) ppm with the 1999-style function to (1.0 ± 1.3) ppm, in Set B from (3.2 ± 1.6) ppm to (3.0 ± 1.6) ppm. The remaining effect of almost 2σ in Set B is not really a wave but rather a statistical shift between detectors 1-12 and 13-24, as can be seen by the constant difference in Figure 35.

Period	$\langle R \rangle$	χ^2/ndof (fit to a constant)
A	125.9921 ± 0.9172	18.17 / 22
B	126.6632 ± 1.1174	28.80 / 22
avr.	126.2623 ± 0.7090	

Table 25: Average R from the individual detector fits, for the two run sets with a start time of $31.8\,\mu\text{s}$. Detector 20 was excluded. The full physics function was used.

Period	R_0	A_{Rc}	A_{Rs}	$\sqrt{A_{Rc}^2 + A_{Rs}^2}$	χ^2/ndof
A	126.0123 ± 0.9177	-0.6984 ± 1.2791	-0.6688 ± 1.3233	0.9670 ± 1.3004	$17.58 / 20$
B	126.5915 ± 1.1181	0.5711 ± 1.5597	2.9872 ± 1.6109	3.0413 ± 1.6091	$25.11 / 20$
avr.	126.2454 ± 0.7094	-0.1879 ± 0.9890	0.8043 ± 1.0225	0.8260 ± 1.0208	

Table 26: R versus detector fitted with a sine + cosine function. The individual detector spectra were fitted with the full physics function. The start time was $31.8 \mu\text{s}$. Detector 20 was excluded.

Period	$\langle R \rangle - R_0$
A	-0.0202 ± 0.0303
B	0.0717 ± 0.0396

Table 27: Difference between fitting R versus detector to a constant and to a wave (Tables 25 and 26).

In Table 28 we give the average CBO amplitudes and the CBO vector sums like in Table 11, except that the weights N_d in Eq. (27) are replaced by $N_d A_d \phi_{a,d} \sin \phi_{a,d}$, as can be seen by expanding the phase modulation in the physics function.

Period	$\langle A_{\text{CBO}} \rangle \times 10^3$	$\langle A_{\text{Rob}} \rangle \times 10^3$	$\langle A_{\text{Jim}} \rangle \times 10^3$	$\langle \phi_{\text{Jim}} - \phi_{\text{Rob}} \rangle$
A	6.28 ± 0.17	2.84 ± 0.28	0.67 ± 0.10	2.36 ± 0.15
B	10.27 ± 0.16	4.10 ± 0.28	0.71 ± 0.10	2.15 ± 0.14

Period	vector sum over all detectors					
	$A_{\text{CBO}} \times 10^3$	ϕ_{CBO}	$A_{\text{Rob}} \times 10^3$	ϕ_{Rob}	$A_{\text{Jim}} \times 10^3$	ϕ_{Jim}
A	1.36 ± 0.15	-0.30 ± 0.09	0.20 ± 0.29	2.25 ± 1.46	0.04 ± 0.10	6.20 ± 2.75
B	2.09 ± 0.13	2.28 ± 0.06	0.84 ± 0.29	0.88 ± 0.34	0.21 ± 0.10	2.27 ± 0.47

Table 28: Upper table: CBO parameters from fits to the individual detectors, averaged over all detectors. Lower Table: coherent sum of the CBO parameters over all detectors. The results should be consistent with the fit parameters obtained from the summed spectra (cf. Table 24).

Again, average amplitude and vector sum of the main CBO are not strongly affected by the inclusion of the phase modulation term (cf. Tables 19 and 28). The same holds for the asymmetry modulation.

The asymmetry and phase modulation vector sums over all detectors reproduce the results from the fit to the sum of detectors (Table 24) within their errors.

Comparison between Fits to the Sum and the Average of Individual Fits

Period	$ \langle R \rangle - R_{\text{sum}} $	$ R_0 - R_{\text{sum}} $
A	0.0767 ± 0.0234	0.0951 ± 0.0234
B	0.0063 ± 0.0149	-0.0616 ± 0.0365

Table 29: *Difference between R from fits to the sum of all detector spectra and the averages $\langle R \rangle$ and R_0 from fits to individual detector spectra.*

5.4.4 Energy-Binned Fits with the Full Physics Function

To shed some more light on the instability of the asymmetry in start-time scans a series of fits in 200 MeV energy bins between 1.8 GeV and 3.4 GeV was performed. Fit convergence was facilitated by excluding double CBO and fixing the CBO lifetime to the result from the fit to the full energy range. The muon loss amplitude was left free even if it took a non-physical negative value. This was done to give the fit an r.s.e.-like freedom for eliminating problems with slow effects which we don't aim to study here.

The pileup error correction was adapted to the binned situation. The coefficients X and γ and their product to be used in Eq. 23 are drawn as a function of E in Figures 39 and 40. X is determined as the ratio of doubles (D) to singles ($N - D + S1 + S2$) counted over the g-2 cycle centred at $34.1 \mu\text{s}$. The factor γ is calculated from the single-pulse energy spectrum obtained from $S2$ pulses which are not suppressed by the 0.9 GeV threshold. Figure 38 serves as illustration of the calculation. Note that all zones with $E_{S1} < 0.9 \text{ GeV}$ are invisible in the Mediterranean pileup subtraction and have to be simulated by reduplication of the corresponding zones with $E_{S2} < 0.9 \text{ GeV}$.

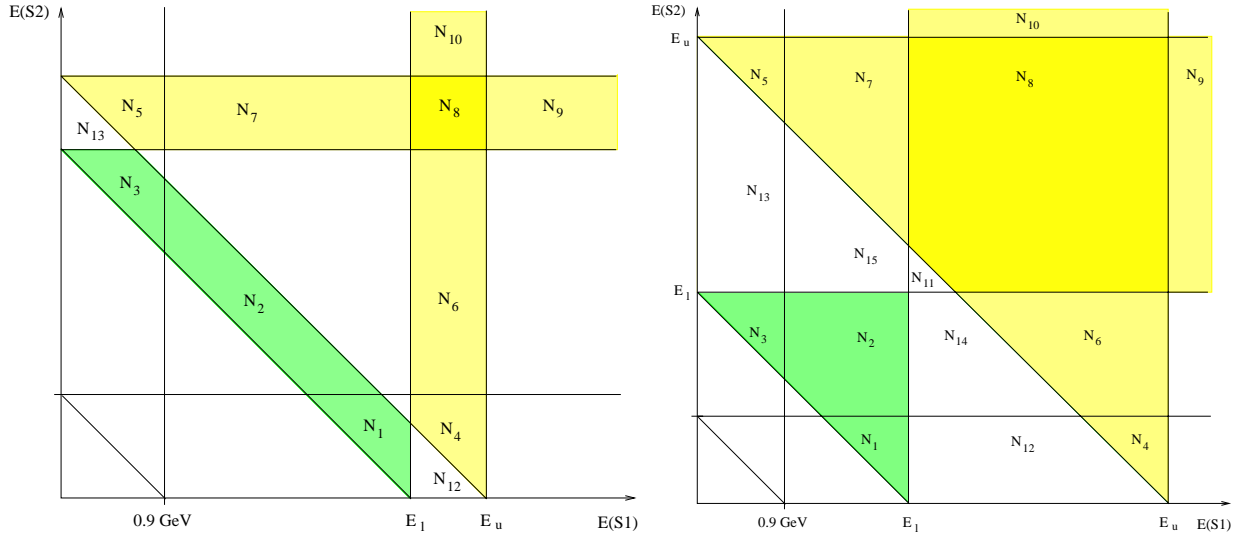


Figure 38: Zones in the $S1$ - vs. $S2$ -pulse energy plane for the calculation of the γ factor in an energy interval $[E_l; E_u]$. Two different cases are shown.

As a first step, the single-pulse energy spectrum $n_S(E)$ is two-dimensionally integrated over each of the zones labelled in the figure:

$$N_i = \int_{\text{Zone } i} dE_{S1} dE_{S2} n_S(E_{S1}) n_S(E_{S2}) \quad (28)$$

Then γ is defined as the ratio

$$\gamma = \frac{N_{\text{extra}} + \sigma_{\text{extra}}^2 + 2 \text{cov}_{\text{raw hist, extra}}}{N_{\text{doubles}}} \quad (29)$$

with

$$N_{\text{extra}} = 2(N_1 - N_4) + N_2 - N_6 - N_7 - 2N_8 - N_9 - N_{10} - N_{11} \quad (30)$$

$$\sigma_{\text{extra}}^2 = 4(N_1 + N_4) + N_2 + N_6 + N_7 + 4N_8 + N_9 + N_{10} + N_{11} \quad (31)$$

$$\text{cov}_{\text{raw hist, extra}} = 2N_4 + N_6 + N_7 + 2N_8 + N_9 + N_{10} + N_{11} \quad (32)$$

$$N_{\text{doubles}} = 2N_1 + N_2 + N_{11} + 2N_{12} + N_{14} + N_{15} \quad (33)$$

At high energies it is important to use the correct coefficients: fitting Set B in the energy bin $[3.2 \text{ GeV}; 3.4 \text{ GeV}]$ with the values from the full energy range yields a χ^2 of 1.066. With the correct values this is reduced to 1.012. Fred points out correctly that there are correlations between the γ -factors of different energy bins. This happens because some zones used for a given bin will also appear in the calculation for another bin. However, we take above formulae as a first-order approach.

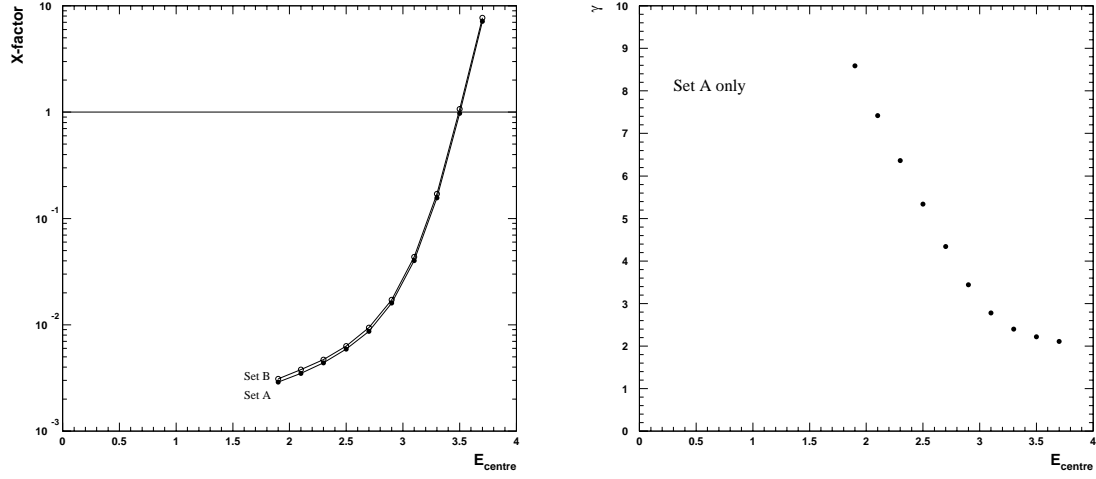


Figure 39: *Pileup error correction coefficients X and γ as a function of the centre of 200 MeV wide energy bins.*

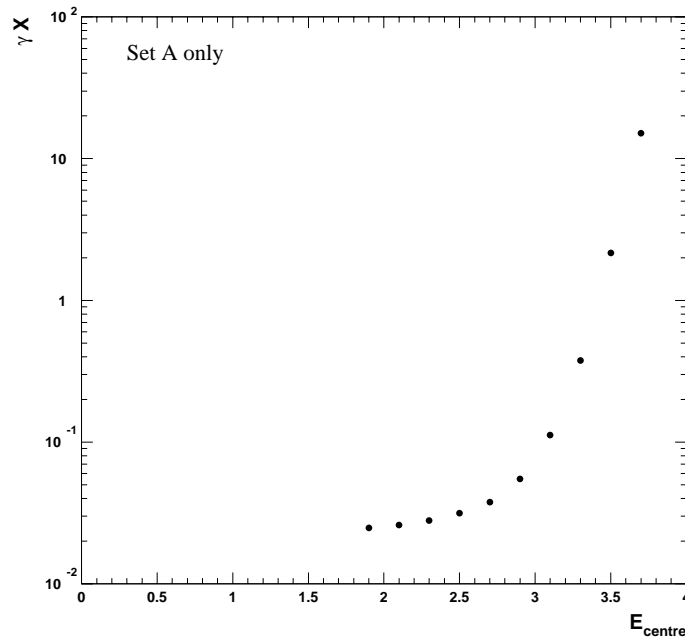


Figure 40: *Product $X\gamma$ from the previous figure.*

Figures 41 to 43 show R , A and χ^2 respectively for a start time of $31.8 \mu\text{s}$ as a function of the centre of the energy bin. The other parameters are given in Appendix D.

Table 30 compares R averaged over the energy bins with the results from fits over the full energy range $1.8 \text{ GeV} - 3.4 \text{ GeV}$. Note the lower statistical errors when energy bins are fitted separately. For Set A the two results agree whereas for Set B they differ by 2.1 standard deviations. The error of the difference may be underestimated by using the simple quadratic error difference.

Set	Fit over $[1.8 \text{ GeV}; 4.3 \text{ GeV}]$	Average of Energy Bins	Difference
A	125.9085 ± 0.9172	126.1537 ± 0.8516	0.2452 ± 0.3406
B	126.6301 ± 1.1169	127.6315 ± 1.0371	1.0014 ± 0.4146
avr.	126.1991 ± 0.7088	126.7488 ± 0.6581	0.5497 ± 0.2633

Table 30: Comparison of R from fits to the full energy range and from the average of individual energy bin results. These numbers represent fits to the sum of all detectors starting at $31.8 \mu\text{s}$.

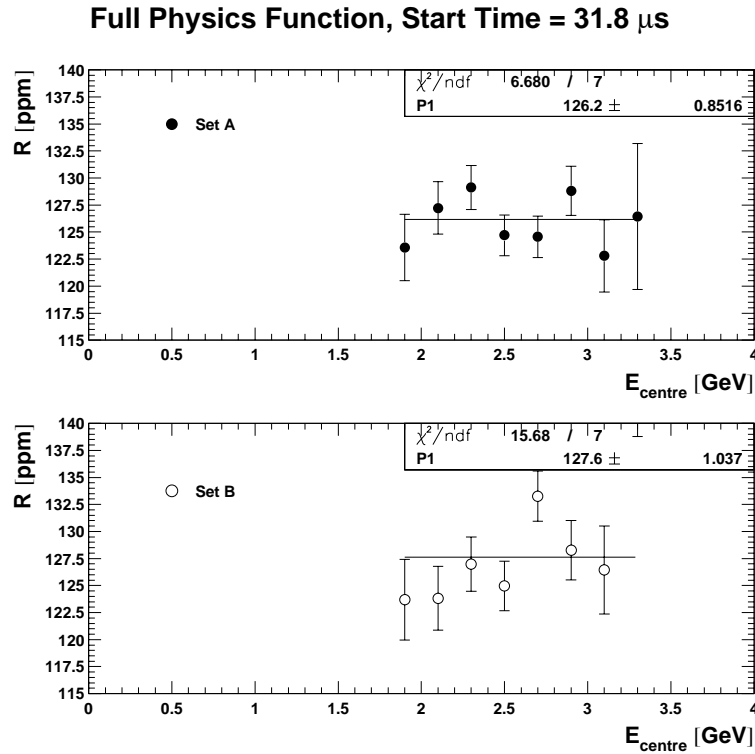
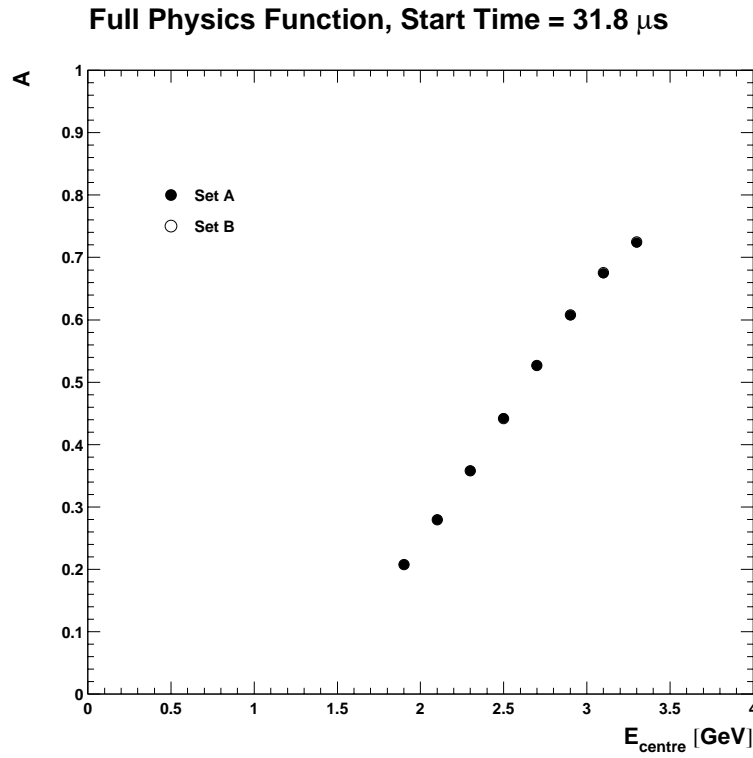
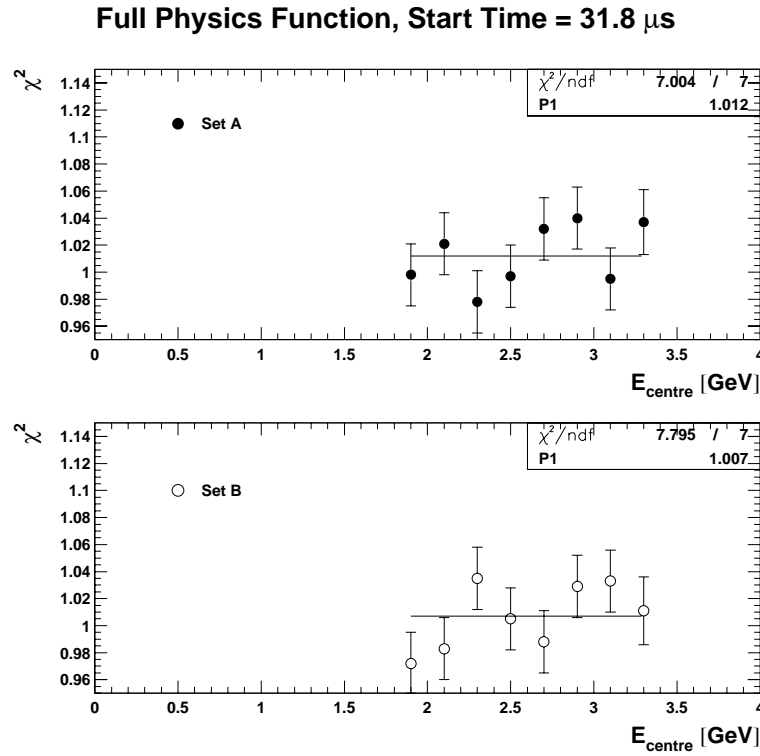


Figure 41: R versus centre of 200 MeV wide energy bins.

Figure 42: A versus centre of 200 MeV wide energy bins.Figure 43: χ^2 versus centre of 200 MeV wide energy bins.

Individual Detector Fits

The same comparison was done for individual detector fits. The fit results are shown in Figure 44.

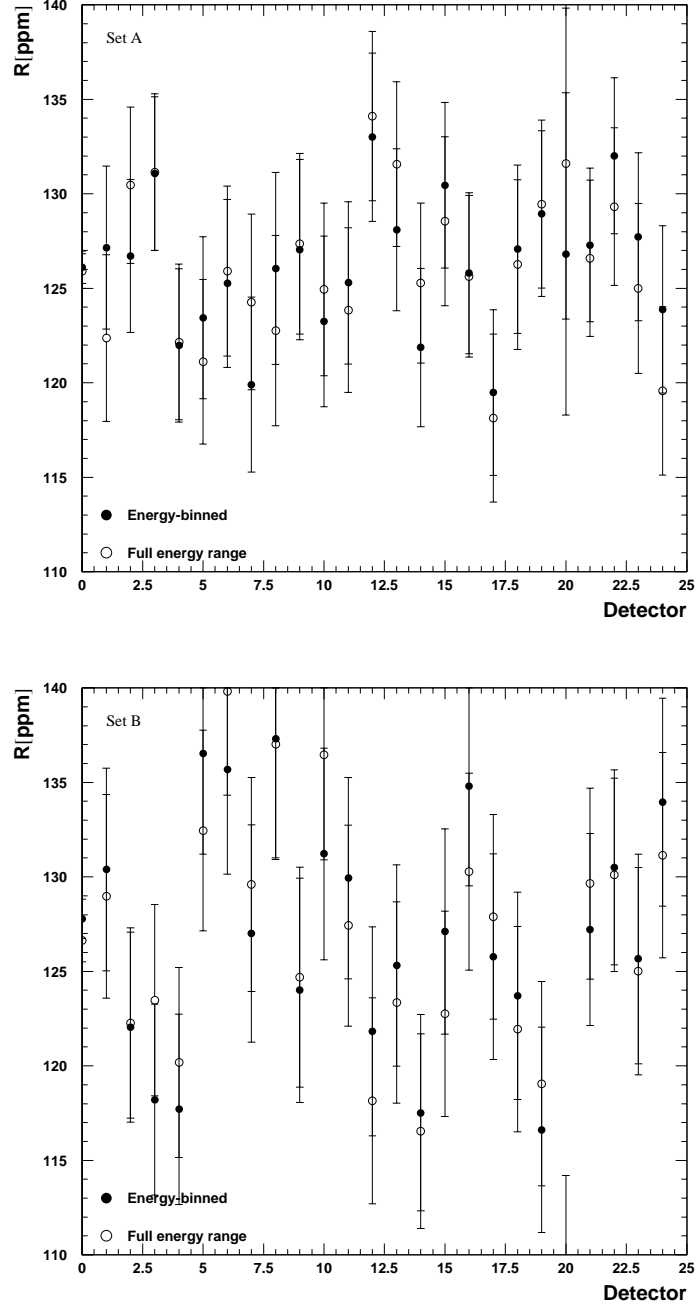


Figure 44: *Comparison of the results from the energy-binned and the combined fits.*

Again, the error of the difference between the binned and the summed analysis is assumed to be the quadratic error difference which may be wrong. Indeed, Figure 45 shows differences up to 10σ for some detectors. No clear pattern of troublesome detectors is visible. Averaging the results over detectors we obtain Table 31.

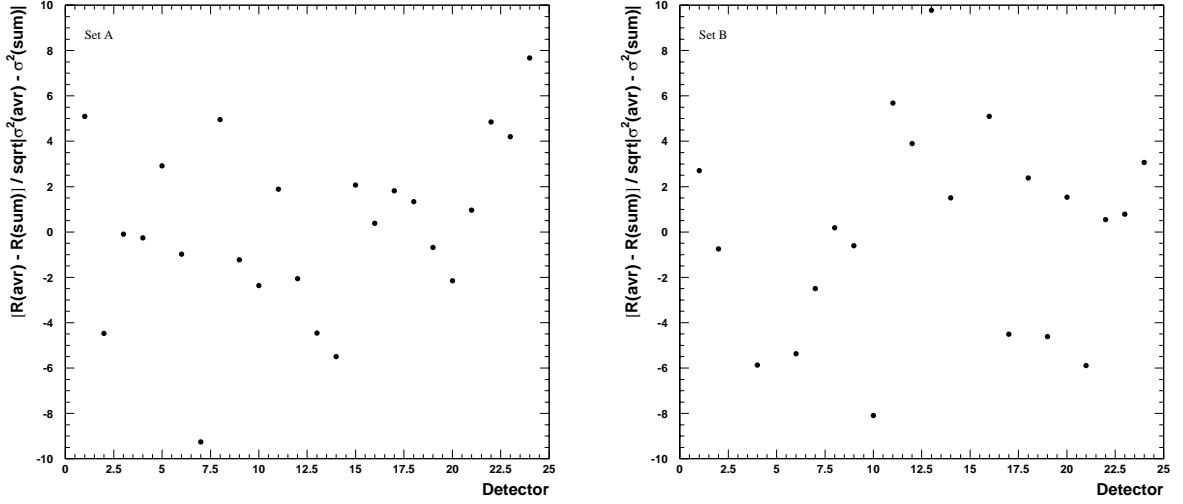


Figure 45: *Difference between the binned and the summed fit results in terms of standard deviations assuming that the errors subtract quadratically.*

Set	Fit over [1.8 GeV; 4.3 GeV] averaged over detectors	Average of Energy Bins and detectors	Difference
A	125.9921 ± 0.9172	126.2570 ± 0.9059	0.2649 ± 0.1435
B	126.6632 ± 1.1174	126.7072 ± 1.1255	0.0440 ± 0.1348
avr.	126.2623 ± 0.7090	126.4340 ± 0.7057	0.1717 ± 0.0683

Table 31: *Comparison of R from fits to the full energy range and from the average of individual energy bin results. These numbers are the averages over individual detector fits starting at $31.8 \mu s$.*

Strangely, unlike the sum of detectors, the average over detectors does not show any obvious problem in Set B.

However, for a conclusive comparison a detailed systematic error analysis for the binned fits would be necessary which is beyond the scope of our approach.

Upon request by the review committee we have also evaluated the normalised differences $\frac{R(E_i) - \langle R(E_i) \rangle}{\sigma(R(E_i))}$ for each detector. The means and RMS of these distributions are plotted versus detector in Figure 46). Their averages over all detectors (except 20) are given in Table 46. For both sets the average means are sufficiently close to 0 whereas the average RMS are about 2σ lower than 1.

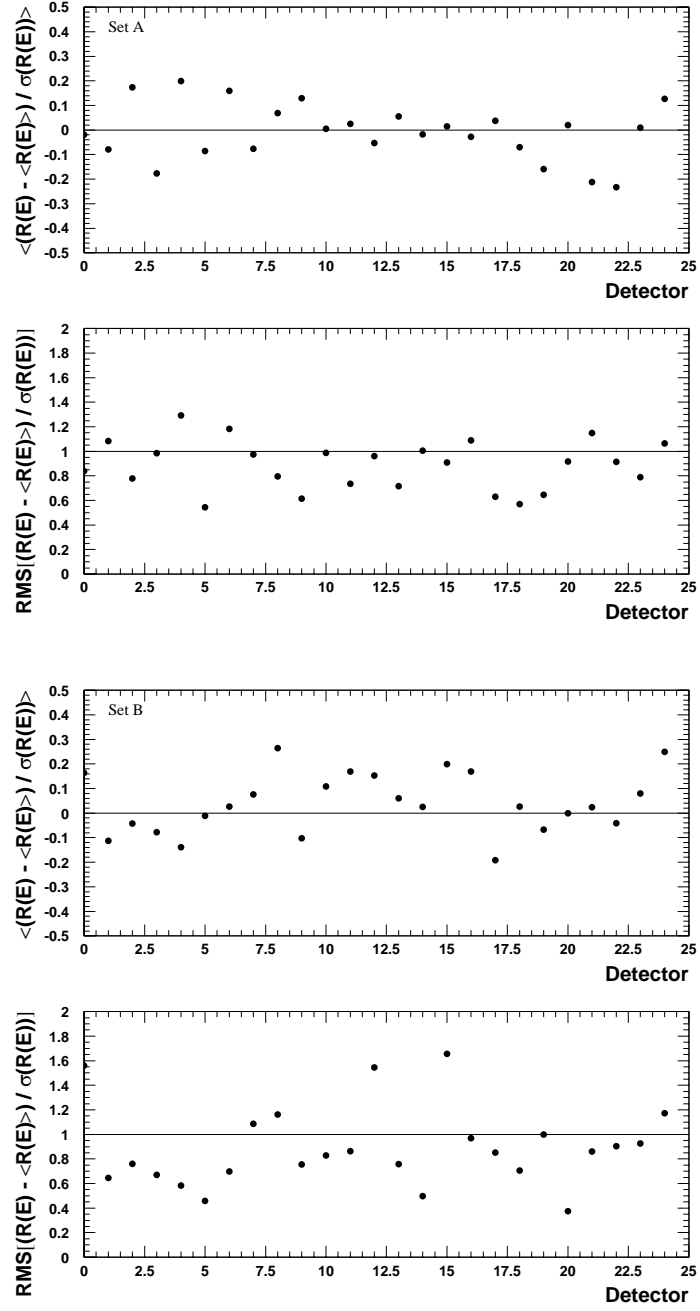


Figure 46: Mean and RMS of the pull distributions $\frac{R(E_i) - \langle R(E_i) \rangle}{\sigma(R(E_i))}$. "Detector 0" corresponds to the detector sum.

Set		
A	-0.0079 ± 0.0252	0.8876 ± 0.0439
B	0.0370 ± 0.0261	0.8850 ± 0.0612

Table 32: Means and RMS from Figure 46 averaged over all detectors.

5.4.5 Comparison of Fit Results with Different Functions

The following results still represent one random seed. The combined results for more seeds will be given in Section 6.10.

Period	1999 Func.	Physics Func. without Phase Modulation	Full Physics Func.
A	125.9420 ± 0.9138	125.9080 ± 0.9161	125.9085 ± 0.9172
B	126.4448 ± 1.1098	126.5474 ± 1.1128	126.6301 ± 1.1169
avr.	126.1452 ± 0.7054	126.1663 ± 0.7073	126.1991 ± 0.7088

Table 33: Comparison of R from fits with the three functions studied. These numbers represent fits to the sum of all detectors starting at $31.8\mu\text{s}$.

Period	1999 Func.	Physics Func. without Phase Modulation	Full Physics Func.
A	1.0375	1.0378	1.0383
B	1.0211	1.0194	1.0194

Table 34: Comparison of χ^2 from fits with the three functions studied. These numbers represent fits to the sum of all detectors starting at $31.8\mu\text{s}$. In all cases the statistical error amounts to 0.0230 .

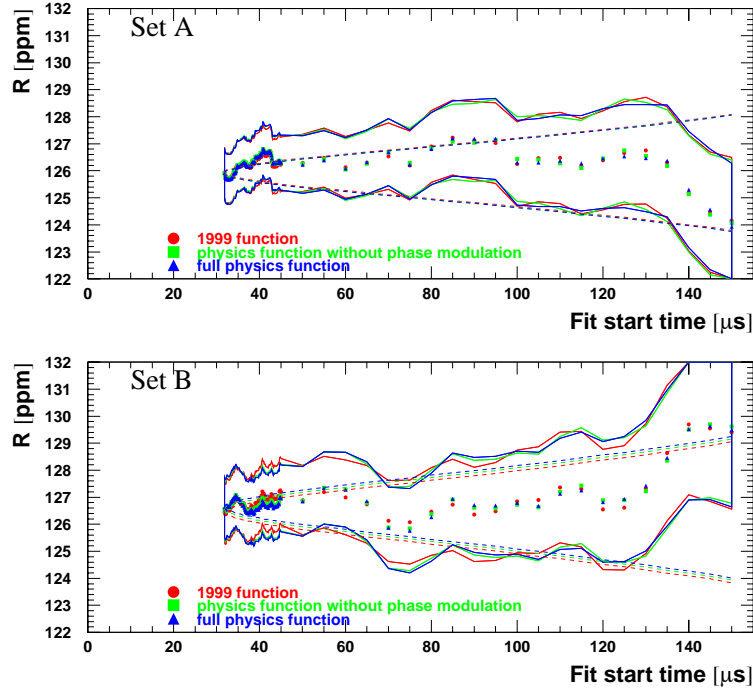
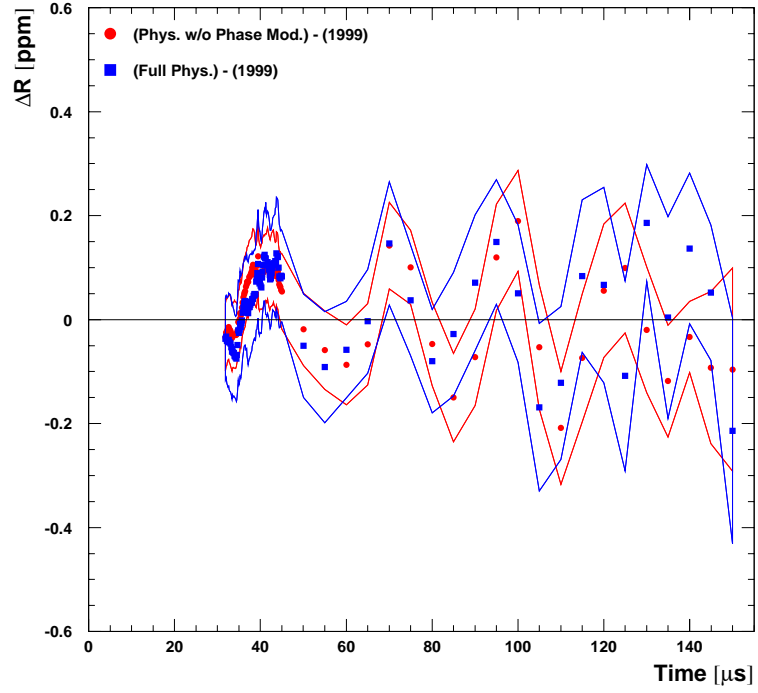
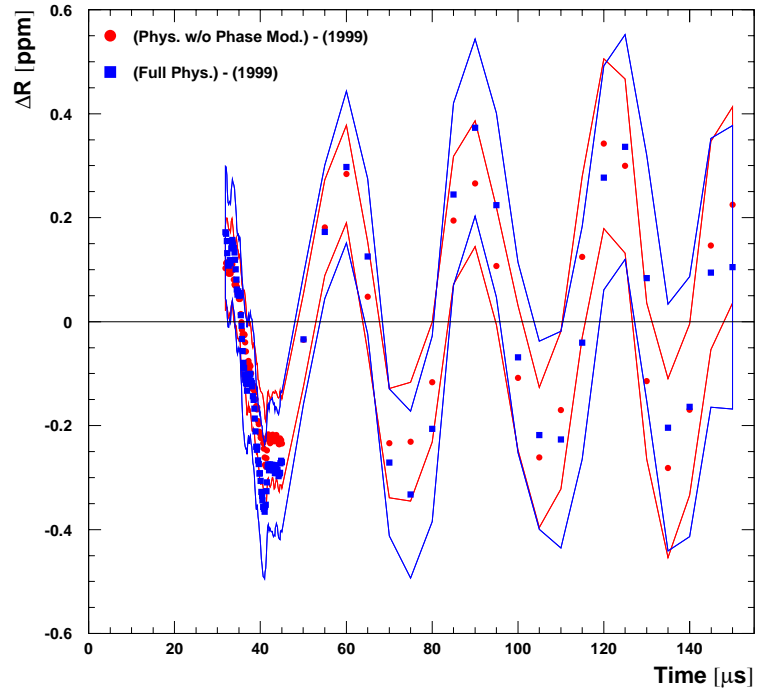


Figure 47: Start-time scans for the three fit functions studied.

Figure 48: *Difference between R results from start-time scans for Set A.*Figure 49: *Difference between R results from start-time scans for Set B.*

6 Systematic Errors at 31.8 μ s Fit Start Time

6.1 Time-Varying CBO Frequency

From the quadrupole circuitry we know that the voltage decay time should be of the order 200 ms. In 2000 we found an empirical optimum at 140 ms. We can expect our knowledge to be correct within about a factor 2 at most. Therefore the fixed parameter τ_{droop} was manually varied as shown in Figures 50 and 51. In the range between 70 ms and 300 ms, R changes by no more than 0.01 ppm. Hence we take 0.01 ppm as systematic error due to the CBO frequency droop.

Figures 82, 83, 94 and 95 show that despite implementing the the CBO frequency droop, the parameter f_{CBO} still sags out of the correlated-error band by about 1σ . Via its correlation, the CBO phase follows this behaviour. Out of curiosity we tried to stabilize ϕ_{CBO} by fixing f_{CBO} to its value from the earliest fit. The reaction of R is shown in Figures 52 to 55. The difference between the results with fixed and with floating f_{CBO} exhibits an oscillation with the left CBO side-band frequency $f_{\text{CBO}} - f_a$ and an average amplitude of about 0.03 ppm. We conclude that artificially fixing a parameter can be a dangerous idea.

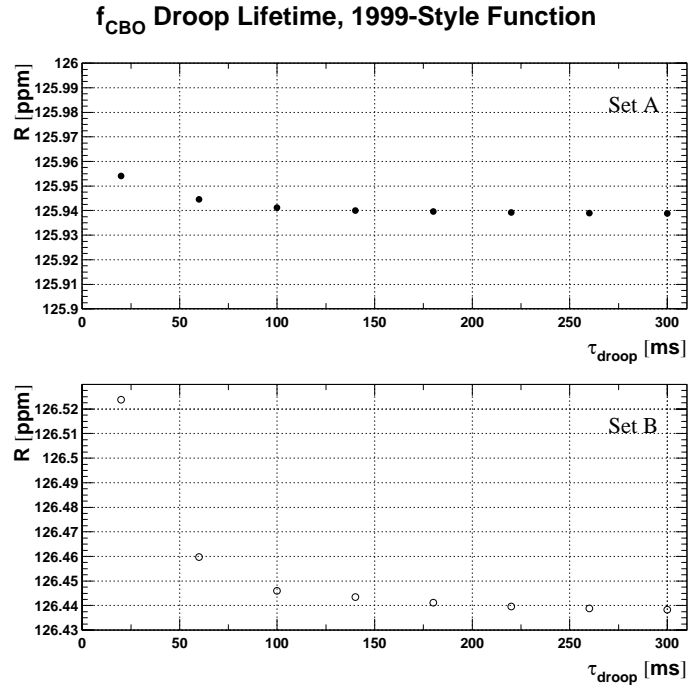


Figure 50: R versus lifetime of the CBO frequency droop for the 1999-style function.

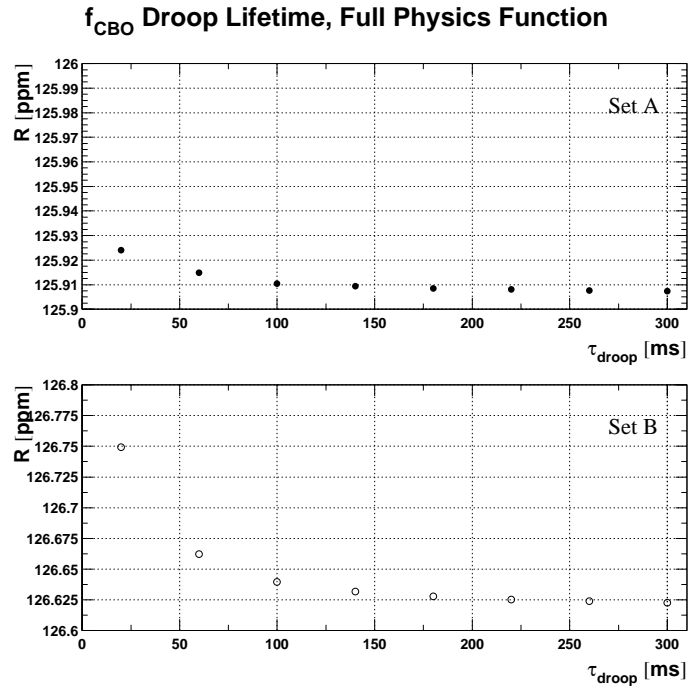


Figure 51: R versus lifetime of the CBO frequency droop for the full physics function.

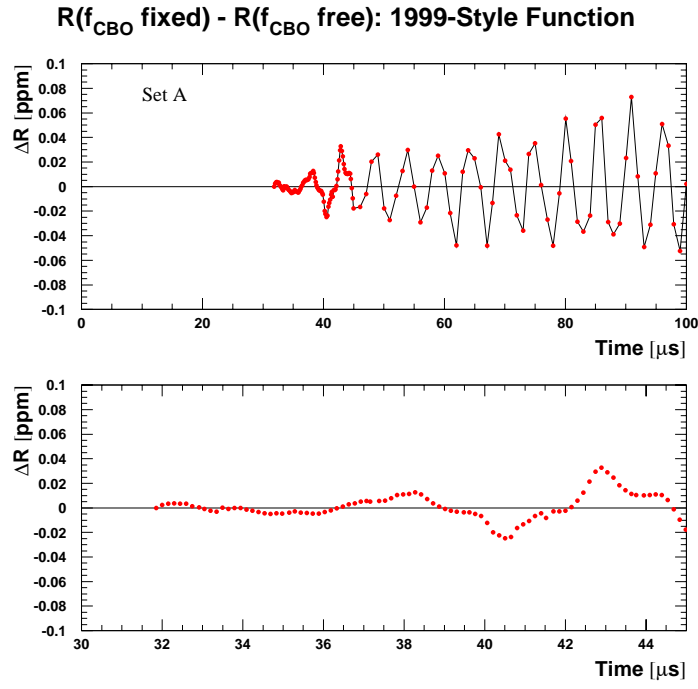


Figure 52: R difference between fits with floating and fixed f_{CBO} for the 1999-style function and Set A.

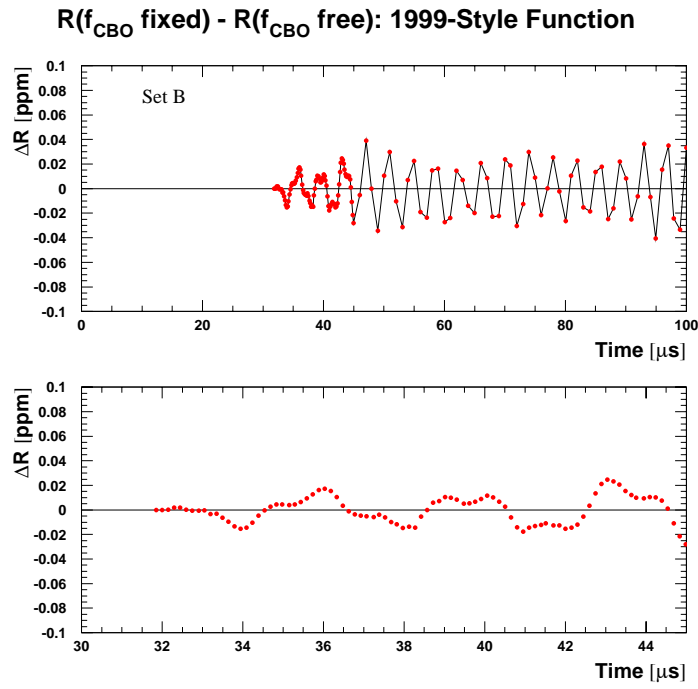


Figure 53: R difference between fits with floating and fixed f_{CBO} for the 1999-style function and Set B.

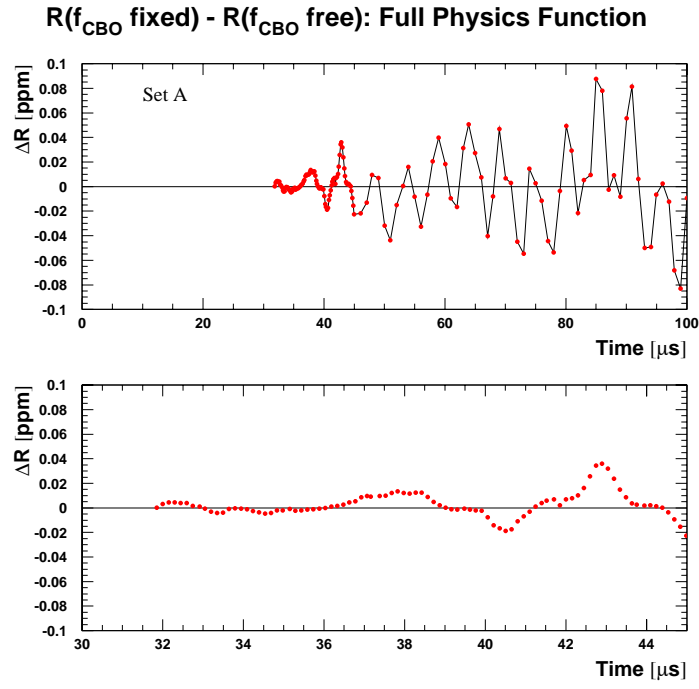


Figure 54: R difference between fits with floating and fixed f_{CBO} for the full physics function and Set A.

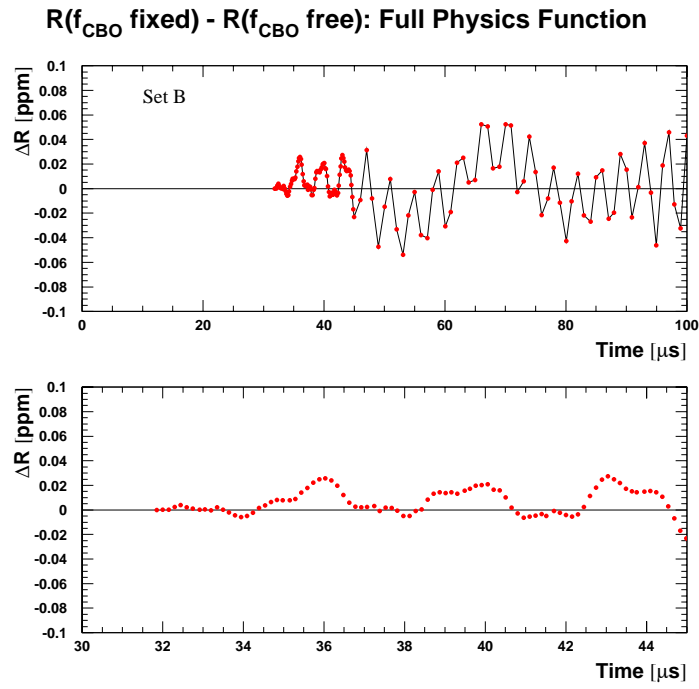


Figure 55: R difference between fits with floating and fixed f_{CBO} for the full physics function and Set B.

6.2 Main (Acceptance) CBO

We follow the procedure of the 2000 analysis ([1], Section 6.1). Yannis' simulation [16] showed that ignoring an additive CBO perturbation with an amplitude of 0.01 leads to phase pulling in R with an amplitude of 6.5 ppm (Set A with $f_{\text{CBO}} = 418$ kHz) or 7.0 ppm (Set B with $f_{\text{CBO}} = 490$ kHz) at a fit start time $t = 0$. At a start time of 31.8 μ s the effect has decayed to

$$\begin{aligned} 6.5 \text{ ppm} \times e^{-31.8/100} &= 4.7 \text{ ppm} \quad (\text{Set A}) \\ 7.0 \text{ ppm} \times e^{-31.8/140} &= 5.6 \text{ ppm} \quad (\text{Set B}) \end{aligned}$$

If – more realistically – a multiplicative CBO term is used in the simulation and then ignored in the fit, the phase pulling amplitude is reduced by a factor 10 to about 0.5 ppm or 0.6 ppm respectively, corresponding to an RMS error of $0.6 \text{ ppm} / \sqrt{2} = 0.4 \text{ ppm}$ (or $0.5 \text{ ppm} / \sqrt{2} = 0.4 \text{ ppm}$). From our fits to the sum of detector spectra with a start time of 31.8 μ s we obtain $A_{\text{CBO}} = 0.0013$ (or 0.0019) (see Tables 7, 15 and 24) instead of the 0.010 assumed in the simulation. This brings the error from completely ignoring the main CBO down to $0.4 \text{ ppm} \times A_{\text{CBO}} / 0.010 = 0.05 \text{ ppm}$ (0.08 ppm). However, we do fit for the CBO, and the systematic error is determined by the amount of remnant CBO that the fit doesn't take care of. The fraction of left-over CBO can be determined from the factor by which the CBO peak in a Fourier spectrum of fit residuals is reduced when the CBO term is included in the fit function. To enhance the sensitivity of the study to CBO effects we align the time spectra of the individual detectors such that the CBO phases are equal. Thus we avoid cancellation around the ring when the individual spectra are added. Figure 56 shows the result.

To quantify the CBO peak in the spectrum we average the amplitude in the range [0.34 MHz, 0.54 MHz] (Set A) or [0.4 MHz, 0.6 MHz] (Set B). The background level is taken as the average over [0.1 MHz, 1 MHz] \setminus {peak area as defined above} in the spectrum after fitting the full physics function.

- Set A:
 - CBO not fitted: average signal = 7.16
 - CBO fitted: average signal = 0.82; background = 0.68.
 - Reduction factor = $\frac{7.16 \ominus 0.68}{0.82 \ominus 0.68} = 15.5$
- Set B:
 - CBO not fitted: average signal = 8.89
 - CBO fitted: average signal = 0.69; background = 0.54.
 - Reduction factor = $\frac{8.89 \ominus 0.54}{0.69 \ominus 0.54} = 20.6$

This yields systematic errors of $0.05 \text{ ppm} / 15.5 = 0.003 \text{ ppm}$ for Set A and $0.08 \text{ ppm} / 20.6 = 0.004 \text{ ppm}$ for Set B.

These systematic errors are common to all three fitting functions because the main CBO peak originates solely from the acceptance CBO which is included in all of them.

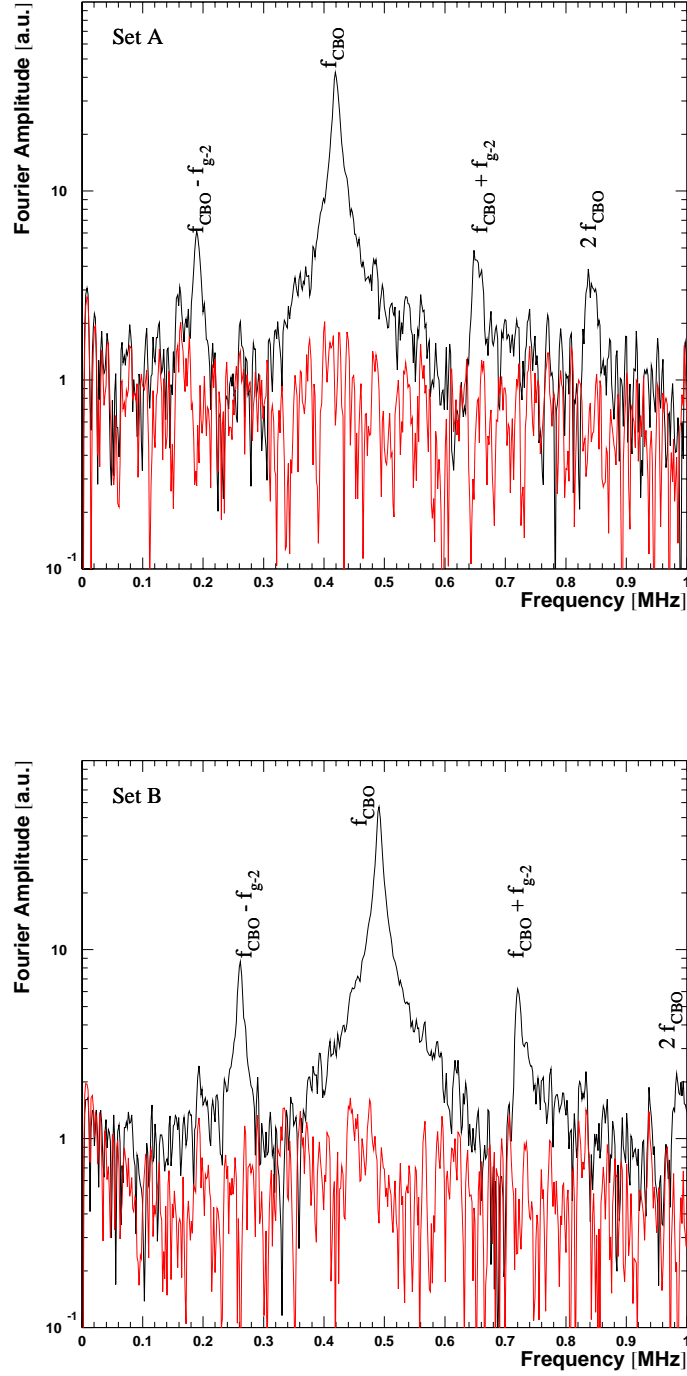


Figure 56: *Residual Fourier spectrum of CBO-aligned data after fits with the (5 parameter + muon loss) function (black) and with the full physics function (red).*

6.3 Acceptance Double CBO

The only uncertain part of the double CBO parametrisation is its envelope. In regular fits, the DCBO lifetime is tied to the CBO lifetime by setting $\tau_{\text{DCBO}} = \frac{1}{2}\tau_{\text{CBO}}$. To study systematic effects from the DCBO envelope we make τ_{DCBO} a fixed parameter, vary it manually and watch R (see Figures 57 and 58 for the 1999-style and the physics function respectively). Since χ^2 as a function of τ_{DCBO} is basically flat (no absolute increase by 1 within $[10, 100] \mu$ s) it cannot be used to define a 1σ interval. But we know that τ_{DCBO} must be about 50-60 μ s and can set conservative limits by assuming that our knowledge is less than a factor 2 off, i.e. $25 \mu\text{s} < \tau_{\text{DCBO}} < 100 \mu\text{s}$. R changes so little that the exact choice of these limits doesn't really matter.

For Set A we observe a change in R of 0.01 ppm (with both the 1999 and the Full Physics Function); for Set B the change is 0.004 ppm.

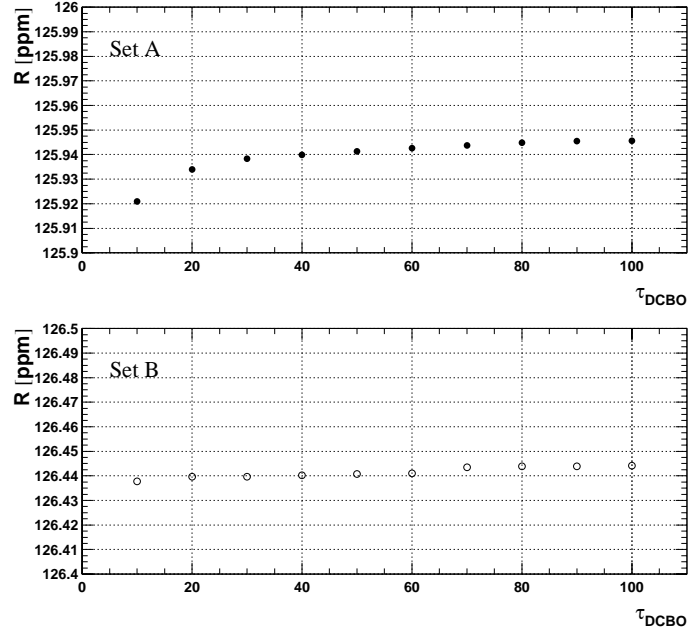


Figure 57: R versus lifetime of the double CBO for the 1999-style function.

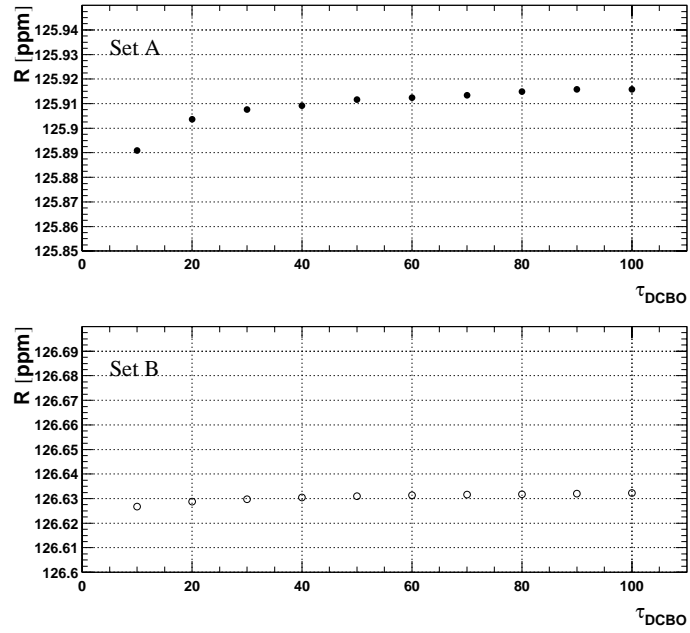


Figure 58: R versus lifetime of the double CBO for the full physics function.

6.4 Asymmetry and Phase CBO – Half-Ring Effect

6.4.1 1999-Style Function

Again, we proceed along the lines of [1] (Section 6.3), only changing the CBO frequencies and lifetimes according to Table 7, and taking the corresponding phase-pulling amplitudes from [16]: for a left side-band amplitude $A_- = 0.01$ the simulation finds 20 ppm (Set A) and 21 ppm (Set B), leading to rms systematic errors

$$\text{Set A: } \delta R = 20 \text{ ppm} \times e^{-31.8/100} / \sqrt{2} \times \frac{A_-}{0.01} = 15 \text{ ppm} \times \frac{A_-}{0.01} \quad (34)$$

$$\text{Set B: } \delta R = 21 \text{ ppm} \times e^{-31.8/140} / \sqrt{2} \times \frac{A_-}{0.01} = 17 \text{ ppm} \times \frac{A_-}{0.01} \quad (35)$$

For determining the left side-band amplitude A_- we repeat the equations derived in the previous analysis:

$$A_-^2 = A_{-, \text{Rob}}^2 + A_{-, \text{Jim}}^2 + 2 A_{-, \text{Rob}} A_{-, \text{Jim}} \cos(\phi_{\text{Jim}} - \phi_{\text{Rob}} - \frac{\pi}{2}) \quad (36)$$

with

$$A_{-, \text{Rob}} = \frac{1}{2} A A_{\text{Rob}} \quad (37)$$

and

$$A_{-, \text{Jim}} = \frac{1}{2} A A_{\text{Jim}} \phi_a \quad (38)$$

The phase difference $\phi_{\text{Jim}} - \phi_{\text{Rob}} - \frac{\pi}{2}$ is known from the fits to individual detectors. From Table 28 we get

$$\phi_{\text{Jim}} - \phi_{\text{Rob}} - \frac{\pi}{2} = 0.78 \pm 0.15 \quad (\text{Set A}) \quad (39)$$

$$\phi_{\text{Jim}} - \phi_{\text{Rob}} - \frac{\pi}{2} = 0.58 \pm 0.14 \quad (\text{Set B}) \quad (40)$$

and hence

$$\cos(\phi_{\text{Jim}} - \phi_{\text{Rob}} - \frac{\pi}{2}) = 0.71 \pm 0.11 \quad (\text{Set A}) \quad (41)$$

$$\cos(\phi_{\text{Jim}} - \phi_{\text{Rob}} - \frac{\pi}{2}) = 0.84 \pm 0.08 \quad (\text{Set B}). \quad (42)$$

Note that the 2001 value of this angle agrees quite well with the one from 2000, $\phi_{2000} = 0.70 \pm 0.10$ and $\cos \phi_{2000} = 0.76 \pm 0.06$.

If both asymmetry and phase modulation cancel by the same factor and mechanism, then this phase difference is preserved after cancellation in the sum of detectors. From Table 24 and the lower block of Table 28 follows:

- Fit to the sum:

$$\phi_{\text{Jim}} - \phi_{\text{Rob}} - \frac{\pi}{2} = 2.40 \pm 5.10 \quad (\text{Set A}) \quad (43)$$

$$\phi_{\text{Jim}} - \phi_{\text{Rob}} - \frac{\pi}{2} = -0.09 \pm 0.74 \quad (\text{Set B}); \quad (44)$$

- Vector sum of individual fit results:

$$\phi_{\text{Jim}} - \phi_{\text{Rob}} - \frac{\pi}{2} = 2.38 \pm 3.11 \quad (\text{Set A}) \quad (45)$$

$$\phi_{\text{Jim}} - \phi_{\text{Rob}} - \frac{\pi}{2} = -0.18 \pm 0.58 \quad (\text{Set B}). \quad (46)$$

Since in the detector sum asymmetry and phase modulation are small effects with large errors, we cannot make a clear conclusion about the conservation of phase differences in the cancellation process. Therefore, like in 2000, the sideband amplitudes will be evaluated for two different cases:

- The cancellation mechanisms and factors of asymmetry and phase modulation are equal and their phase relation is preserved.
- The cancellation factors are different and the phase relation after cancellation is arbitrary, i.e. the expectation value of $\cos(\phi_{\text{Jim}} - \phi_{\text{Rob}} - \frac{\pi}{2})$ is 0.

Comparing the amplitudes A_{Rob} and A_{Jim} for the detector sum (Table 24)

$$\text{Set A: } A_{\text{Rob}} = (0.23 \pm 0.25) \times 10^{-3}, \quad A_{\text{Jim}} = (0.02 \pm 0.09) \times 10^{-3} \quad (47)$$

$$\text{Set B: } A_{\text{Rob}} = (0.71 \pm 0.25) \times 10^{-3}, \quad A_{\text{Jim}} = (0.13 \pm 0.09) \times 10^{-3} \quad (48)$$

with the corresponding average amplitudes for the individual detectors (Table 28, upper block), one finds the following cancellation factors:

	Asymmetry mod.	Phase mod.
Set A	$\frac{0.23 \pm 0.25}{2.84 \pm 0.28} = 0.08 \pm 0.09$	$\frac{0.02 \pm 0.09}{0.67 \pm 0.10} = 0.03 \pm 0.13$
Set B	$\frac{0.71 \pm 0.25}{4.10 \pm 0.28} = 0.17 \pm 0.06$	$\frac{0.13 \pm 0.09}{0.71 \pm 0.10} = 0.18 \pm 0.13$

(49)

The obvious problem here is that both effects are hardly significant in the sum of detectors, and the cancellation factors have huge uncertainties.

To calculate the side-band contributions $A_{-, \text{Rob}}$ and $A_{-, \text{Jim}}$ according to Eqns. (37) and (38), we use A_{Rob} and A_{Jim} from Eqns (47) and (48), and the values $A = 0.350067 \pm 0.000029$ and $\phi_a = 2.96129 \pm 0.00015$ (Set A) and $A = 0.349920 \pm 0.000035$ and $\phi_a = 2.96165 \pm 0.00019$ (Set B):

$$\text{Set A: } A_{-, \text{Rob}} = (0.04 \pm 0.04) \times 10^{-3}, \quad A_{-, \text{Jim}} = (0.01 \pm 0.05) \times 10^{-3} \quad (50)$$

$$\text{Set B: } A_{-, \text{Rob}} = (0.12 \pm 0.04) \times 10^{-3}, \quad A_{-, \text{Jim}} = (0.07 \pm 0.05) \times 10^{-3} \quad (51)$$

Combining directly these amplitudes to the total left side-band amplitude implies the assumption of different cancellation factors and hence an arbitrary phase relation for the two vectors after cancellation. With Eq. (36) and $\cos(\phi_{\text{Jim}} - \phi_{\text{Rob}} - \frac{\pi}{2}) = 0$ we obtain the combined left side-band amplitude

$$\text{Set A: } A_- = (0.041 \pm 0.041) \times 10^{-3} \quad (52)$$

$$\text{Set B: } A_- = (0.139 \pm 0.043) \times 10^{-3} \quad (53)$$

corresponding to a systematic error

$$\text{Set A: } \delta R = (0.06 \pm 0.06) \text{ ppm} \quad (54)$$

$$\text{Set B: } \delta R = (0.24 \pm 0.07) \text{ ppm} \quad (55)$$

Alternatively we can use the average modulation amplitudes from individual detector fits and assume equal cancellation mechanisms for asymmetry and phase modulation with an average cancellation factor of 0.06 ± 0.07 (Set A) or 0.17 ± 0.05 (Set B). In this model we need to use the phase difference (41), (42). This leads to a combined left side-band amplitude

$$\text{Set A: } A_- = (0.047 \pm 0.055) \times 10^{-3} \quad (56)$$

$$\text{Set B: } A_- = (0.178 \pm 0.054) \times 10^{-3} \quad (57)$$

or a systematic error

$$\text{Set A: } \delta R = (0.07 \pm 0.08) \text{ ppm} \quad (58)$$

$$\text{Set B: } \delta R = (0.30 \pm 0.09) \text{ ppm} \quad (59)$$

Both fit-based methods for determining A_- have the drawback of large statistical uncertainties because asymmetry and phase modulation amplitudes have a rather small signal-to-noise ratio.

6.4.2 Full Physics Function

Figure 59 shows the results for R from a manual sweep of τ_{Rob} . It turned out that χ^2 is too insensitive to the asymmetry modulation and cannot be used for determining a confidence interval for τ_{Rob} . Minima of χ^2 are found at unphysical values of τ_{Rob} , i.e. either near 0 or at infinity. This problem persists even with CBO-aligned data. However, we know that τ_{Rob} should have about the same magnitude as τ_{CBO} and can set conservative limits. Assuming $\tau_{\text{Rob}} > \tau_{\text{DCBO}} = 50 \mu\text{s}$ and $\tau_{\text{Rob}} < 200 \mu\text{s}$, we find:

$$\text{Set A: } \delta R_{\text{Rob}} = \frac{1}{2} \times 0.0258 \text{ ppm} = 0.0129 \text{ ppm} \quad (60)$$

$$\text{Set B: } \delta R_{\text{Rob}} = \frac{1}{2} \times 0.0122 \text{ ppm} = 0.0061 \text{ ppm} \quad (61)$$

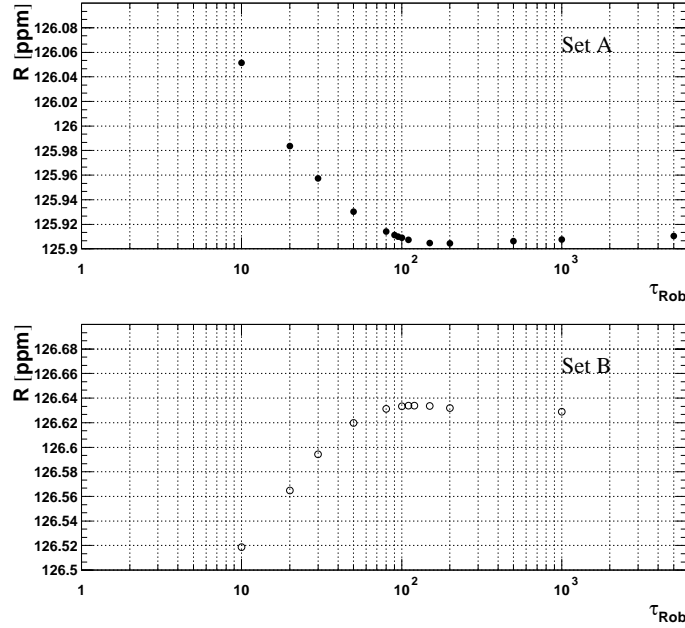


Figure 59: R versus the (exponential) lifetime of the asymmetry modulation.

Similarly, we perform a sweep of τ_{Jim} (Figure 60) and estimate again $\tau_{\text{Jim}} > \tau_{\text{DCBO}} = 50 \mu\text{s}$ and $\tau_{\text{Jim}} < 200 \mu\text{s}$. This yields a systematic uncertainty

$$\text{Set A: } \delta R_{\text{Jim}} = \frac{1}{2} \times 0.0037 \text{ ppm} = 0.0019 \text{ ppm} \quad (62)$$

$$\text{Set B: } \delta R_{\text{Jim}} = \frac{1}{2} \times 0.0437 \text{ ppm} = 0.0219 \text{ ppm} \quad (63)$$

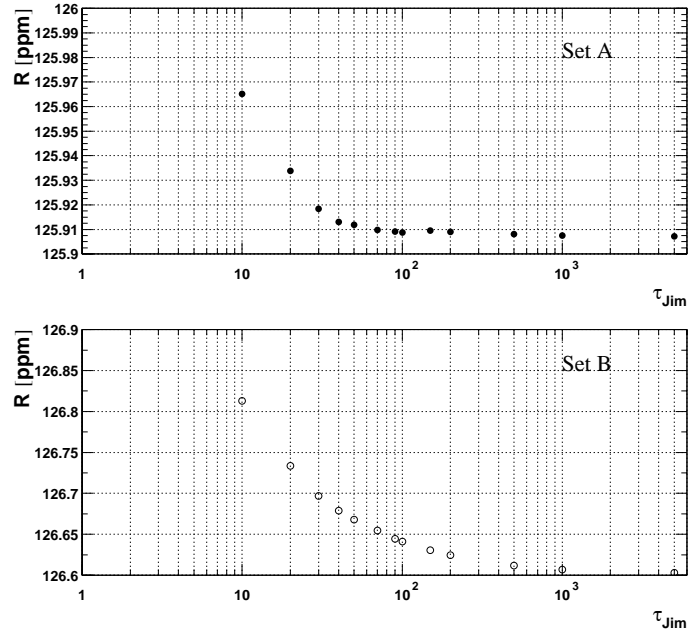


Figure 60: R versus the (exponential) lifetime of the phase modulation.

Using the angle (41, 42) between asymmetry and phase modulation, we get a total halfring-effect systematic uncertainty of:

$$\begin{aligned} \text{Set A: } \delta R_{\text{halfring}} &= \sqrt{0.0129^2 + 0.0019^2 + 2 \times 0.0129 \times 0.0019 \times 0.71} \text{ ppm} & (64) \\ &= 0.0143 \text{ ppm} & (65) \end{aligned}$$

$$\begin{aligned} \text{Set B: } \delta R_{\text{halfring}} &= \sqrt{0.0061^2 + 0.0219^2 + 2 \times 0.0061 \times 0.0219 \times 0.84} \text{ ppm} & (66) \\ &= 0.0272 \text{ ppm} & (67) \end{aligned}$$

6.5 Residual Pileup

There are two aspects to systematic errors due to imperfections in the statistical pileup construction and subtraction:

- Over- or undersubtraction of pileup, but with the correct phase
- Pileup construction with the wrong phase, e.g. by energy-dependent over- and underestimate of pileup. This is also called the “Underwater Effect”.

We will first estimate the fraction of residual pileup, then investigate its influence on R and finally give an upper limit on the Underwater Effect.

6.5.1 Residual Pileup Fraction from Early and Late Energy Spectra

We proceed along the lines of the 2000 analysis [1] (Section 6.5.1).

The pileup $\tilde{P}(t)$ at the early time t can be determined from early and late energy spectra $N(t)$ and $N(t + \Delta t)$ via¹

$$\tilde{P}(t) = \frac{N(t) - e^{\Delta t/\tau} N(t + \Delta t)}{1 - e^{-\Delta t/\tau}} \quad (68)$$

The inefficiency in the pileup subtraction then follows as

$$1 - \eta(t) = 1 - \frac{P(t)}{\tilde{P}(t)} = \frac{[N(t) - P(t)] - e^{\Delta t/\tau} [N(t + \Delta t) - P(t + \Delta t)]}{N(t) - e^{\Delta t/\tau} N(t + \Delta t)} \quad (69)$$

where $P(t)$ is the reconstructed pileup spectrum. For the early spectrum the time slice [31.8; 40.6] μ s was used. The time interval for the late energy spectrum was varied for the purpose of an additional consistency check. For the choice of this interval the bin boundaries 49.2, 66.7, 75.6, 97.3, 123.5, 149.6, 202.0, 315.6, 450.0 and 600.0 μ s were available.

The upper plots in Figure 61 show an early and a late energy spectrum for N and P for the sum of all detectors and the two run sets. Since the pileup spectrum has a zero crossing around 2.6 GeV, the modulus is drawn to avoid conflicts with the logarithmic scale. The middle and lower left-hand graphs compare the constructed pileup spectrum $|D - S1 - S2|$ with the one determined according to Eq. (68). The difference is the residual pileup which is also shown. The middle and lower right-hand plots show the residual pileup fraction. The lower part of the figure zooms into the sub-range from 3 to 6 GeV where this method is usable. Below about 3.2 GeV the pileup spectrum tends towards the 2.6 GeV zero crossing where the uncertainties are big. Above about 5.5 GeV the statistics become poor.

We conclude that the residual pileup fraction ranges within $\pm 10\%$.

¹This concept goes back to earlier analyses, see e.g. [11].

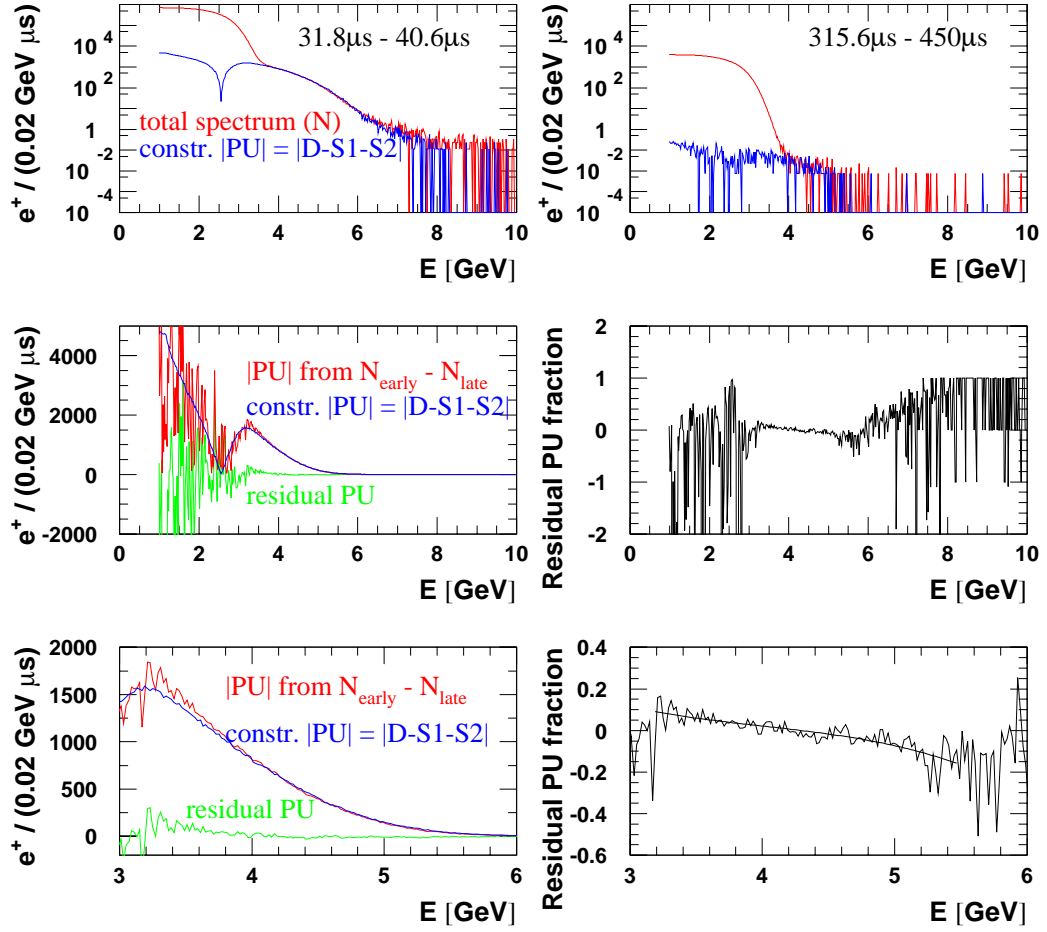
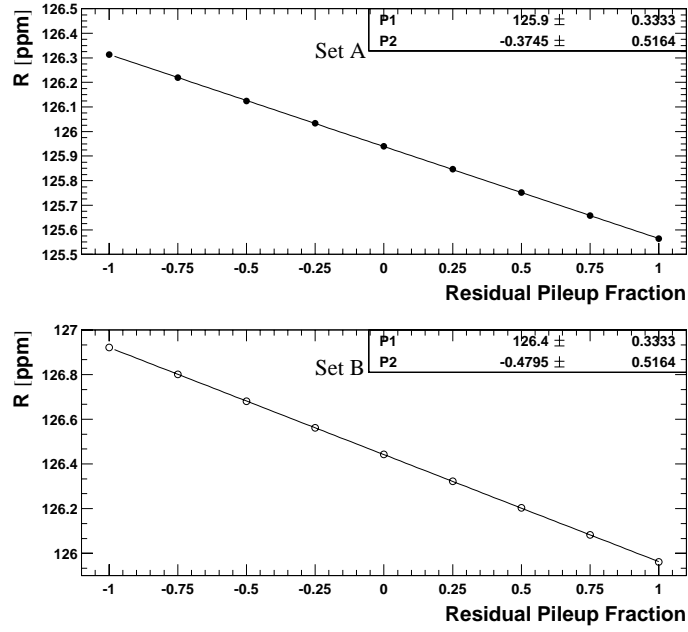
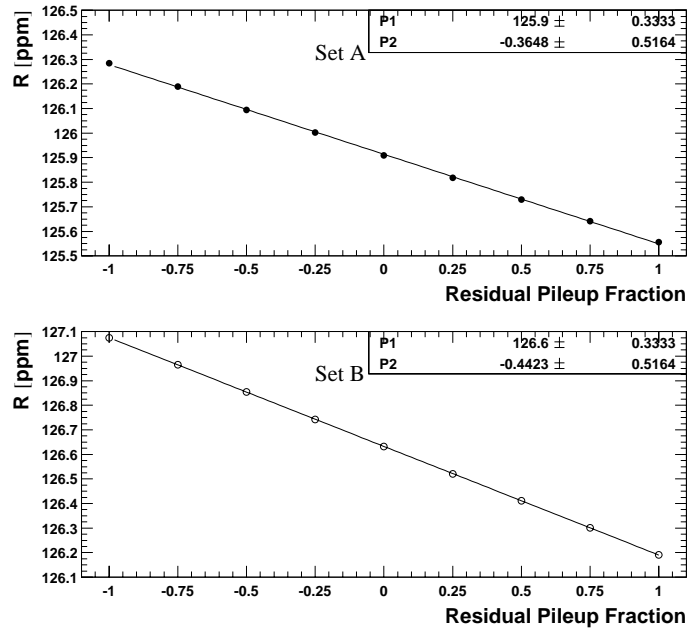


Figure 61: Determination of the residual pileup fraction using the evolution of the energy spectrum from the time bin $[31.8 \mu\text{s}; 40.6 \mu\text{s}]$ to $[315.6 \mu\text{s}; 450.0 \mu\text{s}]$.

6.5.2 Influence of Residual Pileup on R Figure 62: R versus residual pileup fraction $\rho = 1 - \lambda$ for the 1999-style function.Figure 63: R versus residual pileup fraction $\rho = 1 - \lambda$ for the full physics function.

6.5.3 Shift in R due to the Pileup Phase (Underwater Effect)

To estimate the effect of a possible phase deviation in the constructed pileup we use Yannis' approach [12]. Conservatively assuming that the pileup contributions below and above the zero-crossing around 2.6 GeV may be misreconstructed by up to 10 %, he obtains a deviation in R of the order of 20 % of the shift suffered if no pileup subtraction is applied at all. The latter shift can be read off the parameter boxes (P2) in Figures 63 and 62. We give the resulting estimates for the systematic uncertainty due to the Underwater effect in Table 35.

Set	1999 Function	Full Physics Function
A	$0.37 \times 0.2 = 0.07$	$0.37 \times 0.2 = 0.07$
B	$0.48 \times 0.2 = 0.10$	$0.44 \times 0.2 = 0.09$

Table 35: *Systematic uncertainty on R due to a phase error in the reconstructed pileup.*

6.5.4 Unseen Pileup

Pileup involving pulses below 250 MeV is not directly observable and cannot be statistically constructed because the small constituent pulses are not seen [2]. On average, neither the energy nor the time of high energy pulses are changed by the unseen pulses (cancellation). However, there are systematic phase and asymmetry shifts.

Old Approach via Asymmetry Instability

Like for the 2000 data an estimate of an upper limit on the systematic error from unseen pileup was made along the lines of [14] for the sum of all detectors and all runs. The calculations are based on Figures 17, 33 and the numerical values given in Table 37.

With the 1999 function, the asymmetry shows a peak-to-peak variation $\delta A = 0.00019$ for Set A and $\delta A = 0.00023$ for Set B. We take the full value as systematic error on A which is very conservative.

As shown in [14], the sensitivity of ϕ to unseen pileup is at most 0.19 times the sensitivity of A . This gives a maximum systematic error contribution of

$$\delta\phi \leq 0.19 \times \delta A = \begin{cases} 3.6 \times 10^{-5} & \text{(Set A)} \\ 4.4 \times 10^{-5} & \text{(Set B)} \end{cases}$$

for the phase, which is 0.24 (0.23) times the statistical error $\sigma(\phi) = 1.5 \times 10^{-4}$ (1.9×10^{-4}). Since R is strongly correlated with the phase, the contribution of this effect to the systematic error on R is again about 0.24 (0.23) times the statistical error:

$$\frac{\delta R}{R} \approx \frac{\sigma(R)}{R} \frac{\delta\phi}{\sigma(\phi)} = \begin{cases} 0.91 \text{ ppm} \times 0.24 = 0.22 \text{ ppm} & \text{(Set A)} \\ 1.11 \text{ ppm} \times 0.23 = 0.26 \text{ ppm} & \text{(Set B)} \end{cases} \quad (70)$$

For the Full Physics Function, the same procedure yields $\delta A = 0.00019$ (0.00022), and hence $\delta\phi \leq 0.19 \times \delta A = 3.6 \times 10^{-5}$ (4.2×10^{-5}). With the statistical error $\sigma(\phi) = 1.5 \times 10^{-4}$ (1.9×10^{-4}) we obtain

$$\frac{\delta R}{R} \approx \frac{\sigma(R)}{R} \frac{\delta\phi}{\sigma(\phi)} = \begin{cases} 0.92 \text{ ppm} \times 0.24 = 0.22 \text{ ppm} & \text{(Set A)} \\ 1.12 \text{ ppm} \times 0.22 = 0.25 \text{ ppm} & \text{(Set B)} \end{cases} \quad (71)$$

The uncertainties resulting from this approach seem vastly overestimated. Furthermore, the decrease of A with start time is the wrong signature; unseen pileup should increase A . Fortunately Vanya found a method which provides sharper limits for the effects from unseen pileup.

New Approach via Pedestal Spread

Vanya recently calculated the systematic error from unseen pileup by using the amplitude spread of the first samples in WFD islands relative to the average pedestal level [15]. His result amounts to 0.01 ppm. This will be used in the systematic error table.

6.6 Gain Changes and Residual Slow Effects

6.6.1 Gain Correction with Upper Energy Cut

The procedure used for applying a gain correction was the same as in the 2000 analysis [1] (Section 6.6), with the only difference that this time an upper energy cut at 3.4 GeV was applied because we had come to the conclusion that pileup above the energy endpoint has a strong falsifying influence on the average energy and that it is relatively poorly subtracted.

First, the relation

$$\frac{\Delta E}{E} = a \frac{\Delta G}{G} = a \Delta g \quad (72)$$

between gain variations and average energy changes needs to be calibrated [17]. Again, this is done applying two constant energy scale factors $1 + \Delta g_1 = 0.995$ and $1 + \Delta g_2 = 1.005$. to all pulse energies and then determining the modified average energies $E_1(t)$ and $E_2(t)$. Then we can calculate the sensitivity factor a as

$$a(t) = \frac{E_2(t) - E_1(t)}{E_0(t) (\Delta g_2 - \Delta g_1)} \quad (73)$$

Detector	a	Detector	a
1	0.5114 ± 0.0003	13	0.4940 ± 0.0003
2	0.5054 ± 0.0003	14	0.4856 ± 0.0003
3	0.4977 ± 0.0003	15	0.5085 ± 0.0003
4	0.4996 ± 0.0003	16	0.4725 ± 0.0003
5	0.4976 ± 0.0003	17	0.4984 ± 0.0003
6	0.4801 ± 0.0003	18	0.4823 ± 0.0003
7	0.4443 ± 0.0003	19	0.4905 ± 0.0003
8	0.4124 ± 0.0003	(20)	(0.1022 ± 0.0005)
9	0.4615 ± 0.0003	21	0.4868 ± 0.0003
10	0.4954 ± 0.0003	22	0.4765 ± 0.0003
11	0.4967 ± 0.0003	23	0.4809 ± 0.0003
12	0.4656 ± 0.0003	24	0.4745 ± 0.0003

Table 36: *Sensitivity factors for the relation between relative gain change and average energy change for $1.8 \text{ GeV} < E < 3.4 \text{ GeV}$.*

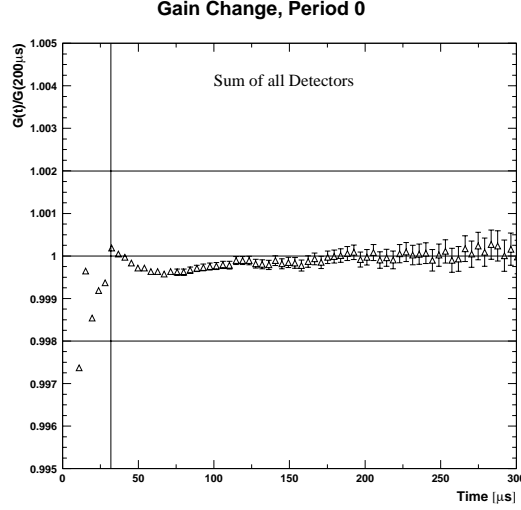
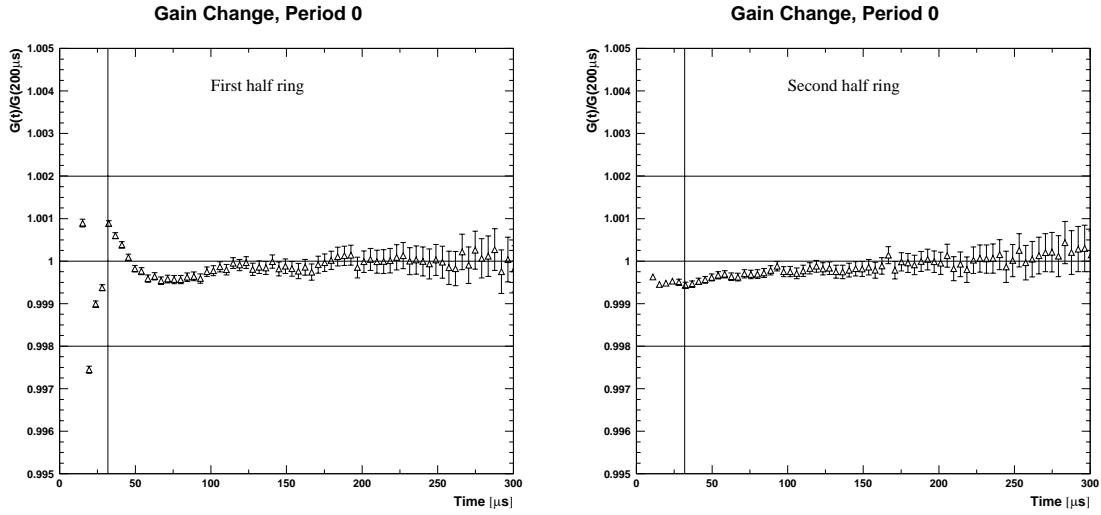
If the relation between gain change and average energy is linear, $a(t)$ should not depend on the time. In Appendix E.1, $a(t)$ is shown for all detectors. Fits to constants are superimposed. The resulting sensitivity factors are given in Table 36.

Figure 64 shows the gain $G(t)$ relative to the reference time $200 \mu\text{s}$, as obtained from the average energy and the sensitivity factor. The corresponding results for the two half rings are displayed in Figure 65.

Gain variation plots for the two run sets and the 24 detectors can be found in Appendix E.2.

Using an empirical parametrisation of $\Delta g(t)$ for each individual detector, a gain correction factor $1/(1 + \Delta g)$ was applied to the pulse energies before filling the time spectra.

The influence of the gain correction on χ^2 and asymmetry stability is summarised in Table 37. Apparently the gain correction with upper energy cut improves χ^2 and reduces the asymmetry sag, however, not perfectly.

Figure 64: *Gain versus time for all runs and all detectors together.*Figure 65: *Gain versus time for the two half rings (all runs together).*

The rows labeled “diff” show the sensitivity of R to the gain correction at $31.8\mu\text{s}$ (i.e. near a zero-crossing). This would be the systematic error if our uncertainty about the gain correction were 100 %.

To study the influence of high-energy pileup on the gain correction and the fit results we applied different upper cuts.

Table 38 shows that χ^2 is not very sensitive to the position of the upper cut. The asymmetry sag (Table 39) is not strongly influenced either, which suggests that pileup is not its dominant origin.

The impact of the upper cut on R is shown in Table 40.

The uncertainty of the R -difference between two cuts was calculated according to [18]:

$$\sigma^2(\Delta R) = \sigma^2(R_2) - \sigma^2(R_1) \left(2 \frac{A_1}{A_2} \cos(\Delta\phi) - 1 \right) \quad (74)$$

where R_1 has been obtained with the higher upper cut. We observe a general difference

Set			1999 Function	Full Physics Function
A	χ^2	raw	1.1057	1.1066
		corr.	1.0395	1.0404
	ΔA [10^{-4}]	raw	2.67	2.75
		corr.	1.90	1.88
	R [ppm]	raw	125.9253 ± 0.9134	125.9236 ± 0.9168
		corr.	125.9420 ± 0.9138	125.9085 ± 0.9172
		diff.	0.0167 ± 0.0270	0.0151 ± 0.0271
B	χ^2	raw	1.0710	1.0698
		corr.	1.0212	1.0195
	ΔA [10^{-4}]	raw	2.94	2.86
		corr.	2.17	2.08
	R [ppm]	raw	126.3820 ± 1.1094	126.5639 ± 1.1164
		corr.	126.4448 ± 1.1098	126.6301 ± 1.1169
		diff.	0.0628 ± 0.0298	0.0662 ± 0.0334

Table 37: Comparison of χ^2 and R at a start time of $31.8\mu s$, and the peak-to-peak variation of the asymmetry for data without and with gain correction (upper cut = 3.4 GeV).

Set	Upper Cut [GeV]	1999 Function	Full Physics Function
A	3.2	1.0404	1.0413
	3.4	1.0395	1.0404
	6.2	1.0402	1.0411
B	3.2	1.0262	1.0247
	3.4	1.0212	1.0195
	6.2	1.0227	1.0208

Table 38: χ^2 at a start time of $31.8\mu s$ for gain-corrected data with different upper energy cuts.

Set	Upper Cut [GeV]	1999 Function	Full Physics Function
A	3.2	2.00 ± 0.66	2.06 ± 0.66
	3.4	1.90 ± 0.66	1.88 ± 0.66
	6.2	2.12 ± 0.66	2.10 ± 0.66
B	3.2	2.11 ± 0.80	2.01 ± 0.81
	3.4	2.17 ± 0.80	2.08 ± 0.80
	6.2	2.38 ± 0.80	2.27 ± 0.80

Table 39: Difference ΔA [10^{-4}] between the start times $31.8\mu s$ and $150\mu s$ for gain-corrected data with different upper energy cuts.

between the sets A and B: B is much more sensitive to the upper cut than A. The reason is unclear.

However, there is also an interesting tendency: the significance of the R -difference between 6.2 GeV and 3.4 GeV is much higher than the one between 3.4 GeV and 3.2 GeV . The reason may be the dominance of residual pileup at energies above 3.4 GeV .

Set	Upper Cuts [GeV]	1999 Function	Full Physics Function
A	(3.4) - (3.2)	$-0.0080 \pm 0.0599 = 0.13 \sigma$	$-0.0003 \pm 0.0613 = 0.01 \sigma$
	(6.2) - (3.4)	$-0.0264 \pm 0.0246 = 1.07 \sigma$	$-0.0181 \pm 0.0204 = 0.89 \sigma$
B	(3.4) - (3.2)	$0.1905 \pm 0.0736 = 2.59 \sigma$	$0.1949 \pm 0.0734 = 2.66 \sigma$
	(6.2) - (3.4)	$-0.1499 \pm 0.0267 = 5.61 \sigma$	$-0.1489 \pm 0.0305 = 4.88 \sigma$

Table 40: *Differences in R [ppm] between two upper cuts for a start time of 31.8 μ s and gain-corrected data.*

6.6.2 Artificial Enhancement of Gain Variations

To improve the handle on the influence of gain changes on the ω_a fit results, artificially enhanced gain variations were introduced. This was done by creating time spectra based on manipulated pulse energies, i.e. modified effective energy thresholds. The energy of a pulse detected at a time t was multiplied by a factor

$$\kappa_g(t) \equiv \frac{1 + \xi \Delta g(t)}{1 + \Delta g(t)} \quad , \quad (75)$$

where the gain multiplier ξ was a fixed coefficient. The value $\xi = 1$ corresponds to untreated energies. For this study, the values $\xi = 5$, $\xi = 10$ and $\xi = -1$ were used. The first two choices magnify the gain changes which are present in the data by a factor 5 or 10; the third choice overcorrects the gain changes by one unit. The case $\xi = 0$ (i.e. corrected energy scale, ideally no gain changes left), was already discussed in the previous section.

Fit results for the five values of ξ and our two fit functions are shown in Figures 66 and 68. The upper plots show phase pulling whose amplitude is proportional to ξ . The fact that there is some phase pulling even for $\xi = 0$ (gain corrected data) is due to a combination of imperfections in the gain correction and residual slow effects like incorrectly parametrised muon loss.

In the zero-crossings of these phase-pulling oscillations the systematic error on R would be zero. However, the actual abscissa position $t_{\text{start},1} = 31.8541 \mu\text{s}$ of our fit start time bin (determined as explained in [1], Section 5.2) does not exactly coincide with the phase-pulling zero-crossings. Moreover, for the $\xi = 0$ curve it is not easy to determine the zero-crossing positions from the graphs. Therefore we use the curves for $\xi = 5$ and $\xi = 10$ which show very pronounced oscillations. We determine their first two extrema with parabolic fits and infer the first zero-crossings near $t_{\text{start},1}$:

ξ	Set A		Set B	
	1999 Func.	Full Phys. Func.	1999 Func.	Full Phys. Func.
5	31.8301 ± 0.0093	31.9496 ± 0.0126	31.8057 ± 0.0181	31.7390 ± 0.0166
10	31.8297 ± 0.0127	31.9666 ± 0.0077	31.8560 ± 0.0101	31.7787 ± 0.0090
avr.	31.8300 ± 0.0075	31.9620 ± 0.0065	31.8441 ± 0.0088	31.7697 ± 0.0079

Table 41: *First zero-crossing times of the gain related phase pulling.*

The same parabolic fits give us the phase-pulling amplitudes which we define as $\text{amplitude} = |\text{first maximum} - \text{first minimum}| / 2$.

Approximating the functional form of the phase-pulling by a sinusoidal curve, the systematic shift ΔR due to the deviation $t_{\text{zero-crossing}} - t_{\text{start},1}$ is given by

$$\Delta R = \text{amplitude} \times \omega_a \times (t_{\text{zero-crossing}} - t_{\text{start},1}) \quad (76)$$

Figures 67 and 69 show ΔR as a function of ξ . The results for the gain-corrected data ($\xi = 0$) are listed in Table 42. Note that these uncertainties include all other slow effects causing phase pulling, in particular muon losses.

Set	1999 Func.	Full Phys. Func.
A	0.010 ppm	0.049 ppm
B	0.004 ppm	0.028 ppm

Table 42: *Estimate of the systematic error from phase pulling due to residual gain variations and other slow effects. Cf. Table 43 for an alternative approach.*

Why not just use the difference between gain corrected and uncorrected results from Table 37? Firstly, because those numbers assume that the gain correction is 100 % uncertain, which is too pessimistic. Secondly we prefer the values in Table 42 because they also cover the other slow effects. In the next section another way of estimating the influence of the combination of slow effects will be given for comparison. As final systematic error we shall take the larger of the two estimates.

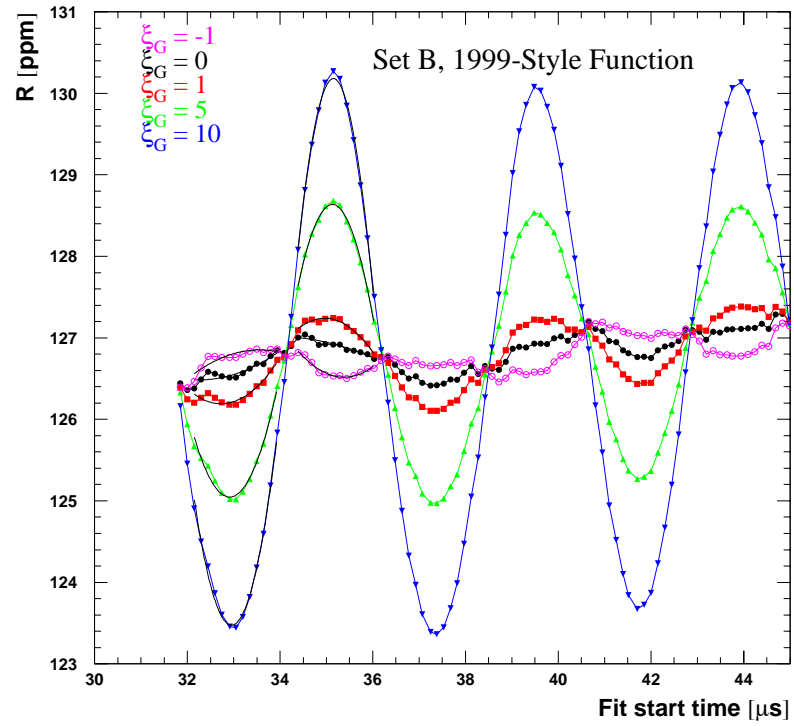
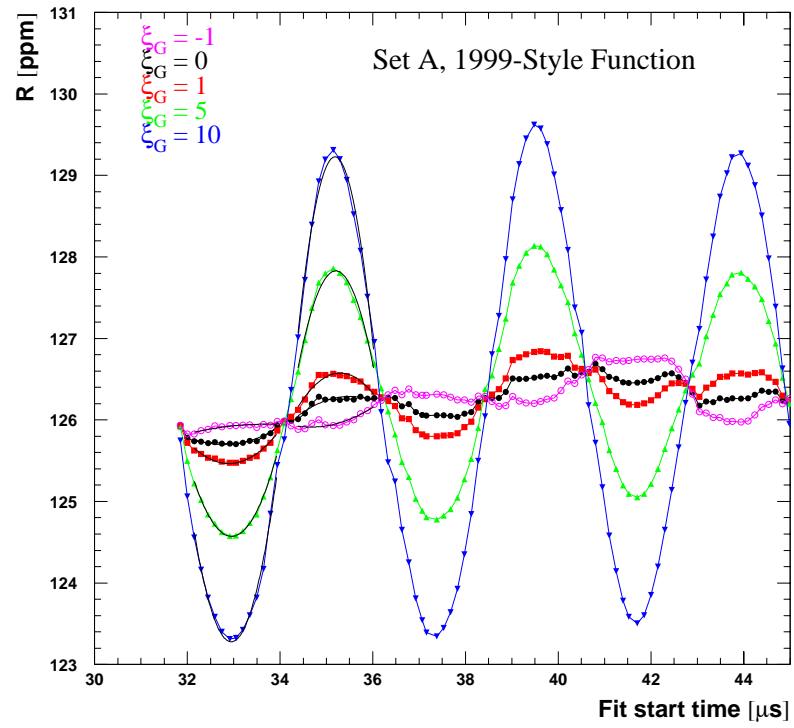


Figure 66: Study of gain correction and artificial gain change for the 1999-style function.

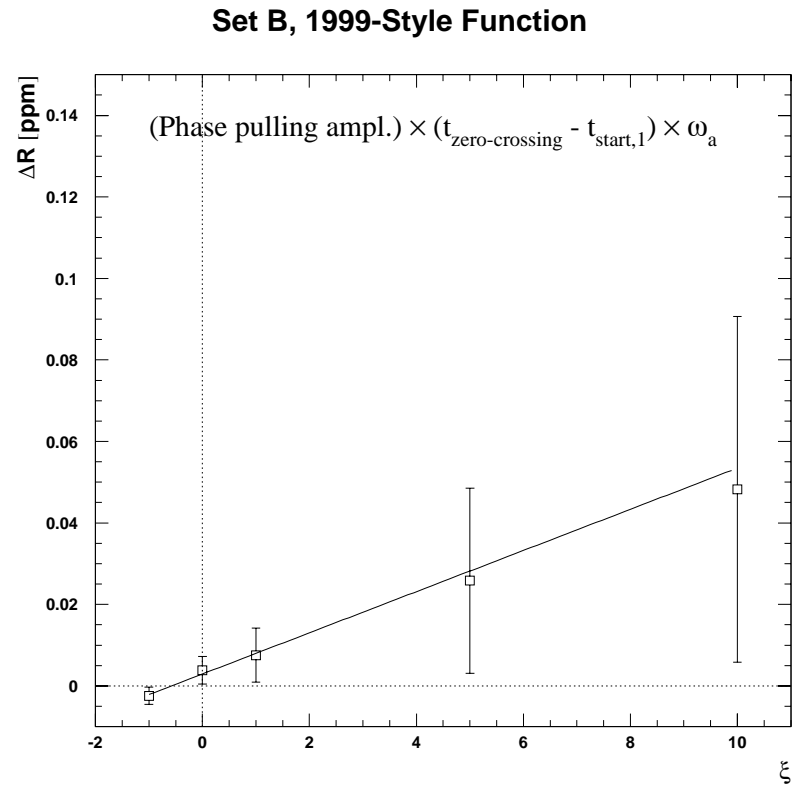
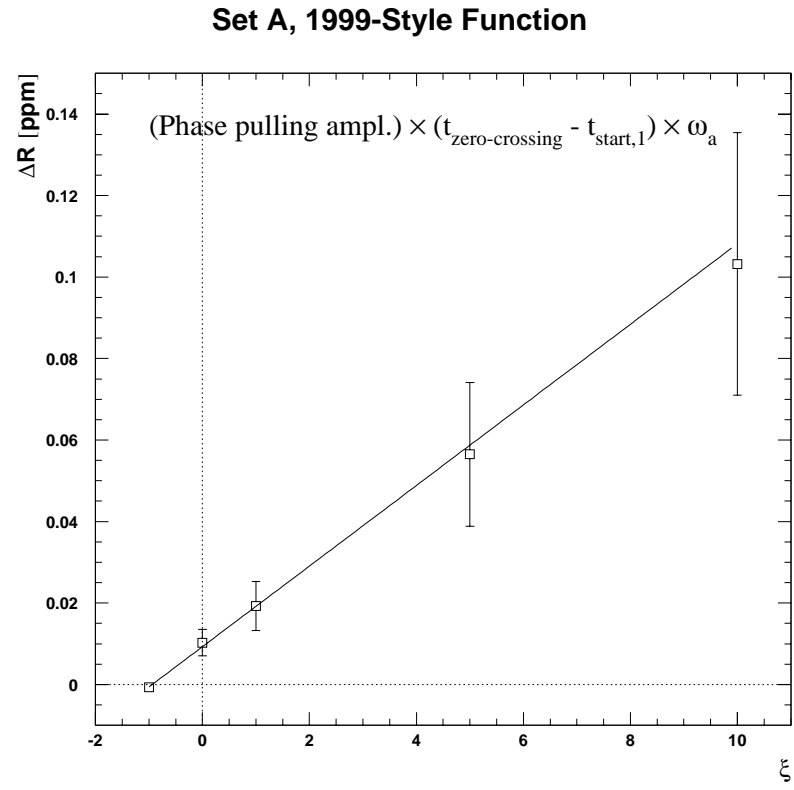


Figure 67: Systematic error from phase pulling induced by gain variations as a function of the gain multiplier. The zero-crossing of the phase pulling was determined from the curves with $\xi = 5$ and $\xi = 10$ in Figure 66.

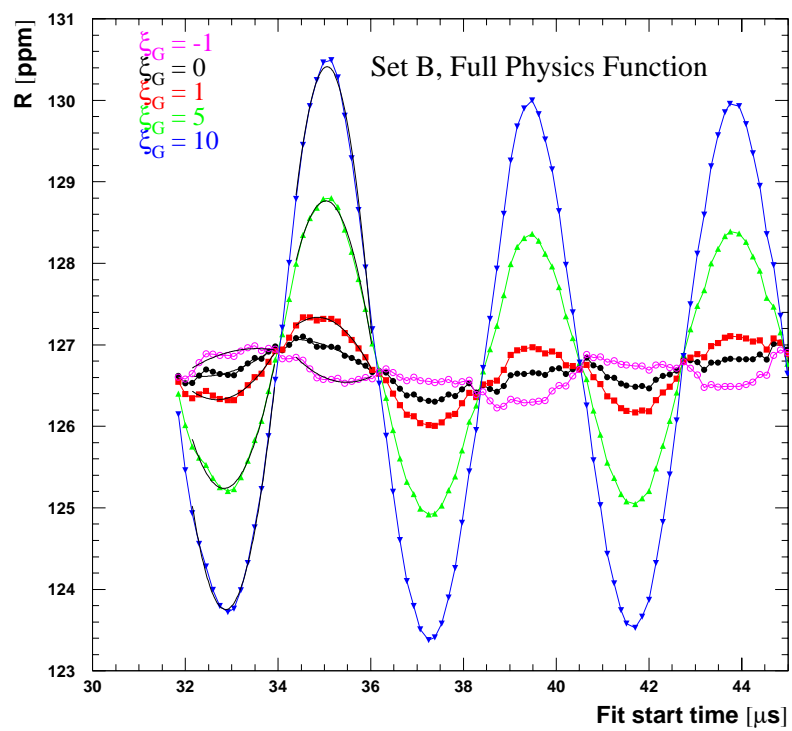
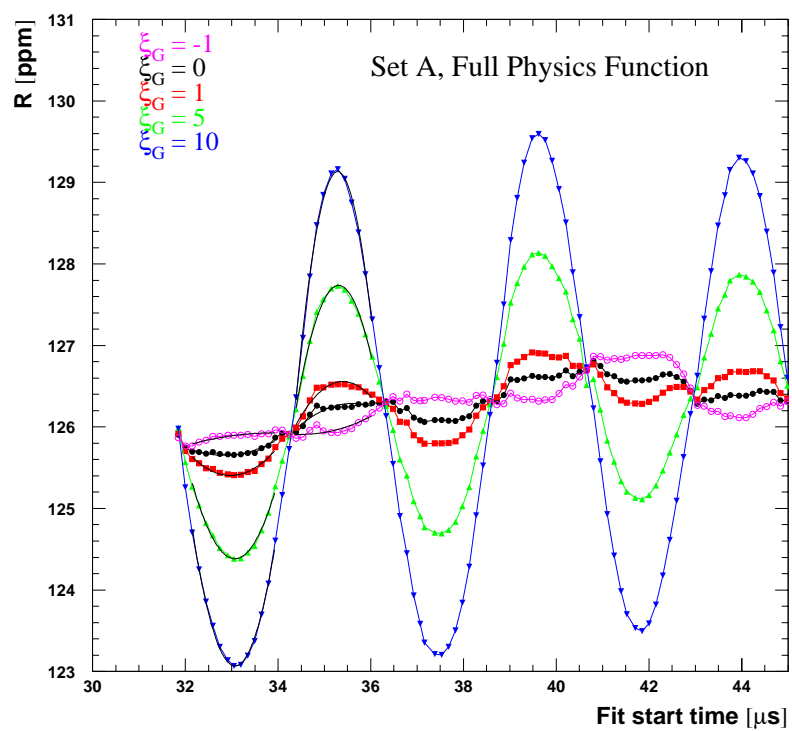


Figure 68: Study of gain correction and artificial gain change for the full physics function.

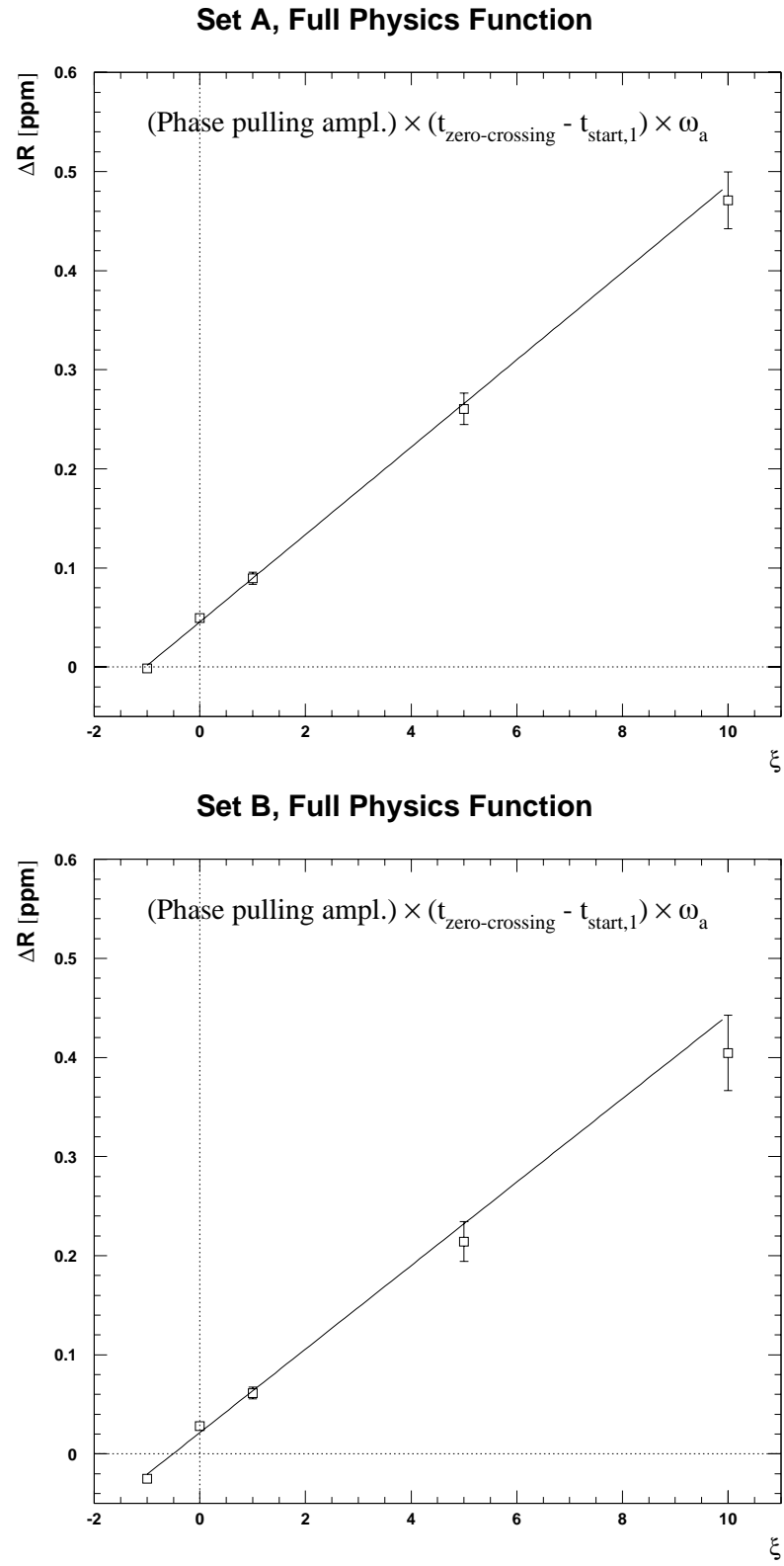


Figure 69: Systematic error from phase pulling induced by gain variations as a function of the gain multiplier. The zero-crossing of the phase pulling was determined from the curves with $\xi = 5$ and $\xi = 10$ in Figure 68.

6.6.3 Effects of an R.S.E. Term

An empirical term describing residual slow effects can be used to correct shortcomings in our knowledge about the non-wiggling component of the decay spectrum (see Eq. (15)).

Figures 70 and 71 demonstrate that the r.s.e. term effectively eliminates phase pulling for $\xi = 0$ and strongly reduces it for larger ξ . The difference between the results for R with and without r.s.e. term for gain-corrected data is shown in Table 43.

Set	1999 Function	full Physics Function
A	-0.0145 ± 0.0000	-0.0408 ± 0.0135
B	-0.0310 ± 0.0149	0.0174 ± 0.0150

Table 43: *Difference $\Delta R = R_{with\ r.s.e.} - R_{without\ r.s.e.}$ [ppm] at a start time of $31.8\mu\text{s}$ for gain-corrected data.*

Since these differences are also a measure for the systematic error from phase pulling, we conservatively use the larger of the values from Tables 42 and 43 as final systematic error.

The disadvantage of including an r.s.e. term is that it cures only the symptoms but not the origins of residual slow effects. Inaccuracies in pileup construction or gain correction may also affect the asymmetry, a consequence which remains after including an r.s.e. term. We therefore chose not to have an r.s.e. term, but to accept phase pulling in R and systematic variations of the fitted muon lifetime in start-time scans.

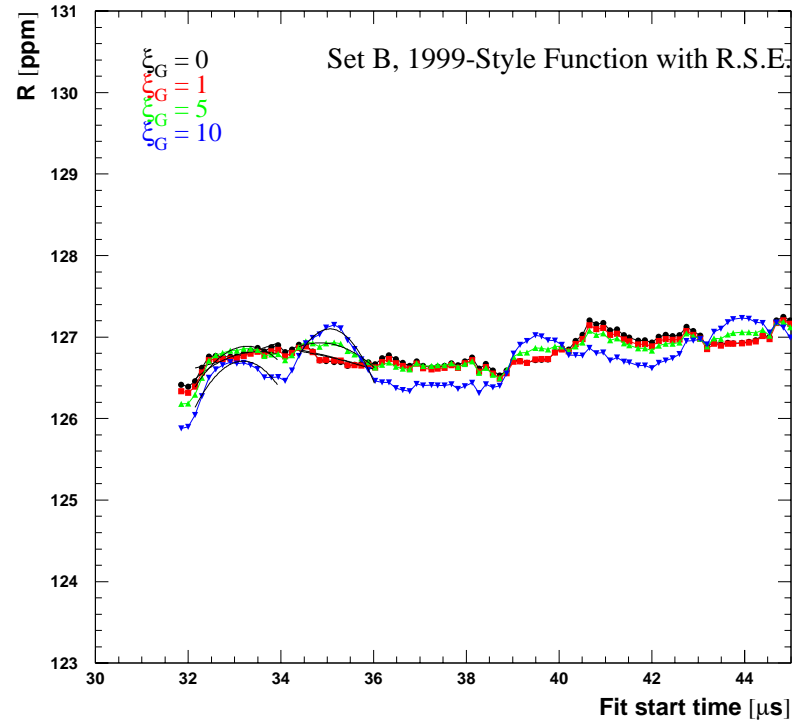
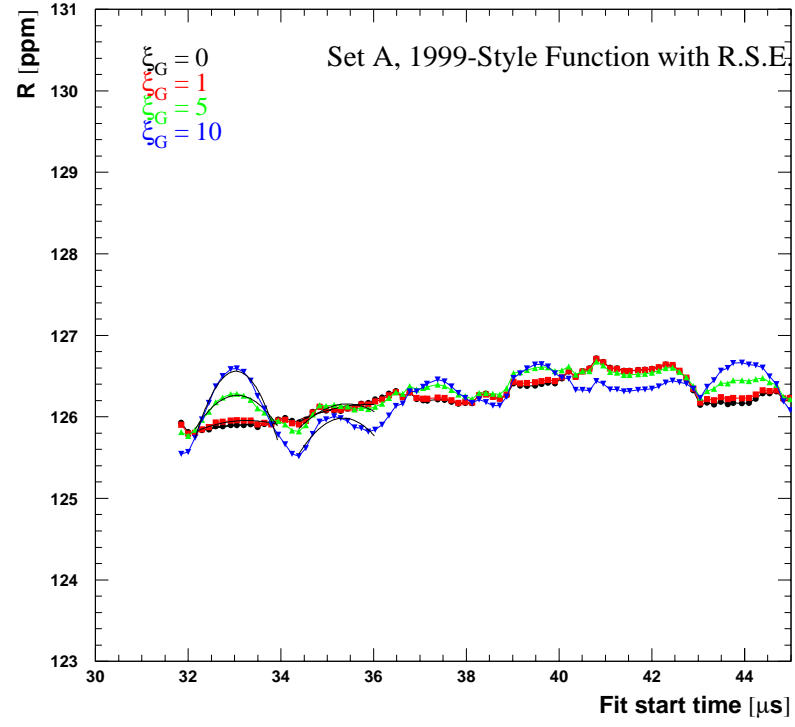


Figure 70: *Study of gain correction and artificial gain change for the 1999-style function with r.s.e. term.*

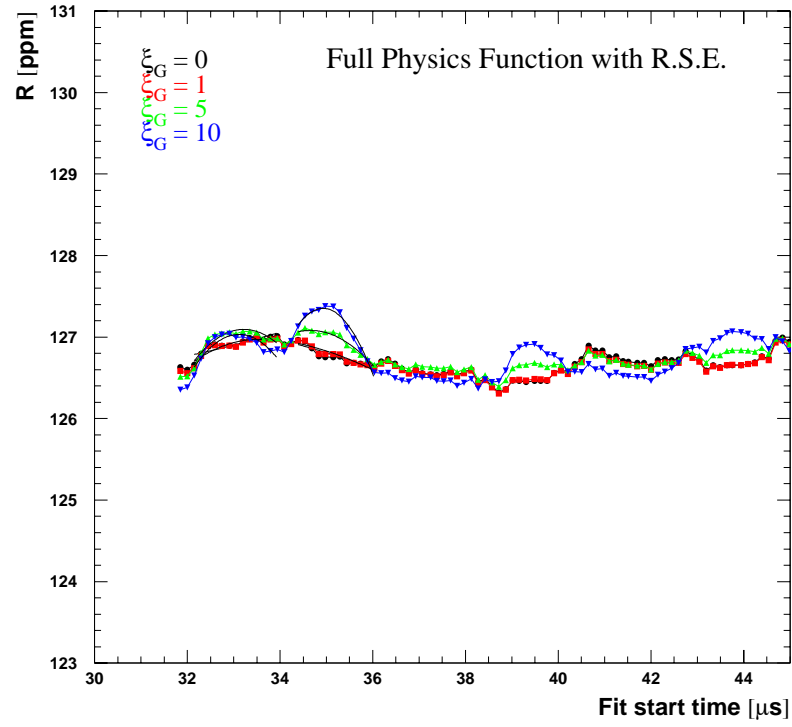
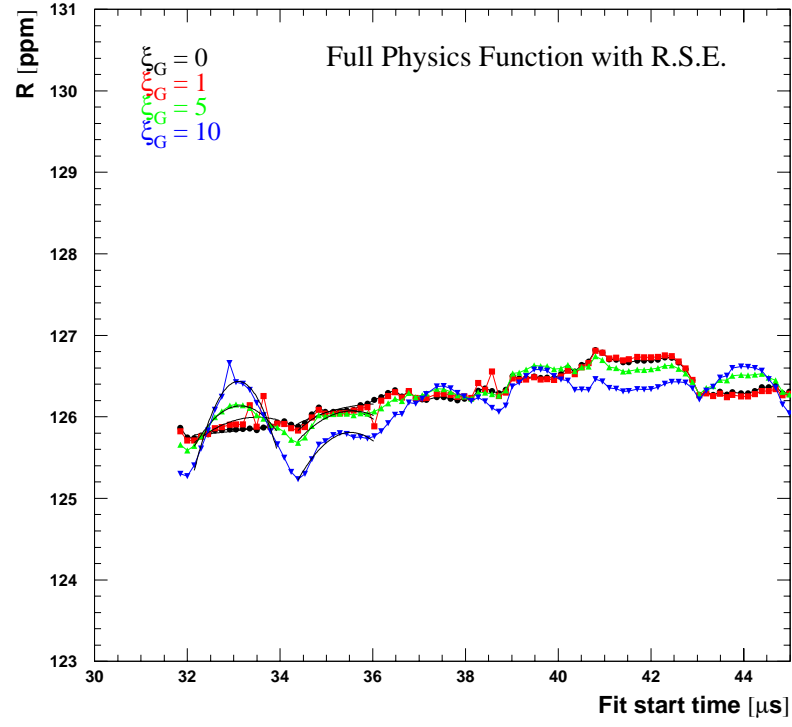


Figure 71: *Study of gain correction and artificial gain change for the full physics function with r.s.e. term.*

6.7 Investigation of the Asymmetry Instability by Energy-Binned Fits

Instabilities in start-time scans for the asymmetry can be caused by gain variations, residual pileup or unseen pileup involving pulses below 250 MeV. The last-mentioned effect cannot be dominant because it would cause a rise of the asymmetry with time rather than a droop as observed in the fit results.

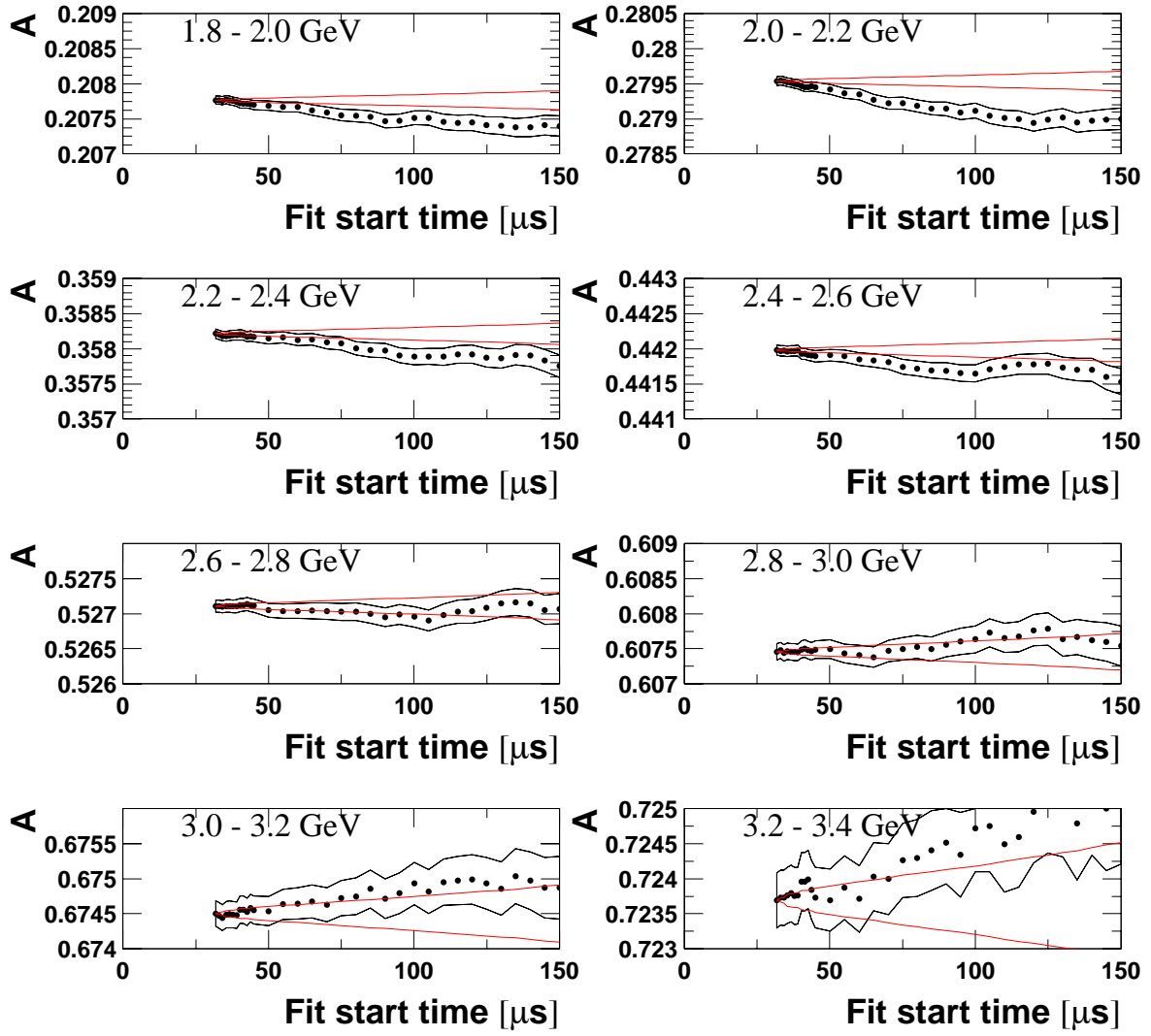
In order to shed some light on the origin of the asymmetry sag we look at its evolution as a function of energy. Figure 72 shows the series of asymmetry start-time scans for Set A; Set B looks similar. These scans reveal a trend: at low energies A tends to sag whereas at high energies it rises with start time. This is even better visible when a figure of merit for the sag – e.g. $A(100\ \mu\text{s}) - A(31.8\ \mu\text{s})$ is drawn as a function of E , see Figure 74.

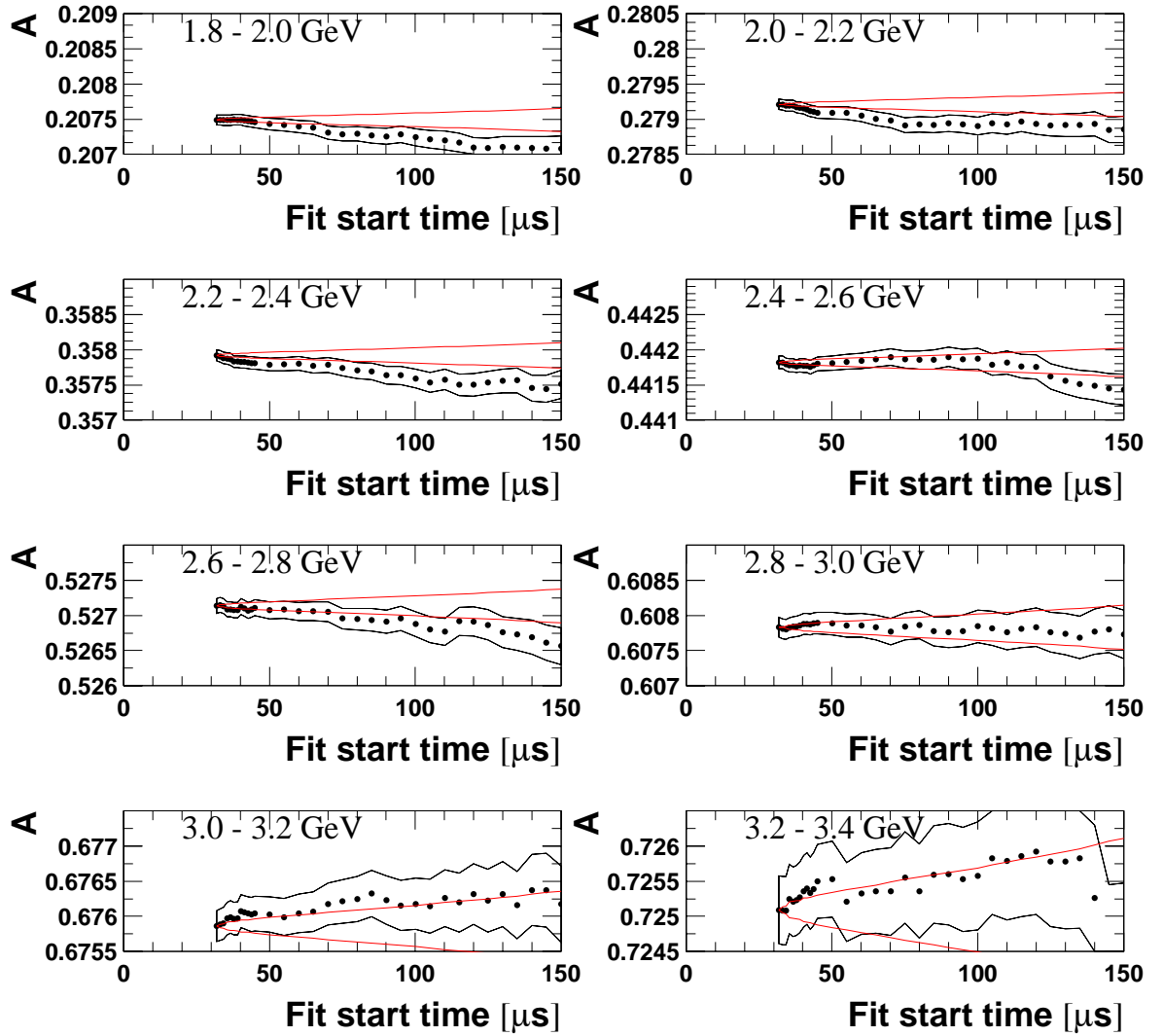
In Section 6.6.1 we have seen that the second half of the ring suffers less from gain variations than the first half. In particular, the second half ring has no detectors showing the whammo effect². The start-time scans for A in the second half ring are shown in Figure 76, and the sag versus energy is given in Figure 75. The asymmetry stability looks better than for all detectors, but one may be misled by the larger statistical errors. The overall trend of asymmetry sag versus energy is still visible. This study suggests that gain changes may cause a part of the asymmetry instability.

Let us now see whether pileup produces the observed structure. For this purpose, non-pileup-subtracted data are fitted. The result is given in Figure 78. Apparently pileup shifts the entire curve and bends it upwards at high energies, but does not reproduce the same shape. The observed behaviour cannot be explained by a globally wrong pileup multiplier but possibly by an energy-dependent pileup subtraction efficiency.

So far the results are not quite conclusive.

²The structures in the average energy versus time of detectors 3 to 7 (Figure 105) are called “whamos” (introduced by Bill).

Set AFigure 72: *Start-time scans for A in energy bins for Set A.*

Set BFigure 73: *Start-time scans for A in energy bins for Set B.*

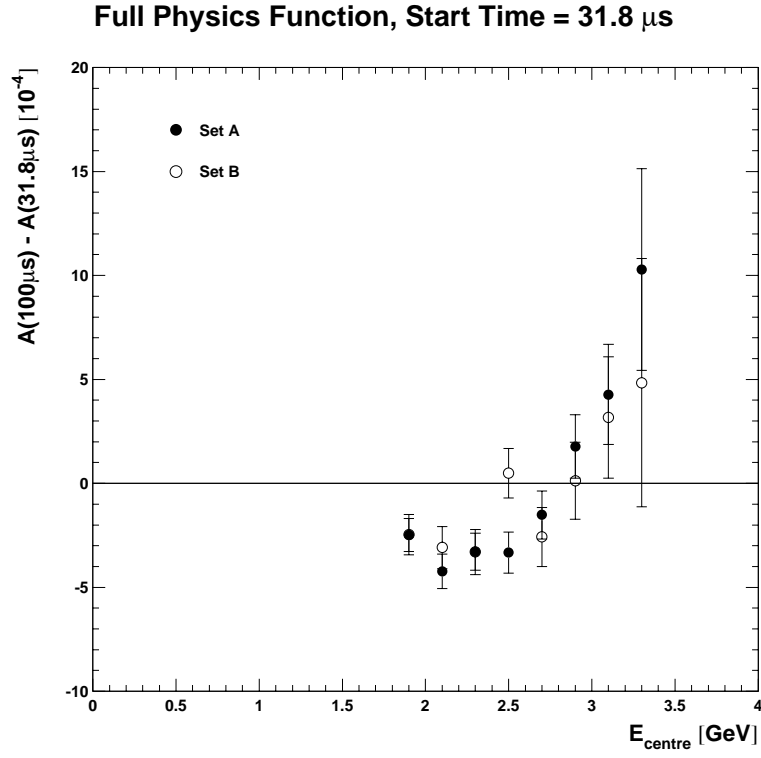


Figure 74: *Asymmetry sag versus centre of 200 MeV wide energy bins.*

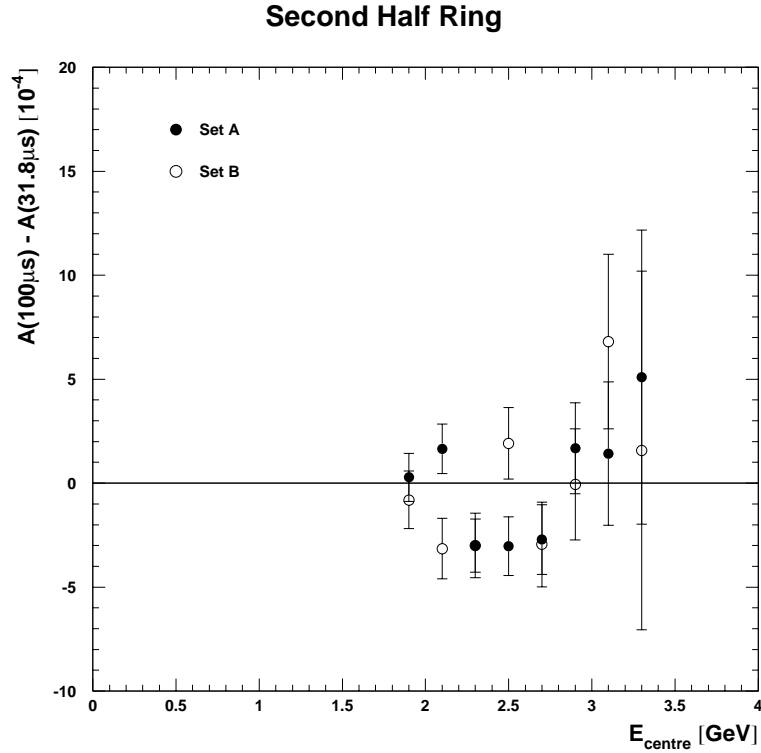


Figure 75: *Asymmetry sag versus centre of 200 MeV wide energy bins, only for detectors 13 to 24.*

Set A, Second Half Ring

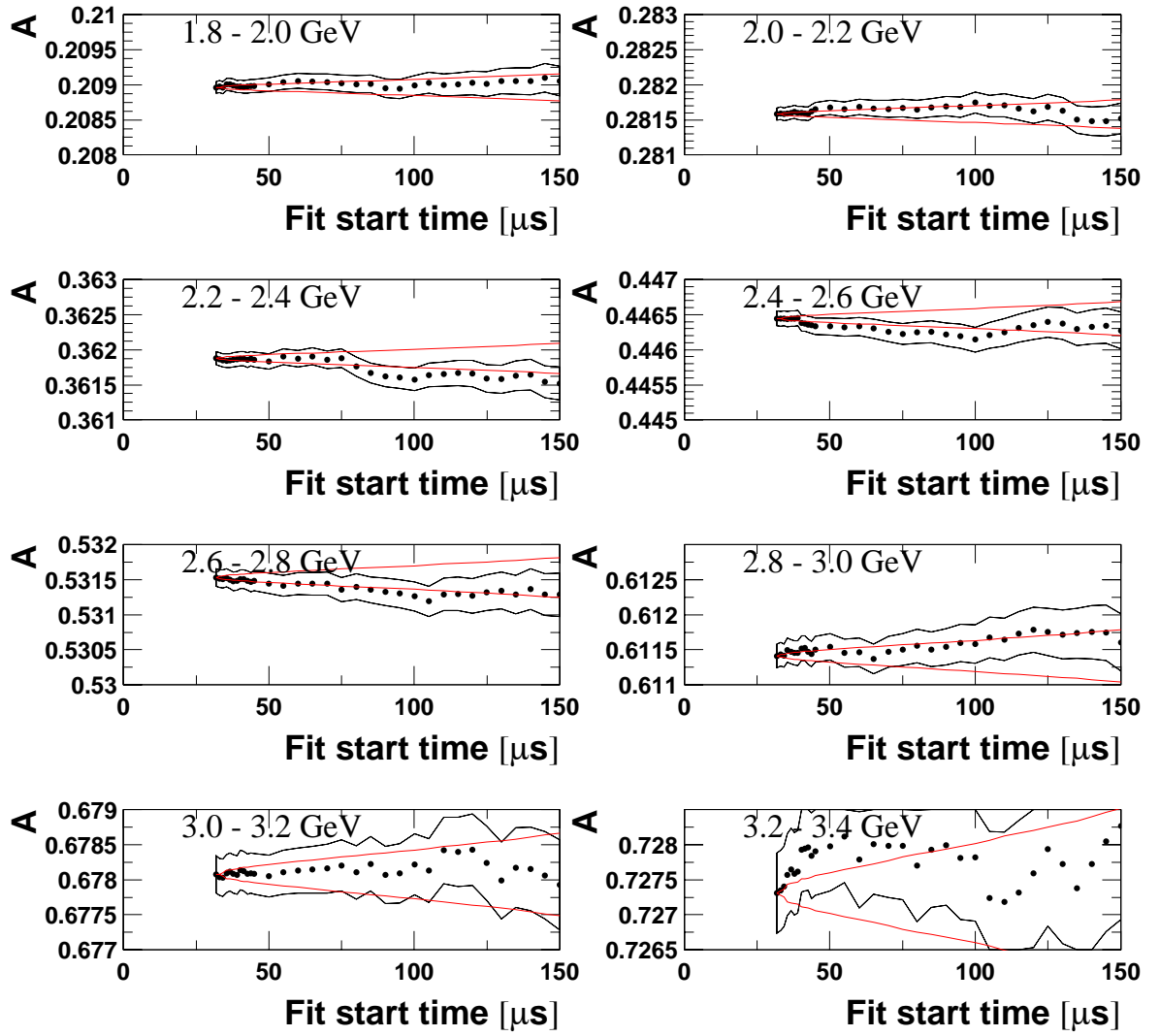


Figure 76: Start-time scans for A in energy bins, only for the second half of the ring (detectors 13 - 24); Set A.

Set B, Second Half Ring

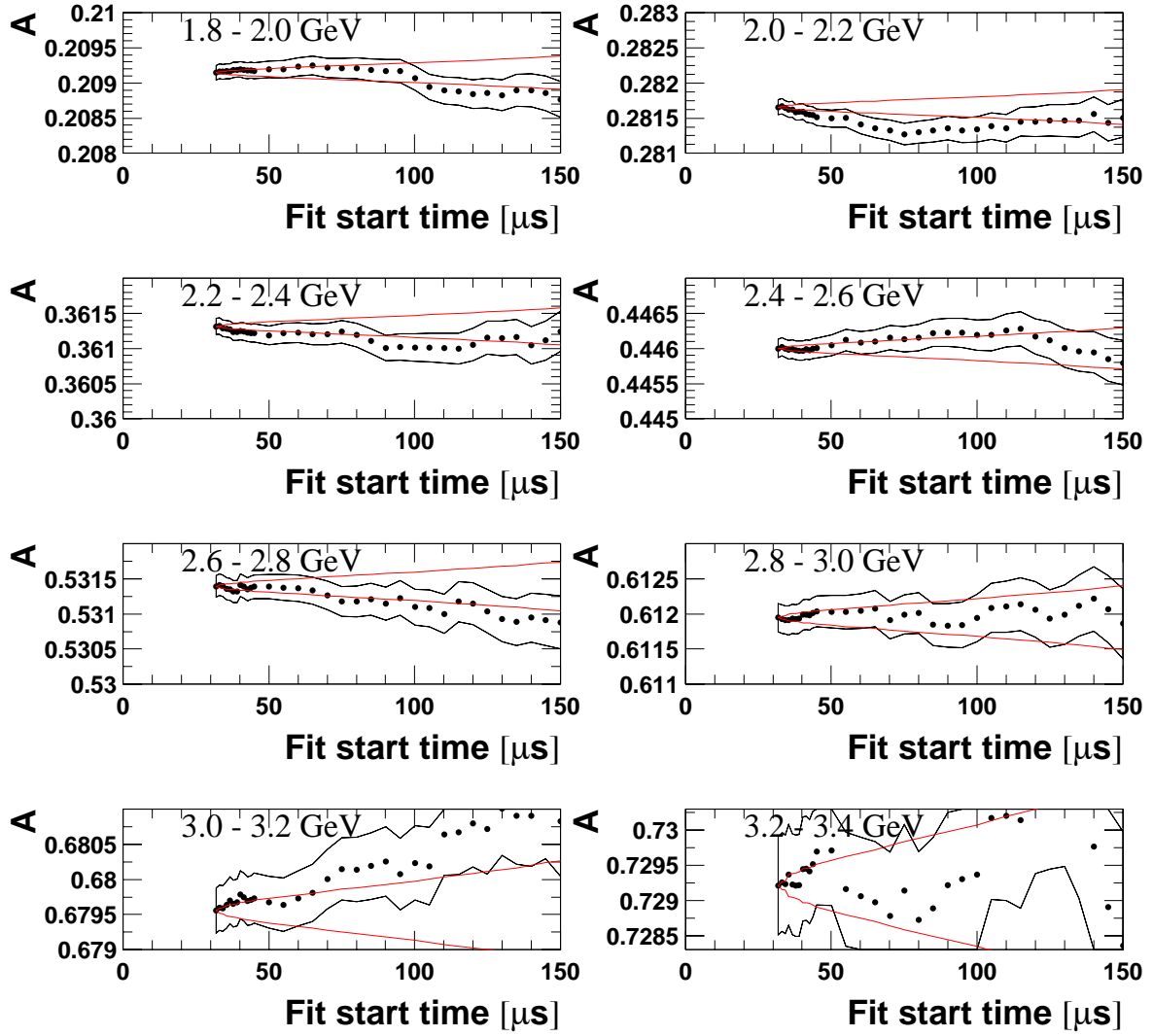


Figure 77: Start-time scans for A in energy bins, only for the second half of the ring (detectors 13 - 24); Set B.

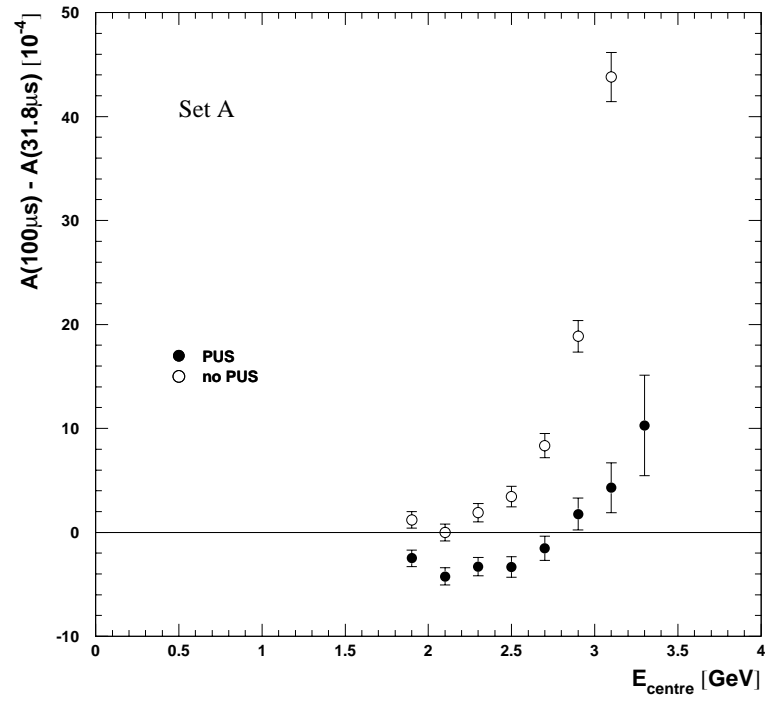


Figure 78: *Asymmetry sag versus centre of 200 MeV wide energy bins with and without pileup subtraction.*

6.8 Muon losses

Inaccuracies in the functional form of the muon losses reveal themselves in phase pulling, i.e. g-2 wiggles in R versus start time. Their systematic error is hence already covered by the evaluation given in Section 6.6 in the context of gain variations. The much more serious influence of muon losses on R comes from differences in the average spin direction between the populations of lost and stored muons. Bill estimated this effect and obtained 0.13 ppm.

It is also interesting to look by how much the two experimental analyses of the muon loss function [9, 10] differ and whether this has any significant impact on R . The two functions are compared in Figure 79.

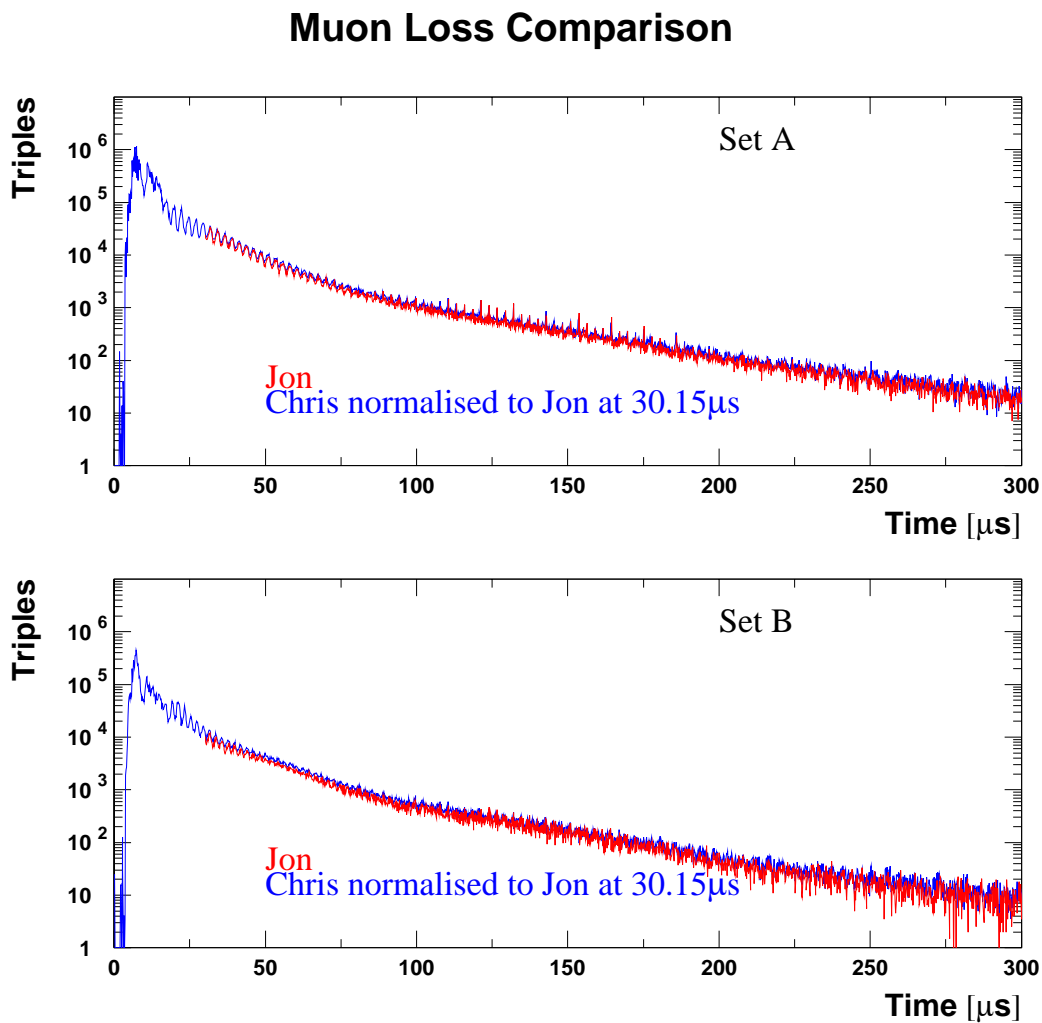


Figure 79: Comparison of Jon's and Chris' muon loss functions. You need a colour copy to distinguish the two curves.

Tables 44 and 45 demonstrate that both muon loss functions produce results for R which agree within 0.01 ppm.

Set	Loss Function	R [ppm]	χ^2
A	Chris	125.9420 ± 0.9138	1.0377
	Jon	125.9446 ± 0.9138	1.0375
B	Chris	126.4447 ± 1.1098	1.0214
	Jon	126.4451 ± 1.1098	1.0214

Table 44: *Comparison of R and χ^2 with Chris' and Jon's muon loss function implemented in the 1999 Function.*

Set	Loss Function	R [ppm]	χ^2
A	Chris	125.9085 ± 0.9173	1.0386
	Jon	125.9106 ± 0.9172	1.0384
B	Chris	126.6301 ± 1.1169	1.0196
	Jon	126.6303 ± 1.1169	1.0196

Table 45: *Comparison of R and χ^2 with Chris' and Jon's muon loss function implemented in the Full Physics Function.*

6.9 Binning Effects

The effect of the bin width was extensively studied in the 2000 analysis and found to be very small: $\delta R \leq (0.06 \pm 0.05)$ ppm. There is nothing new the smaller data set from 2001 can contribute.

6.10 Randomisation

The time spectra were randomised with 5 different random seeds but the same randomisation period given by the cyclotron period of 149.2 ns. Then for each seed the sum of detector spectra was fitted. The means and rms of R and χ^2 are listed in Tables 46 and 47.

Set	$\langle R \rangle$ [ppm]	$\text{rms}(R)$ [ppm]	$\langle \chi^2 \rangle$	$\text{rms}(\chi^2)$
A	125.9913 ± 0.9138	0.0464	1.0222	0.0082
B	126.4103 ± 1.1098	0.0682	1.0200	0.0123
avr.	126.1606 ± 0.7054			

Table 46: *The effects of randomisation on R and χ^2 for the 1999 Function.*

Set	$\langle R \rangle$ [ppm]	$\text{rms}(R)$ [ppm]	$\langle \chi^2 \rangle$	$\text{rms}(\chi^2)$
A	125.9645 ± 0.9173	0.0517	1.0232	0.0085
B	126.5892 ± 1.1168	0.0698	1.0180	0.0125
avr.	126.2162 ± 0.7088			

Table 47: *The effects of randomisation on R and χ^2 for the Full Physics Function.*

We also show start time scans for R with the results of all random seeds combined (Figures 80 and 81). For the purpose of comparison we superimpose the scan for the particular seed for which all studies were done up to this point of the report.

The systematic error on the average of the 5 results is given by $\text{rms}(R)/\sqrt{5-1}$.

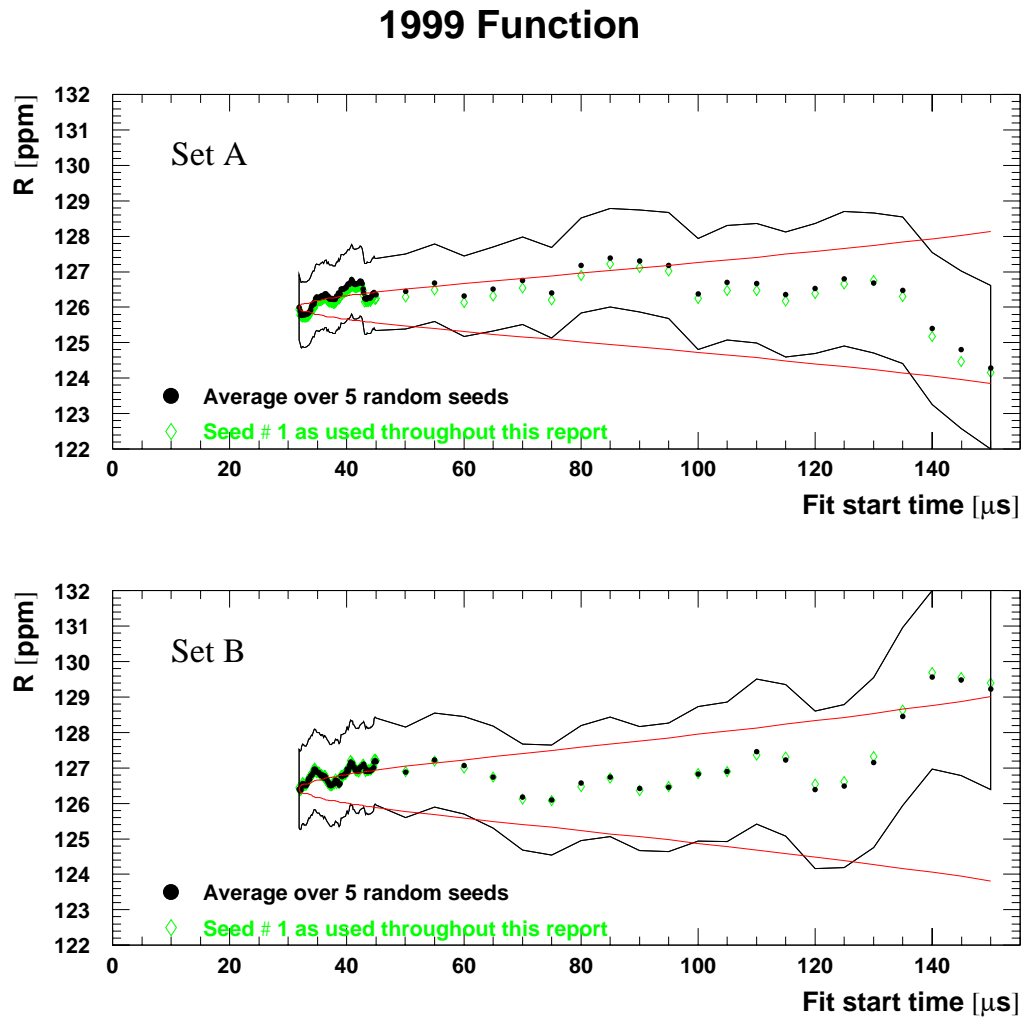


Figure 80: *Start time scans for R averaged over 5 random seeds (1999 function). For comparison we also plot the result for the particular seed used in the rest of this document.*

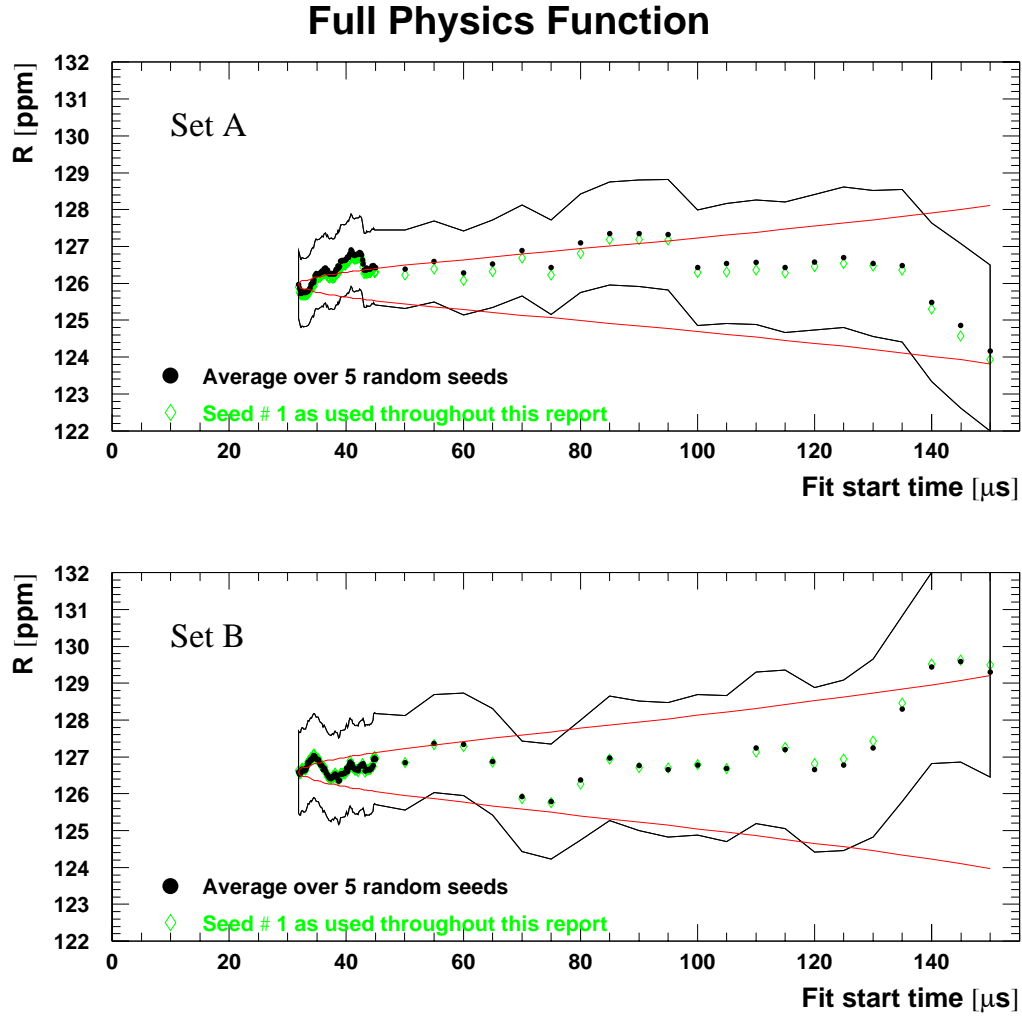


Figure 81: Start time scans for R averaged over 5 random seeds (full physics function). For comparison we also plot the result for the particular seed used in the rest of this document.

7 Summary

7.1 Systematic Error Table

The final systematic error balance is given in Table 48.

Effect	1999 Function		Full Physics Function	
	Set A	Set B	Set A	Set B
CBO frequency droop	0.01	0.01	0.01	0.01
Acceptance CBO residual	0.00	0.00	0.00	0.00
Acceptance DCBO envelope	0.01	0.00	0.01	0.00
Asymmetry and phase CBO (halfring effect)	0.07	0.30	0.01	0.03
Residual pileup (wrong ampl.)	0.04	0.05	0.04	0.04
(wrong phase)	0.07	0.10	0.07	0.09
Unseen pileup	0.01	0.01	0.01	0.01
Detector gain variations, muon loss function and other slow effects	0.01	0.03	0.05	0.03
Muon losses (spin direction)	0.13	0.13	0.13	0.13
Binning	0.06	0.06	0.06	0.06
Randomisation	0.02	0.03	0.03	0.03
AGS Background (*)	0.01	0.01	0.01	0.01
Combination (see text!)	0.18	0.36	0.19	0.19

(*) to be stolen from a yet unknown victim. The values given are from 2000.

Table 48: *Systematic uncertainties of R for a fit start time of $31.8\mu\text{s}$. All numbers are given in ppm.*

Should the errors in Table 48 be added linearly or in quadrature?

We only bother to look at the major entries of the tables, not at the romantics.

The main correlations are expected between residual pileup, unseen pileup and gain variations. We have seen that under- or oversubtracted pileup can easily be (mis-)compensated by the gain correction. We therefore add the uncertainties from gain and from a wrong pileup amplitude **linearly**. The number for the contribution from a wrong pileup phase is a generous upper limit and should not be added linearly.

We have seen that in 2001 the parameters related to the halfring effect are not strongly correlated with the asymmetry, unlike in 2000. The correlations between CBO effects and gain can therefore be expected to be small.

This year, all slow effects are treated together which avoids correlations between entries that would be difficult to separate. The uncertainty given for lost muons represents purely the possible difference in average spin direction between lost and stored muons. This aspect of muon losses is independent from the slow terms modifying the lifetime.

7.2 Combined Result from the two Run Sets

The central values and statistical errors of R for the two run sets are taken from Tables 46 and 47, i.e. averaged over 5 random seeds. We repeat them here:

- 1999-Style Function:

$$\text{Set A: } R = (125.9913 \pm 0.9138) \text{ ppm} \quad (77)$$

$$\text{Set B: } R = (126.4103 \pm 1.1098) \text{ ppm} \quad (78)$$

- Full Physics Function:

$$\text{Set A: } R = (125.9645 \pm 0.9173) \text{ ppm} \quad (79)$$

$$\text{Set B: } R = (126.5892 \pm 1.1168) \text{ ppm} \quad (80)$$

We now need to *add* the partial results *together*, taking into account statistical and systematic errors and their correlations.

7.2.1 Averaging Central Values and Systematic Errors with Statistical Weights

The simplest and most intuitive approach for combining the two subsets is to use the statistical weights $w_i \equiv \frac{1/\sigma_i^2}{1/\sigma_1^2 + 1/\sigma_2^2}$ for the central values and for the systematic errors:

- 1999-Style Function: $w_1 = 0.5980$, $w_2 = 0.4020$
- Full Physics Function: $w_1 = 0.5971$, $w_2 = 0.4029$

Thus we obtain:

- 1999-style function: $R = (126.1606 \pm \underbrace{0.7054 \pm 0.2524}_{0.7492 \text{ ppm}}) \text{ ppm}$

- Full physics function: $R = (126.2162 \pm \underbrace{0.7088 \pm 0.1900}_{0.7338 \text{ ppm}}) \text{ ppm}$

7.2.2 Optimal Weighting including Correlations of Systematic Errors

We define our correlation matrix as

$$V \equiv V_{\text{stat}} + V_{\text{syst}} = \begin{pmatrix} \sigma_1^2 & 0 \\ 0 & \sigma_2^2 \end{pmatrix} + \begin{pmatrix} \tau_1^2 & f \tau_1 \tau_2 \\ f \tau_1 \tau_2 & \tau_2^2 \end{pmatrix} \quad (81)$$

with a correlation coefficient f for the systematic part. Using the formalism discussed in [20], one obtains the combined result for the optimal weighted average and error:

$$R = \frac{\sigma_2^2 + \tau_2^2 - f \tau_1 \tau_2}{\sigma_1^2 + \tau_1^2 + \sigma_2^2 + \tau_2^2 - 2f \tau_1 \tau_2} R_1 + \frac{\sigma_1^2 + \tau_1^2 - f \tau_1 \tau_2}{\sigma_1^2 + \tau_1^2 + \sigma_2^2 + \tau_2^2 - 2f \tau_1 \tau_2} R_2 \quad (82)$$

$$\sigma^2 = \frac{(\sigma_1^2 + \tau_1^2)(\sigma_2^2 + \tau_2^2) - f^2 \tau_1^2 \tau_2^2}{\sigma_1^2 + \tau_1^2 + \sigma_2^2 + \tau_2^2 - 2f \tau_1 \tau_2} \quad (83)$$

These expressions require knowledge of the correlation factor f . We shall now evaluate them for two different assumptions on f .

$f = 0$:

- 1999-style function: $R = (126.1535 \pm 0.7261) \text{ ppm}$
- Full physics function: $R = (126.2182 \pm 0.7219) \text{ ppm}$

This assumption is certainly far too optimistic and underestimates the total error. The systematic errors from the two run sets can be expected to be highly correlated.

$f = 1$:

- 1999-style function: $R = (126.1506 \pm 0.7273) \text{ ppm}$
- Full physics function: $R = (126.2162 \pm 0.7224) \text{ ppm}$

This result is very close to the one from the naive approach in Section 7.2.1. The 100 % correlations are likely to be somewhat overestimated.

Optimal weighting has generally the drawback that the central value of the result depends on the not too well known correlations.

7.2.3 Purely Statistical Weights but Error Analysis with Correlations

Here, we calculate the central value of the result using only statistical weights (like in Section 7.2.1). For the total error however, estimates on the correlations between the systematic errors are used. This leads to a stable central value and a slightly more conservative error.

For weights $w_i = \frac{1/\sigma_i^2}{1/\sigma_1^2 + 1/\sigma_2^2}$ (where σ_i is the statistical error of set i) and a covariance matrix V , the combined error is given by [20]

$$\sigma^2 = \sum_{i,j=1}^2 w_i w_j V_{ij} = \frac{\frac{V_{11}}{\sigma_1^4} + \frac{V_{22}}{\sigma_2^4} + 2 \frac{V_{12}}{\sigma_1^2 \sigma_2^2}}{\left(\frac{1}{\sigma_1^2} + \frac{1}{\sigma_2^2}\right)^2} = \frac{\frac{\sigma_1^2 + \tau_1^2}{\sigma_1^4} + \frac{\sigma_2^2 + \tau_2^2}{\sigma_2^4} + 2 \frac{f \tau_1 \tau_2}{\sigma_1^2 \sigma_2^2}}{\left(\frac{1}{\sigma_1^2} + \frac{1}{\sigma_2^2}\right)^2} \quad (84)$$

$$= \frac{1}{\frac{1}{\sigma_1^2} + \frac{1}{\sigma_2^2}} + \frac{\frac{\tau_1^2}{\sigma_1^4} + \frac{\tau_2^2}{\sigma_2^4} + 2 \frac{f \tau_1 \tau_2}{\sigma_1^2 \sigma_2^2}}{\frac{1}{\sigma_1^4} + \frac{1}{\sigma_2^4} + 2 \frac{1}{\sigma_1^2 \sigma_2^2}} \quad (85)$$

Again, we try $f = 0$ and $f = 1$:

$f = 0$:

- 1999-style function: $R = (126.1606 \pm \underbrace{0.7054 \pm 0.1807}_{0.7282 \text{ ppm}}) \text{ ppm}$
- Full physics function: $R = (126.2162 \pm \underbrace{0.7088 \pm 0.1369}_{0.7219 \text{ ppm}}) \text{ ppm}$

$f = 1$:

- 1999-style function: $R = (126.1606 \pm \underbrace{0.7054 \pm 0.2527}_{0.7493 \text{ ppm}}) \text{ ppm}$
- Full physics function: $R = (126.2162 \pm \underbrace{0.7088 \pm 0.1900}_{0.7338 \text{ ppm}}) \text{ ppm}$

Apparently for both values of f the error penalty from non-optimal weighting is small.

One could refine this procedure by writing V_{sys} as a sum of matrices pertaining to the individual systematic effects and assigning different correlation factors for each of them.

7.2.4 Preferred Result

The preferred result is the one from the Full Physics Function. It has a slightly smaller total error than the 1999 Function. We conservatively combine the run sets according to the approach from Section 7.2.3 with $f = 1$:

$$\text{with my offset:} \quad R = (126.2162 \pm \underbrace{0.7088 \pm 0.1900}_{0.7338 \text{ ppm}}) \text{ ppm} \quad (86)$$

$$\text{with the official offset:} \quad R = 108.3062 \text{ ppm} \quad (87)$$

References

- [1] M. Deile: Multiparameter ω_a Analysis of the g-2 Data from 2000, g-2 Note 421.
- [2] I. Logashenko: FIT Pulse Finding Algorithm, g-2 Note 334, rev. March 1999; Shapes of WFD Pulses and the FIT Pulse Finding Algorithm, g-2 Note 369, September 2000.
- [3] Run selection for 2001, available from
<http://g2muon:precess@www.npl.uiuc.edu/~polly/g-2> .
- [4] A. Lam: Fast-rotation analysis, presented at the October 2002 collaboration meeting.
- [5] C. Özben and Y.K. Semertzidis: Eliminating Pileup from the g-2 Data, g-2 Note 365, July 2000.
- [6] I. Logashenko: energy dependence of f_L and the g2off dead-time, e-mail to g2offline, 22 October 2002.
- [7] F. Farley et al.: Estimation of Error in Differential Pileup Subtracted Data, g-2 Note 377, December 2000.
- [8] Y. Semertzidis et al., The Brookhaven Muon g-2 Storage Ring High Voltage Quadrupoles, accepted for publication in Nucl. Instr. Meth. A.
- [9] C. Polly: Muon losses for the two run sets, presentation at the Illinois analysis workshop, December 2002.
- [10] J. Paley: Muon losses for the two run sets, presentation at the Illinois analysis workshop, December 2002.
- [11] C. Özben: 1999 ω_a Analysis of g-2, g-2 Note 385, January 2001.
- [12] Y.K. Semertzidis: Shift in R due to pileup phase a.k.a. the “Underwater” effect, g-2 Note 426, July 2002.
- [13] W. Morse: relationship between gain and asymmetry; private communication.
- [14] W. Morse: The Low Pulse Height Pile-Down Effect, g-2 Note 373, October 2000.
- [15] I. Logashenko: Estimating the systematic error in ω_a due to low-energy pileup, draft of a g-2 Note, January 2003.
- [16] Y.K. Semertzidis: The Spectrum of χ and Systematic Errors Due to Backgrounds in the 2000 Run Data, g-2 Note 406, January 2002. See remark 3 in Section 4.
- [17] A. Steinmetz: The 98 Systematic Error on the g-2 Frequency, g-2 Note 351, November 1999.
- [18] S. Redin: Statistical Equations for Set-Subset Problem, ..., g-2 Note 387, March 2001.
- [19] Y.K. Semertzidis: On the Question of the Functional Form of the 2000 Run Data, g-2 Note 403, December 2001.
- [20] O. Rind and E. Sichtermann: On Combining the Results for ω_a , g-2 Note 380, January 2001.

A Fit Results for the 1999-Style Function

A.1 Start Time Scans for the Sum of Detectors

1999 Function, Sum of Detectors, Period A

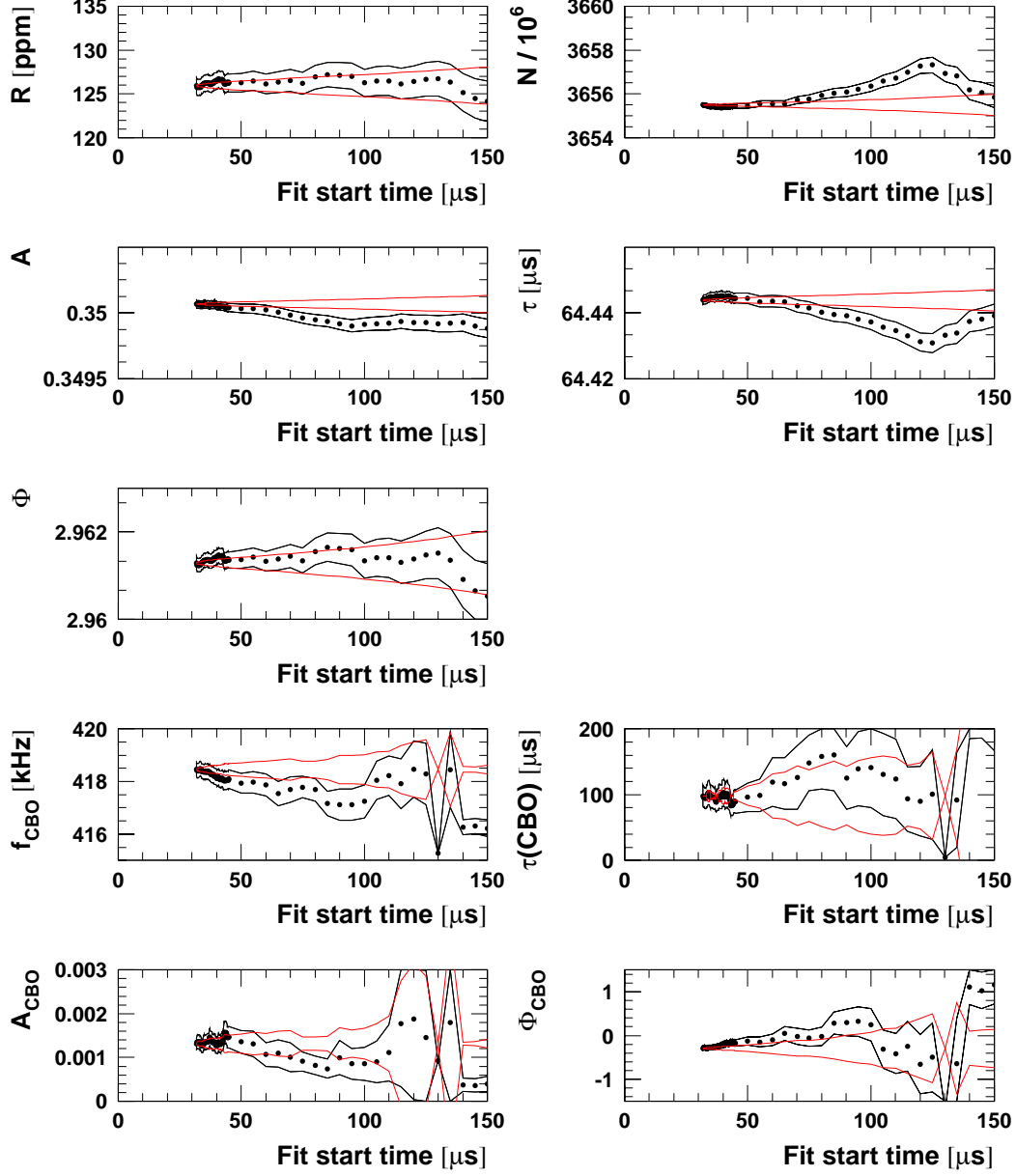
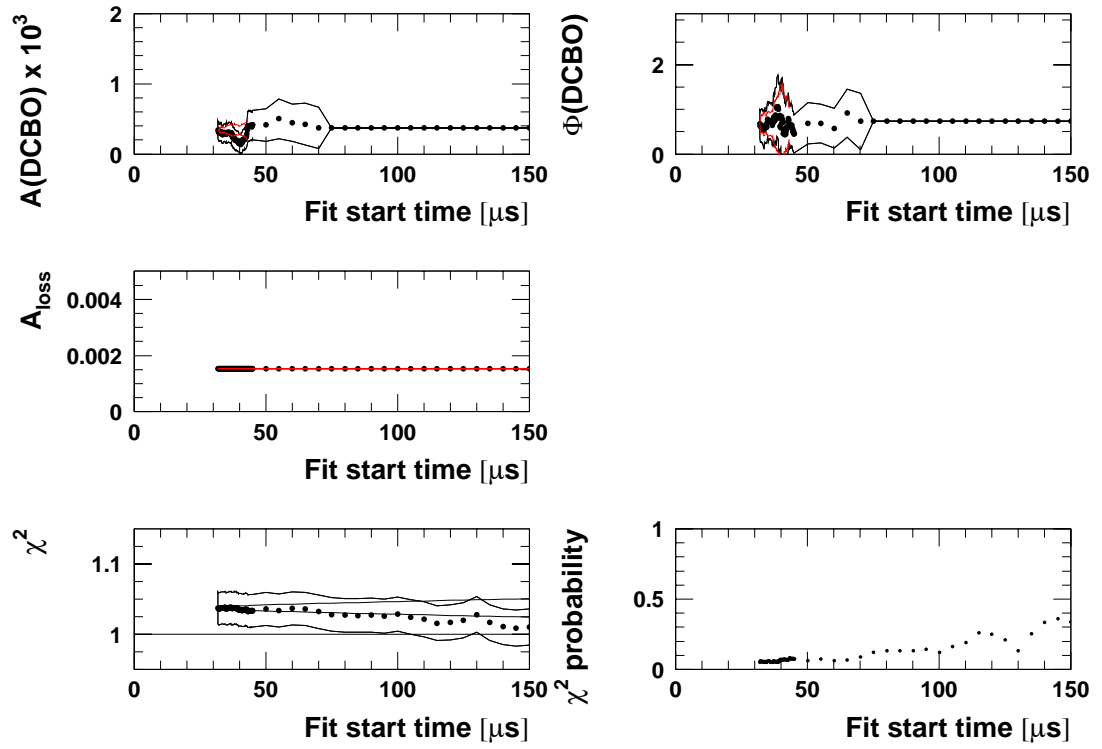


Figure 82: Start time scan with the 1999-style function for Set A.

1999 Function, Sum of Detectors, Period A



1999 Function, Sum of Detectors, Period B

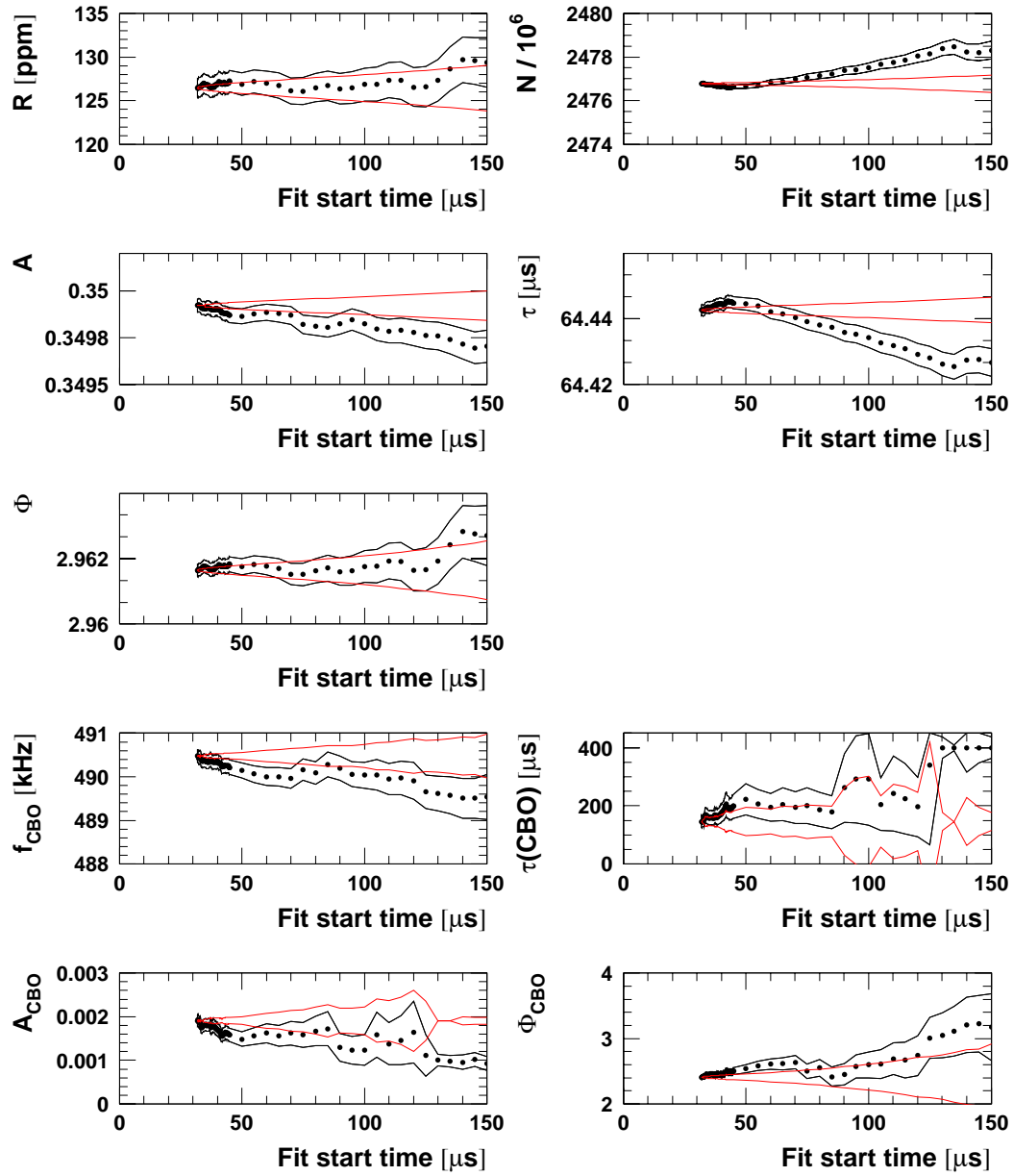
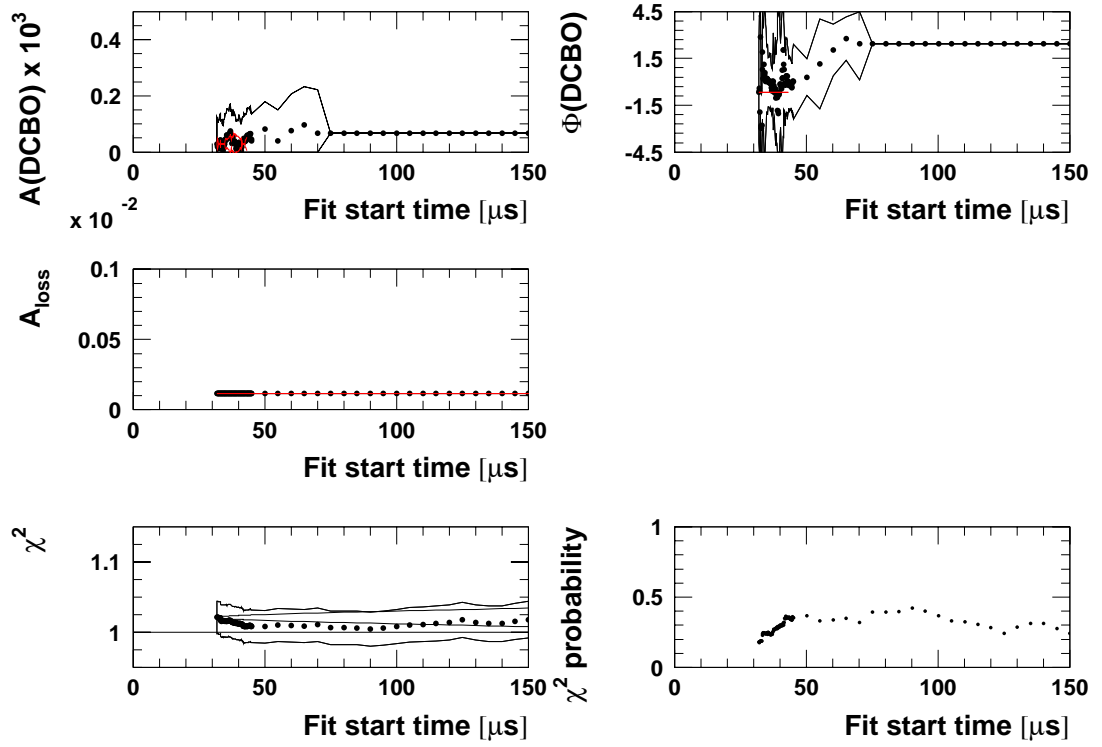


Figure 83: *Start time scan with the 1999-style function for Set B.*

1999 Function, Sum of Detectors, Period B



A.2 Start Time Scans for the Two Half Rings

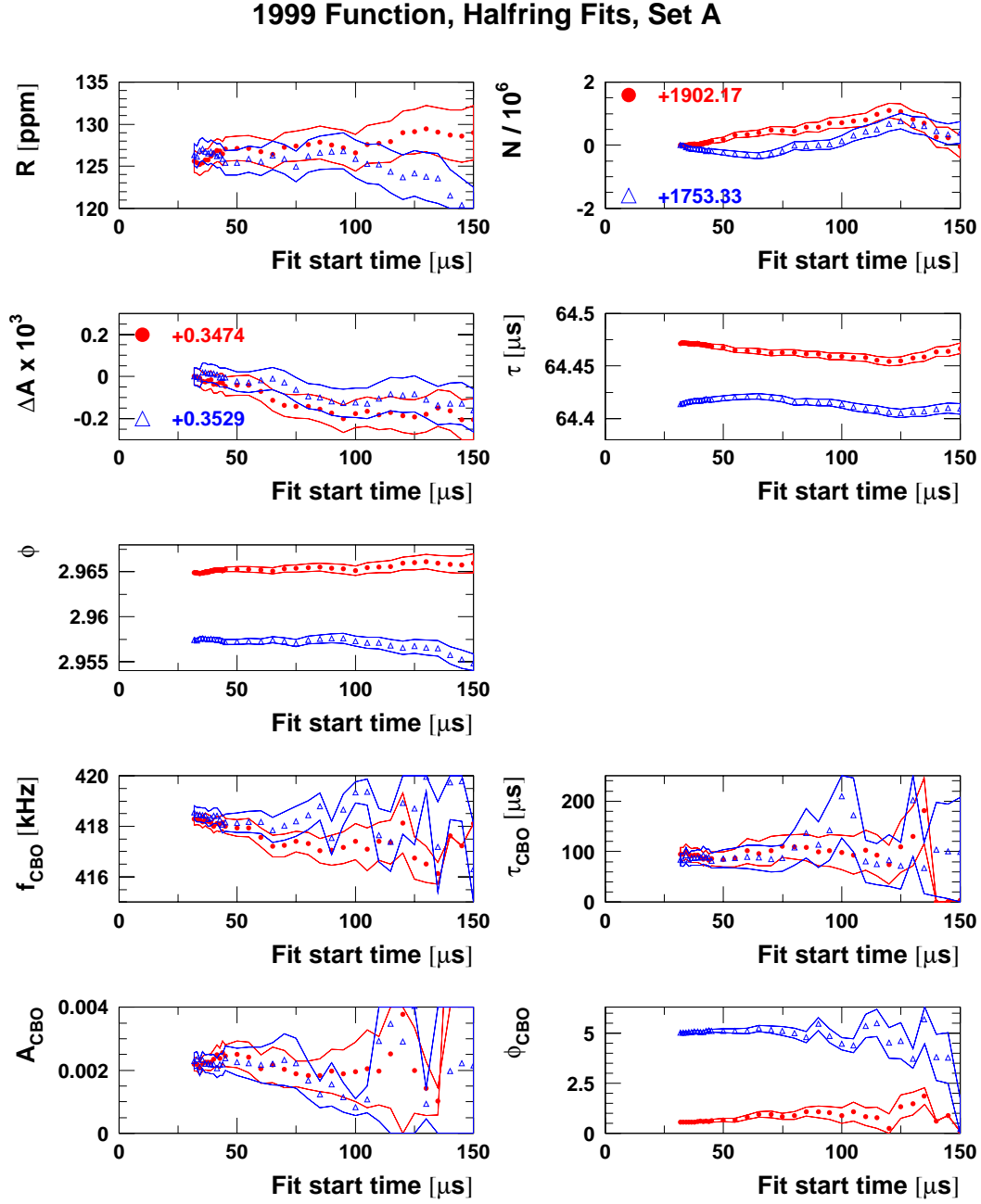
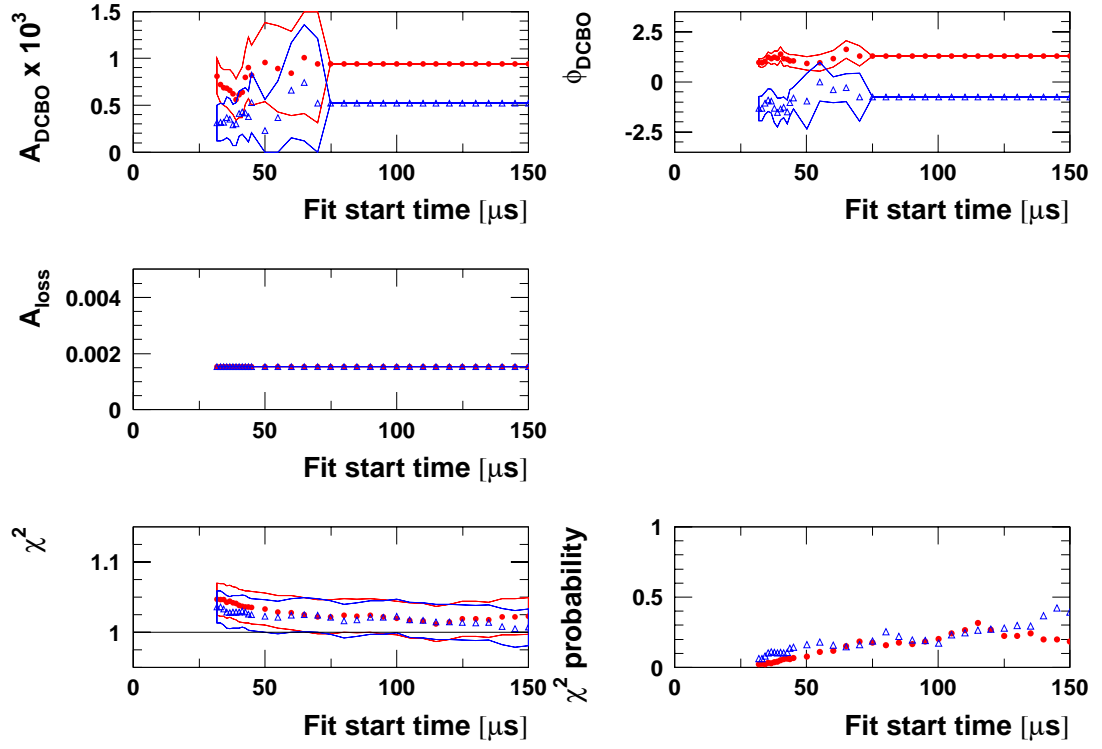


Figure 84: Start time scan for the two half rings separately (red circles = det. 1-12, blue triangles = det. 13-24) with the 1999-style function for Set A.

1999 Function, Halfring Fits, Set A



1999 Function, Halfring Fits, Set B

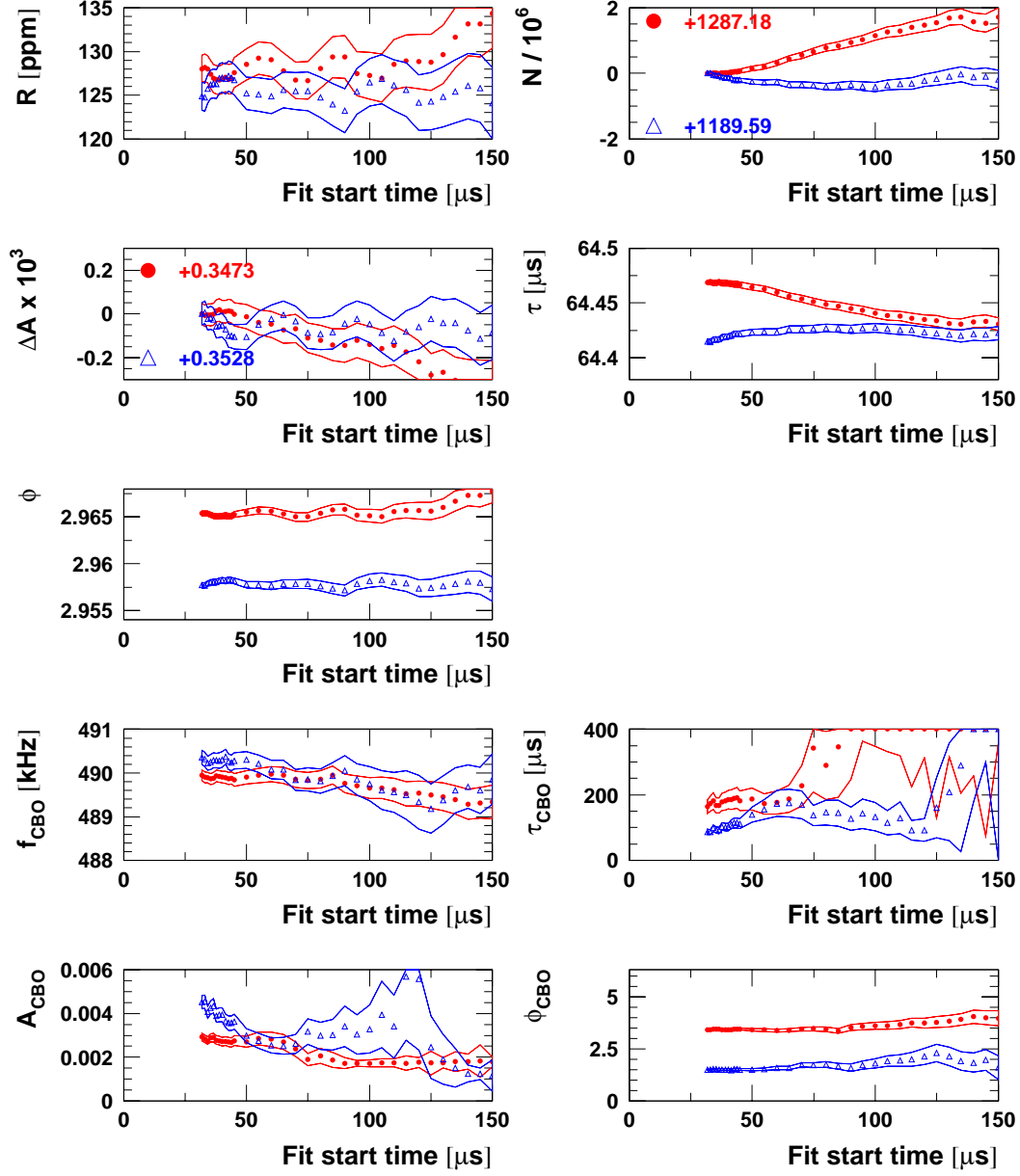
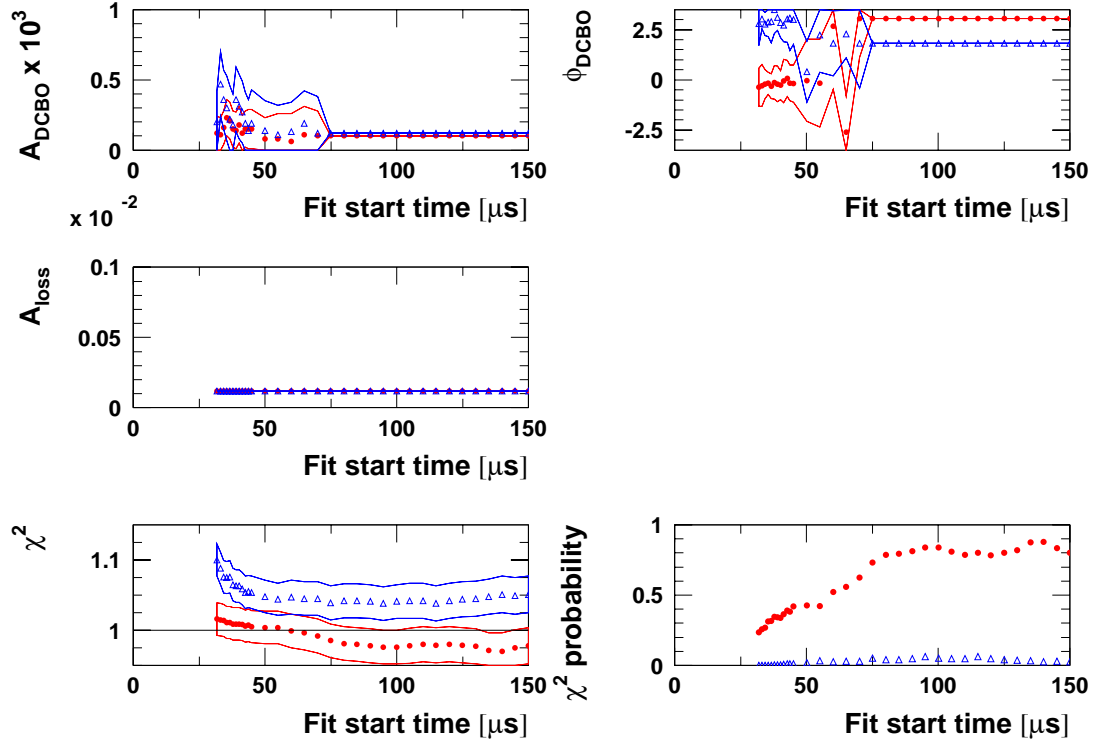


Figure 85: Start time scan for the two half rings separately (red circles = det. 1-12, blue triangles = det. 13-24) with the 1999-style function for Set B.

1999 Function, Halfring Fits, Set B



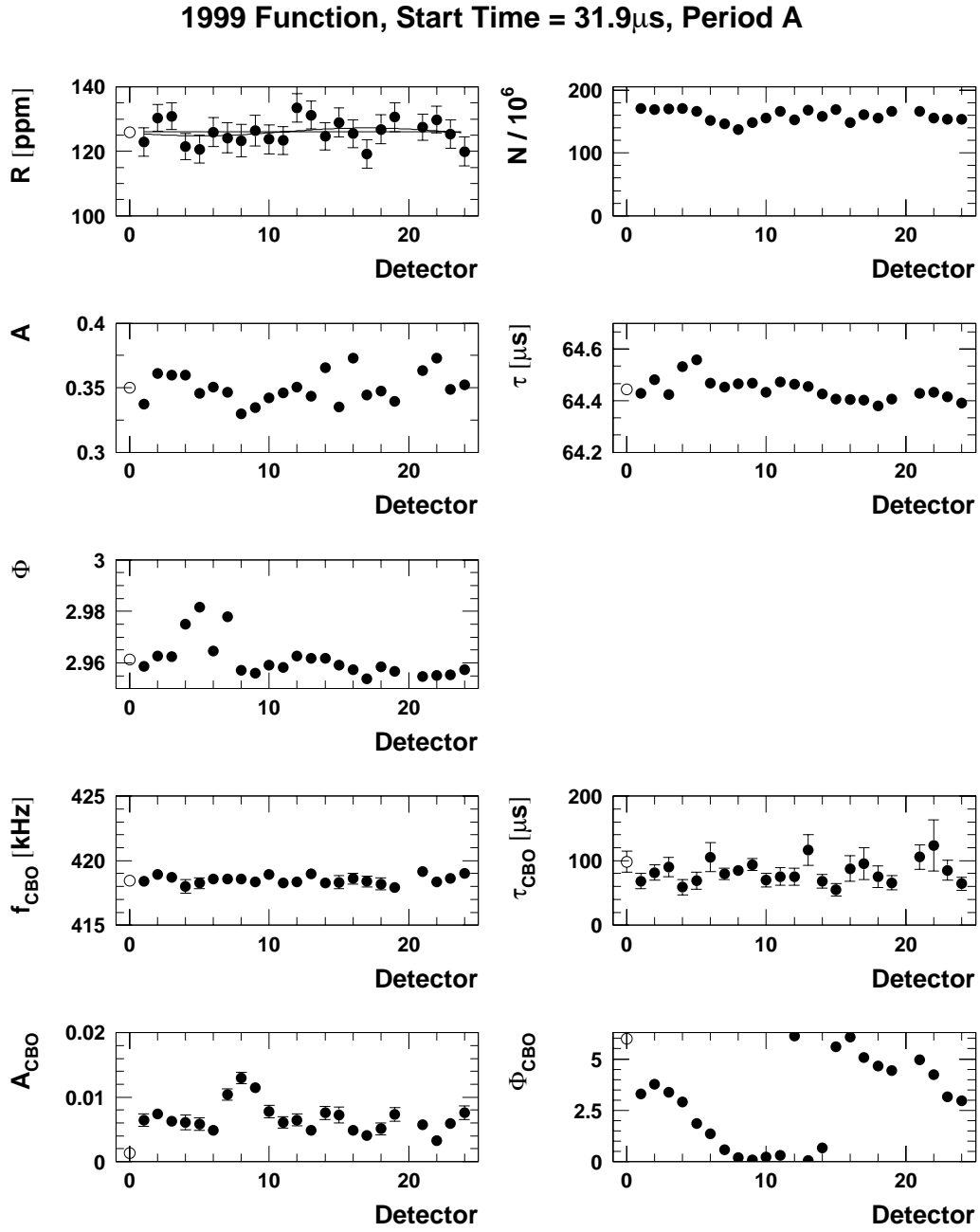
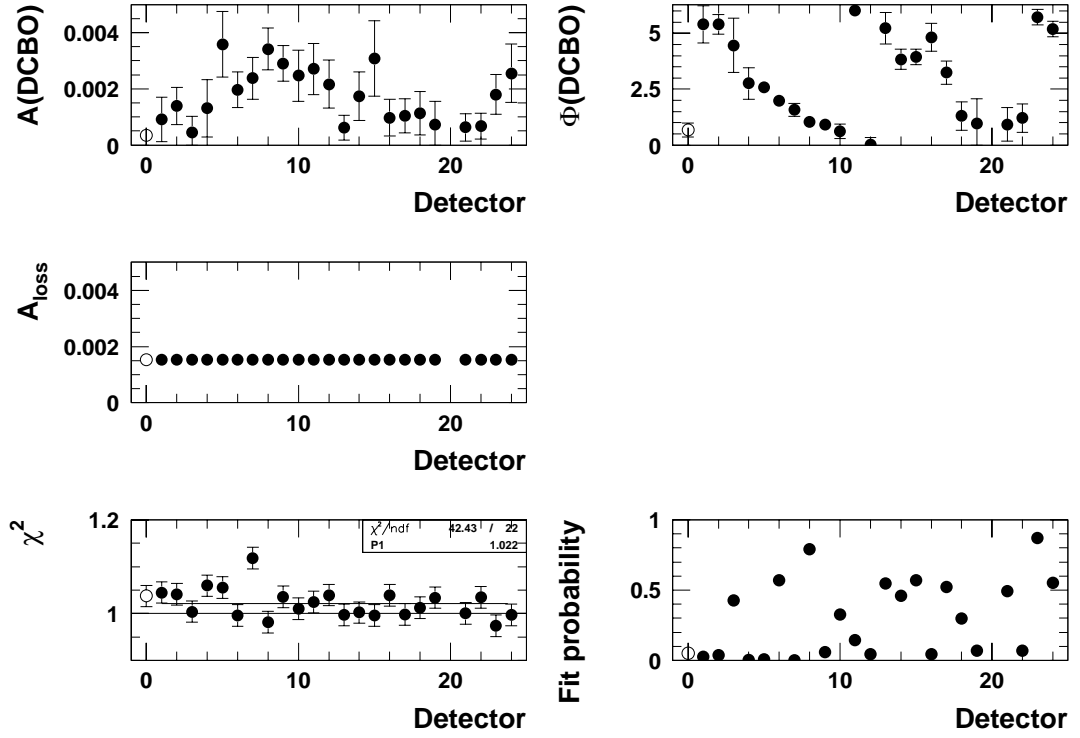
A.3 Individual Detector Fits Starting at $31.8 \mu\text{s}$ 

Figure 86: *Fits of individual detector spectra with the 1999-style function for Set A. The open marker at detector 0 represents the fit to the sum.*

1999 Function, Start Time = $31.9\mu s$, Period A

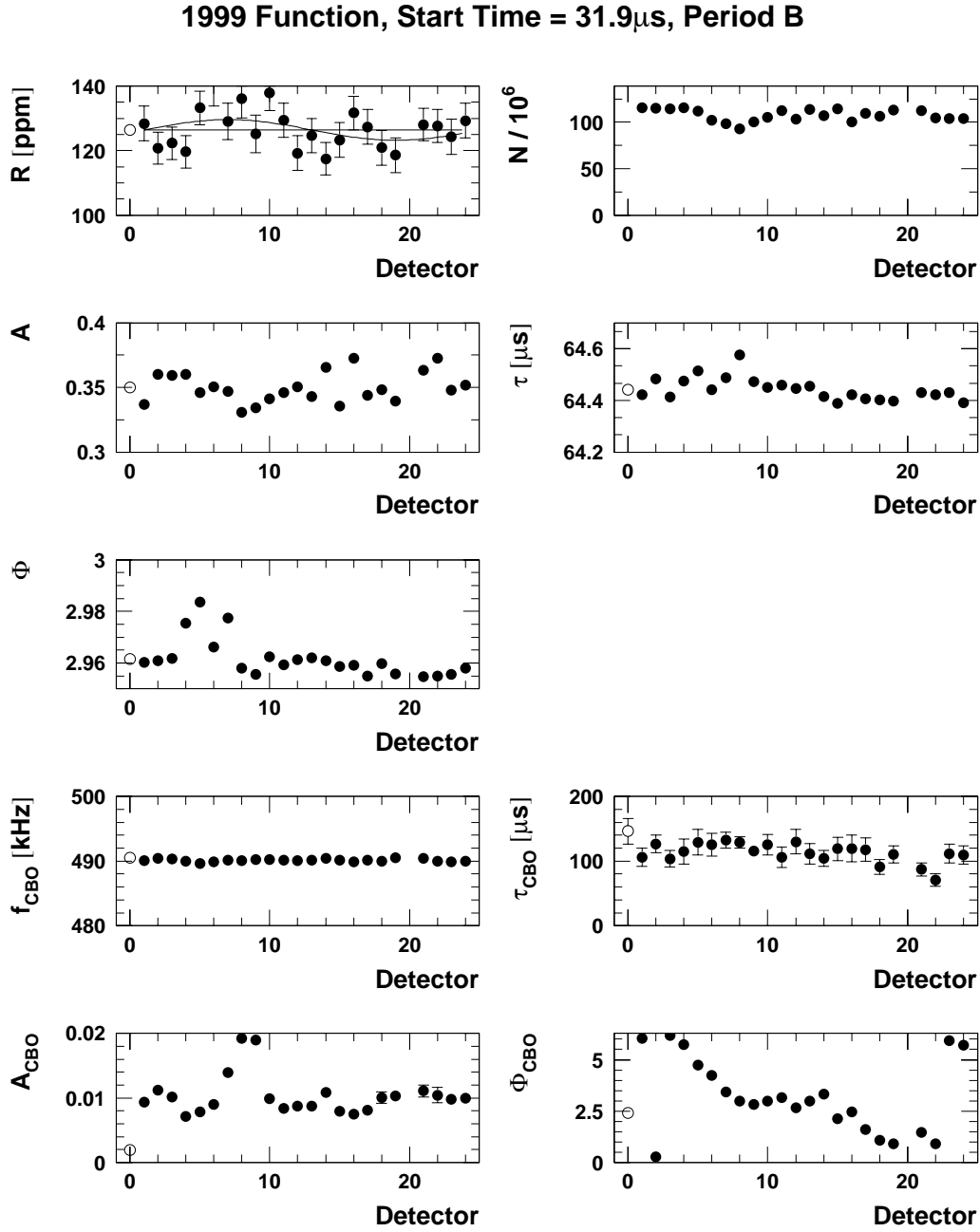
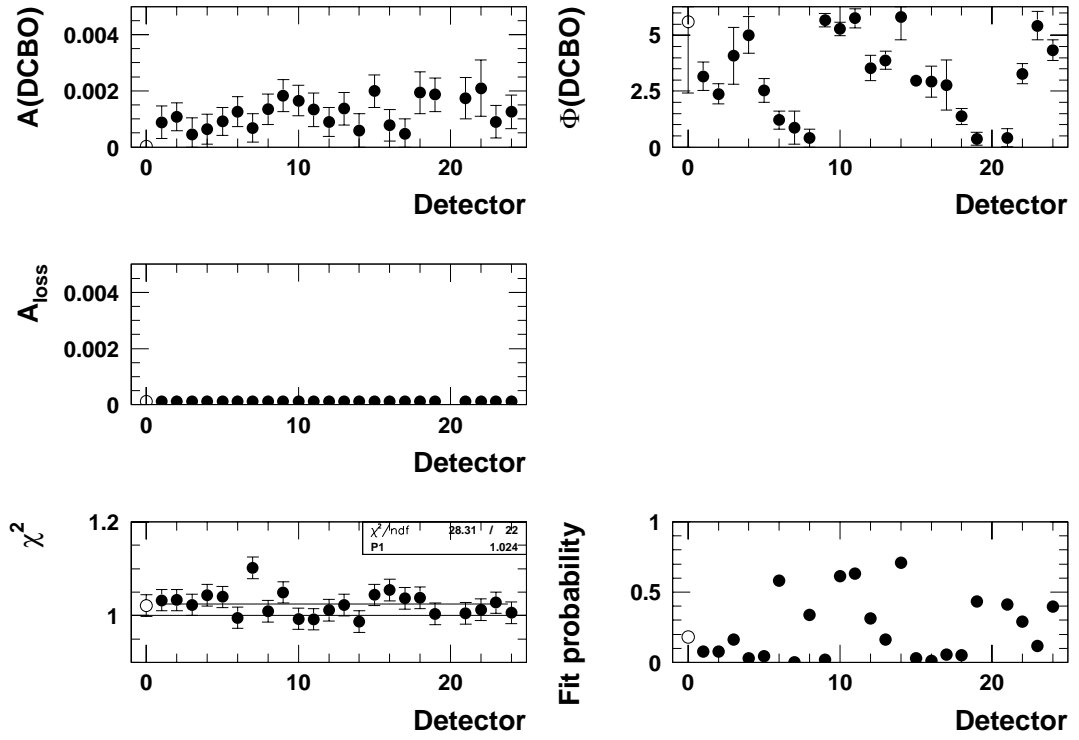


Figure 87: *Fits of individual detector spectra with the 1999-style function for Set B. The open marker at detector 0 represents the fit to the sum.*

1999 Function, Start Time = $31.9\mu s$, Period B



B Fit Results for the Physics Function without Phase Modulation

B.1 Start Time Scans for the Sum of Detectors

Physics Function w/o Phase Modulation, Sum of Detectors, Period A

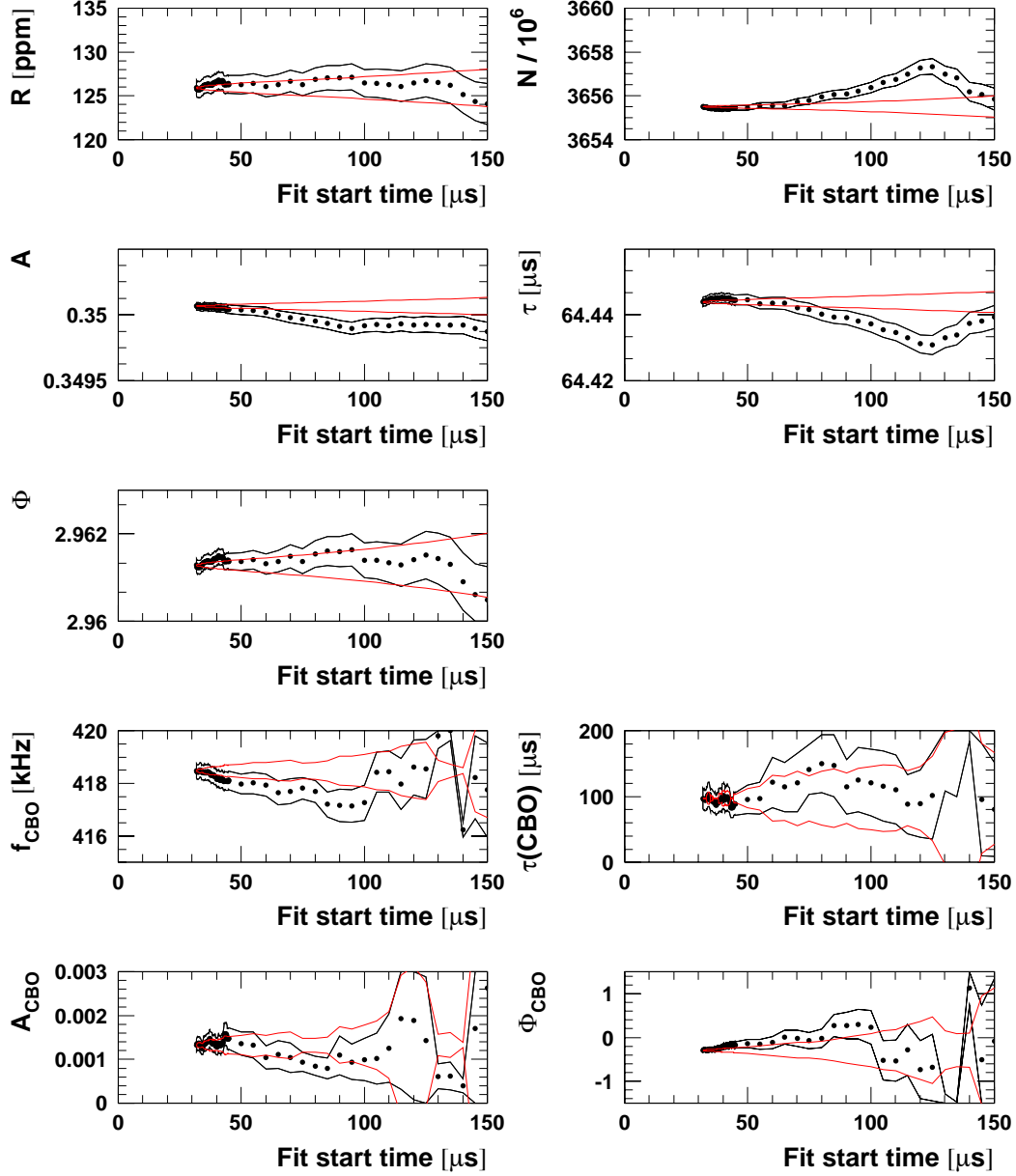
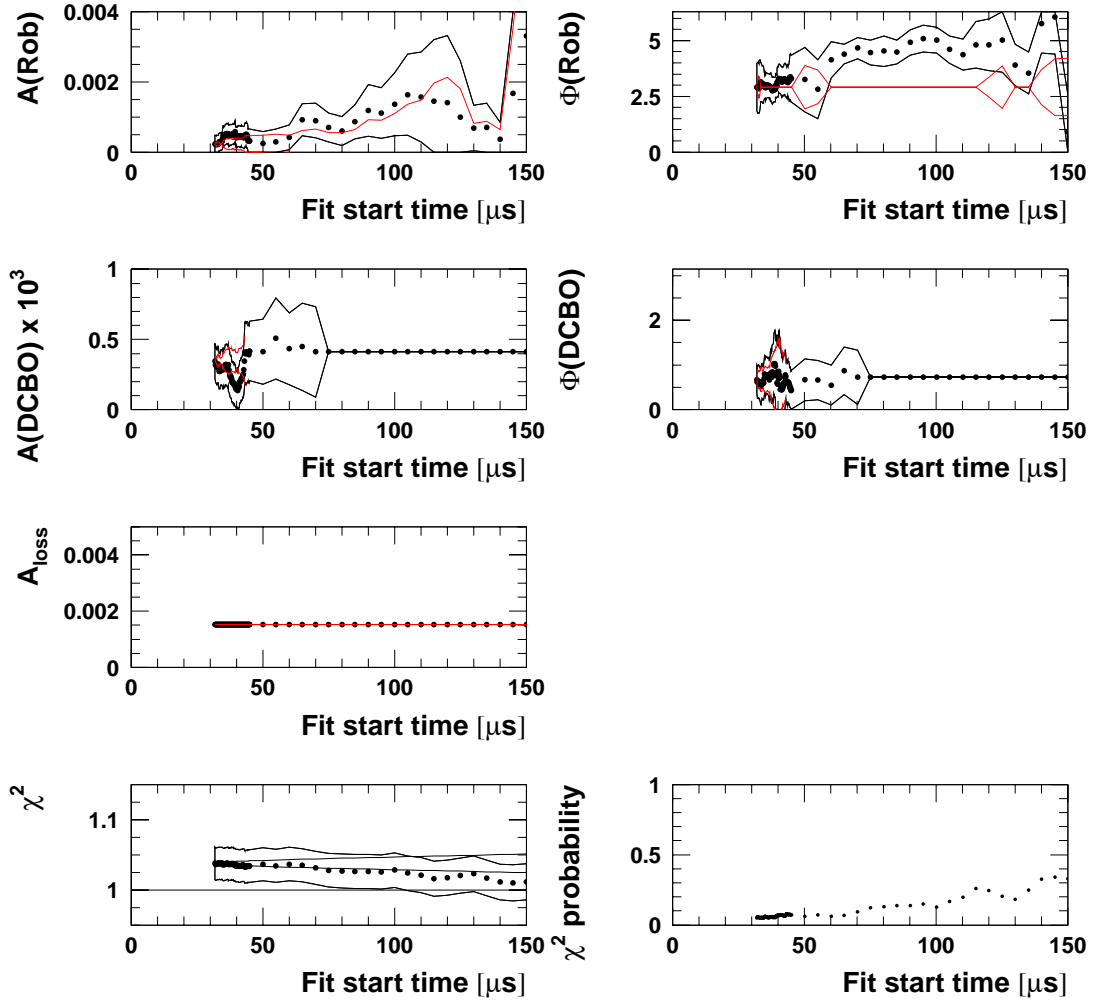


Figure 88: Start time scan with the physics function without phase modulation for Set A.

Physics Function w/o Phase Modulation, Sum of Detectors, Period A



Physics Function w/o Phase Modulation, Sum of Detectors, Period B

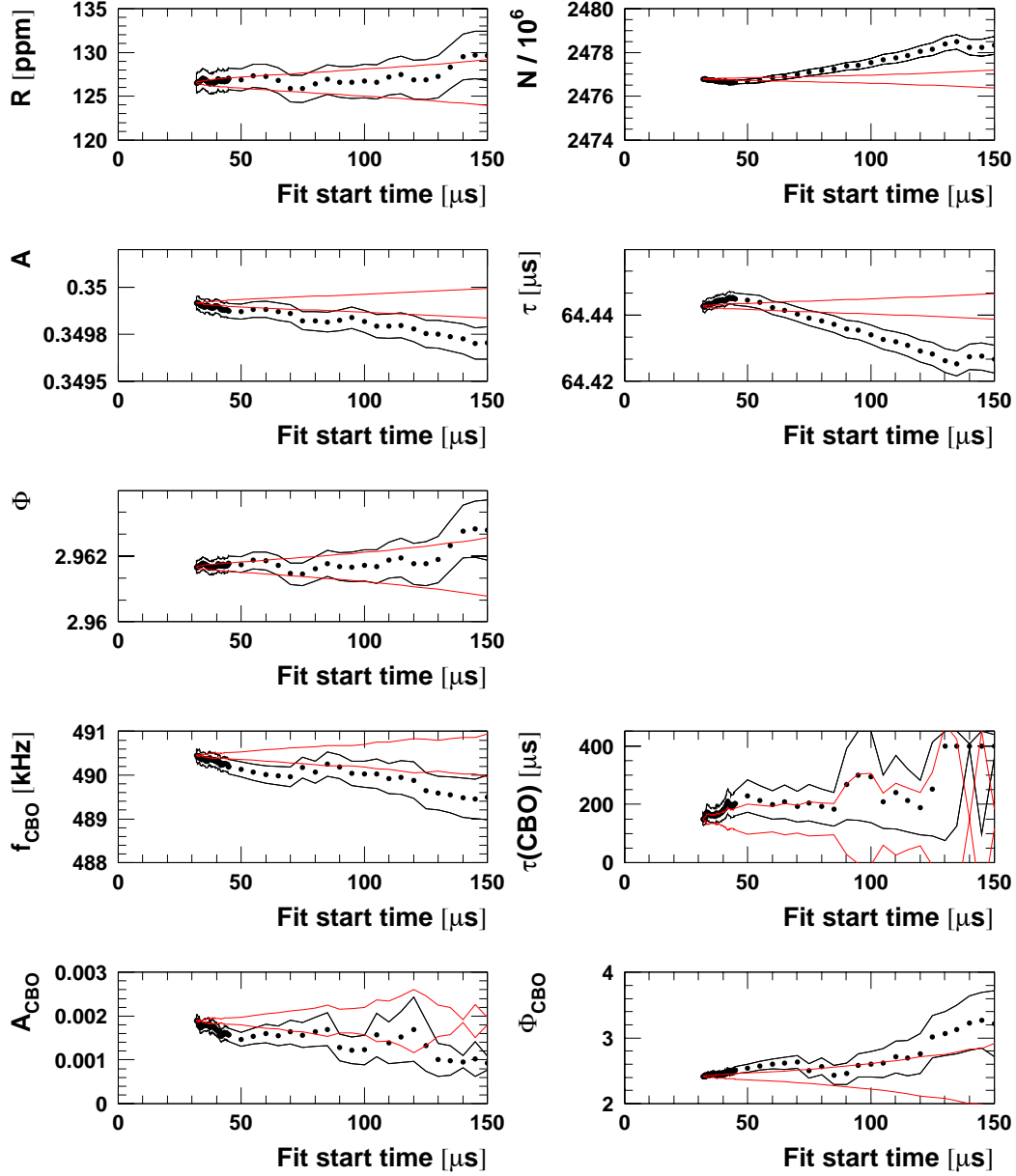
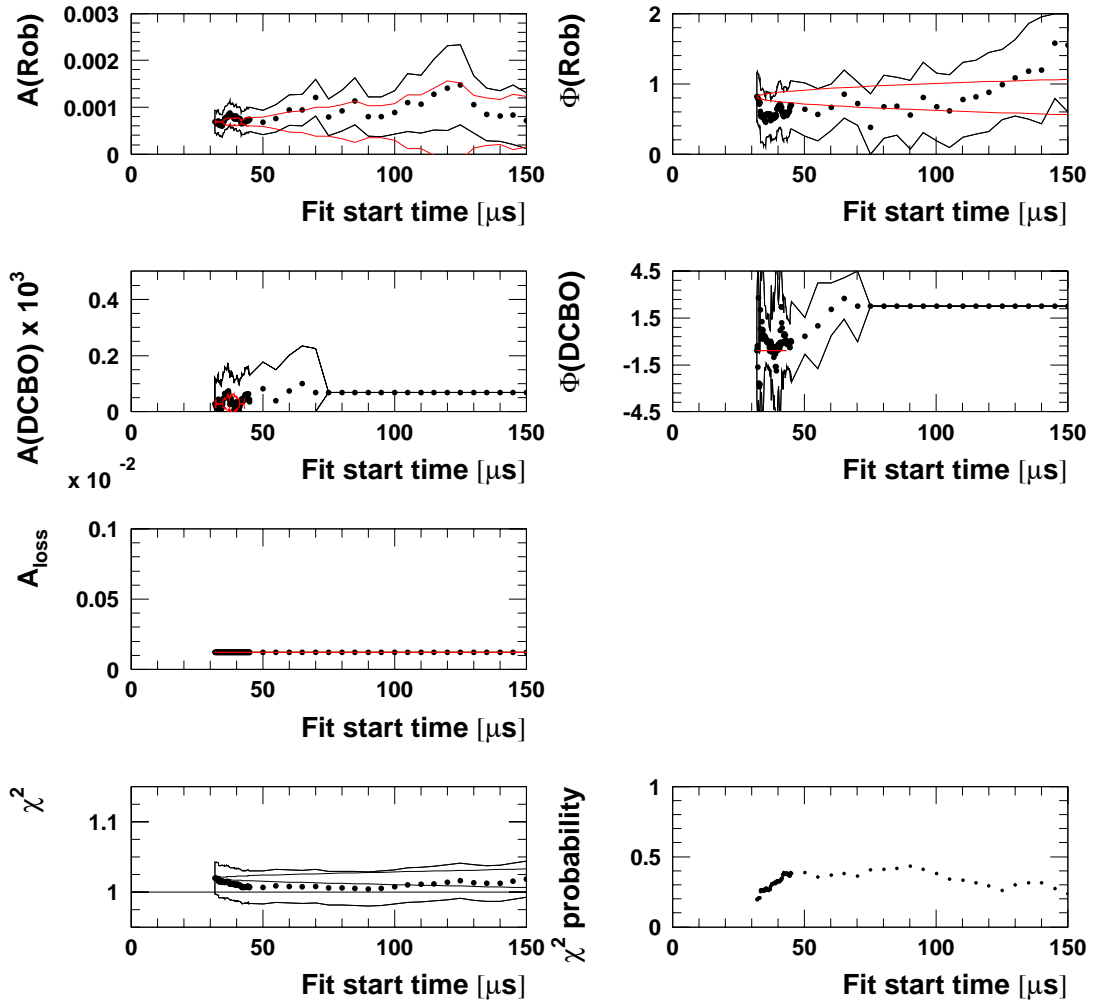


Figure 89: Start time scan with the physics function without phase modulation for Set B.

Physics Function w/o Phase Modulation, Sum of Detectors, Period B



B.2 Start Time Scans for the Two Half Rings

Physics Function w/o Phase Modulation, Halfring Fits, Set A

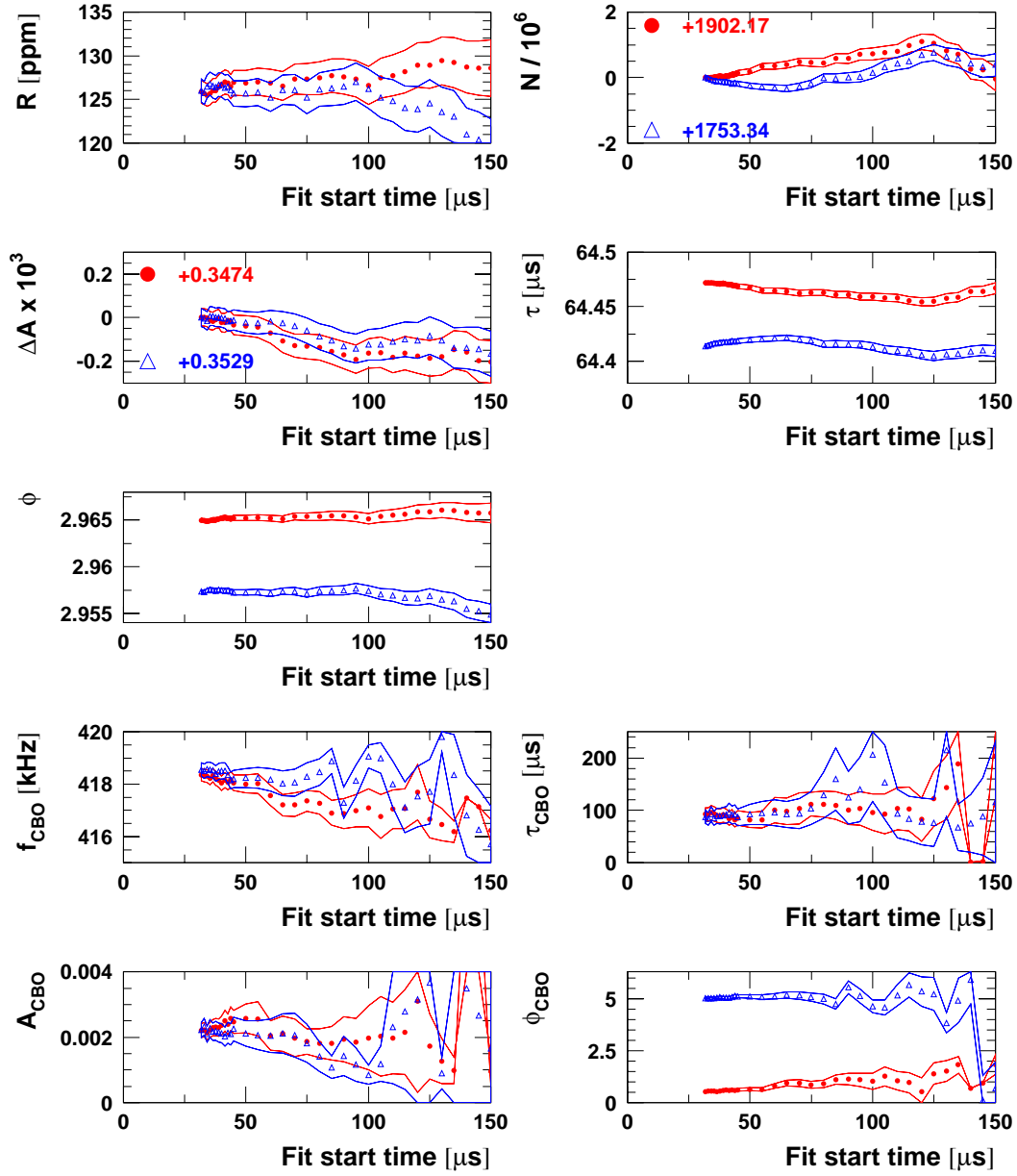
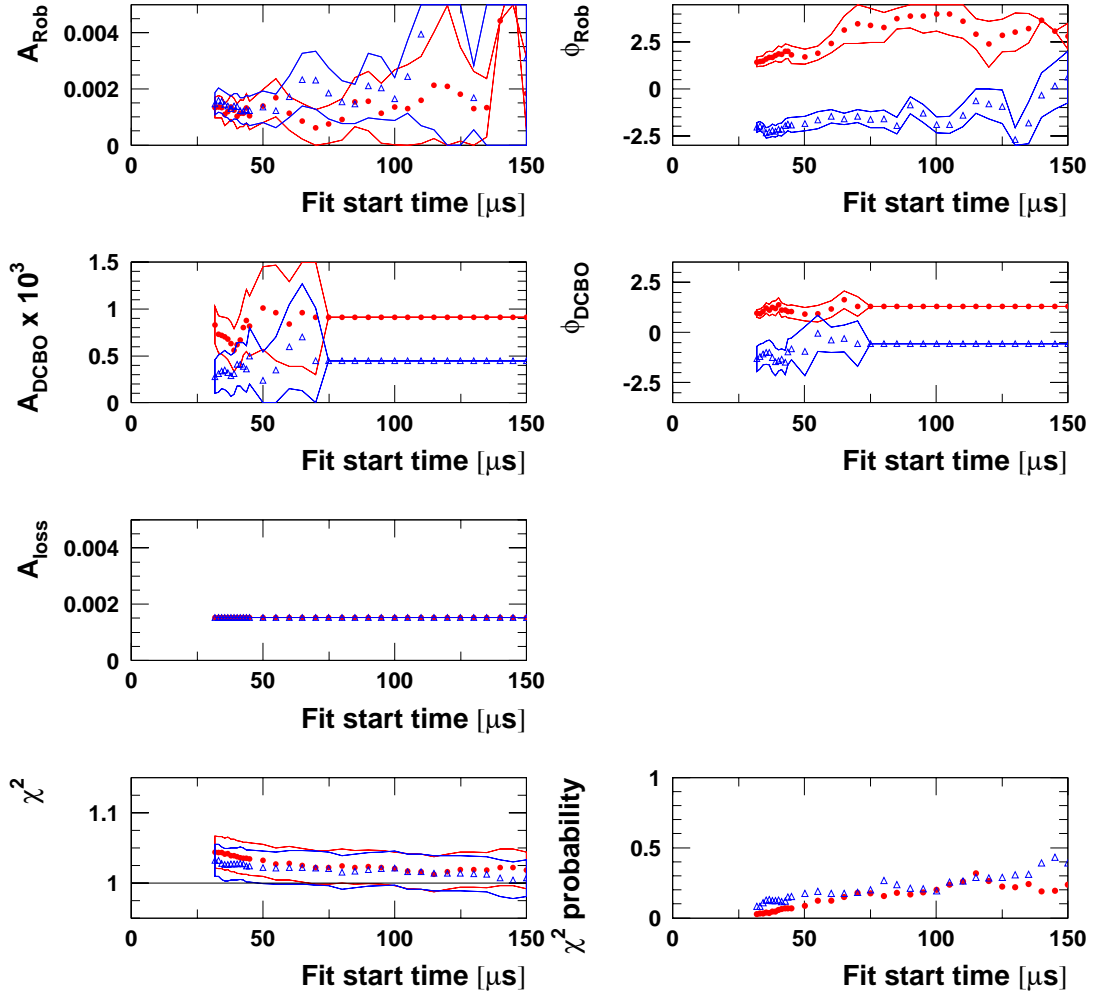


Figure 90: Start time scan for the two half rings separately (red circles = det. 1-12, blue triangles = det. 13-24) with the physics function without phase modulation for Set A.

Physics Function w/o Phase Modulation, Halfring Fits, Set A



Physics Function w/o Phase Modulation, Halfring Fits, Set B

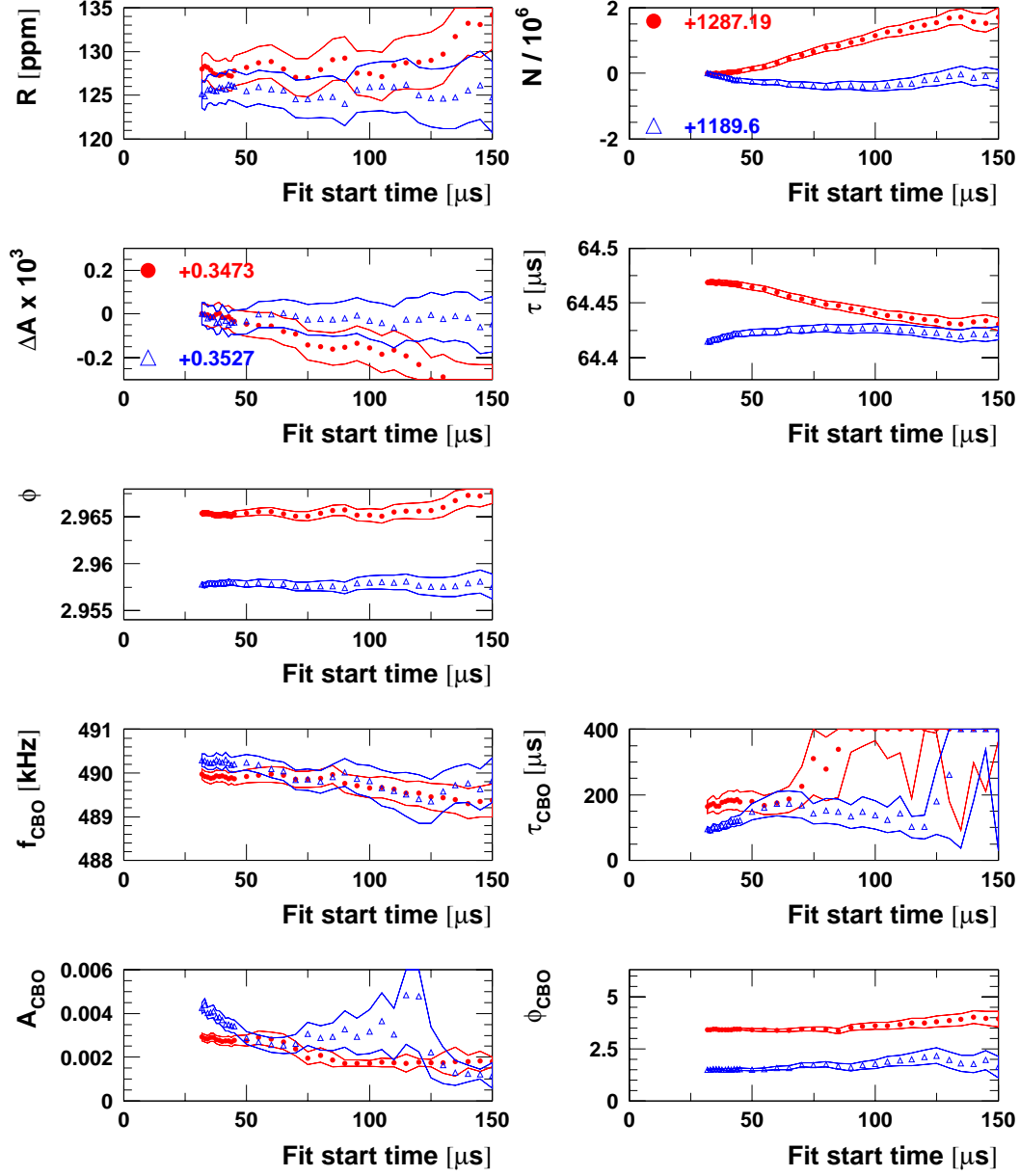
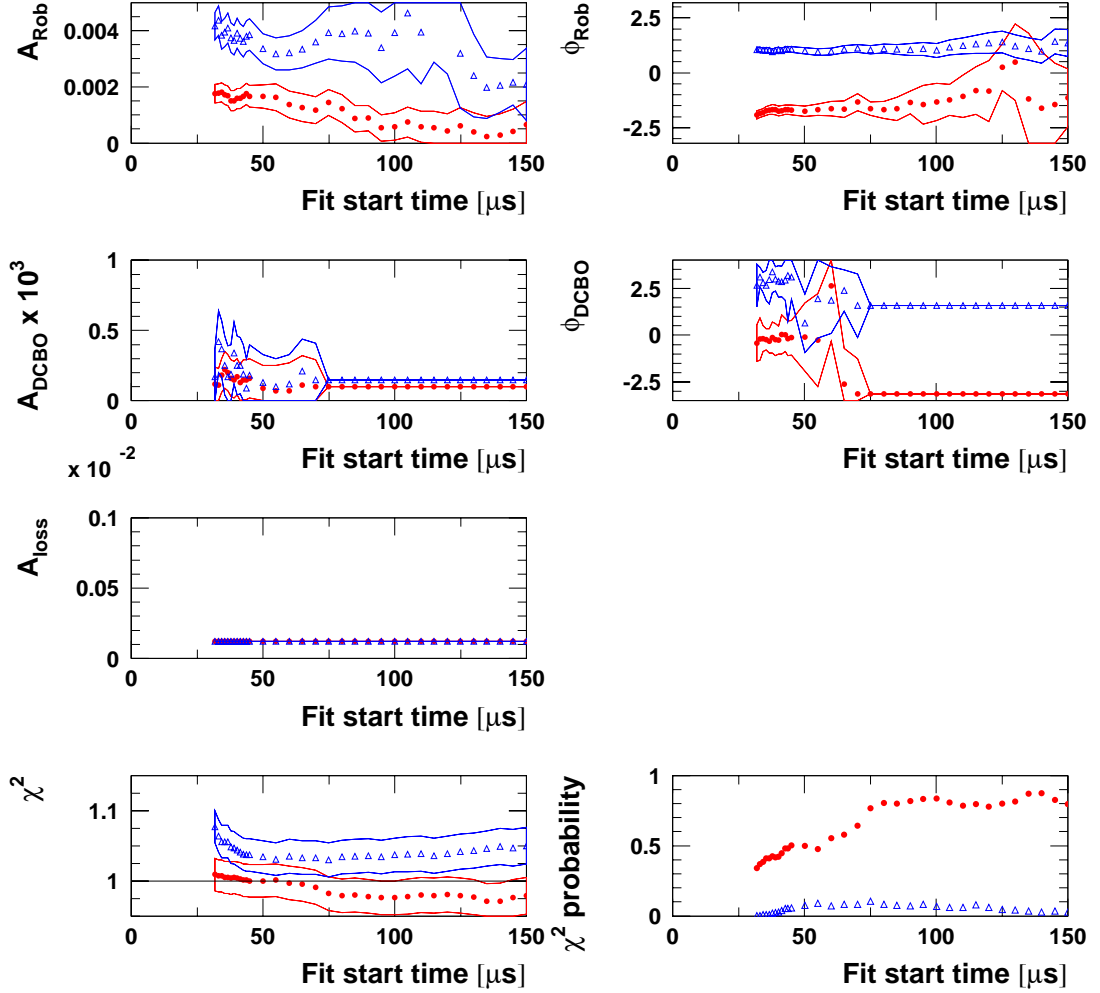


Figure 91: Start time scan for the two half rings separately (red circles = det. 1-12, blue triangles = det. 13-24) with the physics function without phase modulation for Set B.

Physics Function w/o Phase Modulation, Halfring Fits, Set B



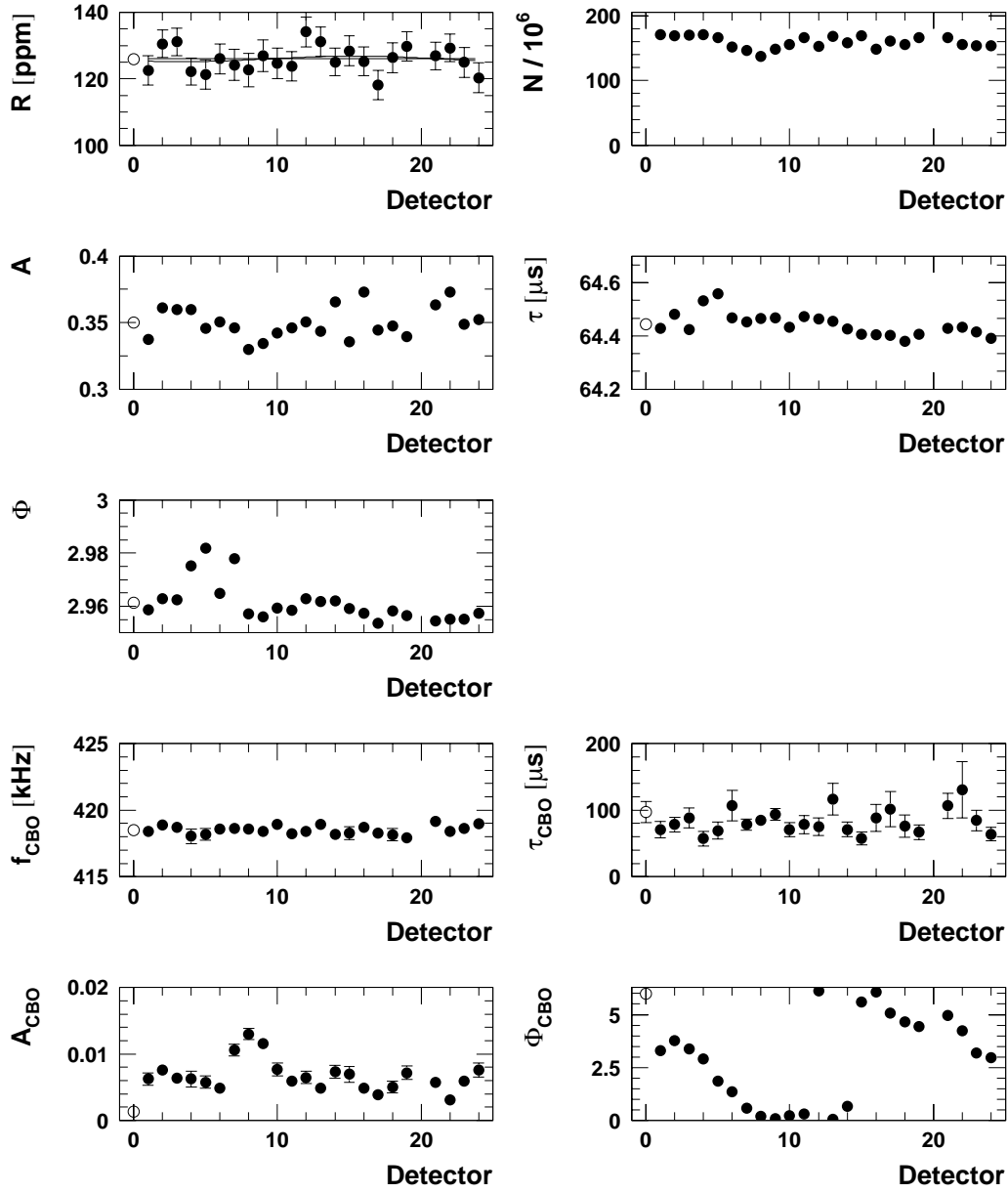
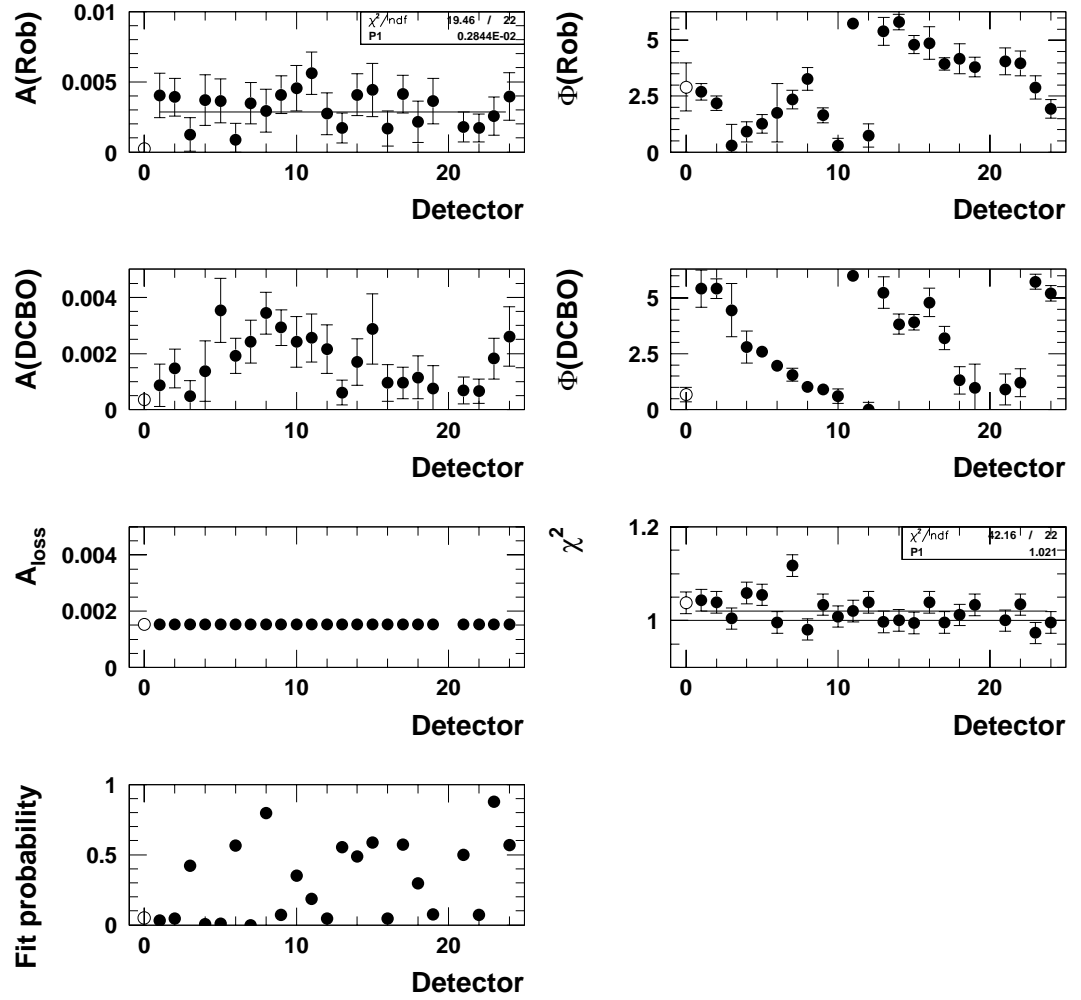
B.3 Individual Detector Fits Starting at $31.8 \mu\text{s}$ Physics Function w/o Phase Modulation, Start Time = $31.9 \mu\text{s}$, Period A

Figure 92: *Fits of individual detector spectra with the physics function without phase modulation for Set A.*

Physics Function w/o Phase Modulation, Start Time = $31.9\mu s$, Period A



Physics Function w/o Phase Modulation, Start Time = 31.9 μ s, Period B

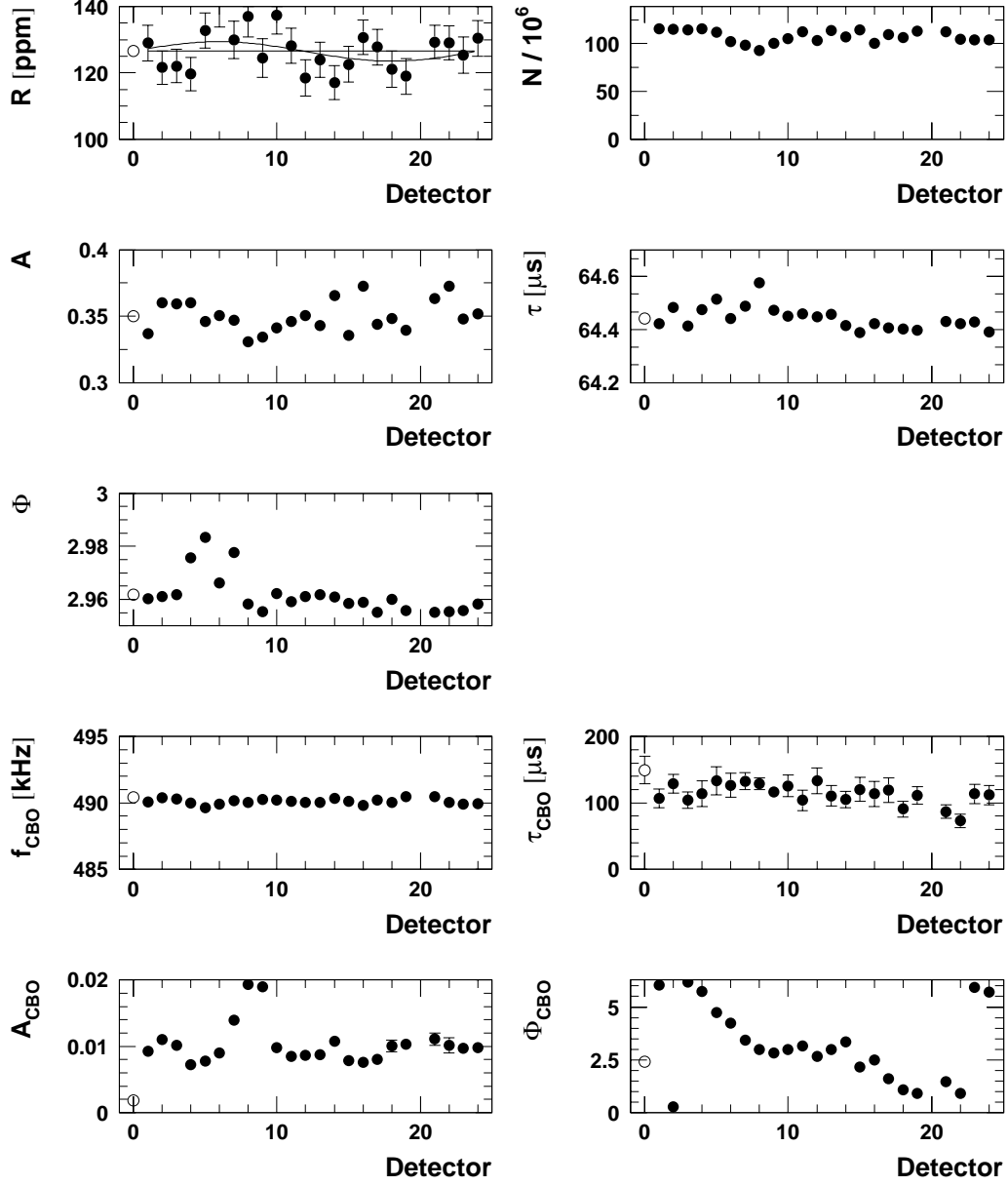
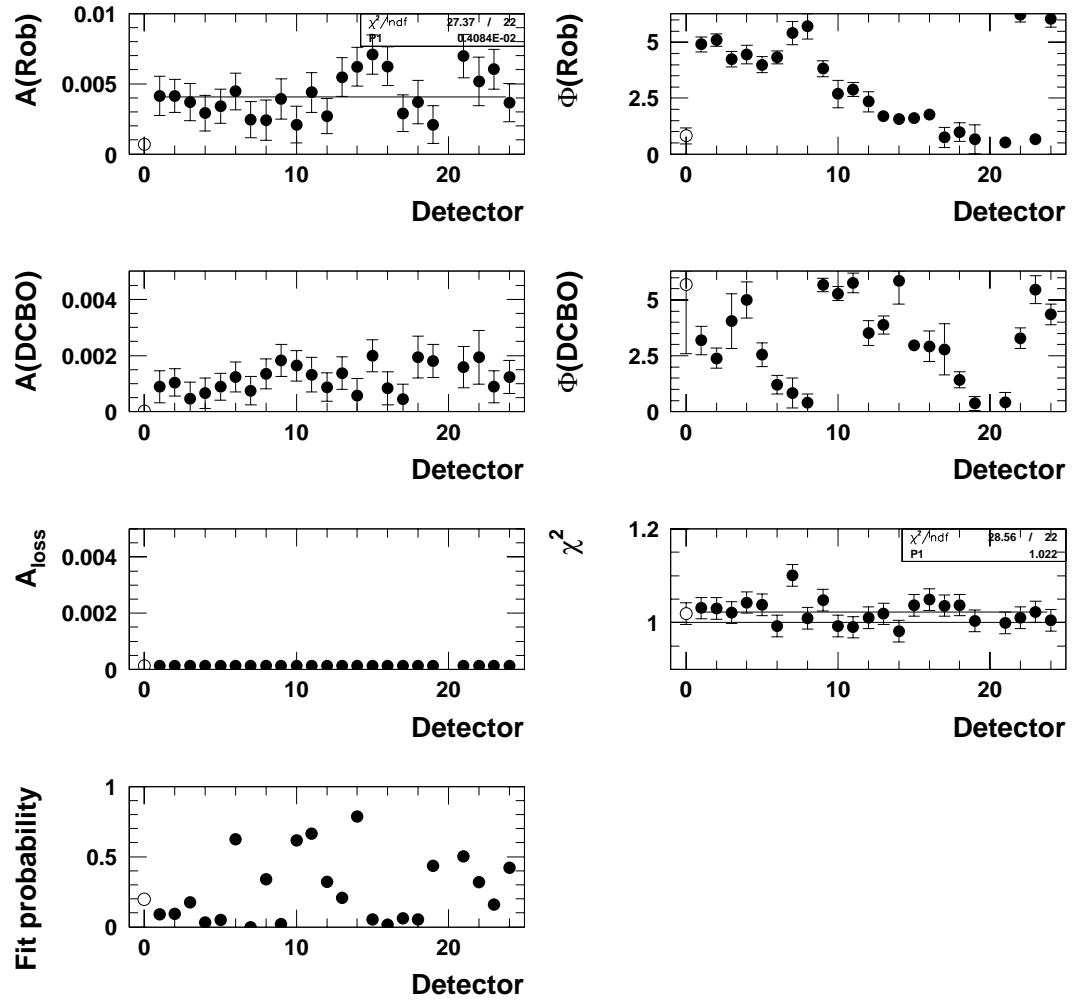


Figure 93: Fits of individual detector spectra with the physics function without phase modulation for Set B.

Physics Function w/o Phase Modulation, Start Time = $31.9\mu s$, Period B



C Fit Results for the Full Physics Function

C.1 Start Time Scans for the Sum of Detectors

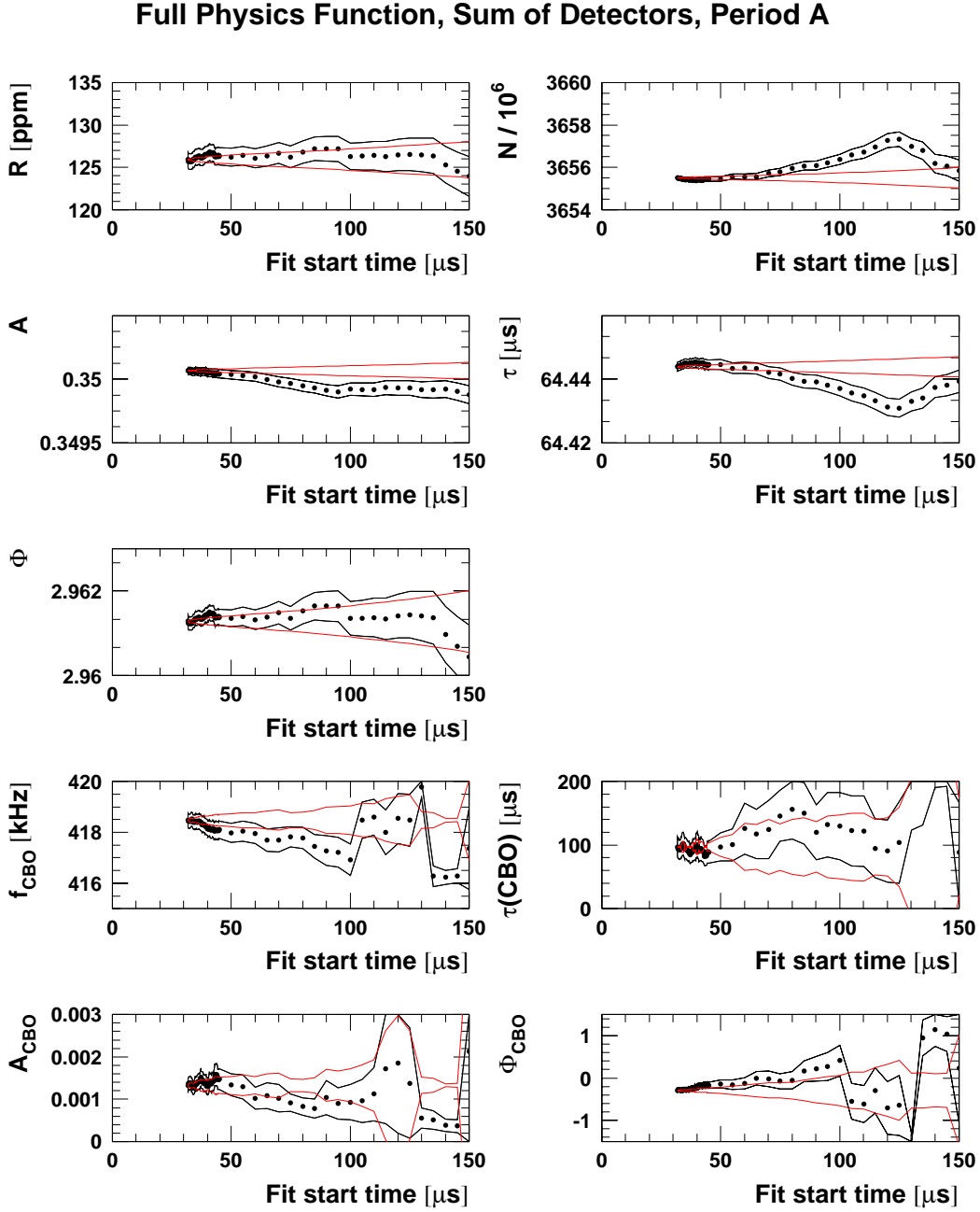
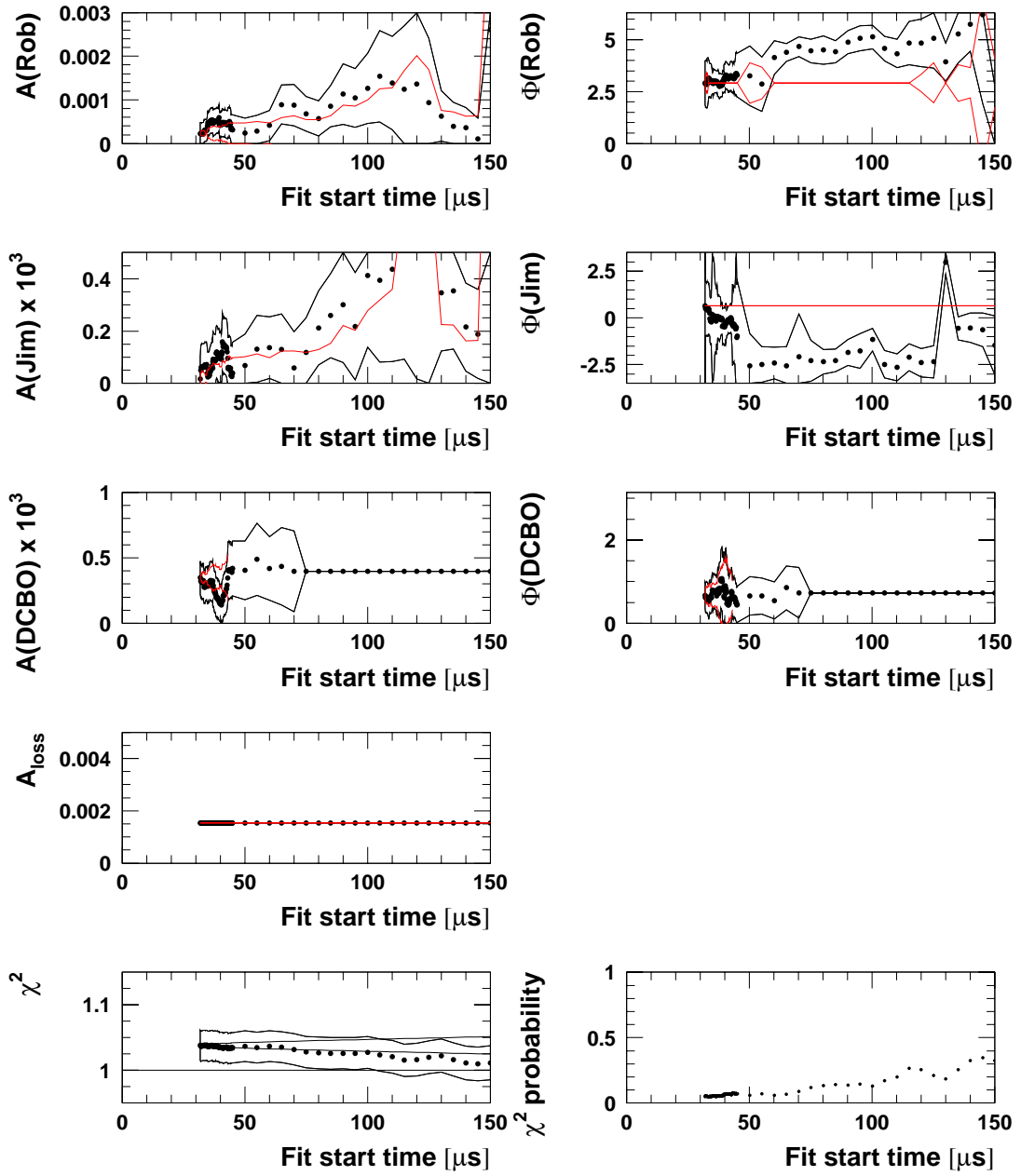


Figure 94: *Start time scan with the full physics function for Set A.*

Full Physics Function, Sum of Detectors, Period A



Full Physics Function, Sum of Detectors, Period B

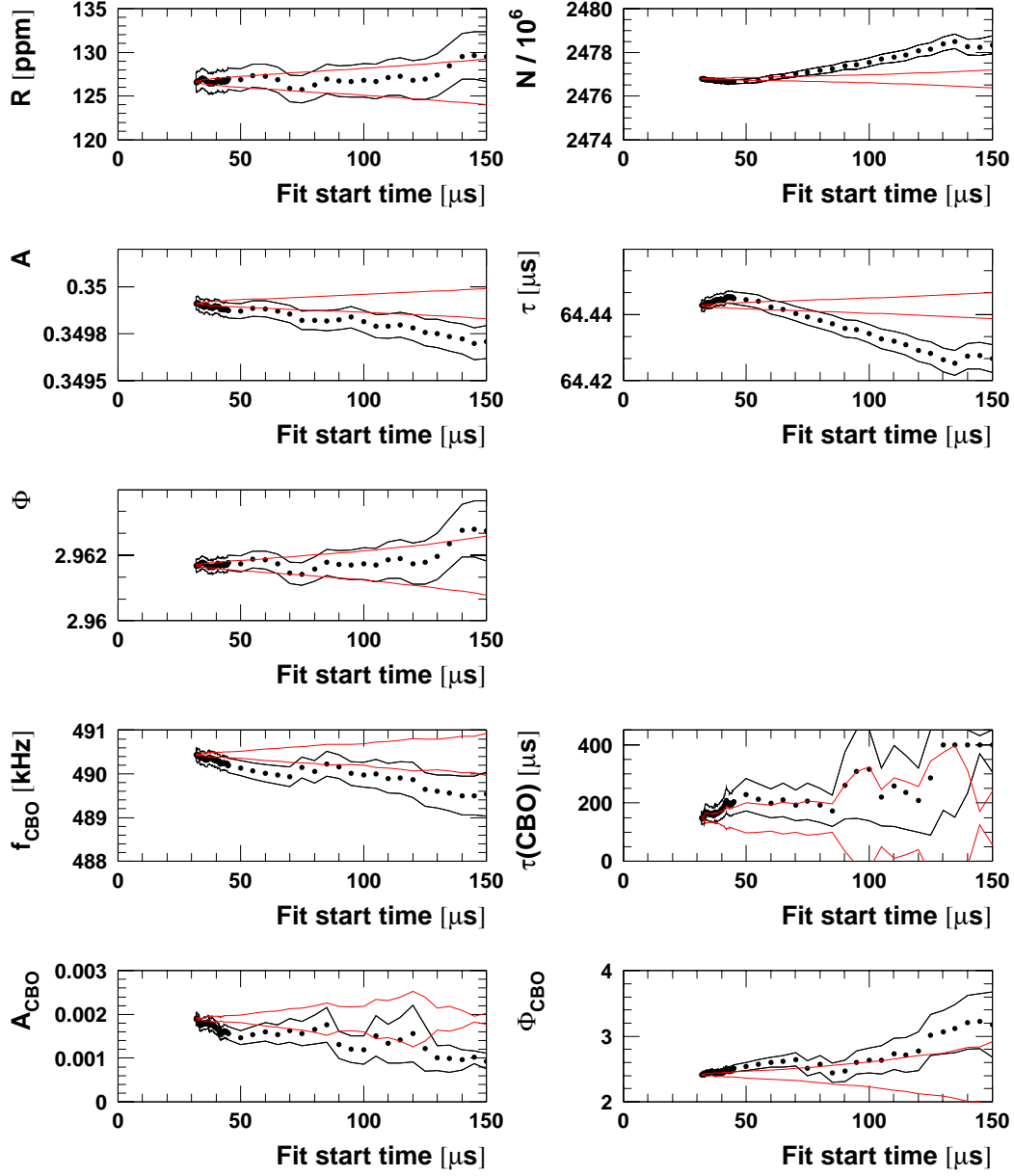
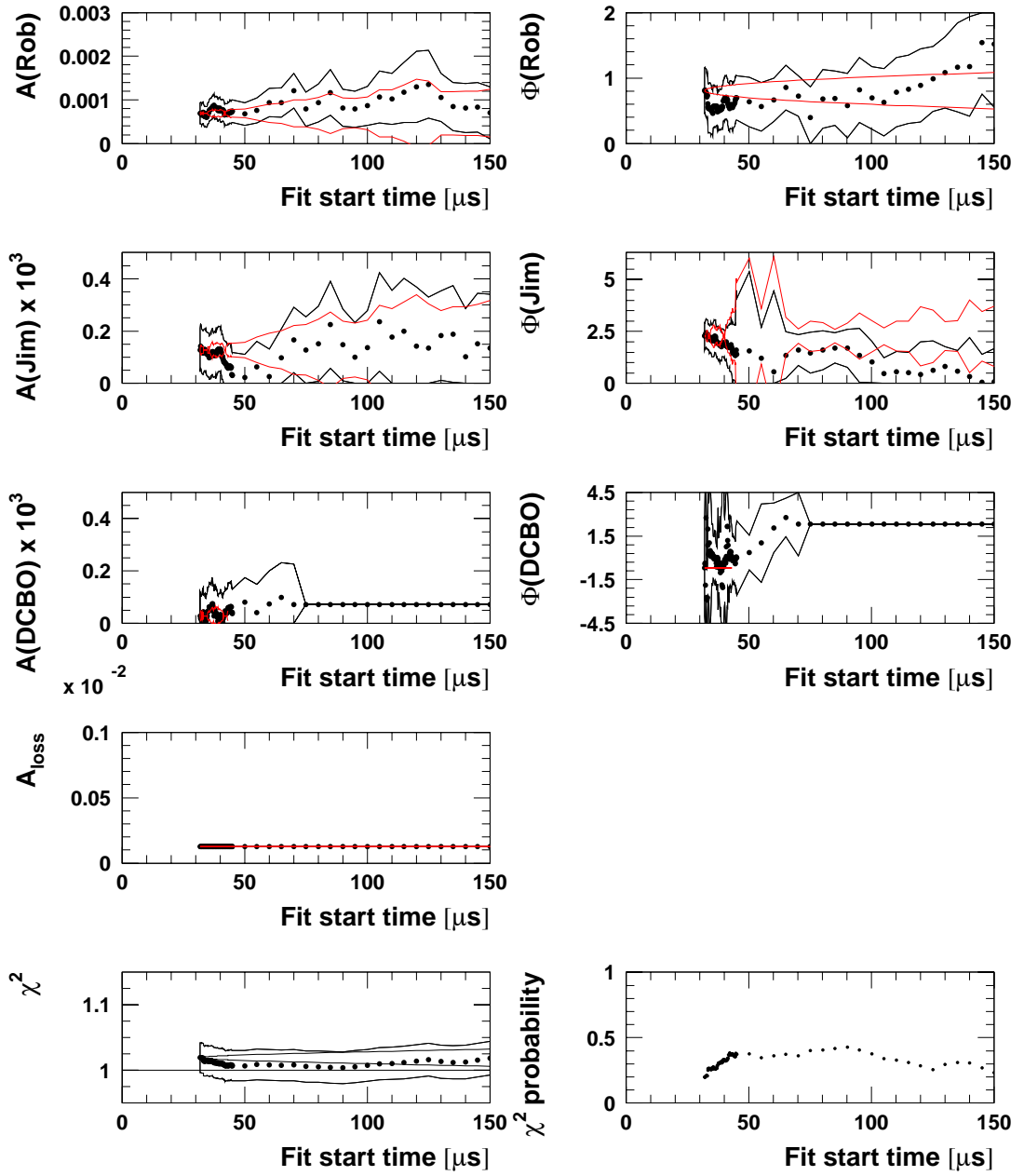


Figure 95: *Start time scan with the full physics function for Set B.*

Full Physics Function, Sum of Detectors, Period B



C.2 Start Time Scans for the Two Half Rings

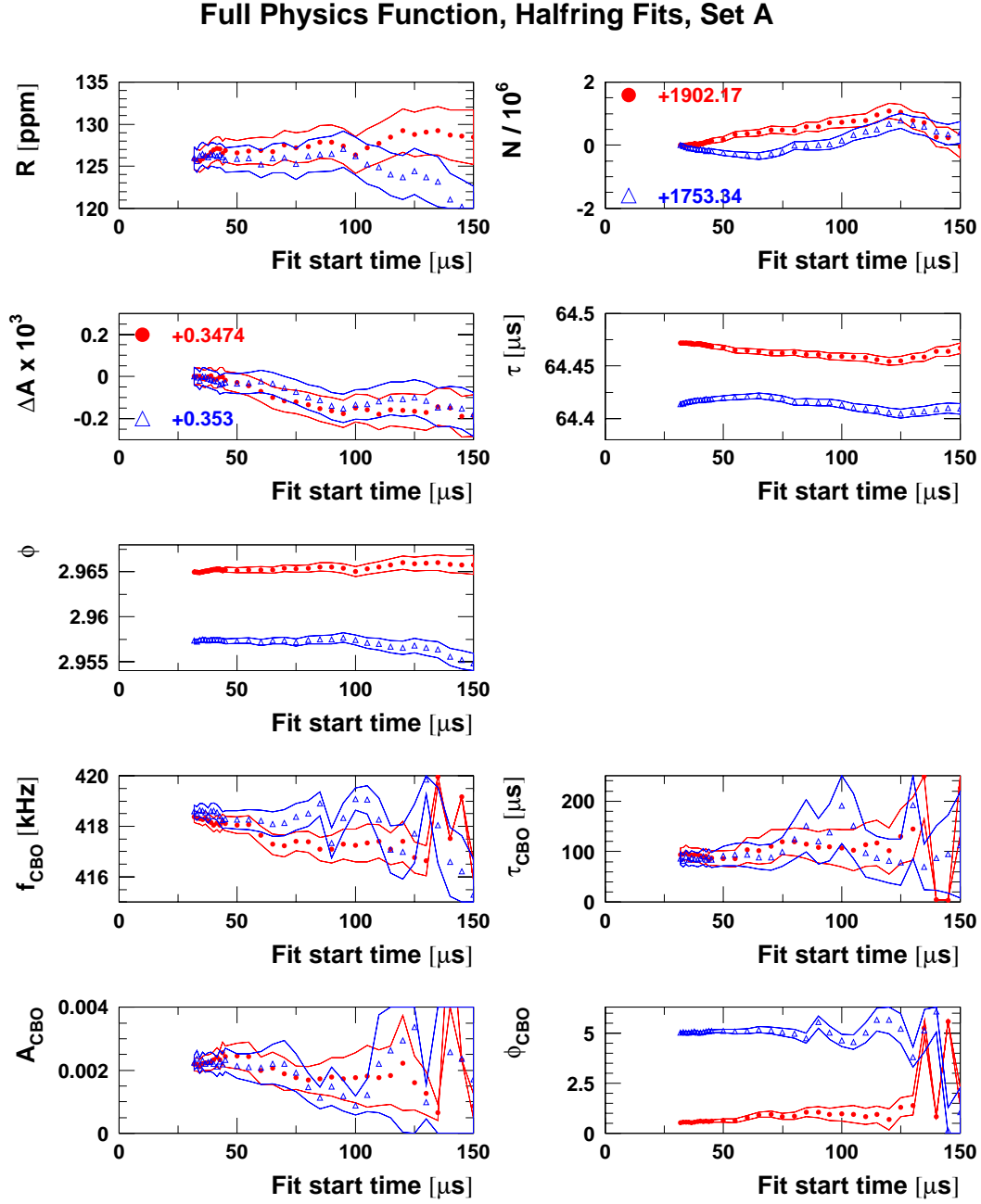
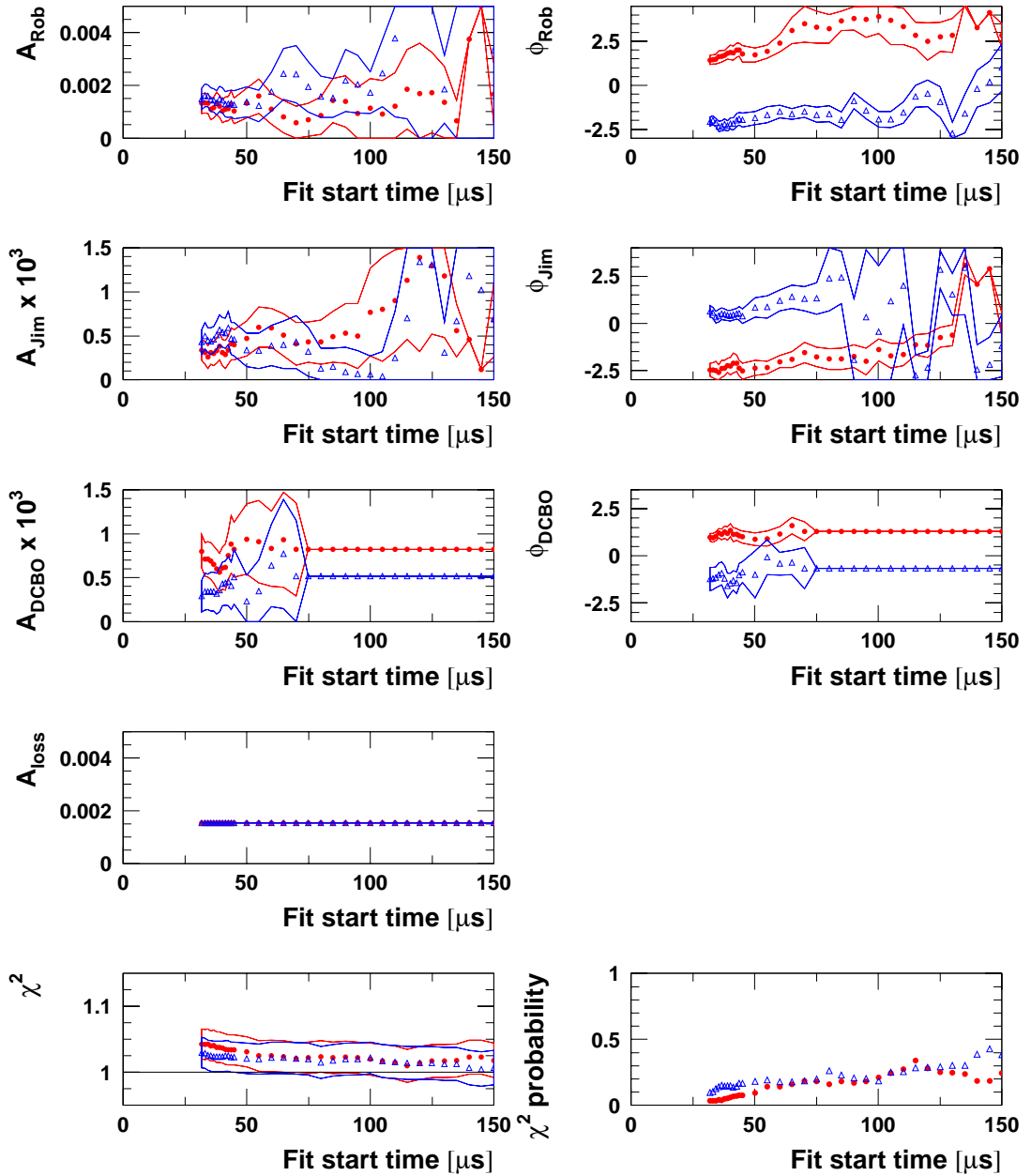


Figure 96: Start time scan for the two half rings separately (red circles = det. 1-12, blue triangles = det. 13-24) with the full physics function for Set A.

Full Physics Function, Halfring Fits, Set A



Full Physics Function, Halfring Fits, Set B

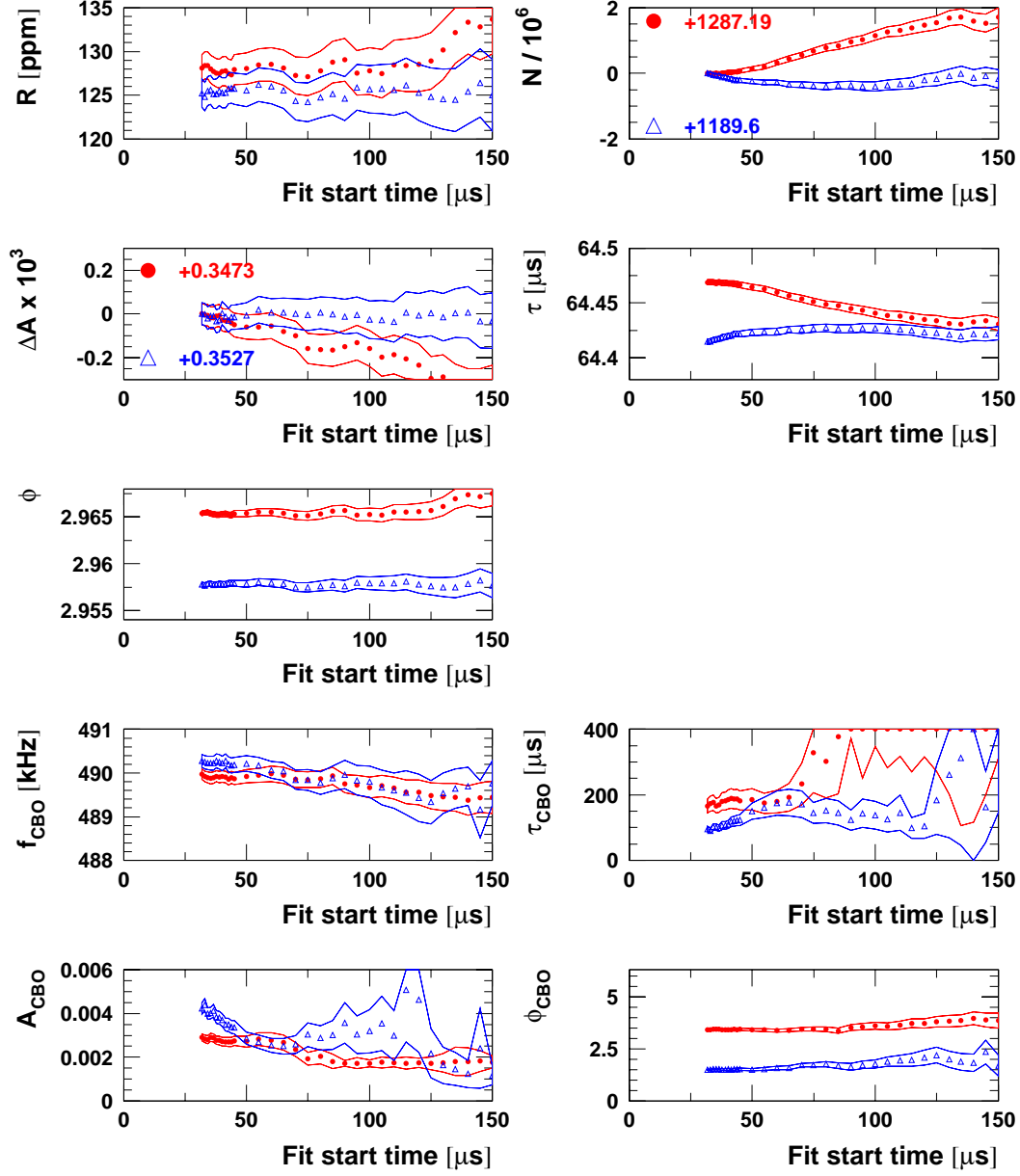
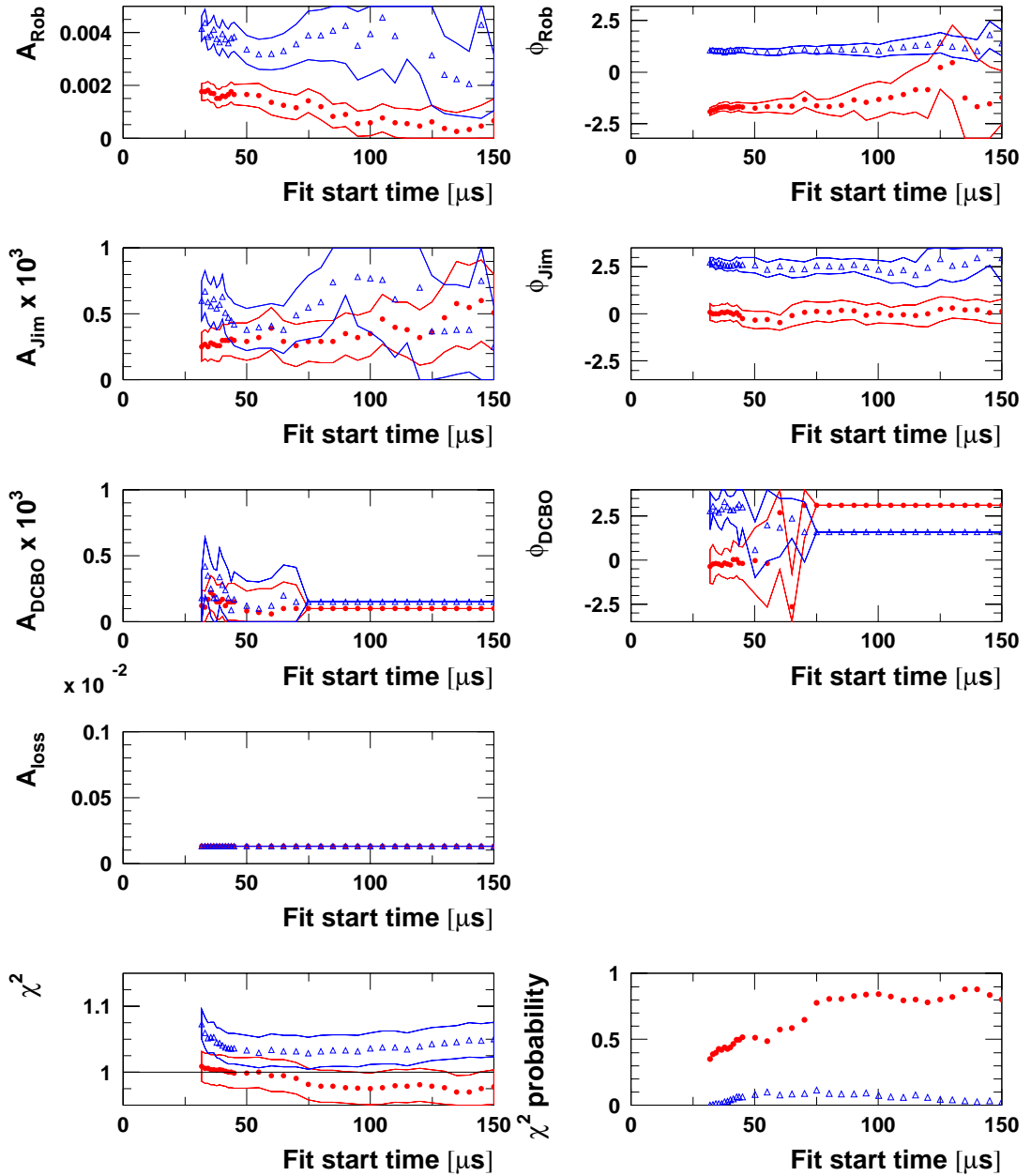
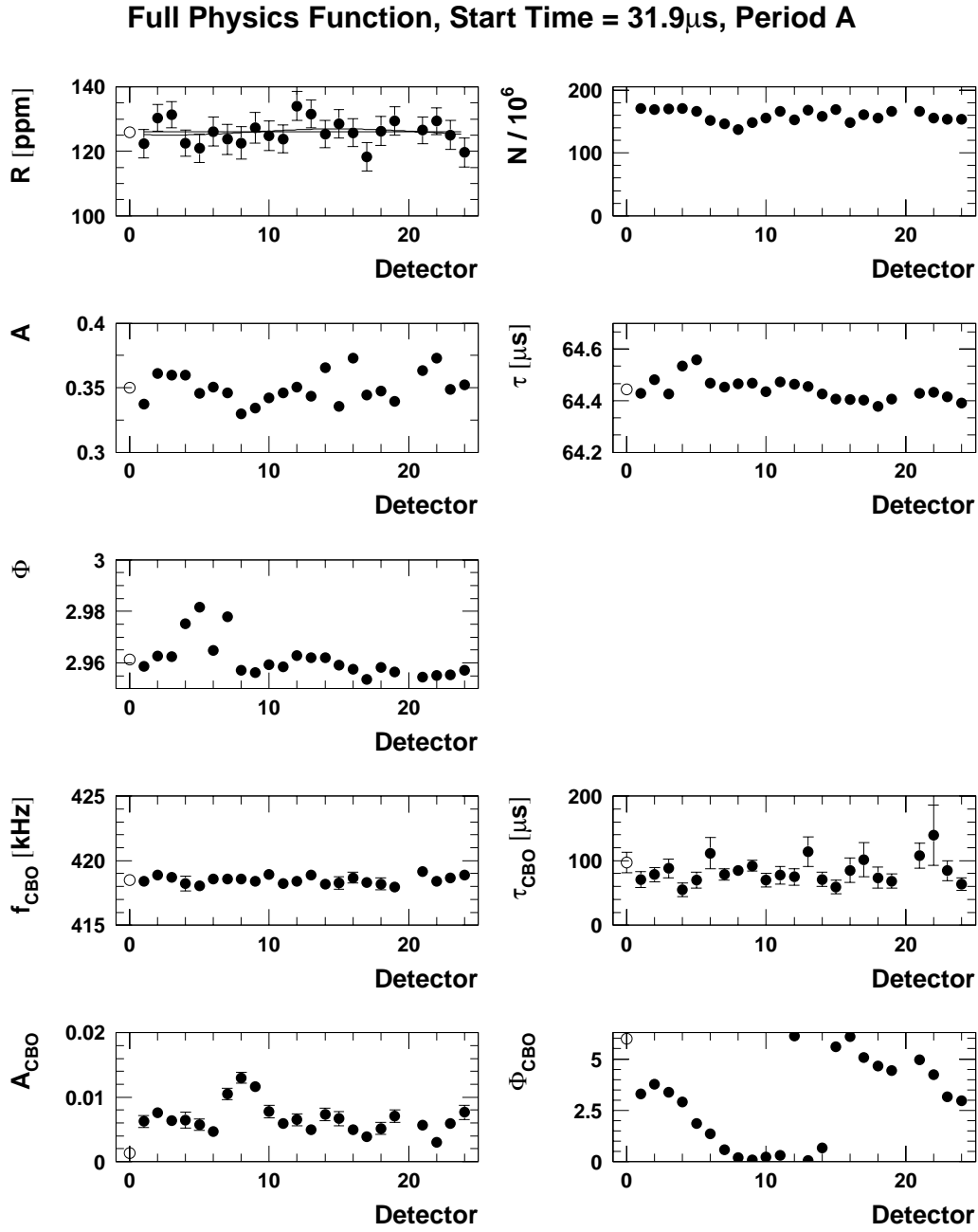
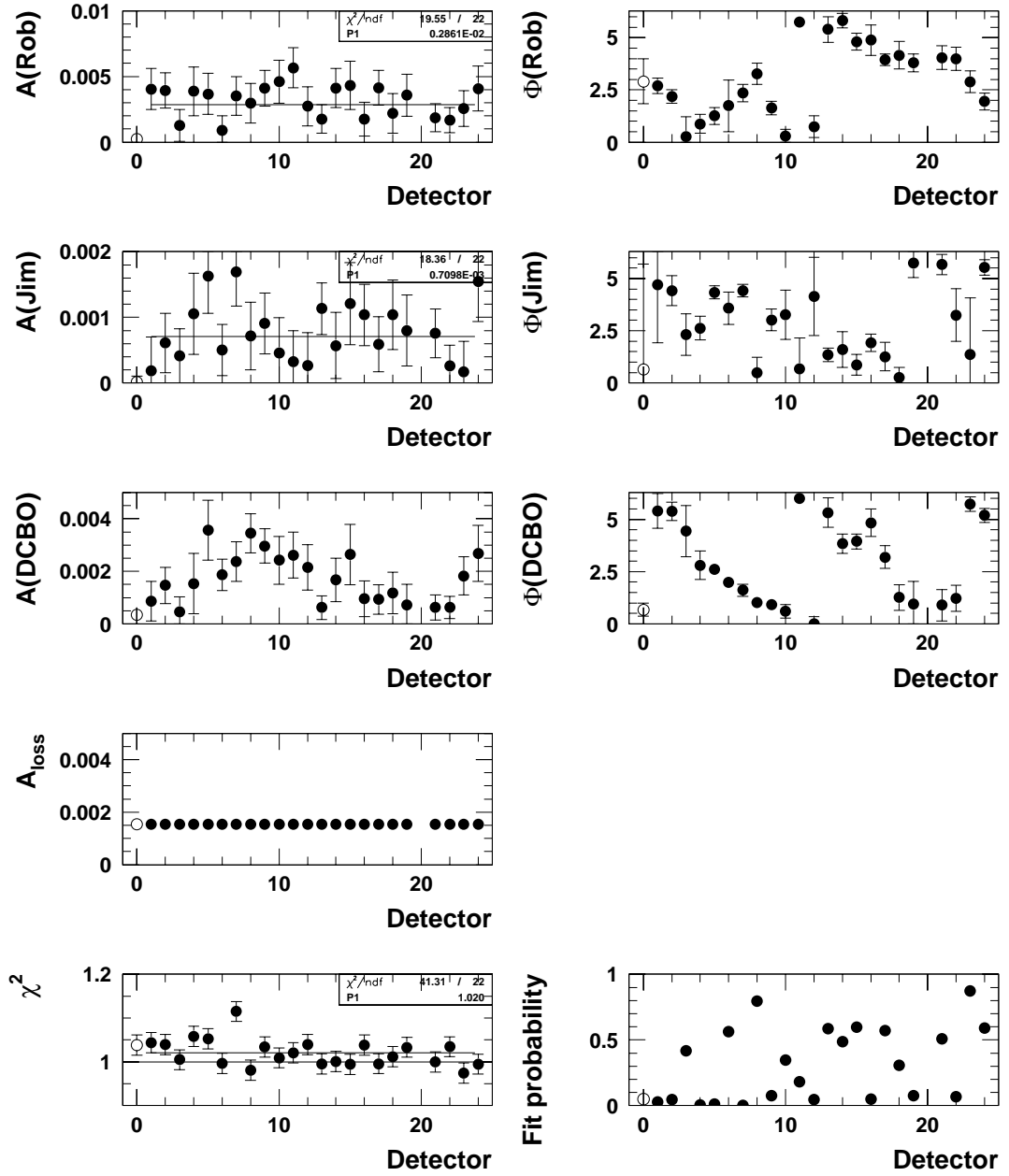


Figure 97: Start time scan for the two half rings separately (red circles = det. 1-12, blue triangles = det. 13-24) with the full physics function for Set B.

Full Physics Function, Halfring Fits, Set B



C.3 Individual Detector Fits Starting at $31.8 \mu\text{s}$ Figure 98: *Fits of individual detector spectra with the full physics function for Set A.*

Full Physics Function, Start Time = 31.9 μ s, Period A

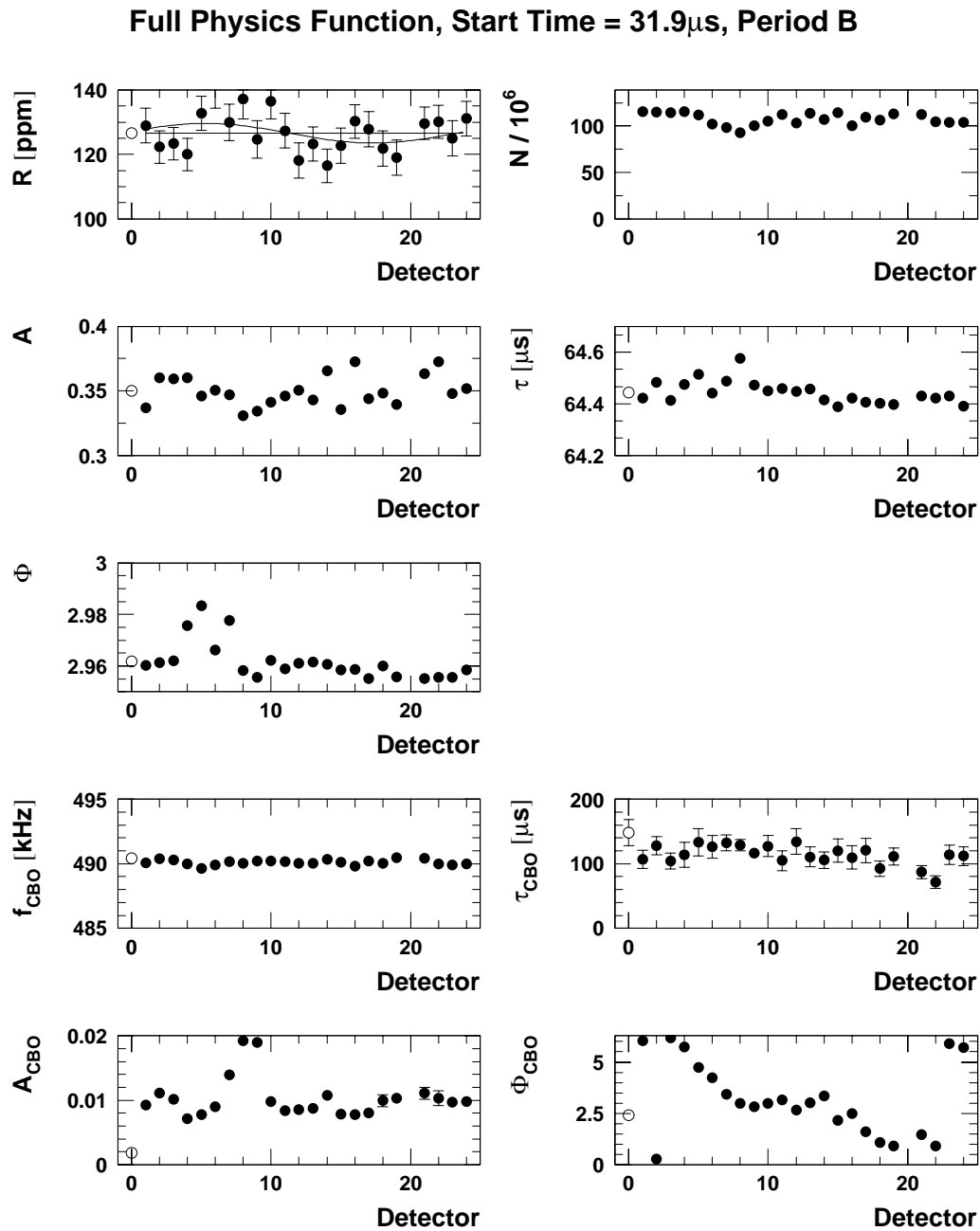
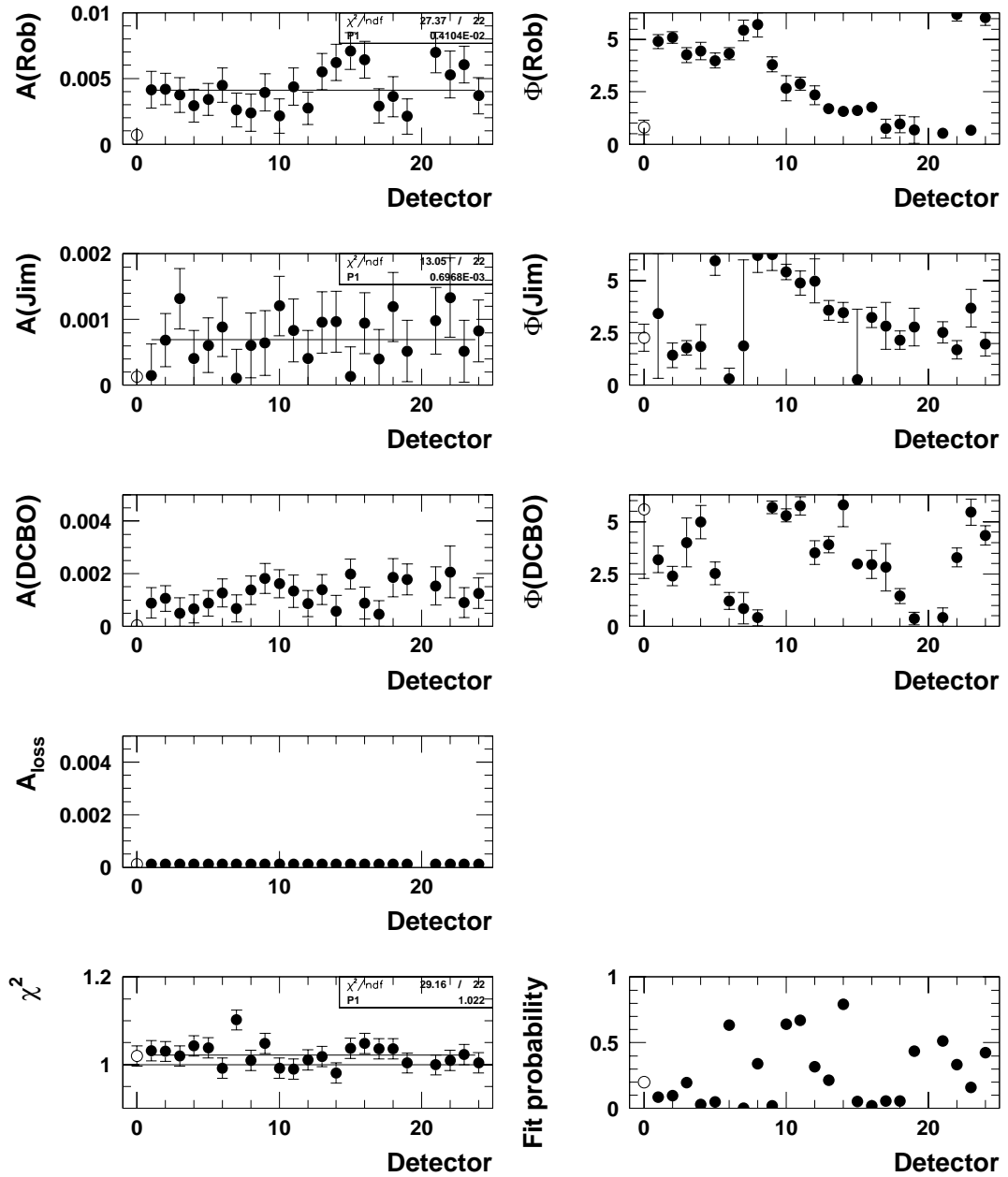


Figure 99: Fits of individual detector spectra with the full physics function for Set B.

Full Physics Function, Start Time = 31.9 μs , Period B

D Results from the Energy-Binned Fits with the Full Physics Function

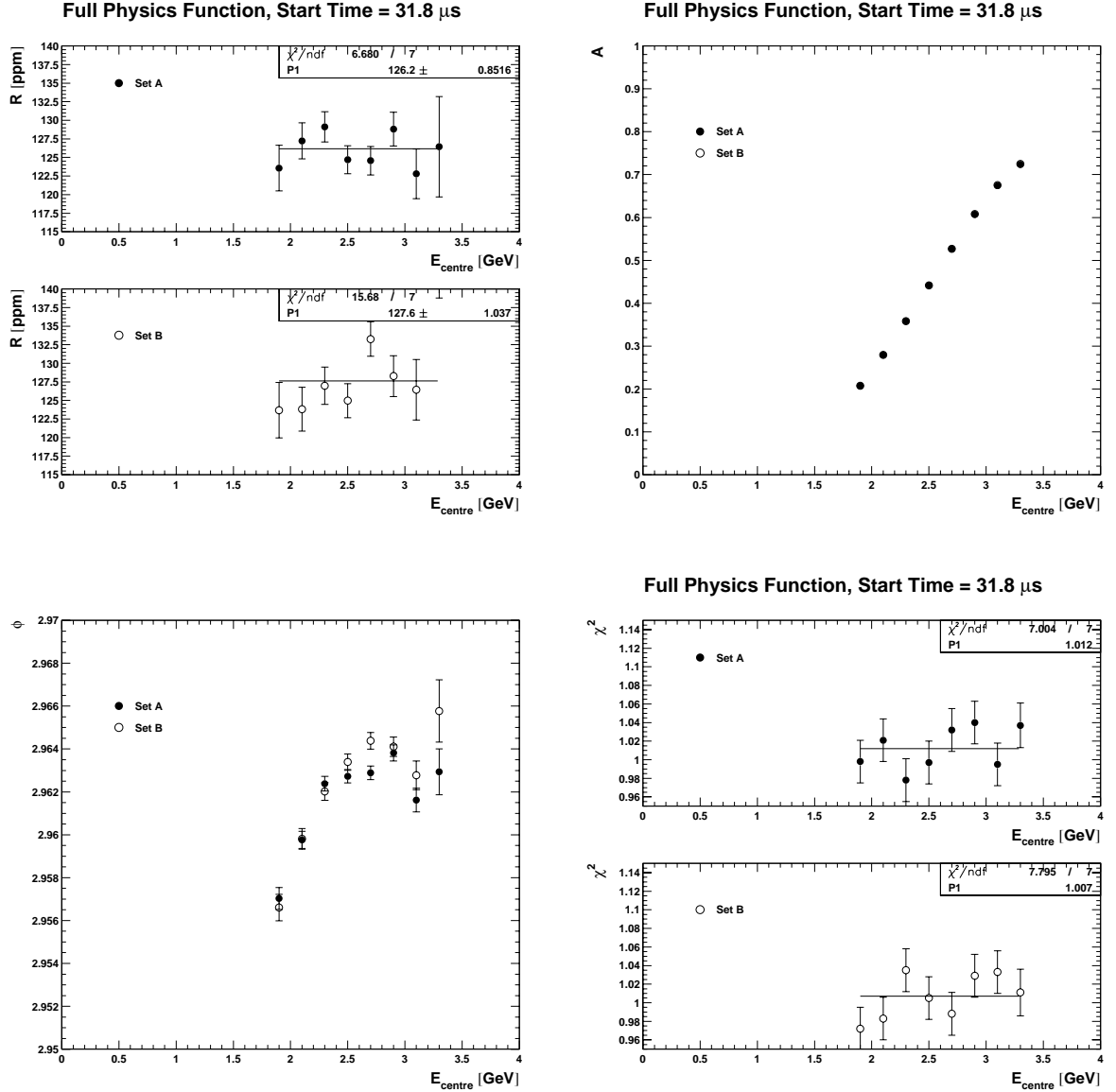


Figure 100: *Fit results versus centre of 200 MeV wide energy bins for a start time of 31.8 μs , performed with the Full Physics Function.*

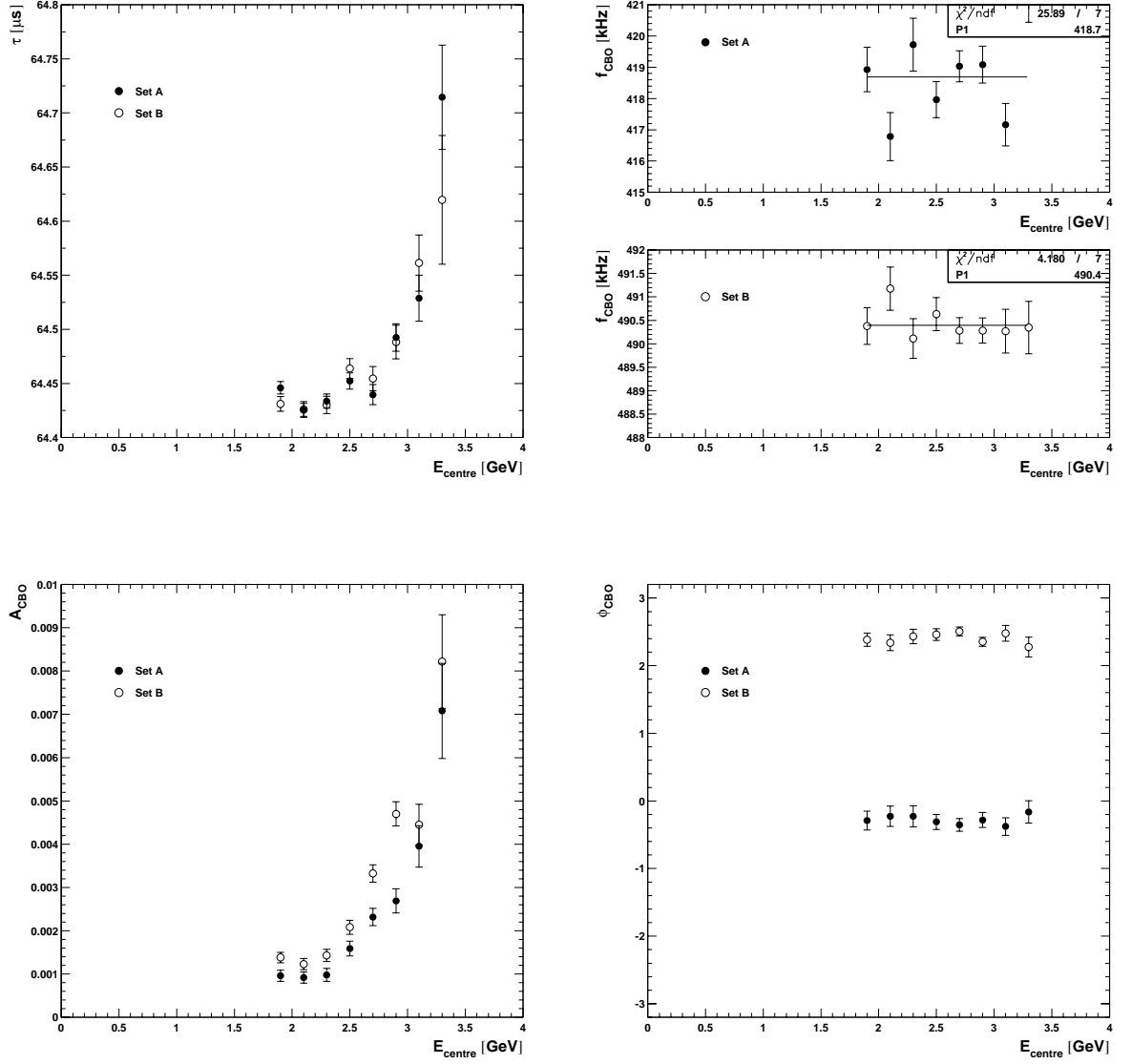


Figure 101: *Fit results versus centre of 200 MeV wide energy bins for a start time of 31.8 μs , performed with the Full Physics Function.*

The instability in f_{CBO} versus E was found to be caused by the inclusion of the asymmetry and phase modulation which are suppressed in narrow energy bins. Fitting with the 1999-style function would be more reasonable in this case.

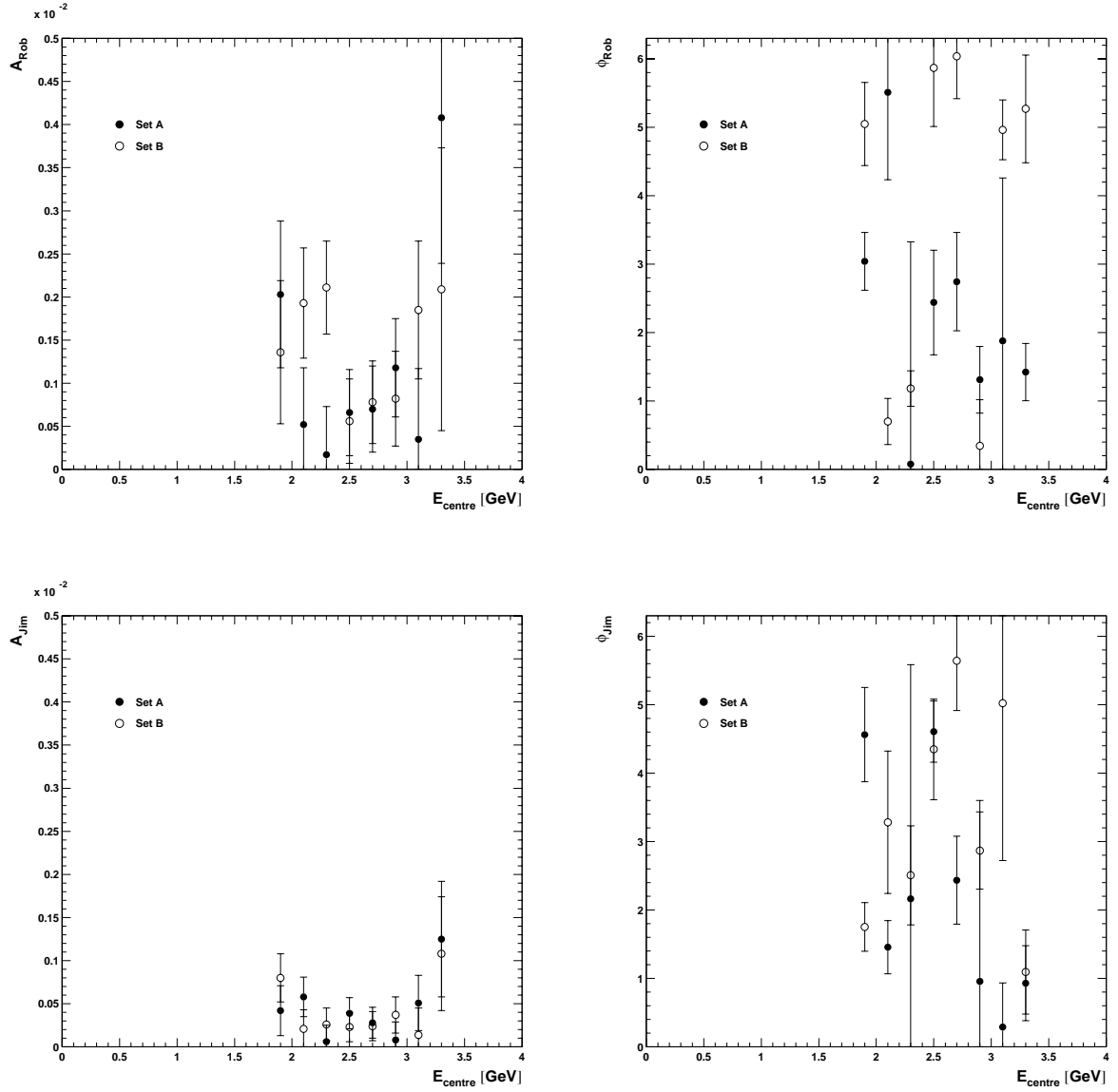


Figure 102: *Fit results versus centre of 200 MeV wide energy bins for a start time of 31.8 μs , performed with the Full Physics Function.*

E Results from the Gain Study

E.1 Average Energy / Gain Sensitivity Factors

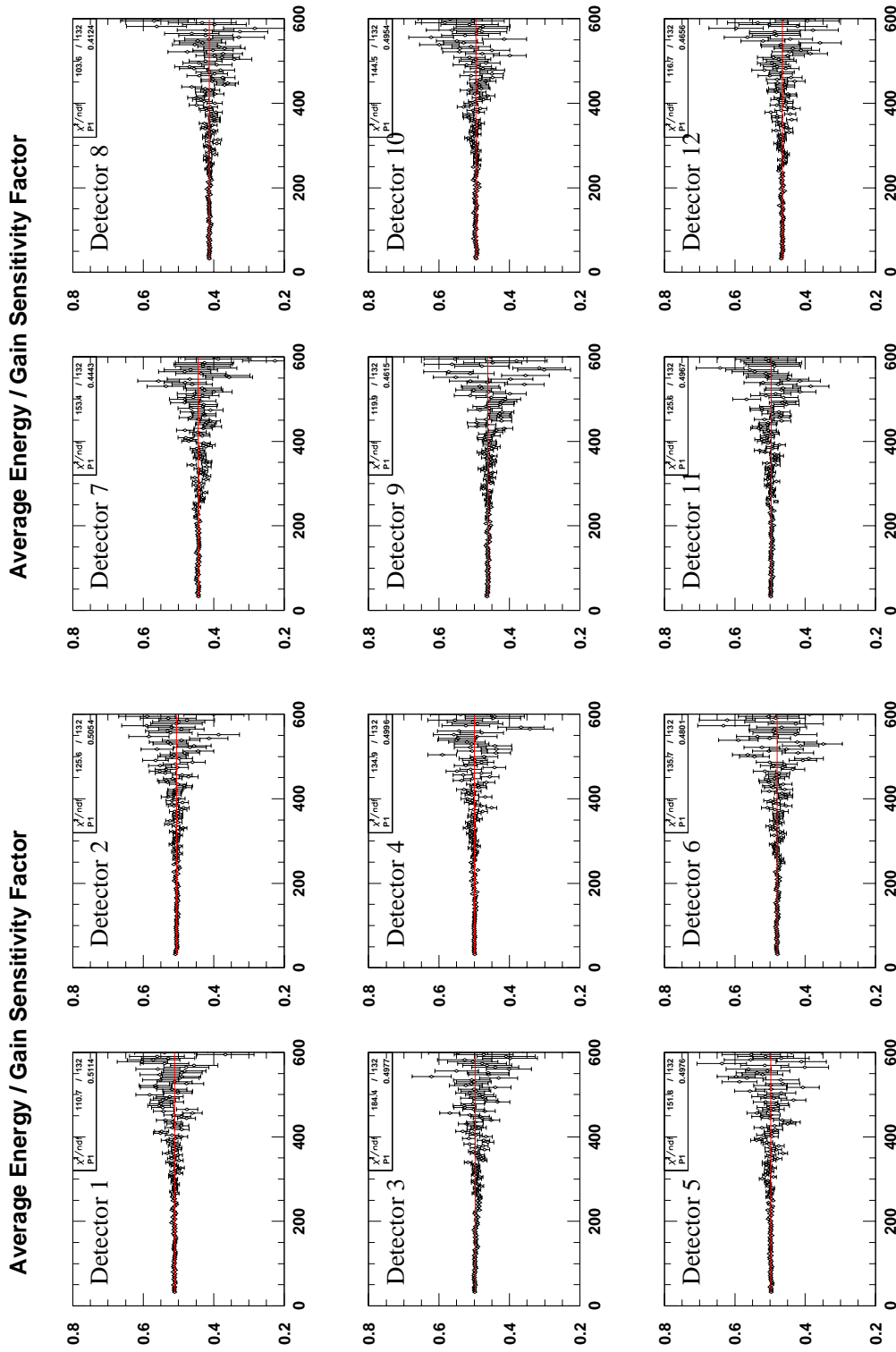


Figure 103: Sensitivity factors for the relation between relative gain change and average energy change for $1.8 \text{ GeV} < E < 3.4 \text{ GeV}$. The two run sets were combined for this study.

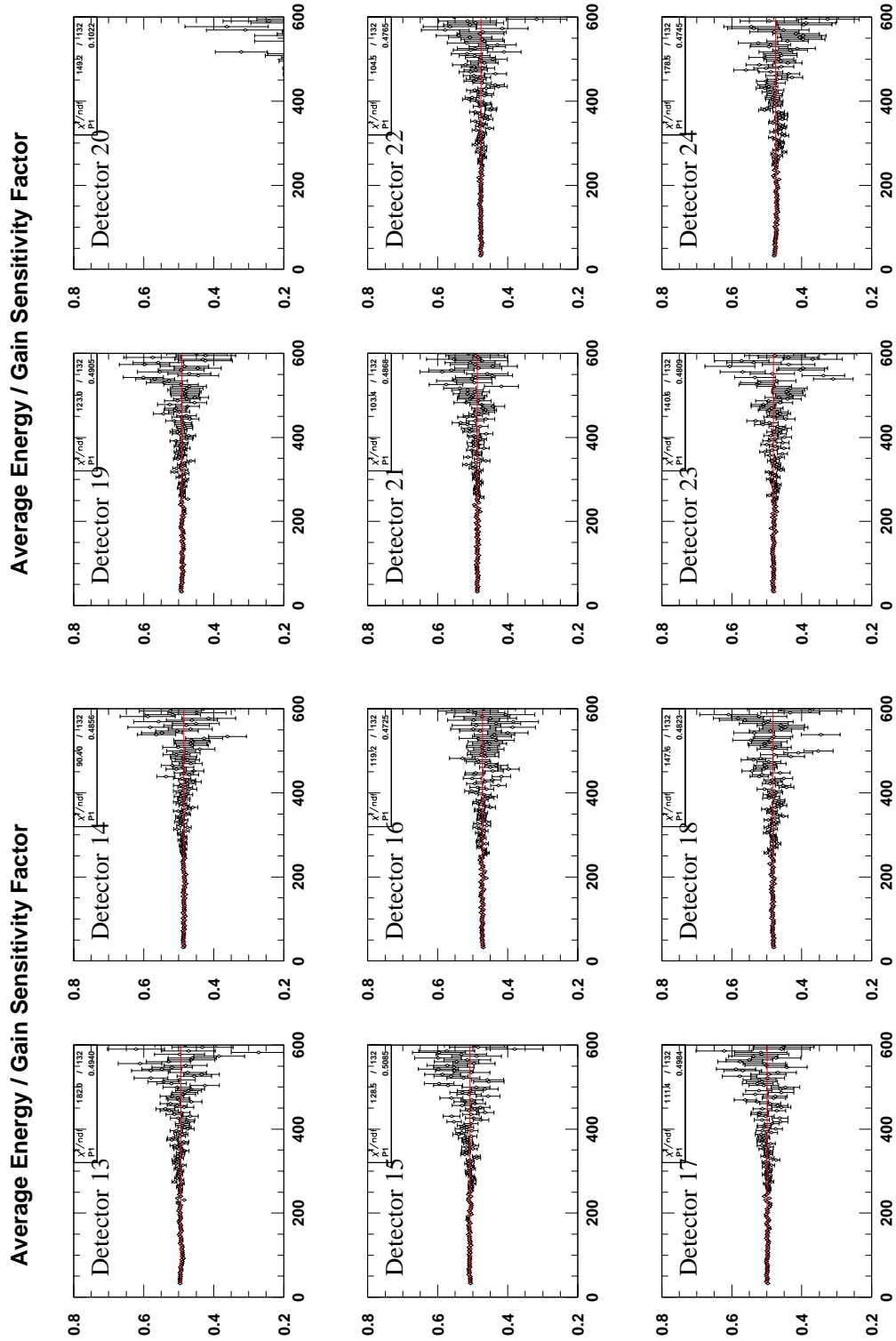
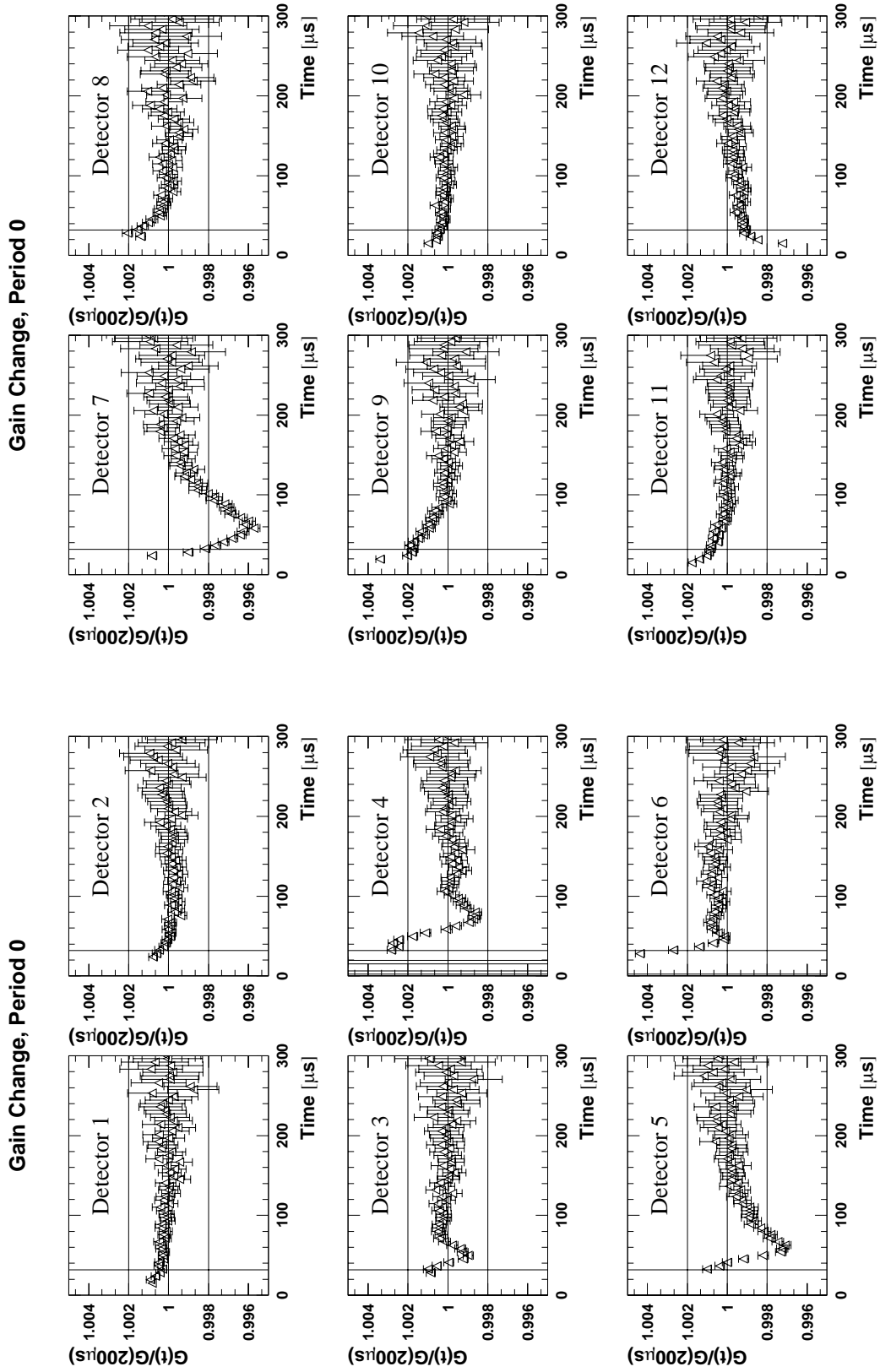


Figure 104: Sensitivity factors for the relation between relative gain change and average energy change for $1.8 \text{ GeV} < E < 3.4 \text{ GeV}$. The two run sets were combined for this study.

E.2 Gain versus Time

Figure 105: *Gain normalised at $200 \mu\text{s}$ for all runs (detectors 1-12).*

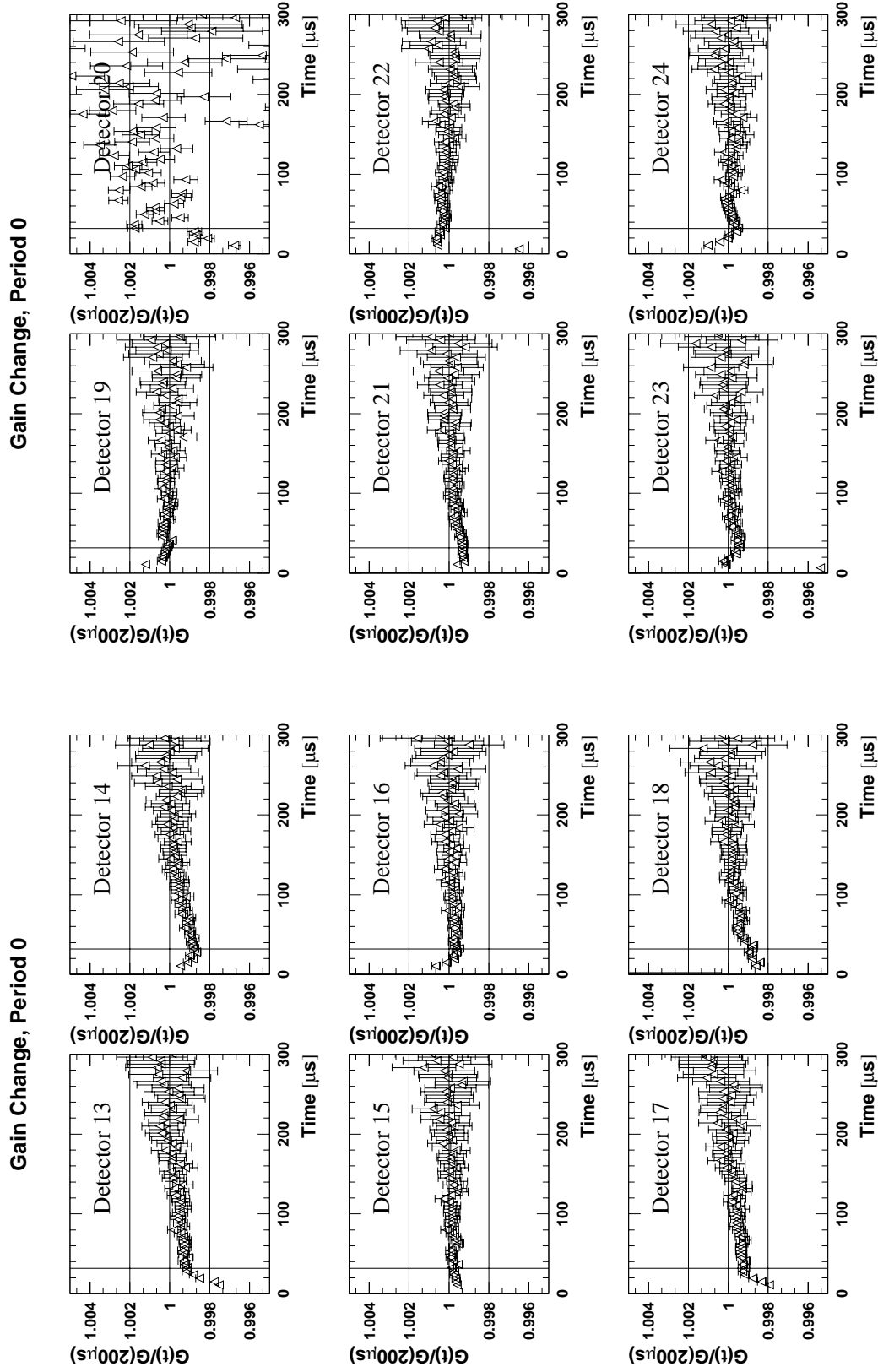


Figure 106: *Gain normalised at 200 μs for all runs (detectors 13-24).*

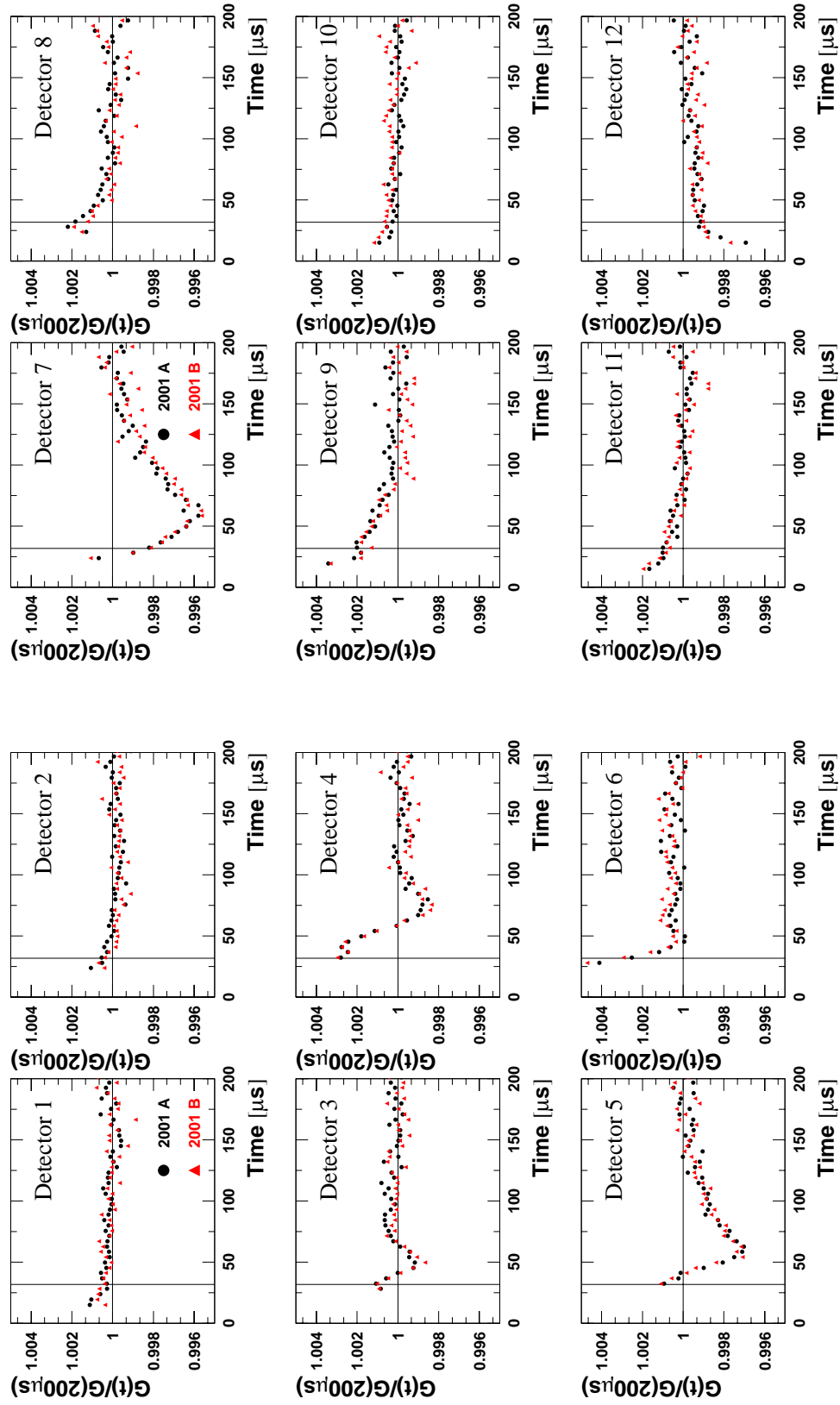


Figure 107: *Gain normalised at $200\mu s$ for Sets A and B separately (detectors 1-12).*

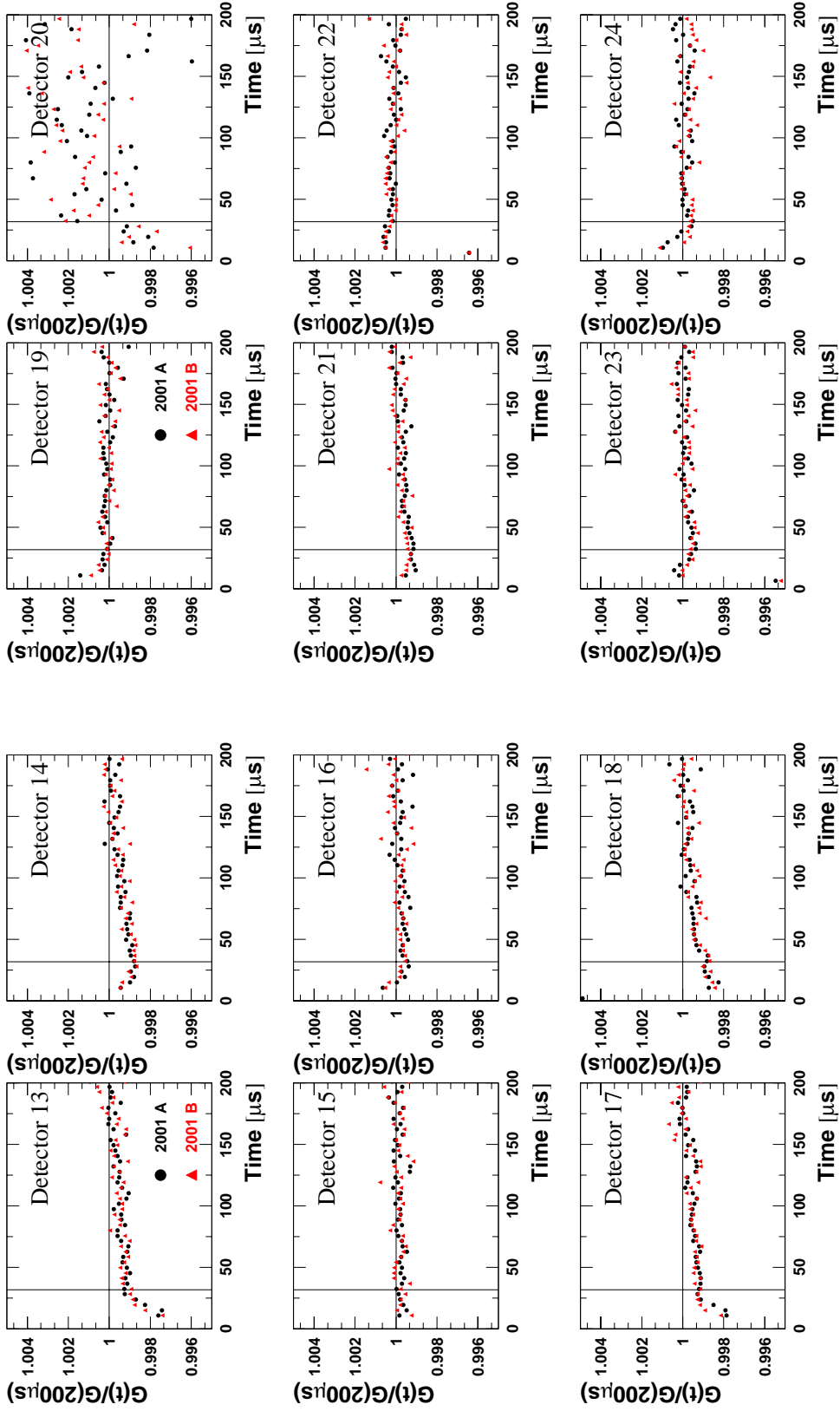


Figure 108: *Gain normalised at 200 μs for Sets A and B separately (detectors 13-24).*

Multiparameter ω_a Analysis of the g-2 Data from 2001

M. Deile
Yale University

April 27, 2003

Version 1.0

Abstract

The present report describes an ω_a analysis for the g-2 data of the run period in the year 2001. The muon spin precession frequency ω_a was determined by fitting a multiparameter function to the combined electron time spectrum from all 23 usable calorimeters in the g-2 ring.

Two fit functions were applied to the data and compared. The first of them neglects the modulations of g-2 asymmetry and phase by coherent betatron oscillations, whereas the second – the so-called full physics function – implements these effects.

In this document the fit results for R are given with our own secret offset. To convert these numbers into the ones with the official offset, you need to subtract 17.91 ppm.

The smallest total uncertainty was obtained with the full physics function. With the official offset the result of this analysis is

$$R = (108.31 \pm 0.71 \pm 0.19) \text{ ppm}.$$

Contents

1	Data Production	4
2	Run Selection and Division into Subsets	4
3	Fill Selection	4
3.1	Quadrupole Cuts	4
3.2	T0 Cuts	7
3.3	Laser Cut	7
4	Construction of the Electron Decay Time Spectra	8
4.1	Energy calibration	8
4.2	T0 subtraction	8
4.3	Binning and Randomisation	8
4.4	Pileup Subtraction	8
4.5	Energy Scale Correction	12
4.6	Electrons after Pileup Subtraction	12
5	Fit of the Time Spectra	13
5.1	Fourier Spectra after 5-Parameter Fits	13
5.2	Fit Function	15
5.2.1	Overview	15
5.2.2	Free and Fixed Fit Parameters	17
5.2.3	The CBO Envelope	18
5.2.4	Implementation of the Muon Loss Function	18
5.3	Fit Procedure	20
5.4	Fit Results	24
5.4.1	Fits without Asymmetry/Phase Modulation (1999 Style)	24
5.4.2	Fits with Asymmetry Modulation but without Phase Modulation	33
5.4.3	Fits with Asymmetry and Phase Modulation	41
5.4.4	Energy-Binned Fits with the Full Physics Function	51
5.4.5	Comparison of Fit Results with Different Functions	58
6	Systematic Errors at 31.8 μs Fit Start Time	60
6.1	Time-Varying CBO Frequency	60
6.2	Main (Acceptance) CBO	64
6.3	Acceptance Double CBO	66
6.4	Asymmetry and Phase CBO – Half-Ring Effect	68
6.4.1	1999-Style Function	68
6.4.2	Full Physics Function	70
6.5	Residual Pileup	72
6.5.1	Residual Pileup Fraction from Early and Late Energy Spectra	72
6.5.2	Influence of Residual Pileup on R	74
6.5.3	Shift in R due to the Pileup Phase (Underwater Effect)	75
6.5.4	Unseen Pileup	75
6.6	Gain Changes and Residual Slow Effects	77
6.6.1	Gain Correction with Upper Energy Cut	77
6.6.2	Artificial Enhancement of Gain Variations	80
6.6.3	Effects of an R.S.E. Term	86
6.7	Investigation of the Asymmetry Instability by Energy-Binned Fits	89

6.8	Muon losses	96
6.9	Binning Effects	97
6.10	Randomisation	98
7	Summary	101
7.1	Systematic Error Table	101
7.2	Combined Result from the two Run Sets	102
7.2.1	Averaging Central Values and Systematic Errors with Statistical Weights	102
7.2.2	Optimal Weighting including Correlations of Systematic Errors . . .	102
7.2.3	Purely Statistical Weights but Error Analysis with Correlations . . .	103
7.2.4	Preferred Result	104
A	Fit Results for the 1999-Style Function	106
A.1	Start Time Scans for the Sum of Detectors	106
A.2	Start Time Scans for the Two Half Rings	110
A.3	Individual Detector Fits Starting at $31.8\ \mu\text{s}$	114
B	Fit Results for the Physics Function without Phase Modulation	118
B.1	Start Time Scans for the Sum of Detectors	118
B.2	Start Time Scans for the Two Half Rings	122
B.3	Individual Detector Fits Starting at $31.8\ \mu\text{s}$	126
C	Fit Results for the Full Physics Function	130
C.1	Start Time Scans for the Sum of Detectors	130
C.2	Start Time Scans for the Two Half Rings	134
C.3	Individual Detector Fits Starting at $31.8\ \mu\text{s}$	138
D	Results from the Energy-Binned Fits with the Full Physics Function	142
E	Results from the Gain Study	145
E.1	Average Energy / Gain Sensitivity Factors	145
E.2	Gain versus Time	147

1 Data Production

This analysis is based on the g2off data production [2].

2 Run Selection and Division into Subsets

The run selection by C. Polly and X. Huang [3] with field input from E. Sichtermann – with some further modifications by E. Sichtermann and myself – was used. Runs with low kicker amplitude ($< 97\%$) were discarded while runs with a scraping amplitude of 4 kV instead of 7 kV were kept. Both scraping times used ($7\mu\text{s}$ and $15\mu\text{s}$) were kept.

The data set was divided in two parts reflecting the two quadrupole voltages 21.7 kV and 25.3 kV which result in very distinct coherent betatron oscillation frequencies (418.4 kHz and 490.3 kHz respectively). The run periods constituting the two data sub-sets are defined in Table 1.

Subset	Runs	V_{Quad} [kV]	Comments
A	9423 - 9754	21.7	B_r changed
B	9755 - 9989	25.3	
A	9990 - 10272	21.7	
B	10273 - 10710	25.3	
A	10711 - 10780	21.7	
A	10788 - 10963	21.7	
B	10964 - 11019	25.3	
A	11026 - 11356	21.7	
B	11357 - 11384	25.3	
0	all runs	–	

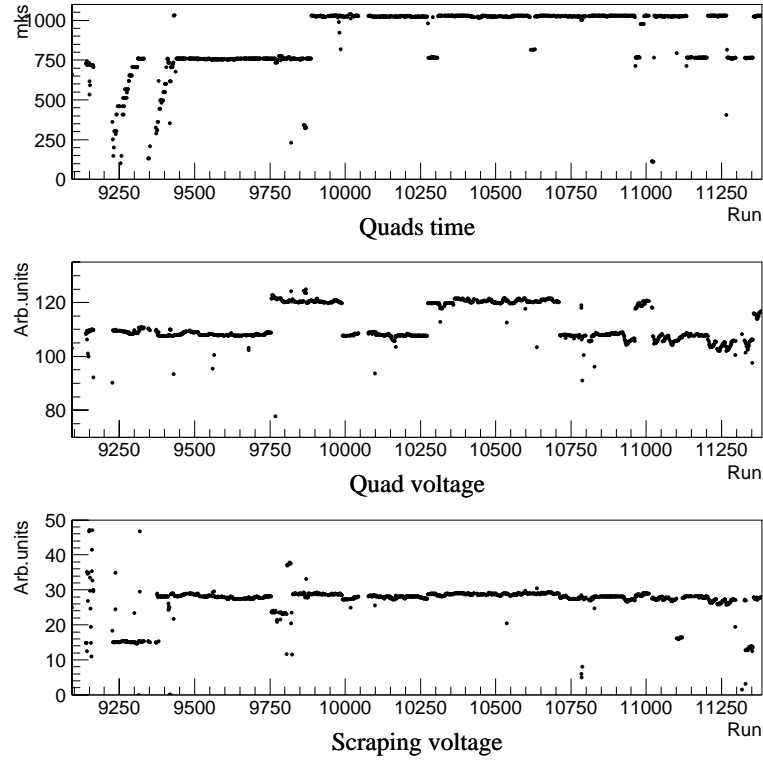
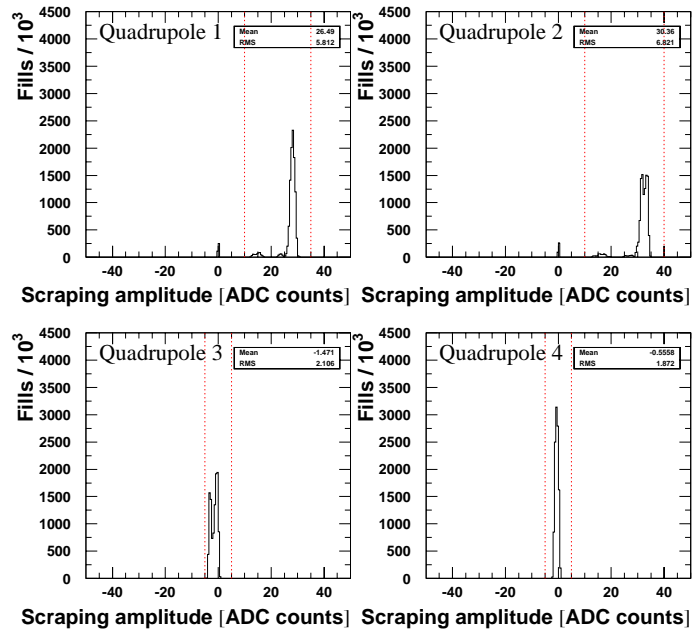
Table 1: *Run periods and the reasons for their distinction.*

3 Fill Selection

3.1 Quadrupole Cuts

A fill passes the quadrupole selection if the following criteria are met:

- The quadrupoles are on for at least $600\mu\text{s}$ after injection. The distribution of quadrupole switch-off times is shown in Figure 1.
- The scraping amplitudes (second minus first quadrupole voltage reading) must be within the limits shown in Figure 2.
- The second and third quadrupole reading must be equal within the limits shown in Figure 3. This requirement discards fills with quadrupole sparks.
- The individual quadrupole readings must lie within $5 \times \text{RMS}$ of their distributions.

Figure 1: *CBO parameters versus run.*Figure 2: *Distribution of the scraping amplitudes in the four quadrupoles. The dotted lines represent the cuts applied.*

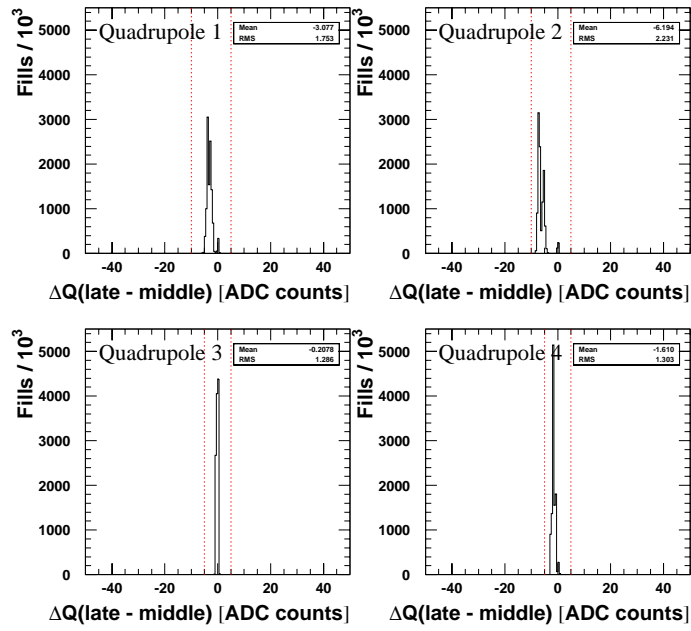


Figure 3: *Distribution of the difference between the third and the second voltage measurement in the four quadrupoles. The dotted lines represent the cuts applied.*

3.2 T0 Cuts

T0 cuts were derived from the distributions of T0 pulse amplitudes and mean times. Outlier fills are discarded.

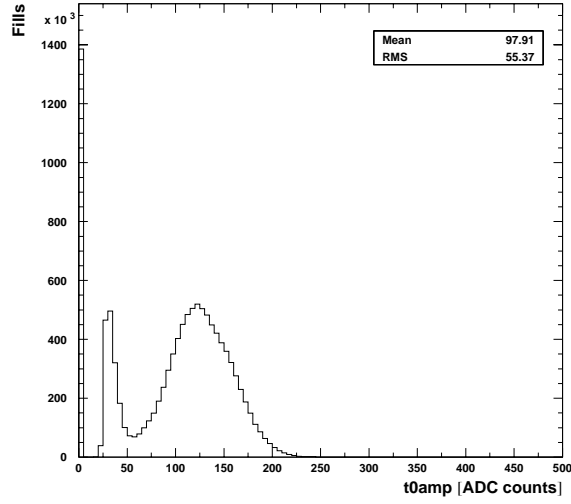


Figure 4: *Distribution of the T0 pulse amplitude. Each entry corresponds to one fill.*

- The pulse amplitude is required to be greater than 10 (see Figure 4).
- The pulse mean time must lie between 59000 ns and 59500 ns (Figure 5). This cut is not very tight and mainly designed for discarding fills without T0 pulse (**t0mean** = 0).

3.3 Laser Cut

Fills with laser pulses in the analysed time window (20 μ s to 600 μ s) were discarded.

4 Construction of the Electron Decay Time Spectra

4.1 Energy calibration

Energy-spectrum end-points (corresponding to 3.2 GeV) were determined for each run by straight-line fits to the trailing parts of the energy spectra later than $200\,\mu\text{s}$. The raw run-by-run end-points were then plotted as a function of the run number and fitted to straight lines in run intervals.

4.2 T0 subtraction

To obtain the electron pulse times with respect to the T0 pulse, the mean time of the T0 pulse (ntuple variable **t0mean**) was subtracted from the raw pulse times.

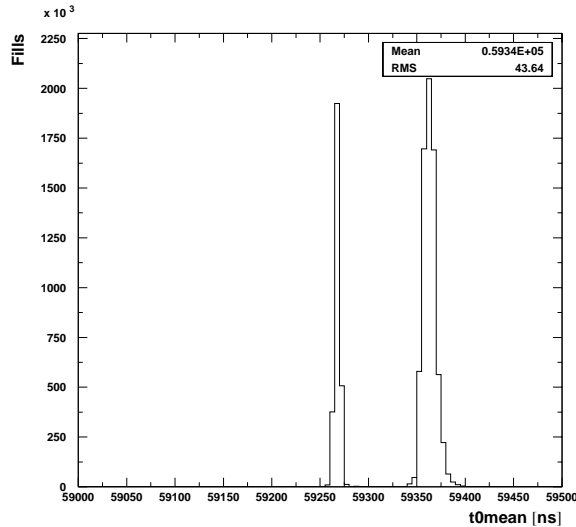


Figure 5: *Distributions of the mean time of the T0 pulse. Each entry corresponds to one fill. There are two peaks because after run 10827 the G10 kicker timing changed.*

4.3 Binning and Randomisation

For each detector and each run a time spectrum was created. The bin width of the time spectra was 149.2 ns, i.e. the fast rotation period determined by A. Lam with a Fourier analysis [4]. Before filling the individual electron times into their histograms, they were randomised by adding a fill-specific random number taken from a flat distribution in the range $[-\frac{149.2\,\text{ns}}{2}, +\frac{149.2\,\text{ns}}{2}]$. This was done to remove the fast rotation structure from the data.

4.4 Pileup Subtraction

Pileup was subtracted with the ‘‘Mediterranean Method’’ [5]. The lower energy cut was 1.8 GeV.

The time window where shadow pulses (‘‘S2’’) for the construction of the artificial pileup were looked for, had its centre 13 ns after the trigger pulse (‘‘S1’’). The window width was twice the g2off pulse fitter dead-time. This dead-time is detector-specific and depends on the energy E_{S2} of the shadow pulse. It is typically about 2.9 ns. The detector

and energy dependence of the dead-time (Figure 6) was provided by Vanya [6] who had obtained them from a simulation.

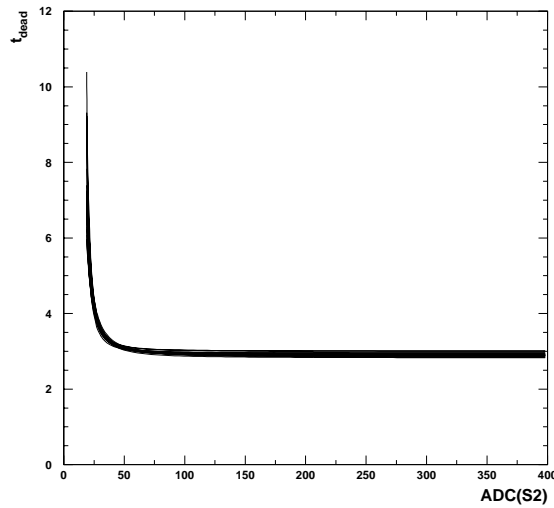


Figure 6: *Dead-time of the pulse finding algorithm as a function of the pulse height of S2 in terms of ADC counts. The conversion from ADC to energy is detector dependent (Section 4.1). Typically $ADC = 60$ corresponds to 1 GeV. The curves for all detectors are superimposed.*

Also, the energy E_D of a constructed double pulse was calculated from the energies E_{S1} and E_{S2} of the two individual overlapping pulses, using Vanya’s simulation results:

$$E_D = f_L(E_{S1}, E_{S2}) \cdot (E_{S1} + E_{S2}) \quad , \quad (1)$$

where the function $f_L(E_{S1}, E_{S2})$ replaces the constant “Logashenko coefficient” of 0.96 which had been used in the past. This function is shown in Figures 7 and 8.

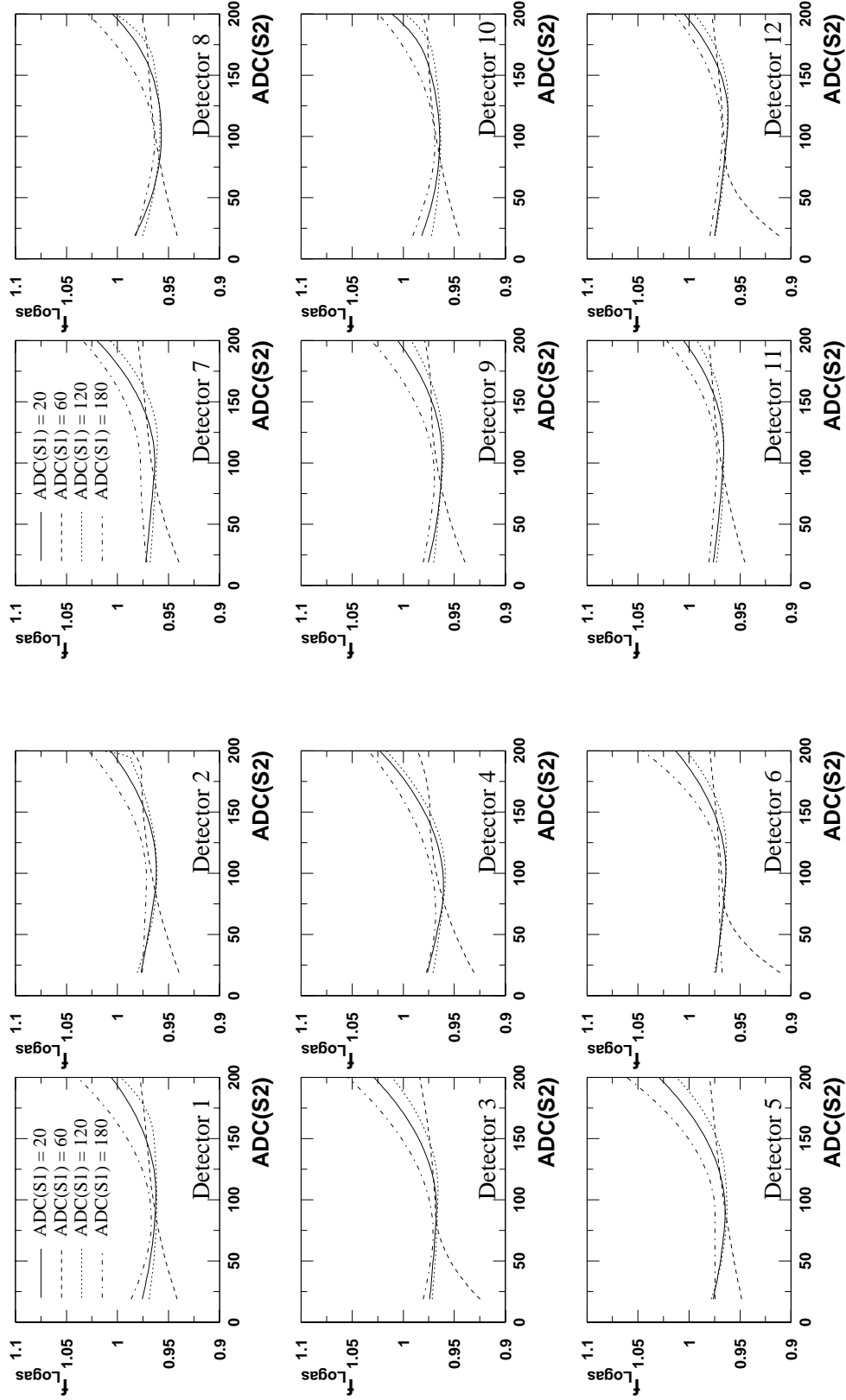


Figure 7: Logashenko function for detectors 1 to 12. Typically $ADC = 60$ corresponds to 1 GeV .

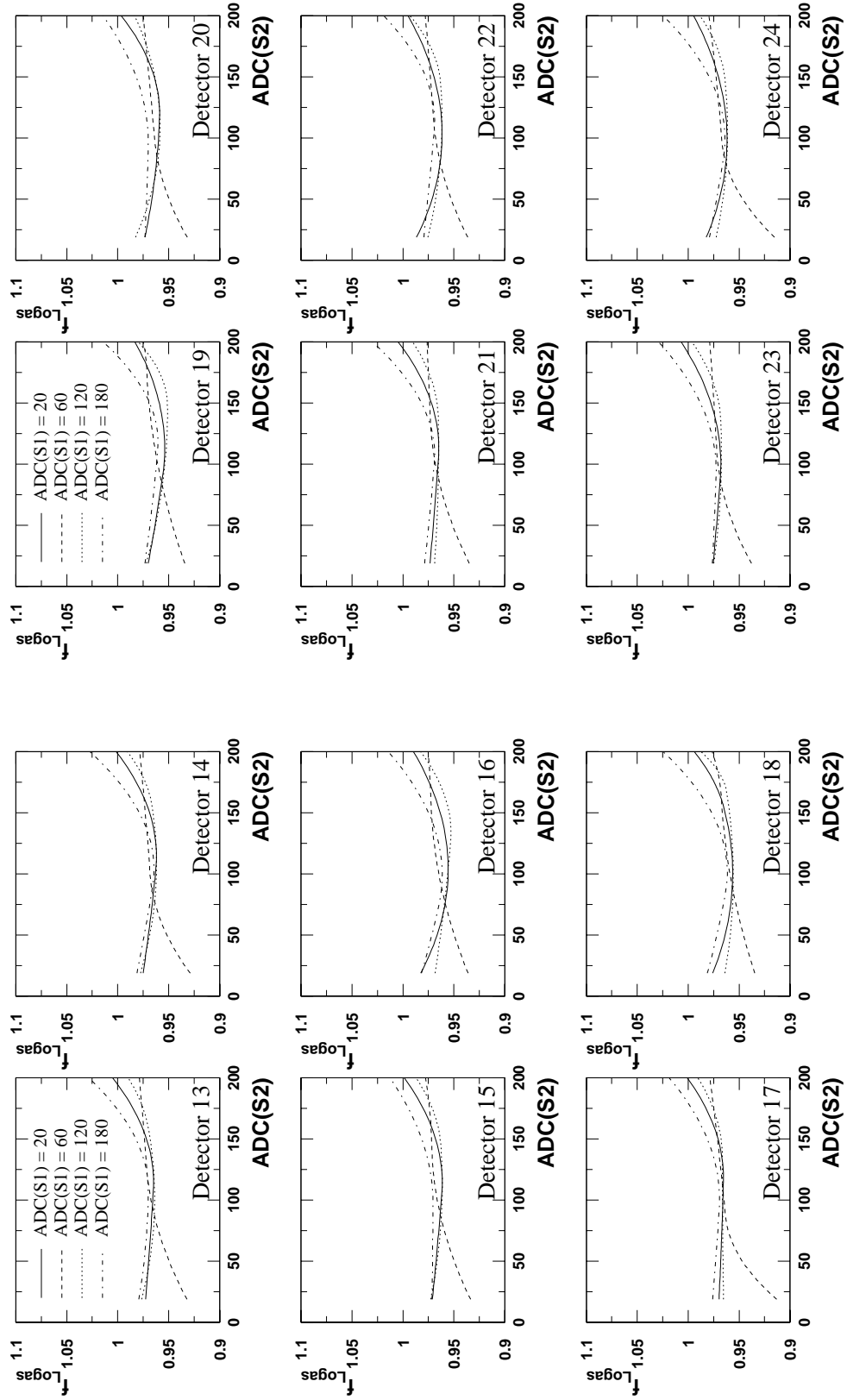


Figure 8: *Logashenko function for detectors 13 to 24. Typically $\text{ADC} = 60$ corresponds to 1 GeV .*

4.5 Energy Scale Correction

Gain variations were corrected for by using the time evolution of the average energy between 1.8 GeV and 3.4 GeV. Method and impact on the fit results are explained in Section 6.6.

4.6 Electrons after Pileup Subtraction

The final number of analysable electrons per detector between $31.8 \mu\text{s}$ and $600 \mu\text{s}$ after all cuts and pileup subtraction is given in Table 2.

Detector	Set A	Set B	Sum
1	104 598 794	70 865 274	
2	103 722 204	70 326 373	
3	103 772 927	70 143 333	
4	104 718 612	70 870 106	
5	101 670 393	68 768 646	
6	92 808 150	62 612 199	
7	89 486 798	60 444 400	
8	84 002 245	56 946 686	
9	90 529 440	61 384 216	
10	94 882 887	64 436 026	
11	101 510 607	68 760 995	
12	93 472 178	63 470 416	
13	103 069 423	69 830 759	
14	96 542 080	65 562 645	
15	103 111 415	70 100 276	
16	90 659 893	61 548 018	
17	98 442 277	66 990 281	
18	95 187 966	65 085 152	
19	101 657 780	69 125 511	
20	(60 966 748)	(40 588 896)	
21	102 012 193	68 873 798	
22	94 927 638	64 246 414	
23	94 084 851	63 798 012	
24	93 891 155	63 771 855	
0	2 238 761 906	1 517 961 391	3 756 723 297

Table 2: *Number of electrons between $31.8 \mu\text{s}$ and $600 \mu\text{s}$ after all cuts and pileup subtraction.*

5 Fit of the Time Spectra

5.1 Fourier Spectra after 5-Parameter Fits

Figures 9 and 10 show the Fourier spectra of residuals after fits to the 5-parameter function

$$\dot{N}(t) = \frac{N_0}{\tau} e^{-t/\tau} [1 + A \cos(\omega_a t + \phi_a)] \quad (2)$$

with a start time of 31.8 μs .

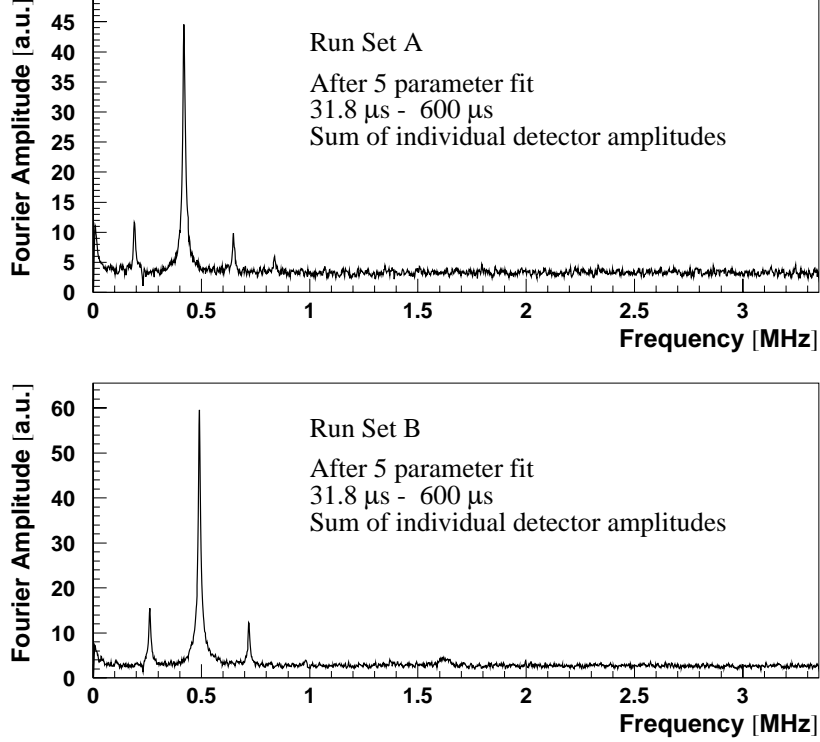


Figure 9: *All detectors were fitted separately to a 5-parameter function in the fit interval 31.8 μs - 600 μs . The residuals after the fit were Fourier-analysed; then the Fourier amplitudes were added.*

This study tells us which perturbation effects need to be accounted for by the fit function. In the first figure, the individual detector residuals were Fourier-analysed and then their Fourier amplitudes added; in the second figure, the residuals from the fit to the sum of detectors were Fourier-analysed.

All spectra shown are dominated by the CBO peak and its satellites from beating with ω_a . Furthermore, there is a peak at zero frequency which is mainly caused by muon losses but also by residual slow effects from gain variations and unsubtracted pileup.

The double CBO is significant for Set A, mainly in the sum of individual Fourier amplitudes. In the spectrum from the fit to the sum of detector it is less pronounced because of cancellation around the ring, but it is still visible. Therefore the DCBO was included in the fit function. In the sum of individual Fourier amplitudes a small peak for the vertical waist (VW) is visible in Set A (around 1.63 MHz). In Set B the VW peak

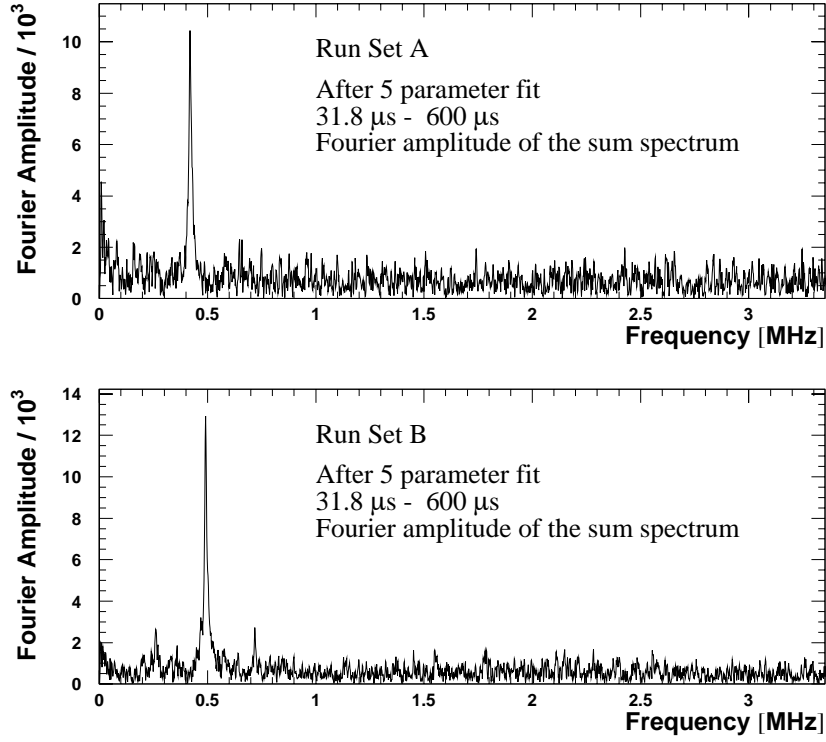


Figure 10: *The sum of detectors was fitted to a 5-parameter function in the fit interval $31.8 \mu\text{s} - 600 \mu\text{s}$. The residuals after the fit were Fourier-analysed.*

would be expected around 2.0 MHz but is not observed. The vertical oscillations (VO, expected around 2.3 MHz in Set A and around 2.5 MHz in Set B) are invisible. Both VW and VO were neglected in the fits.

5.2 Fit Function

5.2.1 Overview

The analysis is based on the following function. Some of its features were only switched on for certain studies.

$$\dot{N}(t) = \frac{N_0}{\tau} A_N(t) \cdot e^{-t/\tau} \cdot \frac{[1 + A \cdot A_R(t) \cdot \cos(\omega_a t + \phi_a \cdot A_J(t))]}{V(t) \cdot g_{\text{slow}}(t)} \quad (3)$$

with

$$\omega_a = 2\pi \cdot 0.2291 \text{ MHz} \cdot [1 - (R - \Delta R) \cdot 10^{-6}] \quad (4)$$

where R is the actual fit parameter and ΔR a secret offset.

This function accounts for horizontal (radial) CBO oscillations modulating the acceptance $A_N(t)$, the asymmetry A and the g-2 phase ϕ_a . There are contributions from oscillations of the beam centre and from width variations. The latter are not harmonic oscillations with the CBO frequency f_{CBO} but also contain components with the frequency $2f_{\text{CBO}}$. However, this double CBO decays with about half the CBO life time (i.e. roughly $50 \mu\text{s}$) and plays a role only at early times. The following functional forms were used for the CBO terms:

- Acceptance modulation by CBO:

$$A_N(t) = 1 + A_{\text{CBO}} \cdot g_{\text{CBO}}(t) \cdot \cos(\phi_{\text{CBO}}(t)) + A_{\text{DCBO}} \cdot g_{\text{CBO}}^2(t) \cdot \cos(\phi_{\text{DCBO}}(t)) \quad (5)$$

The oscillation is described by the terms $\phi_{\text{CBO}}(t)$ (single CBO frequency) and $\phi_{\text{DCBO}}(t)$ (double CBO frequency) which will be further specified below. The time envelope $g_{\text{CBO}}(t)$ was determined as described in Section 5.2.3, and found to be exponential in good approximation. For the double CBO envelope the square of $g_{\text{CBO}}(t)$ was used, i.e. an exponential with half the CBO life time.

- Asymmetry modulation by CBO (“Rob effect”):

$$A_R(t) = 1 + A_R \cdot g_{\text{CBO}}(t) \cdot \cos(\phi_R(t)) \quad (6)$$

For a single detector, this effect is roughly five times smaller than the acceptance CBO. The same exponential time envelope $g_{\text{CBO}}(t)$ was used as for the acceptance CBO. In principle, there is also a double CBO component like for the acceptance CBO. However, it is very small and can be neglected.

- Phase modulation by CBO (“Jim effect”):

$$A_J(t) = 1 + A_J \cdot g_{\text{CBO}}(t) \cdot \cos(\phi_J(t)) \quad (7)$$

Again, the same exponential envelope $g_{\text{CBO}}(t)$ was used.

Vertical waist and vertical oscillation are small, short-lived effects and only observable at very early times. The dominant acceptance part is given by

$$V(t) = 1 + A_{\text{VW}} \cdot e^{-t^2/2\tau_{\text{VW}}^2} \cdot \cos(\phi_{\text{VW}}(t)) + A_{\text{VO}} \cdot e^{-t^2/2\tau_{\text{VO}}^2} \cdot \cos(\phi_{\text{VO}}(t)) \quad , \quad (8)$$

if the time envelopes are approximated by gaussians. This expression was only implemented for systematic studies whereas for the regular fitting function, $V(t)$ was set to 0.

The quadrupole voltage V_Q and thus the field index n were not constant during the fill:

- After the end of scraping, V_Q and n increase with a RC saturation time constant τ_{rise} of about $5 \mu\text{s}$:

$$n(t) = n_{\text{sat}} \left[1 - A_{\text{rise}} e^{-(t-t_{\text{scrap}})/\tau_{\text{rise}}} \right] \quad (9)$$

In 2000, the parameter values were $A_{\text{rise}} = 0.13$, $\tau_{\text{rise}} = 4.3 \mu\text{s}$ and $t_{\text{scrap}} = 15 \mu\text{s}$ [1]. Since τ_{rise} is determined by hardware, it is the same in 2001. A_{rise} depends slightly on the quadrupole-plate voltages during and after scraping, but the order of magnitude is the same in 2000 and 2001. The scraping time however was only $t_{\text{scrap}} = 7 \mu\text{s}$ in 2001. Therefore, the end-of-scraping effect on f_{CBO} which had already been negligible in 2000 after about $30 \mu\text{s}$, was even smaller in 2001 and hence not included in the fitting function.

- After $50 \mu\text{s}$ the quadrupole plates discharge with a time constant of the order 200 ms:

$$n(t) = n(50\mu\text{s}) e^{-(t-50\mu\text{s})/\tau_{\text{droop}}} \quad (10)$$

In 2000, χ^2 minimisation gave an empirical optimum of τ_{droop} at 140 ms. It was used for the 2001 analysis as well since it depends only on the quadrupole circuitry. This parameter is always fixed in the final fits. A systematic error will be assigned.

The time dependence of n translates into a time dependence of the frequencies

$$f_{\text{CBO}}(t) \approx (1 - \sqrt{1 - n(t)}) f_{\text{cyc}} \quad (11)$$

$$f_{\text{VO}}(t) \approx \sqrt{n(t)} f_{\text{cyc}} \quad (12)$$

$$f_{\text{VW}}(t) \approx (1 - 2\sqrt{n(t)}) f_{\text{cyc}} \quad (13)$$

(for a rigorous treatment see [8]). Therefore the arguments $\phi_{\text{CBO}}(t)$, $\phi_{\text{DCBO}}(t)$, $\phi_{\text{VO}}(t)$ and $\phi_{\text{VW}}(t)$ of the horizontal and vertical oscillation cosines are not simply $\omega_{\text{CBO}}t + \phi_{\text{CBO}}(0)$ etc., but have to be obtained from time integration of the respective frequencies, e.g.

$$\phi_{\text{CBO}}(t) = \int_{50 \mu\text{s}}^t dt' 2\pi f_{\text{CBO}}(t') + \phi_{\text{CBO}}(50\mu\text{s}) \quad (14)$$

As fit parameters the frequencies and phases at the reference time $50 \mu\text{s}$ are chosen. Acceptance, asymmetry and phase modulation share the same CBO frequency parameter. By definition, the double CBO frequency was implemented as $2 f_{\text{CBO}}$ and is not an additional free parameter.

The electron time spectrum is further modulated by slow effects $g_{\text{slow}}(t)$ which are dominated by muon losses and residual detector gain variations and pileup. These effects correlate strongly with each other and are difficult to separate. Their individual functional forms are not very well known. In the final fitting function we implement only the muon loss function $g_{\text{loss}}(t)$ derived from FSD triple coincidence measurements [9]. This function is known to about 10%. The details of the implementation of $g_{\text{loss}}(t)$ are explained in Section 5.2.4. To avoid phase pulling in R entirely, an empirical correction term would have to be included:

$$g_{\text{slow}}(t) = (1 + g_{\text{loss}}(t) - A_{\text{rse}} \cdot e^{-t/\tau_{\text{rse}}}) \quad (15)$$

The correction term accounts for lacking knowledge about $g_{\text{loss}}(t)$, for imperfections in the gain correction and pileup subtraction. Therefore it is called “residual slow effects” (“r.s.e.”; if this concept is unclear to you see Figure 16 in [1] for a comprehensive explanation). In the final fits no such term is used, but it was included for studies.

5.2.2 Free and Fixed Fit Parameters

- N_0 : always free.
- τ : always free.
- A : always free.
- R : always free.
- ϕ_a : always free.
- $f_{\text{CBO}}(50\mu\text{s})$: always free.
- A_{CBO} : always free.
- $\phi_{\text{CBO}}(50\mu\text{s})$: always free.
- A_{DCBO} : free for start times up to $80\mu\text{s}$, then fixed.
- $\phi_{\text{DCBO}}(50\mu\text{s})$: free for start times up to $80\mu\text{s}$, then fixed.
- A_{R} : fixed to 0 in the 1999-style function, otherwise free.
- $\phi_{\text{R}}(50\mu\text{s})$: fixed to 0 in the 1999-style function, otherwise free.
- A_{J} : free in the “full physics function”, otherwise fixed to 0.
- $\phi_{\text{J}}(50\mu\text{s})$: free in the “full physics function”, otherwise fixed to 0.
- A_{VO} : free for systematic studies; otherwise fixed to 0.
- $f_{\text{VO}}(50\mu\text{s})$: only used for systematic studies; fixed; determined from a Fourier spectrum.
- τ_{VO} : only used for systematic studies; fixed; determined by manual χ^2 minimisation at early times.
- $\phi_{\text{VO}}(50\mu\text{s})$: only used for systematic studies where it is free; otherwise fixed to 0.
- A_{VW} : free for systematic studies; otherwise fixed to 0.
- $f_{\text{VW}}(50\mu\text{s})$: only used for systematic studies; fixed; determined from a Fourier spectrum.
- τ_{VW} : only used for systematic studies; fixed; determined by manual χ^2 minimisation at early times.
- $\phi_{\text{VW}}(50\mu\text{s})$: only used for systematic studies where it is free; otherwise fixed to 0.
- $\tau_{\text{droop}} = 140\text{ ms}$: always fixed.
- A_{loss} : free at the earliest start time for the sum of all detectors, otherwise fixed to that result.
- A_{rse} : free in special studies, otherwise fixed to 0.
- τ_{rse} : free in special studies, otherwise irrelevant.

There are 12 free parameters if the “1999-style function” is used; the “physics function without phase modulation” has 14 free parameters, and the “full physics function” including the phase modulation has 16 free parameters. In studies at very early start times the inclusion of the vertical oscillation and waist increases the number of parameters to 20.

5.2.3 The CBO Envelope

The CBO envelope was determined as described in the 2000 analysis report [1] (Section 5.1.3). The results for the two data sets are shown in Figure 11 together with exponential fits.

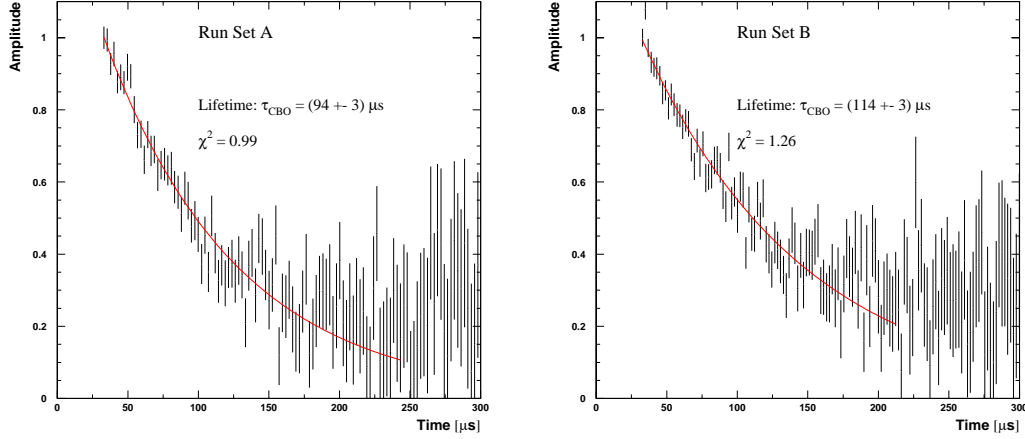


Figure 11: *CBO envelopes for the two run sets, normalised to the value at 31.8 μs. The lines superimposed represent exponential fits.*

Unlike in 2000, the CBO envelopes are sufficiently well parametrised by exponentials, and we do not need empirical envelopes.

5.2.4 Implementation of the Muon Loss Function

Following a suggestion by Chris, the implementation of the muon loss function was slightly changed w.r.t. 2000.

Neglecting the muon spin precession, the time spectrum of the detected electrons $\dot{N}_\mu(t)$ is given by the differential equation

$$\dot{N}_\mu(t) = -\varepsilon_d \lambda_\mu N(t) \quad (16)$$

where $\lambda = 1/\tau$, $N(t)$ is the total number of muons in the ring at the time t , and ε_d is an efficiency and acceptance factor for the electron detection. The muon losses $L(t)$ measured via FSD triple coincidences [9, 10] obey the equation

$$L(t) = -\varepsilon_l \dot{N}_l(t) \quad (17)$$

where ε_l an efficiency and acceptance factor for the detection of muons. The number of muons in the ring follows from combining (16) and (17):

$$\dot{N}(t) = -\lambda_\mu N(t) + \dot{N}_l(t) = -\lambda_\mu N(t) - \frac{1}{\varepsilon_l} L(t) \quad (18)$$

The solution is

$$N(t) = N_0 e^{-\lambda_\mu t} \left(1 - \frac{1}{\varepsilon_l} \int_0^t L(t') e^{\lambda_\mu t'} dt' \right) \quad (19)$$

Hence, the detected electron spectrum is

$$\dot{N}_\mu(t) = -\varepsilon_d \lambda_\mu N_0 e^{-\lambda_\mu t} \left(1 - \frac{1}{\varepsilon_l} \int_0^t L(t') e^{\lambda_\mu t'} dt' \right) \quad (20)$$

With a different choice of constants, this equation can be rewritten as

$$\dot{N}_\mu(t) = \tilde{N}_{\mu,0} \lambda_\mu e^{-\lambda_\mu t} \left(1 - A_l \frac{\int_{t_0}^t L(t') e^{\lambda_\mu t'} dt'}{\int_{t_0}^{t_{max}} L(t') e^{\lambda_\mu t'} dt'} \right) \quad (21)$$

where t_0 is an arbitrary reference time which for this analysis was chosen to be $30 \mu\text{s}$. After the cut-off time $t_{max} = 325 \mu\text{s}$ the measured losses $L(t)$ are taken to be zero because anti-proton losses start to dominate.

In (21) we identify

$$g_{\text{loss}}(t) = \left(1 - A_l \frac{\int_{t_0}^t L(t') e^{\lambda_\mu t'} dt'}{\int_{t_0}^{t_{max}} L(t') e^{\lambda_\mu t'} dt'} \right) \quad (22)$$

5.3 Fit Procedure

The fitting technique was the same as for the 2000 data set [1]. However, due to earlier gate-on times, the fits are also started earlier:

The latest detectors to be gated on were 4 and 5. They are available after about $30 \mu\text{s}$. The closest (g-2) zero-crossing is at $31.8 \mu\text{s}$ which was chosen as the start time for individual detector fits, and as the earliest point of start-time scans for fits to the sum of all detector spectra (excluding detector 20). In these scans, the start times were varied in 150 ns steps before $45 \mu\text{s}$ to look for phase pulling. After $45 \mu\text{s}$ the step size was $5 \mu\text{s}$.

Like in the previous analysis, the fit stop time was $600 \mu\text{s}$ or the time when the number of entries per bin went below 42, whichever was earlier. The latter criterion ensures gaussian statistics in each time bin. However, thanks to the big statistics of the data set, this cut was never active.

Again, the error on the N_i entries of a time bin i was corrected for correlations from our pileup subtraction method:

$$\sigma_i = \sqrt{N_i \cdot (1 + \gamma \cdot X \cdot e^{-\frac{t-34.1\mu\text{s}}{\tau}})} \quad (23)$$

in the first call to the fitting routine (NAGLIB e04ycf). In later iterations, N_i was replaced by the function value from the previous fit. The values of the parameters γ and X are given in Tables 3 and 4.

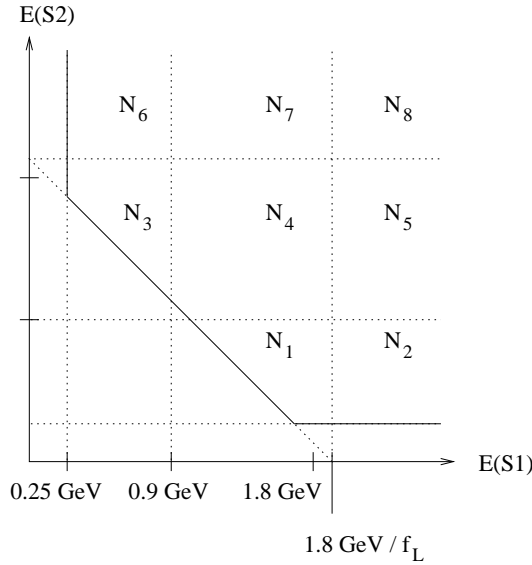


Figure 12: *Illustration of the construction of pileup pulses from single pulses with energies $E(S1)$ and $E(S2)$. For all points above the diagonal line the energy of the constructed double pulse is greater than 1.8 GeV.*

Detector	Set A	Set B
1	1.11	1.10
2	1.12	1.11
3	1.14	1.12
4	1.14	1.13
5	1.13	1.13
6	1.16	1.15
7	1.20	1.20
8	1.22	1.21
9	1.18	1.17
10	1.14	1.13
11	1.13	1.13
12	1.16	1.15
13	1.12	1.12
14	1.14	1.14
15	1.11	1.11
16	1.16	1.16
17	1.13	1.12
18	1.13	1.14
19	1.10	1.10
(20)	(1.31)	(1.32)
21	1.13	1.13
22	1.16	1.16
23	1.15	1.15
24	1.15	1.15
0	1.14	1.14

Table 3: Values of $\gamma \equiv \frac{6N_1+2N_4+2N_8}{2(N_1+N_2)+N_4+N_5+N_7+N_8}$ for all detectors and the two data subsets. Detector 0 stands for the sum of all detectors. For the notation used in the definition of gamma and its derivation see [7] and Figure 12.

Detector	Set A	Set B
1	0.0055	0.0060
2	0.0059	0.0063
3	0.0061	0.0065
4	0.0060	0.0065
5	0.0060	0.0064
6	0.0063	0.0068
7	0.0072	0.0077
8	0.0089	0.0097
9	0.0072	0.0078
10	0.0059	0.0064
11	0.0060	0.0065
12	0.0066	0.0072
13	0.0059	0.0064
14	0.0065	0.0071
15	0.0053	0.0057
16	0.0069	0.0075
17	0.0058	0.0062
18	0.0070	0.0075
19	0.0061	0.0066
(20)	(0.0087)	(0.0094)
21	0.0061	0.0065
22	0.0064	0.0070
23	0.0061	0.0065
24	0.0065	0.0070
0	0.0063	0.0068

Table 4: Values of $X = \frac{\text{doubles at } 34.1 \mu\text{s}}{\text{singles at } 34.1 \mu\text{s}}$ for all detectors and run subsets. Single pulses $N - D + S1 + S2$ and double pulses D are counted over one g -2 period centred at $34.1 \mu\text{s}$. See also Figure 13.

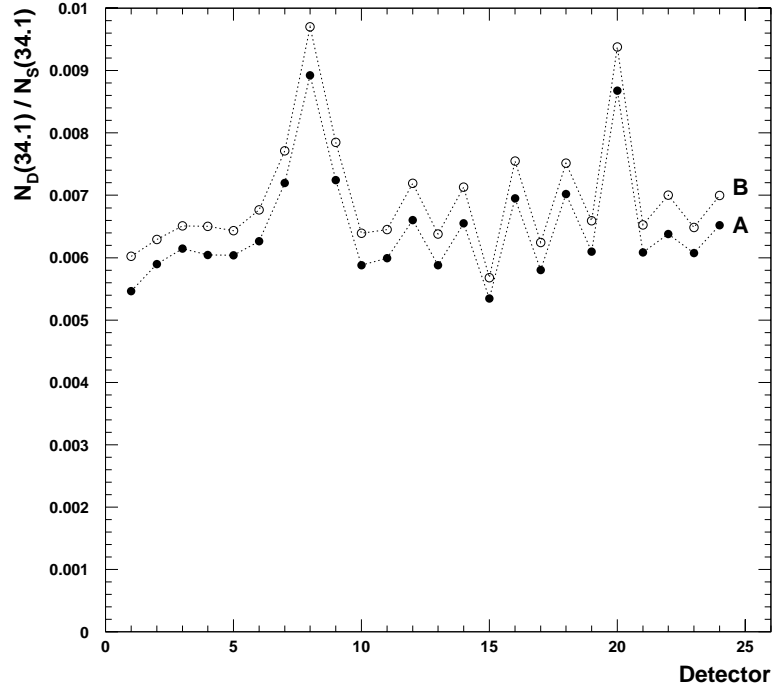


Figure 13: Values of $X = \frac{\text{doubles at } 34.1 \mu\text{s}}{\text{singles at } 34.1 \mu\text{s}}$ as in Table 4. The energy spectra of the kicker detectors 7, 8, 9 have a different shape which impacts the pileup fraction.

5.4 Fit Results

All results in this section are based on a single random seed. More seeds will only be used for a systematic study (Section 6.10).

5.4.1 Fits without Asymmetry/Phase Modulation (1999 Style)

We define the “1999-style function” as Function (3) with the following parameters fixed:

- No asymmetry modulation by CBO: $A_{\text{Rob}} = \phi_{\text{Rob}} = 0$.
- No phase modulation by CBO: $A_{\text{Jim}} = \phi_{\text{Jim}} = 0$.

Thus, the remaining function is

$$\dot{N}(t) = \frac{N_0}{\tau} e^{-t/\tau} [1 + A_{\text{CBO}} \cdot g_{\text{CBO}}(t) \cdot \cos(\phi_{\text{CBO}}(t)) + A_{\text{DCBO}} \cdot g_{\text{CBO}}^2(t) \cdot \cos(\phi_{\text{DCBO}}(t))] \cdot [1 + A \cdot \cos(\omega_a t + \phi_a)] \cdot g_{\text{slow}}(t) \quad (24)$$

The individual terms are explained in Section 5.2.1. For the fits discussed here, $g_{\text{slow}}(t)$ only incorporates the muon losses, no rse term.

Set A	N_0	A	τ	ϕ_a	R	f_{CBO}	τ_{CBO}	A_{CBO}	ϕ_{CBO}	A_{DCBO}	ϕ_{DCBO}	A_{loss}
N_0	1.000	-0.040	0.816	-0.001	-0.001	0.018	-0.021	0.029	-0.026	-0.009	0.019	0.982
A	-0.040	1.000	-0.025	-0.009	-0.005	0.009	0.006	-0.008	-0.012	-0.002	0.003	-0.037
τ	0.816	-0.025	1.000	-0.001	-0.001	0.011	-0.013	0.018	-0.016	-0.006	0.012	0.873
ϕ_a	-0.001	-0.009	-0.001	1.000	0.833	0.014	-0.029	0.040	-0.021	0.001	0.011	-0.002
R	-0.001	-0.005	-0.001	0.833	1.000	0.010	-0.021	0.029	-0.015	0.001	0.008	-0.001
f_{CBO}	0.018	0.009	0.011	0.014	0.010	1.000	-0.004	0.007	-0.321	-0.011	0.016	0.016
τ_{CBO}	-0.021	0.006	-0.013	-0.029	-0.021	-0.004	1.000	-0.902	0.003	-0.462	0.017	-0.019
A_{CBO}	0.029	-0.008	0.018	0.040	0.029	0.007	-0.902	1.000	-0.006	0.416	-0.023	0.027
ϕ_{CBO}	-0.026	-0.012	-0.016	-0.021	-0.015	-0.321	0.003	-0.006	1.000	0.014	-0.016	-0.024
A_{DCBO}	-0.009	-0.002	-0.006	0.001	0.001	-0.011	-0.462	0.416	0.014	1.000	-0.015	-0.008
ϕ_{DCBO}	0.019	0.003	0.012	0.011	0.008	0.016	0.017	-0.023	-0.016	-0.015	1.000	0.017
A_{loss}	0.982	-0.037	0.873	-0.002	-0.001	0.016	-0.019	0.027	-0.024	-0.008	0.017	1.000

Set B	N_0	A	τ	ϕ_a	R	f_{CBO}	τ_{CBO}	A_{CBO}	ϕ_{CBO}	A_{DCBO}	ϕ_{DCBO}	A_{loss}
N_0	1.000	-0.036	0.820	-0.002	-0.001	0.025	-0.004	0.005	-0.033	0.006	0.014	0.982
A	-0.036	1.000	-0.022	-0.009	-0.005	0.001	0.007	-0.010	-0.002	0.004	0.004	-0.033
τ	0.820	-0.022	1.000	-0.002	-0.001	0.015	-0.002	0.003	-0.020	0.002	0.009	0.877
ϕ_a	-0.002	-0.009	-0.002	1.000	0.833	0.023	-0.008	0.011	-0.030	0.003	0.012	-0.002
R	-0.001	-0.005	-0.001	0.833	1.000	0.016	-0.006	0.008	-0.022	0.002	0.009	-0.001
f_{CBO}	0.025	0.001	0.015	0.023	0.016	1.000	0.003	-0.005	-0.422	-0.003	0.005	0.023
τ_{CBO}	-0.004	0.007	-0.002	-0.008	-0.006	0.003	1.000	-0.887	-0.006	-0.027	0.016	-0.003
A_{CBO}	0.005	-0.010	0.003	0.011	0.008	-0.005	-0.887	1.000	0.009	0.022	-0.022	0.004
ϕ_{CBO}	-0.033	-0.002	-0.020	-0.030	-0.022	-0.422	-0.006	0.009	1.000	0.003	-0.010	-0.030
A_{DCBO}	0.006	0.004	0.002	0.003	0.002	-0.003	-0.027	0.022	0.003	1.000	0.001	0.005
ϕ_{DCBO}	0.014	0.004	0.009	0.012	0.009	0.005	0.016	-0.022	-0.010	0.001	1.000	0.013
A_{loss}	0.982	-0.033	0.877	-0.002	-0.001	0.023	-0.003	0.004	-0.030	0.005	0.013	1.000

Table 5: Correlation matrix $\frac{\text{cov}(p_i, p_j)}{\sigma_i \sigma_j}$ from fits to the sum of detectors starting at $31.8\mu\text{s}$; 1999-style function.

With the 1999-style function the fit results for R decouple well from the other fit parameters, as the correlation matrices in Table 5 demonstrate. We shall see that this makes the results relatively insensitive to gain variations and other effects influencing the asymmetry. The disadvantage of this function is that by neglecting the CBO modulations

of g-2 asymmetry and phase it does fully describe the physics. The missing effects need to be addressed in systematic error studies.

Fits to the Sum of Detectors

Start time scans for R is shown in Figure 14 for the two data sets. Figure 15 shows zooms for start times up to $45 \mu\text{s}$ with a step of 150 ns . For both run sets there is phase pulling with the g-2 frequency and an amplitude of about 0.3 ppm which suggests that the muon-loss function alone is not quite adequate to describe the slow varying term $g_{\text{slow}}(t)$. In Section 6.6.3 the resulting systematic error and the effects of including an r.s.e. term will be discussed.

The weighted average of the R values for the two subsets is shown in Figure 16 and Table 6. Figure 17 shows start-time scans for the asymmetry A . Like in 2000, A droops below the allowed 1σ error band, suggesting imperfections in pileup subtraction and/or gain correction.

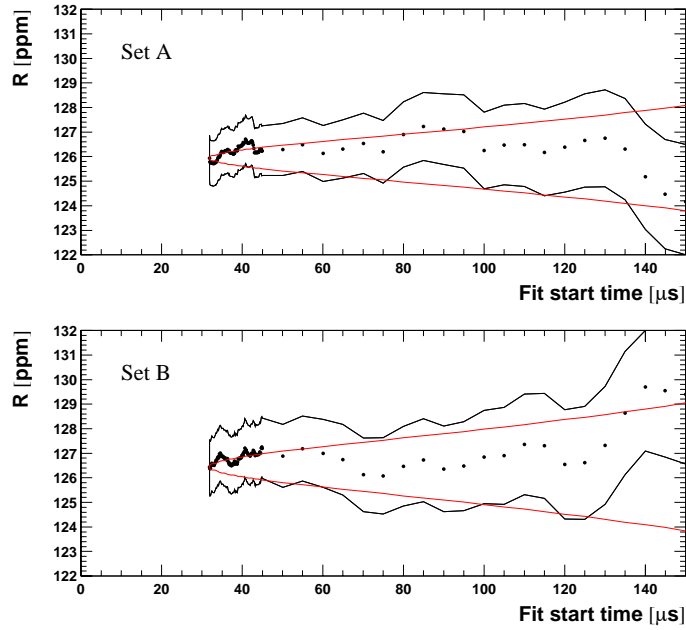
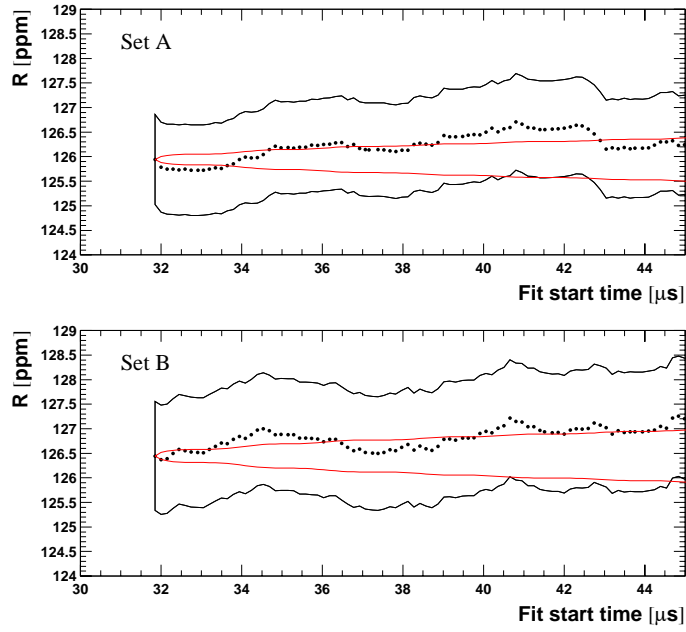
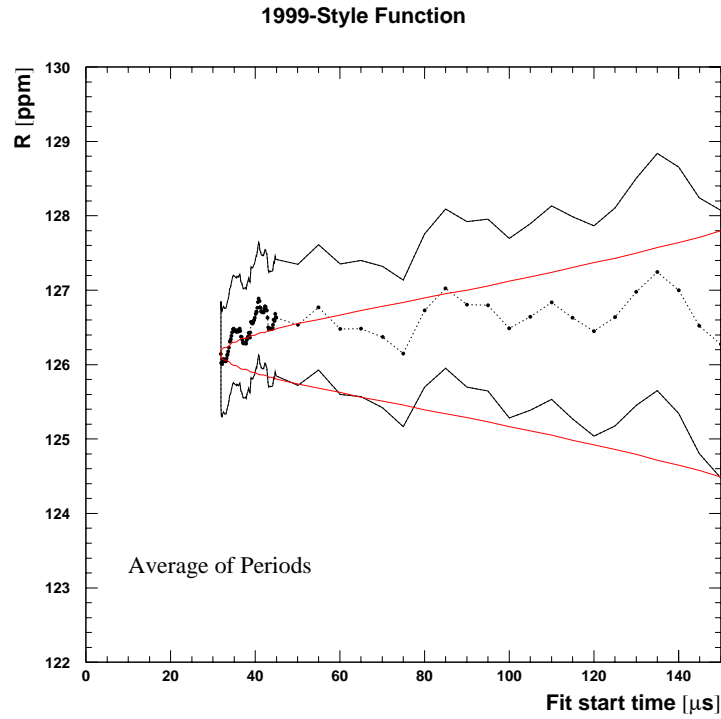
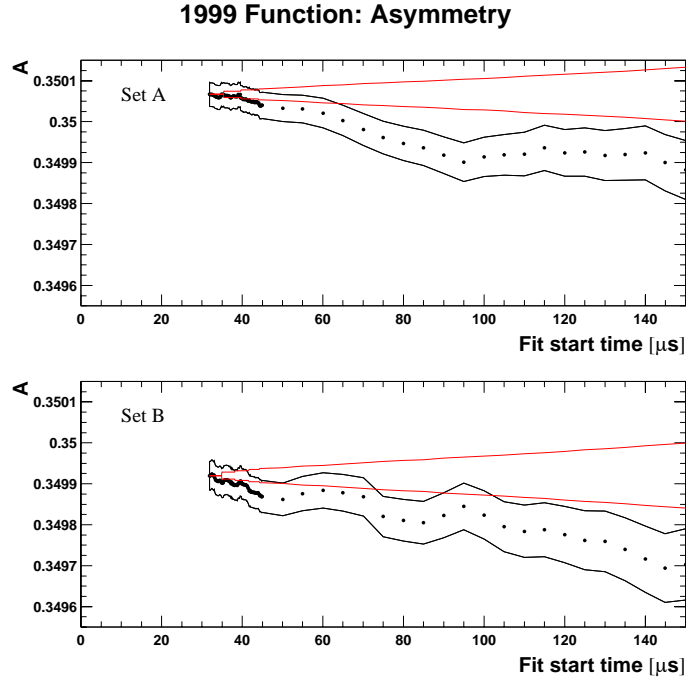


Figure 14: *Start time scans for the sum of all detector spectra of all runs fitted with the 1999-style function.*

Figure 15: *Early-time zoom of Figure 14.*Figure 16: R averaged over the two run sets.

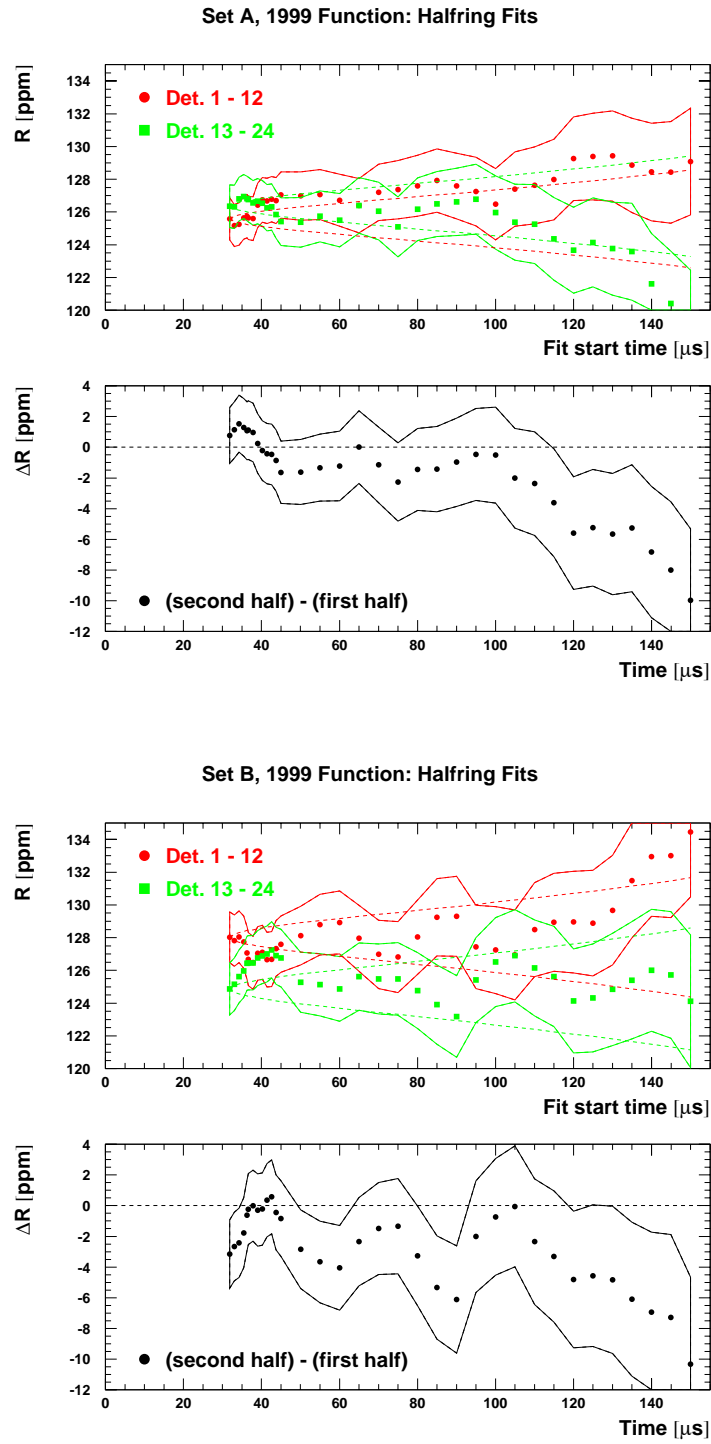
Figure 17: *Start-time scans for A, sum of all detector spectra.*

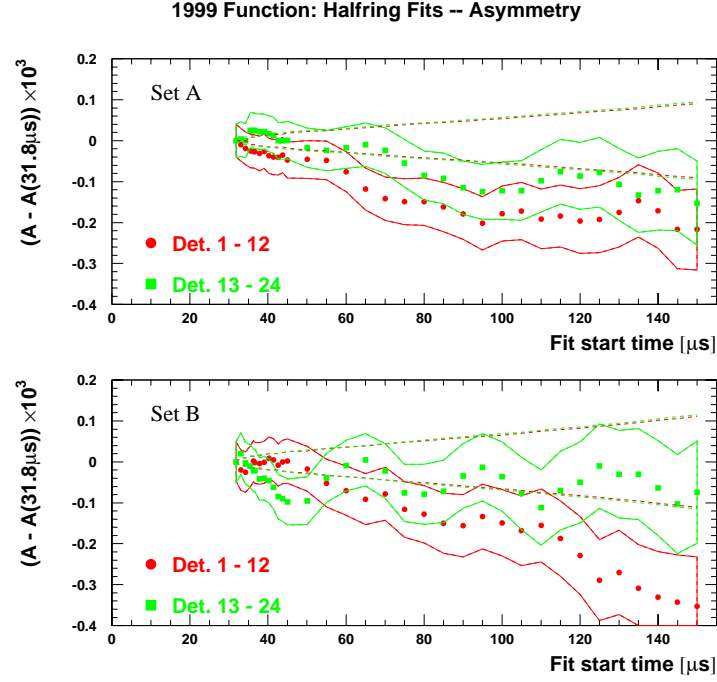
Period	Sum of all detectors	First half	Second half	Average of the halves
A	125.9420 ± 0.9138	125.5806 ± 1.2748	126.3616 ± 1.3079	125.9611 ± 0.9129
B	126.4448 ± 1.1098	128.0083 ± 1.5491	124.8792 ± 1.5874	126.4820 ± 1.1087
avr.	126.1452 ± 0.7054	126.5608 ± 0.9843	125.7622 ± 1.0094	126.1716 ± 0.7047
A - B	0.5028 ± 1.4376	2.4277 ± 2.0062	1.4824 ± 2.0568	0.5209 ± 1.4362

Table 6: *Fit results for R in ppm in the two run periods with a start time of $31.8 \mu\text{s}$. The fits were done with the 1999-style function.*

The omission of the asymmetry and phase modulation manifests itself in the halfring effect on both R and A , see Figures 18 and 19.

Start time scans for all other parameters and for the different run periods are shown in Appendix A.1. Appendix A.2 shows the same for the first and second half of the ring.

Figure 18: *Fit results for R in the two halves of the ring.*

Figure 19: *Fit results for A in the two halves of the ring.*

The CBO parameters are listed in Table 7.

Period	$A_{\text{CBO}} \times 10^3$	ϕ_{CBO}	f_{CBO} [kHz]	τ_{CBO} [μs]
A	1.32 ± 0.15	-0.29 ± 0.05	418.46 ± 0.27	98.28 ± 16.17
B	1.91 ± 0.13	2.41 ± 0.04	490.48 ± 0.15	146.17 ± 20.23

Table 7: *CBO parameters from fits to the sum of all detectors with a start time of 31.8 μs . The fits were done with the 1999-style function.*

Fits to the Individual Detectors

The fit results for individual detectors at a start time of $31.8 \mu\text{s}$ are shown in the figures of Appendix A.3. A bigger version of R versus detector is displayed in Figure 20.

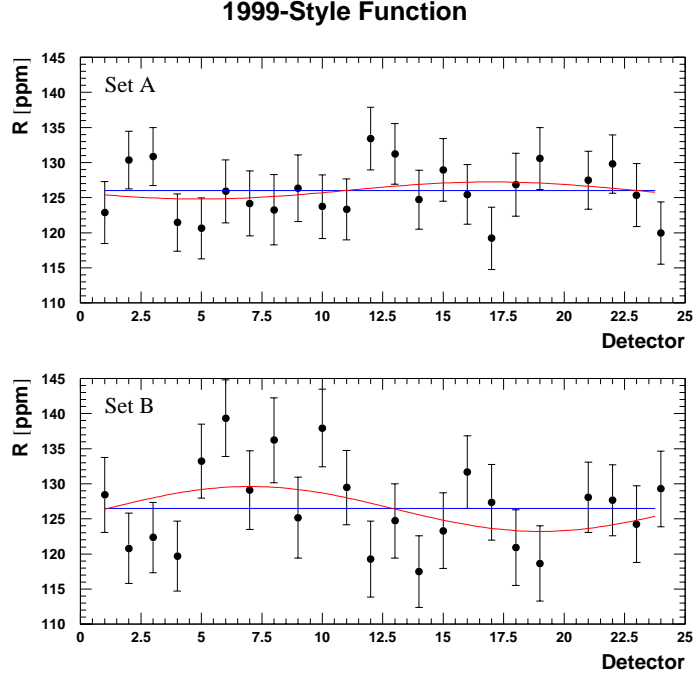


Figure 20: R versus detector with the 1999-style function.

As a consequence of omitting the asymmetry and phase modulation in the fit function, R versus detector may not be constant but follow a sine wave

$$R(d) = R_0 + A_{Rc} \cos(2\pi \frac{d}{24}) + A_{Rs} \sin(2\pi \frac{d}{24}). \quad (25)$$

We find an average amplitude of (0.76 ± 1.00) ppm. The centroid value R_0 of this wave differs by (0.01 ± 0.02) ppm from the weighted average $\langle R \rangle$ (see Table 10).

Set	$\langle R \rangle$	χ^2/dof (fit to a constant)
A	125.9958 ± 0.9133	17.95 / 22
B	126.4789 ± 1.1091	28.77 / 22
avr.	126.1910 ± 0.7050	

Table 8: Average R from the individual detector fits, for the different run periods with a start time of $31.8 \mu\text{s}$. Detector 20 was excluded. The fits were done with the 1999-style function.

Set	R_0	A_{Rc}	A_{Rs}	$\sqrt{A_{Rc}^2 + A_{Rs}^2}$	χ^2/dof
A	126.0255 ± 0.9139	-0.3203 ± 1.2736	-1.1763 ± 1.3175	1.2191 ± 1.3145	$17.05 / 20$
B	126.4110 ± 1.1097	-0.8365 ± 1.5476	3.0848 ± 1.5990	3.1962 ± 1.5955	$24.88 / 20$
avr.	126.1813 ± 0.7055	-0.5287 ± 0.9834	0.5468 ± 1.0168	0.7606 ± 1.0008	

Table 9: R versus detector was fitted with Function (25). The table gives the fit parameters for the two run sets with a start time of $31.8\mu\text{s}$. Detector 20 was excluded. The underlying individual detector fits were done with the 1999-style function.

Set	$\langle R \rangle - R_0$
A	-0.0297 ± 0.0331
B	0.0679 ± 0.0365
avr.	0.0143 ± 0.0245

Table 10: Difference between fitting R versus detector to a constant and to a wave (Tables 8 and 9).

Table 11 lists the CBO amplitude averaged over all detectors for the two run sets.

As an additional detector consistency check, the CBO vectors ($A_{\text{CBO}}, \phi_{\text{CBO}}$) are added coherently (“vector sum” in Table 11) and compared with the result for the sum. This vector sum follows from the addition of the time spectra whose relevant part can be written as

$$N_0 A_{\text{CBO},\text{sum}} \cos(\omega_{\text{CBO}} t + \phi_{\text{CBO},\text{sum}}) = \sum_{d=1}^{24} N_d A_{\text{CBO},d} \cos(\omega_{\text{CBO}} t + \phi_{\text{CBO},d}) \quad (26)$$

In complex notation the amplitude $A_{\text{CBO},\text{sum}}$ and phase $\phi_{\text{CBO},\text{sum}}$ of the sum are given by

$$N_0 A_{\text{CBO},\text{sum}} (\cos \phi_{\text{CBO},\text{sum}} + i \sin \phi_{\text{CBO},\text{sum}}) = \sum_{d=1}^{24} N_d A_{\text{CBO},d} (\cos \phi_{\text{CBO},d} + i \sin \phi_{\text{CBO},d}) \quad (27)$$

These vector sums are in rather good agreement with the results from the fits to the sum of detectors given in Table 7.

Set	$\langle A_{\text{CBO}} \rangle \times 10^3$	vector sum over all detectors	
		$A_{\text{CBO}} \times 10^3$	ϕ_{CBO}
A	6.41 ± 0.17	1.37 ± 0.15	-0.30 ± 0.09
B	10.31 ± 0.16	2.08 ± 0.13	2.27 ± 0.06

Table 11: First column: CBO parameters from fits to the individual detectors, averaged over all detectors. Second and third columns: vector sum of the CBO parameters over all detectors. Amplitude and phase of the vector sum should be consistent with the corresponding parameters obtained from the summed spectra (cf. Table 7).

Comparison between Fits to the Sum and the Average of Individual Fits

The R -value from a fit to the sum of detector spectra should agree with the average $\langle R \rangle$ over the results from individual detector fits. Discrepancies between R_{sum} and the sine wave centroid R_0 are less surprising because the 1999-style function does not include any information about the presence of this sine wave.

Set	$ \langle R \rangle - R_{\text{sum}} $	$ R_0 - R_{\text{sum}} $
A	0.0538 ± 0.0302	0.0835 ± 0.0135
B	0.0341 ± 0.0394	0.0338 ± 0.0149

Table 12: *Difference between R from fits to the sum of all detector spectra and the averages $\langle R \rangle$ or R_0 from fits to individual detector spectra. The 1999 function was used.*

5.4.2 Fits with Asymmetry Modulation but without Phase Modulation

This section describes fits using Function (3) including the asymmetry modulation term (6), but not the phase modulation term (7) (we fix the parameters $A_{\text{Jim}} = \phi_{\text{Jim}} = 0$). This function is only used for a study of fit results. No systematic errors will be determined for it, and it will not be considered for the final result.

A look at the correlation matrices (Table 13) reveals that – unlike in 2000 – the inclusion of the asymmetry modulation into the fit does not lead to additional correlations: neither A nor R correlates strongly with A_{Rob} or ϕ_{Rob} . The reason for the weak correlations is the larger difference $\frac{1}{2}\omega_{\text{CBO}} - \omega_a$ as compared to the 2000 data. R decouples well from all parameters except ϕ .

Fits to the Sum of Detectors

Start time scans for R are shown in Figure 21 for the two data sets. Figure 22 shows a zoom for start times up to $45 \mu\text{s}$ with a step of 150 ns .

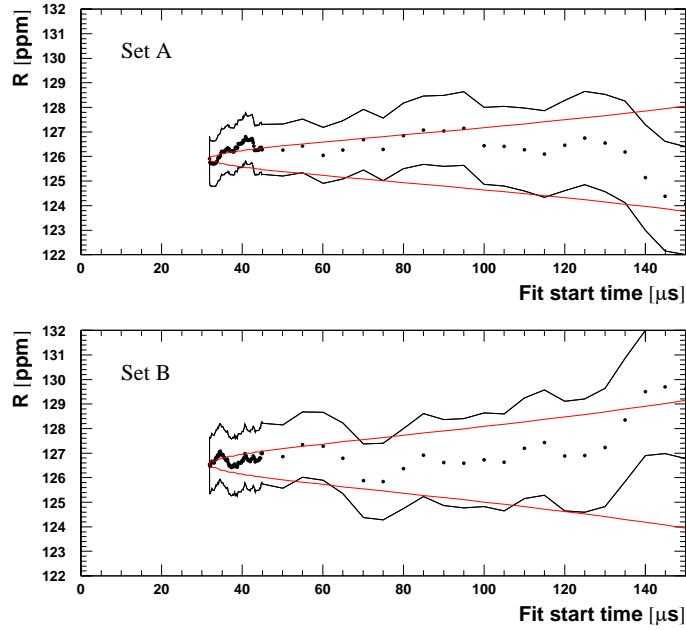


Figure 21: *Start-time scan for the sum of all detector spectra of all runs fitted with the physics function without phase modulation.*

The weighted average of the fit results for R from the two run sets is shown in Figure 23 and Table 14. Figure 24 shows start-time scans for A .

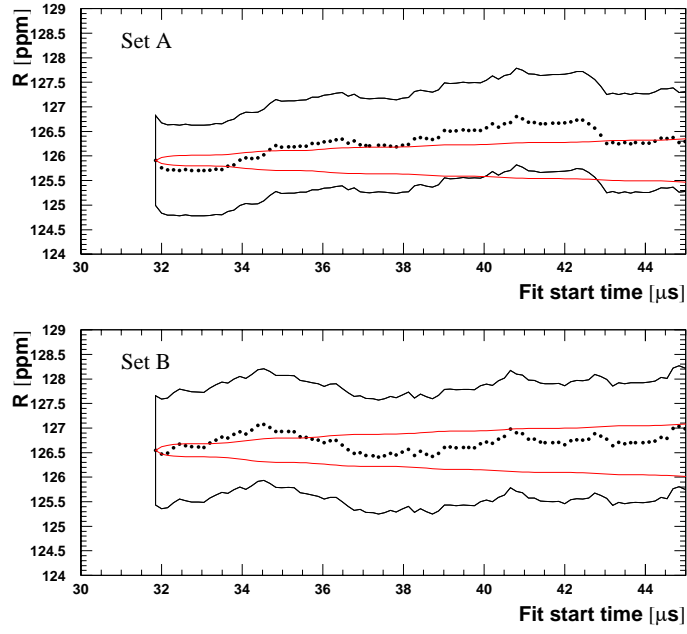
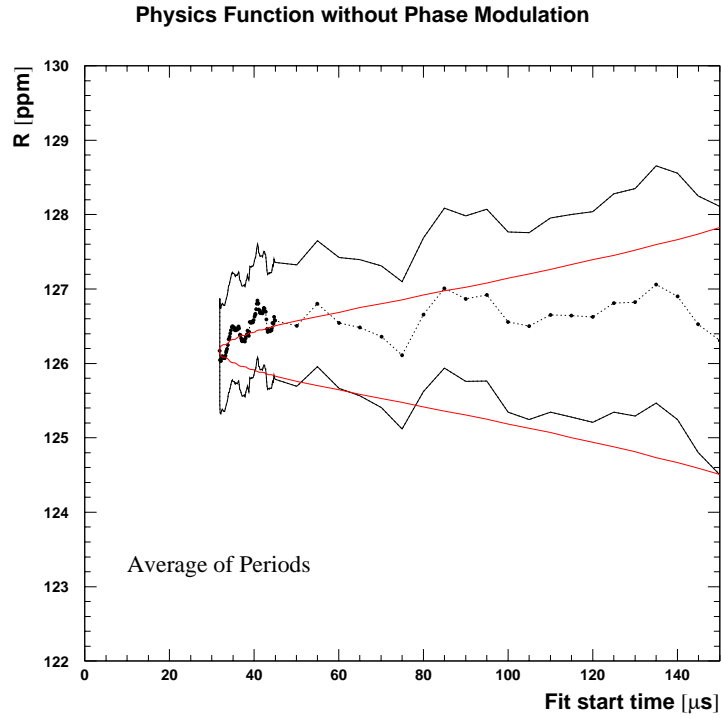
Inclusion of the asymmetry modulation into the fit function almost eliminates the halfring effect, see Figures 25 and 26.

Start time scans for the other parameters and for the different run periods are shown in Appendix B.1. Appendix B.2 shows them for the first and second half of the ring.

Table 13: Correlation matrix $\frac{\text{cov}(\mathbf{p}_i, \mathbf{p}_j)}{\sigma_i \sigma_j}$ from a fit to the sum of detectors starting at 31.8 μs ; physics function without phase modulation.

Set A															
N_0	A	τ	ϕ_a	R	f_{CBO}	τ_{CBO}	A_{CBO}	ϕ_{CBO}	A_{Rob}	ϕ_{Rob}	A_{DCBO}	ϕ_{DCBO}	A_{loss}		
N_0	1.000	-0.040	0.816	-0.005	-0.003	0.015	-0.022	0.031	-0.024	-0.021	0.028	-0.008	0.019	0.982	
A	-0.040	1.000	-0.025	-0.009	-0.005	0.006	0.011	-0.014	-0.011	0.066	0.037	-0.005	0.003	-0.037	
τ	0.816	-0.025	1.000	-0.004	-0.003	0.009	-0.014	-0.015	-0.013	0.018	-0.005	0.012	0.873		
ϕ_a	-0.005	-0.009	-0.004	1.000	0.834	0.019	-0.024	0.035	-0.025	0.053	-0.002	0.009	0.011	0.000	
R	-0.003	-0.005	-0.003	0.834	1.000	0.014	-0.017	0.025	-0.018	0.039	-0.001	0.007	-0.003	0.000	
f_{CBO}	0.015	0.006	0.009	0.019	0.014	1.000	-0.004	-0.004	0.002	-0.049	-0.011	0.016	0.014	0.014	
τ_{CBO}	-0.022	0.011	-0.014	-0.024	-0.017	-0.004	1.000	-0.903	0.003	-0.006	0.003	0.132	-0.003	-0.020	
A_{CBO}	0.031	-0.014	0.019	0.035	0.025	0.008	-0.903	1.000	-0.006	0.046	-0.006	0.015	-0.016	-0.007	
ϕ_{CBO}	-0.024	-0.011	-0.015	-0.025	-0.018	-0.320	-0.006	1.000	-0.003	0.046	-0.003	0.134	-0.007	-0.022	
A_{Rob}	-0.021	0.066	-0.013	0.053	0.039	0.002	0.132	-0.134	1.000	-0.006	0.015	-0.073	-0.003	-0.020	
ϕ_{Rob}	0.028	0.037	0.018	-0.082	-0.058	-0.049	-0.007	-0.007	0.006	1.000	0.005	0.019	0.026	0.018	
A_{DCBO}	-0.008	-0.005	-0.005	-0.002	-0.001	-0.011	-0.465	0.015	-0.073	0.005	1.000	-0.015	-0.007	0.018	
ϕ_{DCBO}	0.019	0.003	0.012	0.009	0.007	0.016	0.017	-0.022	-0.016	-0.003	0.019	1.000	0.018	1.000	
A_{loss}	0.982	-0.037	0.873	-0.005	-0.003	0.014	-0.021	-0.022	-0.020	0.026	-0.007	0.018	1.000	1.000	

Set B															
N_0	A	τ	ϕ_a	R	f_{CBO}	τ_{CBO}	A_{CBO}	ϕ_{CBO}	A_{Rob}	ϕ_{Rob}	A_{DCBO}	ϕ_{DCBO}	A_{loss}		
N_0	1.000	-0.036	0.820	0.001	0.000	0.026	-0.005	0.006	-0.033	0.010	-0.018	0.007	0.014	0.982	
A	-0.036	1.000	-0.022	-0.009	-0.005	0.006	0.012	-0.013	-0.006	-0.066	-0.027	0.004	0.003	-0.033	
τ	0.820	-0.022	1.000	-0.000	-0.000	0.016	-0.003	0.004	-0.020	0.006	-0.011	0.003	0.008	0.877	
ϕ_a	0.001	-0.009	-0.000	1.000	0.834	0.029	-0.016	0.019	-0.033	0.046	-0.090	0.005	0.011	0.000	
R	0.000	-0.005	-0.000	0.834	1.000	0.021	-0.011	0.014	-0.024	0.035	-0.064	0.004	0.008	0.000	
f_{CBO}	0.026	0.006	0.016	0.029	0.021	1.000	0.003	-0.004	-0.426	-0.026	-0.052	-0.002	0.005	0.024	
τ_{CBO}	-0.005	0.012	-0.003	-0.016	-0.011	0.003	1.000	-0.885	-0.008	-0.177	0.028	-0.027	0.014	-0.005	
A_{CBO}	0.006	-0.013	0.004	0.019	0.014	-0.004	-0.885	1.000	0.010	0.155	-0.037	0.021	-0.021	0.006	
ϕ_{CBO}	-0.033	-0.006	-0.020	-0.033	-0.024	-0.426	-0.008	1.000	0.035	0.030	0.002	-0.009	-0.030	0.009	
A_{Rob}	0.010	-0.066	0.006	0.046	0.035	-0.177	0.155	0.010	1.000	-0.005	0.010	0.007	0.003	-0.017	
ϕ_{Rob}	-0.018	-0.027	-0.011	-0.090	-0.064	-0.052	-0.037	0.030	-0.005	1.000	-0.006	0.003	-0.017	0.006	
A_{DCBO}	0.007	0.004	0.003	0.005	0.004	-0.002	0.021	0.002	0.010	-0.006	1.000	0.001	0.001	0.006	
ϕ_{DCBO}	0.014	0.003	0.008	0.011	0.008	0.005	-0.021	-0.009	0.007	0.003	0.001	1.000	0.012	0.012	
A_{loss}	0.982	-0.033	0.877	0.000	0.000	0.024	-0.005	-0.030	0.009	-0.017	0.006	0.012	1.000	1.000	

Figure 22: *Early-time zoom of Figure 21.*Figure 23: *R averaged over the run sets.*

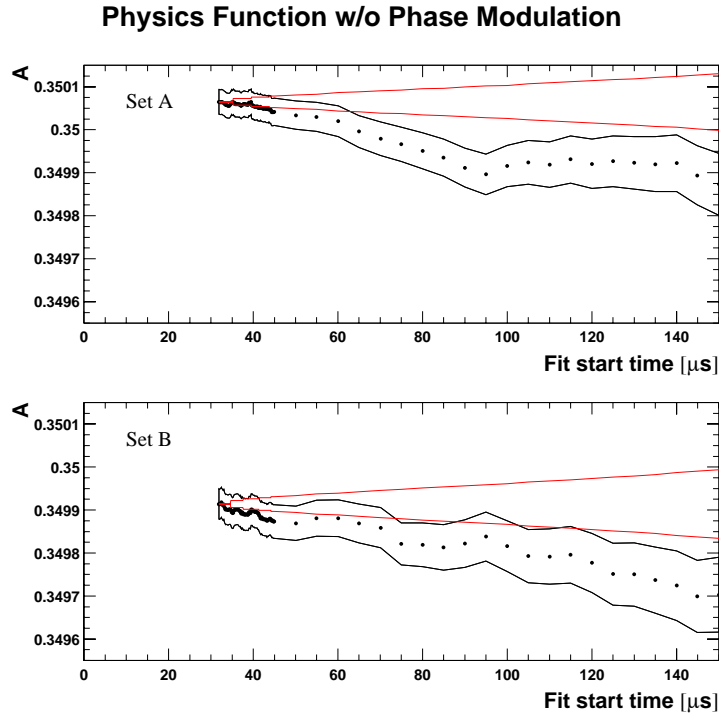


Figure 24: *Start-time scans for A, sum of all detector spectra.*

Set A, Physics Function w/o Phase Mod.: Halfring Fits

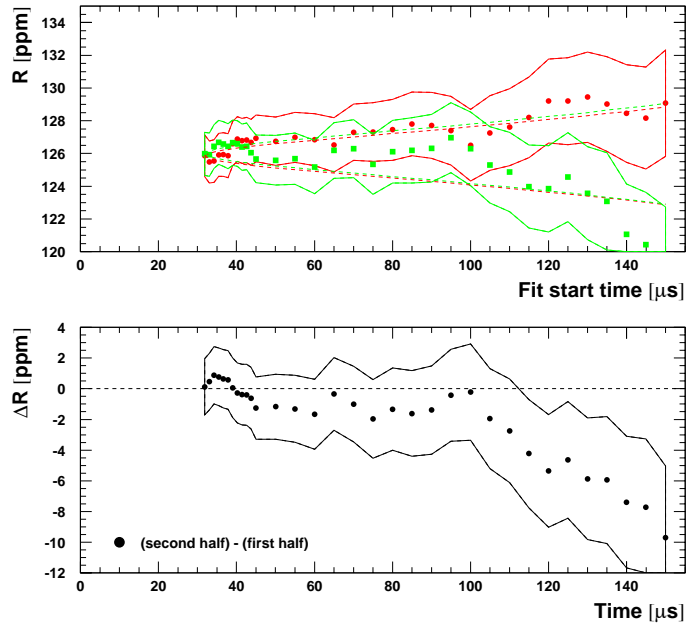
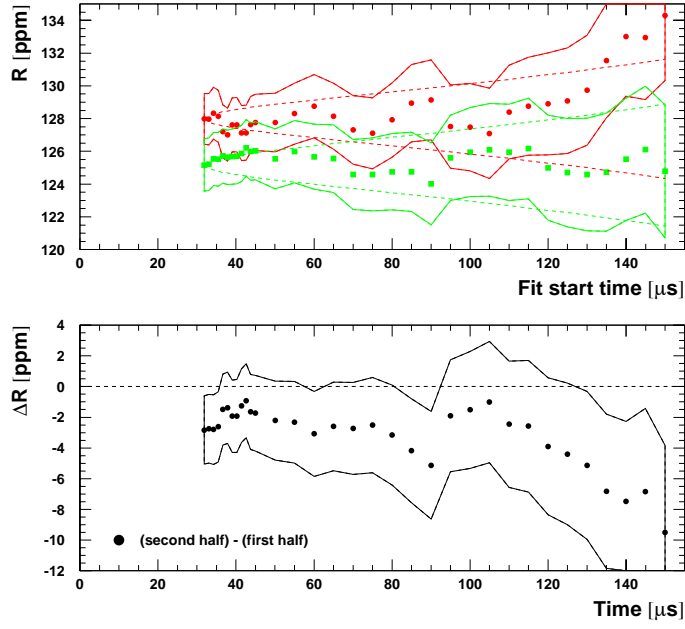


Figure 25: *Fit results for R in the two halves of the ring for Set A.*

Set B, Physics Function w/o Phase Mod.: Halfring Fits

Figure 26: *Fit results for R in the two halves of the ring for Set B.*

Physics Function w/o Phase Mod.: Halfring Fits

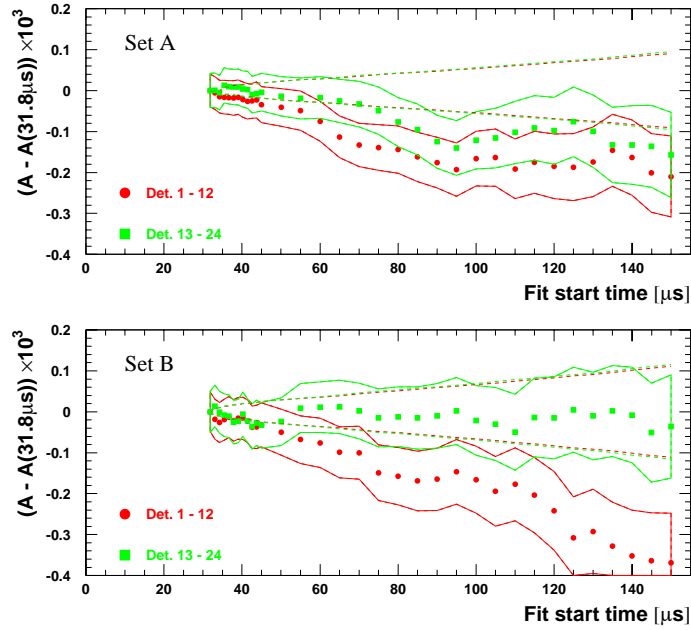
Figure 27: *Fit results for A in the two halves of the ring.*

Table 14 (last line) shows that the results from the two independent run sets are consistent within about 1σ .

Period	Sum of all detectors	First half	Second half	Average of the halves
A	125.9080 ± 0.9161	125.8438 ± 1.2785	126.0064 ± 1.3112	125.9231 ± 0.9154
B	126.5474 ± 1.1128	127.9847 ± 1.5528	125.1480 ± 1.5936	126.6031 ± 1.1121
avr.	126.1663 ± 0.7073	126.7088 ± 0.9870	125.6599 ± 1.0125	126.1977 ± 0.7068
A - B	0.6394 ± 1.4414	2.1409 ± 2.0114	0.8584 ± 2.0637	0.6800 ± 1.4404

Table 14: *Fit results for R in the individual run periods with a start time of $31.8\mu s$. The physics function without phase modulation was used.*

The CBO parameters are shown in Table 15.

Period	$A_{\text{CBO}} \times 10^3$	ϕ_{CBO}	$A_{\text{Rob}} \times 10^3$	ϕ_{Rob}	f_{CBO}	τ_{CBO}
A	1.33 ± 0.15	-0.29 ± 0.05	0.23 ± 0.25	2.91 ± 1.07	418.48 ± 0.27	97.41 ± 15.97
B	1.89 ± 0.13	2.41 ± 0.04	0.69 ± 0.24	0.81 ± 0.35	490.45 ± 0.15	149.53 ± 20.87

Table 15: *CBO parameters from fits to the sum of all detectors.*

Fits to the Individual Detectors

The fit results for individual detectors at a start time of $31.8\mu s$ are shown in the figures of Appendix B.3. A bigger version of R versus detector is displayed in Figure 28.

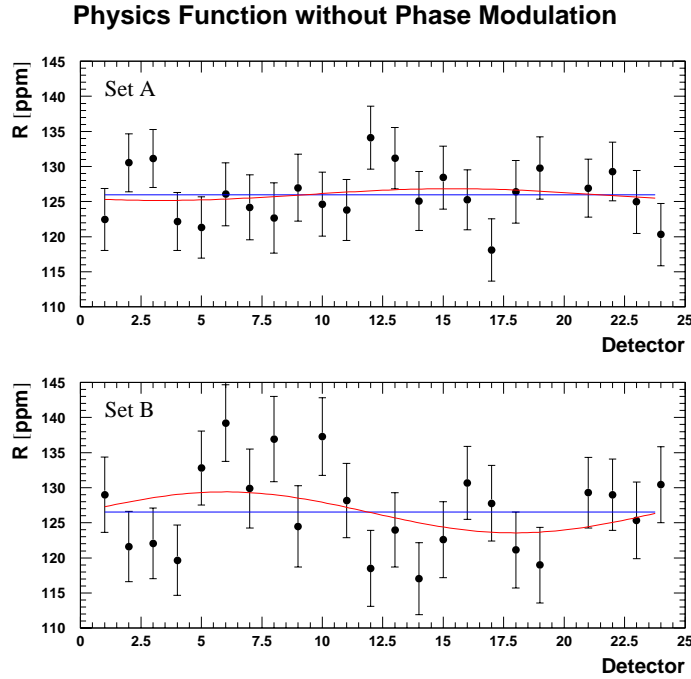


Figure 28: *R versus detector with the physics function without phase modulation.*

R versus detector can be fitted either to a constant or to a sine wave. In both cases satisfactory χ^2 are achieved. The wave amplitude is slightly smaller than for the 1999-style

function. In Set A it decreased from (1.2 ± 1.3) ppm to (0.8 ± 1.2) ppm, in Set B from (3.2 ± 1.6) ppm to (2.9 ± 1.6) ppm. The remaining effect of almost 2σ in Set B is not really a wave but rather a constant statistical shift between detectors 1-12 and 13-24, as can be seen by the rather flat difference in Figure 26.

Period	$\langle R \rangle$	χ^2/ndof (fit to a constant)
A	125.9847 ± 0.9158	17.72 / 22
B	126.5537 ± 1.1127	29.05 / 22
avr.	126.2145 ± 0.7071	

Table 16: Average R from the individual detector fits, for the different run periods with a start time of $31.8\mu\text{s}$. Detector 20 was excluded. The physics function without g -2 phase modulation was used.

Period	R_0	A_{Rc}	A_{Rs}	$\sqrt{A_{Rc}^2 + A_{Rs}^2}$	χ^2/ndof
A	126.0031 ± 0.9164	-0.5328 ± 1.2770	-0.6455 ± 1.3212	0.8370 ± 1.3035	17.28 / 20
B	126.4857 ± 1.1134	0.0304 ± 1.5528	2.9219 ± 1.6046	2.9221 ± 1.6046	25.71 / 20
avr.	126.1980 ± 0.7076	-0.3056 ± 0.9863	0.7959 ± 1.0200	0.8526 ± 1.0157	

Table 17: R versus detector fitted with a sine + cosine function like in Table 9, but for ω_a fits including the asymmetry CBO modulation. The start time was $31.8\mu\text{s}$. As always, detector 20 was excluded.

Period	$\langle R \rangle - R_0$
A	-0.0184 ± 0.0332
B	0.0680 ± 0.0395

Table 18: Difference between fitting R versus detector to a constant and to a wave (Tables 16 and 17).

In Table 19 we give the average CBO amplitudes and the CBO vector sums like in Table 11, except that the weights N_d in Eq. (27) are replaced by $N_d A_d \cos \phi_{a,d}$.

Period	$\langle A_{\text{CBO}} \rangle \times 10^3$	$\langle A_{\text{Rob}} \rangle \times 10^3$
A	6.31 ± 0.17	2.84 ± 0.28
B	10.24 ± 0.16	4.08 ± 0.28

Period	vector sum over all detectors			
	$A_{\text{CBO}} \times 10^3$	ϕ_{CBO}	$A_{\text{Rob}} \times 10^3$	ϕ_{Rob}
A	1.35 ± 0.15	5.98 ± 0.09	0.20 ± 0.29	2.27 ± 1.43
B	2.09 ± 0.13	2.28 ± 0.06	0.84 ± 0.28	0.90 ± 0.34

Table 19: Upper table: CBO parameters from fits to the individual detectors, averaged over all detectors. Lower Table: coherent sum of the CBO parameters over all detectors. The results should be consistent with the fit parameters obtained from the summed spectra (cf. Table 15).

We want to point out the following observations:

- Inclusion of the asymmetry modulation into the fit has very little influence on $\langle A_{\text{CBO}} \rangle$: For Set A we find $(6.31 \pm 0.17) \times 10^{-3}$ instead of $(6.41 \pm 0.17) \times 10^{-3}$ (Table 11); for Set B we find $(10.24 \pm 0.16) \times 10^{-3}$ instead of $(10.31 \pm 0.16) \times 10^{-3}$.
- The same holds for the vector sum of $(A_{\text{CBO}}, \phi_{\text{CBO}})$.
- The agreement between the vector sum $(A_{\text{CBO}}, \phi_{\text{CBO}})$ and the parameter values obtained by fitting the sum of detector spectra is good (compare with Table 15).
- The same is true for $(A_{\text{Rob}}, \phi_{\text{Rob}})$.

Comparison between Fits to the Sum and the Average of Individual Fits

Period	$ \langle R \rangle - R_{\text{sum}} $	$ R_0 - R_{\text{sum}} $
A	0.0767 ± 0.0234	0.0951 ± 0.0234
B	0.0063 ± 0.0149	-0.0617 ± 0.0365

Table 20: *Difference between R from fits to the sum of all detector spectra and the averages $\langle R \rangle$ and R_0 from fits to individual detector spectra.*

5.4.3 Fits with Asymmetry and Phase Modulation

In this section we fit for all three CBO effects: acceptance, asymmetry and phase modulation.

The correlation matrices (Tables 21 and 22) confirm what we have already seen after including the asymmetry modulation into the fit: neither A nor R correlates strongly with A_{Jim} or ϕ_{Jim} .

Fits to the Sum of Detectors

Start time scans for R are shown in Figure 29 for the two data subsets. Figure 30 shows a zoom for start times up to $45 \mu\text{s}$ with a step of 150 ns .

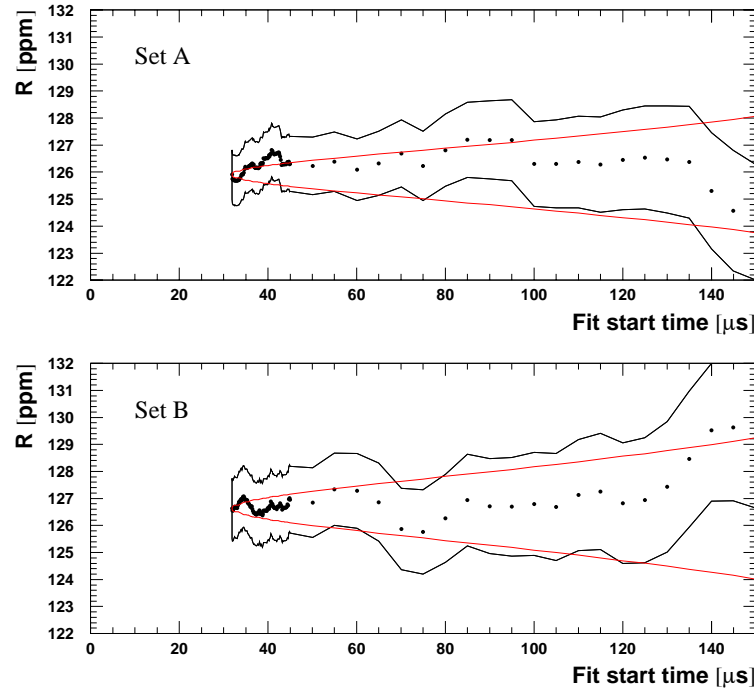


Figure 29: *Start time scans for the sum of all detector spectra fitted with the physics function including phase modulation by CBO.*

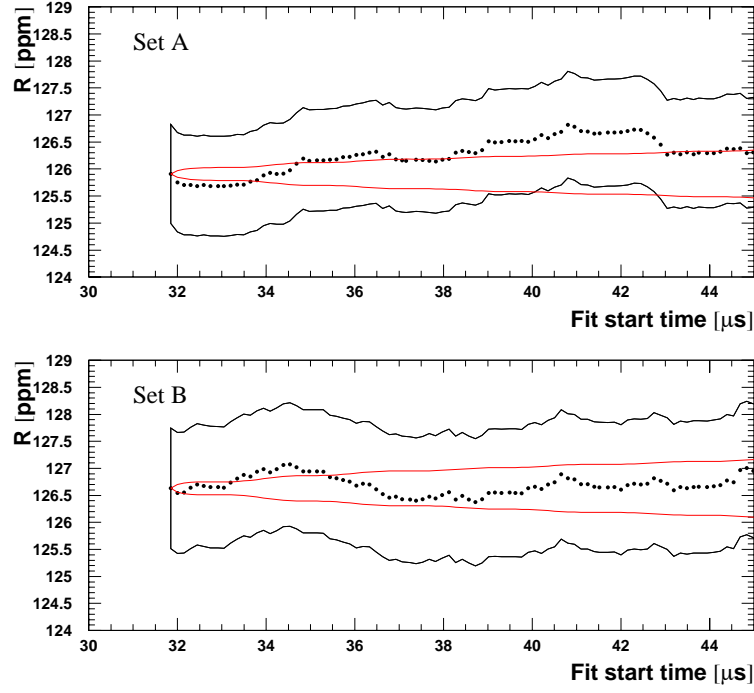
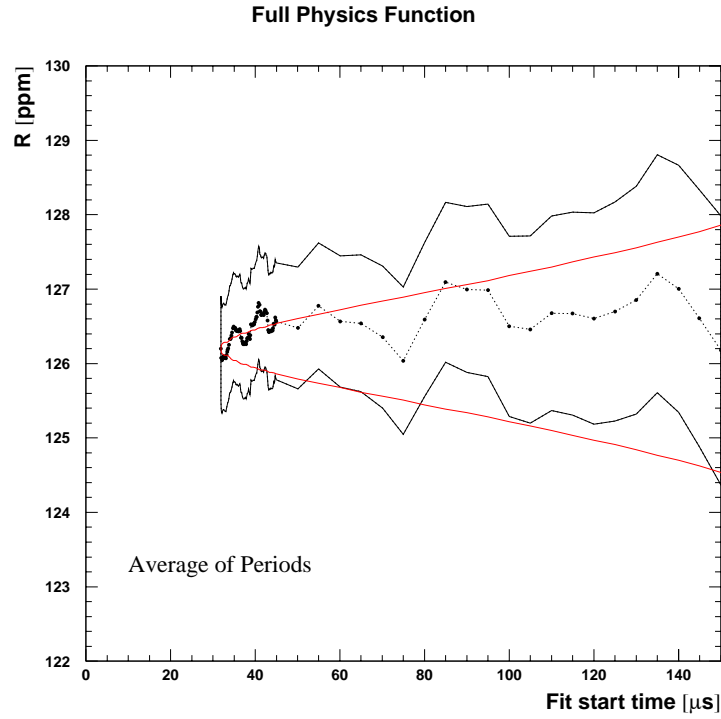
The weighted average of the fit results for R from the two run sets is shown in Figure 31 and Table 23 for R . Scans of the fit stop-time are shown in Figure 32.

Set A	N_0	A	τ	ϕ_a	R	f_{CBO}	τ_{CBO}	A_{CBO}	ϕ_{CBO}	A_{Rob}	ϕ_{Rob}	A_{Jim}	ϕ_{Jim}	A_{DCBO}	ϕ_{DCBO}	A_{loss}
N_0	1.000	-0.040	0.816	-0.010	-0.007	0.017	-0.022	0.030	-0.025	-0.023	0.028	-0.013	-0.071	-0.009	0.018	0.982
A	-0.040	1.000	-0.025	-0.008	-0.004	0.006	0.011	-0.014	-0.010	0.066	0.038	-0.068	0.016	-0.003	0.001	-0.037
τ	0.816	-0.025	1.000	-0.007	-0.005	0.010	-0.013	0.018	-0.015	-0.014	0.018	-0.010	-0.044	-0.006	0.011	0.873
ϕ_a	-0.010	-0.008	-0.007	1.000	0.834	0.018	-0.025	0.035	-0.024	0.054	-0.082	0.004	0.068	-0.000	0.010	-0.009
R	-0.007	-0.004	-0.005	0.834	1.000	0.013	-0.018	0.026	-0.017	0.040	-0.039	0.002	-0.058	-0.000	0.007	-0.007
f_{CBO}	0.017	0.006	0.010	0.018	0.013	1.000	-0.004	0.007	-0.319	0.002	0.132	-0.134	-0.003	-0.012	0.016	0.015
τ_{CBO}	-0.022	0.011	-0.013	-0.025	-0.018	-0.004	1.000	-0.903	0.003	0.132	0.005	-0.007	0.016	-0.466	0.017	-0.020
A_{CBO}	0.030	-0.014	0.018	0.035	0.026	0.007	-0.903	1.000	-0.006	-0.134	-0.007	-0.010	0.008	0.420	-0.022	0.028
ϕ_{CBO}	-0.025	-0.010	-0.015	-0.024	-0.017	-0.319	0.003	-0.006	1.000	-0.003	0.046	-0.001	0.014	-0.016	-0.023	-0.023
A_{Rob}	-0.023	0.066	-0.014	0.054	0.040	0.002	0.132	-0.134	-0.003	1.000	-0.006	-0.009	0.023	-0.073	0.002	-0.021
ϕ_{Rob}	0.028	0.038	0.018	-0.082	-0.058	-0.049	0.005	-0.007	0.046	-0.006	1.000	-0.007	0.005	0.005	0.019	0.026
A_{Jim}	-0.013	-0.068	-0.010	0.004	0.002	-0.002	0.016	-0.010	-0.001	0.009	-0.007	1.000	-0.015	-0.034	0.029	-0.013
ϕ_{Jim}	-0.071	0.016	-0.044	0.068	0.050	-0.016	-0.007	0.008	0.014	0.023	0.005	-0.015	1.000	0.024	0.015	-0.065
A_{DCBO}	-0.009	-0.003	-0.006	-0.000	-0.000	-0.012	-0.466	0.420	0.015	-0.073	0.005	-0.034	0.024	1.000	-0.016	-0.008
ϕ_{DCBO}	0.018	0.001	0.011	0.010	0.007	0.016	0.017	-0.022	-0.016	-0.002	0.019	0.029	0.015	-0.016	1.000	0.016
A_{loss}	0.982	-0.037	0.873	-0.009	-0.007	0.015	-0.020	0.028	-0.023	-0.021	0.026	-0.013	-0.065	-0.008	0.016	1.000

Table 21: Correlation matrix $\frac{\text{cov}(\mathbf{P}_i, \mathbf{P}_j)}{\sigma_i \sigma_j}$ from a fit to the sum of detector spectra of Set A starting at $31.8 \mu\text{s}$.

Set B	N_0	A	τ	ϕ_a	R	f_{CBO}	τ_{CBO}	A_{CBO}	ϕ_{CBO}	A_{Rob}	ϕ_{Rob}	A_{Jim}	ϕ_{Jim}	A_{DCBO}	ϕ_{DCBO}	A_{loss}
N_0	1.000	-0.036	0.820	0.006	0.004	0.028	-0.006	0.007	-0.034	0.010	-0.019	0.024	-0.039	-0.005	0.014	0.982
A	-0.036	1.000	-0.022	-0.010	-0.006	0.009	0.014	-0.016	-0.007	-0.067	-0.027	-0.063	-0.035	-0.004	0.006	-0.033
τ	0.820	-0.022	1.000	0.003	0.002	0.017	-0.003	0.004	-0.021	0.006	-0.012	0.015	-0.023	-0.002	0.009	0.877
ϕ_a	0.006	-0.010	0.003	1.000	0.835	0.034	-0.019	0.021	-0.035	0.046	-0.091	0.066	-0.096	-0.002	0.012	0.005
R	0.004	-0.006	0.002	0.835	1.000	0.024	-0.014	0.015	-0.025	0.035	-0.065	0.050	-0.068	-0.001	0.009	0.004
f_{CBO}	0.028	0.009	0.017	0.034	0.024	1.000	0.003	-0.004	-0.424	-0.027	-0.053	-0.003	-0.033	0.004	0.006	0.026
τ_{CBO}	-0.006	0.014	-0.003	-0.019	-0.014	0.003	1.000	-0.885	-0.008	-0.177	0.028	-0.092	-0.005	0.026	0.016	-0.005
A_{CBO}	0.007	-0.016	0.004	0.021	0.015	-0.004	-0.885	1.000	0.010	0.156	-0.038	0.081	0.007	-0.021	-0.023	0.006
ϕ_{CBO}	-0.034	-0.007	-0.021	-0.035	-0.025	-0.424	-0.008	0.010	1.000	0.035	0.030	0.005	0.021	-0.003	-0.010	-0.031
A_{Rob}	0.010	-0.067	0.006	0.046	0.035	-0.027	-0.177	0.156	0.035	1.000	-0.006	0.022	0.012	-0.009	0.007	0.009
ϕ_{Rob}	-0.019	-0.027	-0.012	-0.091	-0.065	-0.053	0.028	-0.038	0.030	-0.006	1.000	-0.019	0.011	0.006	0.002	-0.018
A_{Jim}	0.024	-0.063	0.015	0.066	0.050	-0.003	-0.092	0.081	0.005	0.022	-0.019	1.000	0.000	0.006	-0.024	0.022
ϕ_{Jim}	-0.039	-0.035	-0.023	-0.096	-0.068	-0.033	-0.005	0.007	0.021	0.012	0.011	0.000	1.000	-0.011	-0.015	-0.035
A_{DCBO}	-0.005	-0.004	-0.002	-0.002	-0.001	0.004	0.026	-0.021	-0.003	-0.009	0.006	0.006	-0.011	1.000	-0.001	-0.004
ϕ_{DCBO}	0.014	0.006	0.009	0.012	0.009	0.006	0.016	-0.023	-0.010	0.007	0.002	-0.024	-0.015	-0.001	1.000	0.013
A_{loss}	0.982	-0.033	0.877	0.005	0.004	0.026	-0.005	0.006	-0.031	0.009	-0.018	0.022	-0.035	-0.004	0.013	1.000

Table 22: Correlation matrix $\frac{\text{cov}(\mathbf{p}_i, \mathbf{p}_j)}{\sigma_i \sigma_j}$ from a fit to the sum of detector spectra of Set B starting at $31.8 \mu\text{s}$.

Figure 30: *Early-time zoom of Figure 29.*Figure 31: R averaged over the two run sets.

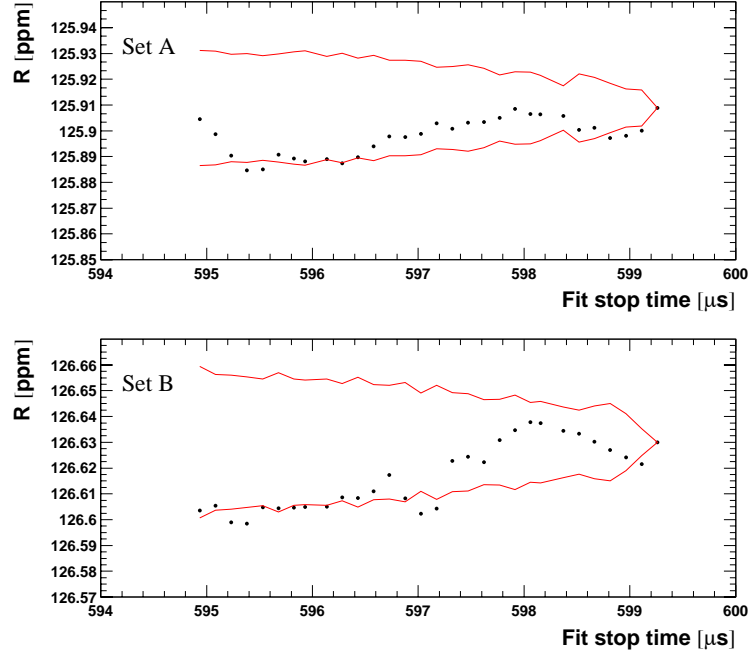
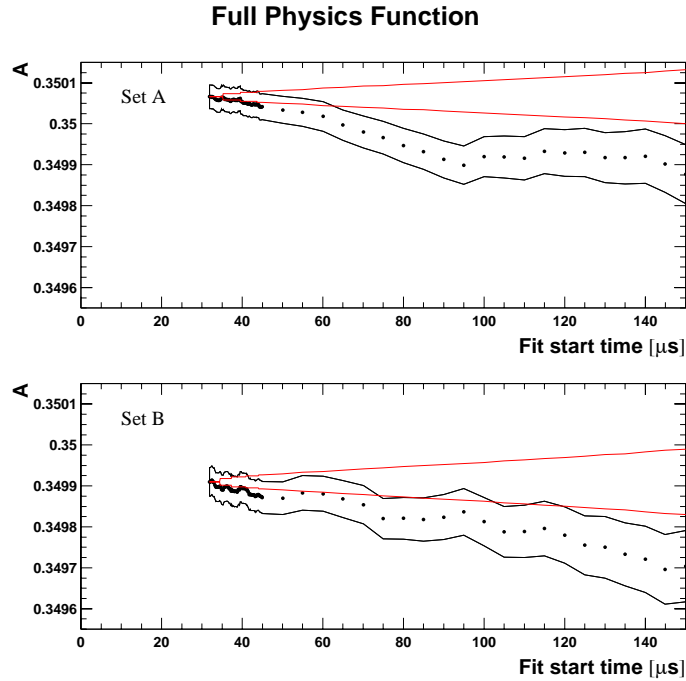
Figure 32: *Fit stop-time scans for R .*

Figure 33 shows start-time scans for A . Unlike in 2000, the start-time stability of A does not improve when amplitude and phase modulation are switched on. This reflects the absence of strong correlations between A and A_{Rob} , A_{Jim} . The reason of the asymmetry sag may be a combination of imperfections in pileup subtraction and energy-scale correction.

Figure 33: *Start-time scans for A , sum of all detector spectra.*

The halfring effect that had already been reduced by inclusion of the asymmetry modulation is mostly eliminated when also the phase modulation is fitted for, see Figures 34 and 35 for R and Figures 36 for A .

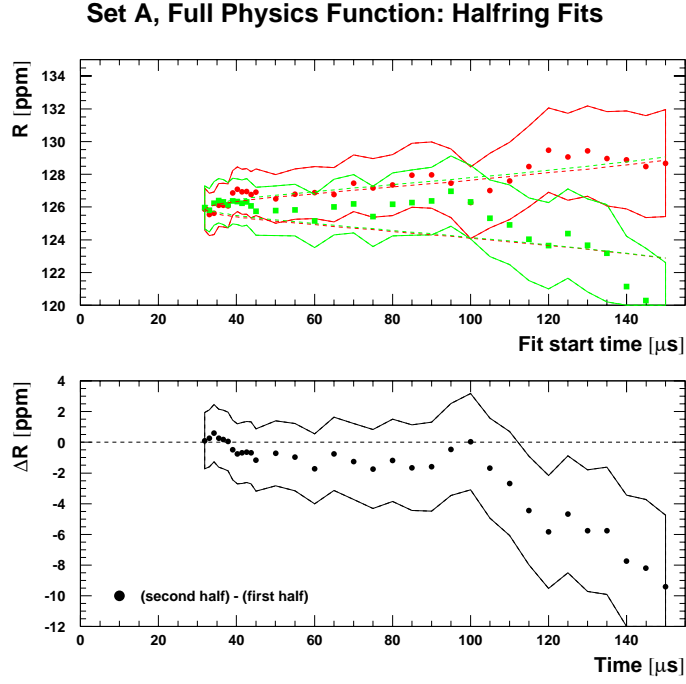


Figure 34: *Fit results for R in the two halves of the ring for Set A.*

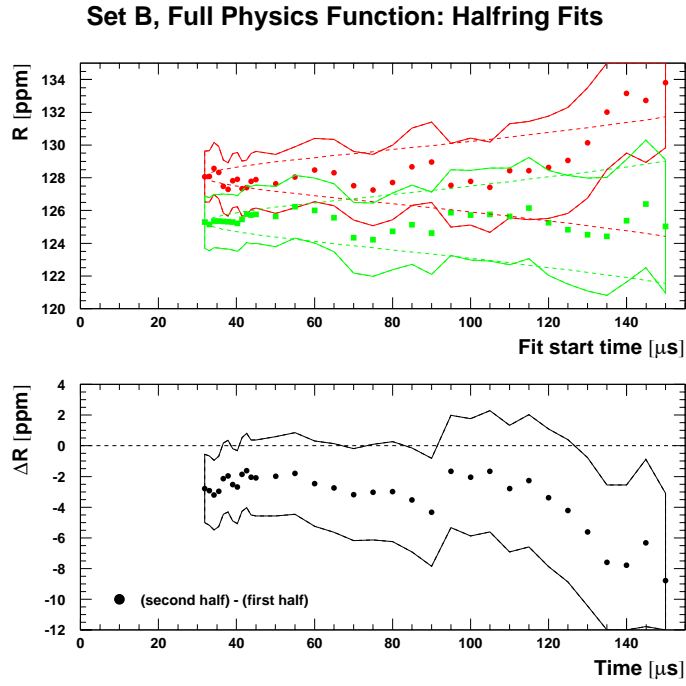


Figure 35: *Fit results for R in the two halves of the ring for Set B.*

Period	Sum of all detectors	First half	Second half	Average of the halves
A	125.9085 ± 0.9172	125.8337 ± 1.2802	126.0115 ± 1.3131	125.9203 ± 0.9166
B	126.6301 ± 1.1169	128.0963 ± 1.5583	125.2315 ± 1.6010	126.7026 ± 1.1167
Avr.	126.1991 ± 0.7088	126.7454 ± 0.9892	125.6978 ± 1.0153	126.2352 ± 0.7085
A - B	0.7216 ± 1.4452	2.2626 ± 2.0167	0.7800 ± 2.0706	0.7823 ± 1.4447

Table 23: R for the sum of all detectors and for the two half rings. The fits were done with the full physics function. The start time was $31.8\mu\text{s}$.

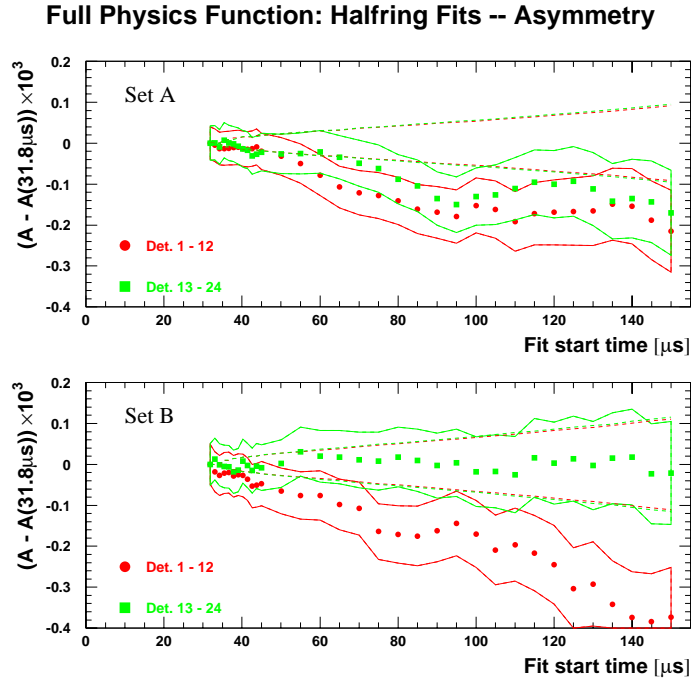


Figure 36: Fit results for A in the two halves of the ring.

Start time scans for the other parameters and for the different run periods are shown in Appendix C.1. Appendix C.2 shows them for the first and second half of the ring.

Period	$A_{\text{CBO}} \times 10^3$	ϕ_{CBO}	$A_{\text{Rob}} \times 10^3$	ϕ_{Rob}	$A_{\text{Jim}} \times 10^3$	ϕ_{Jim}
A	1.33 ± 0.15	-0.29 ± 0.05	0.23 ± 0.25	2.91 ± 1.07	0.02 ± 0.09	0.65 ± 5.03
B	1.89 ± 0.13	2.42 ± 0.04	0.69 ± 0.24	0.81 ± 0.35	0.13 ± 0.08	2.27 ± 0.66
Period	f_{CBO} [kHz]		τ_{CBO} [μs]			
A	418.48 ± 0.27		97.09 ± 15.90			
B	490.44 ± 0.15		148.29 ± 20.58			

Table 24: CBO parameters from fits to the sum of all detectors.

Fits to the Individual Detectors

The fit results for individual detectors at a start time of $49.2 \mu\text{s}$ are shown in the figures of Appendix C.3. A bigger version of R versus detector is displayed in Figure 37.

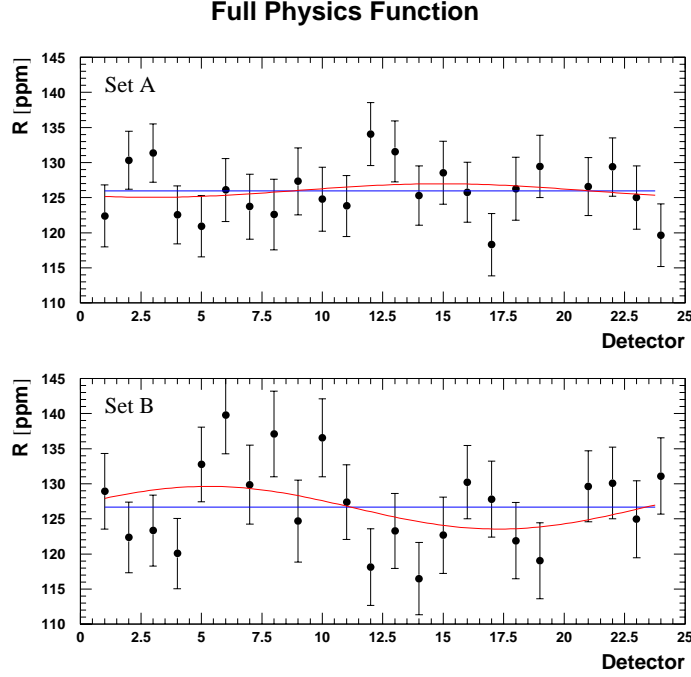


Figure 37: R versus detector with the full physics function.

With the full physics function, R versus detector is very similar to its behaviour for the physics function without phase modulation because the latter is a very small effect. The wave amplitude (Table 26) is reduced from (1.2 ± 1.3) ppm with the 1999-style function to (1.0 ± 1.3) ppm, in Set B from (3.2 ± 1.6) ppm to (3.0 ± 1.6) ppm. The remaining effect of almost 2σ in Set B is not really a wave but rather a statistical shift between detectors 1-12 and 13-24, as can be seen by the constant difference in Figure 35.

Period	$\langle R \rangle$	χ^2/ndof (fit to a constant)
A	125.9921 ± 0.9172	18.17 / 22
B	126.6632 ± 1.1174	28.80 / 22
avr.	126.2623 ± 0.7090	

Table 25: Average R from the individual detector fits, for the two run sets with a start time of $31.8 \mu\text{s}$. Detector 20 was excluded. The full physics function was used.

Period	R_0	A_{Rc}	A_{Rs}	$\sqrt{A_{Rc}^2 + A_{Rs}^2}$	χ^2/ndof
A	126.0123 ± 0.9177	-0.6984 ± 1.2791	-0.6688 ± 1.3233	0.9670 ± 1.3004	17.58 / 20
B	126.5915 ± 1.1181	0.5711 ± 1.5597	2.9872 ± 1.6109	3.0413 ± 1.6091	25.11 / 20
avr.	126.2454 ± 0.7094	-0.1879 ± 0.9890	0.8043 ± 1.0225	0.8260 ± 1.0208	

Table 26: R versus detector fitted with a sine + cosine function. The individual detector spectra were fitted with the full physics function. The start time was $31.8 \mu\text{s}$. Detector 20 was excluded.

Period	$\langle R \rangle - R_0$
A	-0.0202 ± 0.0303
B	0.0717 ± 0.0396

Table 27: Difference between fitting R versus detector to a constant and to a wave (Tables 25 and 26).

In Table 28 we give the average CBO amplitudes and the CBO vector sums like in Table 11, except that the weights N_d in Eq. (27) are replaced by $N_d A_d \phi_{a,d} \sin \phi_{a,d}$, as can be seen by expanding the phase modulation in the physics function.

Period	$\langle A_{\text{CBO}} \rangle \times 10^3$	$\langle A_{\text{Rob}} \rangle \times 10^3$	$\langle A_{\text{Jim}} \rangle \times 10^3$	$\langle \phi_{\text{Jim}} - \phi_{\text{Rob}} \rangle$
A	6.28 ± 0.17	2.84 ± 0.28	0.67 ± 0.10	2.36 ± 0.15
B	10.27 ± 0.16	4.10 ± 0.28	0.71 ± 0.10	2.15 ± 0.14

Period	vector sum over all detectors					
	$A_{\text{CBO}} \times 10^3$	ϕ_{CBO}	$A_{\text{Rob}} \times 10^3$	ϕ_{Rob}	$A_{\text{Jim}} \times 10^3$	ϕ_{Jim}
A	1.36 ± 0.15	-0.30 ± 0.09	0.20 ± 0.29	2.25 ± 1.46	0.04 ± 0.10	6.20 ± 2.75
B	2.09 ± 0.13	2.28 ± 0.06	0.84 ± 0.29	0.88 ± 0.34	0.21 ± 0.10	2.27 ± 0.47

Table 28: Upper table: CBO parameters from fits to the individual detectors, averaged over all detectors. Lower Table: coherent sum of the CBO parameters over all detectors. The results should be consistent with the fit parameters obtained from the summed spectra (cf. Table 24).

Again, average amplitude and vector sum of the main CBO are not strongly affected by the inclusion of the phase modulation term (cf. Tables 19 and 28). The same holds for the asymmetry modulation.

The asymmetry and phase modulation vector sums over all detectors reproduce the results from the fit to the sum of detectors (Table 24) within their errors.

Comparison between Fits to the Sum and the Average of Individual Fits

Period	$ \langle R \rangle - R_{\text{sum}} $	$ R_0 - R_{\text{sum}} $
A	0.0767 ± 0.0234	0.0951 ± 0.0234
B	0.0063 ± 0.0149	-0.0616 ± 0.0365

Table 29: *Difference between R from fits to the sum of all detector spectra and the averages $\langle R \rangle$ and R_0 from fits to individual detector spectra.*

5.4.4 Energy-Binned Fits with the Full Physics Function

To shed some more light on the instability of the asymmetry in start-time scans a series of fits in 200 MeV energy bins between 1.8 GeV and 3.4 GeV was performed. Fit convergence was facilitated by excluding double CBO and fixing the CBO lifetime to the result from the fit to the full energy range. The muon loss amplitude was left free even if it took a non-physical negative value. This was done to give the fit an r.s.e.-like freedom for eliminating problems with slow effects which we don't aim to study here.

The pileup error correction was adapted to the binned situation. The coefficients X and γ and their product to be used in Eq. 23 are drawn as a function of E in Figures 39 and 40. X is determined as the ratio of doubles (D) to singles ($N - D + S1 + S2$) counted over the g-2 cycle centred at $34.1 \mu\text{s}$. The factor γ is calculated from the single-pulse energy spectrum obtained from $S2$ pulses which are not suppressed by the 0.9 GeV threshold. Figure 38 serves as illustration of the calculation. Note that all zones with $E_{S1} < 0.9 \text{ GeV}$ are invisible in the Mediterranean pileup subtraction and have to be simulated by reduplication of the corresponding zones with $E_{S2} < 0.9 \text{ GeV}$.

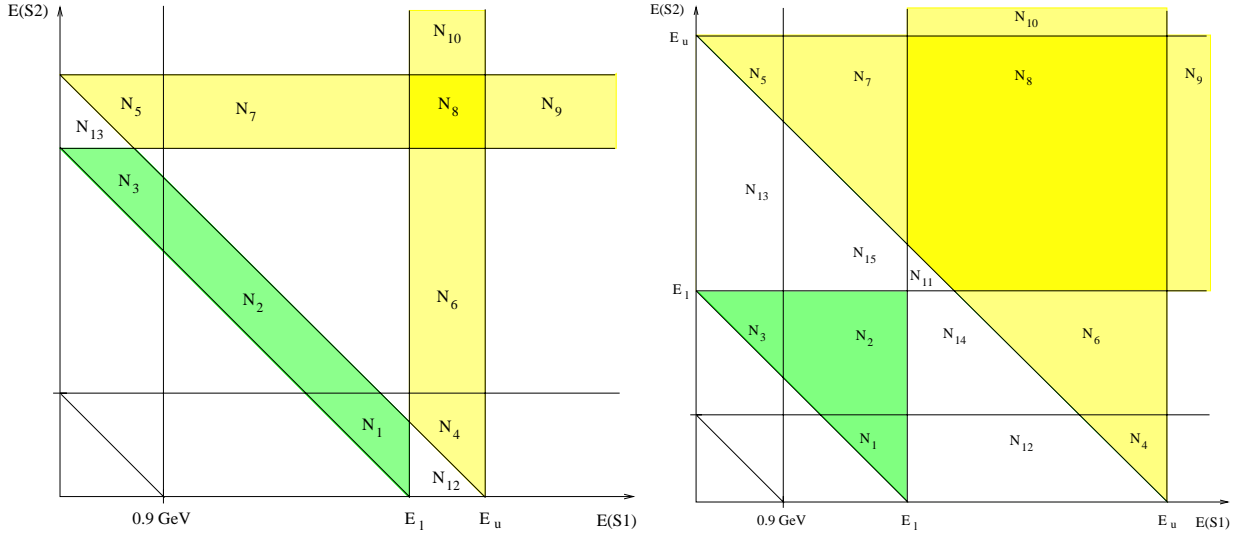


Figure 38: Zones in the $S1$ - vs. $S2$ -pulse energy plane for the calculation of the γ factor in an energy interval $[E_l; E_u]$. Two different cases are shown.

As a first step, the single-pulse energy spectrum $n_S(E)$ is two-dimensionally integrated over each of the zones labelled in the figure:

$$N_i = \int_{\text{Zone } i} dE_{S1} dE_{S2} n_S(E_{S1}) n_S(E_{S2}) \quad (28)$$

Then γ is defined as the ratio

$$\gamma = \frac{N_{\text{extra}} + \sigma_{\text{extra}}^2 + 2 \text{COV}_{\text{raw hist, extra}}}{N_{\text{doubles}}} \quad (29)$$

with

$$N_{\text{extra}} = 2(N_1 - N_4) + N_2 - N_6 - N_7 - 2N_8 - N_9 - N_{10} - N_{11} \quad (30)$$

$$\sigma_{\text{extra}}^2 = 4(N_1 + N_4) + N_2 + N_6 + N_7 + 4N_8 + N_9 + N_{10} + N_{11} \quad (31)$$

$$\text{COV}_{\text{raw hist, extra}} = 2N_4 + N_6 + N_7 + 2N_8 + N_9 + N_{10} + N_{11} \quad (32)$$

$$N_{\text{doubles}} = 2N_1 + N_2 + N_{11} + 2N_{12} + N_{14} + N_{15} \quad (33)$$

At high energies it is important to use the correct coefficients: fitting Set B in the energy bin [3.2 GeV; 3.4 GeV] with the values from the full energy range yields a χ^2 of 1.066. With the correct values this is reduced to 1.012. Fred points out correctly that there are correlations between the γ -factors of different energy bins. This happens because some zones used for a given bin will also appear in the calculation for another bin. However, we take above formulae as a first-order approach.

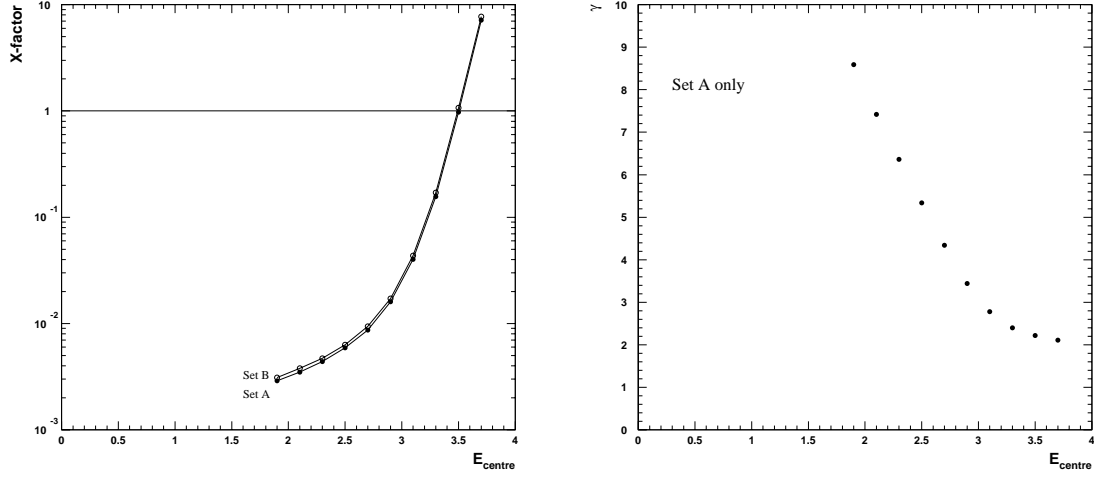


Figure 39: *Pileup error correction coefficients X and γ as a function of the centre of 200 MeV wide energy bins.*

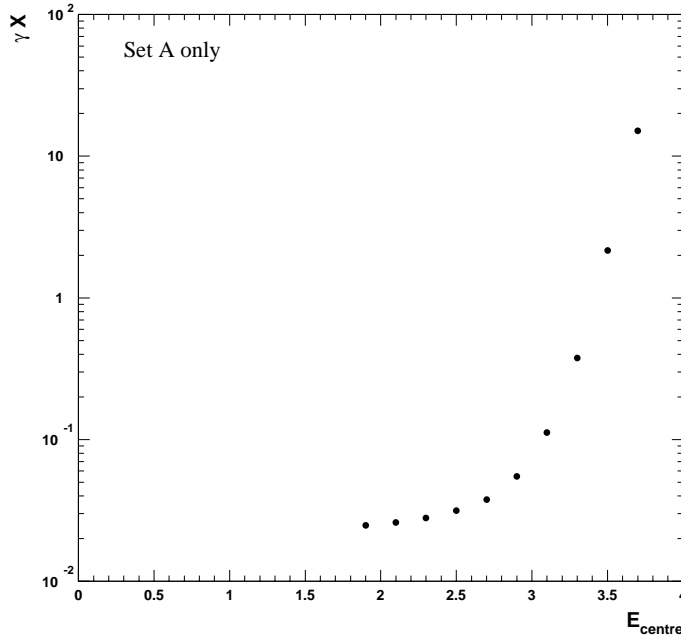


Figure 40: *Product $X\gamma$ from the previous figure.*

Figures 41 to 43 show R , A and χ^2 respectively for a start time of $31.8 \mu\text{s}$ as a function of the centre of the energy bin. The other parameters are given in Appendix D.

Table 30 compares R averaged over the energy bins with the results from fits over the full energy range $1.8 \text{ GeV} - 3.4 \text{ GeV}$. Note the lower statistical errors when energy bins are fitted separately. For Set A the two results agree whereas for Set B they differ by 2.1 standard deviations. The error of the difference may be underestimated by using the simple quadratic error difference.

Set	Fit over $[1.8 \text{ GeV}; 4.3 \text{ GeV}]$	Average of Energy Bins	Difference
A	125.9085 ± 0.9172	126.1537 ± 0.8516	0.2452 ± 0.3406
B	126.6301 ± 1.1169	127.6315 ± 1.0371	1.0014 ± 0.4146
avr.	126.1991 ± 0.7088	126.7488 ± 0.6581	0.5497 ± 0.2633

Table 30: Comparison of R from fits to the full energy range and from the average of individual energy bin results. These numbers represent fits to the sum of all detectors starting at $31.8 \mu\text{s}$.

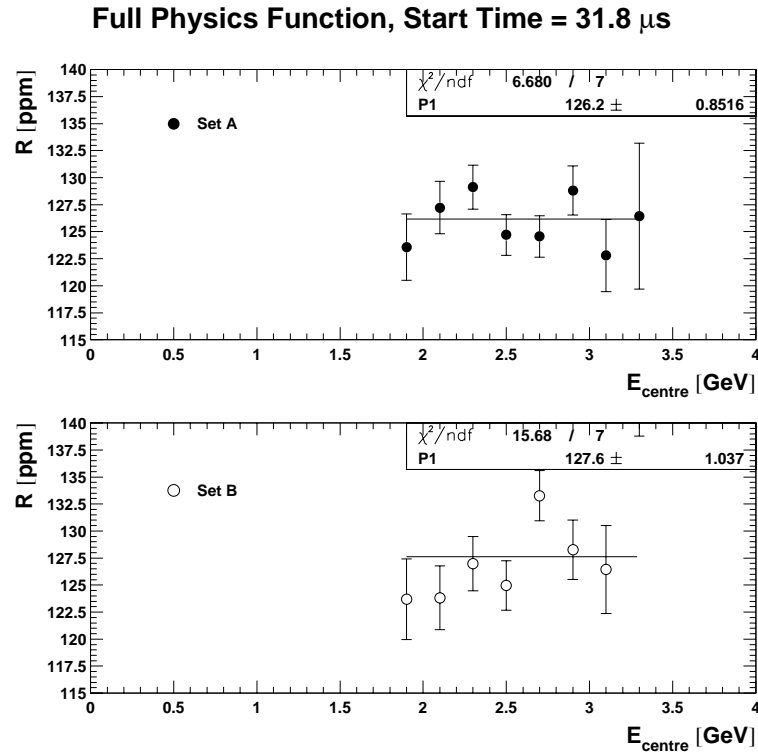
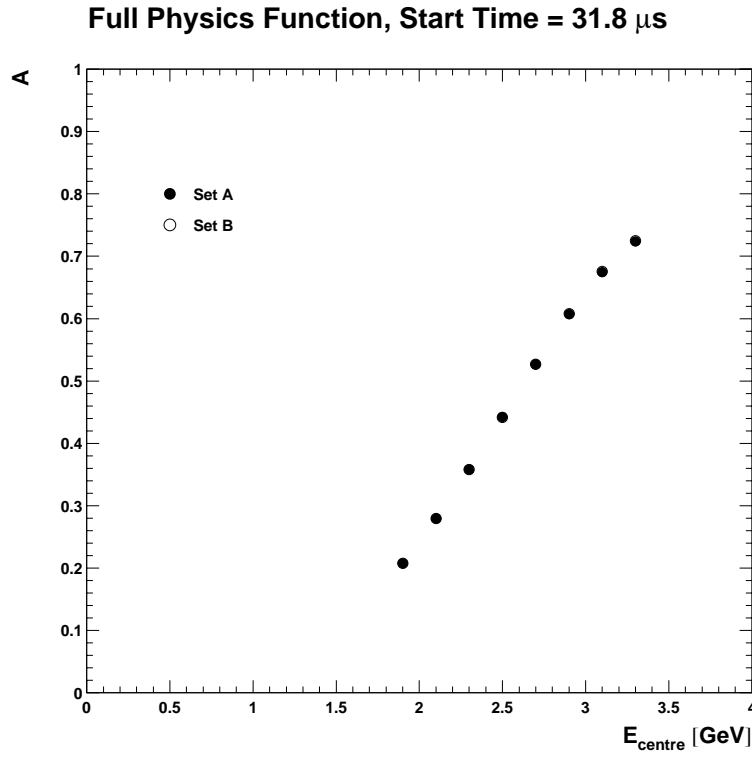
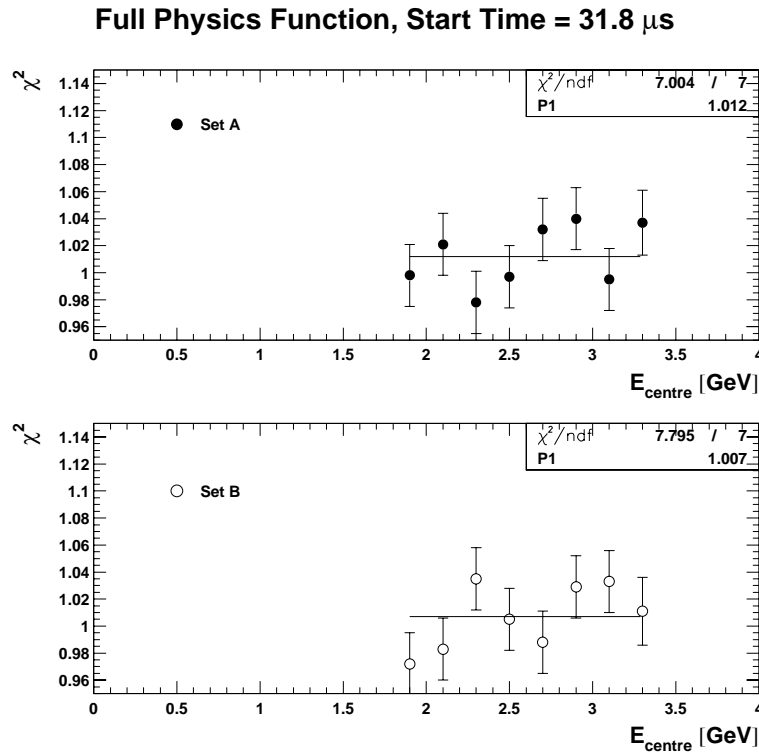


Figure 41: R versus centre of 200 MeV wide energy bins.

Figure 42: A versus centre of 200 MeV wide energy bins.Figure 43: χ^2 versus centre of 200 MeV wide energy bins.

Individual Detector Fits

The same comparison was done for individual detector fits. The fit results are shown in Figure 44.

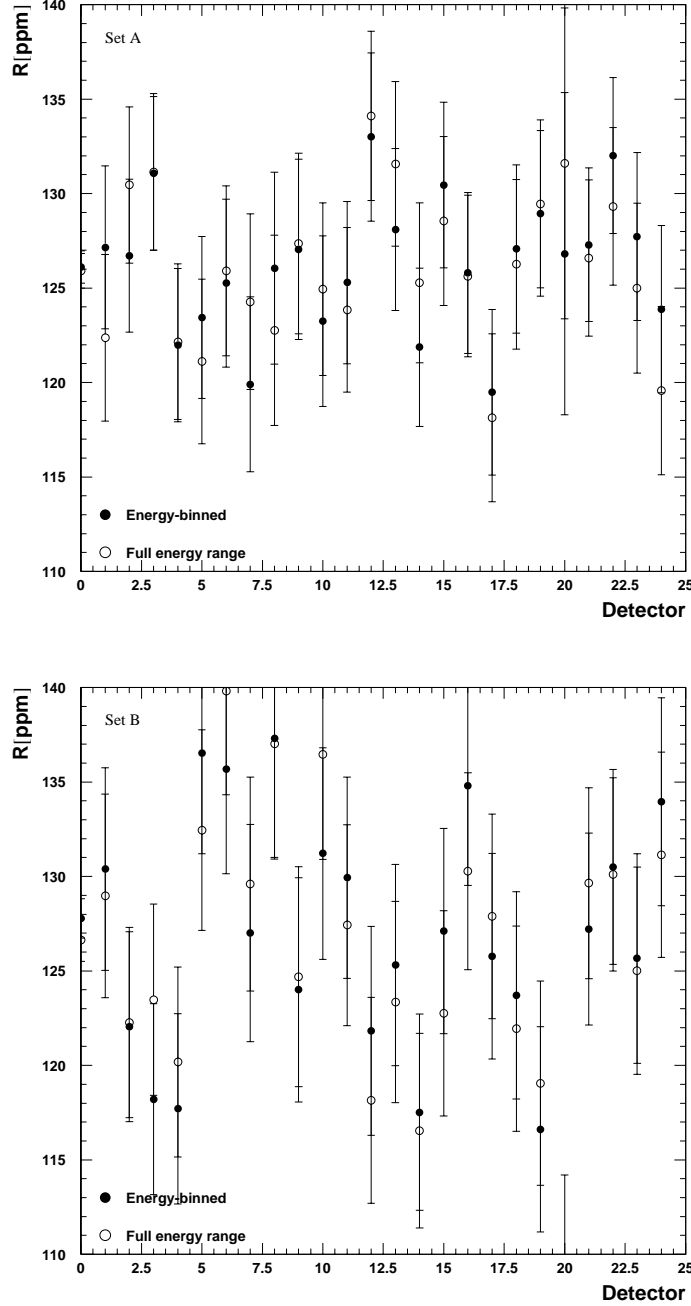


Figure 44: *Comparison of the results from the energy-binned and the combined fits.*

Again, the error of the difference between the binned and the summed analysis is assumed to be the quadratic error difference which may be wrong. Indeed, Figure 45 shows differences up to 10σ for some detectors. No clear pattern of troublesome detectors is visible. Averaging the results over detectors we obtain Table 31.

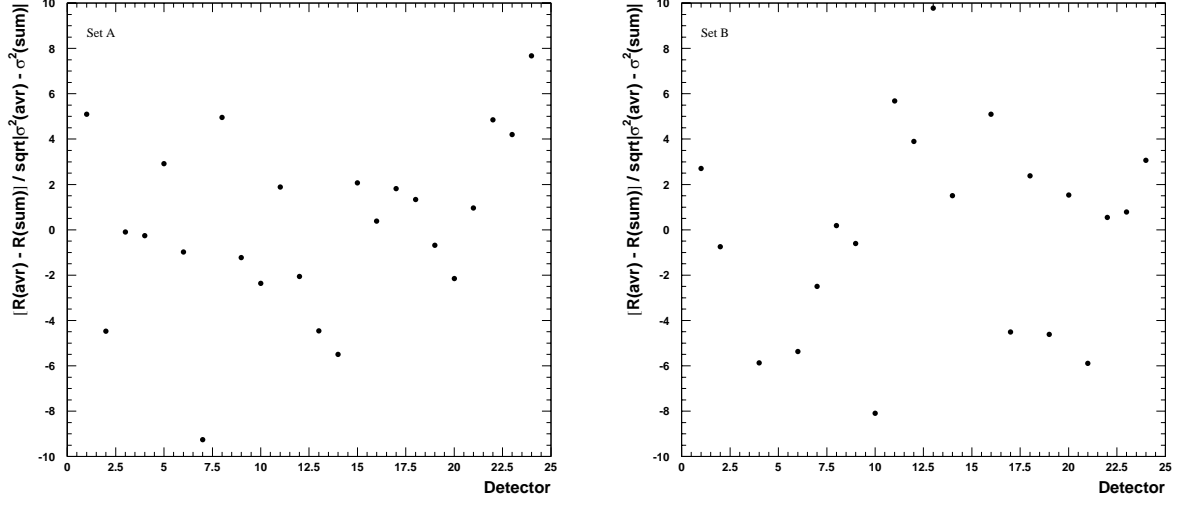


Figure 45: *Difference between the binned and the summed fit results in terms of standard deviations assuming that the errors subtract quadratically.*

Set	Fit over [1.8 GeV; 4.3 GeV] averaged over detectors	Average of Energy Bins and detectors	Difference
A	125.9921 ± 0.9172	126.2570 ± 0.9059	0.2649 ± 0.1435
B	126.6632 ± 1.1174	126.7072 ± 1.1255	0.0440 ± 0.1348
avr.	126.2623 ± 0.7090	126.4340 ± 0.7057	0.1717 ± 0.0683

Table 31: *Comparison of R from fits to the full energy range and from the average of individual energy bin results. These numbers are the averages over individual detector fits starting at $31.8 \mu\text{s}$.*

Strangely, unlike the sum of detectors, the average over detectors does not show any obvious problem in Set B.

However, for a conclusive comparison a detailed systematic error analysis for the binned fits would be necessary which is beyond the scope of our approach.

Upon request by the review committee we have also evaluated the normalised differences $\frac{R(E_i) - \langle R(E_i) \rangle}{\sigma(R(E_i))}$ for each detector. The means and RMS of these distributions are plotted versus detector in Figure 46). Their averages over all detectors (except 20) are given in Table 46. For both sets the average means are sufficiently close to 0 whereas the average RMS are about 2σ lower than 1.

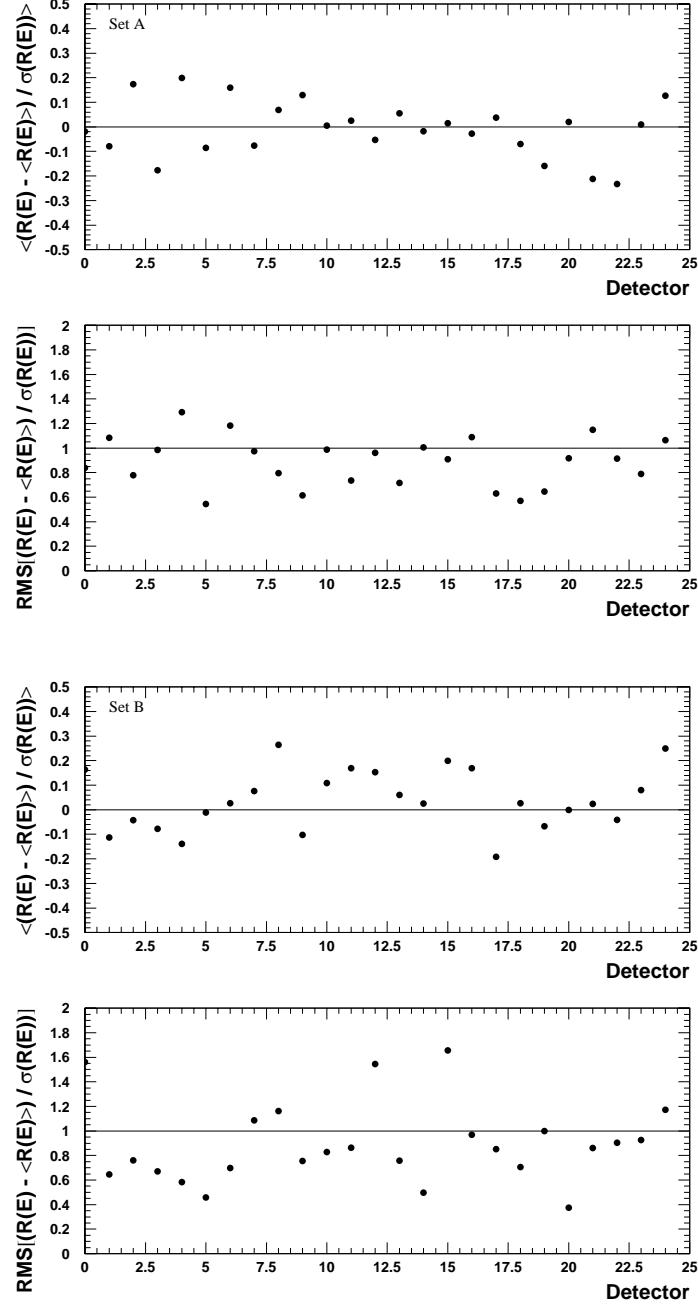


Figure 46: Mean and RMS of the pull distributions $\frac{R(E_i) - \langle R(E_i) \rangle}{\sigma(R(E_i))}$. "Detector 0" corresponds to the detector sum.

Set		
A	-0.0079 ± 0.0252	0.8876 ± 0.0439
B	0.0370 ± 0.0261	0.8850 ± 0.0612

Table 32: Means and RMS from Figure 46 averaged over all detectors.

5.4.5 Comparison of Fit Results with Different Functions

The following results still represent one random seed. The combined results for more seeds will be given in Section 6.10.

Period	1999 Func.	Physics Func. without Phase Modulation	Full Physics Func.
A	125.9420 ± 0.9138	125.9080 ± 0.9161	125.9085 ± 0.9172
B	126.4448 ± 1.1098	126.5474 ± 1.1128	126.6301 ± 1.1169
avr.	126.1452 ± 0.7054	126.1663 ± 0.7073	126.1991 ± 0.7088

Table 33: Comparison of R from fits with the three functions studied. These numbers represent fits to the sum of all detectors starting at $31.8\mu\text{s}$.

Period	1999 Func.	Physics Func. without Phase Modulation	Full Physics Func.
A	1.0375	1.0378	1.0383
B	1.0211	1.0194	1.0194

Table 34: Comparison of χ^2 from fits with the three functions studied. These numbers represent fits to the sum of all detectors starting at $31.8\mu\text{s}$. In all cases the statistical error amounts to 0.0230 .

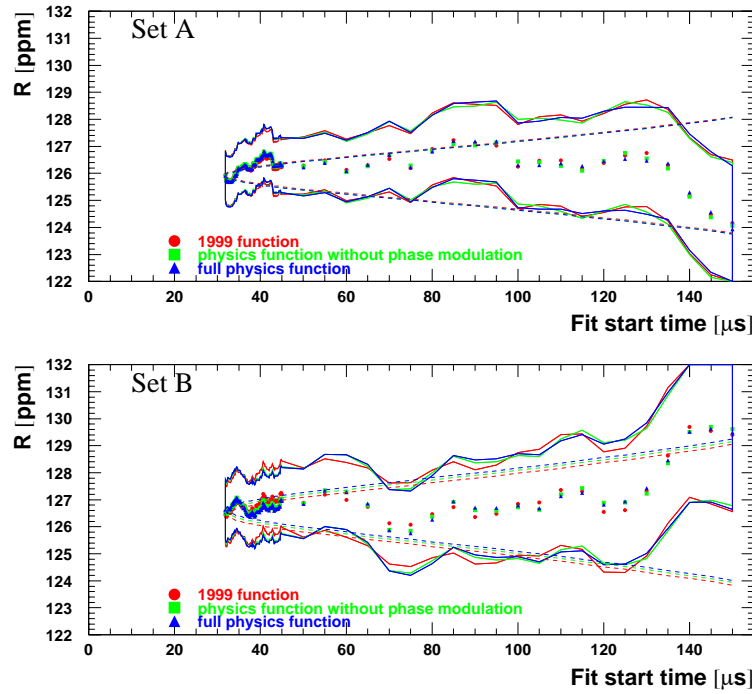


Figure 47: Start-time scans for the three fit functions studied.

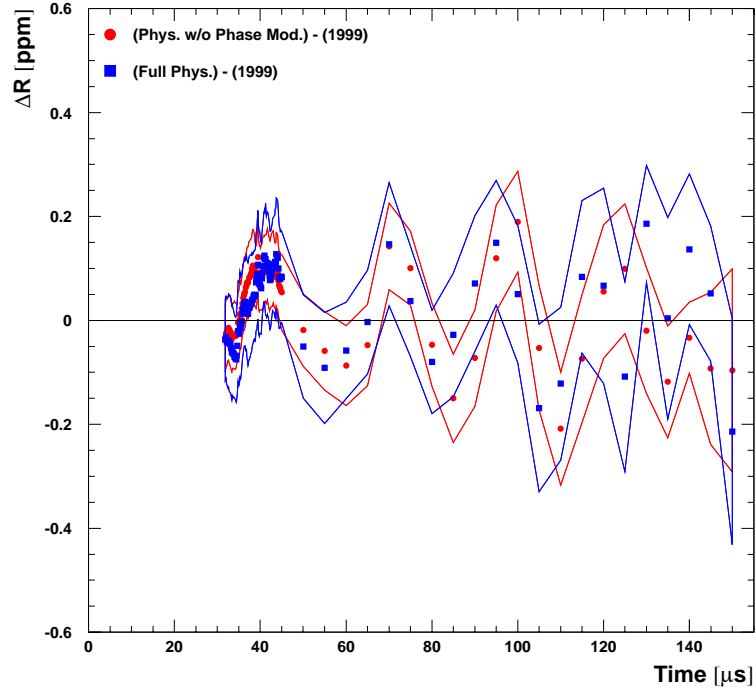


Figure 48: *Difference between R results from start-time scans for Set A.*

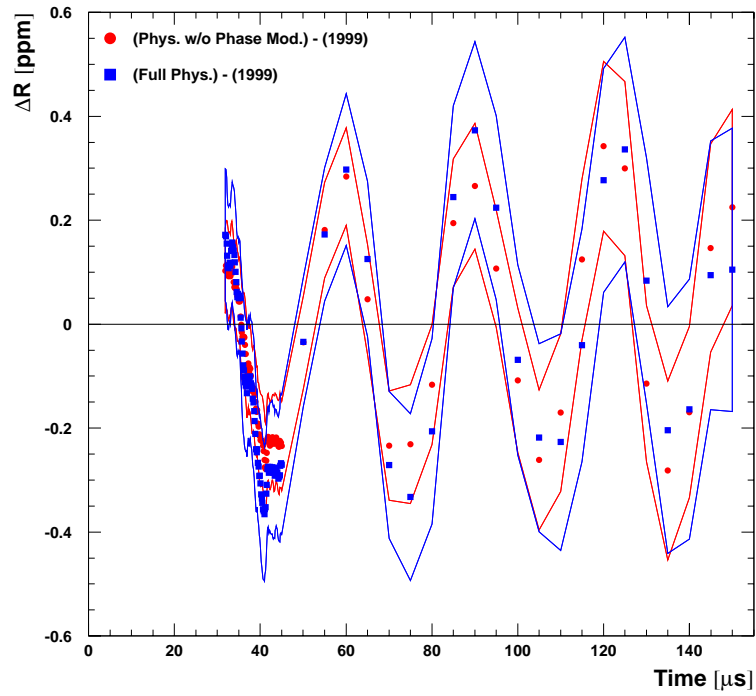


Figure 49: *Difference between R results from start-time scans for Set B.*

6 Systematic Errors at 31.8 μ s Fit Start Time

6.1 Time-Varying CBO Frequency

From the quadrupole circuitry we know that the voltage decay time should be of the order 200 ms. In 2000 we found an empirical optimum at 140 ms. We can expect our knowledge to be correct within about a factor 2 at most. Therefore the fixed parameter τ_{droop} was manually varied as shown in Figures 50 and 51. In the range between 70 ms and 300 ms, R changes by no more than 0.01 ppm. Hence we take 0.01 ppm as systematic error due to the CBO frequency droop.

Figures 82, 83, 94 and 95 show that despite implementing the the CBO frequency droop, the parameter f_{CBO} still sags out of the correlated-error band by about 1σ . Via its correlation, the CBO phase follows this behaviour. Out of curiosity we tried to stabilize ϕ_{CBO} by fixing f_{CBO} to its value from the earliest fit. The reaction of R is shown in Figures 52 to 55. The difference between the results with fixed and with floating f_{CBO} exhibits an oscillation with the left CBO side-band frequency $f_{\text{CBO}} - f_a$ and an average amplitude of about 0.03 ppm. We conclude that artificially fixing a parameter can be a dangerous idea.

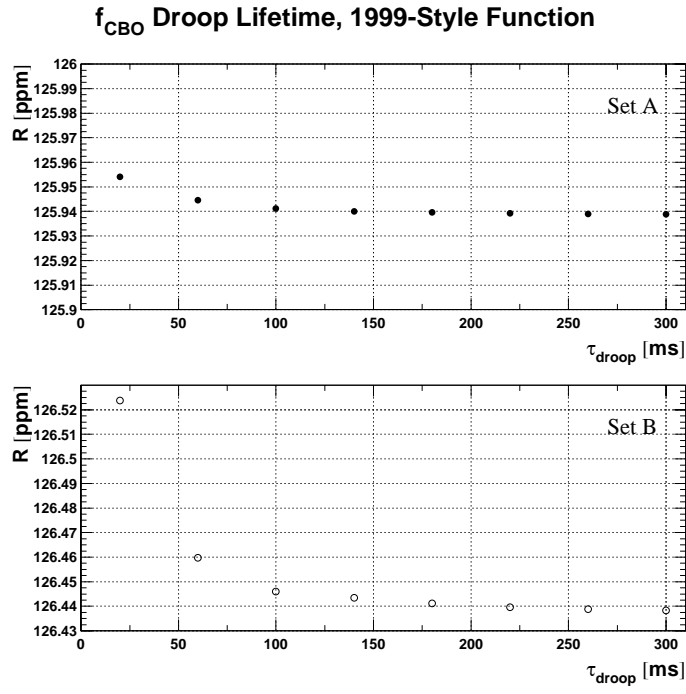


Figure 50: R versus lifetime of the CBO frequency droop for the 1999-style function.

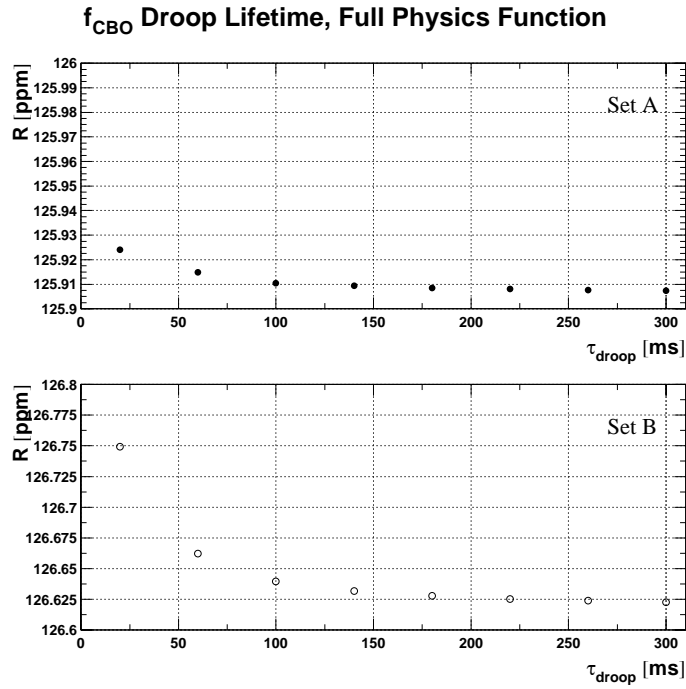


Figure 51: R versus lifetime of the CBO frequency droop for the full physics function.

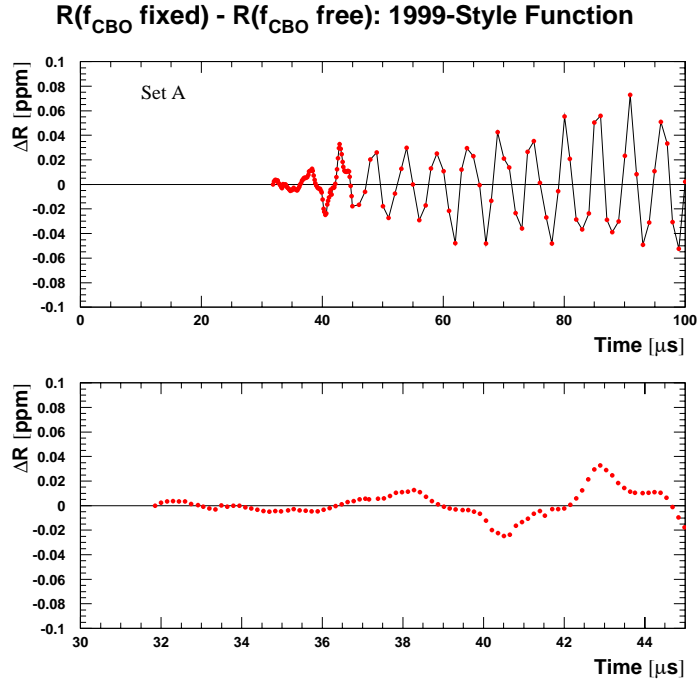


Figure 52: R difference between fits with floating and fixed f_{CBO} for the 1999-style function and Set A.

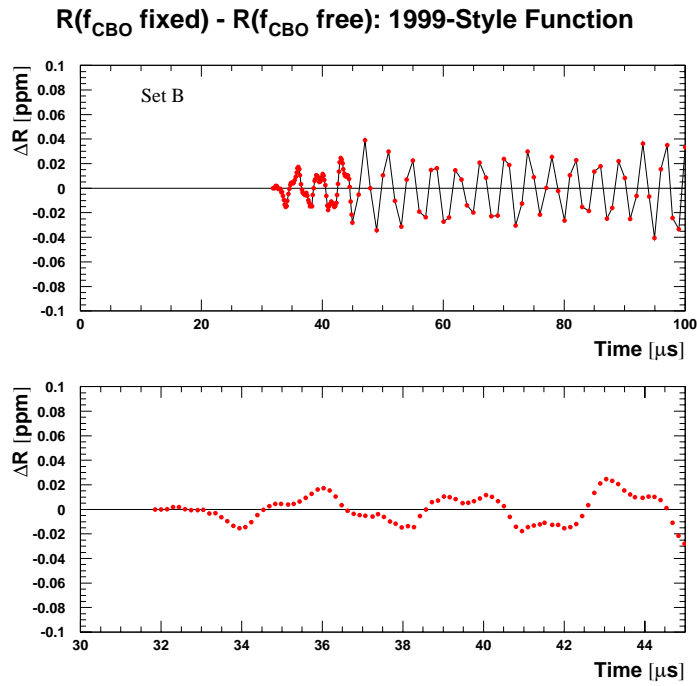


Figure 53: R difference between fits with floating and fixed f_{CBO} for the 1999-style function and Set B.

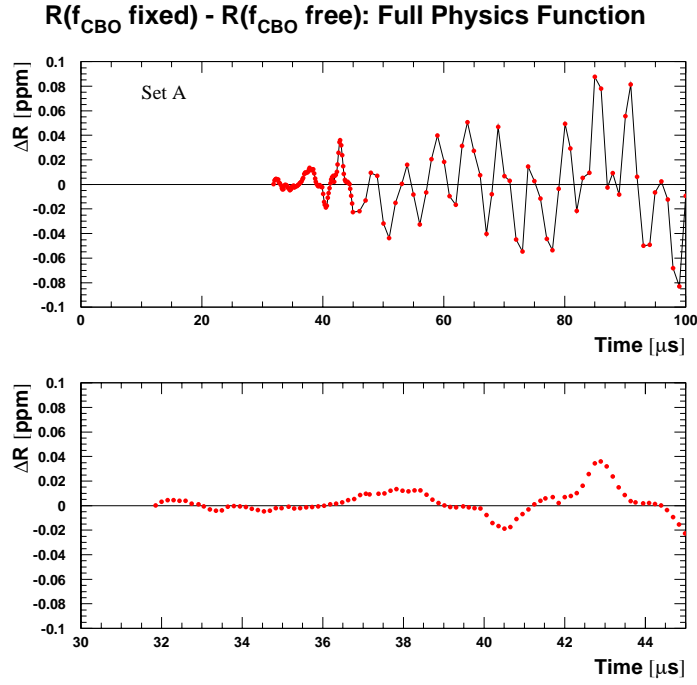


Figure 54: R difference between fits with floating and fixed f_{CBO} for the full physics function and Set A.

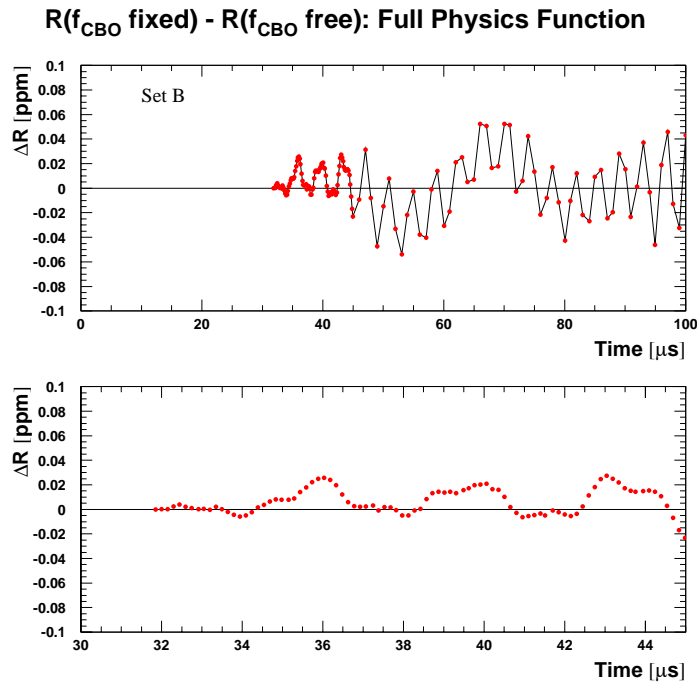


Figure 55: R difference between fits with floating and fixed f_{CBO} for the full physics function and Set B.

6.2 Main (Acceptance) CBO

We follow the procedure of the 2000 analysis ([1], Section 6.1). Yannis' simulation [16] showed that ignoring an additive CBO perturbation with an amplitude of 0.01 leads to phase pulling in R with an amplitude of 6.5 ppm (Set A with $f_{\text{CBO}} = 418$ kHz) or 7.0 ppm (Set B with $f_{\text{CBO}} = 490$ kHz) at a fit start time $t = 0$. At a start time of 31.8 μ s the effect has decayed to

$$\begin{aligned} 6.5 \text{ ppm} \times e^{-31.8/100} &= 4.7 \text{ ppm} \quad (\text{Set A}) \\ 7.0 \text{ ppm} \times e^{-31.8/140} &= 5.6 \text{ ppm} \quad (\text{Set B}) \end{aligned}$$

If – more realistically – a multiplicative CBO term is used in the simulation and then ignored in the fit, the phase pulling amplitude is reduced by a factor 10 to about 0.5 ppm or 0.6 ppm respectively, corresponding to an RMS error of $0.6 \text{ ppm} / \sqrt{2} = 0.4 \text{ ppm}$ (or $0.5 \text{ ppm} / \sqrt{2} = 0.4 \text{ ppm}$). From our fits to the sum of detector spectra with a start time of 31.8 μ s we obtain $A_{\text{CBO}} = 0.0013$ (or 0.0019) (see Tables 7, 15 and 24) instead of the 0.010 assumed in the simulation. This brings the error from completely ignoring the main CBO down to $0.4 \text{ ppm} \times A_{\text{CBO}} / 0.010 = 0.05 \text{ ppm}$ (0.08 ppm). However, we do fit for the CBO, and the systematic error is determined by the amount of remnant CBO that the fit doesn't take care of. The fraction of left-over CBO can be determined from the factor by which the CBO peak in a Fourier spectrum of fit residuals is reduced when the CBO term is included in the fit function. To enhance the sensitivity of the study to CBO effects we align the time spectra of the individual detectors such that the CBO phases are equal. Thus we avoid cancellation around the ring when the individual spectra are added. Figure 56 shows the result.

To quantify the CBO peak in the spectrum we average the amplitude in the range [0.34 MHz, 0.54 MHz] (Set A) or [0.4 MHz, 0.6 MHz] (Set B). The background level is taken as the average over [0.1 MHz, 1 MHz] \ {peak area as defined above} in the spectrum after fitting the full physics function.

- Set A:
 - CBO not fitted: average signal = 7.16
 - CBO fitted: average signal = 0.82; background = 0.68.
 - Reduction factor = $\frac{7.16 \pm 0.68}{0.82 \pm 0.68} = 15.5$
- Set B:
 - CBO not fitted: average signal = 8.89
 - CBO fitted: average signal = 0.69; background = 0.54.
 - Reduction factor = $\frac{8.89 \pm 0.54}{0.69 \pm 0.54} = 20.6$

This yields systematic errors of $0.05 \text{ ppm} / 15.5 = 0.003 \text{ ppm}$ for Set A and $0.08 \text{ ppm} / 20.6 = 0.004 \text{ ppm}$ for Set B.

These systematic errors are common to all three fitting functions because the main CBO peak originates solely from the acceptance CBO which is included in all of them.

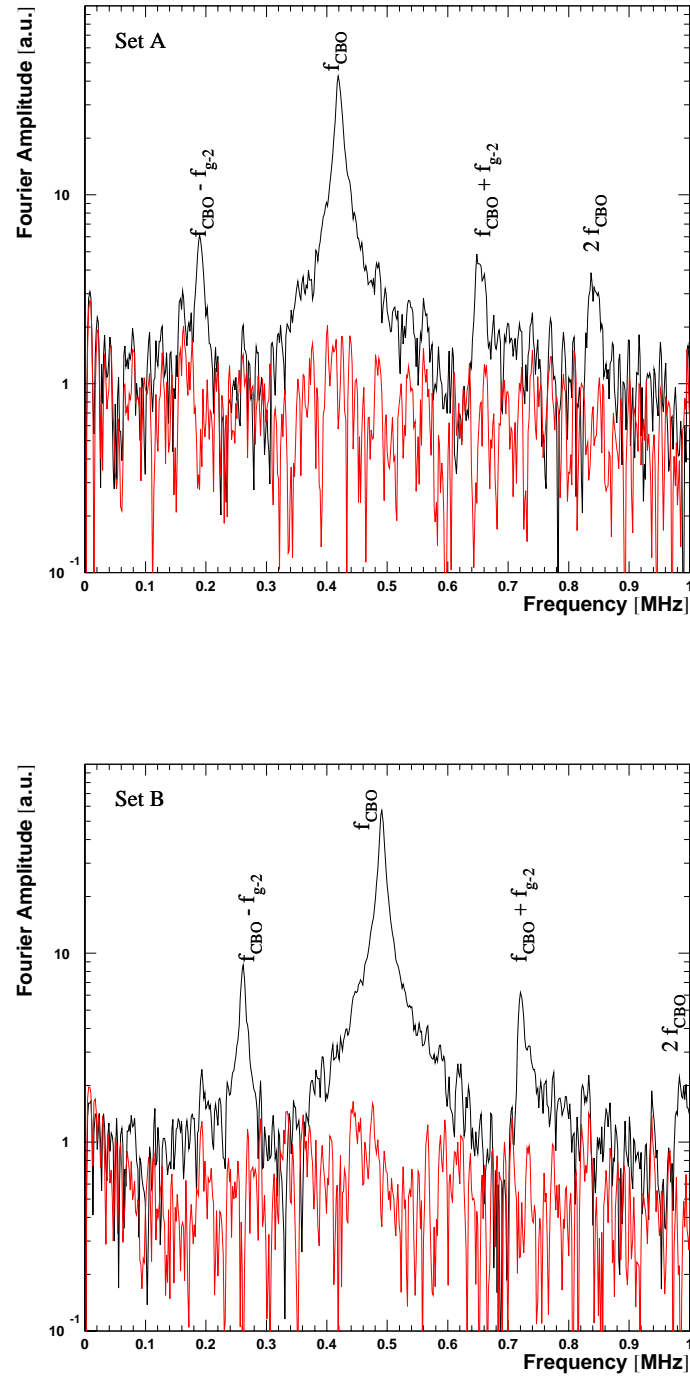


Figure 56: *Residual Fourier spectrum of CBO-aligned data after fits with the (5 parameter + muon loss) function (black) and with the full physics function (red).*

6.3 Acceptance Double CBO

The only uncertain part of the double CBO parametrisation is its envelope. In regular fits, the DCBO lifetime is tied to the CBO lifetime by setting $\tau_{\text{DCBO}} = \frac{1}{2}\tau_{\text{CBO}}$. To study systematic effects from the DCBO envelope we make τ_{DCBO} a fixed parameter, vary it manually and watch R (see Figures 57 and 58 for the 1999-style and the physics function respectively). Since χ^2 as a function of τ_{DCBO} is basically flat (no absolute increase by 1 within $[10, 100]\mu s$) it cannot be used to define a 1σ interval. But we know that τ_{DCBO} must be about $50\text{--}60\mu s$ and can set conservative limits by assuming that our knowledge is less than a factor 2 off, i.e. $25\mu s < \tau_{\text{DCBO}} < 100\mu s$. R changes so little that the exact choice of these limits doesn't really matter.

For Set A we observe a change in R of 0.01 ppm (with both the 1999 and the Full Physics Function); for Set B the change is 0.004 ppm.

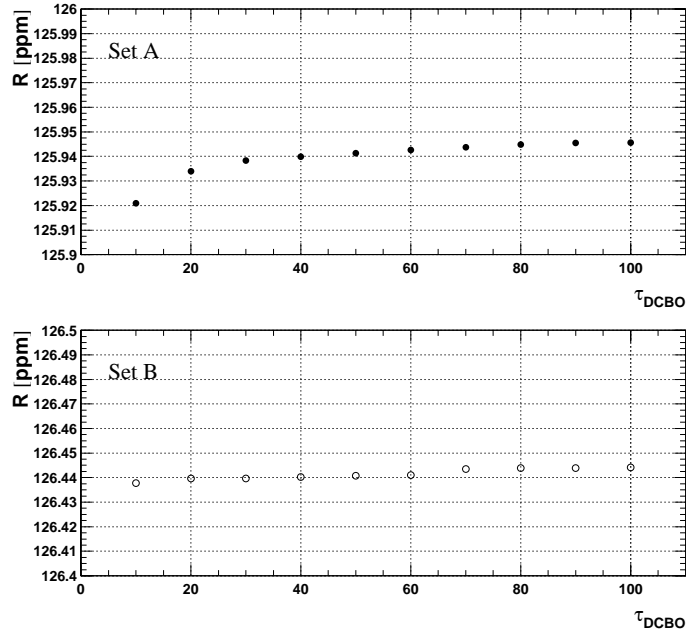


Figure 57: R versus lifetime of the double CBO for the 1999-style function.

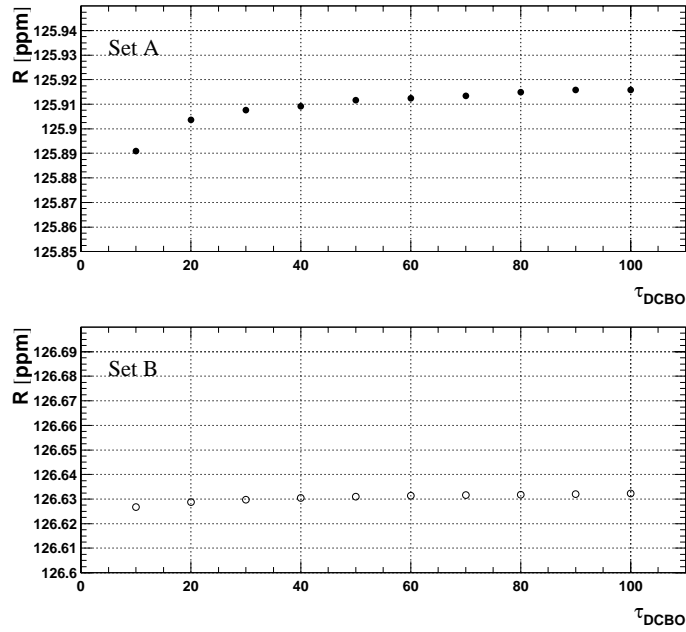


Figure 58: R versus lifetime of the double CBO for the full physics function.

6.4 Asymmetry and Phase CBO – Half-Ring Effect

6.4.1 1999-Style Function

Again, we proceed along the lines of [1] (Section 6.3), only changing the CBO frequencies and lifetimes according to Table 7, and taking the corresponding phase-pulling amplitudes from [16]: for a left side-band amplitude $A_- = 0.01$ the simulation finds 20 ppm (Set A) and 21 ppm (Set B), leading to rms systematic errors

$$\text{Set A: } \delta R = 20 \text{ ppm} \times e^{-31.8/100} / \sqrt{2} \times \frac{A_-}{0.01} = 15 \text{ ppm} \times \frac{A_-}{0.01} \quad (34)$$

$$\text{Set B: } \delta R = 21 \text{ ppm} \times e^{-31.8/140} / \sqrt{2} \times \frac{A_-}{0.01} = 17 \text{ ppm} \times \frac{A_-}{0.01} \quad (35)$$

For determining the left side-band amplitude A_- we repeat the equations derived in the previous analysis:

$$A_-^2 = A_{-, \text{Rob}}^2 + A_{-, \text{Jim}}^2 + 2 A_{-, \text{Rob}} A_{-, \text{Jim}} \cos(\phi_{\text{Jim}} - \phi_{\text{Rob}} - \frac{\pi}{2}) \quad (36)$$

with

$$A_{-, \text{Rob}} = \frac{1}{2} A A_{\text{Rob}} \quad (37)$$

and

$$A_{-, \text{Jim}} = \frac{1}{2} A A_{\text{Jim}} \phi_a \quad (38)$$

The phase difference $\phi_{\text{Jim}} - \phi_{\text{Rob}} - \frac{\pi}{2}$ is known from the fits to individual detectors. From Table 28 we get

$$\phi_{\text{Jim}} - \phi_{\text{Rob}} - \frac{\pi}{2} = 0.78 \pm 0.15 \quad (\text{Set A}) \quad (39)$$

$$\phi_{\text{Jim}} - \phi_{\text{Rob}} - \frac{\pi}{2} = 0.58 \pm 0.14 \quad (\text{Set B}) \quad (40)$$

and hence

$$\cos(\phi_{\text{Jim}} - \phi_{\text{Rob}} - \frac{\pi}{2}) = 0.71 \pm 0.11 \quad (\text{Set A}) \quad (41)$$

$$\cos(\phi_{\text{Jim}} - \phi_{\text{Rob}} - \frac{\pi}{2}) = 0.84 \pm 0.08 \quad (\text{Set B}). \quad (42)$$

Note that the 2001 value of this angle agrees quite well with the one from 2000, $\phi_{2000} = 0.70 \pm 0.10$ and $\cos \phi_{2000} = 0.76 \pm 0.06$.

If both asymmetry and phase modulation cancel by the same factor and mechanism, then this phase difference is preserved after cancellation in the sum of detectors. From Table 24 and the lower block of Table 28 follows:

- Fit to the sum:

$$\phi_{\text{Jim}} - \phi_{\text{Rob}} - \frac{\pi}{2} = 2.40 \pm 5.10 \quad (\text{Set A}) \quad (43)$$

$$\phi_{\text{Jim}} - \phi_{\text{Rob}} - \frac{\pi}{2} = -0.09 \pm 0.74 \quad (\text{Set B}); \quad (44)$$

- Vector sum of individual fit results:

$$\phi_{\text{Jim}} - \phi_{\text{Rob}} - \frac{\pi}{2} = 2.38 \pm 3.11 \quad (\text{Set A}) \quad (45)$$

$$\phi_{\text{Jim}} - \phi_{\text{Rob}} - \frac{\pi}{2} = -0.18 \pm 0.58 \quad (\text{Set B}). \quad (46)$$

Since in the detector sum asymmetry and phase modulation are small effects with large errors, we cannot make a clear conclusion about the conservation of phase differences in the cancellation process. Therefore, like in 2000, the sideband amplitudes will be evaluated for two different cases:

- The cancellation mechanisms and factors of asymmetry and phase modulation are equal and their phase relation is preserved.
- The cancellation factors are different and the phase relation after cancellation is arbitrary, i.e. the expectation value of $\cos(\phi_{\text{Jim}} - \phi_{\text{Rob}} - \frac{\pi}{2})$ is 0.

Comparing the amplitudes A_{Rob} and A_{Jim} for the detector sum (Table 24)

$$\text{Set A: } A_{\text{Rob}} = (0.23 \pm 0.25) \times 10^{-3}, \quad A_{\text{Jim}} = (0.02 \pm 0.09) \times 10^{-3} \quad (47)$$

$$\text{Set B: } A_{\text{Rob}} = (0.71 \pm 0.25) \times 10^{-3}, \quad A_{\text{Jim}} = (0.13 \pm 0.09) \times 10^{-3} \quad (48)$$

with the corresponding average amplitudes for the individual detectors (Table 28, upper block), one finds the following cancellation factors:

	Asymmetry mod.		Phase mod.
Set A	$\frac{0.23 \pm 0.25}{2.84 \pm 0.28} = 0.08 \pm 0.09$		$\frac{0.02 \pm 0.09}{0.67 \pm 0.10} = 0.03 \pm 0.13$
Set B	$\frac{0.71 \pm 0.25}{4.10 \pm 0.28} = 0.17 \pm 0.06$		$\frac{0.13 \pm 0.09}{0.71 \pm 0.10} = 0.18 \pm 0.13$

(49)

The obvious problem here is that both effects are hardly significant in the sum of detectors, and the cancellation factors have huge uncertainties.

To calculate the side-band contributions $A_{-, \text{Rob}}$ and $A_{-, \text{Jim}}$ according to Eqns. (37) and (38), we use A_{Rob} and A_{Jim} from Eqns (47) and (48), and the values $A = 0.350067 \pm 0.000029$ and $\phi_a = 2.96129 \pm 0.00015$ (Set A) and $A = 0.349920 \pm 0.000035$ and $\phi_a = 2.96165 \pm 0.00019$ (Set B):

$$\text{Set A: } A_{-, \text{Rob}} = (0.04 \pm 0.04) \times 10^{-3}, \quad A_{-, \text{Jim}} = (0.01 \pm 0.05) \times 10^{-3} \quad (50)$$

$$\text{Set B: } A_{-, \text{Rob}} = (0.12 \pm 0.04) \times 10^{-3}, \quad A_{-, \text{Jim}} = (0.07 \pm 0.05) \times 10^{-3} \quad (51)$$

Combining directly these amplitudes to the total left side-band amplitude implies the assumption of different cancellation factors and hence an arbitrary phase relation for the two vectors after cancellation. With Eq. (36) and $\cos(\phi_{\text{Jim}} - \phi_{\text{Rob}} - \frac{\pi}{2}) = 0$ we obtain the combined left side-band amplitude

$$\text{Set A: } A_- = (0.041 \pm 0.041) \times 10^{-3} \quad (52)$$

$$\text{Set B: } A_- = (0.139 \pm 0.043) \times 10^{-3} \quad (53)$$

corresponding to a systematic error

$$\text{Set A: } \delta R = (0.06 \pm 0.06) \text{ ppm} \quad (54)$$

$$\text{Set B: } \delta R = (0.24 \pm 0.07) \text{ ppm} \quad (55)$$

Alternatively we can use the average modulation amplitudes from individual detector fits and assume equal cancellation mechanisms for asymmetry and phase modulation with an average cancellation factor of 0.06 ± 0.07 (Set A) or 0.17 ± 0.05 (Set B). In this model we need to use the phase difference (41), (42). This leads to a combined left side-band amplitude

$$\text{Set A: } A_- = (0.047 \pm 0.055) \times 10^{-3} \quad (56)$$

$$\text{Set B: } A_- = (0.178 \pm 0.054) \times 10^{-3} \quad (57)$$

or a systematic error

$$\text{Set A: } \delta R = (0.07 \pm 0.08) \text{ ppm} \quad (58)$$

$$\text{Set B: } \delta R = (0.30 \pm 0.09) \text{ ppm} \quad (59)$$

Both fit-based methods for determining A_- have the drawback of large statistical uncertainties because asymmetry and phase modulation amplitudes have a rather small signal-to-noise ratio.

6.4.2 Full Physics Function

Figure 59 shows the results for R from a manual sweep of τ_{Rob} . It turned out that χ^2 is too insensitive to the asymmetry modulation and cannot be used for determining a confidence interval for τ_{Rob} . Minima of χ^2 are found at unphysical values of τ_{Rob} , i.e. either near 0 or at infinity. This problem persists even with CBO-aligned data. However, we know that τ_{Rob} should have about the same magnitude as τ_{CBO} and can set conservative limits. Assuming $\tau_{\text{Rob}} > \tau_{\text{DCBO}} = 50 \mu\text{s}$ and $\tau_{\text{Rob}} < 200 \mu\text{s}$, we find:

$$\text{Set A: } \delta R_{\text{Rob}} = \frac{1}{2} \times 0.0258 \text{ ppm} = 0.0129 \text{ ppm} \quad (60)$$

$$\text{Set B: } \delta R_{\text{Rob}} = \frac{1}{2} \times 0.0122 \text{ ppm} = 0.0061 \text{ ppm} \quad (61)$$

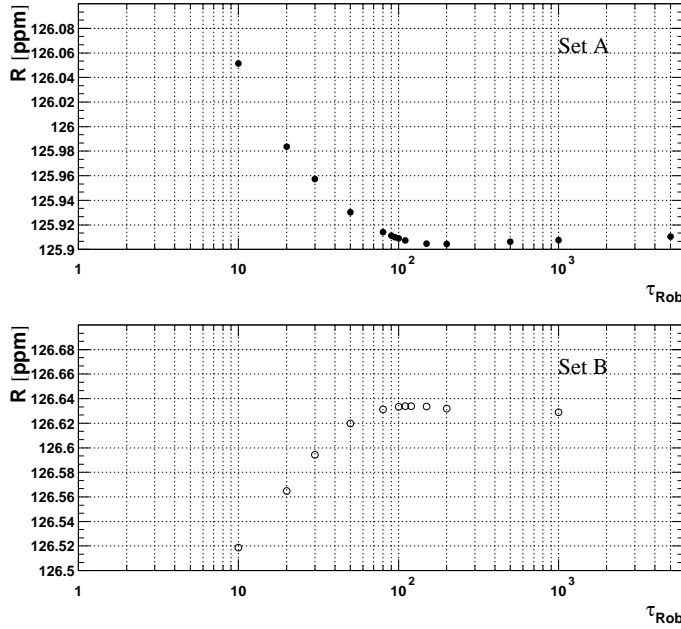


Figure 59: R versus the (exponential) lifetime of the asymmetry modulation.

Similarly, we perform a sweep of τ_{Jim} (Figure 60) and estimate again $\tau_{\text{Jim}} > \tau_{\text{DCBO}} = 50 \mu\text{s}$ and $\tau_{\text{Jim}} < 200 \mu\text{s}$. This yields a systematic uncertainty

$$\text{Set A: } \delta R_{\text{Jim}} = \frac{1}{2} \times 0.0037 \text{ ppm} = 0.0019 \text{ ppm} \quad (62)$$

$$\text{Set B: } \delta R_{\text{Jim}} = \frac{1}{2} \times 0.0437 \text{ ppm} = 0.0219 \text{ ppm} \quad (63)$$

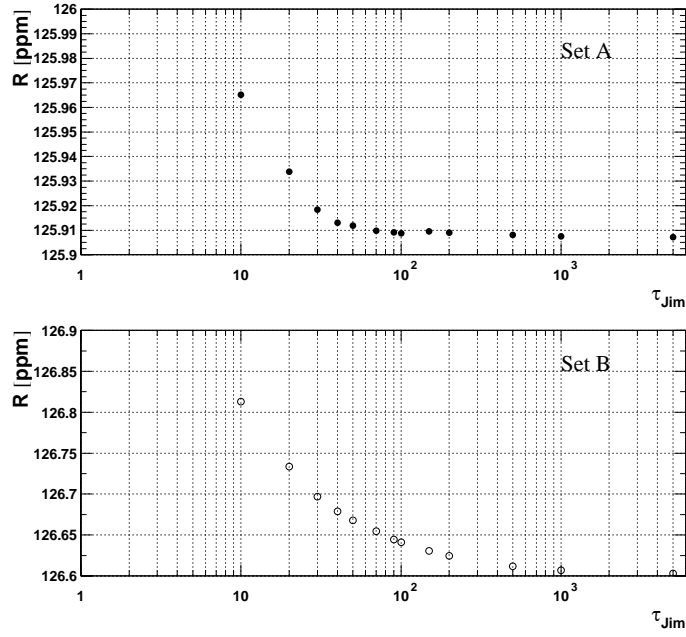


Figure 60: R versus the (exponential) lifetime of the phase modulation.

Using the angle (41, 42) between asymmetry and phase modulation, we get a total half-ring-effect systematic uncertainty of:

$$\text{Set A: } \delta R_{\text{half-ring}} = \sqrt{0.0129^2 + 0.0019^2 + 2 \times 0.0129 \times 0.0019 \times 0.71} \text{ ppm} \quad (64)$$

$$= 0.0143 \text{ ppm} \quad (65)$$

$$\text{Set B: } \delta R_{\text{half-ring}} = \sqrt{0.0061^2 + 0.0219^2 + 2 \times 0.0061 \times 0.0219 \times 0.84} \text{ ppm} \quad (66)$$

$$= 0.0272 \text{ ppm} \quad (67)$$

6.5 Residual Pileup

There are two aspects to systematic errors due to imperfections in the statistical pileup construction and subtraction:

- Over- or undersubtraction of pileup, but with the correct phase
- Pileup construction with the wrong phase, e.g. by energy-dependent over- and underestimate of pileup. This is also called the “Underwater Effect”.

We will first estimate the fraction of residual pileup, then investigate its influence on R and finally give an upper limit on the Underwater Effect.

6.5.1 Residual Pileup Fraction from Early and Late Energy Spectra

We proceed along the lines of the 2000 analysis [1] (Section 6.5.1).

The pileup $P(t)$ at the early time t can be determined from early and late energy spectra $N(t)$ and $N(t + \Delta t)$ via¹

$$\tilde{P}(t) = \frac{N(t) - e^{\Delta t/\tau} N(t + \Delta t)}{1 - e^{-\Delta t/\tau}} \quad (68)$$

The inefficiency in the pileup subtraction then follows as

$$1 - \eta(t) = 1 - \frac{P(t)}{\tilde{P}(t)} = \frac{[N(t) - P(t)] - e^{\Delta t/\tau} [N(t + \Delta t) - P(t + \Delta t)]}{N(t) - e^{\Delta t/\tau} N(t + \Delta t)} \quad (69)$$

where $P(t)$ is the reconstructed pileup spectrum. For the early spectrum the time slice [31.8; 40.6] μ s was used. The time interval for the late energy spectrum was varied for the purpose of an additional consistency check. For the choice of this interval the bin boundaries 49.2, 66.7, 75.6, 97.3, 123.5, 149.6, 202.0, 315.6, 450.0 and 600.0 μ s were available.

The upper plots in Figure 61 show an early and a late energy spectrum for N and P for the sum of all detectors and the two run sets. Since the pileup spectrum has a zero crossing around 2.6 GeV, the modulus is drawn to avoid conflicts with the logarithmic scale. The middle and lower left-hand graphs compare the constructed pileup spectrum $|D - S1 - S2|$ with the one determined according to Eq. (68). The difference is the residual pileup which is also shown. The middle and lower right-hand plots show the residual pileup fraction. The lower part of the figure zooms into the sub-range from 3 to 6 GeV where this method is usable. Below about 3.2 GeV the pileup spectrum tends towards the 2.6 GeV zero crossing where the uncertainties are big. Above about 5.5 GeV the statistics become poor.

We conclude that the residual pileup fraction ranges within $\pm 10\%$.

¹This concept goes back to earlier analyses, see e.g. [11].

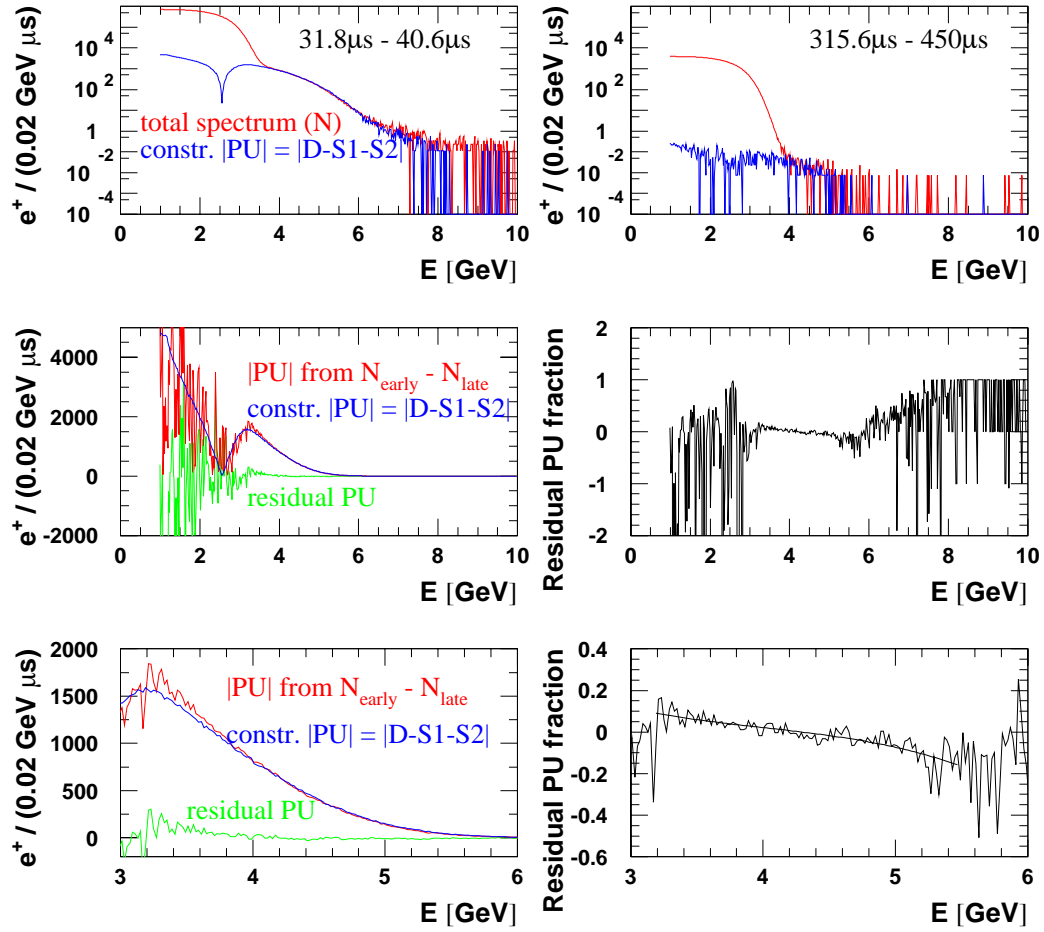
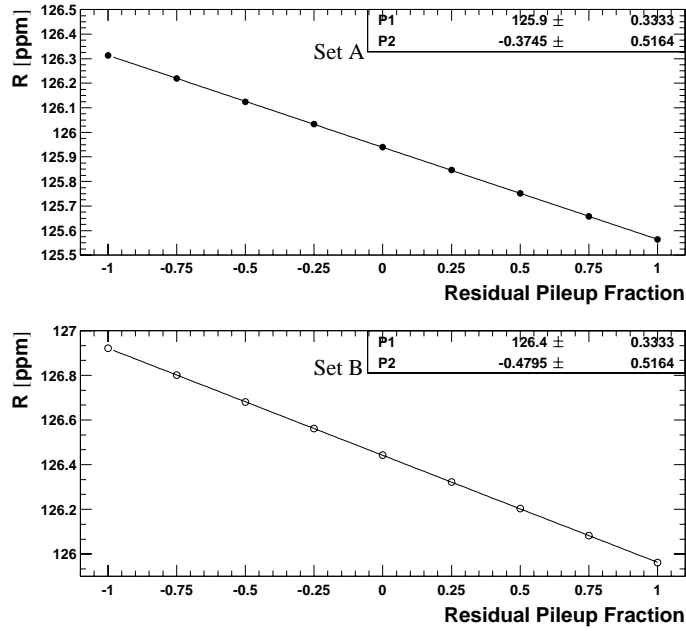
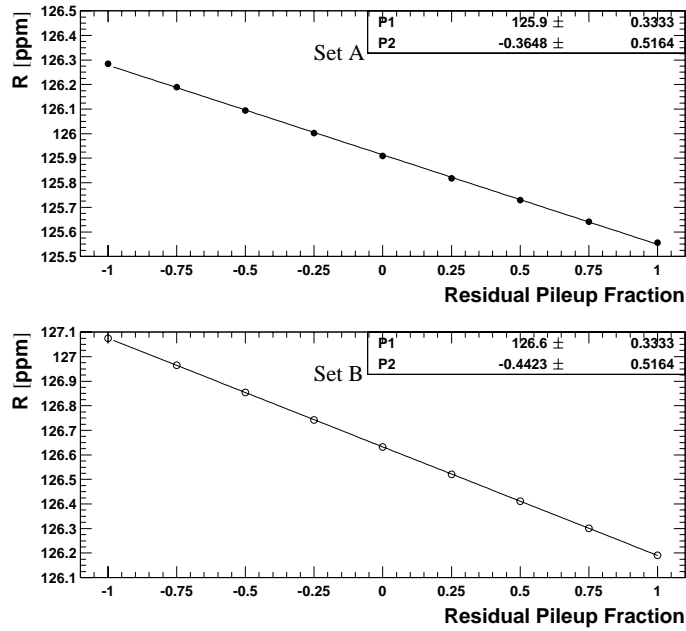


Figure 61: Determination of the residual pileup fraction using the evolution of the energy spectrum from the time bin $[31.8 \mu\text{s}; 40.6 \mu\text{s}]$ to $[315.6 \mu\text{s}; 450.0 \mu\text{s}]$.

6.5.2 Influence of Residual Pileup on R Figure 62: R versus residual pileup fraction $\rho = 1 - \lambda$ for the 1999-style function.Figure 63: R versus residual pileup fraction $\rho = 1 - \lambda$ for the full physics function.

6.5.3 Shift in R due to the Pileup Phase (Underwater Effect)

To estimate the effect of a possible phase deviation in the constructed pileup we use Yannis' approach [12]. Conservatively assuming that the pileup contributions below and above the zero-crossing around 2.6 GeV may be misreconstructed by up to 10 %, he obtains a deviation in R of the order of 20 % of the shift suffered if no pileup subtraction is applied at all. The latter shift can be read off the parameter boxes (P2) in Figures 63 and 62. We give the resulting estimates for the systematic uncertainty due to the Underwater effect in Table 35.

Set	1999 Function	Full Physics Function
A	$0.37 \times 0.2 = 0.07$	$0.37 \times 0.2 = 0.07$
B	$0.48 \times 0.2 = 0.10$	$0.44 \times 0.2 = 0.09$

Table 35: *Systematic uncertainty on R due to a phase error in the reconstructed pileup.*

6.5.4 Unseen Pileup

Pileup involving pulses below 250 MeV is not directly observable and cannot be statistically constructed because the small constituent pulses are not seen [2]. On average, neither the energy nor the time of high energy pulses are changed by the unseen pulses (cancellation). However, there are systematic phase and asymmetry shifts.

Old Approach via Asymmetry Instability

Like for the 2000 data an estimate of an upper limit on the systematic error from unseen pileup was made along the lines of [14] for the sum of all detectors and all runs. The calculations are based on Figures 17, 33 and the numerical values given in Table 37.

With the 1999 function, the asymmetry shows a peak-to-peak variation $\delta A = 0.00019$ for Set A and $\delta A = 0.00023$ for Set B. We take the full value as systematic error on A which is very conservative.

As shown in [14], the sensitivity of ϕ to unseen pileup is at most 0.19 times the sensitivity of A . This gives a maximum systematic error contribution of

$$\delta\phi \leq 0.19 \times \delta A = \begin{cases} 3.6 \times 10^{-5} & \text{(Set A)} \\ 4.4 \times 10^{-5} & \text{(Set B)} \end{cases}$$

for the phase, which is 0.24 (0.23) times the statistical error $\sigma(\phi) = 1.5 \times 10^{-4}$ (1.9×10^{-4}). Since R is strongly correlated with the phase, the contribution of this effect to the systematic error on R is again about 0.24 (0.23) times the statistical error:

$$\frac{\delta R}{R} \approx \frac{\sigma(R)}{R} \frac{\delta\phi}{\sigma(\phi)} = \begin{cases} 0.91 \text{ ppm} \times 0.24 = 0.22 \text{ ppm} & \text{(Set A)} \\ 1.11 \text{ ppm} \times 0.23 = 0.26 \text{ ppm} & \text{(Set B)} \end{cases} \quad (70)$$

For the Full Physics Function, the same procedure yields $\delta A = 0.00019$ (0.00022), and hence $\delta\phi \leq 0.19 \times \delta A = 3.6 \times 10^{-5}$ (4.2×10^{-5}). With the statistical error $\sigma(\phi) = 1.5 \times 10^{-4}$ (1.9×10^{-4}) we obtain

$$\frac{\delta R}{R} \approx \frac{\sigma(R)}{R} \frac{\delta\phi}{\sigma(\phi)} = \begin{cases} 0.92 \text{ ppm} \times 0.24 = 0.22 \text{ ppm} & \text{(Set A)} \\ 1.12 \text{ ppm} \times 0.22 = 0.25 \text{ ppm} & \text{(Set B)} \end{cases} \quad (71)$$

The uncertainties resulting from this approach seem vastly overestimated. Furthermore, the decrease of A with start time is the wrong signature; unseen pileup should increase A . Fortunately Vanya found a method which provides sharper limits for the effects from unseen pileup.

New Approach via Pedestal Spread

Vanya recently calculated the systematic error from unseen pileup by using the amplitude spread of the first samples in WFD islands relative to the average pedestal level [15]. His result amounts to 0.01 ppm. This will be used in the systematic error table.

6.6 Gain Changes and Residual Slow Effects

6.6.1 Gain Correction with Upper Energy Cut

The procedure used for applying a gain correction was the same as in the 2000 analysis [1] (Section 6.6), with the only difference that this time an upper energy cut at 3.4 GeV was applied because we had come to the conclusion that pileup above the energy endpoint has a strong falsifying influence on the average energy and that it is relatively poorly subtracted.

First, the relation

$$\frac{\Delta E}{E} = a \frac{\Delta G}{G} = a \Delta g \quad (72)$$

between gain variations and average energy changes needs to be calibrated [17]. Again, this is done applying two constant energy scale factors $1 + \Delta g_1 = 0.995$ and $1 + \Delta g_2 = 1.005$. to all pulse energies and then determining the modified average energies $E_1(t)$ and $E_2(t)$. Then we can calculate the sensitivity factor a as

$$a(t) = \frac{E_2(t) - E_1(t)}{E_0(t) (\Delta g_2 - \Delta g_1)} \quad (73)$$

Detector	a	Detector	a
1	0.5114 ± 0.0003	13	0.4940 ± 0.0003
2	0.5054 ± 0.0003	14	0.4856 ± 0.0003
3	0.4977 ± 0.0003	15	0.5085 ± 0.0003
4	0.4996 ± 0.0003	16	0.4725 ± 0.0003
5	0.4976 ± 0.0003	17	0.4984 ± 0.0003
6	0.4801 ± 0.0003	18	0.4823 ± 0.0003
7	0.4443 ± 0.0003	19	0.4905 ± 0.0003
8	0.4124 ± 0.0003	(20)	(0.1022 ± 0.0005)
9	0.4615 ± 0.0003	21	0.4868 ± 0.0003
10	0.4954 ± 0.0003	22	0.4765 ± 0.0003
11	0.4967 ± 0.0003	23	0.4809 ± 0.0003
12	0.4656 ± 0.0003	24	0.4745 ± 0.0003

Table 36: *Sensitivity factors for the relation between relative gain change and average energy change for $1.8 \text{ GeV} < E < 3.4 \text{ GeV}$.*

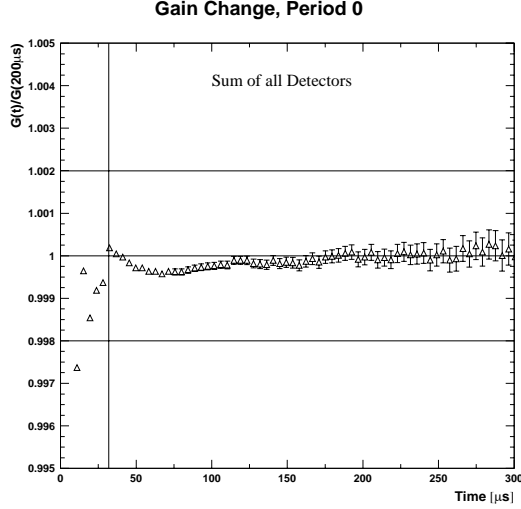
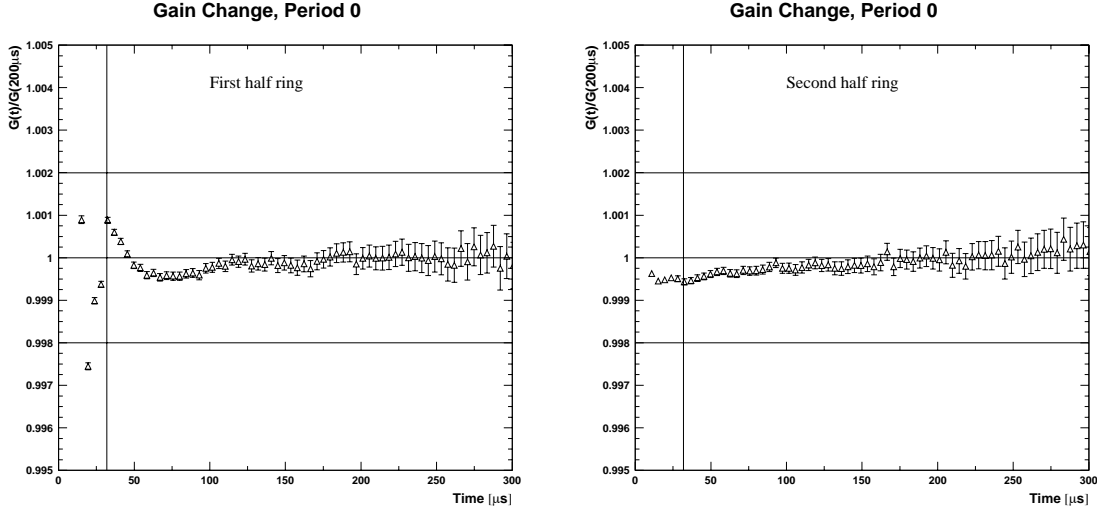
If the relation between gain change and average energy is linear, $a(t)$ should not depend on the time. In Appendix E.1, $a(t)$ is shown for all detectors. Fits to constants are superimposed. The resulting sensitivity factors are given in Table 36.

Figure 64 shows the gain $G(t)$ relative to the reference time $200 \mu\text{s}$, as obtained from the average energy and the sensitivity factor. The corresponding results for the two half rings are displayed in Figure 65.

Gain variation plots for the two run sets and the 24 detectors can be found in Appendix E.2.

Using an empirical parametrisation of $\Delta g(t)$ for each individual detector, a gain correction factor $1/(1 + \Delta g)$ was applied to the pulse energies before filling the time spectra.

The influence of the gain correction on χ^2 and asymmetry stability is summarised in Table 37. Apparently the gain correction with upper energy cut improves χ^2 and reduces the asymmetry sag, however, not perfectly.

Figure 64: *Gain versus time for all runs and all detectors together.*Figure 65: *Gain versus time for the two half rings (all runs together).*

The rows labeled “diff” show the sensitivity of R to the gain correction at $31.8\mu\text{s}$ (i.e. near a zero-crossing). This would be the systematic error if our uncertainty about the gain correction were 100 %.

To study the influence of high-energy pileup on the gain correction and the fit results we applied different upper cuts.

Table 38 shows that χ^2 is not very sensitive to the position of the upper cut. The asymmetry sag (Table 39) is not strongly influenced either, which suggests that pileup is not its dominant origin.

The impact of the upper cut on R is shown in Table 40.

The uncertainty of the R -difference between two cuts was calculated according to [18]:

$$\sigma^2(\Delta R) = \sigma^2(R_2) - \sigma^2(R_1) \left(2 \frac{A_1}{A_2} \cos(\Delta\phi) - 1 \right) \quad (74)$$

where R_1 has been obtained with the higher upper cut. We observe a general difference

Set			1999 Function	Full Physics Function
A	χ^2	raw	1.1057	1.1066
		corr.	1.0395	1.0404
	$\Delta A [10^{-4}]$	raw	2.67	2.75
		corr.	1.90	1.88
	$R [\text{ppm}]$	raw	125.9253 ± 0.9134	125.9236 ± 0.9168
		corr.	125.9420 ± 0.9138	125.9085 ± 0.9172
		diff.	0.0167 ± 0.0270	0.0151 ± 0.0271
B	χ^2	raw	1.0710	1.0698
		corr.	1.0212	1.0195
	$\Delta A [10^{-4}]$	raw	2.94	2.86
		corr.	2.17	2.08
	$R [\text{ppm}]$	raw	126.3820 ± 1.1094	126.5639 ± 1.1164
		corr.	126.4448 ± 1.1098	126.6301 ± 1.1169
		diff.	0.0628 ± 0.0298	0.0662 ± 0.0334

Table 37: Comparison of χ^2 and R at a start time of $31.8\mu\text{s}$, and the peak-to-peak variation of the asymmetry for data without and with gain correction (upper cut = 3.4 GeV).

Set	Upper Cut [GeV]	1999 Function	Full Physics Function
A	3.2	1.0404	1.0413
	3.4	1.0395	1.0404
	6.2	1.0402	1.0411
B	3.2	1.0262	1.0247
	3.4	1.0212	1.0195
	6.2	1.0227	1.0208

Table 38: χ^2 at a start time of $31.8\mu\text{s}$ for gain-corrected data with different upper energy cuts.

Set	Upper Cut [GeV]	1999 Function	Full Physics Function
A	3.2	2.00 ± 0.66	2.06 ± 0.66
	3.4	1.90 ± 0.66	1.88 ± 0.66
	6.2	2.12 ± 0.66	2.10 ± 0.66
B	3.2	2.11 ± 0.80	2.01 ± 0.81
	3.4	2.17 ± 0.80	2.08 ± 0.80
	6.2	2.38 ± 0.80	2.27 ± 0.80

Table 39: Difference $\Delta A [10^{-4}]$ between the start times $31.8\mu\text{s}$ and $150\mu\text{s}$ for gain-corrected data with different upper energy cuts.

between the sets A and B: B is much more sensitive to the upper cut than A. The reason is unclear.

However, there is also an interesting tendency: the significance of the R -difference between 6.2 GeV and 3.4 GeV is much higher than the one between 3.4 GeV and 3.2 GeV . The reason may be the dominance of residual pileup at energies above 3.4 GeV .

Set	Upper Cuts [GeV]	1999 Function	Full Physics Function
A	(3.4) - (3.2)	$-0.0080 \pm 0.0599 = 0.13 \sigma$	$-0.0003 \pm 0.0613 = 0.01 \sigma$
	(6.2) - (3.4)	$-0.0264 \pm 0.0246 = 1.07 \sigma$	$-0.0181 \pm 0.0204 = 0.89 \sigma$
B	(3.4) - (3.2)	$0.1905 \pm 0.0736 = 2.59 \sigma$	$0.1949 \pm 0.0734 = 2.66 \sigma$
	(6.2) - (3.4)	$-0.1499 \pm 0.0267 = 5.61 \sigma$	$-0.1489 \pm 0.0305 = 4.88 \sigma$

Table 40: *Differences in R [ppm] between two upper cuts for a start time of 31.8 μ s and gain-corrected data.*

6.6.2 Artificial Enhancement of Gain Variations

To improve the handle on the influence of gain changes on the ω_a fit results, artificially enhanced gain variations were introduced. This was done by creating time spectra based on manipulated pulse energies, i.e. modified effective energy thresholds. The energy of a pulse detected at a time t was multiplied by a factor

$$\kappa_g(t) \equiv \frac{1 + \xi \Delta g(t)}{1 + \Delta g(t)} \quad , \quad (75)$$

where the gain multiplier ξ was a fixed coefficient. The value $\xi = 1$ corresponds to untreated energies. For this study, the values $\xi = 5$, $\xi = 10$ and $\xi = -1$ were used. The first two choices magnify the gain changes which are present in the data by a factor 5 or 10; the third choice overcorrects the gain changes by one unit. The case $\xi = 0$ (i.e. corrected energy scale, ideally no gain changes left), was already discussed in the previous section.

Fit results for the five values of ξ and our two fit functions are shown in Figures 66 and 68. The upper plots show phase pulling whose amplitude is proportional to ξ . The fact that there is some phase pulling even for $\xi = 0$ (gain corrected data) is due to a combination of imperfections in the gain correction and residual slow effects like incorrectly parametrised muon loss.

In the zero-crossings of these phase-pulling oscillations the systematic error on R would be zero. However, the actual abscissa position $t_{\text{start},1} = 31.8541 \mu\text{s}$ of our fit start time bin (determined as explained in [1], Section 5.2) does not exactly coincide with the phase-pulling zero-crossings. Moreover, for the $\xi = 0$ curve it is not easy to determine the zero-crossing positions from the graphs. Therefore we use the curves for $\xi = 5$ and $\xi = 10$ which show very pronounced oscillations. We determine their first two extrema with parabolic fits and infer the first zero-crossings near $t_{\text{start},1}$:

ξ	Set A		Set B	
	1999 Func.	Full Phys. Func.	1999 Func.	Full Phys. Func.
5	31.8301 ± 0.0093	31.9496 ± 0.0126	31.8057 ± 0.0181	31.7390 ± 0.0166
10	31.8297 ± 0.0127	31.9666 ± 0.0077	31.8560 ± 0.0101	31.7787 ± 0.0090
avr.	31.8300 ± 0.0075	31.9620 ± 0.0065	31.8441 ± 0.0088	31.7697 ± 0.0079

Table 41: *First zero-crossing times of the gain related phase pulling.*

The same parabolic fits give us the phase-pulling amplitudes which we define as $\text{amplitude} = |\text{first maximum} - \text{first minimum}| / 2$.

Approximating the functional form of the phase-pulling by a sinusoidal curve, the systematic shift ΔR due to the deviation $t_{\text{zero-crossing}} - t_{\text{start},1}$ is given by

$$\Delta R = \text{amplitude} \times \omega_a \times (t_{\text{zero-crossing}} - t_{\text{start},1}) \quad (76)$$

Figures 67 and 69 show ΔR as a function of ξ . The results for the gain-corrected data ($\xi = 0$) are listed in Table 42. Note that these uncertainties include all other slow effects causing phase pulling, in particular muon losses.

Set	1999 Func.	Full Phys. Func.
A	0.010 ppm	0.049 ppm
B	0.004 ppm	0.028 ppm

Table 42: *Estimate of the systematic error from phase pulling due to residual gain variations and other slow effects. Cf. Table 43 for an alternative approach.*

Why not just use the difference between gain corrected and uncorrected results from Table 37? Firstly, because those numbers assume that the gain correction is 100 % uncertain, which is too pessimistic. Secondly we prefer the values in Table 42 because they also cover the other slow effects. In the next section another way of estimating the influence of the combination of slow effects will be given for comparison. As final systematic error we shall take the larger of the two estimates.

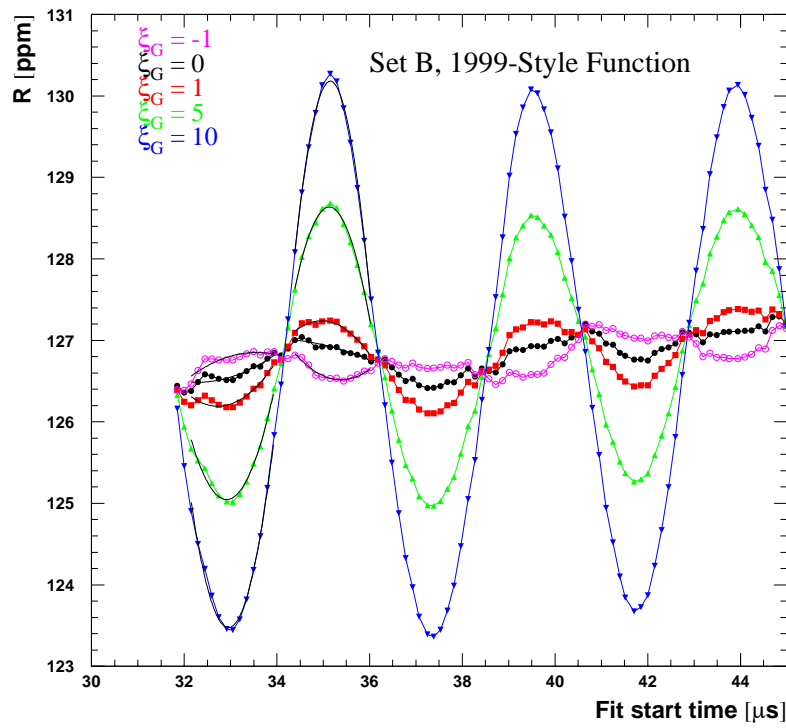
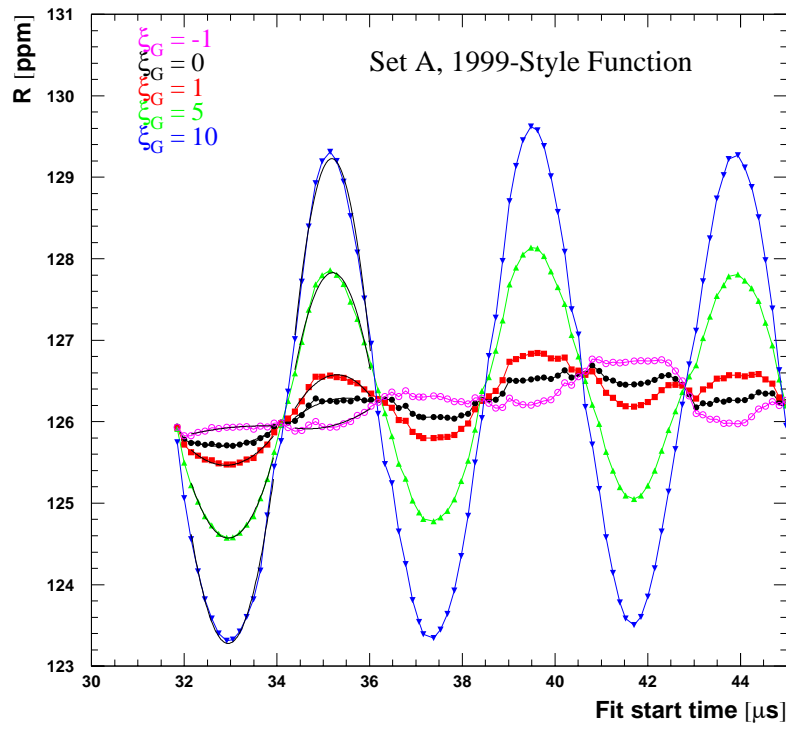


Figure 66: Study of gain correction and artificial gain change for the 1999-style function.

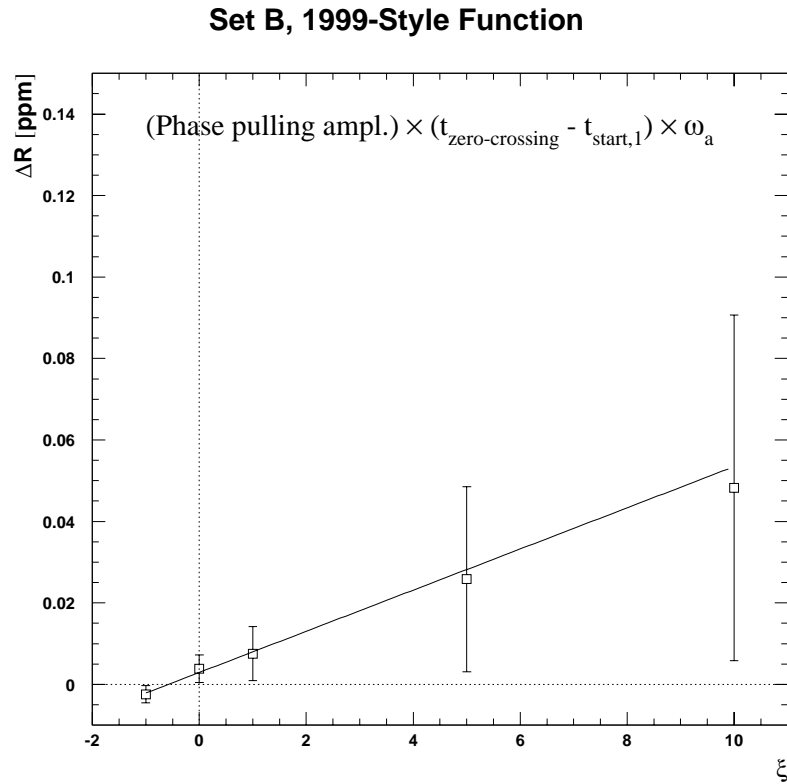
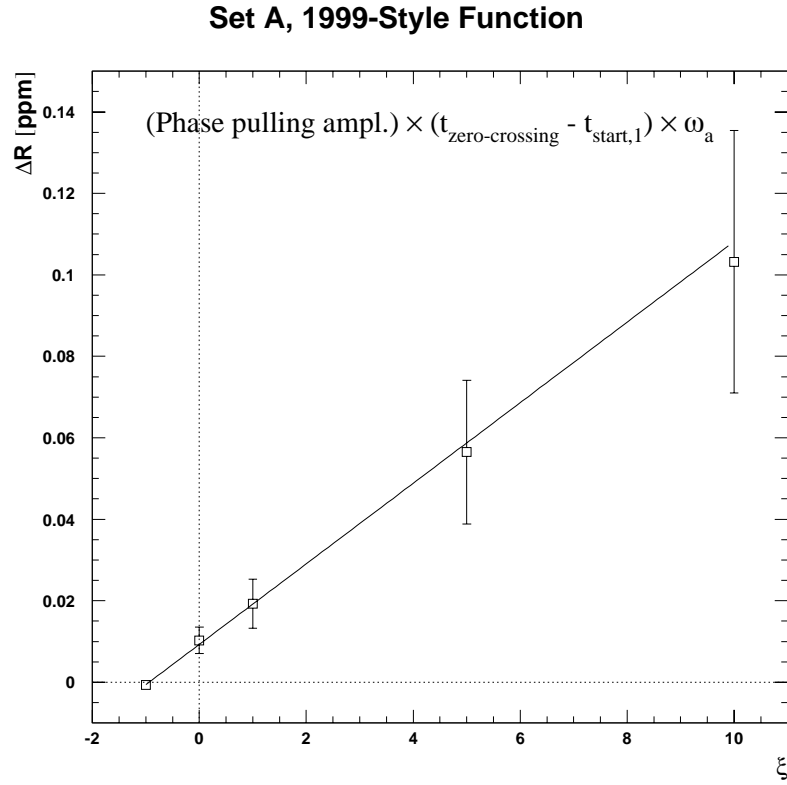


Figure 67: Systematic error from phase pulling induced by gain variations as a function of the gain multiplier. The zero-crossing of the phase pulling was determined from the curves with $\xi = 5$ and $\xi = 10$ in Figure 66.

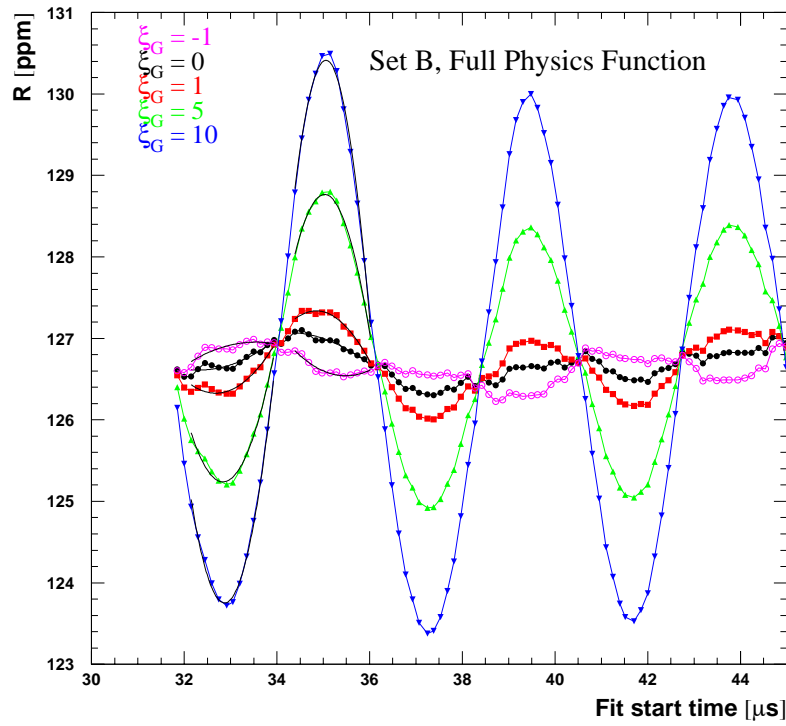
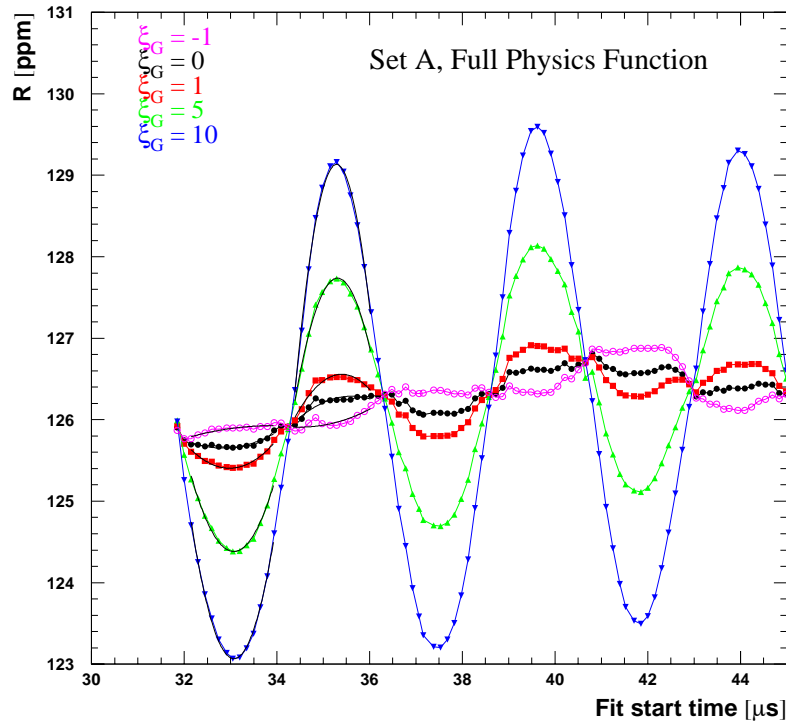


Figure 68: Study of gain correction and artificial gain change for the full physics function.

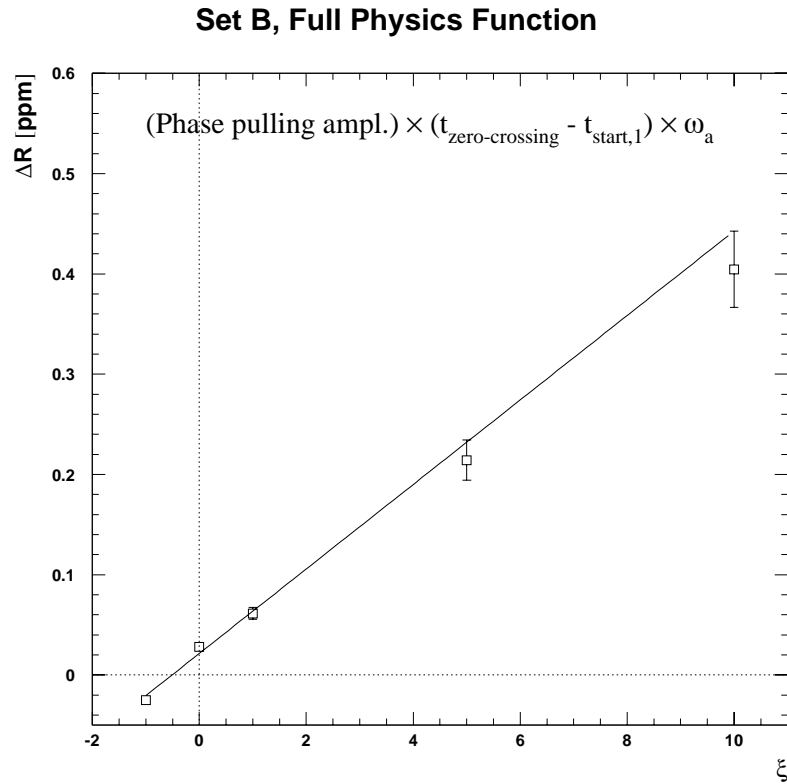
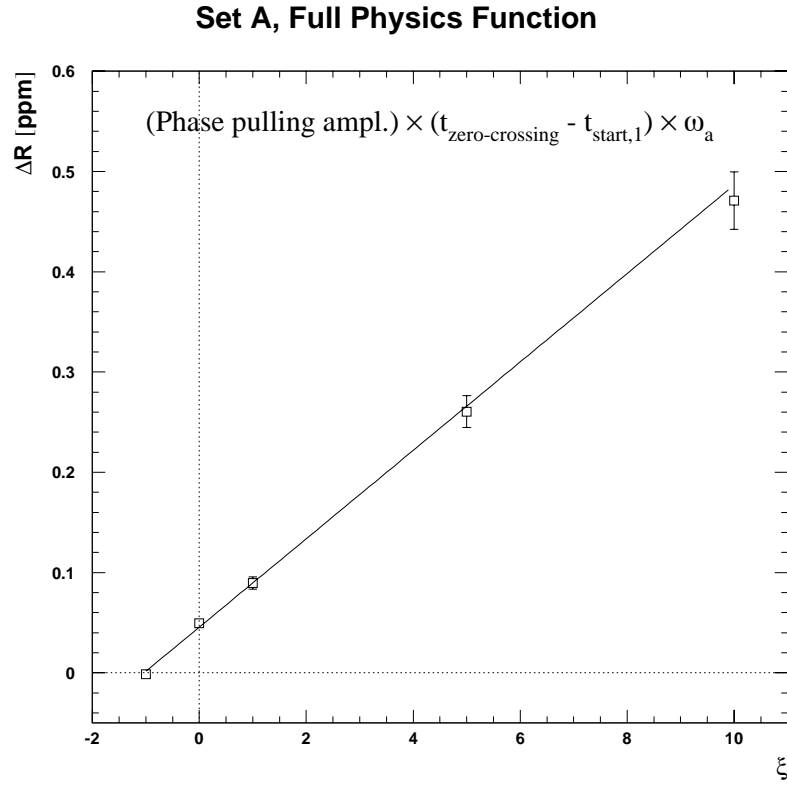


Figure 69: Systematic error from phase pulling induced by gain variations as a function of the gain multiplier. The zero-crossing of the phase pulling was determined from the curves with $\xi = 5$ and $\xi = 10$ in Figure 68.

6.6.3 Effects of an R.S.E. Term

An empirical term describing residual slow effects can be used to correct shortcomings in our knowledge about the non-wiggling component of the decay spectrum (see Eq. (15)).

Figures 70 and 71 demonstrate that the r.s.e. term effectively eliminates phase pulling for $\xi = 0$ and strongly reduces it for larger ξ . The difference between the results for R with and without r.s.e. term for gain-corrected data is shown in Table 43.

Set	1999 Function	full Physics Function
A	-0.0145 ± 0.0000	-0.0408 ± 0.0135
B	-0.0310 ± 0.0149	0.0174 ± 0.0150

Table 43: *Difference $\Delta R = R_{with\ r.s.e.} - R_{without\ r.s.e.}$ [ppm] at a start time of $31.8\mu\text{s}$ for gain-corrected data.*

Since these differences are also a measure for the systematic error from phase pulling, we conservatively use the larger of the values from Tables 42 and 43 as final systematic error.

The disadvantage of including an r.s.e. term is that it cures only the symptoms but not the origins of residual slow effects. Inaccuracies in pileup construction or gain correction may also affect the asymmetry, a consequence which remains after including an r.s.e. term. We therefore chose not to have an r.s.e. term, but to accept phase pulling in R and systematic variations of the fitted muon lifetime in start-time scans.

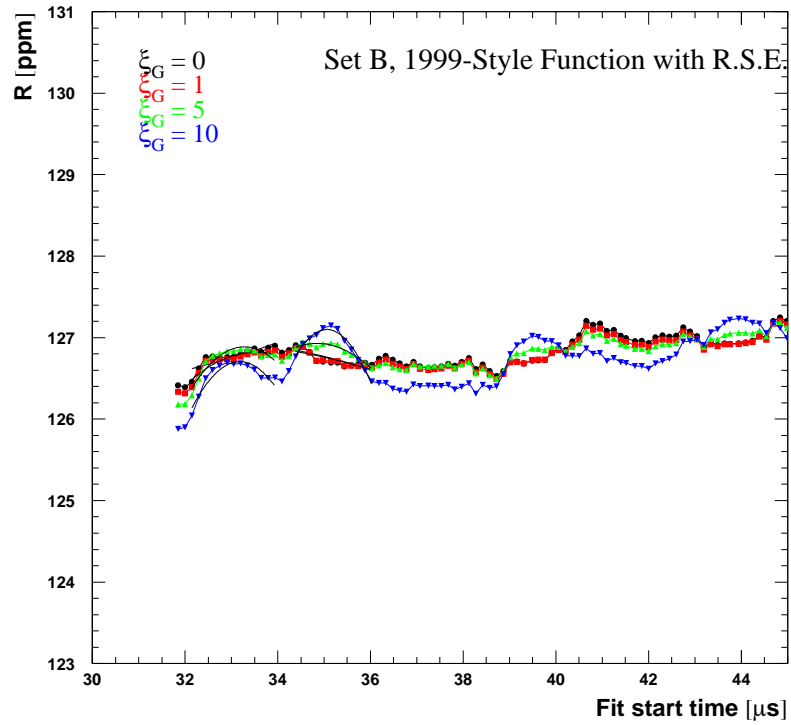
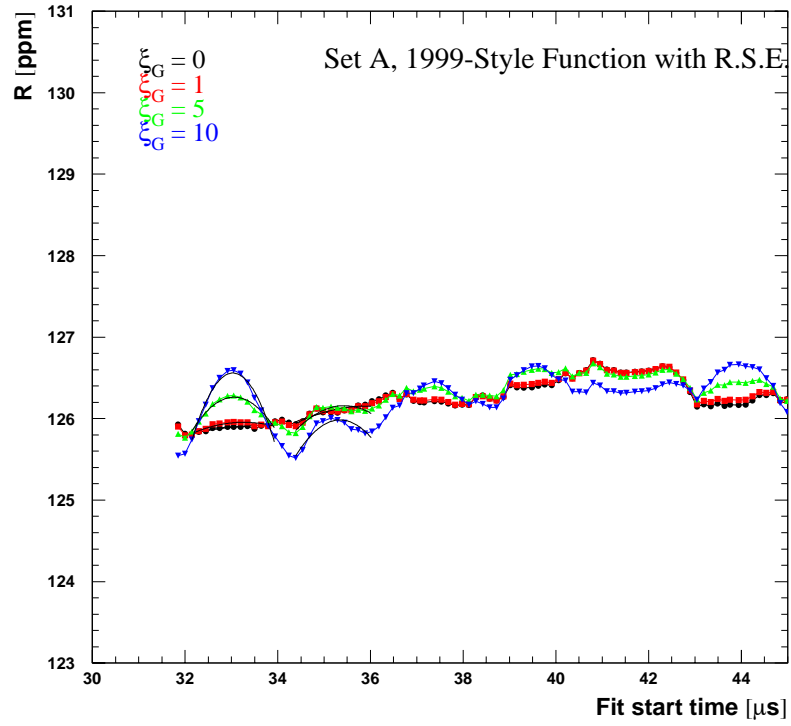


Figure 70: *Study of gain correction and artificial gain change for the 1999-style function with r.s.e. term.*

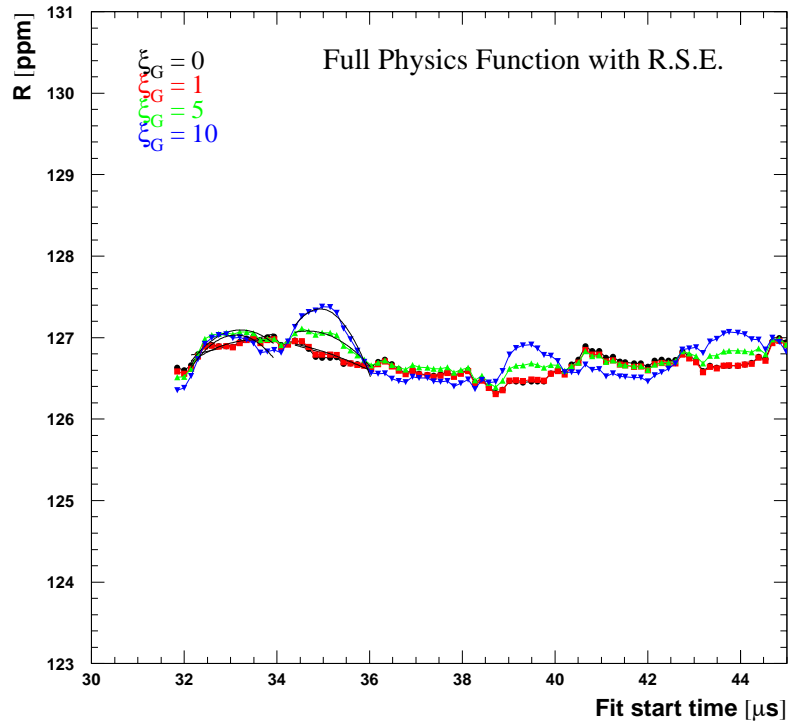
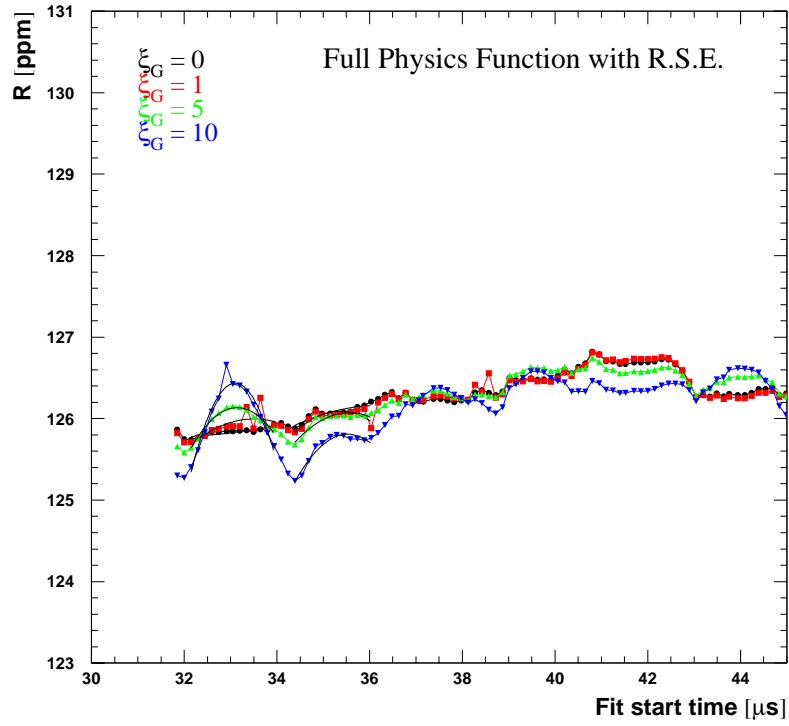


Figure 71: *Study of gain correction and artificial gain change for the full physics function with r.s.e. term.*

6.7 Investigation of the Asymmetry Instability by Energy-Binned Fits

Instabilities in start-time scans for the asymmetry can be caused by gain variations, residual pileup or unseen pileup involving pulses below 250 MeV. The last-mentioned effect cannot be dominant because it would cause a rise of the asymmetry with time rather than a droop as observed in the fit results.

In order to shed some light on the origin of the asymmetry sag we look at its evolution as a function of energy. Figure 72 shows the series of asymmetry start-time scans for Set A; Set B looks similar. These scans reveal a trend: at low energies A tends to sag whereas at high energies it rises with start time. This is even better visible when a figure of merit for the sag – e.g. $A(100\ \mu\text{s}) - A(31.8\ \mu\text{s})$ is drawn as a function of E , see Figure 74.

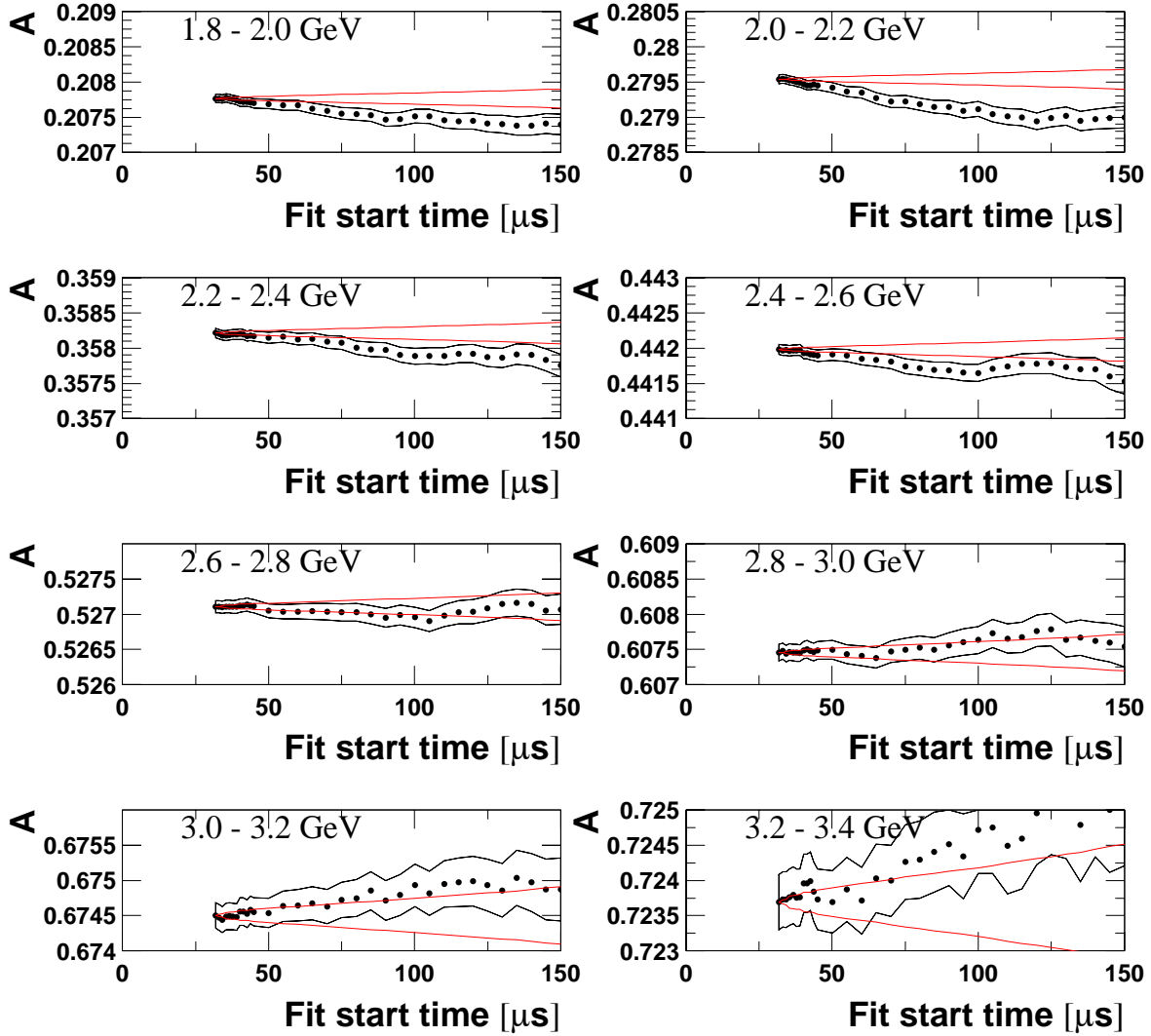
In Section 6.6.1 we have seen that the second half of the ring suffers less from gain variations than the first half. In particular, the second half ring has no detectors showing the whammo effect². The start-time scans for A in the second half ring are shown in Figure 76, and the sag versus energy is given in Figure 75. The asymmetry stability looks better than for all detectors, but one may be misled by the larger statistical errors. The overall trend of asymmetry sag versus energy is still visible. This study suggests that gain changes may cause a part of the asymmetry instability.

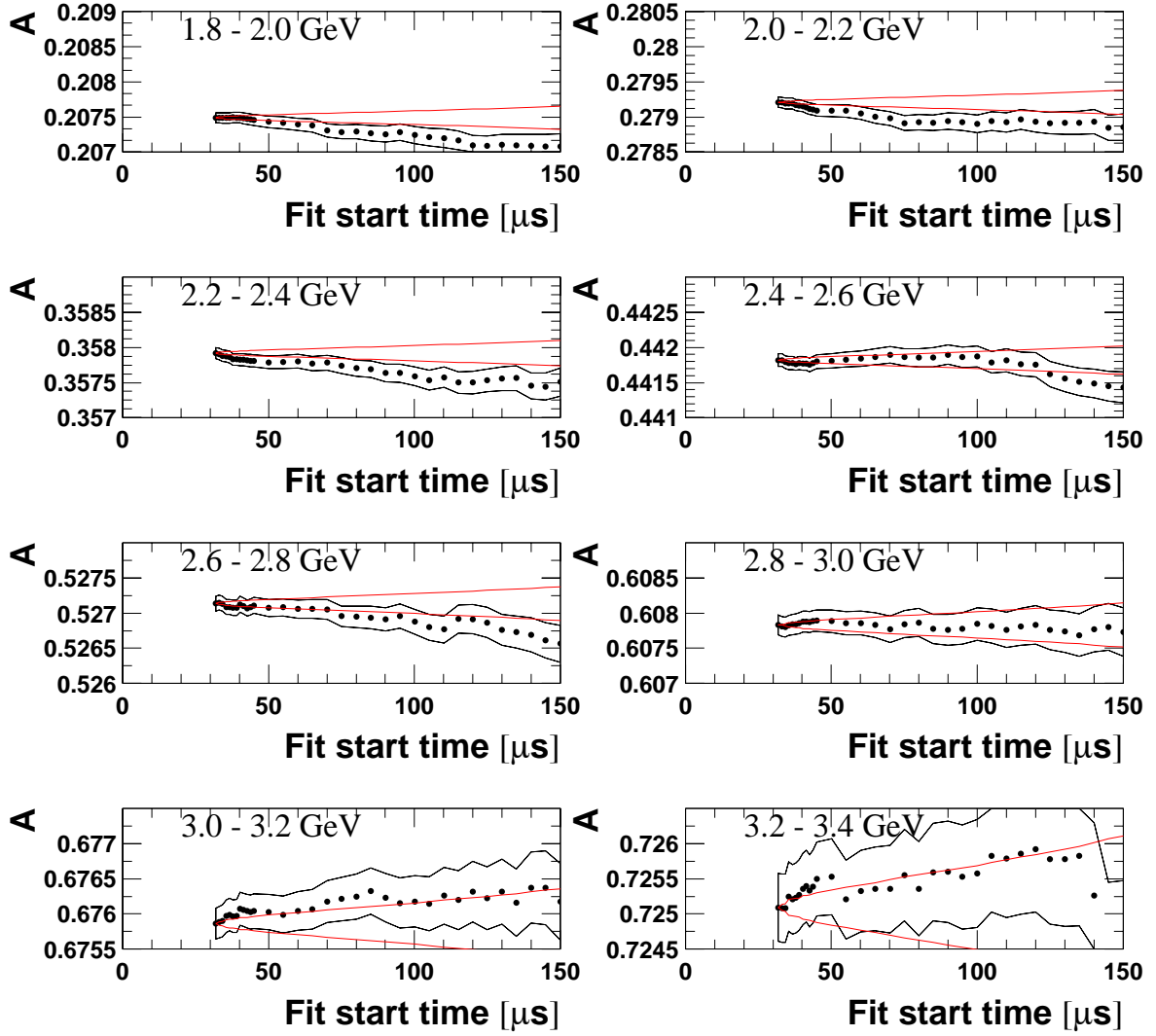
Let us now see whether pileup produces the observed structure. For this purpose, non-pileup-subtracted data are fitted. The result is given in Figure 78. Apparently pileup shifts the entire curve and bends it upwards at high energies, but does not reproduce the same shape. The observed behaviour cannot be explained by a globally wrong pileup multiplier but possibly by an energy-dependent pileup subtraction efficiency.

So far the results are not quite conclusive.

²The structures in the average energy versus time of detectors 3 to 7 (Figure 105) are called “whammos” (introduced by Bill).

Set A

Figure 72: *Start-time scans for A in energy bins for Set A.*

Set BFigure 73: *Start-time scans for A in energy bins for Set B.*

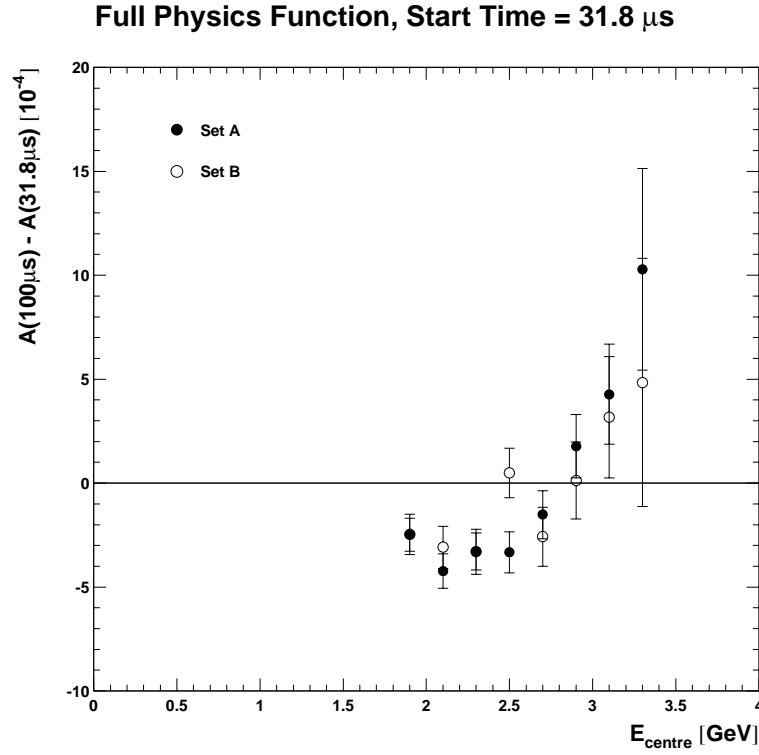


Figure 74: *Asymmetry sag versus centre of 200 MeV wide energy bins.*

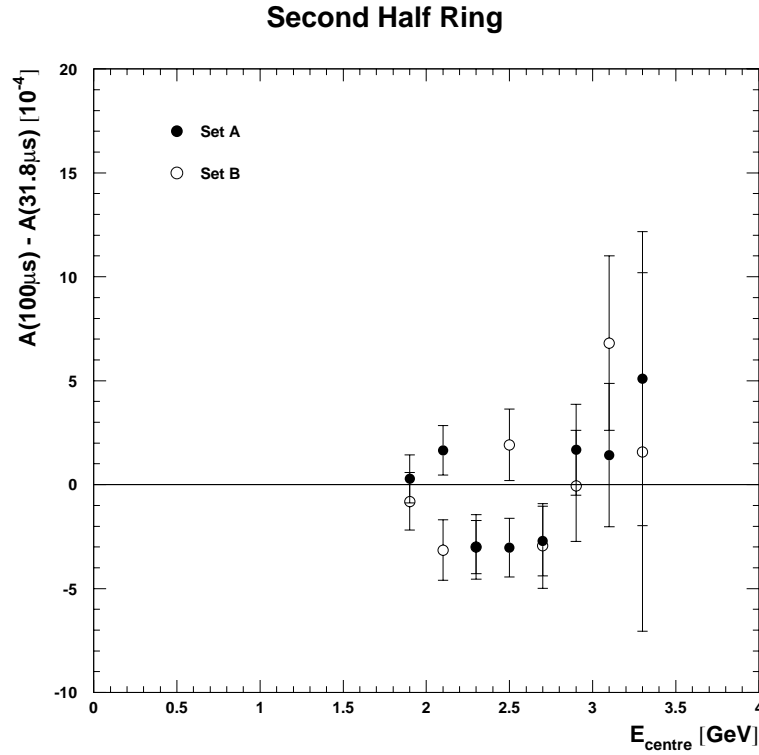


Figure 75: *Asymmetry sag versus centre of 200 MeV wide energy bins, only for detectors 13 to 24.*

Set A, Second Half Ring

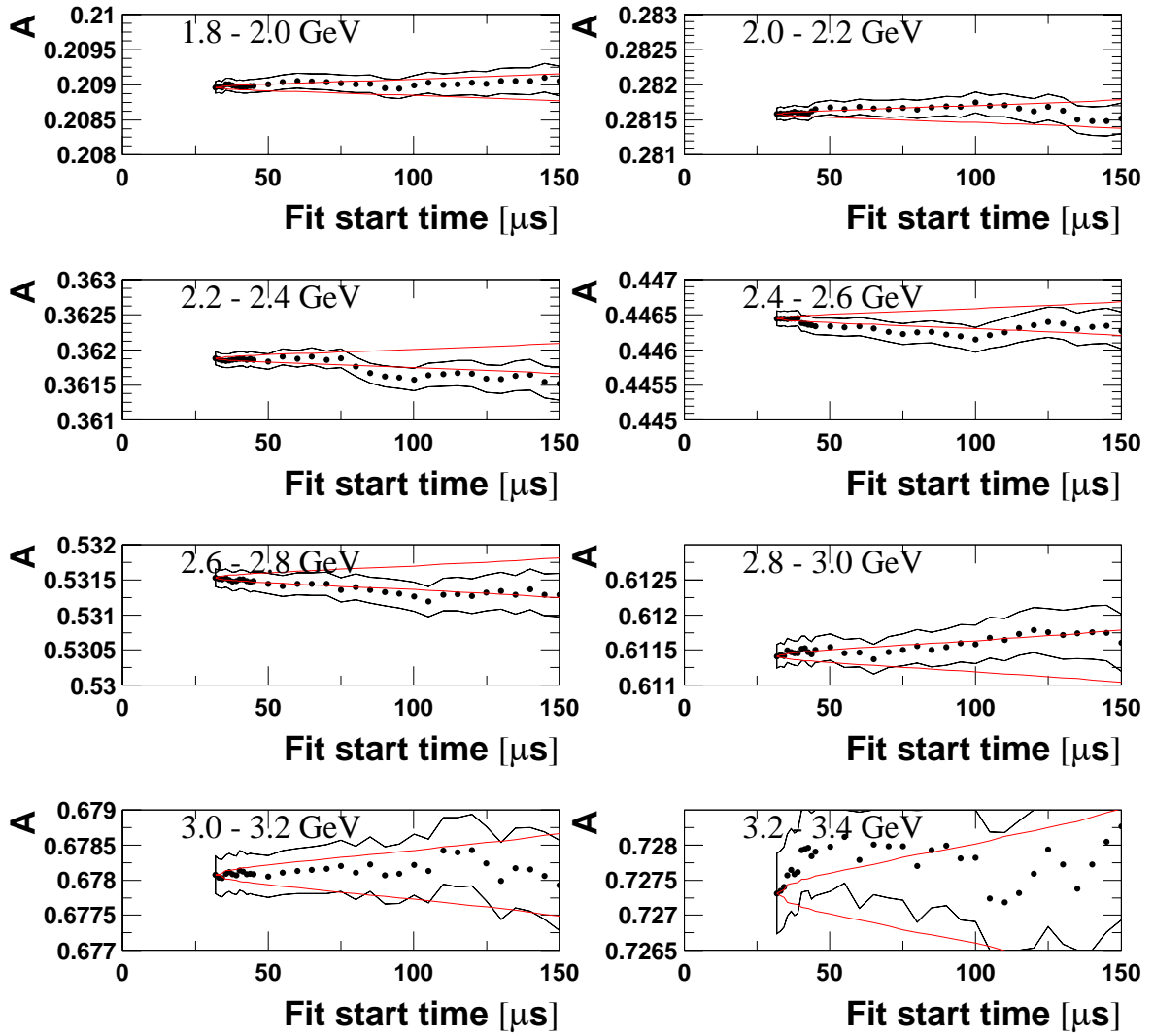


Figure 76: Start-time scans for A in energy bins, only for the second half of the ring (detectors 13 - 24); Set A.

Set B, Second Half Ring

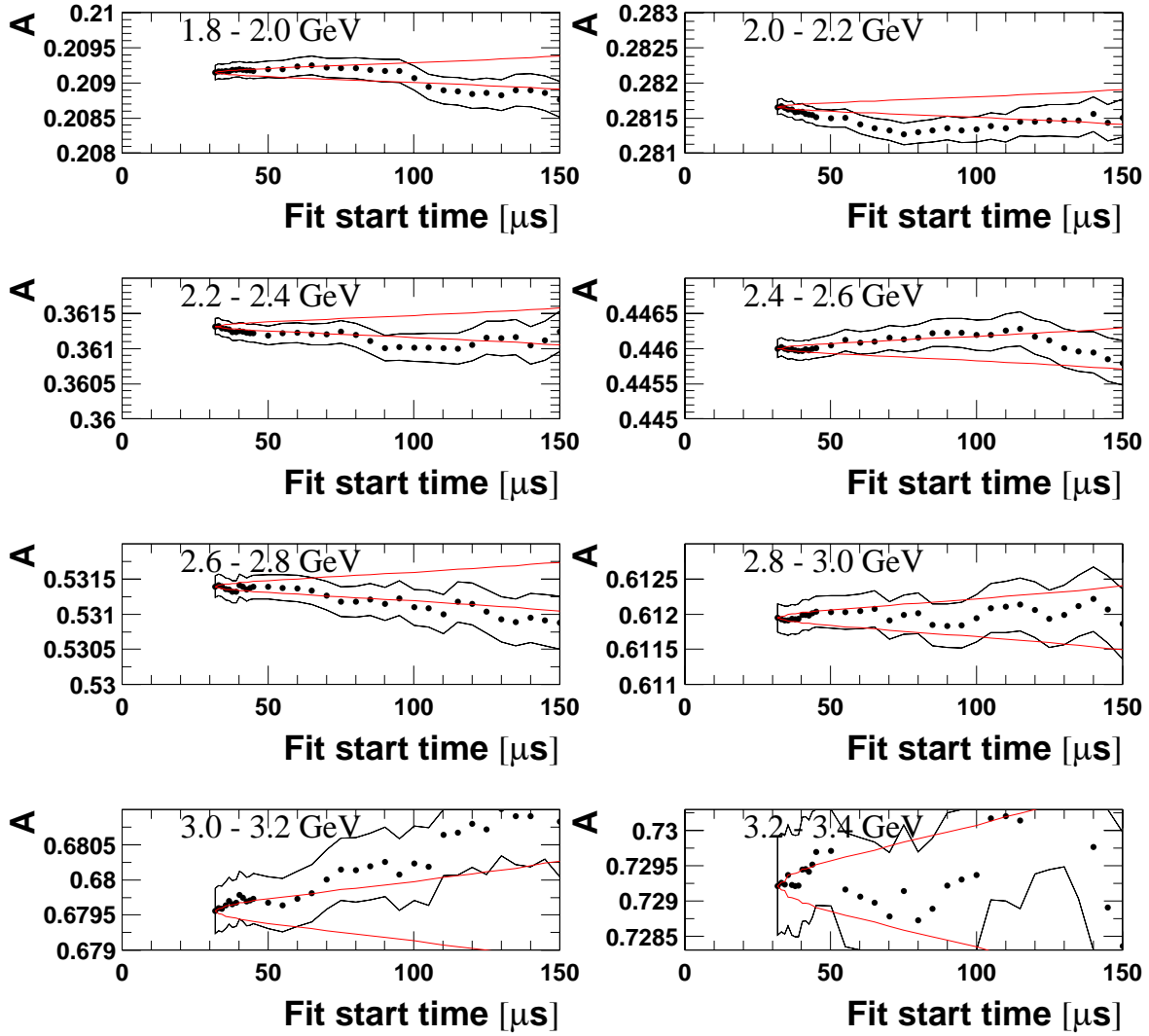


Figure 77: Start-time scans for A in energy bins, only for the second half of the ring (detectors 13 - 24); Set B.

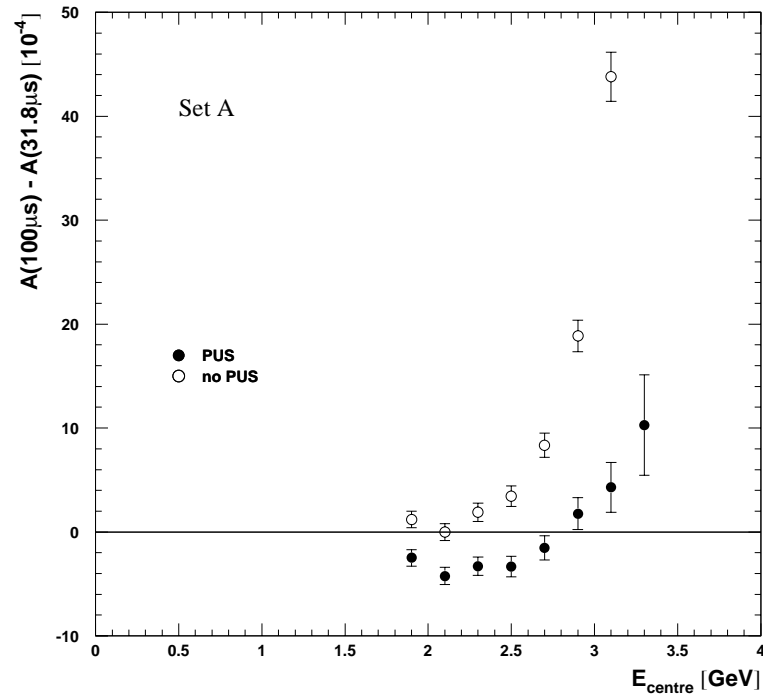


Figure 78: *Asymmetry sag versus centre of 200 MeV wide energy bins with and without pileup subtraction.*

6.8 Muon losses

Inaccuracies in the functional form of the muon losses reveal themselves in phase pulling, i.e. g-2 wiggles in R versus start time. Their systematic error is hence already covered by the evaluation given in Section 6.6 in the context of gain variations. The much more serious influence of muon losses on R comes from differences in the average spin direction between the populations of lost and stored muons. Bill estimated this effect and obtained 0.13 ppm.

It is also interesting to look by how much the two experimental analyses of the muon loss function [9, 10] differ and whether this has any significant impact on R . The two functions are compared in Figure 79.

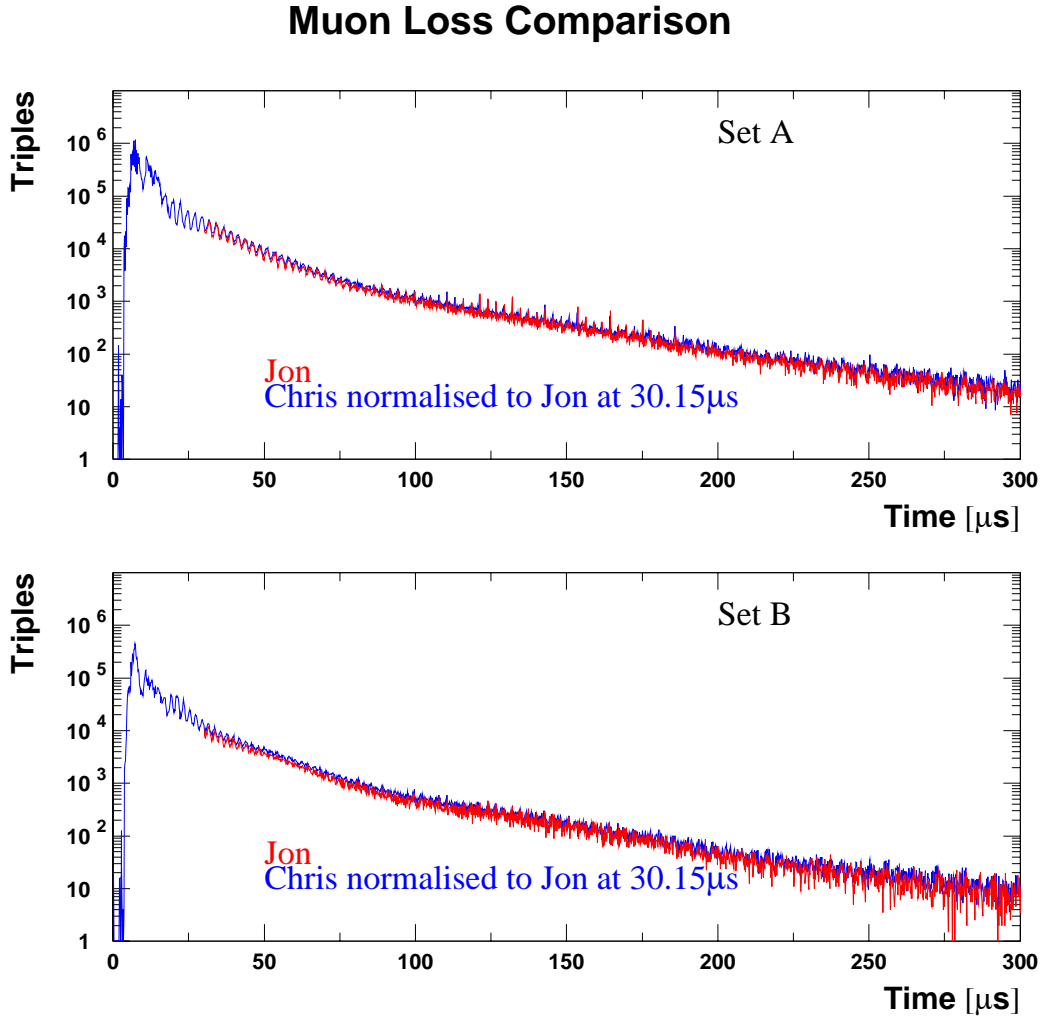


Figure 79: Comparison of Jon's and Chris' muon loss functions. You need a colour copy to distinguish the two curves.

Tables 44 and 45 demonstrate that both muon loss functions produce results for R which agree within 0.01 ppm.

Set	Loss Function	R [ppm]	χ^2
A	Chris	125.9420 ± 0.9138	1.0377
	Jon	125.9446 ± 0.9138	1.0375
B	Chris	126.4447 ± 1.1098	1.0214
	Jon	126.4451 ± 1.1098	1.0214

Table 44: *Comparison of R and χ^2 with Chris' and Jon's muon loss function implemented in the 1999 Function.*

Set	Loss Function	R [ppm]	χ^2
A	Chris	125.9085 ± 0.9173	1.0386
	Jon	125.9106 ± 0.9172	1.0384
B	Chris	126.6301 ± 1.1169	1.0196
	Jon	126.6303 ± 1.1169	1.0196

Table 45: *Comparison of R and χ^2 with Chris' and Jon's muon loss function implemented in the Full Physics Function.*

6.9 Binning Effects

The effect of the bin width was extensively studied in the 2000 analysis and found to be very small: $\delta R \leq (0.06 \pm 0.05)$ ppm. There is nothing new the smaller data set from 2001 can contribute.

6.10 Randomisation

The time spectra were randomised with 5 different random seeds but the same randomisation period given by the cyclotron period of 149.2 ns. Then for each seed the sum of detector spectra was fitted. The means and rms of R and χ^2 are listed in Tables 46 and 47.

Set	$\langle R \rangle$ [ppm]	$rms(R)$ [ppm]	$\langle \chi^2 \rangle$	$rms(\chi^2)$
A	125.9913 ± 0.9138	0.0464	1.0222	0.0082
B	126.4103 ± 1.1098	0.0682	1.0200	0.0123
avr.	126.1606 ± 0.7054			

Table 46: *The effects of randomisation on R and χ^2 for the 1999 Function.*

Set	$\langle R \rangle$ [ppm]	$rms(R)$ [ppm]	$\langle \chi^2 \rangle$	$rms(\chi^2)$
A	125.9645 ± 0.9173	0.0517	1.0232	0.0085
B	126.5892 ± 1.1168	0.0698	1.0180	0.0125
avr.	126.2162 ± 0.7088			

Table 47: *The effects of randomisation on R and χ^2 for the Full Physics Function.*

We also show start time scans for R with the results of all random seeds combined (Figures 80 and 81). For the purpose of comparison we superimpose the scan for the particular seed for which all studies were done up to this point of the report.

The systematic error on the average of the 5 results is given by $rms(R)/\sqrt{5-1}$.

1999 Function

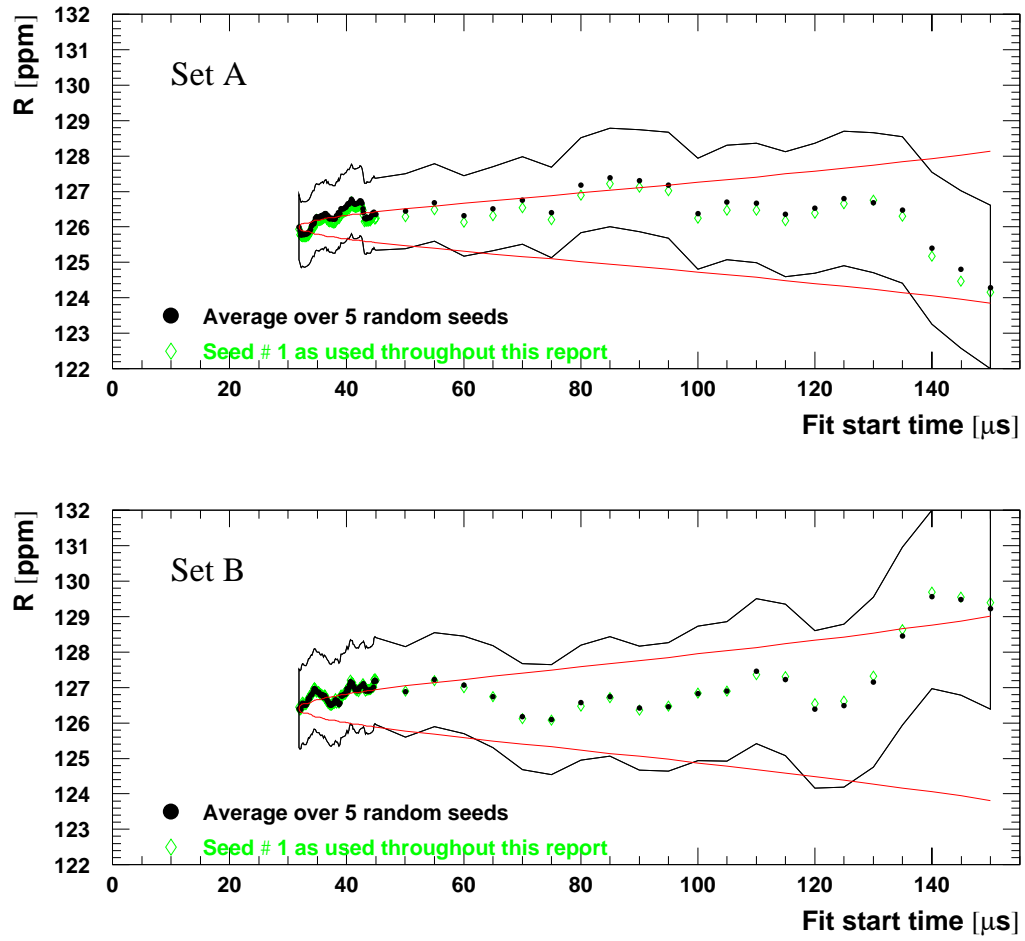


Figure 80: *Start time scans for R averaged over 5 random seeds (1999 function). For comparison we also plot the result for the particular seed used in the rest of this document.*

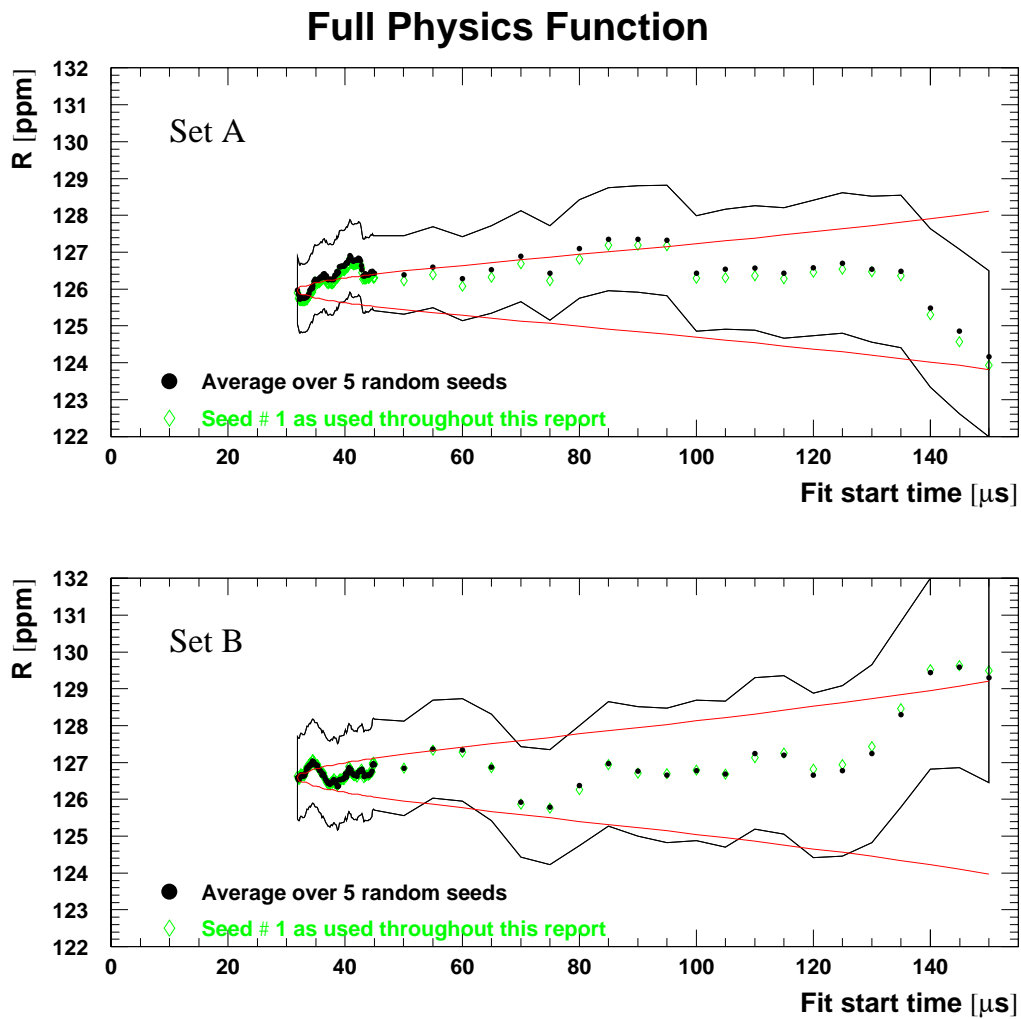


Figure 81: Start time scans for R averaged over 5 random seeds (full physics function). For comparison we also plot the result for the particular seed used in the rest of this document.

7 Summary

7.1 Systematic Error Table

The final systematic error balance is given in Table 48.

Effect	1999 Function		Full Physics Function	
	Set A	Set B	Set A	Set B
CBO frequency droop	0.01	0.01	0.01	0.01
Acceptance CBO residual	0.00	0.00	0.00	0.00
Acceptance DCBO envelope	0.01	0.00	0.01	0.00
Asymmetry and phase CBO (halfring effect)	0.07	0.30	0.01	0.03
Residual pileup (wrong ampl.)	0.04	0.05	0.04	0.04
(wrong phase)	0.07	0.10	0.07	0.09
Unseen pileup	0.01	0.01	0.01	0.01
Detector gain variations, muon loss function and other slow effects	0.01	0.03	0.05	0.03
Muon losses (spin direction)	0.13	0.13	0.13	0.13
Binning	0.06	0.06	0.06	0.06
Randomisation	0.02	0.03	0.03	0.03
AGS Background (*)	0.01	0.01	0.01	0.01
Combination (see text!)	0.18	0.36	0.19	0.19

(*) to be stolen from a yet unknown victim. The values given are from 2000.

Table 48: *Systematic uncertainties of R for a fit start time of $31.8\mu\text{s}$. All numbers are given in ppm.*

Should the errors in Table 48 be added linearly or in quadrature?

We only bother to look at the major entries of the tables, not at the romantics.

The main correlations are expected between residual pileup, unseen pileup and gain variations. We have seen that under- or oversubtracted pileup can easily be (mis-)compensated by the gain correction. We therefore add the uncertainties from gain and from a wrong pileup amplitude **linearly**. The number for the contribution from a wrong pileup phase is a generous upper limit and should not be added linearly.

We have seen that in 2001 the parameters related to the halfring effect are not strongly correlated with the asymmetry, unlike in 2000. The correlations between CBO effects and gain can therefore be expected to be small.

This year, all slow effects are treated together which avoids correlations between entries that would be difficult to separate. The uncertainty given for lost muons represents purely the possible difference in average spin direction between lost and stored muons. This aspect of muon losses is independent from the slow terms modifying the lifetime.

7.2 Combined Result from the two Run Sets

The central values and statistical errors of R for the two run sets are taken from Tables 46 and 47, i.e. averaged over 5 random seeds. We repeat them here:

- 1999-Style Function:

$$\text{Set A: } R = (125.9913 \pm 0.9138) \text{ ppm} \quad (77)$$

$$\text{Set B: } R = (126.4103 \pm 1.1098) \text{ ppm} \quad (78)$$

- Full Physics Function:

$$\text{Set A: } R = (125.9645 \pm 0.9173) \text{ ppm} \quad (79)$$

$$\text{Set B: } R = (126.5892 \pm 1.1168) \text{ ppm} \quad (80)$$

We now need to *add* the partial results *together*, taking into account statistical and systematic errors and their correlations.

7.2.1 Averaging Central Values and Systematic Errors with Statistical Weights

The simplest and most intuitive approach for combining the two subsets is to use the statistical weights $w_i \equiv \frac{1/\sigma_i^2}{1/\sigma_1^2 + 1/\sigma_2^2}$ for the central values and for the systematic errors:

- 1999-Style Function: $w_1 = 0.5980$, $w_2 = 0.4020$
- Full Physics Function: $w_1 = 0.5971$, $w_2 = 0.4029$

Thus we obtain:

- 1999-style function: $R = (126.1606 \pm \underbrace{0.7054 \pm 0.2524}_{0.7492 \text{ ppm}}) \text{ ppm}$

- Full physics function: $R = (126.2162 \pm \underbrace{0.7088 \pm 0.1900}_{0.7338 \text{ ppm}}) \text{ ppm}$

7.2.2 Optimal Weighting including Correlations of Systematic Errors

We define our correlation matrix as

$$V \equiv V_{\text{stat}} + V_{\text{syst}} = \begin{pmatrix} \sigma_1^2 & 0 \\ 0 & \sigma_2^2 \end{pmatrix} + \begin{pmatrix} \tau_1^2 & f \tau_1 \tau_2 \\ f \tau_1 \tau_2 & \tau_2^2 \end{pmatrix} \quad (81)$$

with a correlation coefficient f for the systematic part. Using the formalism discussed in [20], one obtains the combined result for the optimal weighted average and error:

$$R = \frac{\sigma_2^2 + \tau_2^2 - f \tau_1 \tau_2}{\sigma_1^2 + \tau_1^2 + \sigma_2^2 + \tau_2^2 - 2f \tau_1 \tau_2} R_1 + \frac{\sigma_1^2 + \tau_1^2 - f \tau_1 \tau_2}{\sigma_1^2 + \tau_1^2 + \sigma_2^2 + \tau_2^2 - 2f \tau_1 \tau_2} R_2 \quad (82)$$

$$\sigma^2 = \frac{(\sigma_1^2 + \tau_1^2)(\sigma_2^2 + \tau_2^2) - f^2 \tau_1^2 \tau_2^2}{\sigma_1^2 + \tau_1^2 + \sigma_2^2 + \tau_2^2 - 2f \tau_1 \tau_2} \quad (83)$$

These expressions require knowledge of the correlation factor f . We shall now evaluate them for two different assumptions on f .

$f = 0$:

- 1999-style function: $R = (126.1535 \pm 0.7261) \text{ ppm}$
- Full physics function: $R = (126.2182 \pm 0.7219) \text{ ppm}$

This assumption is certainly far too optimistic and underestimates the total error. The systematic errors from the two run sets can be expected to be highly correlated.

$f = 1$:

- 1999-style function: $R = (126.1506 \pm 0.7273) \text{ ppm}$
- Full physics function: $R = (126.2162 \pm 0.7224) \text{ ppm}$

This result is very close to the one from the naive approach in Section 7.2.1. The 100 % correlations are likely to be somewhat overestimated.

Optimal weighting has generally the drawback that the central value of the result depends on the not too well known correlations.

7.2.3 Purely Statistical Weights but Error Analysis with Correlations

Here, we calculate the central value of the result using only statistical weights (like in Section 7.2.1). For the total error however, estimates on the correlations between the systematic errors are used. This leads to a stable central value and a slightly more conservative error.

For weights $w_i = \frac{1/\sigma_i^2}{1/\sigma_1^2 + 1/\sigma_2^2}$ (where σ_i is the statistical error of set i) and a covariance matrix V , the combined error is given by [20]

$$\sigma^2 = \sum_{i,j=1}^2 w_i w_j V_{ij} = \frac{\frac{V_{11}}{\sigma_1^4} + \frac{V_{22}}{\sigma_2^4} + 2 \frac{V_{12}}{\sigma_1^2 \sigma_2^2}}{(\frac{1}{\sigma_1^2} + \frac{1}{\sigma_2^2})^2} = \frac{\frac{\sigma_1^2 + \tau_1^2}{\sigma_1^4} + \frac{\sigma_2^2 + \tau_2^2}{\sigma_2^4} + 2 \frac{f \tau_1 \tau_2}{\sigma_1^2 \sigma_2^2}}{(\frac{1}{\sigma_1^2} + \frac{1}{\sigma_2^2})^2} \quad (84)$$

$$= \frac{1}{\frac{1}{\sigma_1^2} + \frac{1}{\sigma_2^2}} + \frac{\frac{\tau_1^2}{\sigma_1^4} + \frac{\tau_2^2}{\sigma_2^4} + 2 \frac{f \tau_1 \tau_2}{\sigma_1^2 \sigma_2^2}}{\frac{1}{\sigma_1^4} + \frac{1}{\sigma_2^4} + 2 \frac{f}{\sigma_1^2 \sigma_2^2}} \quad (85)$$

Again, we try $f = 0$ and $f = 1$:

$f = 0$:

- 1999-style function: $R = (126.1606 \pm \underbrace{0.7054 \pm 0.1807}_{0.7282 \text{ ppm}}) \text{ ppm}$
- Full physics function: $R = (126.2162 \pm \underbrace{0.7088 \pm 0.1369}_{0.7219 \text{ ppm}}) \text{ ppm}$

$f = 1$:

- 1999-style function: $R = (126.1606 \pm \underbrace{0.7054 \pm 0.2527}_{0.7493 \text{ ppm}}) \text{ ppm}$
- Full physics function: $R = (126.2162 \pm \underbrace{0.7088 \pm 0.1900}_{0.7338 \text{ ppm}}) \text{ ppm}$

Apparently for both values of f the error penalty from non-optimal weighting is small.

One could refine this procedure by writing V_{sys} as a sum of matrices pertaining to the individual systematic effects and assigning different correlation factors for each of them.

7.2.4 Preferred Result

The preferred result is the one from the Full Physics Function. It has a slightly smaller total error than the 1999 Function. We conservatively combine the run sets according to the approach from Section 7.2.3 with $f = 1$:

$$\text{with my offset:} \quad R = (126.2162 \pm \underbrace{0.7088 \pm 0.1900}_{0.7338 \text{ ppm}}) \text{ ppm} \quad (86)$$

$$\text{with the official offset:} \quad R = 108.3062 \text{ ppm} \quad (87)$$

References

- [1] M. Deile: Multiparameter ω_a Analysis of the g-2 Data from 2000, g-2 Note 421.
- [2] I. Logashenko: FIT Pulse Finding Algorithm, g-2 Note 334, rev. March 1999; Shapes of WFD Pulses and the FIT Pulse Finding Algorithm, g-2 Note 369, September 2000.
- [3] Run selection for 2001, available from
<http://g2muon:precess@www.npl.uiuc.edu/~polly/g-2> .
- [4] A. Lam: Fast-rotation analysis, presented at the October 2002 collaboration meeting.
- [5] C. Özben and Y.K. Semertzidis: Eliminating Pileup from the g-2 Data, g-2 Note 365, July 2000.
- [6] I. Logashenko: energy dependence of f_L and the g2off dead-time, e-mail to g2offline, 22 October 2002.
- [7] F. Farley et al.: Estimation of Error in Differential Pileup Subtracted Data, g-2 Note 377, December 2000.
- [8] Y. Semertzidis et al., The Brookhaven Muon g-2 Storage Ring High Voltage Quadrupoles, accepted for publication in Nucl. Instr. Meth. A.
- [9] C. Polly: Muon losses for the two run sets, presentation at the Illinois analysis workshop, December 2002.
- [10] J. Paley: Muon losses for the two run sets, presentation at the Illinois analysis workshop, December 2002.
- [11] C. Özben: 1999 ω_a Analysis of g-2, g-2 Note 385, January 2001.
- [12] Y.K. Semertzidis: Shift in R due to pileup phase a.k.a. the “Underwater” effect, g-2 Note 426, July 2002.
- [13] W. Morse: relationship between gain and asymmetry; private communication.
- [14] W. Morse: The Low Pulse Height Pile-Down Effect, g-2 Note 373, October 2000.
- [15] I. Logashenko: Estimating the systematic error in ω_a due to low-energy pileup, draft of a g-2 Note, January 2003.
- [16] Y.K. Semertzidis: The Spectrum of χ and Systematic Errors Due to Backgrounds in the 2000 Run Data, g-2 Note 406, January 2002. See remark 3 in Section 4.
- [17] A. Steinmetz: The 98 Systematic Error on the g-2 Frequency, g-2 Note 351, November 1999.
- [18] S. Redin: Statistical Equations for Set-Subset Problem, ..., g-2 Note 387, March 2001.
- [19] Y.K. Semertzidis: On the Question of the Functional Form of the 2000 Run Data, g-2 Note 403, December 2001.
- [20] O. Rind and E. Sichtermann: On Combining the Results for ω_a , g-2 Note 380, January 2001.

A Fit Results for the 1999-Style Function

A.1 Start Time Scans for the Sum of Detectors

1999 Function, Sum of Detectors, Period A

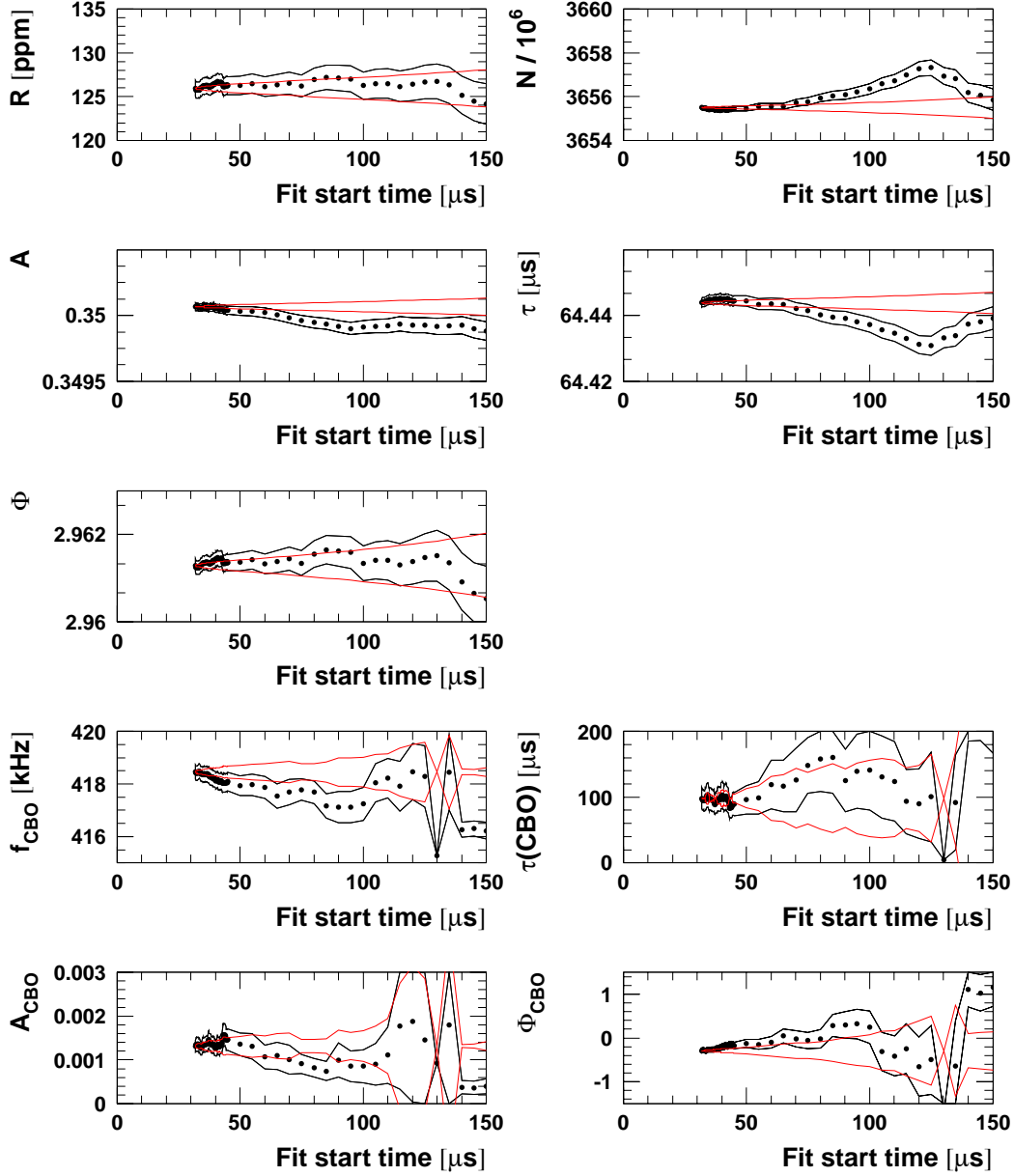
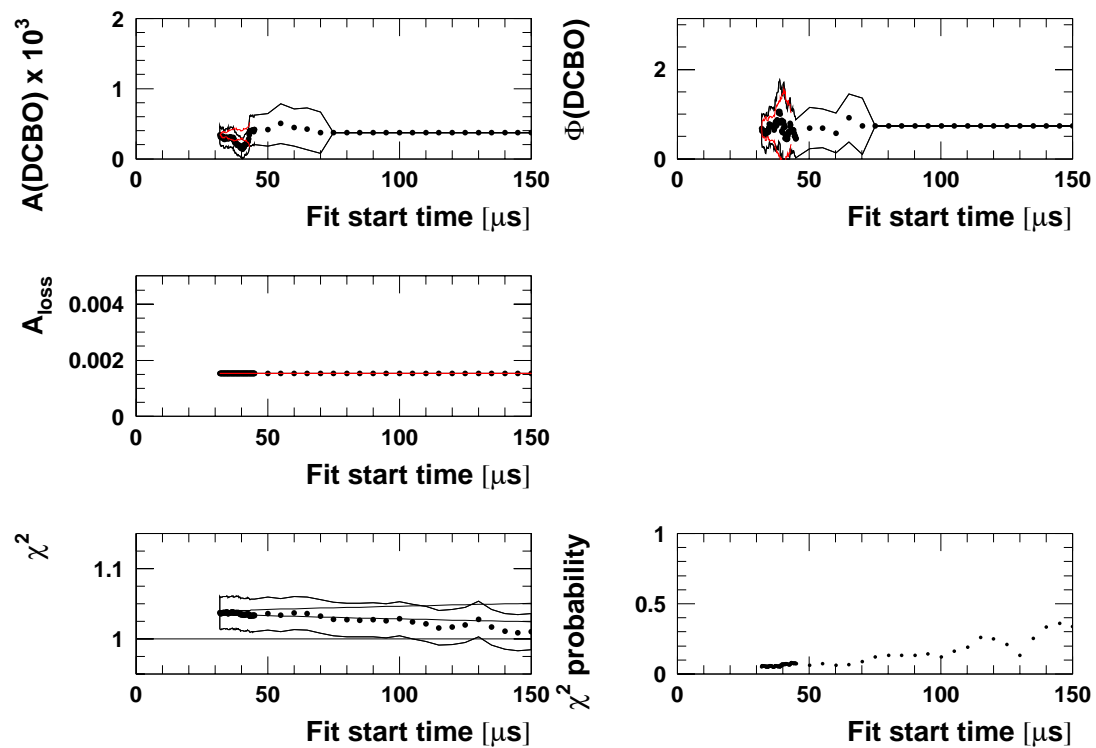


Figure 82: *Start time scan with the 1999-style function for Set A.*

1999 Function, Sum of Detectors, Period A



1999 Function, Sum of Detectors, Period B

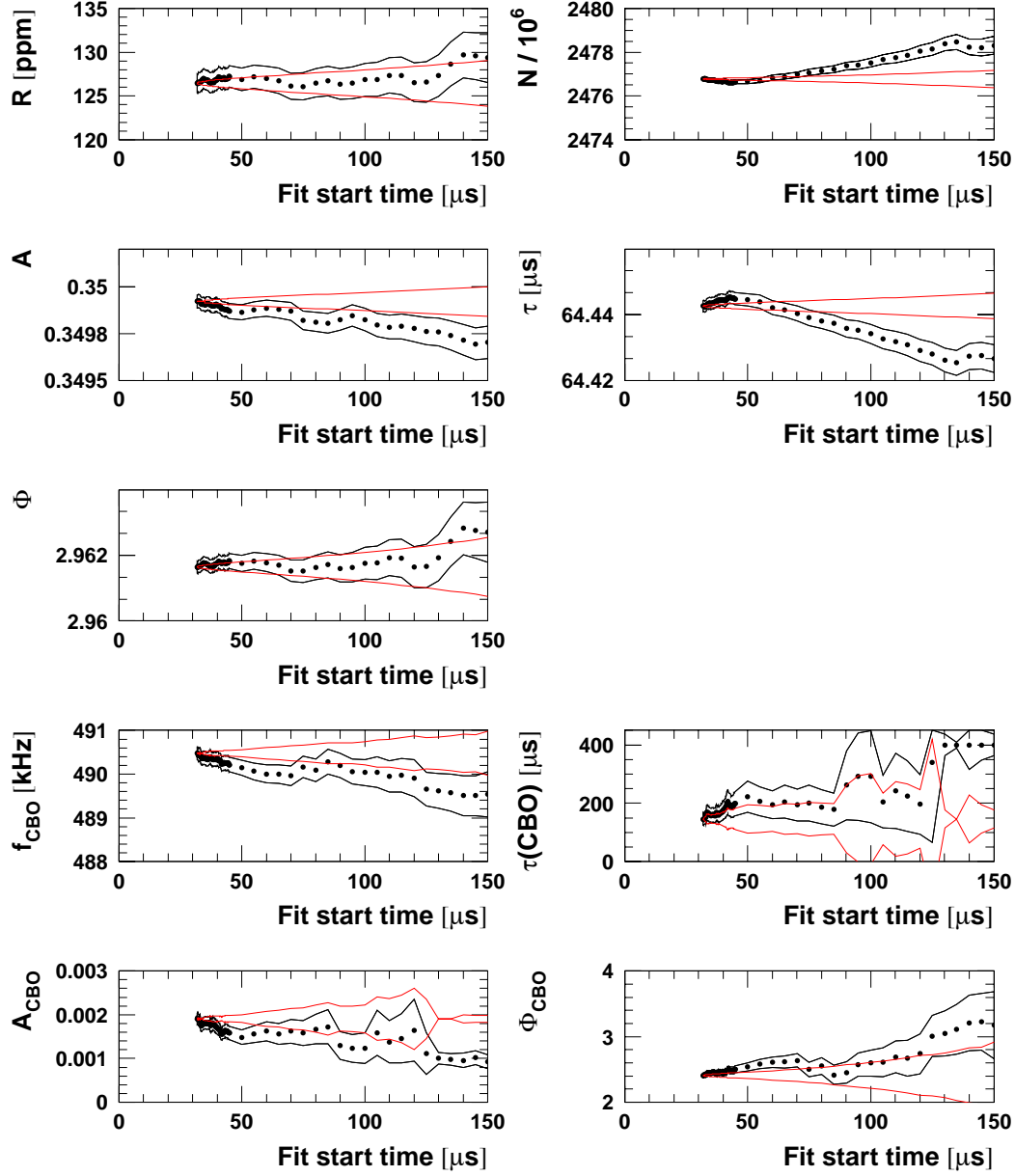
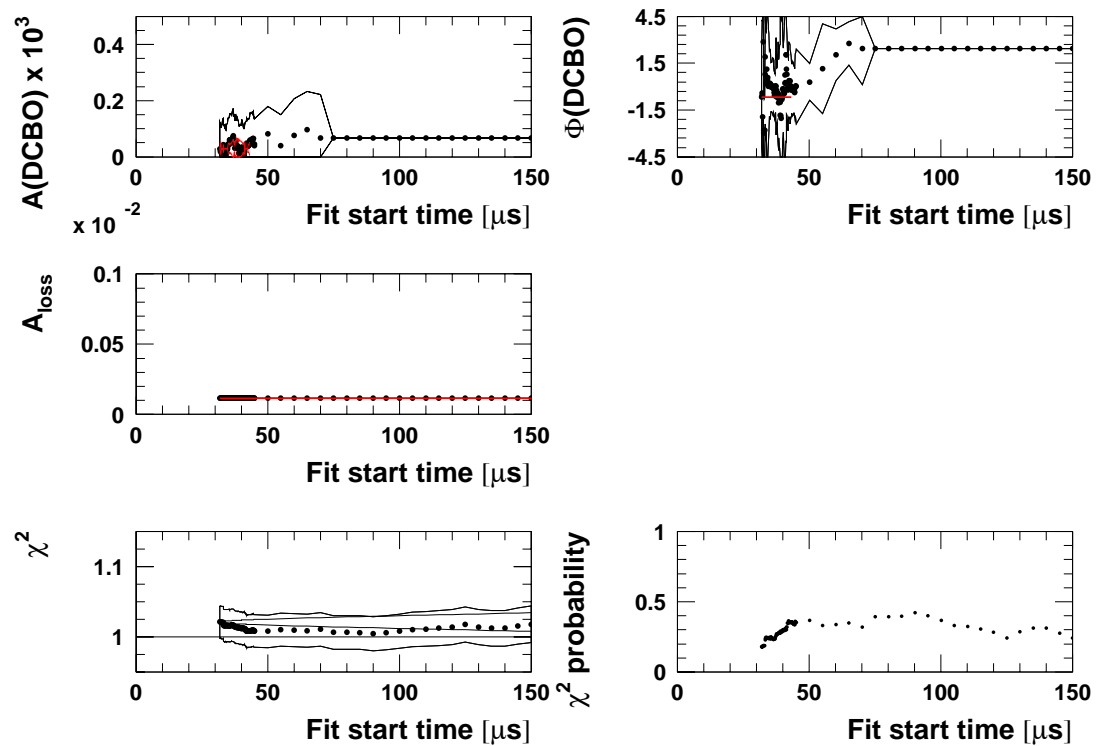


Figure 83: *Start time scan with the 1999-style function for Set B.*

1999 Function, Sum of Detectors, Period B



A.2 Start Time Scans for the Two Half Rings

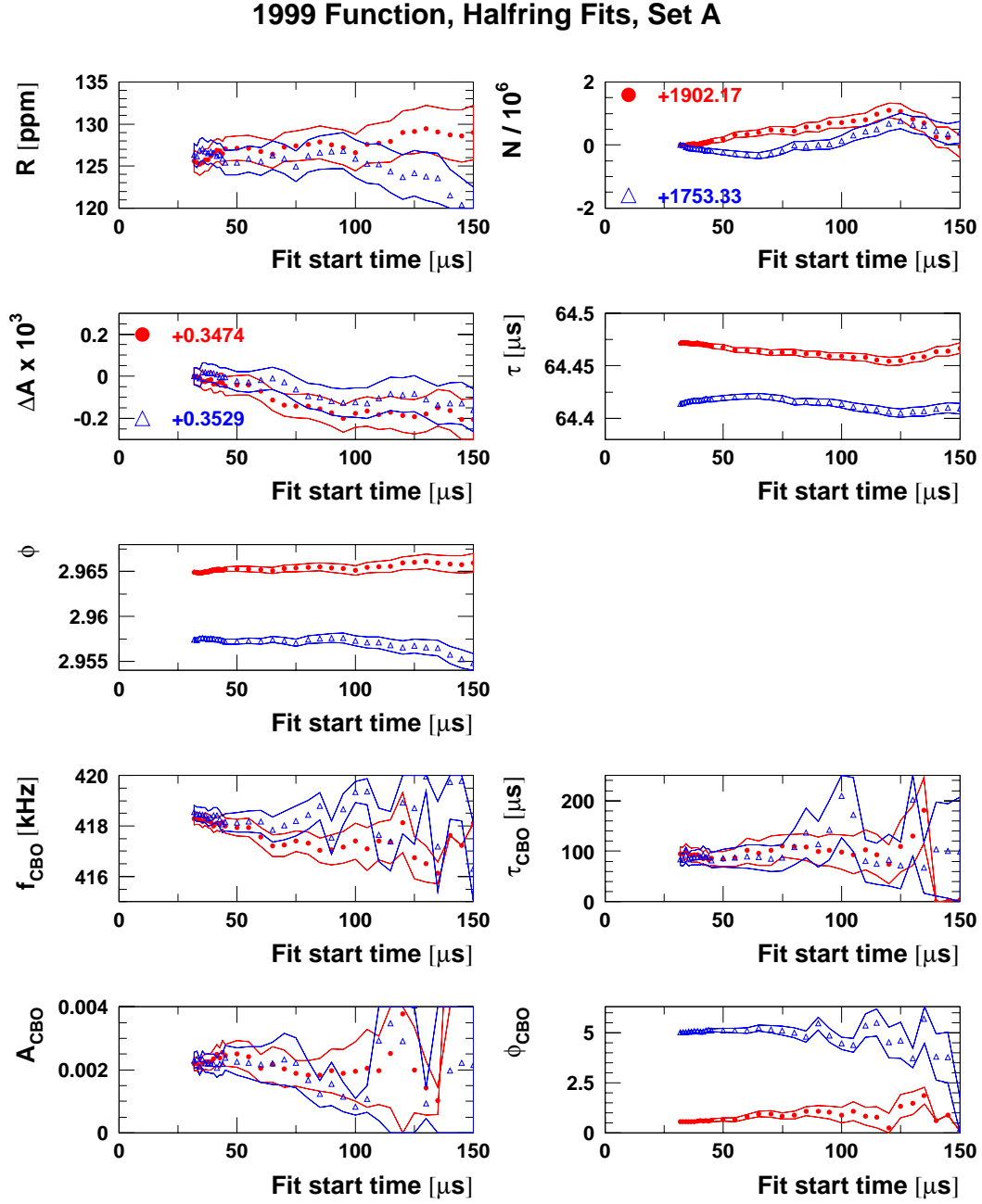
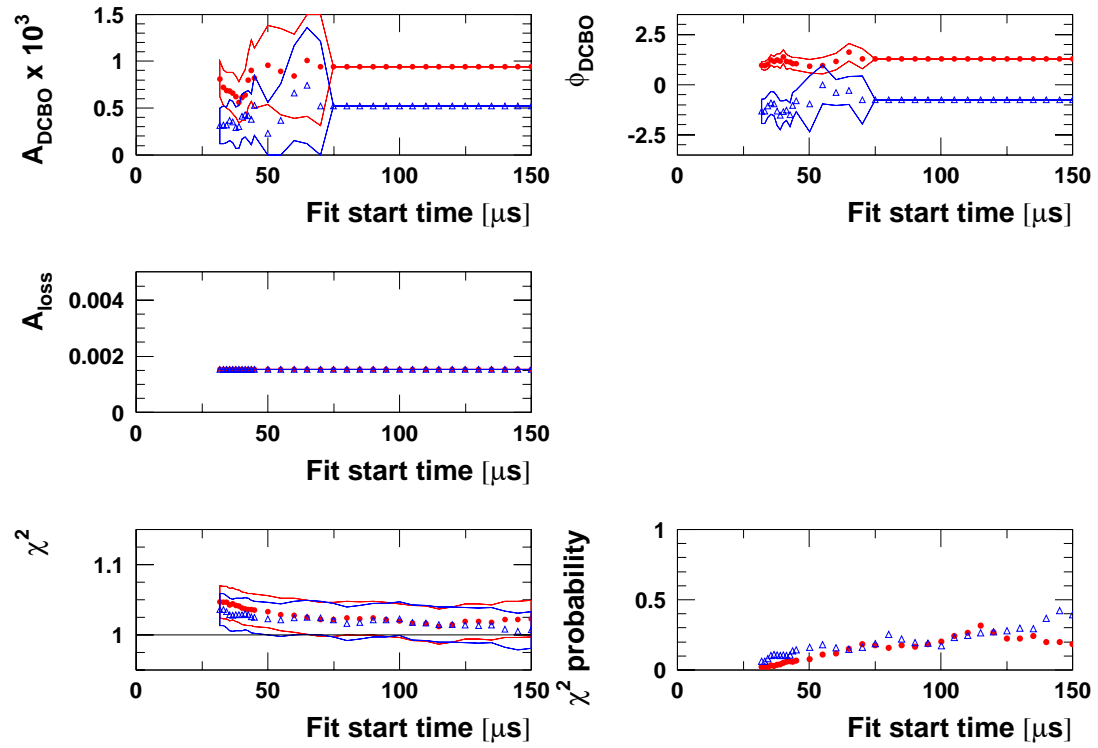


Figure 84: Start time scan for the two half rings separately (red circles = det. 1-12, blue triangles = det. 13-24) with the 1999-style function for Set A.

1999 Function, Halfring Fits, Set A



1999 Function, Halfring Fits, Set B

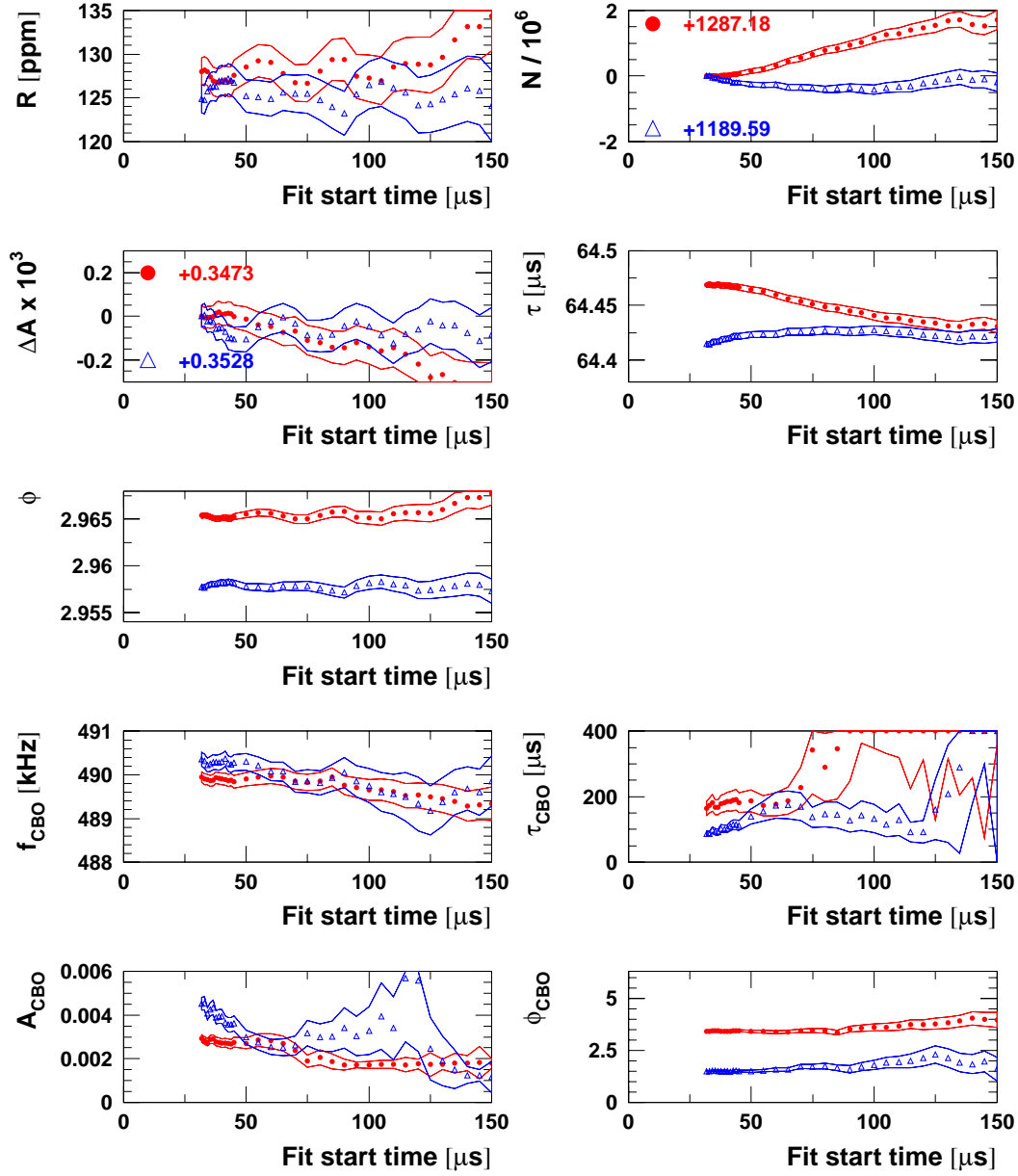
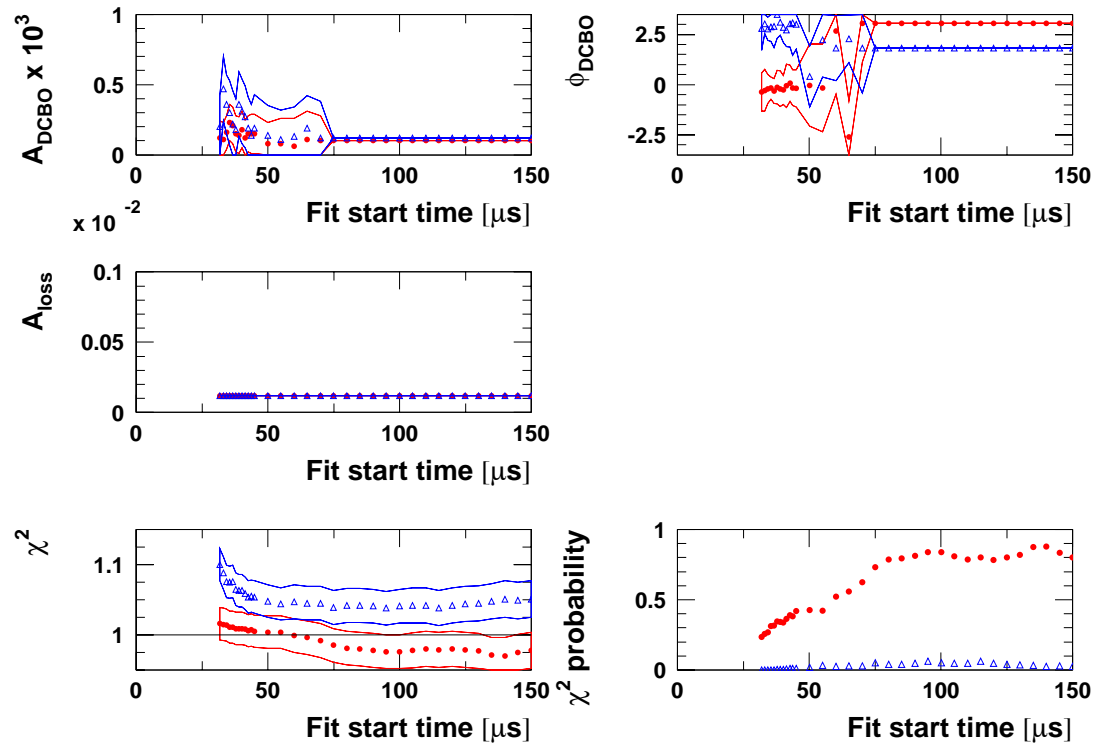


Figure 85: Start time scan for the two half rings separately (red circles = det. 1-12, blue triangles = det. 13-24) with the 1999-style function for Set B.

1999 Function, Halfring Fits, Set B



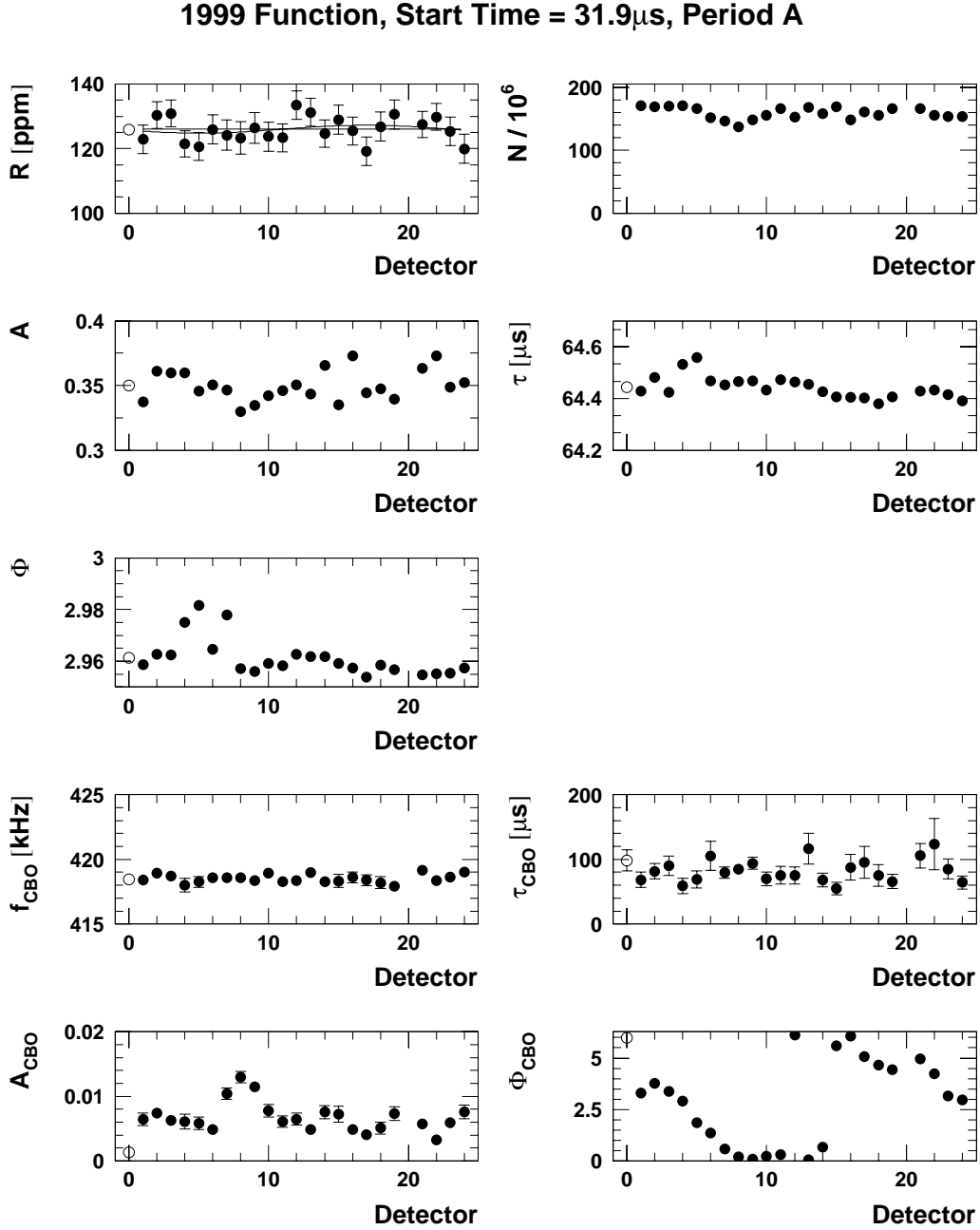
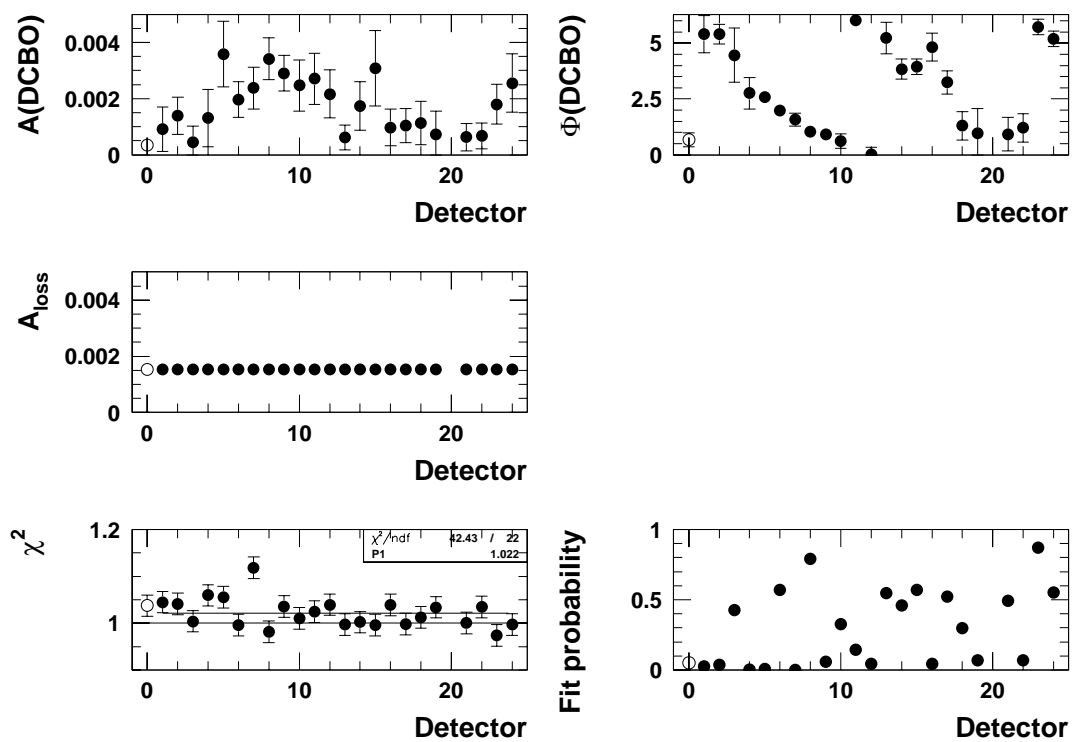
A.3 Individual Detector Fits Starting at $31.8\ \mu\text{s}$ 

Figure 86: *Fits of individual detector spectra with the 1999-style function for Set A. The open marker at detector 0 represents the fit to the sum.*

1999 Function, Start Time = $31.9\mu\text{s}$, Period A

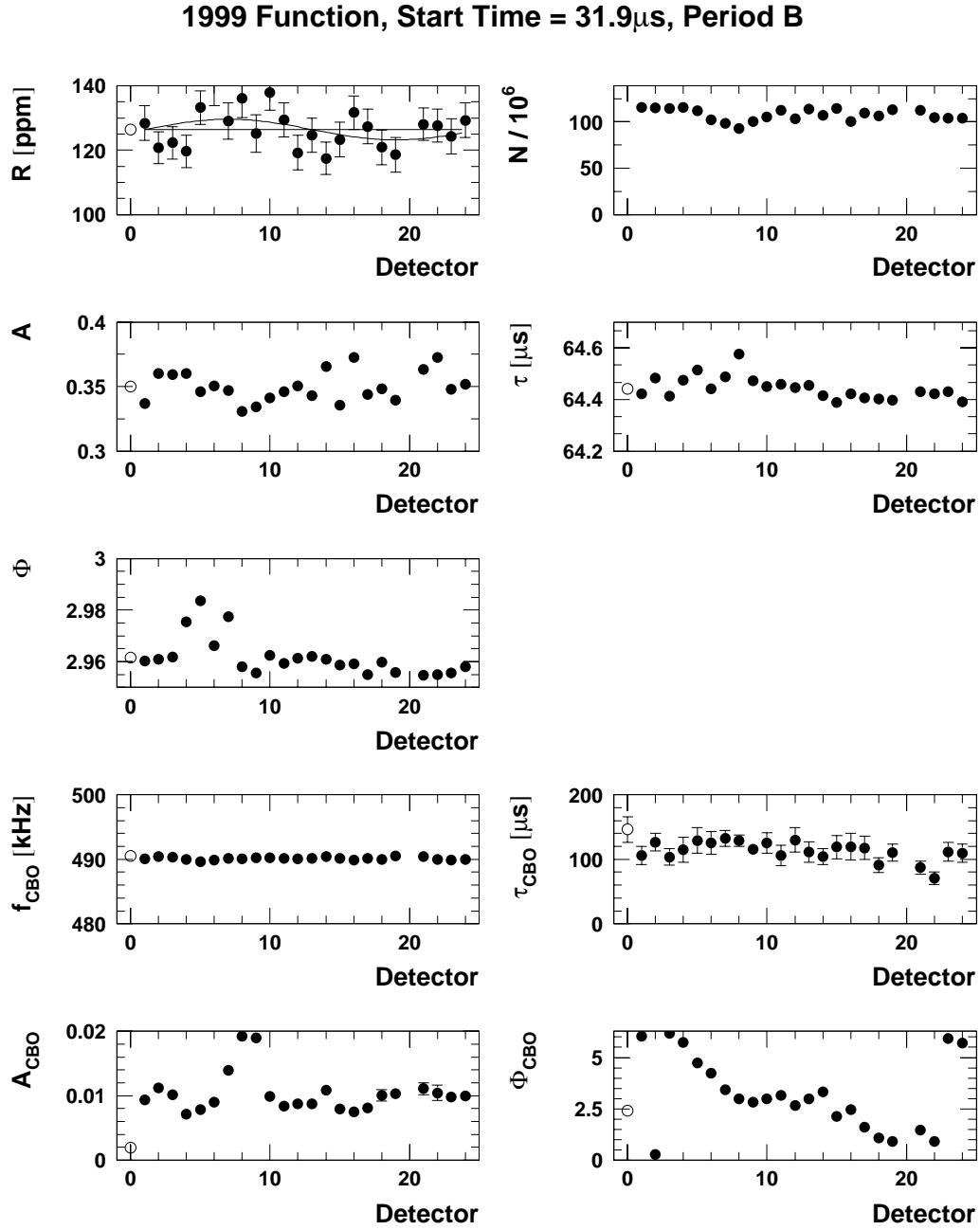
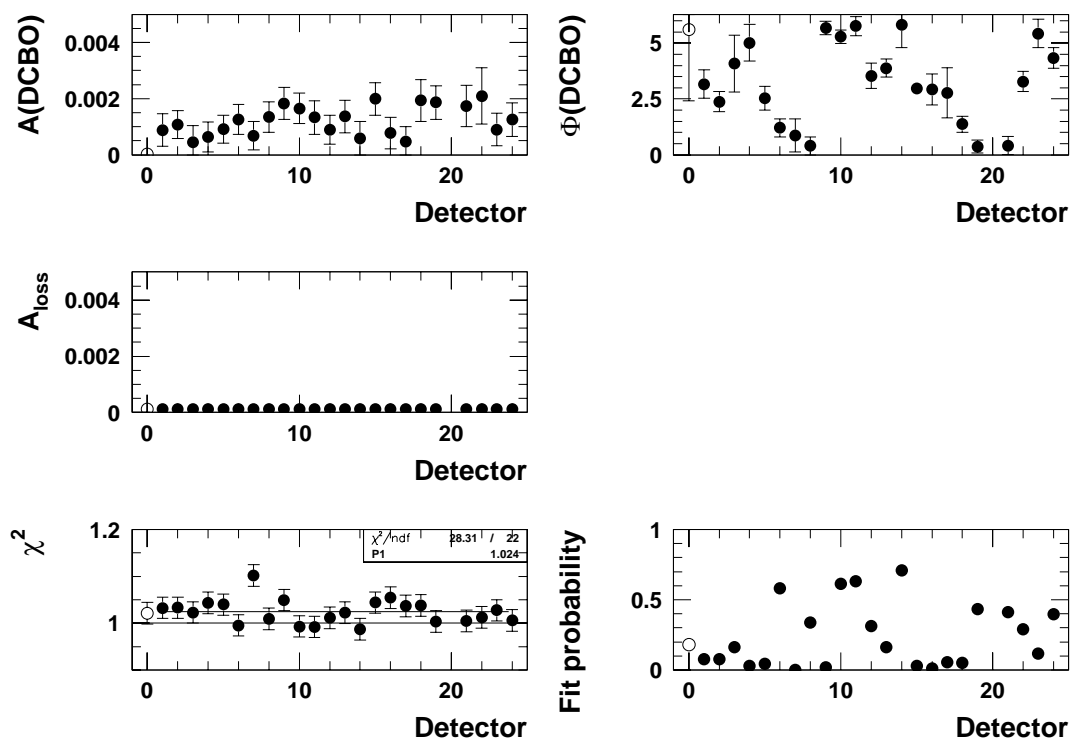


Figure 87: *Fits of individual detector spectra with the 1999-style function for Set B. The open marker at detector 0 represents the fit to the sum.*

1999 Function, Start Time = $31.9\mu\text{s}$, Period B

B Fit Results for the Physics Function without Phase Modulation

B.1 Start Time Scans for the Sum of Detectors

Physics Function w/o Phase Modulation, Sum of Detectors, Period A

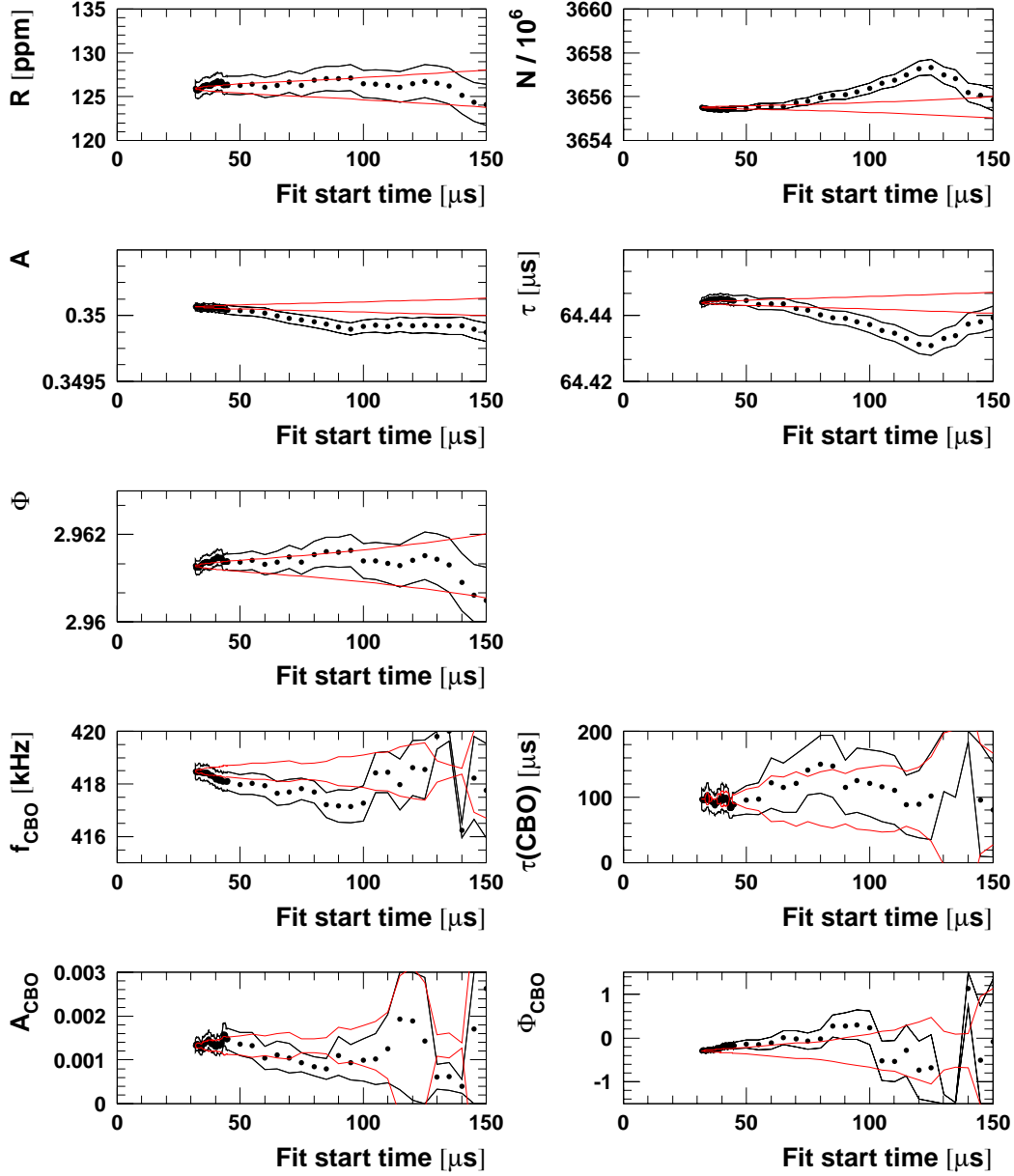
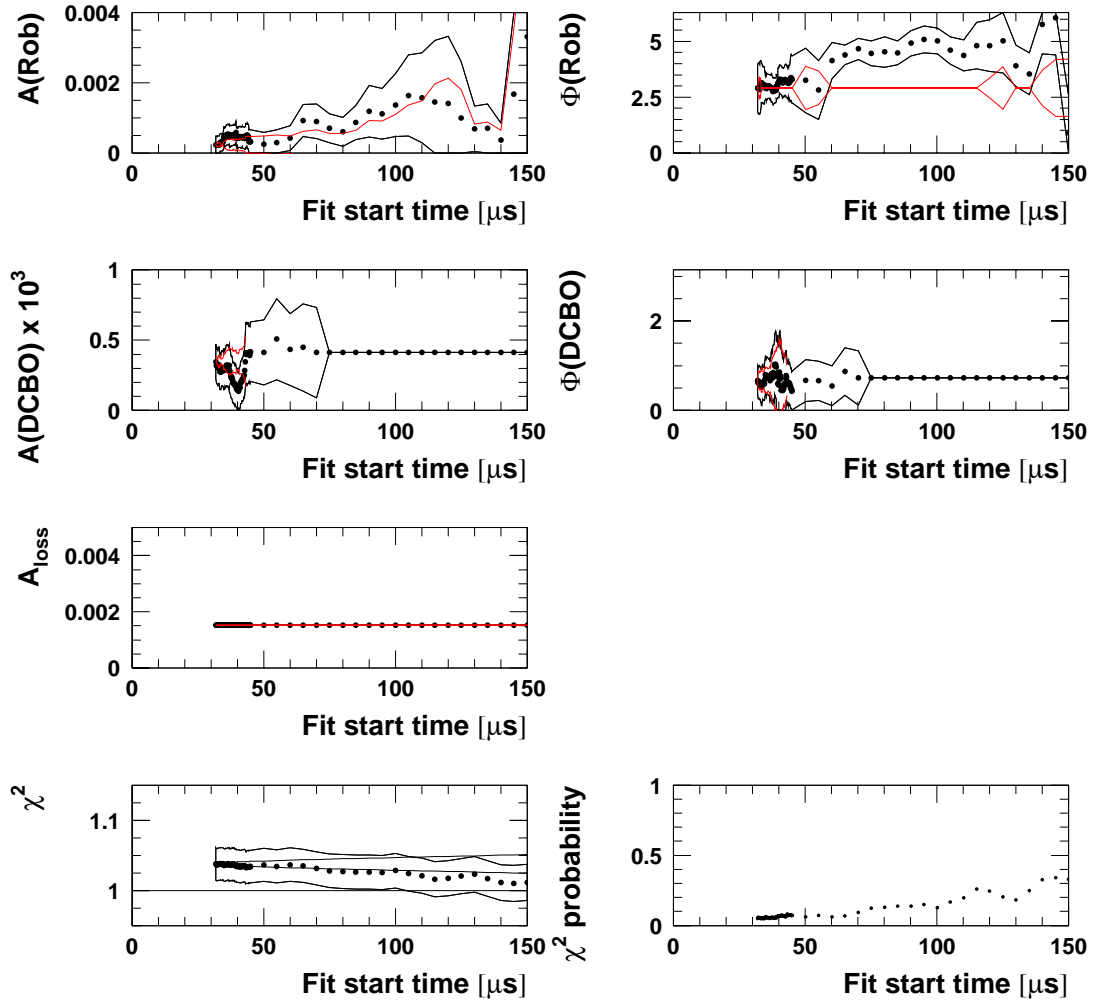


Figure 88: Start time scan with the physics function without phase modulation for Set A.

Physics Function w/o Phase Modulation, Sum of Detectors, Period A



Physics Function w/o Phase Modulation, Sum of Detectors, Period B

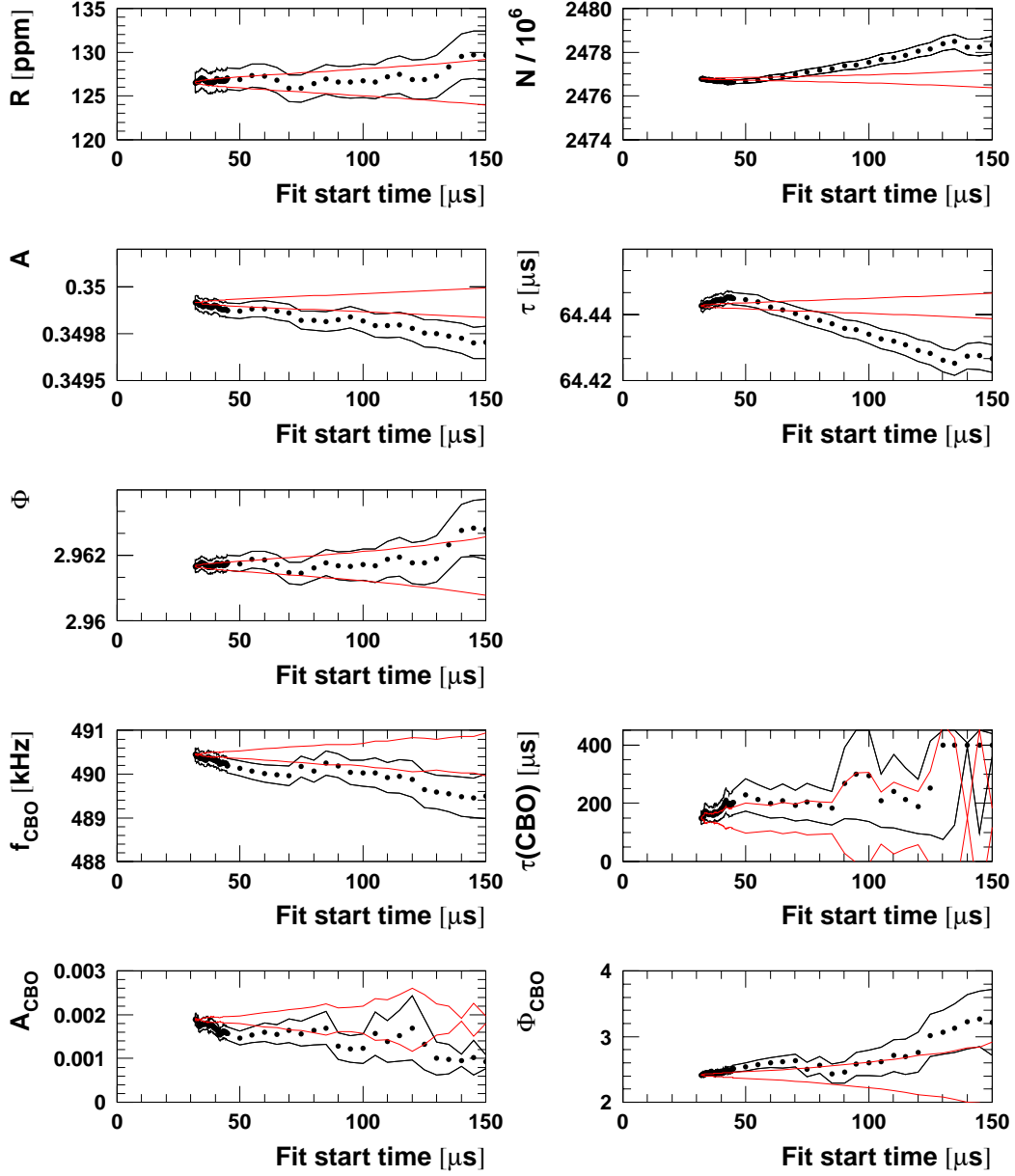
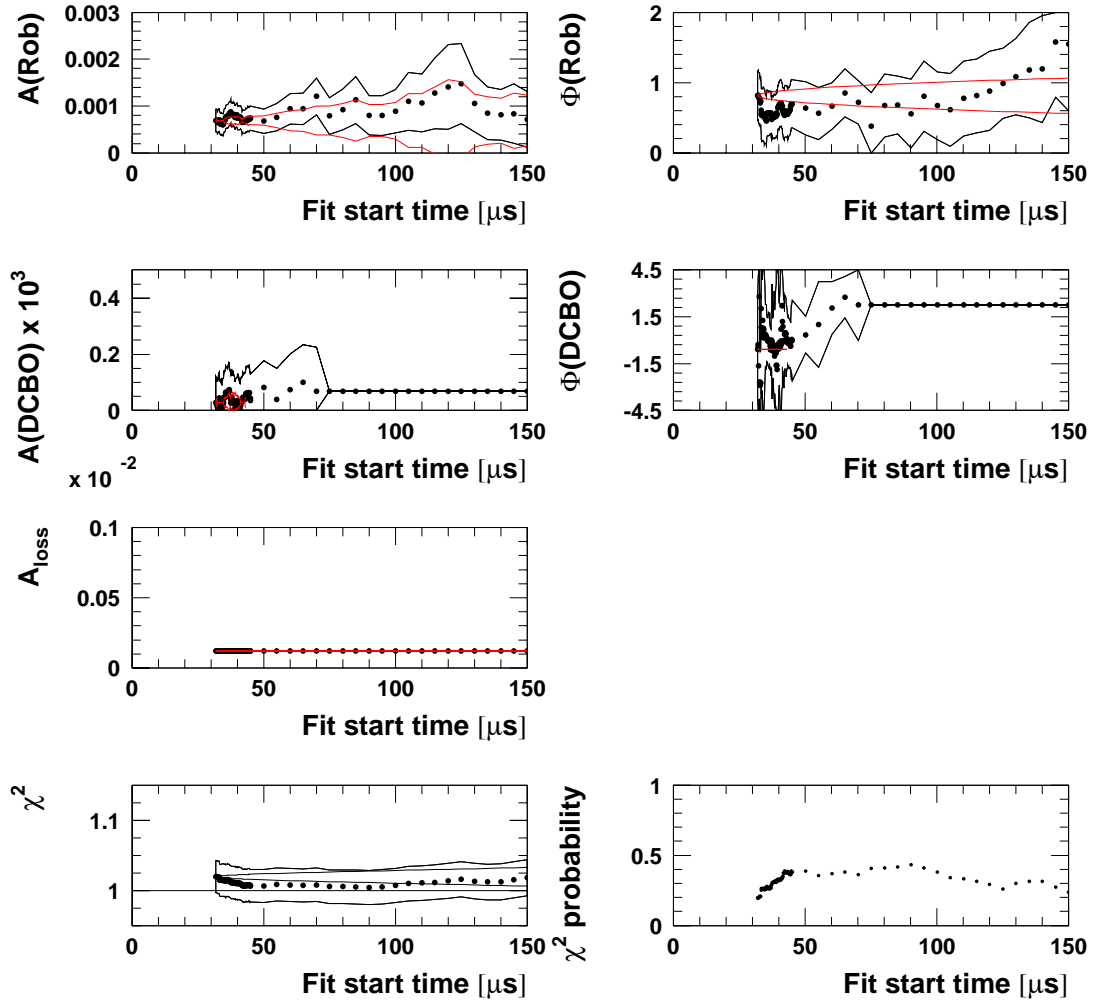


Figure 89: Start time scan with the physics function without phase modulation for Set B.

Physics Function w/o Phase Modulation, Sum of Detectors, Period B



B.2 Start Time Scans for the Two Half Rings

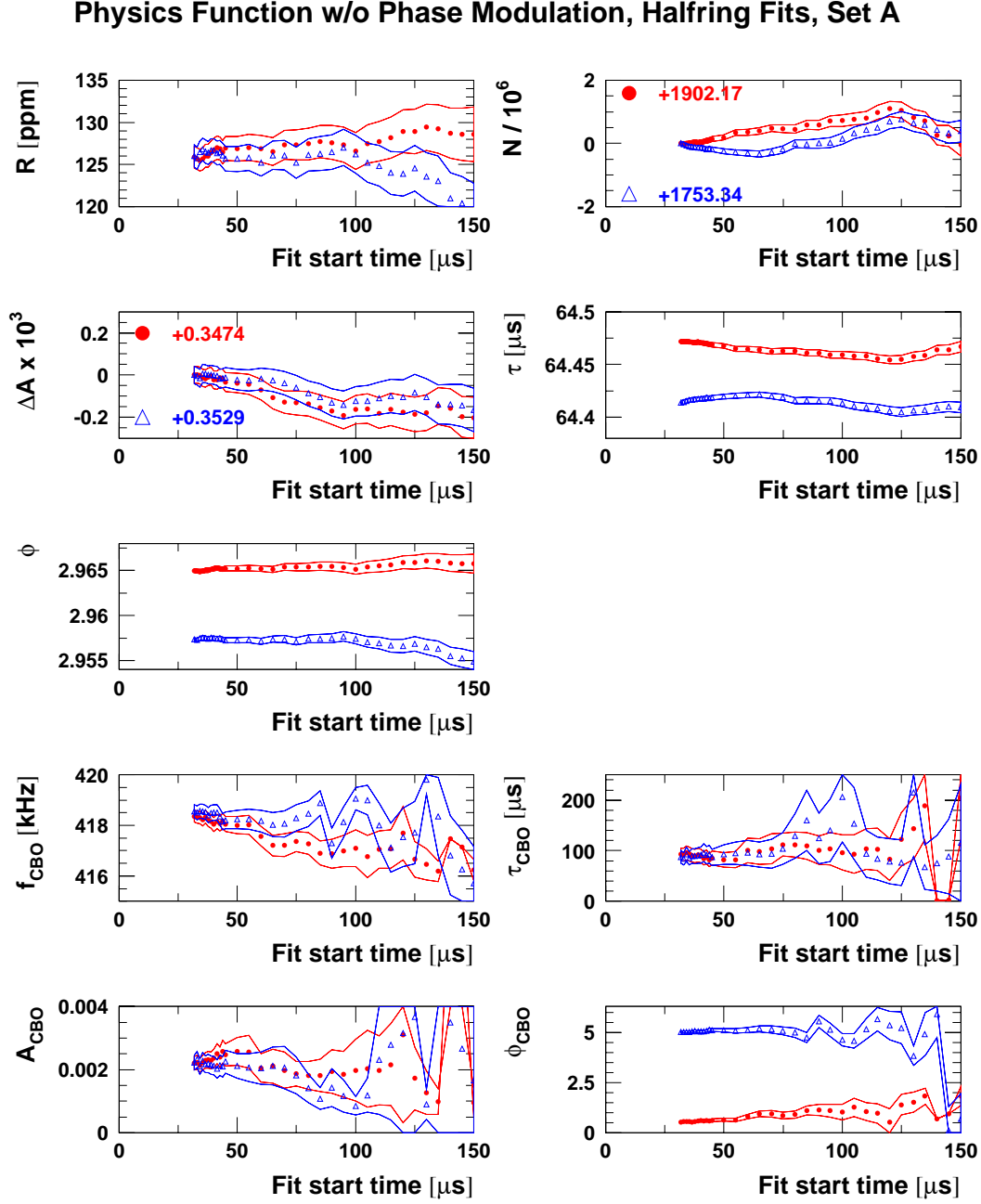
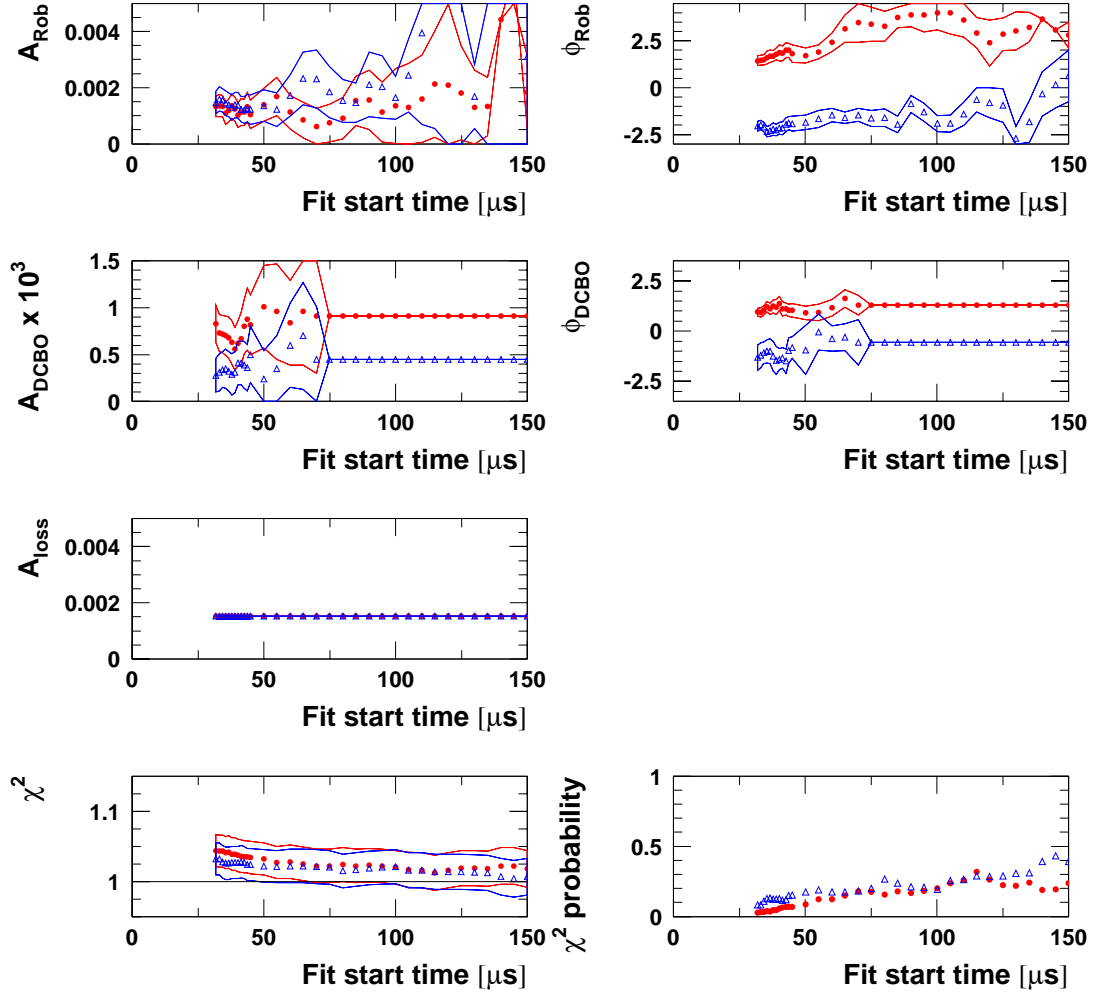


Figure 90: Start time scan for the two half rings separately (red circles = det. 1-12, blue triangles = det. 13-24) with the physics function without phase modulation for Set A.

Physics Function w/o Phase Modulation, Halfring Fits, Set A



Physics Function w/o Phase Modulation, Halfring Fits, Set B

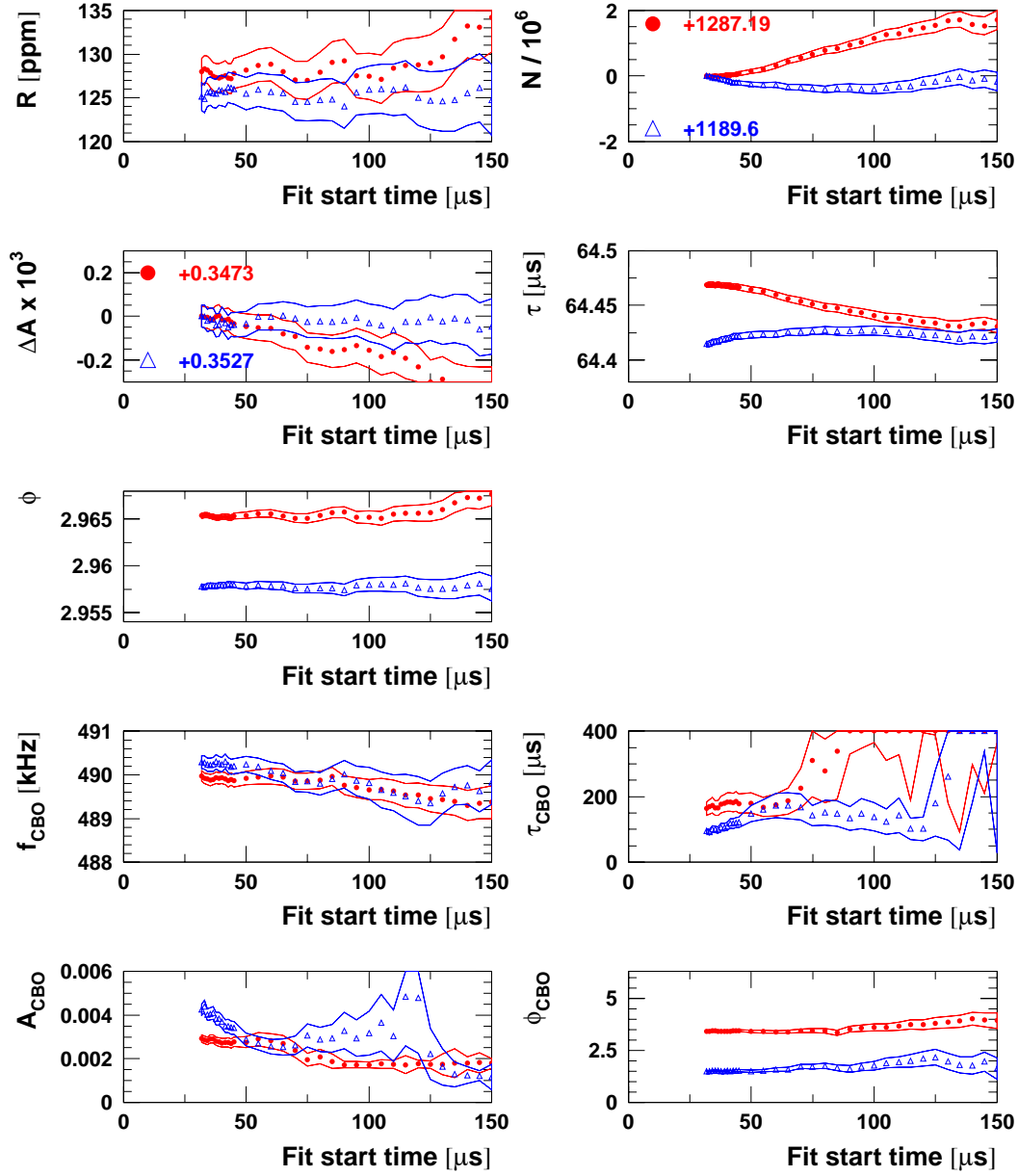
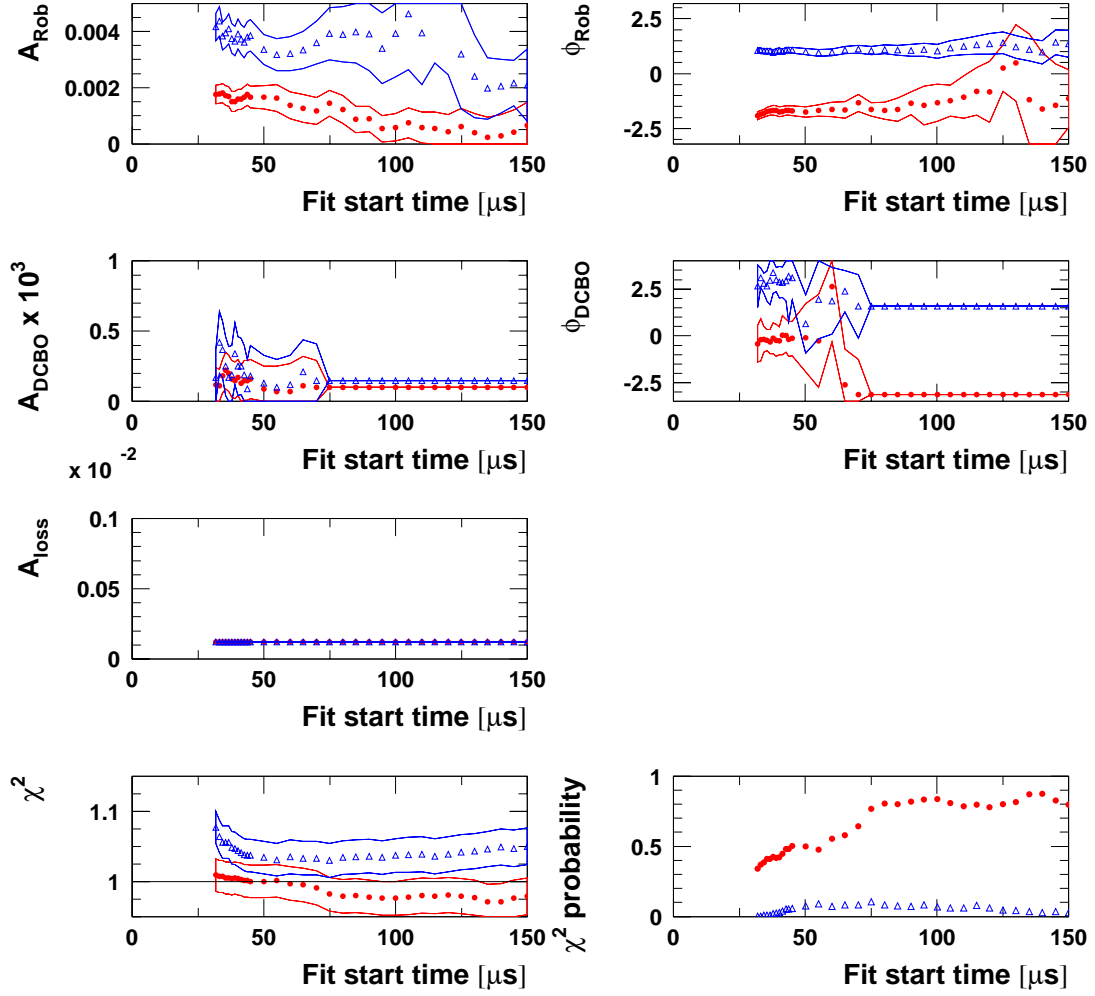


Figure 91: Start time scan for the two half rings separately (red circles = det. 1-12, blue triangles = det. 13-24) with the physics function without phase modulation for Set B.

Physics Function w/o Phase Modulation, Halfring Fits, Set B



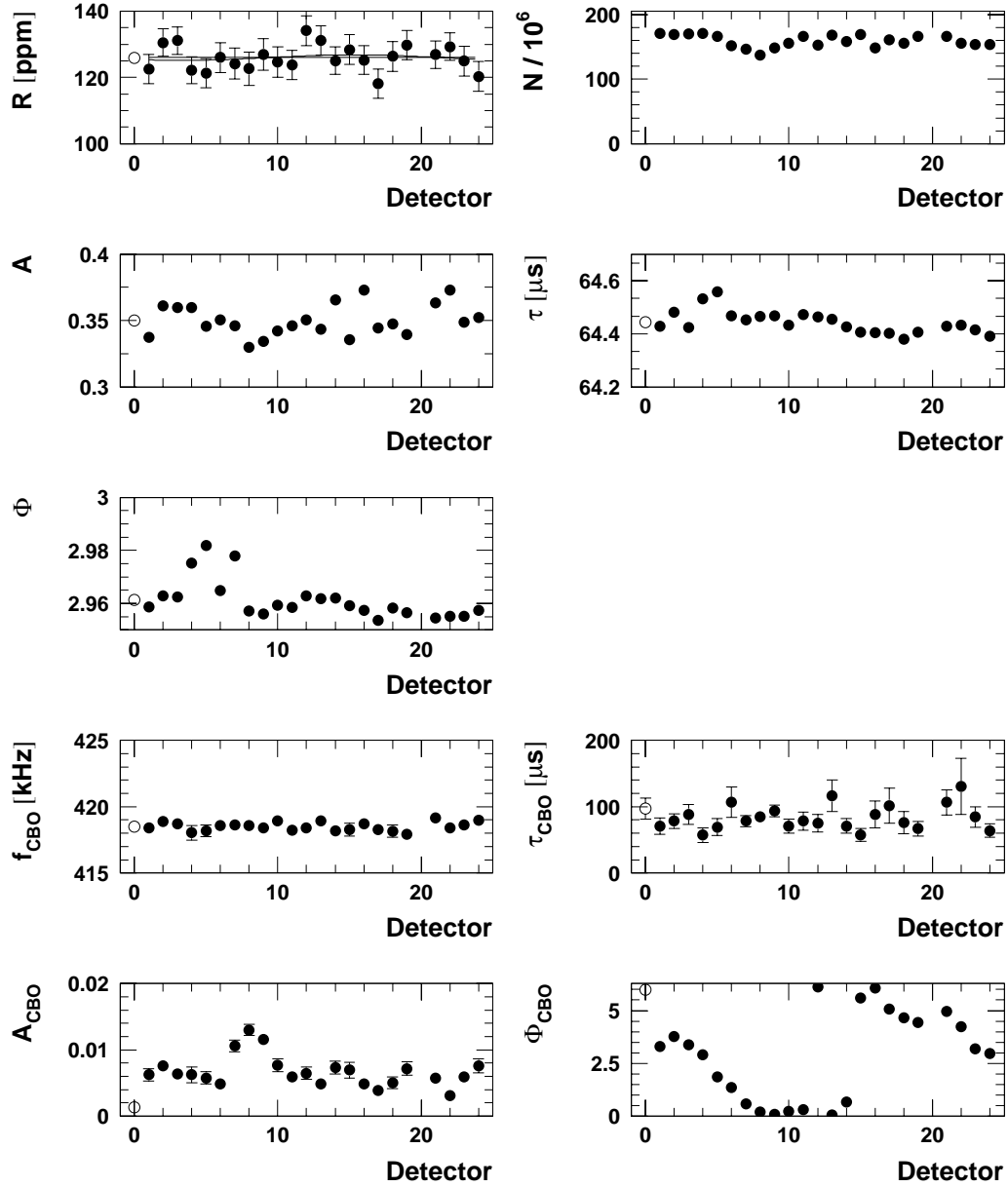
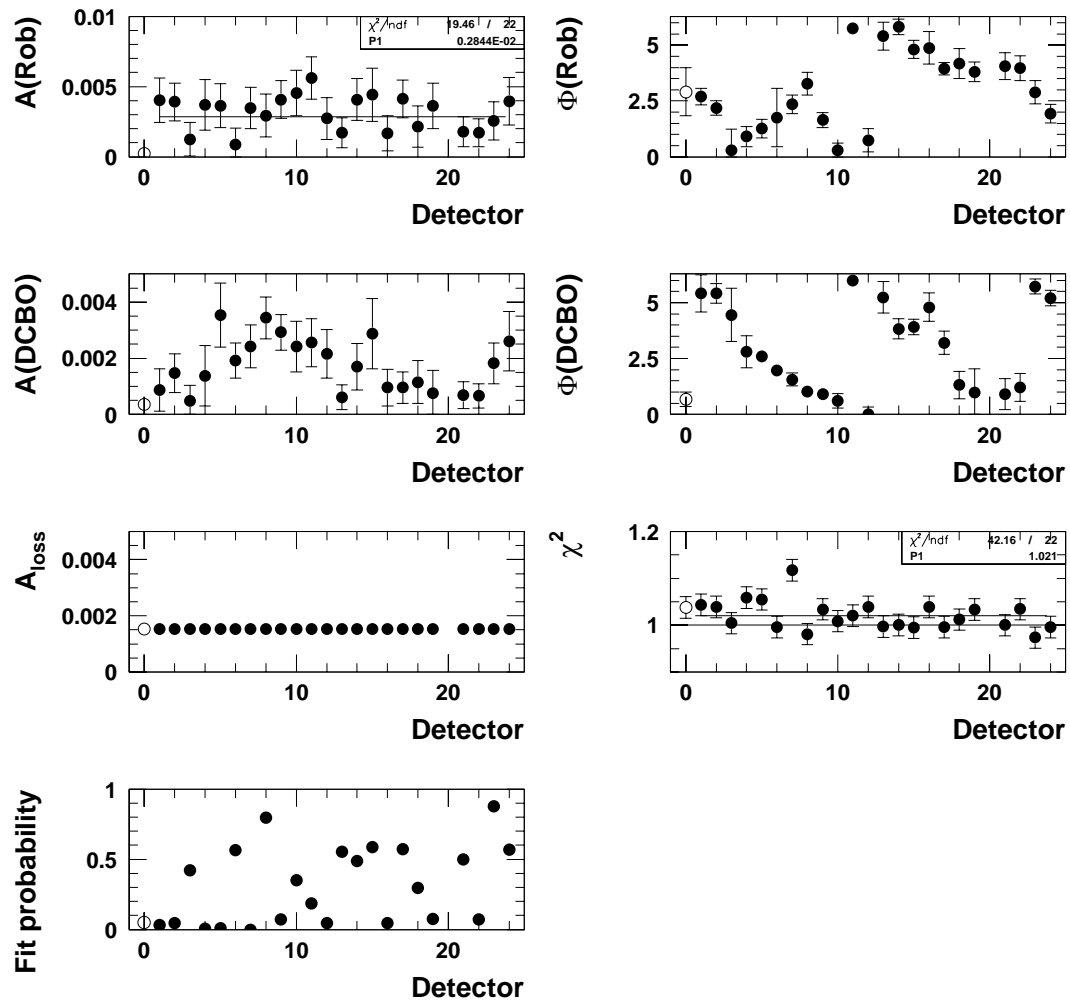
B.3 Individual Detector Fits Starting at $31.8\mu\text{s}$ Physics Function w/o Phase Modulation, Start Time = $31.9\mu\text{s}$, Period A

Figure 92: Fits of individual detector spectra with the physics function without phase modulation for Set A.

Physics Function w/o Phase Modulation, Start Time = $31.9\mu\text{s}$, Period A



Physics Function w/o Phase Modulation, Start Time = 31.9 μ s, Period B

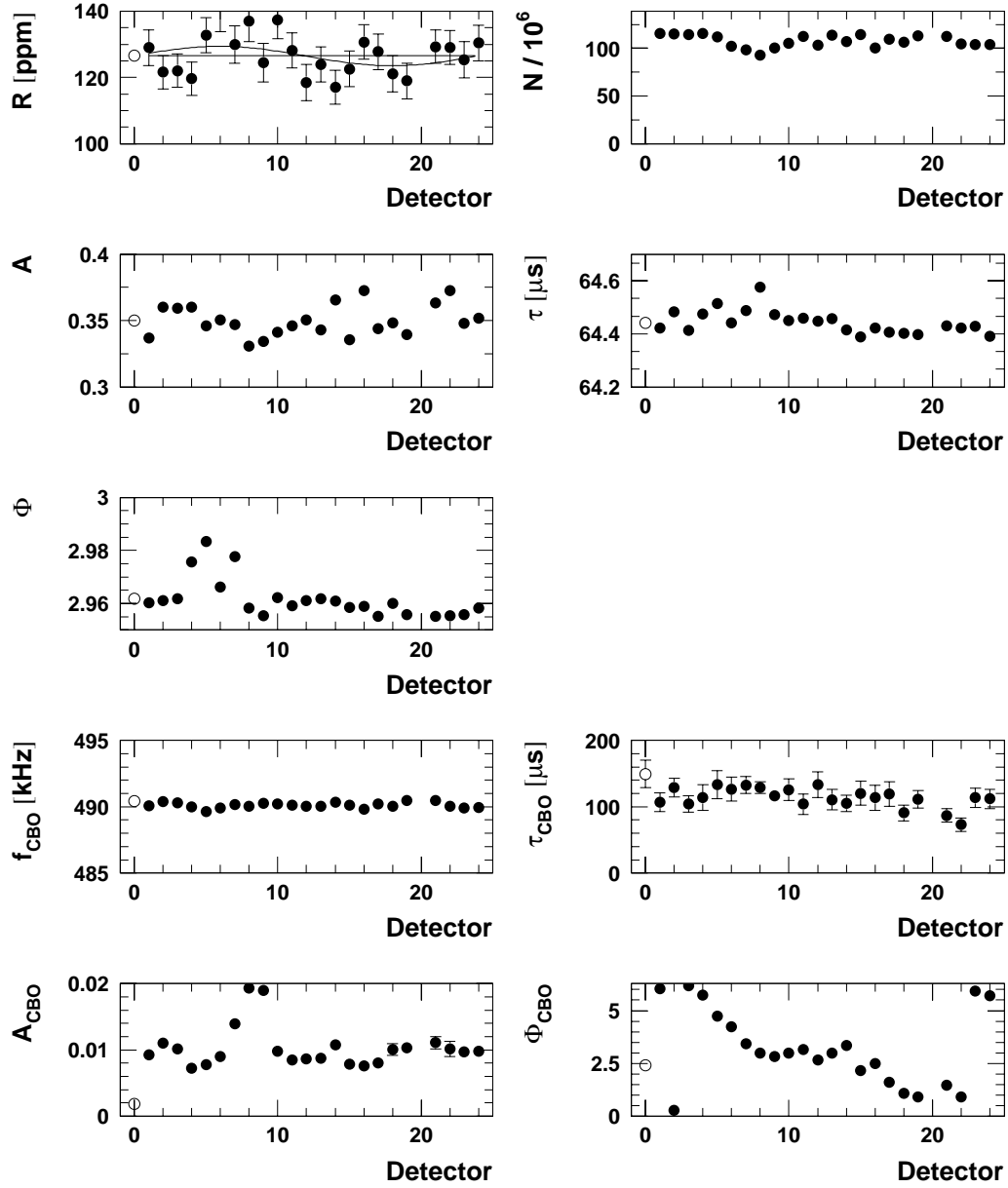
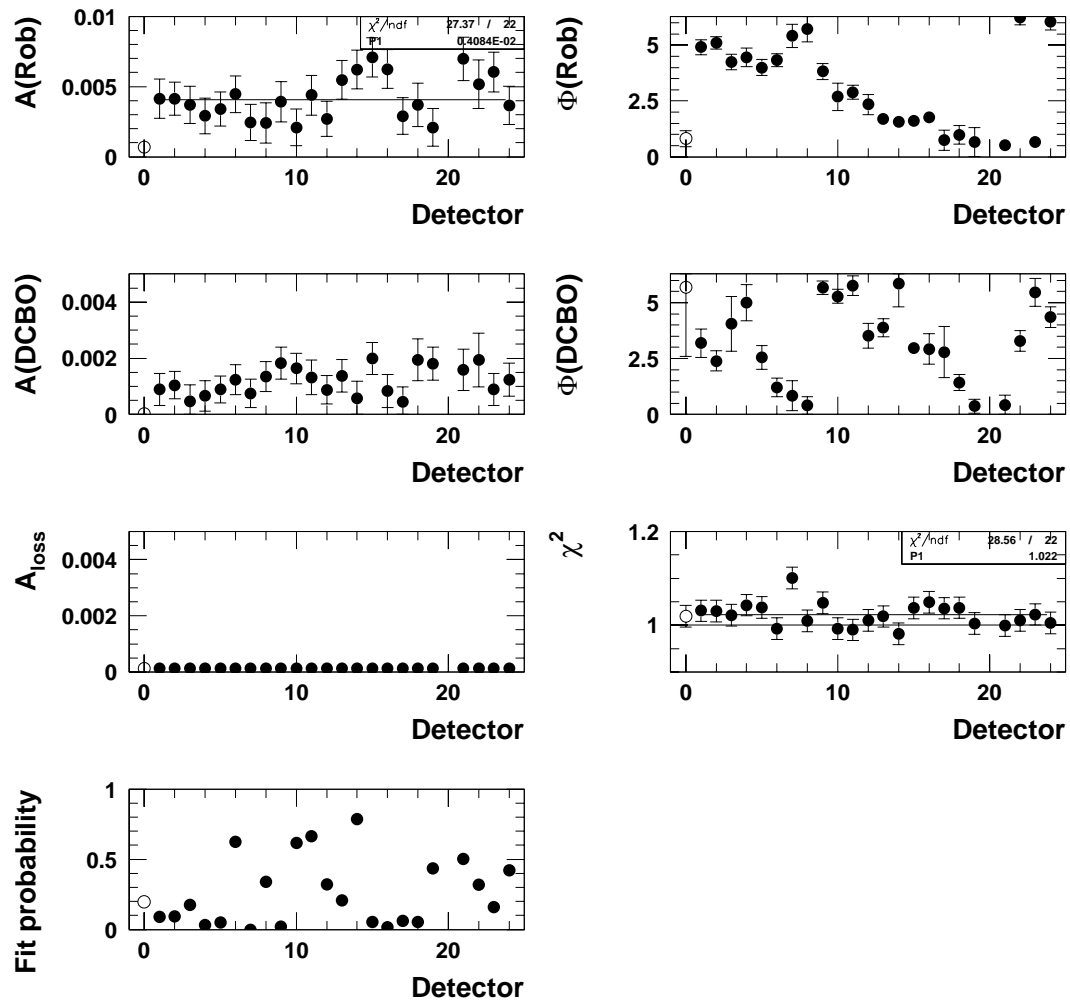


Figure 93: *Fits of individual detector spectra with the physics function without phase modulation for Set B.*

Physics Function w/o Phase Modulation, Start Time = 31.9 μs , Period B



C Fit Results for the Full Physics Function

C.1 Start Time Scans for the Sum of Detectors

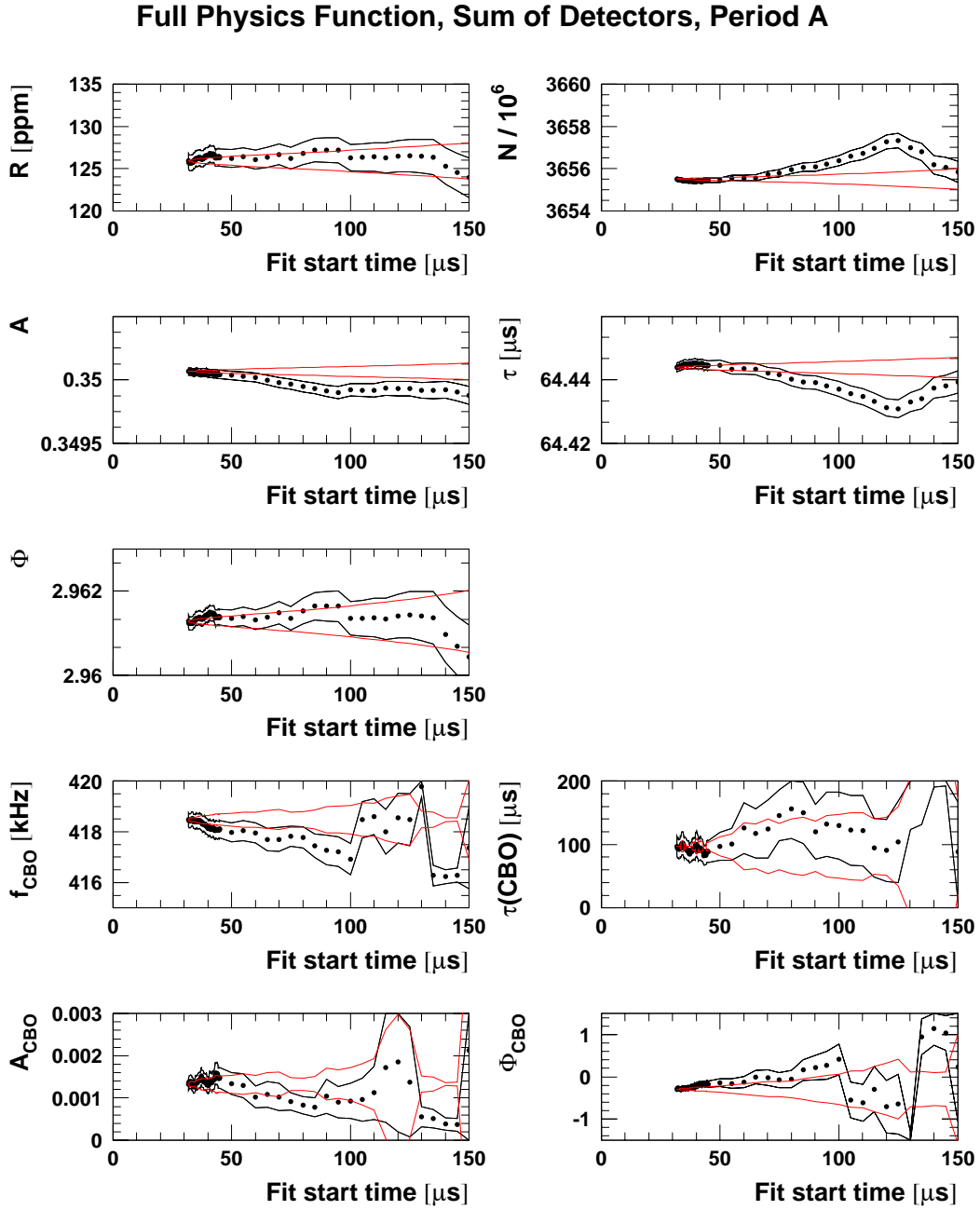
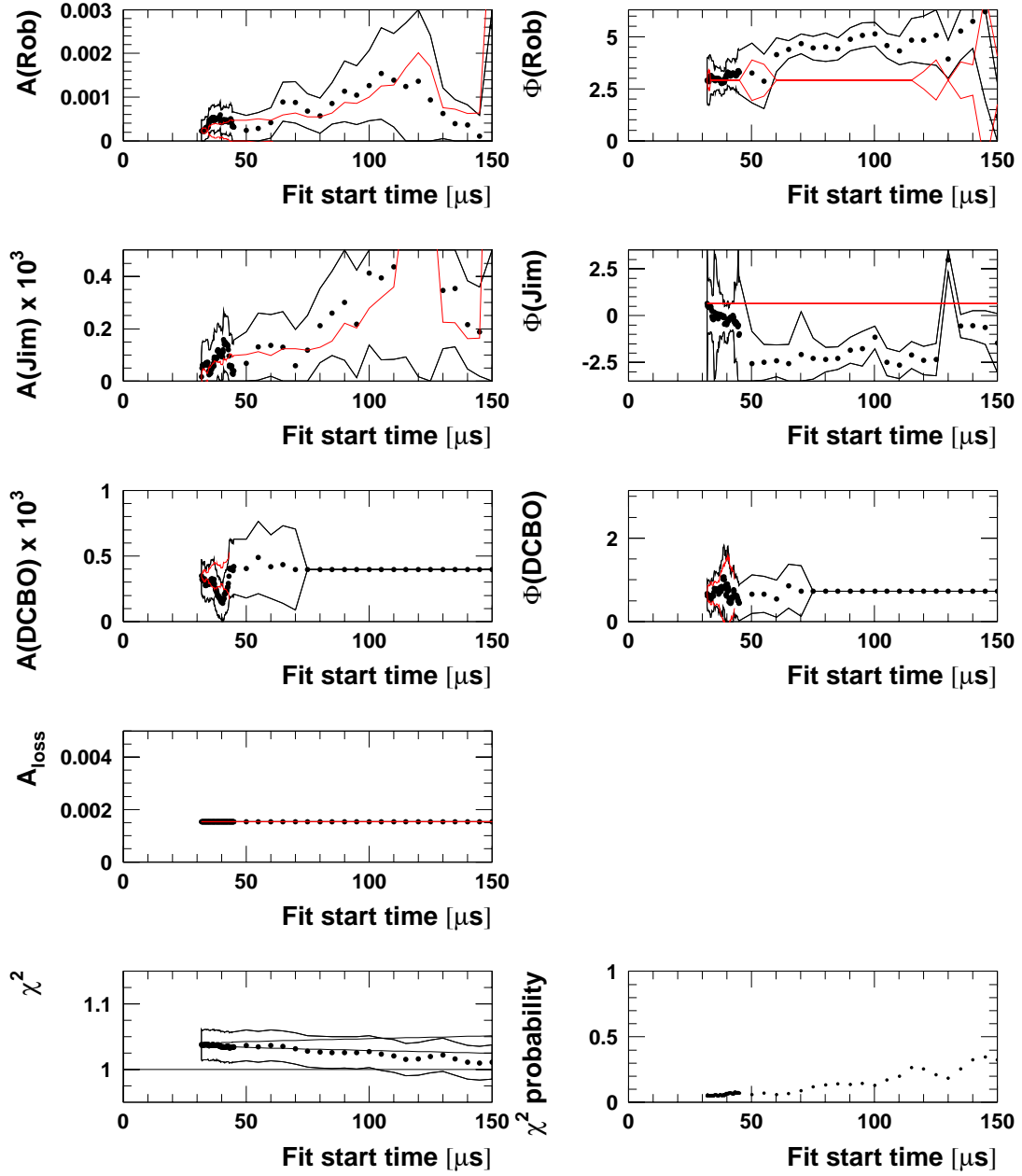


Figure 94: *Start time scan with the full physics function for Set A.*

Full Physics Function, Sum of Detectors, Period A



Full Physics Function, Sum of Detectors, Period B

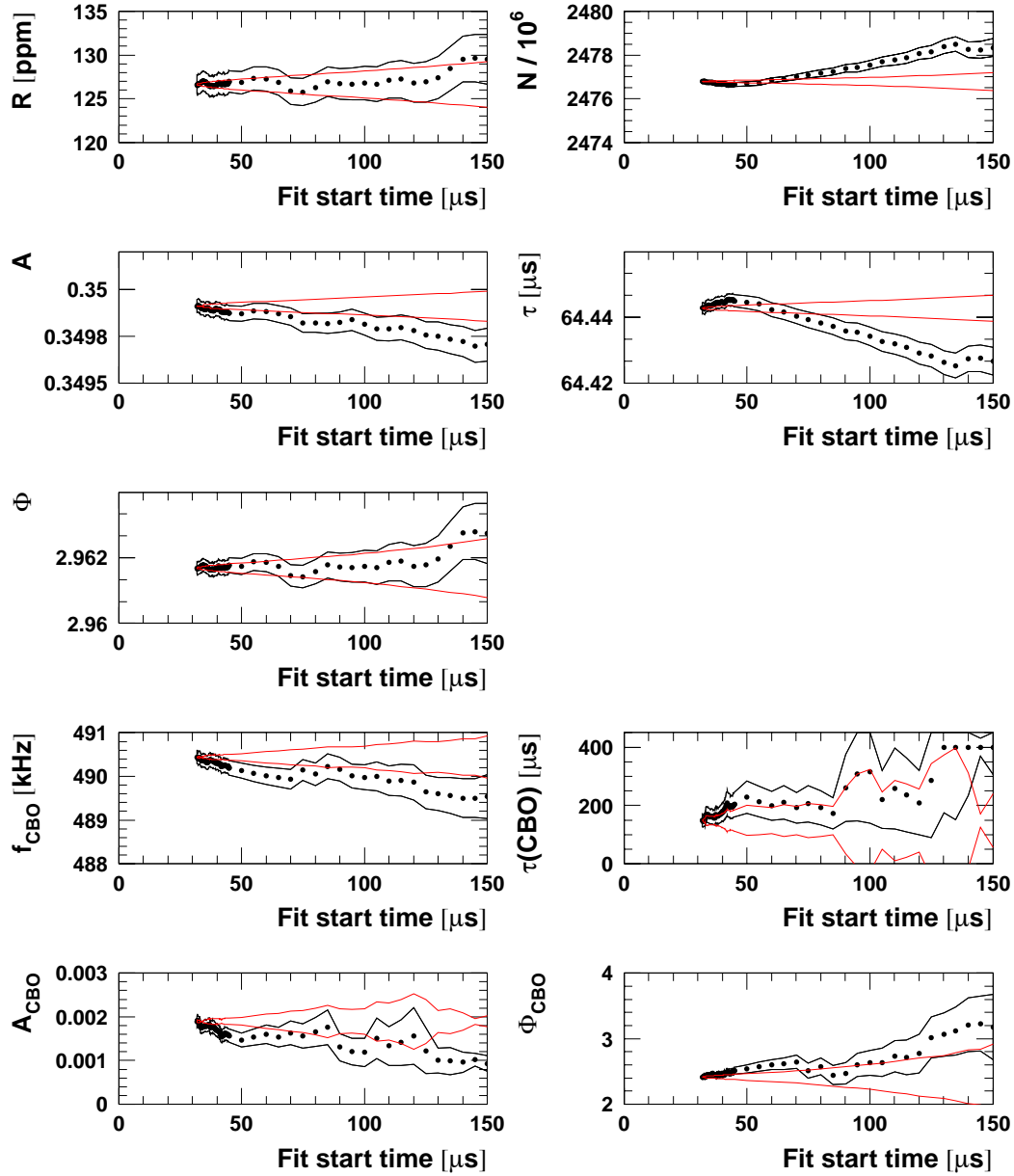
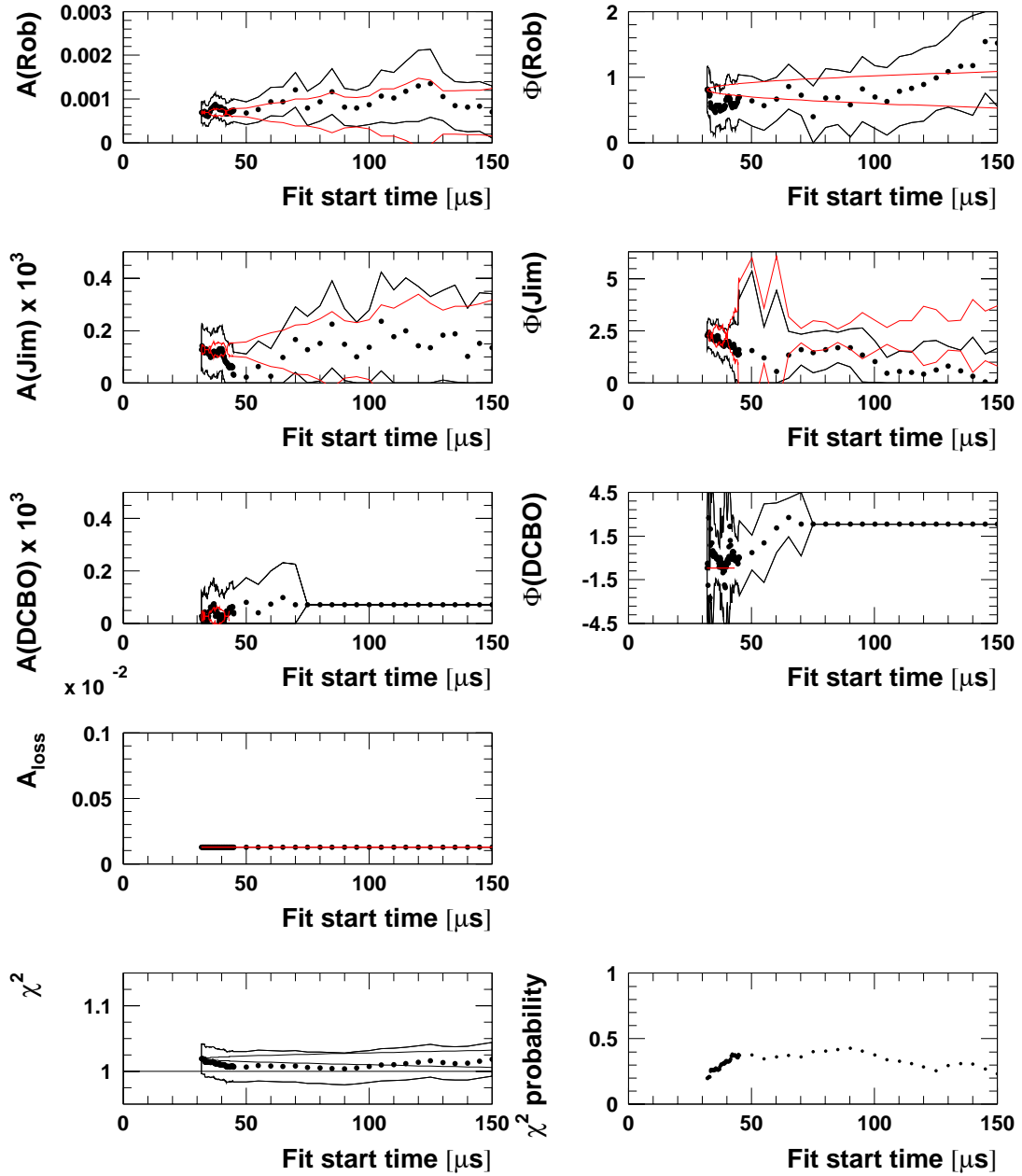


Figure 95: *Start time scan with the full physics function for Set B.*

Full Physics Function, Sum of Detectors, Period B



C.2 Start Time Scans for the Two Half Rings

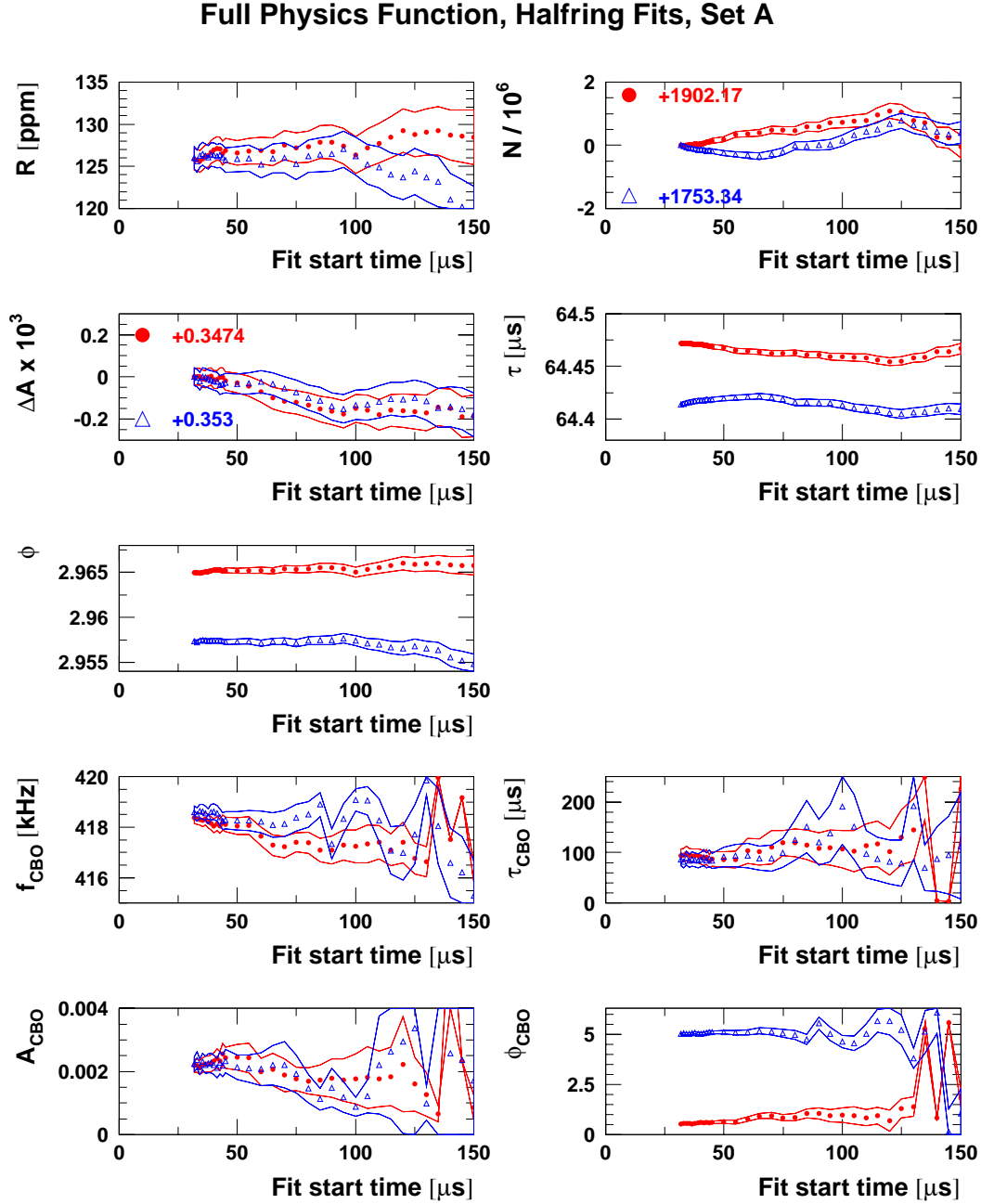
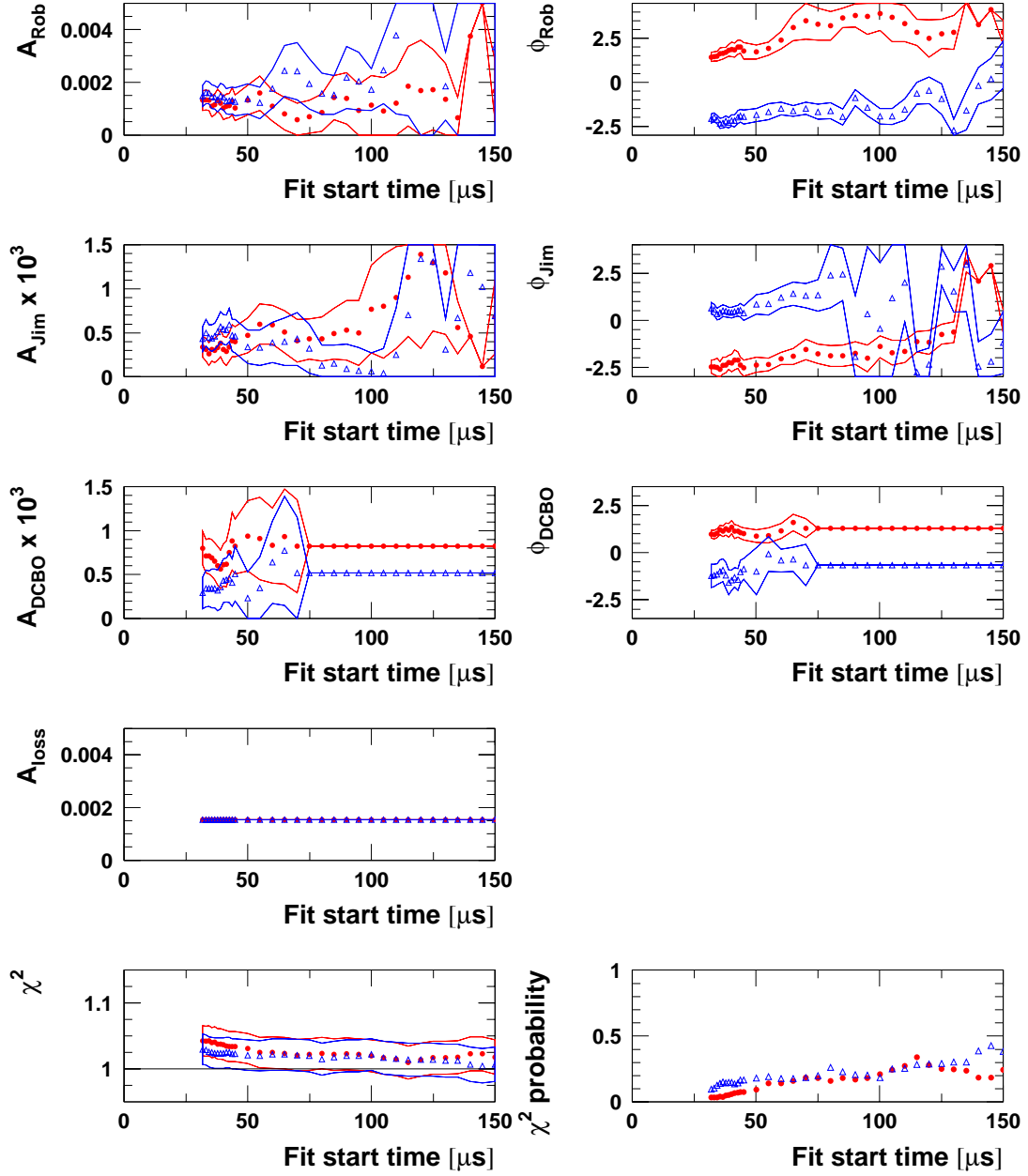


Figure 96: Start time scan for the two half rings separately (red circles = det. 1-12, blue triangles = det. 13-24) with the full physics function for Set A.

Full Physics Function, Halfring Fits, Set A



Full Physics Function, Halfring Fits, Set B

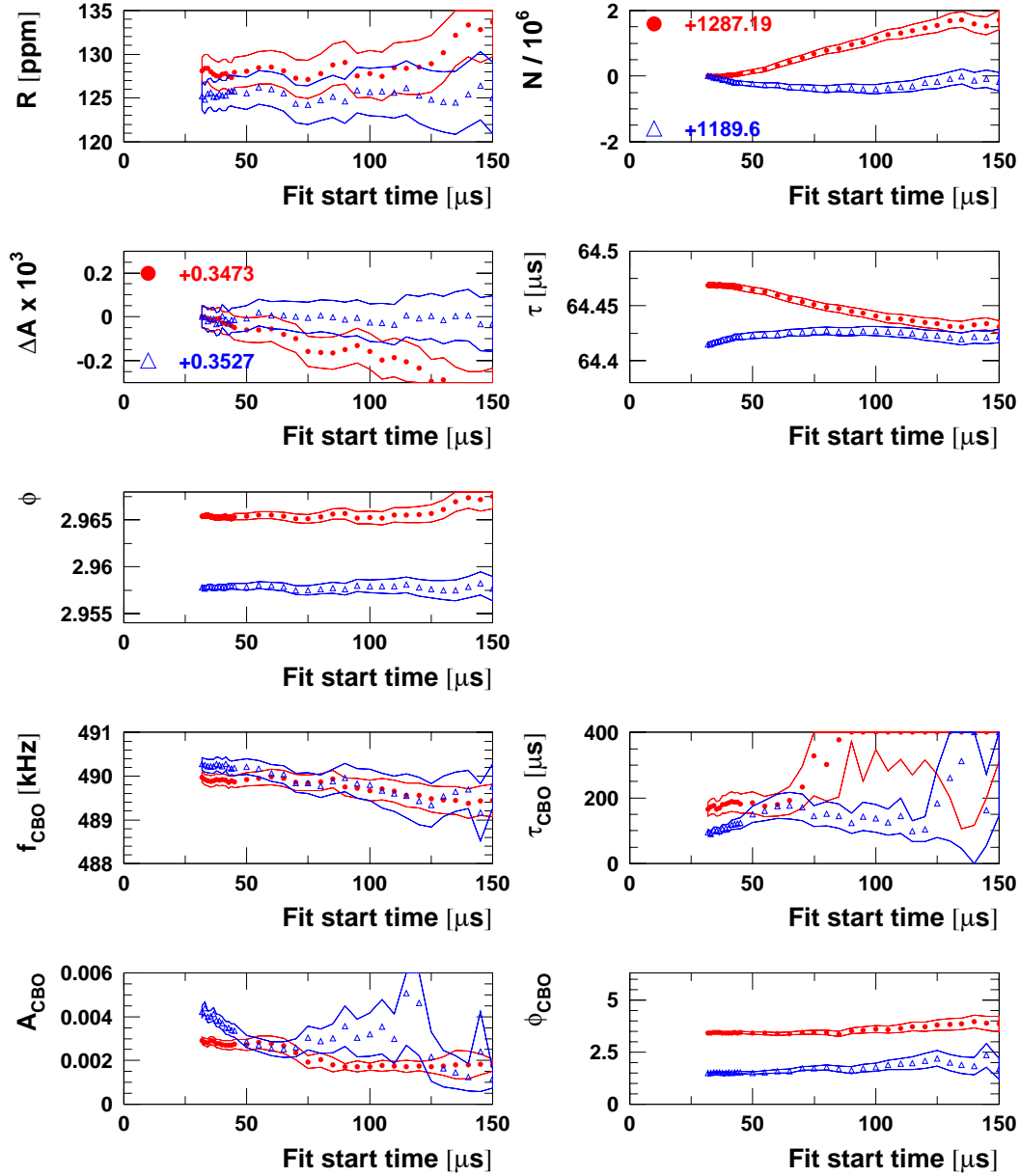
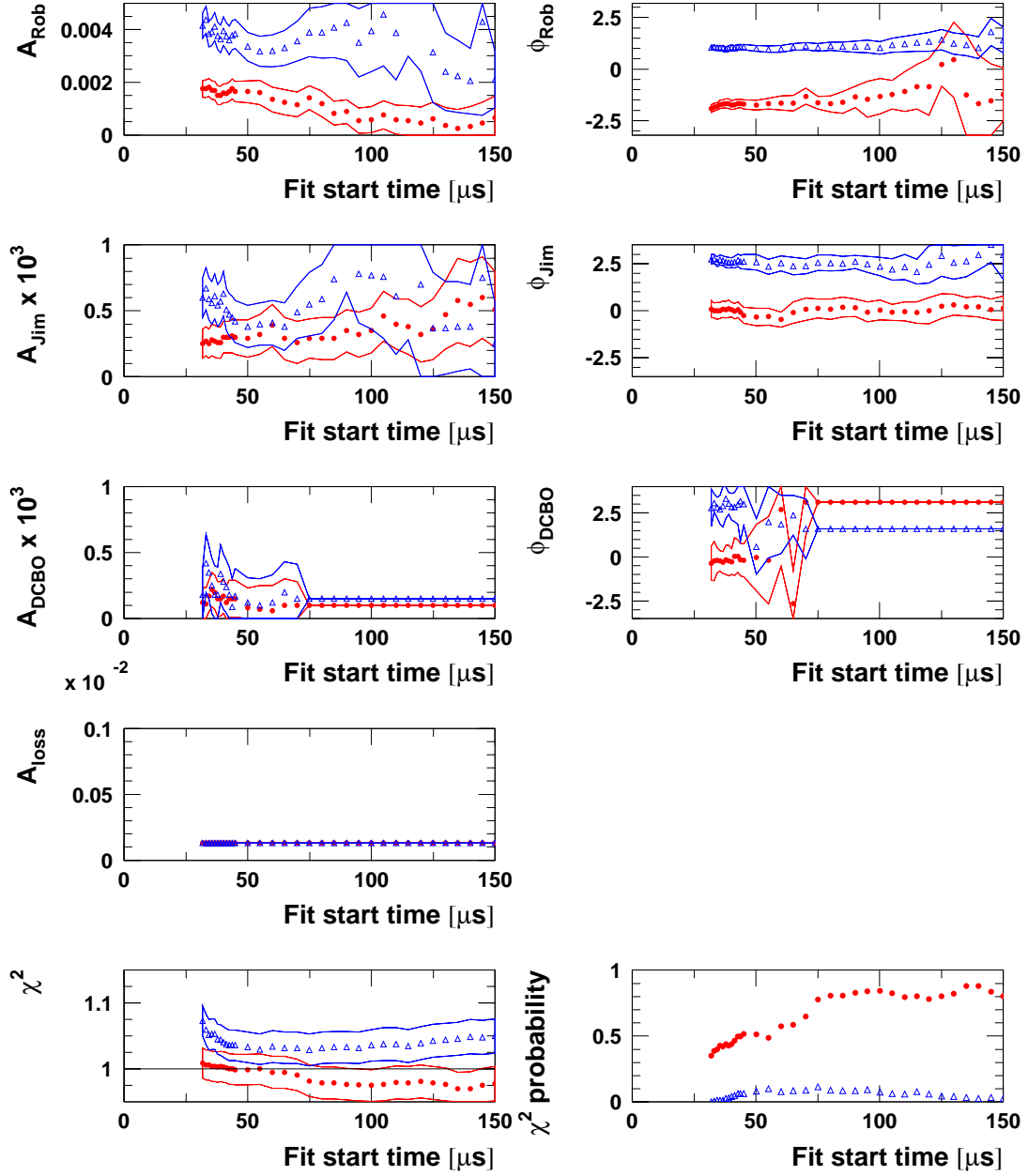
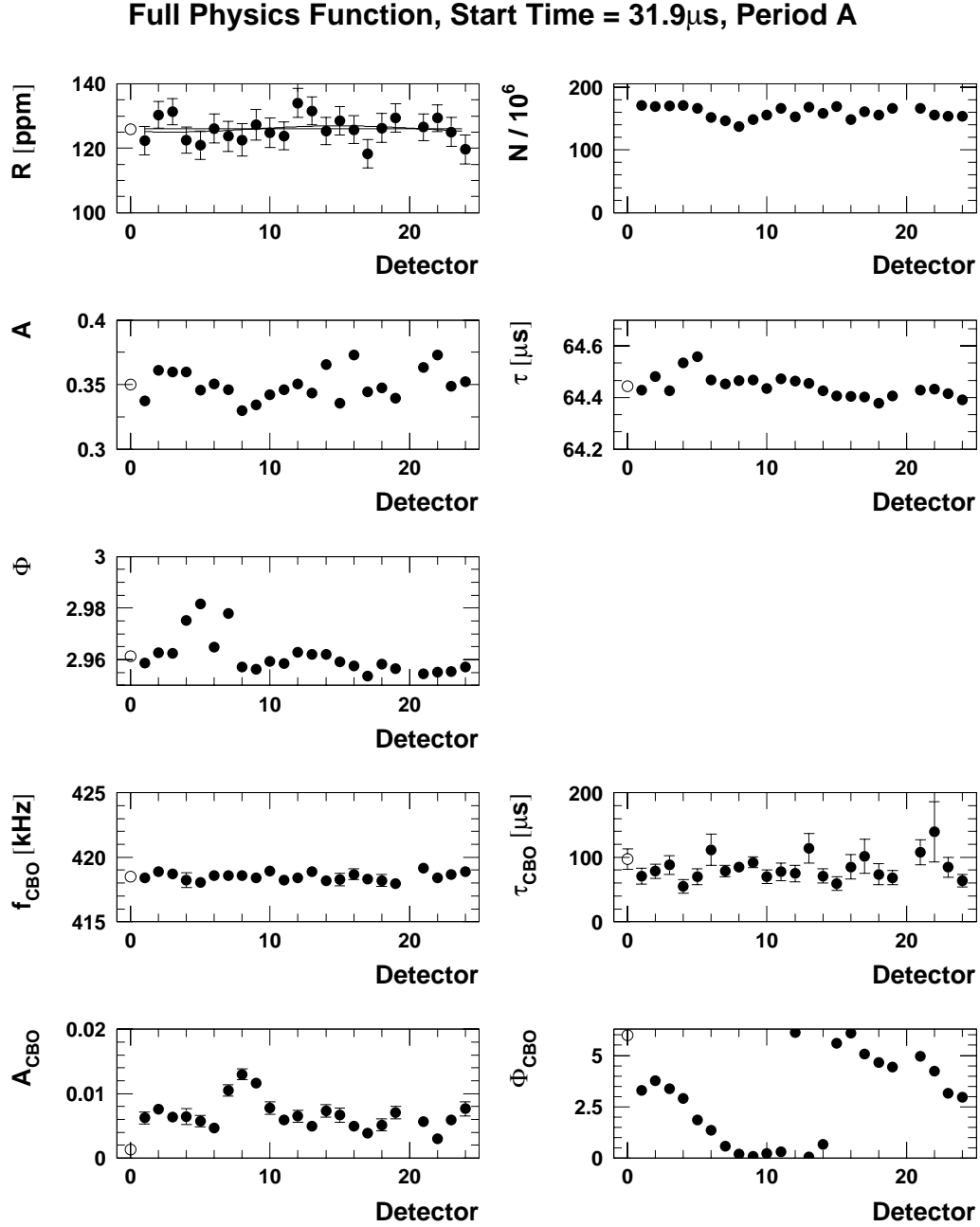
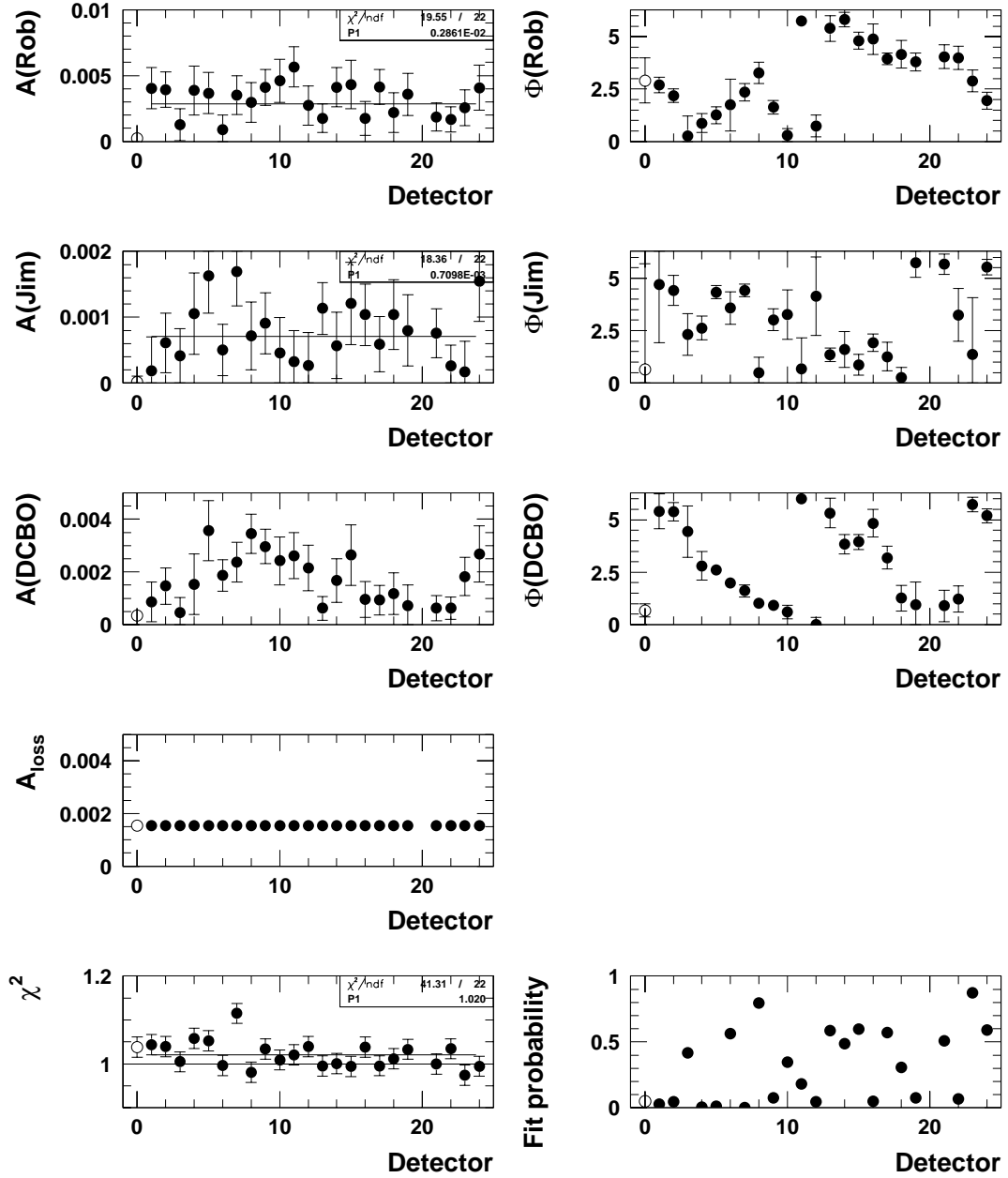


Figure 97: Start time scan for the two half rings separately (red circles = det. 1-12, blue triangles = det. 13-24) with the full physics function for Set B.

Full Physics Function, Halfring Fits, Set B



C.3 Individual Detector Fits Starting at $31.8\,\mu\text{s}$ Figure 98: *Fits of individual detector spectra with the full physics function for Set A.*

Full Physics Function, Start Time = $31.9\mu\text{s}$, Period A

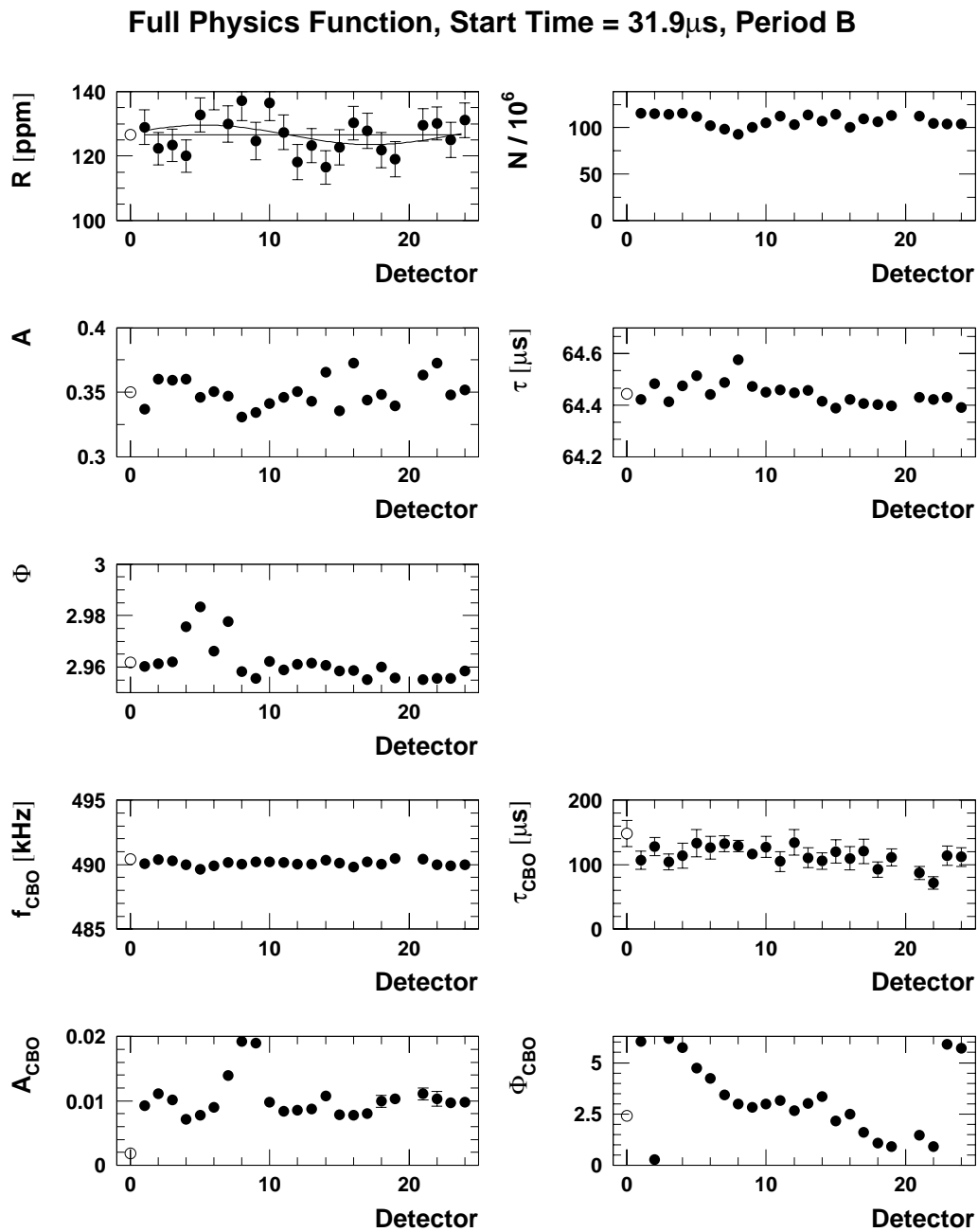
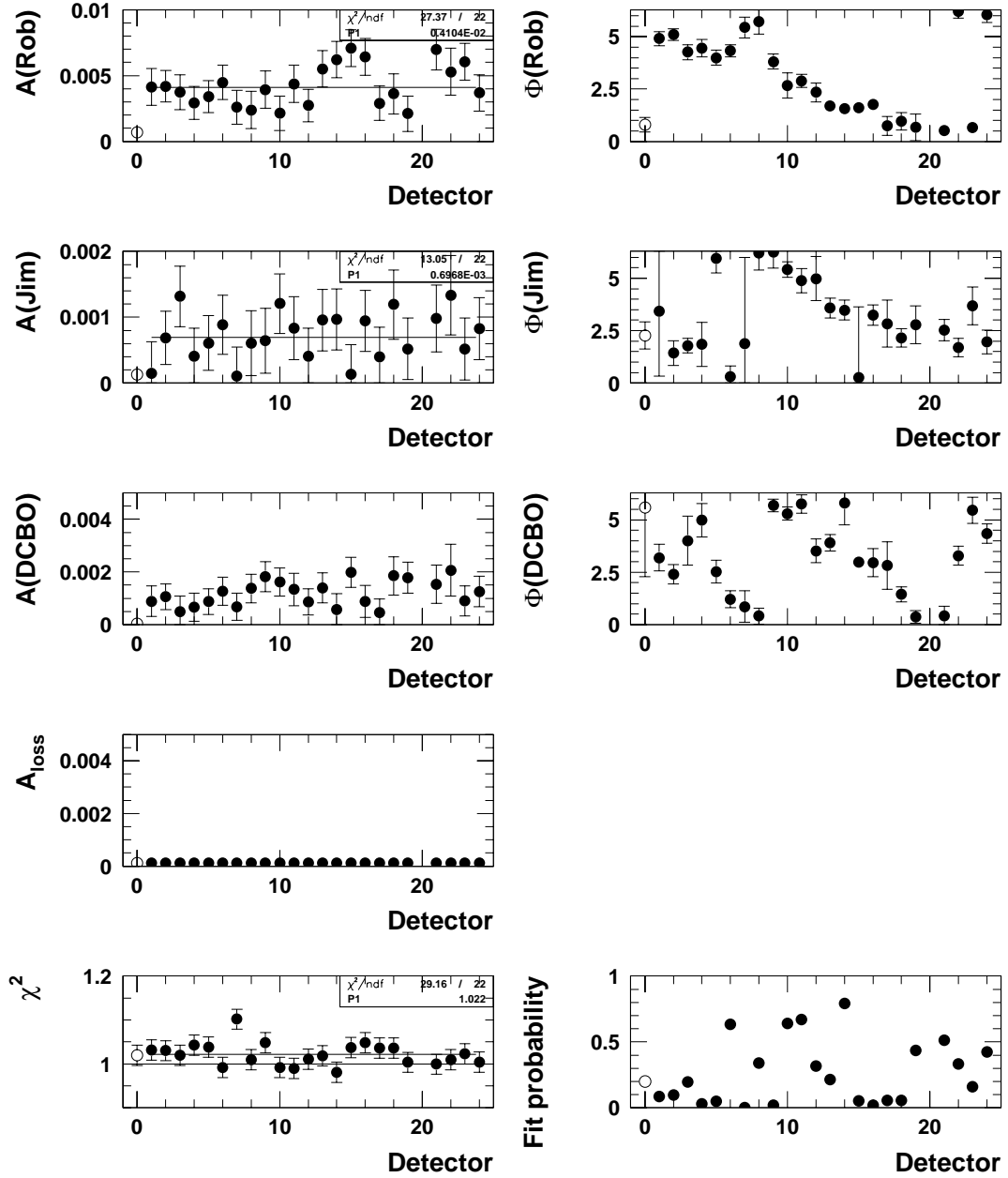


Figure 99: *Fits of individual detector spectra with the full physics function for Set B.*

Full Physics Function, Start Time = $31.9\mu\text{s}$, Period B

D Results from the Energy-Binned Fits with the Full Physics Function

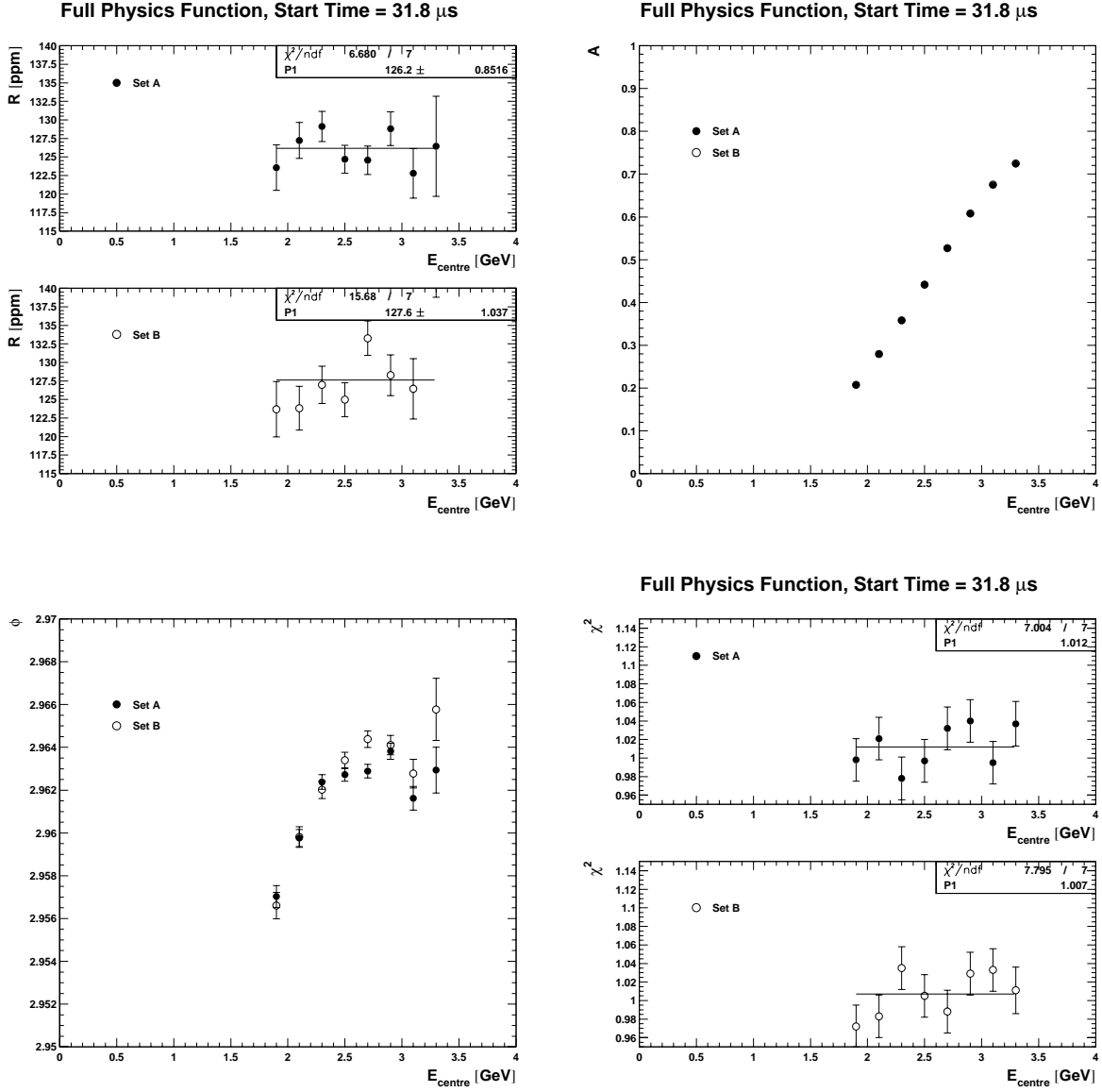


Figure 100: *Fit results versus centre of 200 MeV wide energy bins for a start time of 31.8 μs , performed with the Full Physics Function.*

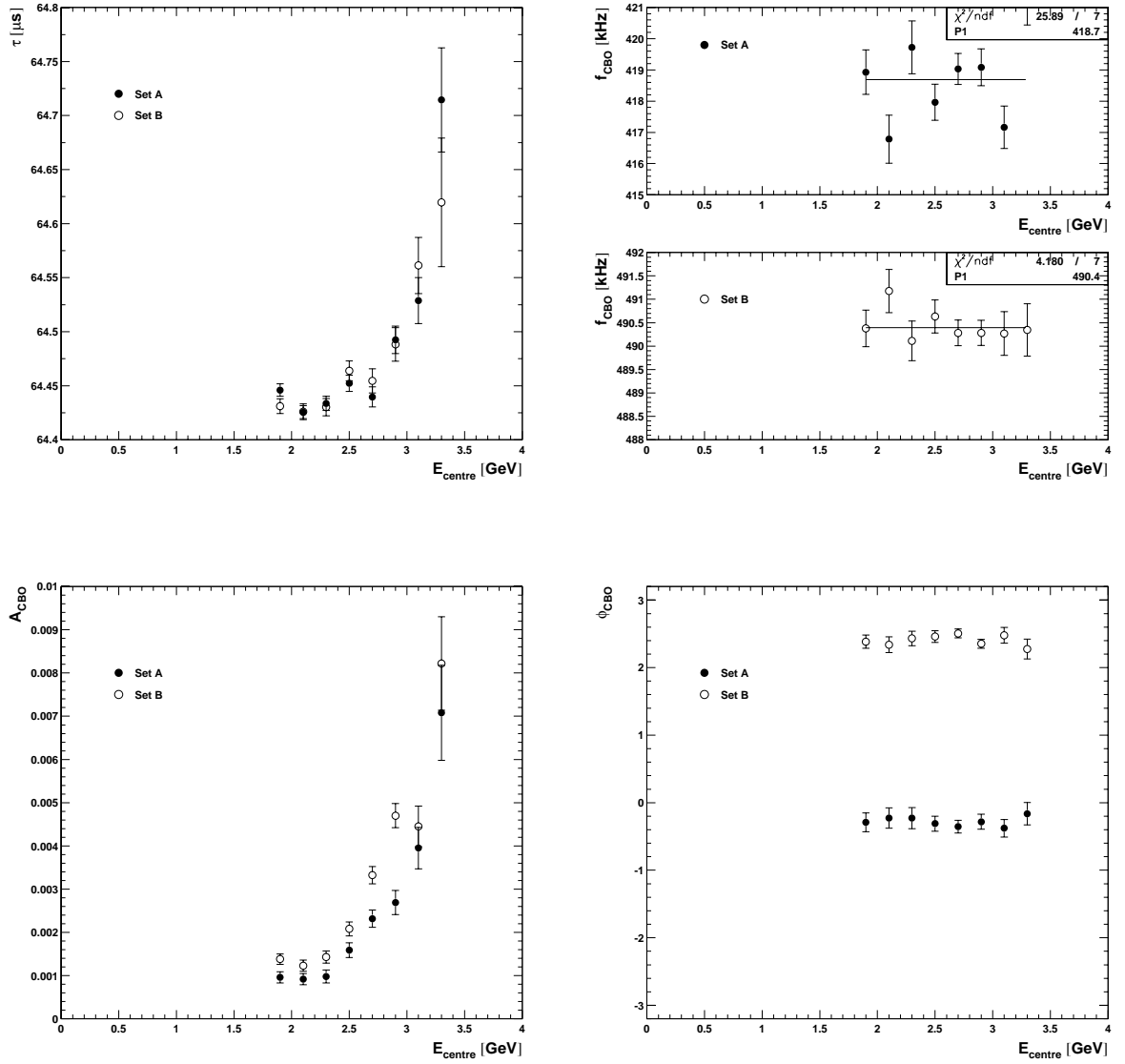


Figure 101: *Fit results versus centre of 200 MeV wide energy bins for a start time of 31.8 μs , performed with the Full Physics Function.*

The instability in f_{CBO} versus E was found to be caused by the inclusion of the asymmetry and phase modulation which are suppressed in narrow energy bins. Fitting with the 1999-style function would be more reasonable in this case.

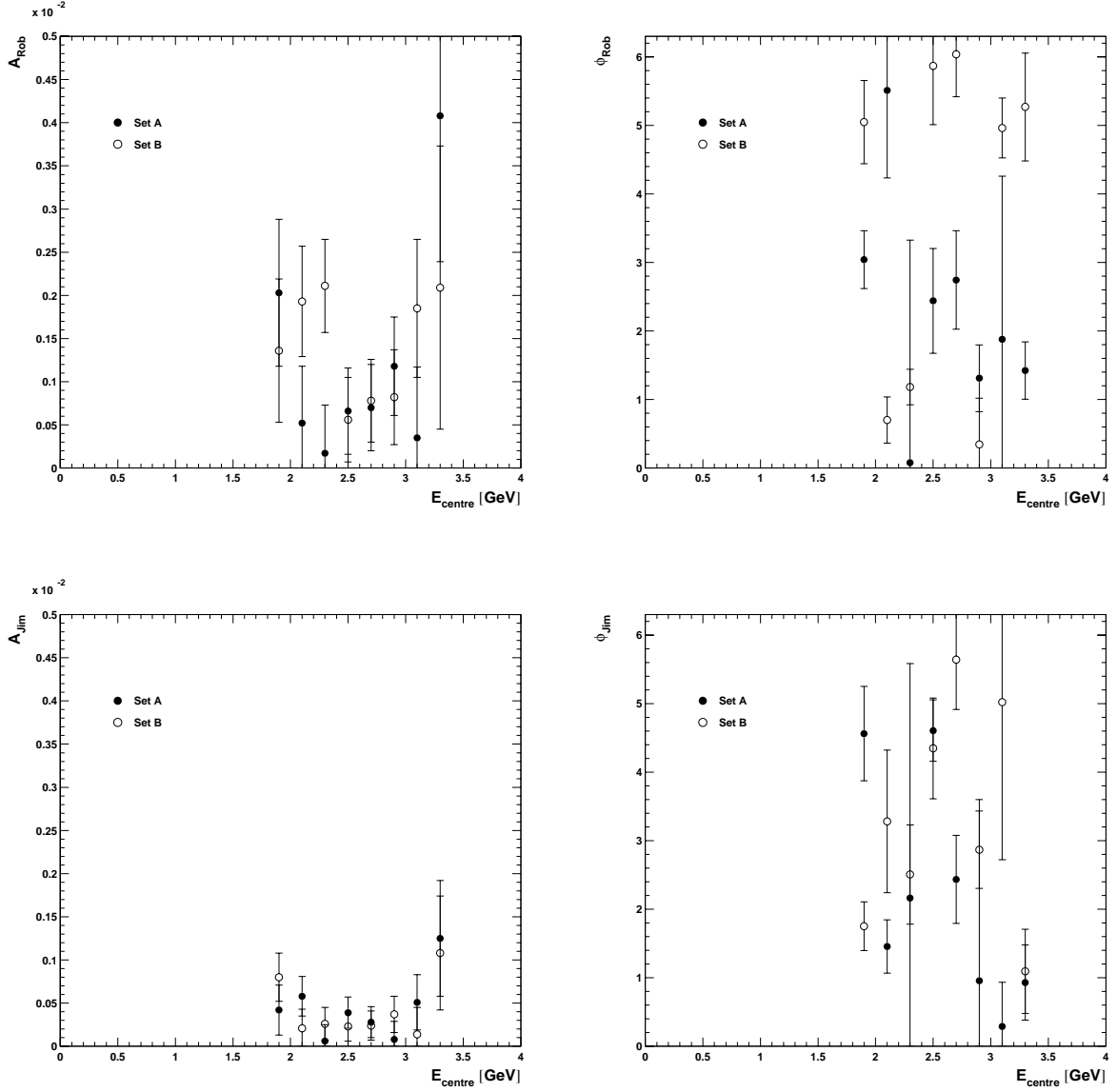


Figure 102: *Fit results versus centre of 200 MeV wide energy bins for a start time of 31.8 μs , performed with the Full Physics Function.*

E Results from the Gain Study

E.1 Average Energy / Gain Sensitivity Factors

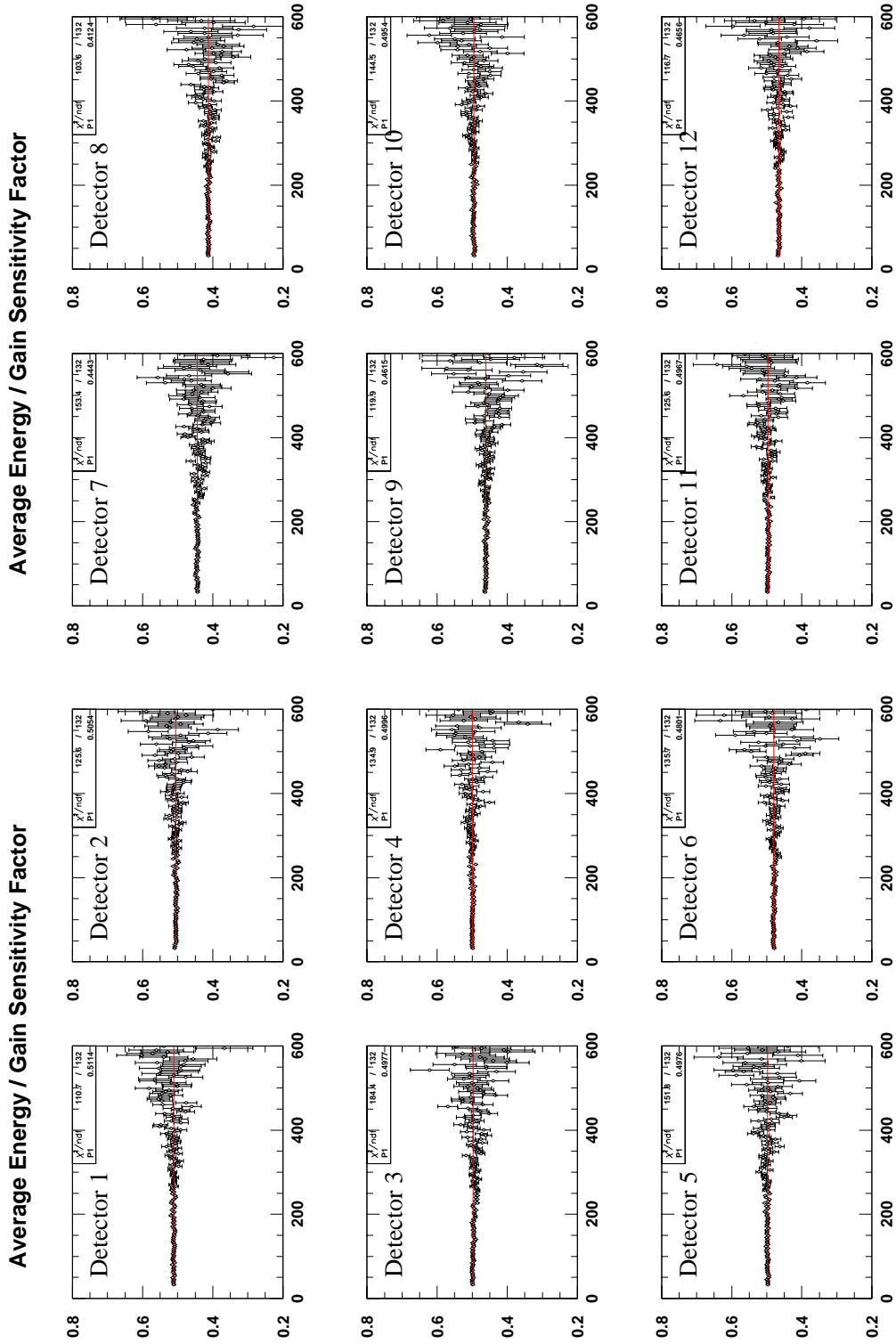


Figure 103: Sensitivity factors for the relation between relative gain change and average energy change for $1.8 \text{ GeV} < E < 3.4 \text{ GeV}$. The two run sets were combined for this study.

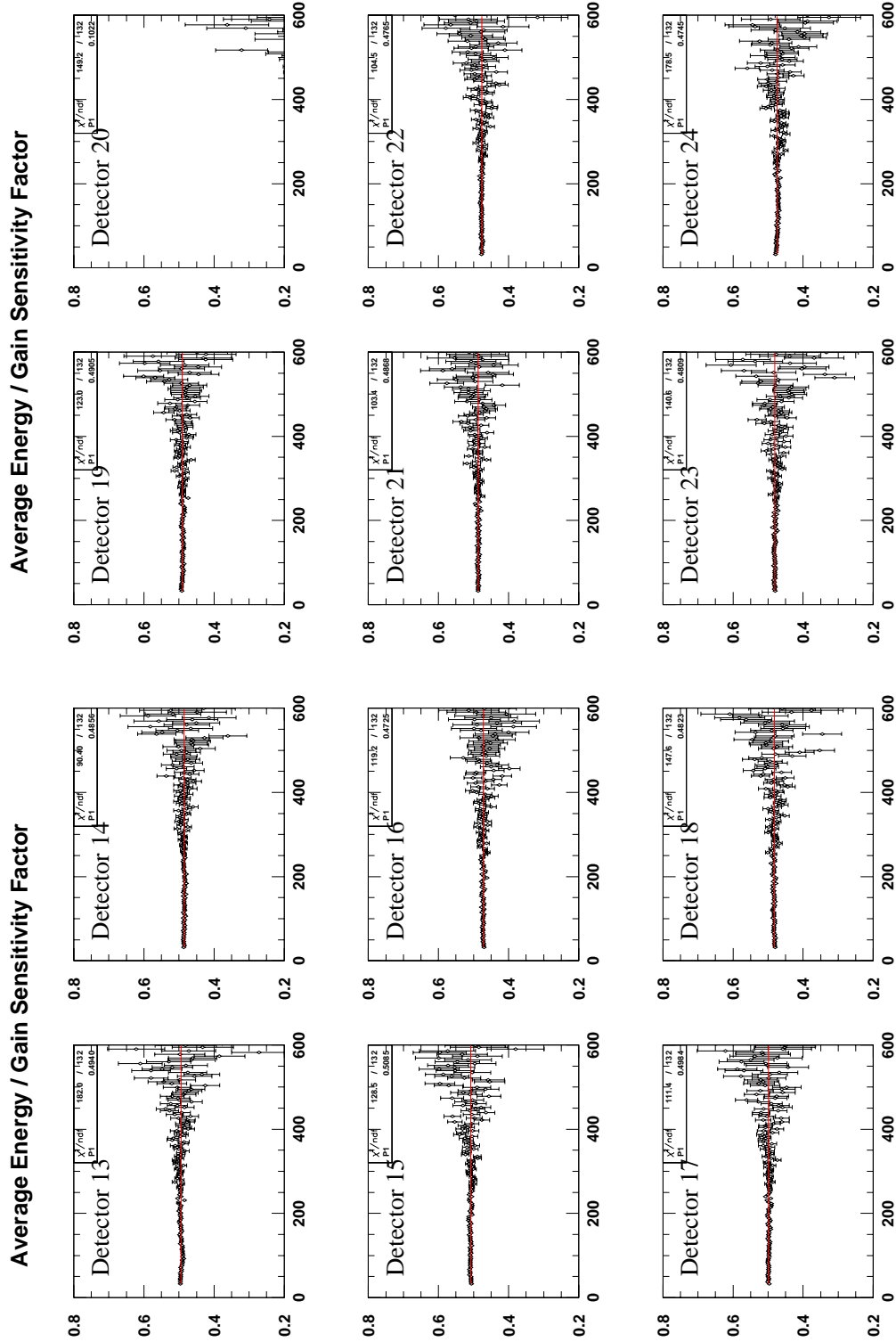
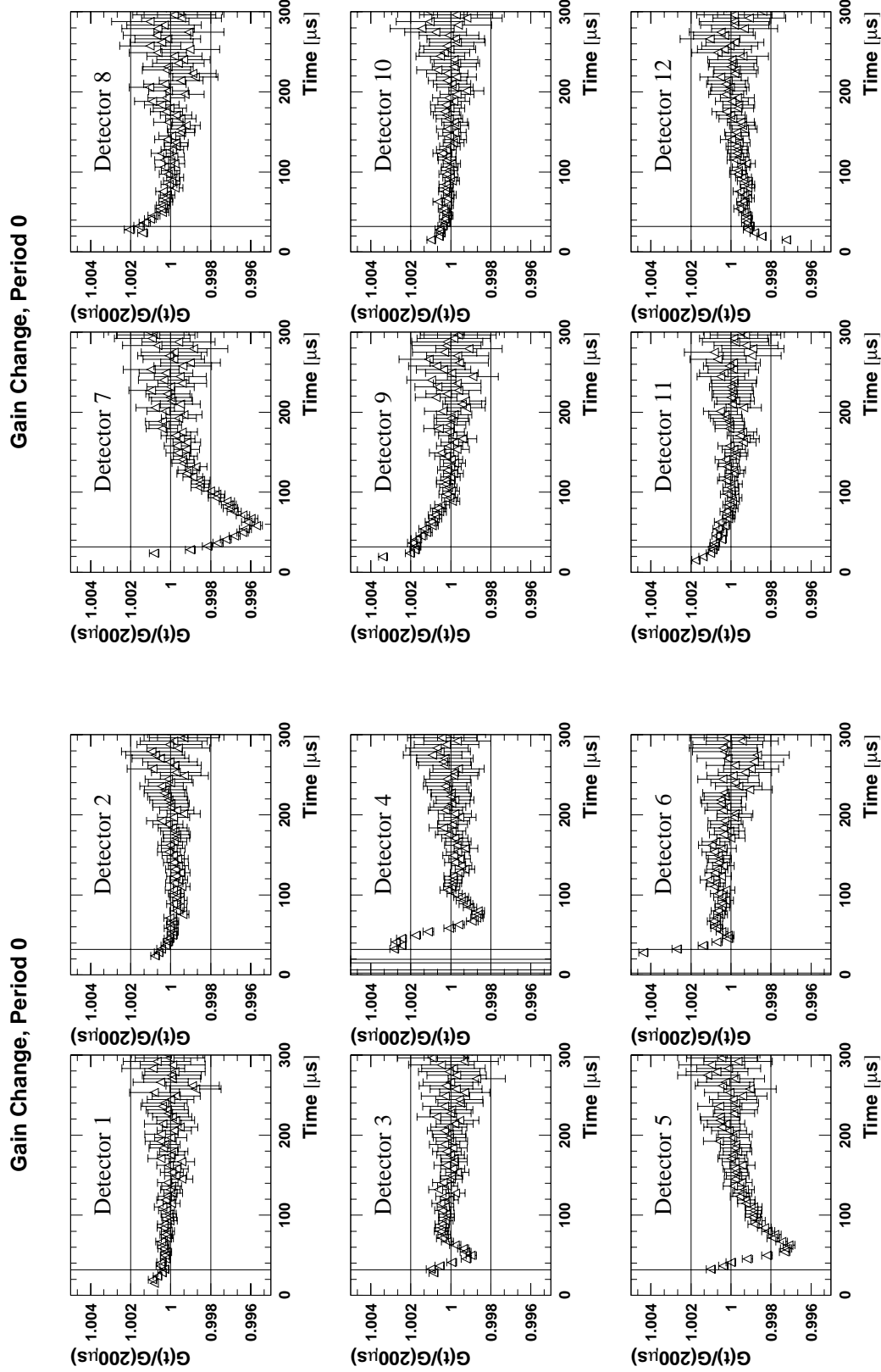


Figure 104: Sensitivity factors for the relation between relative gain change and average energy change for $1.8 \text{ GeV} < E < 3.4 \text{ GeV}$. The two run sets were combined for this study.

E.2 Gain versus Time

Figure 105: *Gain normalised at 200 μs for all runs (detectors 1-12).*

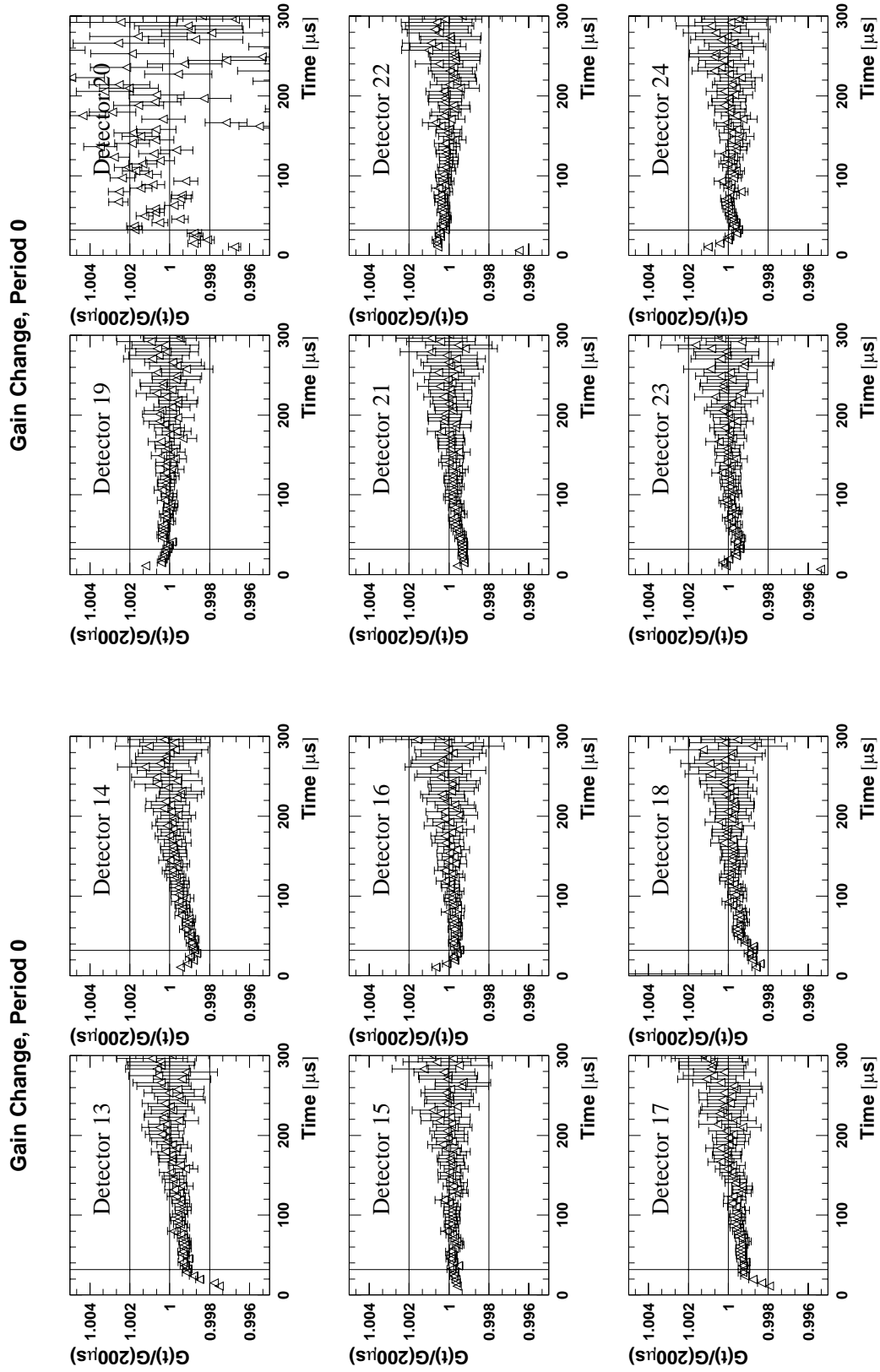
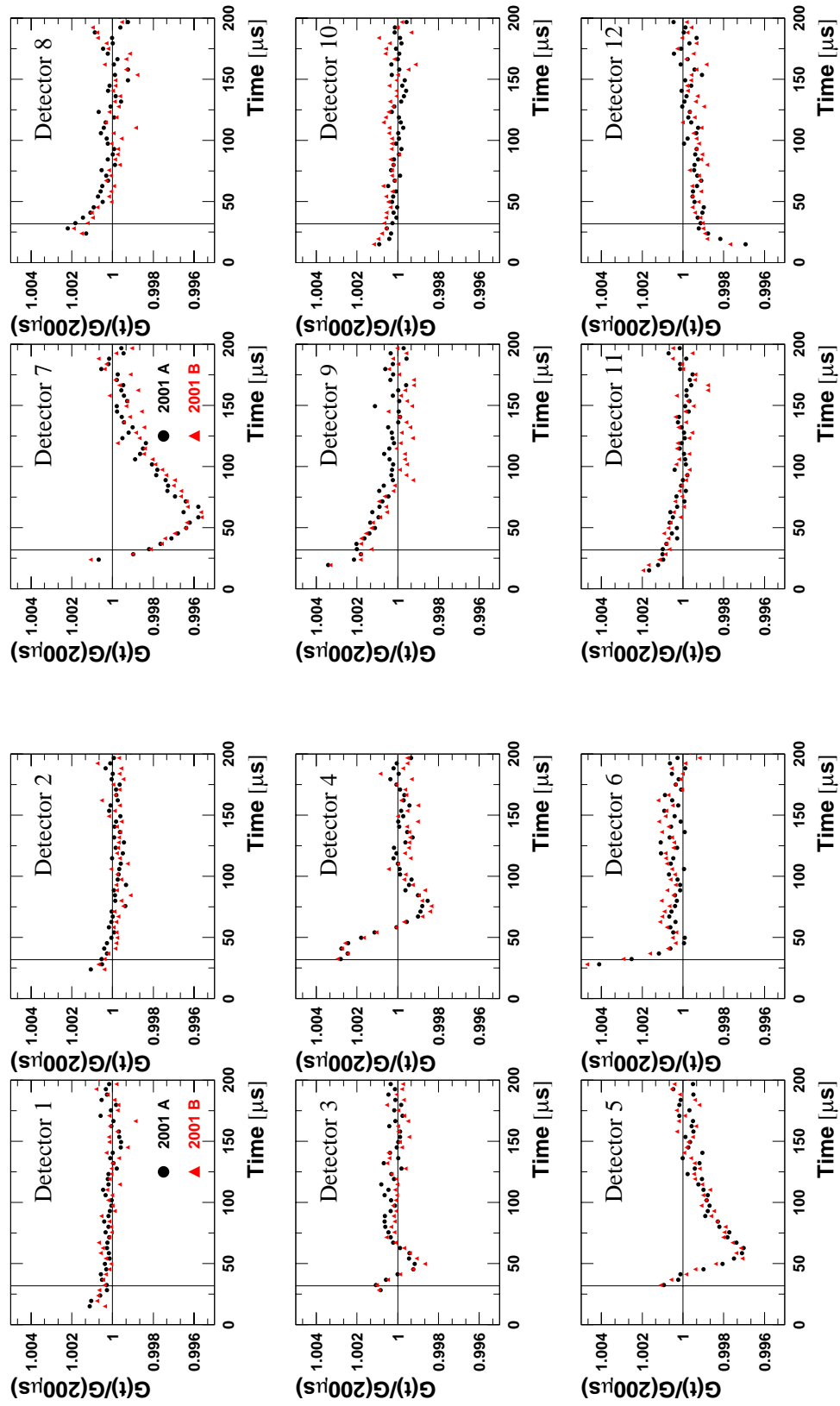


Figure 106: *Gain normalised at 200 μs for all runs (detectors 13-24).*

Figure 107: Gain normalised at $200\mu s$ for Sets A and B separately (detectors 1-12).

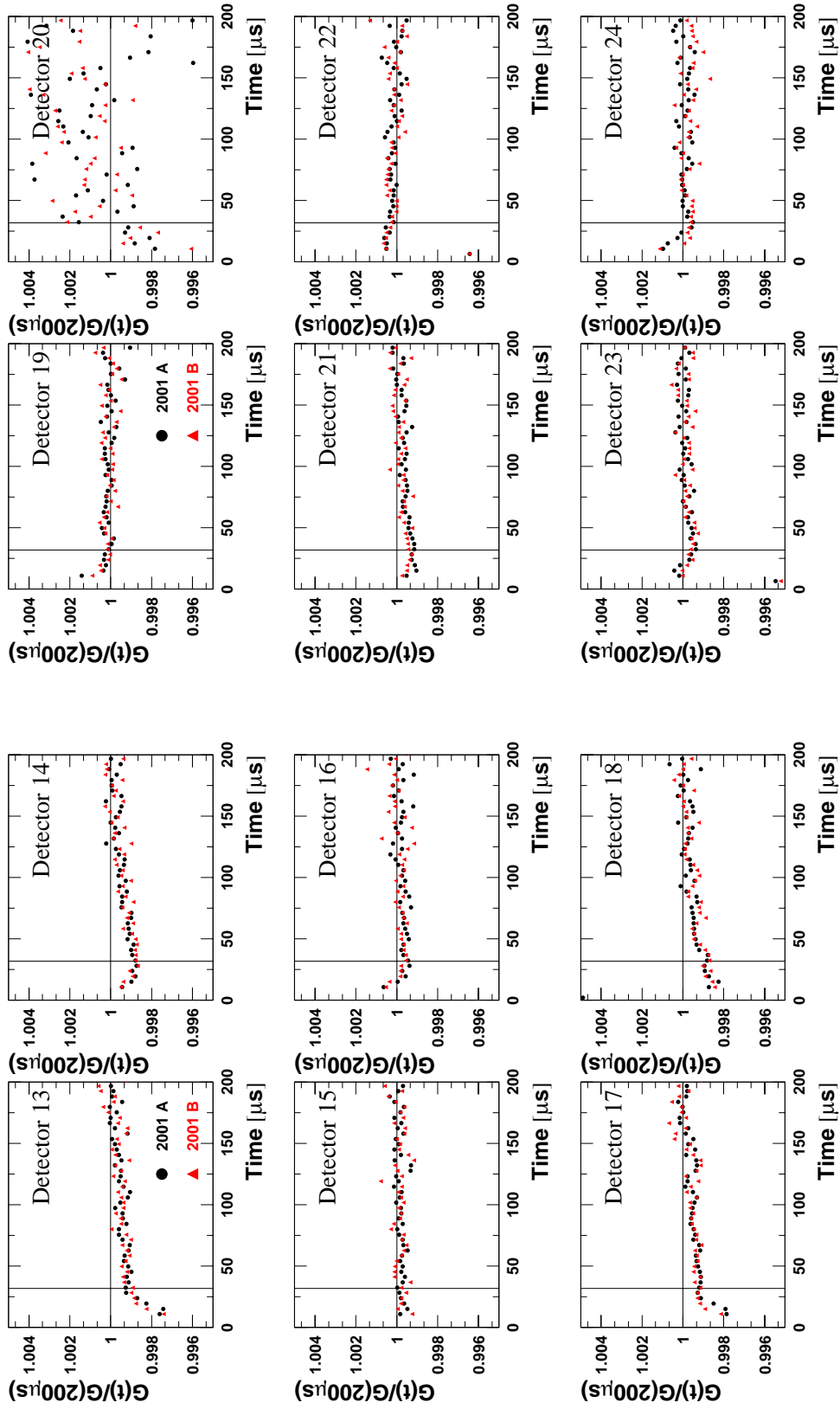


Figure 108: *Gain normalised at 200 μs for Sets A and B separately (detectors 13-24).*